

Chemical Profiling and Toxicological Assessment of Atmospheric Aerosol Using Human Lung Cells



by Faria Khan



IChF

Instytut Chemii Fizycznej PAN



THE UNIVERSITY
of NORTH CAROLINA
at CHAPEL HILL

Ph.D. Thesis

**Chemical Profiling and Toxicological Assessment of
Atmospheric Aerosol Using Human Lung Cells**

Faria Khan

Supervisors: Professor Rafal Szmigielski, Professor Jason D. Surratt

The present thesis was prepared within the International Doctoral Studies in Chemistry at the Institute of Physical Chemistry of Polish Academy of Sciences in collaboration with the Department of Environmental Science and Engineering, Gillings School of Global Public Health at the University of North Carolina at Chapel Hill, NC, USA

Warsaw, November 2021

Biblioteka Instytutu Chemii Fizycznej PAN

F-B.546/22



80000000343608

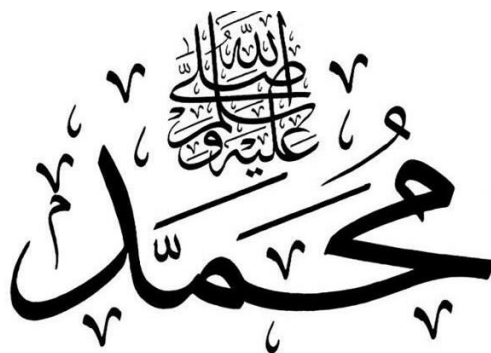
i

<http://rcin.org.pl>



B. 546/22

To



The Seal of all Knowledge

My Lovely Parents,

Maj Khalid Iqbal Khan (retd.) & Sana Khalid

My Husband, Naveed Iqbal

& Grandfather, Mian Haq Nawaz

who left us all before I could complete this journey.

Acknowledgments

I have dreamed a lot about this moment, where the journey to obtain my Ph.D. degree will be near completion. All those years that got me to this point transformed me from a girl who had big dreams to the believer, who knows now everything is possible if you have the right kind of dedication. It wasn't easy- there were so many challenges. Sometimes, I wondered if I chose the right path by getting enrolled in a Ph.D. program so far away from home and family- but then I knew that this need to get the knowledge will get me to a better place in this world. All of this became true because I was always surrounded by people who supported me and lifted me up when life was pulling me down.

I would like to thank my research advisors:

Professor Rafal Szmigielski: I am truly blessed to have a mentor and supervisor like you in my Ph.D. You believed in me and my crazy ideas when I started this research, always drawing the line when I went too over-board. Thank you for always keeping your office door opened for me and allowing me to ignore that "silence zone" sign on it. Your faith in my abilities and polishing them subtly led me to complete this Ph.D. Thank you for giving me this opportunity to gain experience and grow more as a scientist and an individual. Your kind heart and passion for science made my last 4.5 years most awarding experience of life.

Professor Jason D. Surratt: From the day I first met you, there wasn't a single day in which I haven't learned from you. Thank you for being an amazing teacher, supervisor, and a mentor. From long hour meetings in your office (and then virtually), you drew me deep into the world of environmental toxicology. The research questions you raised, made me probe deeper into the research. The detailed inputs in my manuscripts were exhausting yet made me realize how incredibly one can present their research in writing. You kept me motivated when the labs closed due to pandemic and made sure I completed and excelled in the project during my visit to UNC. Now, I am taking with me, a renewed passion for research from you.

I would further like to acknowledge.

Dr Krzysztof Rudziński: For your help in my research (including your persistence to correct my wrong graphs), to arranging real life matters, when I was finding it hard to come to a sane conclusion. Also showing me new and interesting ways to fight for my right.

Dr Karina Kwapiszewska: For the first day in the H9 cell culture lab in 2017 till the last day of my research work in the confocal microscopy lab in 2021. You are the best senior ever.

Dr Nasir Jalal: For helping me understand cell and cancer biology from my undergraduate times and design experiments till my Ph.D., while teaching me important life lessons along the way.

Magda Claeys and Willy Maenhaut: For their guidance, support, and encouragement when I started this research and following up with my progress throughout this journey. Magda you are truly inspirational.

Professor Rebecca C. Fry: For your kind eyes and your guidance. There were times when I thought I can never achieve the end goals of my project due to pandemic, yet you believed in me and allowed me to work in your lab on priority basis. Thank you for believing me till the end and making sure I got an access to all the guidance that I needed for my research.

Dr Mohammed Jaoui: For being my US family and your research collaboration from Environmental Protection Agency (EPA), US, in our nitrophenols project.

Dr Alicia Martinez-Romero: For your collaboration in my three projects, your trainings in the lab with flow cytometry and help in designing experiments.

Dr Yue Zhang: For your help in the monoterpene and isoprene SOA projects and being a warm host in the US.

Dr Yuzhi Chen: For your training with the PAM reactor and practically showing me how the chemistry behind isoprene SOA works in the lab. Also, for help in the monoterpene and isoprene SOA manuscripts,

Hadley Hartwell: For being my only lab-mate during the pandemic times. When I thought the cells won't grow or there is no way to run multiple samples in the lab; you helped me in designing the experiments and in running hundreds of samples in a day. Thank you!

Dr Ying-Hsuan Lin: For teaching me the genome networking and PCA analysis.

Jin Yan: For your help in the isoprene SOA project and running the PAM reactor for days so that I can complete work on time.

Anastasia Freedman: For the last week at UNC, when I had so much to do, and with your help I was able to complete the last set of experiments.

Dr Avram Gold: For your important insights and comments on my projects.

Dr Marta Majewska and Dr Piotr Pieta: For their collaboration on the project related to the nitrophenols exposure in model eukaryotic membrane.

Also, thanks to my professors, Prof Robert Kolos, Robert Nowakowski, and Prof Adam Kubas at ICHF, who helped me gain new knowledge in physical chemistry. Finally, my lab mates Dr Monika, Dr Agatha, Paulina, Klara, Ola, and Kumar for the wonderful time we all shared together in the past 4.5 years. There are people outside of research who are close to my heart and made me who I am today:

My Father: Thank you papa jaan for always supporting me, believing in me, guarding my dreams, and making sure each of them come true. When the men in our society want son as an heir, you made me your whole heirloom. From holding my hands when I was a toddler to going to the schools, exam-halls, universities and even my Ph.D. research institute with me. When I wanted to know the right path, you subtly taught me which one was it. Thank you, papa, for those long hours on phone when I wanted to talk and being my best friend. For that wink, saying mom will be okay and encouraging me to follow my heart. For making sure I am well provided for and calling me first thing in the morning, holding up all your meetings in the office, so that you could talk with me. I know how hard it must have been for you to see your precious struggle so far away and alone in life, yet your trust in me made me a successful human in every walk of life. I owe this Ph.D. to you and mama.

My Mother: My inspiration in life- I have learned so many things from you, in each walk of life. You taught me how to hold the pencil and understand the most complicated writings. I learned how to read a lot of books from you, share the views and research on a topic. When I wrote childish literature at 8, and drew silly diagrams, you read it and encouraged me to write and draw. When I worked for long hours before exams, your love and support kept me motivated. Before my O-levels first exam, our walk and the discussion over can of soda is still engraved to my heart. When I was making the cover of this Ph.D. thesis, you helped me design it amidst all your commitments. You trained me to be a fighter, a winner and taught me never to give up. How difficult it must have been for you to let me go and live my dreams- an average

mom in our society does not have this kind of wisdom. I hired the wisdom and intelligence from you mom and promise to pass it on to the generations to come.

My Husband: The love of my life, Naveed. You came in the most challenging year of my life and then you changed it all in a beautiful way. The passion in your eyes for me, trust and patience help my heart blossom and your encouragement keeps me motivated. When you tell me *دے دو مجھے آؤں میرے خوابوں کو سچا کر لو* (Give me your dreams and I will make them come true), I feel each dream has already come true. Thank you for waiting long hours and days for me while I was completing this Ph.D. and planning my future career goals with me, owning them as yours. For reassuring me you will take care of everything for me and holding my hands tight whenever I get tired in life. With you by my side, I can conquer the world.

Sania Baji (Rumaisa): My baji, who keeps saying “kheir ha” (it’s okay) whenever it gets exasperating, for teaching me how to be patient in life and her lovely doll Alvina, who has my heart with her.

Shabinda: My dolly, who would give me silly pep talks, which never work out, and bringing me food whenever I was studying. You are my best friend; I missed you the most when I left home for the university, and I still miss the beautiful, simple things in life that we used to share together as a team.

Manahil: My kid sister- sometimes I feel like you are the elder one. Your wisdom and wittiness are beautiful. Thank you for keeping a check on me and for long calls when I was in the US and Poland. For listening to my whining, pep talks, lectures and making me laugh. For being so annoying sometimes that I forget about science and feel normal. This journey in science has developed a special bond between us and I look forward to seeing you as a next successful scientist in the family. You are so precious to my heart.

My grandparents: Although you are no more with us, I know you would have been the one most proud of me Abu. I know how you felt about me studying, travelling, and living my life and telling mama “She is like a son, it is possible to travel as a married woman to all those places, but she is doing it all on her own, and that itself is beautiful about her”. I still miss your “waah” (wow) and “kamaal hai” (amazing) when I used to tell you about my life experiences. Thank you Amma, for sitting and waiting for me for long hours at home when I was going to the university and listening to my daily routine when I would return.

My Aunt and Uncle. Thank you, Anny (Saira Moazzam), for being my guardian angel, for the first day in Europe and travelling with me from Barcelona to Poland. For making sure I was in the safe hands of Rafal and Krystof (lol) and coming to my rescue whenever I made a blunder. Thank you for taking care of me, listening to my worries, and providing me with a solution. Thank you Khaloo (Dr Moazzam Ali) for being a source of inspiration, guiding me through my professional journey, teaching me how to deal with the people from distinct cultural backgrounds and being a guardian in my journey as a researcher. Also, thanks to their kids, Mashaal (for her love, calls and silly jokes), Daniyal (for trying to be a responsible elder brother, getting exasperated when I used to make errors in booking flights and planning exciting travel plans with me) and Hassan (for being my darling kid brother, annoying and loving me unconditionally).

My friend, Nabila: This Ph.D. journey would have been really boring without you. We shared so much things- happiness, our first experimental success, our blunders, crazy research ideas, our silly future plans. But most importantly, we co-existed in each other’s challenging times and listened patiently to each other over a cup of coffee in the office, when after long weeks and hours of working (which ultimately turned into months), we would not get good results in the lab. You made it all so much beautiful and I will cherish the memories with you for years to come.

Aisha: For her support and being my family during my Ph.D. in Poland.

Statement of Originality

I, *Faria Khan*, confirm that the research included within the present thesis was conducted by myself or in collaboration with and supported by others, as described in the acknowledgments section. Moreover, the previously published material is listed below.

I attest that I have exercised reasonable care to ensure that the work is original, and does not, to the best of my knowledge, violate any Polish or International law, infringe any third party's copyright or other Intellectual Property Right, or contains any confidential material.

I accept that the Polish Academy of Sciences has the right to use plagiarism detection software to check the electronic version of the thesis.

I confirm that my thesis has previously not been submitted for the award of a degree by IPC PAS or any other institute or university.

The copyright of this thesis rests with the author, and no quotation from it or information derived from it may be published without the author's prior written consent.

Signature:

Date:

Funding

The undertaken research work was financed by:

- The European Union's Horizon 2020 research and innovation program under the Marie Skłodowska-Curie grant agreement No. 711859 and by financial resources for science in 2017–2021 awarded by the Polish Ministry of Science and Higher Education for the implementation of an international co-financed project.
- U.S. National Science Foundation grant number 1703535 for supporting the chemical analysis of the SOA samples collected from the PAM reactor.
- Research on methyl-tetrol sulfates was supported by the National Institute of Environmental Health Sciences (NIEHS) of the National Institutes of Health (NIH) under award number P30ES010126, the University of North Carolina Center for Environmental Health and Susceptibility (UNC-CEHS).



Horizon 2020
European Union Funding
for Research & Innovation



National
Science
Centre
Poland



List of Publications Included in this Study

Faria Khan, Karina Kwapiszewska, Yue Zhang, Yuzhi Chen, Andrew T. Lambe, Agata Kołodziejczyk, Nasir Jalal, Krzysztof Rudzinski, Alicia Martínez-Romero, Rebecca C. Fry, Jason D. Surratt, and Rafal Szmigielski, *Chemical Research in Toxicology*, 2021, 34 (3), 817-832, DOI: 10.1021/acs.chemrestox.0c00409

Marta Majewska, **Faria Khan**, Izabela S. Pieta, Aleksandra Wróblewska, Rafal Szmigielski, Piotr Pieta, Toxicity of selected airborne nitrophenols on eukaryotic cell membrane models, *Chemosphere*, 2021, Volume 266, 128996, ISSN, 0045-6535, DOI: 10.1016/j.chemosphere.2020.128996.

Faria Khan, Yuzhi Chen, Hadley J. Hartwell, Jin Yan, Ying-Hsuan Lin, Anastasia Freedman, Zhenfa Zhang, Yue Zhang, Andrew T. Lambe, Avram Gold, Andrew P. Ault, Rafal Szmigielski, Rebecca C. Fry, and Jason D. Surratt, Heterogeneous Oxidation Products of Particulate Isoprene Epoxydiol-Derived Methyltetrol Sulfates Increase the Oxidative Stress and Inflammatory Gene Responses in Human Lung Cells. (Submitted in ES&T), 2021.

Faria Khan, Mohammed Jaoui, Krzysztof Rudziński, Karina Kwapiszewska, Alicia Martínez-Romero, Domingo Gil-Casanova, Michael Lewandowski, Tadeusz E. Kleindienst, John H. Offenberg, Jonathan D. Krug, Jason D. Surratt and Rafal Szmigielski, Cytotoxicity and Oxidative Stress Induced by Atmospheric Mono-Nitrophenols in Human Lung Cells. (Submitted in ES&T), 2021.

Faria Khan, Karina Kwapiszewska, Alicia Martínez-Romero, Domingo Gil-Casanova, Krzysztof Rudziński, Jason D. Surratt, and Rafal Szmigielski, Exposure to Biomass Burning Aerosol Components Impair Mitochondrial Function to induce Cytotoxicity in Human Lung Cells. (Under Preparation), 2021.

Other List of Publications

Faria Khan, Sajid Iqbal, Nauman Khalid, Irshad Hussain, Zajif Hussain, Rafal Szmigielski & Hussnain A. Janjua, Screening and stability testing of commercially applicable *Heliotropium crispum* silver nanoparticle formulation with control over aging and biostability. *Appl Nanosci* **10**, 1941–1956 (2020). DOI:10.1007/s13204-020-01333-x

Faria Khan, Rafal Szmigielski, Alvina Gul, Volkan Altay and Munir Ozturk, Advancements in plant transgenomics approach for the biopharmaceutics and vaccines production, July 2020. In book: Biodiversity and Biomedicine - Our Future Publisher: Academic Press-Elsevier.

Moazzam Ali, Joanna Paula Cordero, **Faria Khan** & Rachel Folz, Leaving no one behind': a scoping review on the provision of sexual and reproductive health care to nomadic populations. *BMC Women's Health* **19**, 161, 2019. DOI:10.1186/s12905-019-0849-4

Faria Khan, Naeem Akhtar, Nasir Jalal, Irshad Hussain, Rafal Szmigielski, M. Qasim Hayat, Hasfiz B. Ahmad, W. A. El-Said, M. Yang and Hussnain. A. Janjua, 2019, Carbon-dot wrapped ZnO nanoparticle-based photoelectrochemical sensor for selective monitoring of H₂O₂ released from cancer cells, *Microchimica Acta* 186(2): 127. DOI:10.1007/s00604-019-3227-x

Javaria Hanif, Nauman Khalid, Rao Sanaullah Khan, Muhammad Faraz Bhatti, Mohammad Qasim Hayat, Muhammad Ismail, Saadia Andleeb, Qaisar Mansoor, **Faria Khan**, Faheem Amin, Rumeza Hanif, Muhammad Uzair Hashmi, Hussnain Ahmed Janjua, Formulation of active packaging system using Artemisia scoparia for enhancing shelf life of fresh fruits, 2019, *Materials Science and Engineering: C*, Volume 100, 2019, Pages 82-93, ISSN 0928-4931, DOI: 10.1016/j.msec.2019.02.101

Faria Khan, Zaineb Sohail, Tahira Khan, Bukhtawar Fatima, Fatima Malik, Syeda Fatma Hassan Bukhari, Sameen Ruqia Imadi, and Alvina Gul. Deforestation: A Continuous Battle—A Case Study from Central Asia and Other Countries. 2018. In *Vegetation of Central Asia and Environs*, edited by Dilfuza.

Muhammad Uzair Hashmi, **Faria Khan**, Nauman Khalid, Asad Abdullah Shahid, Aqib Javed, Tehseen Alam, Nasir Jalal, Muhammad Qasim Hayat, Shah Rukh Abbas, Hussnain Ahmed Janjua, Hydrogels incorporated with silver nanocolloids prepared from antioxidant rich *Aerva javanica* as disruptive agents against burn wound infections disruptive agents against burn wound infections, 2017. *Colloids and Surfaces a Physicochemical and Engineering Aspects*. DOI: 10.1016/j.colsurfa.2017.06.036

Faria Khan, Amjad Ali and Alvina Gul, Omics approaches and engineering against Superbug, 2017. in *Omics Technologies and Bioengineering: Towards Improving Quality of Life*, Chapter: 41, Publisher: Elsevier, Editors: Debmalya Barh, Vasco Azevedo

Faria Khan, Muhammad Uzair Hashmi, Nauman Khalid, Muhammad Qasim Hayat, Aamer Ikram, Hussnain A. Janjua, Controlled assembly of silver nano-fluid in *Heliotropium crispum* extract: A potent anti-biofilm and bactericidal formulation, *Applied Surface Science*, Volume 387, 2016, Pages 317-331, ISSN 0169-4332, DOI:10.1016/j.apsusc

Uzair Hashmi, Samia Shafqat, **Faria Khan**, Misbah Majid, Harris Hussain, Alvina Gul Kazi, Riffat John & Parvaiz Ahmad (2015) Plant exomics: Concepts, applications and methodologies in crop improvement, *Plant Signaling & Behavior*, 10:1, DOI: 10.4161/15592324.2014.976152

Poster Presentations at International Conferences

Faria Khan, Karina Kwapiszewska, Mohammad Jaoui, Alicia Martinez-Romero, Krzysztof Rudzinski, Jason Surratt and Rafal Szmigielski, *Toxicological Profiling of Environmental 2-, 3- and 4-Nitrophenols using Human Lung Cells*, 17-21 May 2021, European Union Commission's JRC Virtual Summer School on Non-animal Approaches in Science: The Three R Evolution (Virtual).

Faria Khan, Karina Kwapiszewska, Alicia M. Romero, Nasir Jalal, Krzysztof Rudzinski, Jason D. Surratt, Rafal Szmigielski, *Exposure to Atmospheric 4-Nitrocatechol causes Mitochondrial Dysfunction to Induce Apoptosis in the BEAS-2B Cells*, 12-16 March 2021, Annual Meeting of the Society of Toxicology (Virtual).

Faria Khan, Karina Kwapiszewska, Yue Zhang, Yuzhi Chen, Agata Kołodziejczyk, Nasir Jalal, Krzysztof Rudzinski, Rebecca Fry, Jason D. Surratt, Rafal Szmigielski, *Toxicological Responses of α -Pinene-Derived Secondary Organic Aerosol in Human Lung Cell Lines* (North Carolina, US), 17-23 September 2020, Annual Conference of North Carolina Chapter Society of Toxicology, USA (Virtual).

Faria Khan, Karina Kwapiszewska, Nasir Jalal, Krzysztof Rudzinski, Jason D. Surratt and Rafal Szmigielski. *The monitoring of air quality through impact of the aerosol components on human health*, 8-14 July 2018, Euro Science Open Forum, Toulouse, France.

Faria Khan, Nauman Khalid, Irshad Hussain, Rafal Szmigielski, Hussnain A. Janjua *Stability Testing of Antimicrobial Heliotropium Crispum Silver- Nanoparticles as a Commercial Formulation for treatment against Drug Resistant Bacterial Pathogens*, 20-24 October 2018. New York Academy of Sciences, New York, USA.

Oral Presentations at International Conferences

Faria Khan, Karina Kwapiszewska, Alicia M. Romero, Krzysztof Rudzinski, Jason D. Surratt, Rafal Szmigielski, *Biomass Burning Aerosol Components Impair Mitochondrial Functioning to Induce Toxicological Response in Lung Cell Lines*, 5-9 October 38th The American Association for Aerosol Research, Raleigh, North Carolina, USA (Virtual).

Faria Khan, Karina Kwapiszewska, Nasir Jalal, Krzysztof Rudzinski, Jason D. Surratt and Rafal Szmigielski., *Acute Exposure Effects of Biomass Burning Aerosol Components in BEAS-2B Cell Lines: Dosage-Time Dependent Cellular Response*, 25-30 August 2019, European Aerosol Conference, Gothenburg, Sweden

List of Abbreviations

- 2MGS**- Glycolic Acid Sulfate
2NP- 2-Nitrophenol
3NP-3-Nitrophenol
4NP- 4-Nitrophenol
AU- Arbitrary Unit
AFM- Atomic Force Microscopy
APHEA- Air Pollution and Health: a European Approach
ARDS- Acute Respiratory Distress Syndrome
ARE- Antioxidant Response Element
ASOA- Anthropogenic Secondary Organic Aerosol
BBA- Biomass Burning Aerosol
BBOA- Biomass Burning-Derived Organic Aerosol
BC- Black Carbon
BEGM- Bronchial Epithelial Cell Growth Medium
BrC- Brown Carbon
BSOA- Biogenic Secendory Organic Aerosol
BSTFA- Trimethylsilyl Trifluoroacetamide: 1% Trimethylchlorosilane
BVOCs- Biogenic Volatile Organic Compounds
Carboxy-H₂DCHF- 6-Carboxy-2',7'-Dichlorodihydrofluorescein Diacetate
CCR- Carbon-Centred Radicals
cdNA- Complimentary DNA
COPD- Chronic Obstructive Pulmonary Disease
COX2- Cyclo-oxygenase 2
CRP- C-Reactive Protein
DEP- Diesel Exhaust-Particulate
DMEM- Dulbecco's Modified Eagle's Medium
DMPC- 1,2-Dimyristoyl-Sn-Glycero-3-Phosphocholine
DMSO- Dimethyl Sulfoxide
DPBS- Dulbecco's Phosphate-Buffered Saline
DPPC-1,2-Dipalmitoyl-Sn-Glycero-3-Phosphocholine
DTT- Dithiothreitol

EIC – Extracted Ion Current Chromatogram
EIS– Electrochemical Impedance Spectroscopy
ELVOCs– Extremely Low-Volatility Organic Compounds
EPA– Environmental Protection Agency
ET-1– Endothelin
ESI – Electrospray Ionization Mass Spectrometry
FCCP– Carbonyl cyanide 4-(trifluoromethoxy) phenylhydrazone
FITC– Fluorescein Isothiocyanate
GCLC– Glutamate-Cysteine Ligase Catalytic Subunit
GCLM– Glutamate-Cysteine Ligase Modifier Subunit
GC-MS– Gas Chromatography Interfaced to Mass Spectrometry
GSH –Glutathione
GST– Glutathione-S-Transferases
H₂SO₄– Sulfuric Acid
HILIC/ESI-HR-QTOFMS– Hydrophilic Interaction Liquid Chromatography Interfaced to Electrospray Ionization High-Resolution Quadrupole Time-of-Flight Mass Spectrometry
HMOX-1– Heme Oxygenase-1
HNO₃–Nitric Acid
IC– Ion Chromatography
IC₅₀– Inhibitory Concentration-50
IEPOX– Isoprene Epoxy Diols
IL10– Interleukin 10
IL6– Interleukin 6
IL8– Interleukin 8
IPF– Idiopathic Pulmonary Fibrosis
ISOPOOH– Isoprene Hydroxy Hydroperoxides
KEAP1– Kelch-like ECH-associated protein 1
KPA– Ketopinic Acid
LD₅₀– Lethal Dose, 50%
LDH– Lactate Dehydrogenase
LG– Levoglucosan
LRP– Lung Resistance-Related Protein
MAE– Methacrylic Acid Epoxide

MBTCA- 3-Methyl-1,2,3-Butanetricarboxylic Acid
MLR -Multiple Linear Regression
MMP9- Matrix Metalloproteinase
MPPD- Multiple Path Particle Dosimetry
MSA- Methane Sulfonic Acid
mtROS- Mitochondrial Reactive Oxygen Species
2-MTSs- 2-Methyltetrol Sulfates
MTT- Mitochondrial Toxicity Testing
NACs- Nitro-Aromatic Compounds
NADPH- Nicotinamide Adenine Dinucleotide Phosphate Oxidase
NC- 4-Nitrocatechol
NG- 4-Nitroguaiacol
NitroPAHS- Nitro-Polyaromatic Hydrocarbons
NMMAPS- National Mortality, Morbidity and Air Pollution Studies
NMOC- Non-Methane Organic Carbon
NO₃- Nitrate Radicals
Nrf2- Nuclear Factor (Erythroid Derived 2)-Like 2
NS- 3-Nitrosalicylic Acid
NSOA- Naphthalene-Derived Secondary Organic Aerosol
O₃- Ozone
OC- Organic Carbon
OH- Hydroxyl Radical
OSs- Organosulfates
PAM – Potential Aerosol Mass Flow Oxidation Reactor
PC- Phosphatidylcholines
PC- Principal Components
PG- Phosphatidylglycerol
PI- Propidium Iodide
PM- Particulate Matter
PM_{0.1}- Ultra-Fine Particles with Aerodynamic Diameter $\leq 0.1 \mu\text{m}$
PM₁₀- Coarse PM Of Aerodynamic Diameter $\leq 10 \mu\text{m}$
PM_{2.5}- Fine PM Of Aerodynamic Diameter $\leq 2.5 \mu\text{m}$
POA- Primary Organic Aerosol

POPC-1-Palmitoyl-2-Oleoyl-Sn-Glycero-3-Phosphocholine
PS- Phosphatidylserine
RH- Relative Humidity
RNS- Reactive Nitrogen Species
RO₂[•]-Peroxy Radicals
ROS- Reactive Oxygen Species
RT-qPCR -Real Time Quantitative Polymerase Chain Reaction
SMPS- Scanning Mobility Particle Sizer
Sulf_{inorg}- Inorganic Sulfates
TBARS-Thiobarbituric Acid Reactive Substance
TC-Tissue Culture
TIC – Total Ion Current Chromatogram
Tg Yr⁻¹-Teragram Per Year
TGF-β- Tumor Growth Factor
TMRM- Tetramethyl Rhodamine Methyl Ester
TNF-α- Tumor Necrosis Factor Alpha
UPLC/ESI-HR-QTOFMS- Ultra-Performance Liquid Chromatography Interfaced to
Electrospray Ionization High-Resolution Quadrupole Time-of-Flight Mass Spectrometry
VOCs- Volatile Organic Compounds
WHO- World Health Organization
ΔΨ_m- Mitochondrial Membrane Potential

Abstract (in English)

The main objective of this research was to determine the exposure health effects of various types of atmospherically-relevant submicron organic aerosol (OA) by using human lung cell lines. Airborne fine particulate matter of aerodynamic diameters $< 2.5 \mu\text{m}$ ($\text{PM}_{2.5}$) contributes to poor air quality, climatic change and exhibits adverse health effects upon inhalation. $\text{PM}_{2.5}$ exposures trigger lung-associated pathologies, including asthma, allergy, chronic obstructive pulmonary disease (COPD), bronchitis, emphysema, decreased lung function, and increased instances of lung cancer. This research aimed to decipher changes in lung cells at the molecular, cellular, biochemical, and/or genomic levels, which were induced by submicron OA exposures originating from four different atmospheric sources, including from: (i) monoterpene-derived secondary organic aerosol (SOA) obtained through the ozonolysis of α -pinene, (ii) heterogeneously-aged isoprene-derived particulate 2-methyltetrol sulfates (2-MTSs), which are the most abundant particulate organosulfates (OS) detected in ambient $\text{PM}_{2.5}$ and contribute greatly to isoprene SOA, and (iii) atmospheric-relevant mono-nitrophenols (NPs), and (iv) other key components of biomass burning aerosol (BBA).

Two *in vitro* cell models, BEAS-2B (i.e., immortalized human bronchial epithelial cells) and A549 (i.e., adenocarcinoma human alveolar epithelial cells) were selected in the current thesis projects to determine acute exposure effects. In the first two sections of this thesis, an oxidation flow reactor (OFR) was used to produce SOA from α -pinene ozonolysis, and OS mixtures produced from the heterogeneous hydroxyl radical ($\cdot\text{OH}$)-mediated oxidation of particulate 2-MTSs (equivalent to 0-22 days of atmospheric aging), respectively. The aerosol mixtures were analysed using liquid chromatography interfaced to high-resolution electrospray ionization tandem mass spectrometry (LC/ESI-HR-MS/MS) to detect organic acids and peroxides from α -pinene ozonolysis SOA, and multifunctional OSs from heterogeneously aged particulate 2-MTSs. Furthermore, qualitative chemical analyses of ambient $\text{PM}_{2.5}$ and SOA generated from the photooxidation of a series of monocyclic aromatic hydrocarbons in the United States (US) Environmental Protection Agency (EPA) smog chamber was conducted for atmospheric NPs.

The aerosol mixtures of known and characterized OA markers were then exposed to lung cells and assessed for the percentage of cellular proliferation using high throughput

assays; subsequent time- and concentration-dependent viability values were used to determine the inhibitory concentration-50 (IC₅₀) of each atmospheric OA system. In addition, functional assays with fluorescent probes were used to detect cellular reactive oxygen species (ROS) and mitochondrial ROS (mtROS) post-exposure; these assays used flow cytometry and confocal microscopy, respectively. Changes in cellular viability were analysed through live/dead staining under a fluorescent microscope, whereas cells death mechanisms were determined through the Annexin V/Propidium Iodide assay using flow cytometry. Real-time quantitative polymerase chain reaction (RT-qPCR) was utilized to evaluate genomic changes that could result from exposures to heterogeneously-aged particulate 2-MTSs to determine the post-exposure responses via modulation of oxidative stress and inflammatory genes.

In the first part of this thesis, we quantified an increasing concentration response of three well-established α -pinene SOA tracers (pinic, pinonic, and 3-methyl-1,2,3-butanetricarboxylic acids) and a complete mixture of α -pinene ozonolysis SOA in A549 and BEAS-2B cell lines. The atmospheric ozonolysis of α -pinene (C₁₀H₁₆), an abundantly emitted monoterpene from terrestrial vegetation, contributes significantly to the global SOA budget; however, its impact on pulmonary pathophysiology remains uncertain. Cellular proliferation, cell viability, and oxidative stress were assessed as toxicological endpoints in this study. The three aforementioned tracers contributed ~57% of the α -pinene ozonolysis SOA mass; however, multifunctional hydroperoxides identified in the SOA could have contributed more than these individual SOA tracers to the toxicological changes observed.

The second part of this thesis focused on examining the inhalation toxicity associated with the isoprene-derived aerosol particles in the atmosphere. Isoprene (C₅H₈) is the most abundant reactive hydrocarbon released into Earth's atmosphere from vegetation. Once emitted to the atmosphere and exposed therein to \cdot OH under low-NO_x conditions, isoprene oxidation yields high quantities of gaseous epoxydiols (IEPOX). These reactive intermediates interact with acidic sulfate aerosol (generated from human activities) to afford a wide variety of low-volatility particle-bound reaction products, such as OSs. One of the most abundant atmospheric OSs is 2-MTSs. 2-MTSs can undergo further chemical changes in the atmosphere, which leads to the formation of photochemically-aged particles of far more complex chemical compositions. The goal of this portion of the thesis was to gain insights into how these changes might contribute to increased oxidative stress and inflammatory responses in BEAS-2B cells.

The third project of this thesis involved toxicological profiling of atmospherically-relevant NPs using BEAS-2B and A549 cell lines. NPs are found as trace pollutants in various environmental matrices, including PM_{2.5}, agricultural residues, cloud water, rain-water, wildfires, and industrial wastes. First, an equimolar mixture of NPs was exposed to the eukaryotic lipid bilayer membrane to determine the exposure effects on the cell membrane surface. In addition, comparative toxicology of 2-nitrophenol (2NP), 3-nitrophenol (3NP), 4-nitrophenol (4NP), and their equimolar mixture was provided using several ROS, mtROS, cellular viability, and cellular death assays.

The last part of this thesis conducted a detailed toxicological analysis of four important BBA components in the A549 and BEAS-2B cell lines. BB is a major pollution source, particularly in urban, suburban, and rural areas, and was hypothesized to induce increased morbidity and mortality through long-term inhalation. The four BBA components included levoglucosan (LG), 3-nitrosalicylic acid (NS), 4-nitrocatechol (NC), and 4-nitroguaiacol (NG). The exposed cells were analysed for changes in general ROS and mtROS to predict altered biochemical pathways at different exposure concentrations and times. This study was concluded by proposing cellular death mechanisms upon exposure to these chemicals.

The profiling of atmospheric aerosol mixtures and their individual markers from four atmospherically-relevant aerosol systems provide a comparative toxicology in lung cells. We predict the atmospheric system with nitro-aromatics have the highest potential for adverse effects following inhalation. The response was predicted using the IC₅₀ values and the number of atmospherically relevant years required to achieve that effect. This thesis also determines the pathophysiological changes in lungs at the molecular and cellular levels after exposure, which varied significantly with the chemical composition and chemical structure of the markers, as well as time and concentration of exposure. The study further highlights the need to develop regulations and control strategies to mitigate the emission rates of a few emission types due to their potential adverse effects following acute exposure.

Abstrakt (w języku polskim)

Wiodącym kierunkiem opisanych tu badań była próba określenia skutków zdrowotnych ekspozycji na różne składniki submikronowych cząstek aerozolu organicznego (OA) o znaczeniu atmosferycznym przy użyciu dwóch linii komórkowych pochodzących z ludzkich płuc. Unoszące się w powietrzu drobne cząstki stałe o średnicach aerodynamicznych $< 2,5 \mu\text{m}$ (tzw. *frakcja respirabilna PM_{2.5}*) są główną przyczyną pogorszenia jakości powietrza, zmian klimatycznych, a nade wszystko – wykazują niekorzystne skutki zdrowotne podczas wdychania. Ekspozycja na cząstki PM_{2.5} wywołuje liczne patologie układu oddechowego, w tym: astmę, alergie, przewlekłą obturacyjną chorobę płuc (POChP), zapalenie oskrzeli, rozedmę płuc, zmniejszoną czynność płuc i liczne przypadki raka płuc. Badania opisane w niniejszej pracy mają na celu próbę rozszyfrowanie zmian zachodzących w ludzkich komórkach płuc na poziomie molekularnym, biochemicznym i/lub genowym, które to zmiany zostały wywołane ekspozycją na respirabilny pył aerozolowy OA. Pył ów pochodził z czterech istotnych źródeł: (i) procesy utleniania nienasyconych węglowodorów monoterpenuwch w reakcjach ozonu z α -pinenem (**α -pinenowe SOA**), (ii) procesy chemicznego starzenia aerozolu izoprenowego wzbogaconego we polarną frakcję organosiarczanową, w tym siarczan 2-metylotetrolu (2-MTS) (**poddane starzeniu izoprenowe SOA**), (iii) utlenianie węglowodorów aromatycznych w powietrzu zanieczyszczonym tlenkami azotu (**atmosferyczny mono-nitrofenolowy aerozol**) oraz (iv) procesy spalania biomasy (BBA) (**aerozol spalania biomasy**).

W celu określenia skutków ostrej ekspozycji na kluczowe składniki pyłów z wyżej wymienionych źródeł do badań *in vitro* wybrałam dwa modele komórkowe: BEAS-2B (tj. unieśmiertelnione ludzkie komórki nabłonka oskrzeli) i A549 (tj. komórki ludzkiego gruczolaka). W pierwszych dwóch projektach opisanych w niniejszej rozprawie, cząstki α -pinenowe SOA oraz aerozolu izoprenowego zostały wytwarzane w laboratorium w przepływowym reaktorze utleniającym (OFR) z użyciem chemii rodników hydroksylowych ($\bullet\text{OH}$). W przypadku aerozolu izoprenowego proces jego starzenia chemicznego prowadziłam w układzie heterogenicznym, co odzwierciedla procesy starzenia atmosferycznego w czasie od 0 do 22 dni. Tak wytworzony aerozol poddałam analizom chemicznym z użyciem wysokosprawnej chromatografii cieczowej sprzężonej z wysokorozdzielczym tandemowym spektrometrem mas wyposażonym w źródło

elektrosprej (LC/ESI-HR-MS/MS). Analizy te były ukierunkowane na oznaczenie głównych składników chemicznych wytworzonego aerozolu, w tym: kwasów karboksylowych, nadtlenków oraz związków wielofunkcyjnych. W celu porównawczym przeprowadziłam analizy składu chemicznego rzeczywistego aerozolu frakcji PM_{2.5} oraz aerozolu wytworzonego w komorach aerozolowych Amerykańskiej Agencji Środowiska (US EPA) w procesach fotoutleniania monocyklicznych węglowodorów aromatycznych. Wyniki tych ostatnich analiz opisałam w trzecim rozdziale niniejszej pracy.

Wytworzone laboratoryjnie mieszaniny aerozolowe, zawierające zarówno znane markery, jak również nowe składniki, wprowadzałam do hodowli komórkowych płuc celem oceny ich działania cytotoksycznego na owe komórki ze szczególnym uwzględnieniem procesów proliferacji. Wyznaczona eksperymentalnie żywotność komórkowa (zależna od czasu i/lub stężenia badanego składnika SOA) posłużyła mi do określenia stężenia hamującego IC₅₀ tego składnika lub ich mieszanin. Ponadto zastosowałam testy funkcjonalne z sondami fluorescencyjnymi do detekcji tworzących się komórkowych (ROS) i mitochondrialnych (mtROS) reaktywnych form tlenu po ekspozycji; testy te wykorzystywały odpowiednio cytometrię przepływową oraz mikroskopię konfokalną. Zmiany żywotności komórkowej analizowałam z użyciem mikroskopii fluorescencyjnej i testów barwnych dla żywych i/lub martwych komórek, podczas gdy procesy apoptozy komórkowej – w teście aneksyny V/jodku propidyny przy użyciu cytometrii przepływowej. Wykorzystałam ilościową reakcję łańcuchową polimerazy w czasie rzeczywistym (RT-qPCR) do oceny zmian genowych, które były wynikiem ekspozycji aerozolu na badane komórki, indukowanych przez modulację stresu oksydacyjnego i ekspresję genów zapalnych.

W pierwszej części niniejszej pracy określiłam ilościowo reakcję na wzrastające stężenia trzech znanych składników α -pinenowego SOA, tzn. kwasu pinowego, pinonowego i 3-metylo-1,2,3-butanotrikarboksylowego oraz pełnej mieszaniny α -pinenowego SOA w liniach komórkowych A549 i BEAS-2B. W trakcie badań oznaczałam zmiany w proliferacji komórkowej, żywotność komórek oraz stres oksydacyjny. Procesy ozonolizy α -pinenu (C₁₀H₁₆) – obficie emitowanego lotnego związku organicznego klasy monoterpenu przez roślinność lądową, ma znaczący udział w budżecie SOA na poziomie globalnym; jednak co ciekawe, jego wpływ na patofizjologię płuc pozostawał ciągle niepewny. Badania składu chemicznego α -pinenowego SOA udowodniły ~57 % udział w jego masie kwasu pinowego, pinonowego i 3-metylo-1,2,3-

butanotrikarboksylowego oraz znaczący wkład wielofunkcyjnych wodoronadtlenków. Postawiłam hipotezę, że te ostatnie są główną przyczyną obserwowanych zmian toksykologicznych badanego aerozolu.

Druga część niniejszej pracy dotyczy badań toksyczności inhalacyjnej związanej z cząsteczkami aerozolu pochodzenia izoprenowego. Izopren (C_5H_8) to najobficiej (po metanie) emitowany do atmosfery węglowodór przez ekosystemy roślinne. Po przedostaniu się do dolnych warstw atmosfery izopren ulega reakcjom z rodnikami hydroksylowymi $\bullet OH$. W warunkach niskiego stężenia NO_x ($NO_x = NO + NO_2$) reakcja ta prowadzi do tworzenia bardzo reaktywnych produktów pośrednich w fazie gazowej, w tym epoksydioli (IEPOX). Te ostatnie reagują dalej, co dostarcza szerokiej gamy produktów o malejących prężnościach par, takich jak organiczne siarczany (organosiarczany, OS), w tym najbardziej rozpowszechniony w atmosferze siarczan 2-metylotetrolu (2-MTS). 2-MTS może ulegać dalszym przemianom chemicznym, co prowadzi do powstania fotochemicznie starzejących się cząstek o znacznie bardziej złożonym składzie chemicznym. W badaniach opisanych w tej części pracy pokazałam, że chemiczne starzenie cząstek aerozolu izoprenowego nasila stres oksydacyjny oraz indukuje procesy zapalne w liniach komórkach BEAS-2B.

Trzeci zrealizowany projekt badawczy dotyczył oznaczania profilu toksykologicznego mono-nitrofenoli. Związki te stanowią powszechne i niebezpieczne zanieczyszczenia środowiska, w formie – pyłów respirabilnych w atmosferze, pozostałości rolniczych w glebie, wód atmosferycznych i lądowych, produktów niekontrolowanych pożarów i odpadów przemysłowych. We współpracy z Amerykańską Agencją Środowiska pokazałam, że jednym z ważnych źródeł mono-nitrofenoli w atmosferze są produkty utleniania węglowodorów aromatycznych, które to produkty wchodzi w skład cząstek aerozolu. W pierwszej fazie badań zweryfikowałam hipotezę negatywnego oddziaływania mono-nitrofenoli na powierzchnię błony komórkowej płuc. Wykorzystałam tu zarówno sztuczną dwuwarstwową błonę lipidów eukariotycznych (otrzymaną w laboratorium), jak również żywe komórki pochodzące obu linii komórkowych. W drugiej fazie przedstawiłam porównawcze badania toksykologiczne 2-nitrofenolu (2NP), 3-nitrofenolu (3NP), 4-nitrofenolu (4NP) oraz ich równomolowej mieszaniny przy użyciu testów ROS, mtROS, żywotności komórek i śmierci komórkowej.

W ostatniej części pracy przeprowadziłam szczegółową analizę toksykologiczną czterech ważnych składników procesów spalania biomasy (BBA) z użyciem linii

komórkowych A549 i BEAS-2B. Spalanie biomasy jest głównym źródłem zanieczyszczenia powietrza, szczególnie na obszarach miejskich, podmiejskich i wiejskich. Postawiłam hipotezę, że długotrwałe wdychanie tak zanieczyszczonego powietrza może indukować zwiększoną zachorowalność i śmiertelność. Cztery badane składniki BBA obejmowały: lewoglukoza (LG), kwas 3-nitrosalicylowy (NS), 4-nitrokatechol (4NC) i 4-nitrogwajakol (4NG). Komórki z obu linii poddałam ekspozycji na te składniki i analizowałam je pod kątem zachodzących zmian ogólnych ROS i mtROS przy różnych stężeniach i czasach ekspozycji. Pozwoliło to mi przewidzieć zachodzące zmiany w szlakach biochemicznych. Ta seria prac zakończyła się propozycją opracowania mechanizmów śmierci komórkowej po ekspozycji.

Zrozumienie składu chemicznego aerozolu pochodzącego z czterech rozpatrywanych źródeł dostarczyła mi możliwości wykonania porównawczego profilu toksykologicznego jego głównych składników na ludzkie komórki płuc. Zebrane dane pozwoliły określić źródło(a) pyłów z największymi negatywnymi skutkami po inhalacji, dzięki wyznaczonym wartościom toksykologicznym, w tym – IC₅₀. Dodatkowo, opisane badania pozwoliły mi szeroko nakreślić zmiany patofizjologiczne w płucach na poziomie molekularnym i komórkowym po ekspozycji na składniki pyłów, które różniły się istotnie w zależności pochodzenia, składu chemicznego i parametrów ekspozycji (czas, stężenia próbki). Przeprowadzone badania pokazują pilną potrzebę opracowania przepisów i strategii kontroli w celu złagodzenia skutków emisji pyłów, szczególnie tych pochodzących ze spalania biomasy, ze względu na ich potwierdzoną toksyczność inhalacyjną już krótkim czasie ekspozycji.

Table of Contents

ACKNOWLEDGMENTS.....	VII
STATEMENT OF ORIGINALITY.....	X
FUNDING.....	XII
LIST OF PUBLICATIONS INCLUDED IN THIS STUDY.....	XIII
OTHER LIST OF PUBLICATIONS.....	XIV
POSTER PRESENTATIONS AT INTERNATIONAL CONFERENCES.....	XV
ORAL PRESENTATIONS AT INTERNATIONAL CONFERENCES.....	XVI
LIST OF ABBREVIATIONS.....	XVII
ABSTRACT (IN ENGLISH).....	XXI
ABSTRAKT (W JĘZYKU POLSKIM).....	XXIV
TABLE OF CONTENTS.....	XXVIII
CHAPTER 1: LITERATURE REVIEW.....	1
1.1- ATMOSPHERIC AEROSOL CHEMISTRY.....	1
1.1.1- PARTICULATE MATTER (PM) IN THE ATMOSPHERE.....	1
1.1.2- FORMATION OF SECONDARY ORGANIC AEROSOL (SOA).....	2
1.2- ENVIRONMENTAL POLLUTION AND HEALTH EFFECTS.....	4
1.2.1- EXPOSURE EFFECTS OF PM AND SOA.....	5
1.2.2- <i>IN VITRO</i> CELL MODELS TO STUDY INHALATION EXPOSURE RESPONSE OF PM _{2.5}	7
1.2.3- MOLECULAR AND CELLULAR CONSEQUENCES OF EXPOSURE TO PM.....	9
1.3- AEROSOL SYSTEMS INCLUDED IN THE THESIS.....	10
1.3.1- α -PINENE EMISSIONS AND ITS SOA MOLECULAR MARKERS.....	11
1.3.1.1- <i>Formation of SOA Constituents from α-Pinene Ozonolysis</i>	11
1.3.1.2- <i>Toxicological Studies of α-Pinene SOA Markers</i>	12
1.3.2- ISOPRENE EMISSIONS.....	13
1.3.2.1- <i>Atmospheric Aging of Fine Particulate 2-Methyltetrol Sulfates</i>	13
1.3.2.2- <i>Toxicological Assessment of Isoprene SOA Emissions</i>	14
1.3.3- NITROPHENOLS IN THE ATMOSPHERE.....	15
1.3.3.1- <i>Atmospheric Sources of Nitrophenols</i>	15
1.3.3.2- <i>Toxicological Assessment of Nitrophenols</i>	16
1.3.4- ATMOSPHERIC CONTEXT OF BBA.....	17
1.3.4.1- <i>Formation of Important BBA Components</i>	18
1.3.4.2- <i>Toxicological Profiling of Biomass Burning Aerosol</i>	19
1.4. OBJECTIVES OF THESIS.....	20

CHAPTER 2: EXPERIMENTAL SECTION	22
2.1- MATERIALS AND CHEMICALS.....	22
2.1.1- CHEMICALS.....	22
2.1.2- PROBES AND ASSAYS.....	23
2.1.3- MATERIALS AND CELL CULTURE	23
2.2- METHODOLOGY AND EXPERIMENTAL PROCEDURE.....	24
2.2.1- GENERATION, QUANTIFICATION & CHEMICAL ANALYSIS OF SOA	24
2.2.1.1- <i>Generation of α-Pinene SOA through the Ozonolysis of α-Pinene</i>	24
2.2.1.2- <i>Filter Extraction of α-Pinene SOA</i>	25
2.2.1.3- <i>RPLC/ESI-HR-QTOFMS Analysis of α-Pinene SOA</i>	26
2.2.1.4- <i>Generation of Heterogeneously Oxidized 2-Methyltetrol Sulfates Aerosol</i>	27
2.2.1.5- <i>Filter Extraction of 2MTS Originated Aged SOA Products</i>	29
2.2.1.6- <i>Chemical Analysis of Organosulfates</i>	30
2.2.1.7- <i>Principal Component Analysis (PCA)</i>	31
2.2.1.8- <i>Collection and analysis of mono-NPs in SOA and ambient PM_{2.5}</i>	31
2.2.2- MODEL EUKARYOTIC MEMBRANES.....	33
2.2.2.1- <i>Preparation of Model Eukaryotic-Like Cell Membrane</i>	33
2.2.2.2- <i>Atomic Force Microscopy Imaging</i>	33
2.2.3- IN VITRO CELL CULTURES	34
2.2.3.1- <i>A549 Cell</i>	34
2.2.3.2- <i>BEAS-2B Cells</i>	34
2.2.4- HIGH THROUGH-PUT SCREENING USING SPECTROPHOTOMETER.....	35
2.2.4.1- <i>Cell Count Optimization</i>	35
2.2.4.2- <i>Mitochondrial Toxicity Testing (MTT Assay)</i>	37
2.2.4.3- <i>Lactate Dehydrogenase Assay (LDH Assay)</i>	38
2.2.4.4- <i>Resazurin Viability Assay</i>	38
2.2.4.5- <i>Carboxy-H₂DCHF Assay</i>	39
2.2.4.6- <i>Inhibitory Concentration-50 (IC₅₀) Calculations</i>	39
2.2.4.7- <i>Statistical Analysis</i>	40
2.2.5- FLUORESCENT MICROSCOPY AND CELLULAR IMAGING	40
2.2.5.1- <i>Phase Contrast Images</i>	40
2.2.5.2- <i>Calcein-AM Propidium Iodide</i>	41
2.2.5.3- <i>Image-J Analysis</i>	41
2.2.6- FLOW CYTOMETRY SINGLE CELL ANALYSIS.....	42
2.2.6.1- <i>Sample Preparation for Flow Cytometric Analysis</i>	43
2.2.6.2- <i>Annexin-V/Propidium Iodide Staining Assay</i>	44

2.2.6.3-	<i>Tetramethyl rhodamine Methyl Ester Perchlorate (TMRM Assay)</i>	44
2.2.6.4-	<i>MitoSox Assay</i>	45
2.2.6.5-	<i>Carboxy-H₂DCHF Analysis</i>	45
2.2.6.6-	<i>MitoPY1 Analysis</i>	46
2.2.6.7-	<i>Statistical Analysis</i>	46
2.2.7-	CONFOCAL MICROSCOPY IMAGING	46
2.2.7.1-	<i>Oxidative Stress Studies</i>	46
2.2.8-	GENOMIC ANALYSIS	48
2.2.8.1-	<i>Cell Exposure</i>	48
2.2.8.1-	<i>RNA Extraction</i>	48
2.2.8.2-	<i>Complementary DNA (cDNA) Preparation</i>	50
2.2.8.3-	<i>Real-Time PCR Gene Expression Analysis</i>	51
2.2.8.4-	<i>Statistical Analysis on Fold Change of Gene Expression</i>	51
2.2.8.5-	HEAT MAP	53
2.2.8.6-	MULTIVARIATE ANALYSIS AND PEARSON R CORRELATION MATRIX	53
	CHAPTER 3: RESULTS AND DISCUSSION	54
3.1-	TOXICOLOGICAL PROFILING OF α-PINENE OZONOLYSIS SOA AND ITS IMPORTANT ATMOSPHERIC MARKERS IN THE LUNG CELLS	55
3.1.1-	ABSTRACT A-PINENE SOA PROJECT	57
3.1.2-	TIME-DEPENDENT INCREASING CONCENTRATION RESPONSE (ICR) USING THE MTT ASSAY	58
3.1.3-	LIVE/DEAD CELL STAINING ASSAY	64
3.1.4-	OXIDATIVE STRESS MEASUREMENTS USING FLOW CYTOMETRY	70
3.1.5-	RPLC/ESI-HR-QTOFMS ANALYSIS OF PAM-GENERATED A-PINENE SOA	75
3.1.6-	CONCLUSION	83
3.2-	HETEROGENEOUS OXIDATION PRODUCTS OF PARTICULATE ISOPRENE EPOXYDIOL-DERIVED METHYLTETROL SULFATES INCREASE THE OXIDATIVE STRESS AND INFLAMMATORY GENE RESPONSES IN HUMAN LUNG CELLS	84
3.2.1-	ABSTRACT 2MTS PROJECT	86
3.2.2-	CHEMICAL COMPOSITION AND PCA OF PARTICULATE 2-MTSS AND ITS AGING PRODUCTS	87
3.2.3-	IC₅₀ VALUES OF THE 2-MTS AND ITS AGING PRODUCTS IN BEAS-2B CELLS	93
3.2.4-	GENE EXPRESSION ANALYSIS AFTER EXPOSURE TO 2MTS AND ITS HETEROGENEOUSLY AGED OXIDATION PRODUCTS IN THE BEAS-2B CELLS	97
3.2.5-	MULTIPLE LINEAR REGRESSION (MLR) MODEL AND ALTERED GENE EXPRESSION	106
3.2.6-	CONCLUSION	112

3.3- MONO-NITROPHENOLS: ANALYSIS FOR ATMOSPHERIC PREVALENCE AND TOXICOLOGICAL PROFILING IN THE MODEL EUKARYOTIC MEMBRANES AND HUMAN LUNG CELLS	113
3.3.1- ABSTRACT OF NPS PROJECT	116
3.3.2- NPS MIXTURE AND ITS EFFECT ON EUKARYOTIC PHOSPHOLIPID BILAYER	117
3.3.3- AFM IMAGING OF MODEL EUKARYOTIC MEMBRANE REARRANGEMENT FOLLOWING NP-MIXTURE TREATMENT	118
3.3.4- PHASE-CONTRAST MICROSCOPY (PCM) IMAGING OF BEAS-2B AND A549 CELLS TREATED WITH NP-MIXTURE	122
3.3.5- QUALITATIVE ANALYSIS OF MONO-NPS IN AMBIENT PM _{2.5} AND SMOG CHAMBER-GENERATED SOA	125
3.3.6- INHIBITORY CONCENTRATION-50 (IC ₅₀) OF NP	133
3.3.7- ANALYSIS OF CYTOTOXICITY IN THE NITROPHENOLS TREATED CELLS	137
3.3.8- THE MECHANISM OF CELLULAR DEATH: APOPTOSIS VERSUS NECROSIS	142
3.3.9- THE BUILD-UP OF OXIDATIVE STRESS FOLLOWING NITROPHENOL EXPOSURE	148
3.3.10- CHANGES IN MITOCHONDRIAL MEMBRANE POTENTIAL ($\Delta\Psi$ M)	155
3.3.11- CONCLUSION	158
3.4- PRIMARY VERSUS SECONDARY ORGANIC EMISSIONS OF BIOMASS BURNING AEROSOL: NITRATED AROMATIC COMPONENTS INDUCE MITOCHONDRIAL STRESS AND APOPTOSIS IN HUMAN LUNG CELLS	159
3.4.1- ABSTRACT OF BBA PROJECT	161
3.4.2- TOXICOLOGICAL PROFILE OF LG	162
3.4.2.1- <i>IC₅₀ and Cellular Death Analysis in LG-Treated Lung Cells</i>	162
3.4.2.2- <i>General and Mitochondrial ROS buildup in LG-Treated Lung Cells</i>	166
3.4.2.3- <i>Mechanism of Cell Death in LG-Treated Lung Cells</i>	172
3.4.3- TOXICOLOGICAL PROFILE OF NS	175
3.4.3.1- <i>IC₅₀ and Cellular Death Analysis in NS-Treated Lung Cells</i>	175
3.4.3.2- <i>General and Mitochondrial ROS buildup in NS-Treated Lung Cells</i>	179
3.4.3.3- <i>Mechanism of Cell Death in the NS-Treated Lung Cells</i>	184
3.4.4- TOXICOLOGICAL PROFILE OF NG	187
3.4.4.1- <i>IC₅₀ and Cellular Death Analysis in NG-Treated Lung Cells</i>	187
3.4.4.2- <i>General and Mitochondrial ROS buildup in NG-Treated Lung Cells</i>	190
3.4.4.3- <i>Mechanism of Cellular Death Following NG Treatments</i>	195
3.4.5- TOXICOLOGICAL PROFILING OF NC	198
3.4.5.1- <i>IC₅₀ Profiles and Cellular Death Analyses of NC-Treated Lung Cells</i>	198
3.4.5.2- <i>General and Mitochondrial ROS build-up in NC-Treated Lung Cells</i>	201

3.4.4.1-	<i>Mechanism of Cellular Death following NC Treatments</i>	207
3.4.6-	TOXICOLOGICAL PROFILING OF THE 4BBA MIXTURES	213
3.4.6.1-	<i>IC₅₀ Profiles and Cellular Death Analyses of the 4BBA-Treated Lung Cells</i>	213
3.4.6.2-	<i>General and Mitochondrial ROS build-up in the 4BBA Mixture-Treated Lung Cells</i> ..	216
3.4.6.3-	<i>Mechanism of Cellular Death Following the 4BBA Mixture Treatments</i>	221
3.4.1-	COMPARATIVE TOXICOLOGY OF THE BBA MARKERS AND CONCLUSIONS	224
CHAPTER 4: RESEARCH SUMMARY AND FUTURE PROSPECTIVE		231
CHAPTER 5: REFERENCES		235

CHAPTER 1: Literature Review

This chapter is conceived as a general introduction to atmospheric aerosol chemistry and the adverse exposure effects it imposes on human health. It is organized as follows: the first section gives a general overview of the type of particulate matter (PM) present in the atmosphere and the mechanisms for the formation of secondary organic aerosol (SOA); the second section covers the human health implications that arise following exposure to atmospheric PM, which includes an introduction to *in vitro* models that allow for the toxicological screening of hazardous pollutants in the atmosphere as well as molecular mechanisms that can be studied for toxicological assessment; and the third, and final, section reviews the literature on four major PM systems or subtypes (i.e., α -pinene SOA, isoprene SOA, mono-nitrophenols and biomass burning aerosol components) that are examined in detail as a part of this thesis, which encompasses the formation, sources, and toxicological data currently available on them.

1.1- Atmospheric Aerosol Chemistry

The atmosphere comprises a thin layer of mixed gases covering the Earth's surface and is divided into several sublayers based on vertical temperature profiles. Two of the most significant layers of Earth's atmosphere includes the troposphere (spanning up to 15 km from the Earth's surface) and the stratosphere (15-50 km in altitude from Earth's surface).¹ Atmospheric chemistry deals with the extensive photochemical reactions occurring in these two sublayers, and covers the formation of secondary gases (e.g., ozone) and *particulates* (liquid or solid aerosol particles suspended in the air with diameters $\leq 100 \mu\text{m}$).² This section of the thesis briefly covers the literature on the sources and formation of important primary and secondary organic aerosol constituents formed in the troposphere, emphasizing their contributions to particulate matter (PM).

1.1.1- Particulate Matter (PM) in the Atmosphere

Atmospheric aerosol comprises fine liquid and/or solid particles suspended in ambient air with an aerodynamic diameter size $\leq 100 \mu\text{m}$.³ The US EPA defines PM as “*a complex mixture of particles and gases, including acids, organic emissions, metals, soils, and*

dust of size less than micron level.”⁴ These particles are a complex mixture of dynamically altering physio-chemical properties that impacts the environment and life on Earth. At a global scale, the aerosol drives a strong effect on the Earth’s climate, radiation balance, abundance and distributions of trace gases, and formation of cloud condensation nuclei.⁵ ⁶ In addition to this, the ambient PM and air pollution substantially impacts the quality of life, mortality rates, and human health, as demonstrated through various epidemiological studies.^{3, 7, 8} With the increased industrialization and urbanization, transportation development, population growth, decreased forestry and frequent wild-fire emission events, PM is increasing of submicron particle sizes; it has also lead to the increased instances of smog over the recent years.² ⁹ The inhalable PM fractions are also increasing in the atmosphere (aerodynamic diameter ≤ 2.5 μm), and there is an urgent need to understand their physio-chemical composition, formation mechanism and direct impact on air quality and human health.¹⁰ ¹¹

The size of PM ranges from ten micrometres (10 μm) to a few nanometres (nm).⁷ The PM of the aerodynamic diameter ≤ 10 μm are “coarse” inhalable particles that can infiltrate the human respiratory system.⁷ ¹² Airborne fine and inhalable PM of aerodynamic diameter ≤ 2.5 μm (fine particulate matter, PM_{2.5}) and ultra-fine particles with aerodynamic diameter ≤ 0.1 μm (PM_{0.1}) provides a high degree of permeation deep within the cilia and alveoli of the lungs.¹³ PM_{2.5} and PM_{0.1} are associated with poor air quality,¹⁴ climatic change,¹⁵ and exhibits long-term adverse health effects.¹¹ The sources of PM are through primary origin (i.e., natural or anthropogenic emissions), including organic carbon (OC), soil mineral,¹⁶ black carbon, wood combustion,¹⁷ plants and vegetations, wildfire emissions,¹⁸ road vehicles and fuel burning,¹⁹ industrial processes and livestock and animals.¹⁶ Once primary sources of organic aerosol (POA) enter the lower atmosphere (troposphere), they undergo further chemical reactions and atmospheric aging to form complex mixtures of SOA.⁶

1.1.2- Formation of Secondary Organic Aerosol (SOA)

An estimate of 10^3 to 10^4 organic compounds has been measured in the atmosphere, adding to the complexity and diversity of tropospheric SOA formation.²⁰ SOA constituents the most significant mass fractions of PM_{2.5} (contributing upwards of 90%),²¹ formed from the atmospheric oxidation of volatile organic compounds (VOCs) by ozone (O₃), hydroxyl radical (*OH), and nitrate radicals (NO₃*).⁶ Emissions of both biogenic (derived from

terrestrial vegetation) and anthropogenic VOCs contribute to SOA formation through the nucleation, condensation, or multiphase (or heterogeneous) chemical reactions of their semi- and/or low-volatility atmospheric organic oxidation products.^{6, 22, 23} The processes that govern the enhancement of aerosol particle mass in the atmosphere, including vapor condensation through sulfuric acid (H₂SO₄), nitric acid (HNO₃) and secondary organics (SO) can do so without altering the particle numbers in the atmosphere. ^{20, 24} Both the particle size (mass) and particle number determine the climate and health effects of the aerosol in the troposphere.²⁴ Owing to the dynamic atmospheric aging processes and diverse emission sources of SOA, the formation mechanisms of SOA and its composition remains poorly understood.⁶ To assess the health impacts of SOA on a global scale, it is important to elucidate the sources, composition and SOA formation mechanisms in the atmosphere. A brief summary of the processes involved in the emission and formation of SOA and effects of its associated PM_{2.5} are summarized in **Figure 1.1** below.

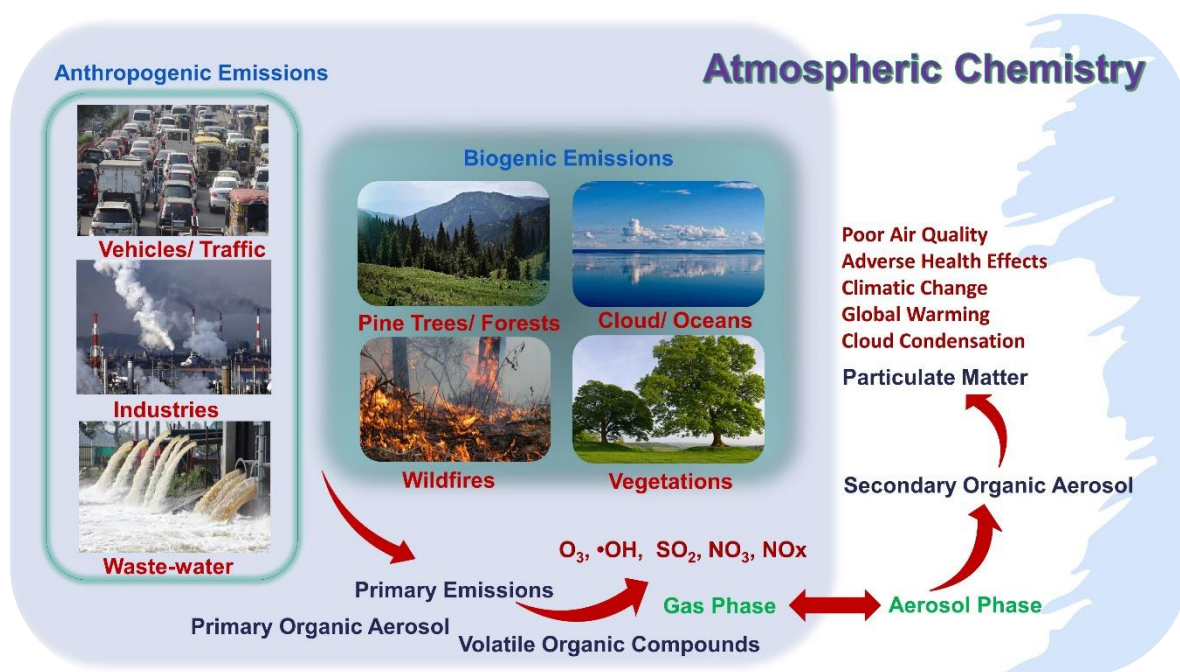


Figure 1.1. Atmospheric chemistry involves the study of primary sources of atmospheric emissions and the subsequent formation of secondary pollutants (e.g., SOA and O₃). This thesis lays particular emphasis on PM_{2.5} formation and its inhalation effects.

Biogenic SOA (BSOA) is primarily derived from the terrestrial environment, biomass burning (BB), and oceans, with an estimated flux of 70-1200 Tg yr⁻¹.^{6, 25-27}

Contributions from anthropogenic SOA (ASOA), e.g., fossil fuel burning fall in the range 12-100 Tg yr⁻¹, with an estimated 67% increase in emission rates per decade.²⁸ Almost two-thirds of non-methane VOCs from biogenic sources are emitted from vegetation, which includes the hemiterpene (e.g., isoprene) (C₅H₈) with total emissions of ~350-800 Tg yr⁻¹,^{27, 29, 30} monoterpenes (α -pinene, β -pinene, δ -limonene) (C₁₀H₁₆) with total emissions of ~120-170 Tg yr⁻¹ ^{27, 29, 30}, sesquiterpene (C₁₅H₂₄) with emissions of ~25 Tg yr⁻¹,^{27, 29, 30} and other oxygenated hydrocarbons with total emissions of 90-260 Tg yr⁻¹.²⁷ Radiocarbon analysis exhibit that the most of carbon content from OA is modern, implying the role of BSOA precursors in driving the composition of tropospheric chemistry.^{6, 31, 32} Although, BSOA emissions may be considered uncontrollable, studies have shown a direct correlation between BSOA formation and ASOA pollutant emissions.³² Hence, to predict the long-term effects of SOA on the environment, climate, and human health, the study of the interactions of BSOA with ASOA and their emission rates is essential to unravel. Furthermore, to elucidate the exposure effects of SOA on human health, it is crucial to understand the sources and atmospheric processes that drive their concentrations in the ambient air.⁷

1.2- Environmental Pollution and Health Effects

The 1952 London Fog event is one of the most referenced fog events in history that led to public awareness of the dangers of air pollution.^{33, 34} A study published two years after this major environmental and public health crisis revealed that mortality rates increased (reported to be 50-300% higher than the previous year) with enhanced concentrations of smog and sulfur dioxide.³⁴ This same study also reported that the mortality rate did not return to normal even after 2 weeks of the incidence.^{34, 35} This notable air pollution event, along with the 1948 Donora Smog event in Pennsylvania, which reported increased mortality rate and cardiovascular diseases,³⁶ inspired subsequent large-scale epidemiological studies, exposure assessment study cohorts, and the development of policies aimed at protecting public health from adverse air pollution exposures. This section covers key results from prior epidemiological studies on health effects of air pollution, alternative approaches to animal testing to systematically study environmental pollutants, and screening methods of certain PM/SOA subtypes at the cellular and molecular levels to elucidate their exposure effects inside human lung cells.

1.2.1- Exposure effects of PM and SOA

PM_{2.5} is linked to adverse human health effects ranging from exacerbation of asthma symptoms to mortality associated with lung cancer and cardiopulmonary disease.[37](#), [38](#) In addition, PM_{2.5} has been associated with negative health outcomes with an estimated contribution of more than 103.1 million indirect disabilities,[39](#) and 9 million premature deaths in 2015 worldwide.[12](#), [40](#) Though the general public is adversely affected by PM_{2.5} exposure, susceptible populations such as the elderly, immuno-compromised individuals, under-nourished individuals with low socioeconomic status, pregnant women, children, and those with health disparities are at higher risk of morbidities and increased underlying systematic pathophysiologies.[41](#) Studies by APHEA (Air Pollution and Health: a European Approach)[42](#), [43](#) and USA, the National Mortality, Morbidity and Air Pollution Studies (NMMAPS)[44](#), [45](#) have provided insights into the epidemiological effects of PM_{2.5} in the past 20 years. The data from APEHA estimated the combined impact of daily mortality increased by 0.6% (95% CI 0.4–0.8) for each 10 µg m⁻³ increase in PM₁₀ in 21 cities.[43](#) In APEHA-2 studies, hospital admissions for asthma and COPD increased in people older than 65 years by 1.0% (0.4–1.5) per 10 µg m⁻³ increase in PM₁₀. Similarly, NMMAPS showed the mortality rate increased by 0.5% (0.1–0.9) for each 10 µg m⁻³ increase in PM₁₀ in 20 metropolitan cities of US. The World Health Organization (WHO) air quality guidelines suggests the PM_{2.5} levels threshold to be 5 µg m⁻³ annual mean and 15 µg m⁻³ 24-hr mean while PM₁₀ levels below 20 µg m⁻³ annual mean and 50 µg m⁻³ 24-h mean for significant decrease in chronic and acute health risks that may arise due to air pollution.[10](#)

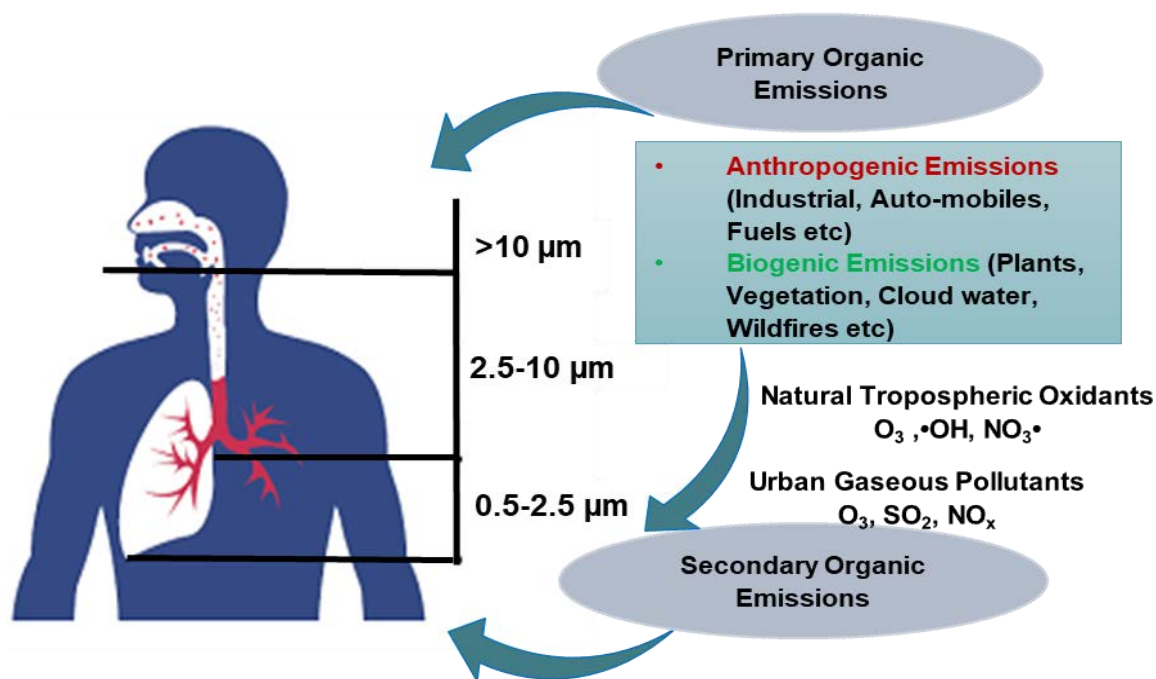


Figure 1.2. Inhalation exposure to PM induces the acute and chronic health effects. The sources of POA and SOA have varying particle sizes, mass, and chemical composition, which can have different adverse effects on human health upon respiration.

Owing to its small particle size and high surface area-to-volume ratio, PM_{2.5} is able to deposit deep into bronchial and alveolar lung tissues, and thus, enter the blood circulation to induce chronic effects on the cardiovascular system.^{46, 47} Exposure to PM_{2.5} triggers lung-associated pathologies including asthma, allergy,⁴⁸ COPD, bronchitis, emphysema, decreased lung function, and increased instances of lung cancer.⁴⁹ Once PM_{2.5} gets deposited inside the lungs, it causes the induction of inflammatory cascades,^{50, 51} including pro-inflammatory cytokines such as interleukin-6 (IL-6), interleukin-8 (IL-8),⁵² c-reactive protein (CRP),⁵³ etc. These inflammatory cytokines are associated with endothelial dysfunction, systemic inflammation, cardiological diseases, and exacerbated myocardial ischemia.⁵⁴ In addition to PM_{2.5} direct exposure, other gaseous pollutants (e.g., CO, NO_x, O₃ and SO₂) were associated with increased instances of cardio-pulmonary diseases.^{55, 56} The summary of inhalation effects of PM_{2.5} are summarized in **Figure 1.2**.

Furthermore, exposure to particle sizes \leq PM_{2.5} increases susceptibility to lower and upper respiratory tract infections.¹¹ Clinical studies provided evidence that PM_{2.5} exposure was positively correlated with increased numbers of hospitalization and outpatient visits.^{11, 57} In one study, it was noted that increased instances of smog enhanced the morbidity

associated with asthma, influenza and acute respiratory tract infections.[11](#), [58](#) Mechanisms of toxicity in lung cells include generation of free reactive oxygen species (ROS), decreased anti-oxidant response,[59](#) and $\cdot\text{OH}$ -induced DNA oxidation damage and susceptibility to mutagenesis and other irreversible damage.[60](#) The dysregulation of calcium (Ca^{2+}) homeostasis is another mechanism through which $\text{PM}_{2.5}$ induces damage inside lung cells, ROS increases lipid peroxidation inside cells, which in turn elevates the Ca^{2+} levels thereby inducing cellular apoptosis or necrosis in the lungs.[61](#) Recruitment of inflammatory cytokines and over-expression of inflammation-related cytokine genes are other indicators of $\text{PM}_{2.5}$ -induced inflammatory injury in lung cells.[62](#) To determine the exact exposure effects, there is a need to identify the chemical composition, structure, atmospheric aging, and source of $\text{PM}_{2.5}$, which can help identify the intracellular responses in the cardio-pulmonary system.

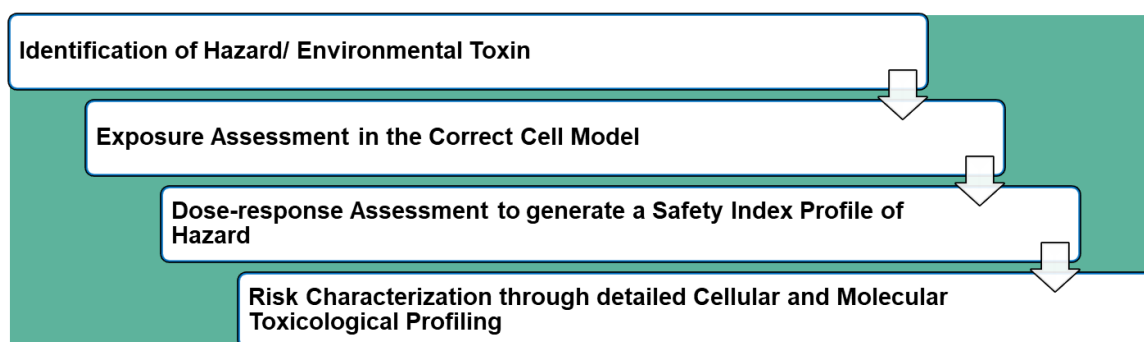
1.2.2- *In vitro* Cell Models to Study Inhalation Exposure Response of $\text{PM}_{2.5}$

There have been many *in vivo* and *in vitro* studies carried out over the years to determine the molecular and cellular changes associated with $\text{PM}_{2.5}$ exposure. Even though there is some evidence that $\text{PM}_{2.5}$ composition affects toxicity in cell lines of lung origin, fewer studies focus on the link between $\text{PM}_{2.5}$ chemical composition and biological outcomes associated with its exposures.[63](#) Various cell models are now developed and tested to study the effects of environmental pollutants on human health. Scientists have been trying to elucidate the toxicological impact more efficiently, which constrains the use of *in vivo* models. Several governments and chemical regulatory authorities have been trying to conduct screening of potentially toxic, genotoxic, metabolic stressors, or carcinogenic chemicals. Mass screening of chemical compounds and pollutants through *in vitro* and *in vivo* analysis has allowed the collection and maintenance of online databases such as USA's ToxCast program,[64](#) EnviroTox for aquatic compounds screening,[65](#) and the European Union's REACH program.[66](#) These initiatives highlight the importance of an alternative to expensive/time-consuming animal testing approaches and have helped develop the validity and reliability of cell models to screen out the toxicological and safety profiles of exposed chemicals.[67](#)

Various cell models were reported to study the toxicological effects of environmental pollutants on human cells; these are either derived from a tumour or immortalized from

primary cell lines.⁶⁸ Normal bronchial epithelial cell lines, such as BEAS-2B (immortalized by SV40/adenovirus 12 hybrid and cloned), and adenocarcinoma alveolar basal epithelial cancer cell lines, such as A549, are established *in vitro* cell models that are utilized in high-throughput screening approaches.⁶⁸ These two cell lines have been frequently used to study the impact of SOA from anthropogenic and biogenic sources,⁶⁹⁻⁷¹ wood burning, gasoline exhaust, and diesel emissions, and biomass combustion products in PM_{2.5}.^{17, 72} Many studies report the use of these cell lines for *in vitro* assessment of oxidative stress and cytotoxicity following exposure to PM_{2.5} and gas-phase toxic pollutants.^{19, 70, 73-77}

Studying the molecular mechanisms associated with the changes in the proteome, genome, and ROS build up in cells and mitochondria may help establish the toxicological profile of different PM exposed to the lungs.⁷⁸ It is vital to select the correct cellular model for exposure assessment as the PM exhibit a response inside the cells based on physiochemical properties, including zeta potential, particle size, and composition. In contrast, this response is modulated with exposure time and concentration.⁷⁸ The four essential components of risk assessment can be divided into the following steps shown in [Scheme 1.1.1](#)



Scheme 1.1. The four major steps of environmental pollutants' hazard assessment adopted in toxicological studies.

When conducting toxicological assessment of a pollutant/compound not previously studied, it is essential to identify the source of the emission followed by the exposure assessment in the correct cell model (e.g., from lung, liver, or heart with the right organism source). The first step in acquiring toxicological data is the establishment of the dose-response curve to generate a safety index of the pollutant/ hazard. This is followed by detailed functional, molecular, biochemical, cellular, or genomic assessment at a dose lower than its inhibitory concentration-50 (IC₅₀) value.¹

1.2.3- Molecular and Cellular Consequences of Exposure to PM

The toxicological endpoints that can be incorporated within *in vitro models* to predict the exposure-outcome of the atmospheric pollutants include cellular proliferation rate/ viability, genomic and epigenomic analysis, a proteomics-based approach, and functional assays.⁶⁸ These are high-throughput screening assays developed to rapidly screen and discern the exposure responses at single-cell levels. Cellular toxicology can arise from disruption of biomolecular functions (enzymes, receptor, agonist/antagonist), cellular metabolism dysregulation, altered cellular signalling, and cytotoxicity-mediated processes.⁷⁹

The processes that modulate cellular signalling include protein, DNA, and lipid reactivity; physiochemical disruption of enzymatic function and proteins or membranes degradation.^{68: 79} The biochemical changes subsequently result in the activation of cellular processes such as apoptosis/ necrosis, oxidative stress signalling, mitochondrial dysfunction, endoplasmic reticulum (ER) stress and microtubule disruption.^{68: 79} The build-up of ROS and altered proliferation rate in pollutant exposed cells proved the occurrence of underlying pathophysiological lung conditions.^{74: 80} Exposure of lung cells to known air pollutants, such as black carbon (BC), brown carbon (BrC), and nitro-aromatic compounds (NACs), induced the cellular death mechanism (apoptosis induction).^{81: 82} Chronic exposures to atmospheric nitro-aromatic compounds, biomass burning-derived organic aerosol (BBOA), SOA from biogenic sources, and fuel-burning molecular markers could complicate the pre-existing cardio-pulmonary pathologies such as allergy, asthma, and respiratory infections as well as induce premature death, which could be attributed to ROS build up and apoptosis induction at the cellular level.^{74: 83: 84} Furthermore, mitochondrial dysfunction, ER stress, and protein/ lipid damage is now linked with underlying lung pathologies, respiratory diseases, and mitochondrial-ROS (mtROS) signal-induced apoptosis.⁸⁵⁻⁸⁷ Disturbances in mtROS signals may be an early sign of mitochondrial dysfunction after exposure to atmospheric pollutants.⁸⁸ This is summarized in **Figure 1.3** below.

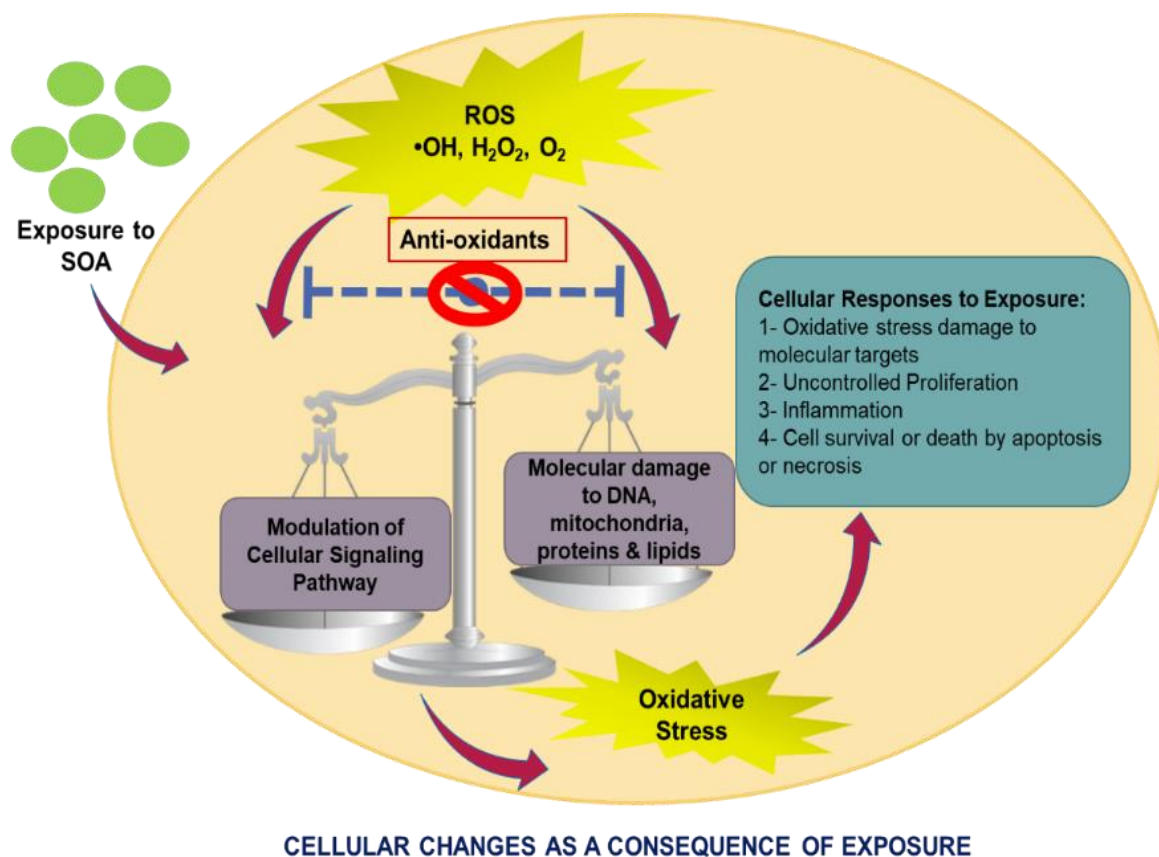


Figure 1.3. Potential cellular consequences resulting from air pollutant exposure, including the modulation of signalling and ROS build-up.


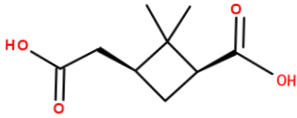
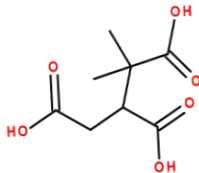
1.3- Aerosol Systems included in the Thesis

The section reviews the literature on the atmospheric prevalence, sources, emission rates, and formation mechanisms of the four types of aerosol components included in the thesis. It further provides the currently available toxicology and exposure assessment data for these aerosol systems. The four aerosol systems examined in the thesis include SOA from α -pinene ozonolysis as well as its three known SOA markers (i.e., pinonic acid, pinic acid and 3-methyl-1,2,3-butanetricarboxylic acid (MBTCA)), isoprene SOA derived from the heterogenous $\cdot\text{OH}$ oxidation of particulate 2MTS, mono-NP and their associated mixtures, and lastly, four important atmospheric markers of BBOA i.e., levoglucosan (LG), 3-nitro salicylic acid (NS), 4-nitrocatechol (NC), and 4-nitroguaiacol (NG).

1.3.1- α -Pinene Emissions and its SOA Molecular Markers

Monoterpene ($C_{10}H_{16}$) emissions contribute up to 15% of the total Biogenic Volatile Organic Compounds (BVOCs) emitted into the troposphere each year,⁸⁹⁻⁹⁰ with α -pinene being the most abundant monoterpene from tree emissions.⁹¹⁻⁹² The global emission rate of α -pinene varies with vegetation type and geographical location; however, its average emission is estimated to be 66 Tg yr^{-1} .²⁹ Because of its high emission rate and SOA yield,⁶⁻²² prior studies have begun examining how exactly α -pinene-derived SOA may adversely affect human health.⁶⁹⁻⁷⁶⁻⁹³⁻⁹⁹ However, detailed toxicological properties of α -pinene SOA and/or its individual molecular tracers are not currently available. Chemical structures for 3 crucial molecular markers for atmospheric α -pinene SOA included in this shown are found in [Table 1.1](#).

Table 1.1. Important molecular markers of atmospheric α -pinene SOA, which are included in this study.

Pinic Acid	Pinonic Acid	MBTCA
		

1.3.1.1- Formation of SOA Constituents from α -Pinene Ozonolysis

First-generation oxidation products of α -pinene that were measured in SOA, including pinonaldehyde as well as pinic, pinonic, and 10-hydroxypinonic acids.¹⁰⁰⁻¹⁰² Another important molecular-level marker for α -pinene-derived SOA formation MBTCA, which is formed via $\bullet\text{OH}$ -mediated oxidation of pinonic acid.¹⁰³⁻¹⁰⁴ In addition to aldehydes and carboxylic acids, α -pinene SOA may contain organic peroxides,¹⁰⁵ dimer esters,¹⁰⁶⁻¹⁰⁷ organosulfates¹⁰⁸ and/or extremely low-volatility organic compounds (ELVOCs).⁹² ELVOCs are believed to form from the autooxidation of first-generation peroxy radicals ($\text{RO}_2\bullet$) generated by either α -pinene + O_3 or α -pinene + $\bullet\text{OH}$ reactions.⁹² These ELVOCs may generate toxicological effects within human lung cells upon inhalation

to α -pinene SOA,⁶⁹ especially since prior studies have demonstrated that multifunctional organic hydroperoxides form within SOA.⁹² Owing to their low-volatile nature, monoterpene-derived SOA constituents within PM_{2.5}^{109, 110} may have atmospheric lifetimes of ~ 2 weeks,²³. Consequently, it can result in inhalation exposures by populations living close proximity or downwind of their initial formations. The first thesis's chapter provides the toxicological profiling of three important SOA constituents (or molecular-level markers) formed through α -pinene ozonolysis (i.e., pinic acid, pinonic acid and MBTCA) and compares it with the full mixture of SOA produced from α -pinene ozonolysis.

1.3.1.2- Toxicological Studies of α -Pinene SOA Markers

Previous studies have demonstrated that pro-inflammatory and inflammatory-related genes can be activated within lung cells when exposed to PM_{2.5}.¹¹¹ Chemical-based assays, such as dithiothreitol (DTT) consumption, have measured oxidative stress of biogenic SOA.^{112, 113} *In vitro* and *in vivo* studies have measured the expression of pro-inflammatory protein biomarkers, such as interleukin-8 (IL-8), interleukin-6 (IL-6) and tumor necrosis factor-alpha (TNF- α), upon exposure to α -pinene SOA.^{76, 97, 98} Evidence of oxidative stress build-up illustrates the underlying cellular pathophysiology contributing to chronic and acute lung diseases.¹¹⁴⁻⁸⁰ Repeated or prolonged exposures to the pollutant particles can trigger obstructive lung diseases, resulting in increased morbidity and overall decreased quality of life.¹¹⁵ A prior study reported using a deposition chamber to expose α -pinene SOA to lung macrophages for up to 2 hours, which did not induce observable cytotoxicity.⁹⁶ Another study demonstrated that the ROS content of α -pinene SOA increases with its corresponding photochemical age,⁹⁴ suggesting a potential association between SOA chemical composition and toxicity that is not currently understood. Increasing concentration-response and subsequent changes in the biological pathway can help us determine the health effects of certain inhalable aerosol particles.³⁹ This is partly because the concentration and time-dependent response following exposure to individual molecular components of α -pinene SOA and comparison with the full mixture of SOA generated from α -pinene ozonolysis has not been reported in the literature.

1.3.2- Isoprene Emissions

Isoprene (C_5H_8) is the most abundant non-methane VOC emitted into Earth's atmosphere ($\sim 500 \text{ Tg yr}^{-1}$), and is primarily derived from vegetation.[29](#), [90](#) Isoprene hydroxy hydroperoxides (ISOPOOH) are the main first-generation reaction products (i.e., $\sim 70\%$ yield) resulting from the hydroxyl radical ($\cdot OH$)-initiated oxidation of isoprene under low- NO_x conditions.[116](#) The $\cdot OH$ -mediated oxidation of ISOPOOH predominantly occurs during the daytime, which generates a high yield ($\sim 75\%$) of gaseous isoprene epoxy diols (IEPOX).[117-120](#) In the presence of inorganic sulfate ($Sulf_{inorg}$) aerosol that is mainly derived from human activities, IEPOX undergoes acid-driven multiphase chemistry to form a variety of low-volatility organo-sulfates (OSs) that have been shown to contribute significantly to SOA mass in $PM_{2.5}$ collected from densely-forested areas of the South Eastern U.S. and Amazon.[121-123](#)

1.3.2.1- Atmospheric Aging of Fine Particulate 2-Methyltetrol Sulfates

Particulate methyl-tetrol sulfates (MTSs) are major products formed from this multiphase chemistry, with 2-methyltetrol sulfate diastereomers (2-MTSs) being its predominant isomers, and the single-most abundant known SOA tracers.[124](#) 2-MTSs contributes up to 13% of the organic carbon,[123-126](#) and up to 15% of the organic mass, in $PM_{2.5}$ collected from certain U.S. and Amazonian ground sites. We recently demonstrated that the heterogeneous $\cdot OH$ oxidation of particulate 2-MTSs leads to the substantial formation of multifunctional particulate OSs, which are also detected in atmospheric $PM_{2.5}$.[127](#) Increasing the IEPOX-to- $Sulf_{inorg}$ aerosol ratio causes the extensive conversion of $Sulf_{inorg}$ to OSs, resulting in the formation of SOA particles with inorganic core-organic shell morphologies.[128](#) Global warming will likely cause larger isoprene emissions into the future,[129](#), [130](#) while regulatory controls on SO_2 emissions might cause $Sulf_{inorg}$ within $PM_{2.5}$ to primarily exist in OS forms.[128](#) Hence, systematically examining the early biological changes resulting from inhalation exposures of atmospherically-aged particulate 2-MTSs, which occurs through its heterogeneous $\cdot OH$ oxidation, and its multifunctional particulate OS products is needed in order to aid in the prediction of its acute and long-term exposure responses in humans.

The second chapter of the thesis systematically examines how the heterogeneous $\cdot OH$ oxidation of fine particulate 2MTSs leads to the formation of multifunctional OSs, and how

this alters oxidative stress within an *in vitro* model of exposure. The outline of formation of enhanced multifunctional particulate OSs from isoprene is shown in **Figure 1.4** below.

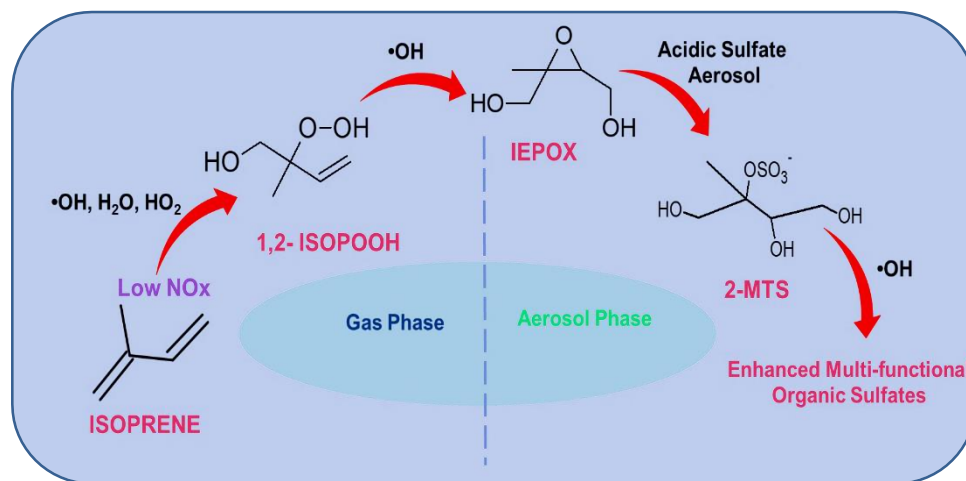


Figure 1.4. Enhanced multifunctional OSs are formed from the heterogeneous $\bullet\text{OH}$ oxidation of fine particulate 2MTSSs, and these OSs are molecular-level markers of atmospheric aging of isoprene-based emissions.

1.3.2.2- Toxicological Assessment of Isoprene SOA Emissions

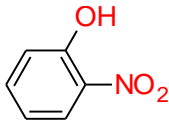
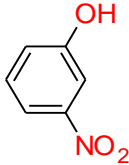
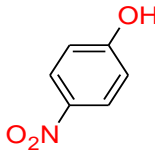
In previous *in vivo* studies, mice exposed to mixtures of isoprene and oxidants (O_3 and NO_2) exhibited an upper respiratory pathway irritation.^{131, 132} Wilkins et al. demonstrated a dependence of the reaction time, relative humidity (*RH*) and O_3 concentration on airway irritation when isoprene and other SOA mixtures were exposed to mice models.¹³³ Few prior studies have focused on *in vitro* inhalation responses following exposure to freshly-generated isoprene-derived SOA.^{70, 75, 134} Prior studies have used the dithiothreitol (DTT) assay to measure the oxidative potential (OP) of isoprene-derived SOA generated under low- and high- NO_x conditions, which found higher OPs of certain low- NO_x SOA types that were comparable or exceeded those of fresh and aged diesel particles.¹¹² In an *in vitro* model using A549 lung cells, exposure to the gas-phase photo-oxidation products of isoprene and 1,3-butadiene in the presence of NO_x , resulted in increased cytotoxicity and up-regulation of the *IL-8* gene (i.e., a marker of inflammatory response).¹³⁵ Similarly, IEPOX-derived SOA induced less fold change in expression of reactive oxygen species (ROS)-associated genes when compared with methacrylic acid epoxide (MAE)-derived SOA (a high- NO_x SOA type) in BEAS-2B cells.^{136, 137} *IL-8* and Cyclooxygenase 2

(COX-2) expression were significantly upregulated at a dose of 0.067 $\mu\text{g cm}^{-2}$ following exposure of BEAS-2B cells at an air-liquid interface to photochemically-generated isoprene SOA in the presence of initially high-NO_x conditions.⁷⁵ We have also previously found that 29 micro-RNAs, controlling inflammatory- and ROS-associated epigenetic factors, were differentially expressed in the presence of IEPOX- and MAE-derived SOA.¹³⁸ In both SOA types, significantly altered gene expression was associated with the nuclear factor (erythroid derived 2)-like 2 (Nrf2) transcription factor network.⁷⁰

1.3.3- Nitrophenols in the Atmosphere

2-Nitrophenol (2NP), 3-nitrophenol (3NP), and 4-nitrophenol (4NP) are aromatic compounds that contain one benzene ring, one OH group bound to the ring at position 1, and one NO₂ group attached at positions 2 (*ortho*, *o*-), 3 (*meta*, *m*-), and 4 (*para*, *p*-), respectively. Their chemical structures are provided in Table 1.2 below.

Table 1.2. The chemical structures of three SOA-bound nitrophenols (NPs) included in the thesis.

2-Nitrophenol	3-Nitrophenol	4-Nitrophenol
		

1.3.3.1- Atmospheric Sources of Nitrophenols

NPs originate mainly from the combustion of vehicle fuels,¹³⁹⁻¹⁴⁵ BB/wildfire emissions,¹⁴², ¹⁴⁶⁻¹⁴⁸ exhausts from incineration plants,¹⁴⁹ degradation of pesticides,¹⁵⁰⁻¹⁵² exhausts from industrial processes,¹⁵² manufacturing of dyes, resins, explosives, and pharmaceuticals,¹⁵³ and through atmospheric chemical processes involving the gas-phase oxidation of aromatic compounds in the presence of nitrogen oxides (NO_x = NO + NO₂).¹⁵³⁻¹⁵⁸ Trace amounts of NPs have been detected in water, fog, rain, clouds, soil, snow, and in PM_{2.5}, at several locations around the world,¹⁵³ including the southeaster US,¹⁵⁹ Europe,¹⁶⁰ and Asia,¹⁶¹ which poses a real threat to people and living organisms.

Furthermore, NPs are delivered to the environment in industrial chemical waste, such as insecticides, pharmaceuticals, pesticides, dyes, plasticizers,[162](#) and wood preservatives.[163](#) NPs were also reported to be released by waste incineration. The regulation of their atmospheric release is of particular concern because NPs were reported to be harmful to plants, which impact forestry and vegetation.[164](#) 2NP and 4NP are recognized as priority (or hazardous) pollutants.[165-168](#) Hence, understanding the sources and behaviour of atmospheric NPs is important to determine their impact on the Earth's climate by contributing to the formation of light-absorbing OA (i.e., BrC)[142, 143, 146, 155, 159, 161, 169, 170](#) as well as their potential adverse effects on human health.[171](#) The three NPs (i.e., 2NP, 3NP and 4NP) as well as their equimolar mixtures were included in the third chapter of this thesis to determine the environmental abundance and the toxicological profiling of these compounds.

1.3.3.2- Toxicological Assessment of Nitrophenols

NPs are reported to induce genotoxic effects on cells and cause respiratory implications.[172](#) Generally, mono- and di-NPs were reported to be toxic in plants and mammals,[171](#) while 4NP was highly toxic in humans.[173](#) There are limited *in-vitro* studies on NPs, while only a few *in-vivo* studies have been reported concerning the oral exposure to NPs.[152, 174](#) The oral LD₅₀ (lethal dose, 50%) values for 2NP were 2830–5376 mg kg⁻¹ body weight in rats and 1300–2080 mg kg⁻¹ body weight in mice, for 3NP were 930 mg kg⁻¹ body weight in rats and 1070 mg kg⁻¹ body weight in mice, and for 4NP were 220 – 620 mg kg⁻¹ body weight in rats.[152, 174](#) 4NP and 2NP were not considered carcinogenic by the US EPA,[150](#) and no conclusions could be made regarding the mutagenicity of 2NP, 3NP, and 4NP by the year 2000.[152](#) However, a recent *in-vitro* experiment showed that 2NP could destroy DNA,[175](#) while a genotoxic risk assessment of 3NP as a drug impurity showed that a threshold limit of 4 mg day⁻¹ was safe for its intra-dermal application.[176](#)

Transfer of NPs into lung fluids during inhalation exposures is highly probable in industrial and urban settings, as well as in regions adversely affected by BBA emissions.[152, 153](#) Their Henry's law constants and water solubilities warrant partitioning from the inhaled gas phase and PM_{2.5} into lung fluids.[177-180](#) However, those parameters can only roughly estimate the dissolution of NPs in lung fluids that differ in composition from pure water. Thus, the assessment of NPs in bio-accessibility during inhalation exposure

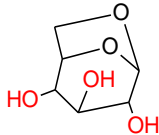
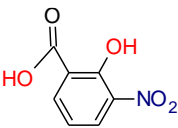

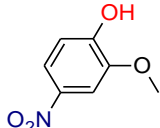
requires that the mass transfer parameters determined for solutions are similar to lung fluids.¹⁸¹ For instance,¹⁸² it was previously found that artificial lung fluid (at pH = 4.5) leached on average 78 % of 4NP contained within PM_{2.5} collected at the Kladno and Ostrava sites (Czech Republic), and the Gamble's Solution (at pH = 7.4) leached 64 % of 4NP from these same PM_{2.5} samples. These estimates may help determine the uptake probability of NPs through inhalation exposure at the site of release.

1.3.4- Atmospheric Context of BBA

BBA emission is one of the largest sources of fine carbonaceous aerosol in the troposphere and the second-largest source of trace gases worldwide.¹⁸³ It contributes to 62% of BC and 93% of primary OC emissions, including BrC.¹⁸⁴ The BC and OC parts of BBA absorb light at different wavelengths, affecting the Earth's radiative balance by potentially contributing to global warming.^{185, 186} Biomass burning (BB) can be defined as open combustion of non-fossilized, vegetative or organic fuels, including residential burning for cooking, open fires in forests, agricultural and crop residues, charcoal or brick making, industrial biofuel consumption, forest fires and savanna fires.^{143, 147, 183, 187}

BB emits one of the largest non-methane organic carbon (NMOC) of around 400 Tg yr⁻¹.¹⁴⁷ The trace gases emitted by BB also have major contributions to the formation of smog and tropospheric O₃.¹⁸⁸ O₃ can adversely affect air quality, as one study shows that enhanced concentrations of O₃ downwind of a rural area of California following wild-fire events.¹⁸⁹ Trace gases from BB can also contribute to the formation of SOA.^{190, 191} Furthermore, both BB and fossil fuel combustion can lead to the formation of aromatic VOCs, which can lead to the formation of secondary nitro-aromatic compounds (NACs) via their photo-oxidation in the presence of NO_x.¹⁴⁷ Hence, NACs are important markers of BBA and are also a component of BrC aerosol. NACs need to be characterized for their role in the atmosphere as a part of BB emissions.^{147, 192} LG is anhydrous sugar and a primary emission of pyrolysis of BB emissions, while some important NACs (i.e., NC, NG and NS) are formed as a secondary product of pyrolysis in presence of NO_x.¹⁴³ These four important BBA components were systematically evaluated for their toxicological profile in human lung cells in the fourth chapter of this thesis; their molecular structures are provided in [Table 1.3](#).

Table 1.3. Four BBA markers included in the current study for toxicological profiling.

Levogluconan	3-Nitrosalicylic Acid	4-Nitrocatechol	4-Nitroguaiacol
			

1.3.4.1- Formation of Important BBA Components

Compounds derived from the pyrolysis of lignin, cellulose, wood combustion, and bio-fuel burning are emitted as POA. One of the molecular-levels markers of this primary atmospheric BBA is an anhydrous sugar called levoglucosan, which is a by-product of thermal degradation of cellulose.¹⁹³ LG is emitted along with its isomers mannosan and galactosan under ambient conditions as POA, while aging of BB emission results in the formation of SOA that include NACs and methylated-NACs.¹⁹³ NACs are important components of ambient aerosol, present in both fresh or aged BBA samples, and represent a significant fraction (~21%) of OA, including BrC, which absorbs light.¹⁹⁴ Major sources of NACs to the atmosphere are BB emissions. Owing to their large atmospheric concentrations, some classes of NACs such as nitro-polyaromatic hydrocarbons (nitro-PAHS), NC, NG and NPs have gained much attention over the past few years.¹⁹⁵ In one study at BB emission sites, a strong correlation was found between LG and 4NC, 3NS, and 4NG, implying these three compounds were SOA components formed from photochemical oxidations of BB emissions.¹⁹⁵ Along with direct emissions, NACs are also formed as a result of oxidation of VOCs containing benzene ring, anthropogenic emissions from industries, manufacturing and military activities, herbicides, and fungicides in the soil.¹⁹⁶ 4NC could also be formed via the $\cdot\text{OH}$ -initiated oxidation of guaiacol (a methoxyphenol emitted from BB) in the presence of NO_2 , while under high- NO_x conditions 4NG is formed.¹⁹⁷ The average total concentration of NACs in urban samples was found to be around 6.63 ng m^{-3} , with 4NP and 4NC being the most prevalent in the quantified samples.^{194, 195} In another study, the NACs concentration was found to be 115 ng m^{-3} for the wintertime samples (typical for smog instances) and 770 ng m^{-3} for the brushfire-influenced aerosol samples.¹⁹⁸ Hence, typically, NACs are present in the urban environment under high- NO_x conditions; the concentration of NACs increase in the instances of wild-fire burning, where

high BB emissions are present in the atmosphere.¹⁹⁹ With increased urbanization, increased occurrences of wild-fire instances, rapid utilization of BB sources (domestic fuel and industrial development), the BBA contribute towards worsening of air quality, decreased visibility, increased climate variation, and may pose a severe health risk upon inhalation.²⁰⁰ Hence, identification of BB emission sources and contributions of individual molecular-level markers of BBA in the total burden of lung-associated pathologies are adamant to develop regulations to control their emission rates in the atmosphere.

1.3.4.2- Toxicological Profiling of Biomass Burning Aerosol

The wide-spread use of NACs by industries worldwide release them into the atmosphere through BB emissions poses a pollution threat, mainly as their removal procedures are not effectively developed.¹⁹⁶ Inhalation, ingestion or direct contact with NACs may result in acute and/or chronic exposures, and are known to pose serious health threats including ROS build up, mutagenesis, DNA damage, hypersensitivity and systematic or localized (pulmonary) inflammatory responses.¹⁹⁶ For example, nitro-PAHs were found to induce DNA damage, mutagenesis and apoptosis.²⁰¹ There are also several extensive studies on the exposure effects of PM_{2.5} originating from wood and fuel combustion and BB.^{17, 77, 200, 202-209} PM_{2.5} from wood combustion enhanced ROS/RNS levels and DNA damage in the lung cells (A549).^{17,204} The water-soluble fraction of PM derived from wood combustion exhibited ROS build up, apoptosis induction, mitochondrial dysfunction and increased lipid peroxidation within BEAS-2B cells and mice,²⁰⁷ while another *in vitro* study exhibited chemical composition based pro-inflammatory and ROS response, and could not differentiate between primary v/s atmospherically-aged wood combustion fractions.²⁰⁶ PM_{2.5} from different types of wood combustion and flaming v/s smoldering conditions exhibited varying potentials of toxicity and mutagenicity in a mice model,²⁰² and significant cellular proliferation and increased migration, and mortality within A549 cells with a dosage of 250-500 µg mL⁻¹. NG was found to be more toxic than NG in a bioluminescence toxicity analysis,²⁰⁹ implying the role of nitration in increasing the toxicity of the aromatic VOC-derived aerosol. A recent cohort study on wild-fire emissions from Southern California found enhanced hospital admissions due to respiratory stress, and caused a greater impact on respiratory health than any other PM_{2.5} source.²⁰⁰ In an *in vitro* study and DTT analysis by Tuet et al.,²⁰⁸ BBA emissions from the Brazilian Amazon was

found to induce the highest toxicity compared to other ambient and/or lab-generated SOA examined in that study. This prior study also highlighted a significant correlation between LG and ROS/RNS even though LG alone did not exhibit significant ROS increases.[208](#) Previous studies provide evidence of increased respiratory stress following exposure to BBA and wood combustion, but none of them identify the molecular-level markers of BBA that are potentially toxic for inhalation.

1.4. Objectives of Thesis

As reviewed in the preceding sections, the formation of SOA in the atmosphere may adversely impact air quality, and thus, public health. However, there are limited studies that compare the formation mechanism and acute inhalation responses of different biogenic/anthropogenic sources of SOA. This thesis covers the formation mechanisms of SOA from two natural plant-based emissions (i.e., SOA from α -pinene ozonolysis and the heterogeneous $\cdot\text{OH}$ oxidation of fine particulate 2MTSs). It compares them to the emission source and exposure impact of NPs and BBA. Two well-established lung cell lines, BEAS-2B and A549, were used as exposure models to compare the inhalation responses of the four different atmospheric PM (or SOA) systems examined in this thesis. The approaches used in this thesis included: (i) an OFR, commercially known as the PAM reactor) was used to generate SOA from either α -pinene ozonolysis or from the heterogeneous $\cdot\text{OH}$ oxidation of fine particulate 2MTSs, with the latter mimicking the atmospheric aging of IEPOX-derived SOA. LC/MS analyses were carried out to identify the various markers and aging products from the aerosol samples; (ii) Model eukaryotic cell membranes were used to carry out *in situ* analysis following exposure to atmospheric NPs. It included electrochemical and atomic force microscopy (AFM) measurements. (iii) High throughput screening to elucidate the cellular proliferation rates after exposure, and the calculation of IC_{50} values to compare the relative toxicities of the four PM (or SOA) systems examined; and (iv) Functional assays, including microscopy, genomic analysis, and flow cytometry, were carried out to determine the intra-cellular mechanisms of toxicity. ROS build-up and mitochondrial dysfunction were observed in cells after exposure. Cells were examined for the cytotoxicity mechanism (i.e., apoptosis or necrosis) at various concentrations and exposure timepoints. The third chapter of this thesis is divided into four sections, covering the atmospheric

sources and mechanisms of toxicity in the lung cells. The key research questions addressed in each chapters were:

- a- The cellular toxicity of the full SOA mixture from α -pinene ozonolysis was compared with the individual and known molecular-level markers of α -pinene SOA, including pinic acid, pinonic acid and MBTCA to see how atmospheric aging affected the ROS build up and IC_{50} in the exposed BEAS-2B and A549 cells.
- b- The genomic analysis was carried out in the 2MTS aerosol system to determine the intra-cellular changes (ROS, anti-ROS, inflammatory and glutathione detoxification) following exposure to atmospherically aged 2MTS aerosol particles. This included the assessment of how atmospheric aging by heterogeneous $\cdot OH$ oxidation of fine particulate 2MTSs changes the aerosol chemical composition, and thus, potentially altering the toxicology profile within BEAS-2B cells.
- c- The equimolar mixture of 2NP, 3NP, and 4NP was exposed to the model lung eukaryotic membrane, and changes in the membrane were assessed through AFM. In the second part of the study, the three NPs (i.e., 2NP, 3NP, and 4NP) were qualitatively analysed in the ambient and lab-generated SOA samples to predict the source of the NPs. These NPs were then assessed for comparative toxicity in the BEAS-2B and A549 cell lines using IC_{50} analysis, determination of the mechanism of cytotoxicity and ROS build-up with special emphasis on mitochondrial dysregulation.
- d- The final section of this thesis covers the exposure assessment of the four molecular-level markers of BBA in the BEAS-2B and A549 lung cell lines. This includes the prediction of how nitration of aromatic aerosol within BB emissions forms the NACs in the atmosphere that modulates the toxicity in the lung cells when compared to the primary emission of BB such as LG

This thesis provides novel insights into how important the exposure assessment of POA and SOA from different sources in the same in vitro model is to predict which of the aerosol systems is more toxic for inhalation and could potentially impact public health. This information can aid air regulatory authorities in designing and implementing control strategies to mitigate emission rates of harmful aerosol systems into the atmosphere.

CHAPTER 2: Experimental Section

2.1- Materials and Chemicals

2.1.1- Chemicals

α -pinene (>99% purity), *cis*-pinonic acid (98% purity), dimethyl sulfoxide (DMSO, MolBio-Grade, USA), Methanol (ChromaSolv-Grade), 0.1 % acetic acid in methanol (Optima LC/MS Grade) were purchased from Sigma-Aldrich (Merck, Poland). Acetonitrile (ACN, HPLC grade) and high-purity methanol (optima LC/MS Grade) were purchased from Fisher Scientific (USA). MBTCA (3-methyl-1,2,3-butanetricarboxylic acid, 99% purity) and *cis*-pinic acid (99.5% purity) were synthesized in the Institute of Physical Chemistry Polish Academy of Sciences (IPC PAS) laboratory, as described previously.²¹⁰²¹¹ A diastereomeric mixture of racemic ammonium 2-MTSs, i.e., (2R,3S)/(2S,3R)- and (2S,3S)/(2R,3R)-1,3,4-trihydroxy-2-methylbutan-2-yl sulfates, used in the study, was synthesized at the University of North Carolina at the Chapel Hill (UNC) as previously described.¹²⁴

2-Nitrophenol, 3-Nitrophenol, 4-Nitrophenol, 4-Nitrocatechol, Levoglucosan, 3-Nitrosalicylic Acid, 4-Nitroguaiacol ((all 99% purity grade) were purchased from Sigma-Aldrich (Merck), USA. All chemicals used for gas chromatography interfaced to mass spectrometry (GC-MS) analysis were purchased at the highest purity available from Aldrich Chemical Co. (Milwaukee, WI) and were used without further purification. Solvents used in GC-MS (GC² quality) analysis were from Burdick and Jackson (Muskegon, MI, USA).

1,2-dimyristoyl-sn-glycero-3-phosphocholine, DMPC(14:0-14:0), 1,2-dipalmitoyl-sn-glycero-3-phosphocholine, DPPC(16:0-16:0), 1-palmitoyl-2-oleoyl-sn-glycero-3-phosphocholine, POPC(16:0-18:1) were purchased from Sigma-Aldrich and used without further purification. 1-Thio- β -D-glucose, β -Tg, was purchased from Sigma-Aldrich and used as a hydrophilic monolayer on the electrode surface. Phosphate buffered saline (tablets, Sigma-Aldrich), PBS, was used to prepare 0.01 M buffer, pH = 7.4. Chloroform (\geq 99%, Sigma-Aldrich) and methanol (HPLC grade, POCH) were used for the preparation of phospholipid stock solutions. A Milli-Q water advantage system (Merck, Poland) was used to obtain Milli-Q water (resistivity 18.2 M Ω x cm at 25°C) to dissolve all the standards and probes.

2.1.2- Probes and Assays

Trypan blue solution and Triton X-100 solutions were purchased from Merk, Poland. All assays and fluorescent probes including PierceTM lactate dehydrogenase (LDH) cytotoxicity assay kit, Vybrant MTT assay kit (3-(4,5-dimethylthiazol-2-yl)-2,5-diphenyltetrazolium bromide), Calcein-AM (a live cell marker), propidium iodide (PI, a fluorescent DNA intercalating probe), 6-carboxy-2',7'-dichlorodihydrofluorescein diacetate (carboxy-H₂DCFDA, a general oxidative stress indicator), MitoSoxTM red (mitochondrial superoxide indicator), Hoechst 33342 solution (fluorescent live-cell nucleus probe), tetramethyl rhodamine methyl ester (TMRM) (mitochondrial membrane potential state), DAPI ((4',6-diamidino-2-phenylindole) and live-cell imaging solution (physiological live-cell imaging medium) were purchased from Invitrogen (ThermoFisher Scientific, USA). MitoPY1 and HEPES (bio ultra for molecular biology grade) were purchased from Merk, Annexin V- FITC kit was purchased from Miltenyi Biotec, USA.

Resazurin sodium salt, a cellular viability indicator dye, was purchased from Alfa Aesar, USA. All Prep DNA/RNA/miRNA universal kit was used to extract the RNA from the cells, and QuantiTect SYBR[®] Green real time quantitative polymerase chain reaction (RT-qPCR) Kit was used for RT-PCR analysis. Both were purchased from Qiagen, USA. A high-capacity cDNA reverse transcription kit from Applied Biosystems, Foster City, CA, USA, was used to synthesize complimentary DNA (cDNA) from RNA.

2.1.3- Materials and Cell Culture

BEAS-2B (ATCC[®] CRL-9609TM) and A549 (ATCC[®] CCL-185TM) cell lines were purchased from ATCC. Bronchial epithelial cell growth medium (BEGM), complete with supplements and growth factors, were purchased from either BEpiCM, ScienCell, USA, or Lonza, USA. Dulbecco's modified eagle's medium (DMEM) with phenol-red was purchased from Institute of Immunology and Experimental Technology, Wrocław, Poland. Phenol-red free DMEM, heat-inactivated fetal bovine serum (FBS), L-glutamine (L/G, 2 mM) and penicillin-streptomycin (P/S, 100 mg mL⁻¹) and Trypsin-EDTA (0.25% solution with phenol red) were purchased from Merk (USA). Dulbecco's phosphate-buffered saline (DPBS), and 0.05% Trypsin-EDTA were purchased from Merck, USA.

Quartz-fiber filters (Tissuquartz™, Pall Life Sciences, USA), 47-mm quartz-fibre filters (PALL Corp part number, May 2020), PTFE syringe filters (Agilent Technologies, 0.2-µm pore size, USA), Tissue culture (TC) treated T75 flasks (Cell Star, Greiner Bio-One, Austria), 96-well advanced TC™ treated µclear® microplates (Greiner Bio-One, Austria), 96-well advanced TC™ clear bottom black-welled microplates, 24 well TC-treated multiple well plates (Corning Co-star, USA) and µ-slide ibidi-polymer, tissue culture treated 8 well coverslip (Ibidi, Germany) were also used in the study. For Real-time polymerase chain reaction (RT-PCR) analysis MicroAmp™ Optical 96-well reaction plates and adhesive PCR plate seals were purchased from ThermoFisher Scientific, USA.

2.2- Methodology and Experimental Procedure

2.2.1- Generation, Quantification & Chemical Analysis of SOA

2.2.1.1- Generation of α -Pinene SOA through the Ozonolysis of α -Pinene

SOA particles from the α -pinene ozonolysis were produced in a Potential Aerosol Mass (PAM) oxidation flow reactor (Aerodyne Research, Inc.)²¹²⁻²¹⁴ under dry (relative humidity, RH < 5%) and dark conditions. A syringe pump (Chemyx, Fusion 100) was employed to continuously inject α -pinene mixed with 3 L min⁻¹ clean, dry N₂ (g) inside a glass bulb to entrain the vapor into the reactor. At the injection rate that was used, the α -pinene mixing ratio was approximately 5 ppm. A separate flow of 2 L min⁻¹ filtered clean air was introduced into a separate O₃ generator to produce 30 ppm of O₃ subsequently injected into the reactor. Following SOA generation in the reactor, the sample flow was passed through activated charcoal denuders and an O₃ denuder to remove excess α -pinene and O₃, respectively. SOA number concentrations and mobility size distributions were obtained with a scanning mobility particle sizer (SMPS, TSI Inc., Model 3080). Integrated filter samples were obtained following the collection of SOA particles onto pre-baked 47-mm quartz-fibre filters at 3 L min⁻¹ (treated at 600°C for 24 h). Typical SOA mass concentrations were approximately 6 mg m⁻³, estimated from SMPS measurements assuming a particle density of 1.2 g cm⁻³.²¹⁵ At these concentrations, 20 mg filter samples were obtained following 18.5 hours of continuous collection. While significantly lower SOA concentrations are easily achieved in the reactor, the longer collection times necessary to

achieve 20 mg samples were not practical. After collection, filters were stored under dark conditions at -20 °C until analysis. The experimental setup for the PAM reactor used in the study is provided in [Figure 2.1](#).

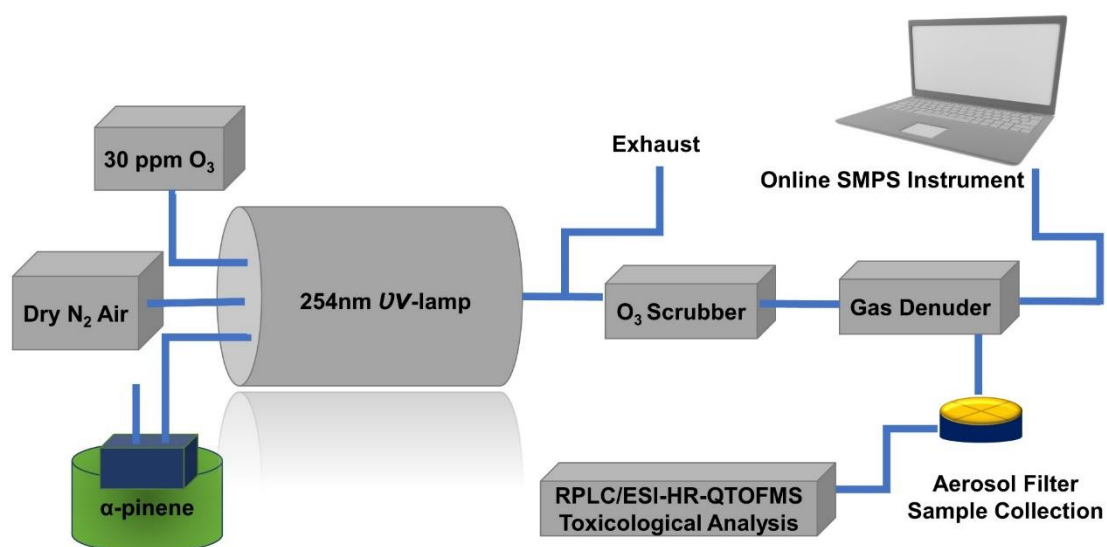


Figure 2.1. Experimental setup for the generation of the α -pinene SOA through the ozonolysis using PAM reactor.

2.2.1.2- Filter Extraction of α -Pinene SOA

The α -pinene SOA constituents were extracted from quartz-fibre filters with 10 mL of high-purity methanol by sonication for 45 min in a pre-cleaned 22 mL scintillation vial. The methanol extracts were blown dry under a gentle N₂ (g); ~ 2mg of mass was reconstituted in 1 mL of deionized water before the exposure studies with the two cell types. Prior to drying, extracts were filtered through 0.2- μ m PTFE syringe filters to remove insoluble particles or quartz filter fibres. The methanol extracts were blown dry under a gentle N₂ (g) stream at ambient temperature. The dried extracts were reconstituted with 300 μ L of a 50:50 (v/v) solvent mixture of methanol and water for RPLC/ESI-HR-QTOFMS analysis.

2.2.1.3- RPLC/ESI-HR-QTOFMS Analysis of α -Pinene SOA

The chemical characterization of α -pinene SOA was performed by ultra-performance liquid chromatography interfaced to electrospray ionization high-resolution quadrupole time-of-flight mass spectrometry (UPLC/ESI-HR-QTOFMS, 6520 Series, Agilent) operated in the negative and positive ion modes to measure organic acids and organic peroxides, respectively.^{124, 128} The reconstituted aerosol extracts were further diluted by a factor of 20 for quantifications of three α -pinene SOA tracers i.e., pinonic acid, pinic acid, and MBTCA. In the negative ion mode, a six-point calibration of the three α -pinene SOA tracers was construed in the range between 0.5 and 50 ppm (Figure 2.2). It was analysed along with the SOA samples produced from α -pinene ozonolysis. It is noted here from the 6-point calibration that the three α -pinene SOA tracers showed the linear response only up to 10 ppm and that the samples fell within this linear dynamic range. 5- μ L aliquots of the calibration standards and samples were injected onto the UPLC column (Waters ACQUITY UPLC HSS T3 column, 2.1×100 mm, 1.8- μ m particle size) at a flow rate of 0.3 mL min⁻¹; the UPLC column was a reversed-phase liquid chromatography (RPLC) column, and thus, we will refer to this method as RPLC/ESI-HR-QTOFMS hereafter. The mobile phases consisted of (A) 0.1 % acetic acid in Milli-Q water and eluent (B) 0.1 % acetic acid in methanol. The applied 15-min gradient elution program was as follows: the concentration of eluent B was 0 % for the first 2 min, increased to 90 % from 2 to 10 min, held at 90 % from 10 to 11 min, and decreased to 0 % from 11 to 15 min.

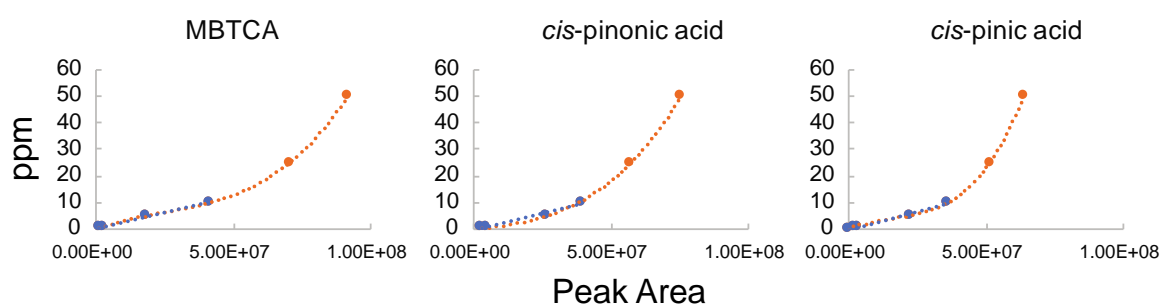


Figure 2.2. Six-point calibration curves obtained for MBTCA, *cis*-pinonic acid, and *cis*-pinic acid before a negative ion RPLC/ESI-HR-QTOFMS analysis. Note that the data points within the linear range and the linear fit are shown in blue, while the non-linear data points and the polynomial fit are shown in orange.

Detailed operating procedures e.g., mass calibration, tuning, voltages, etc. of the RPLC/ESI-HR-QTOFMS method have been published elsewhere.[210](#), [216-218](#) The analogous mobile phases and gradient elution program were employed for the RPLC/ESI-HR-QTOFMS analysis operated in the positive ion mode to aid in the detection of additional α -pinene SOA constituents, including organic peroxides (namely, hydroxy hydroperoxides). The injection volume used for positive ion mode was 10 μ L. Previously, we have demonstrated that isoprene-derived hydroxy hydroperoxides (1-2-ISPOOH; specifically, 2-hydroperoxy-2-methylbut-3-en-1-ol) synthesized at UNC could be measured by the RPLC/ESI-HR-QTOFMS method operated in the positive ion mode.[117](#)

As a result, we injected the 1,2-ISPOOH standard synthesized at UNC onto the RPLC/ESI-HR-QTOFMS to demonstrate how organic hydroperoxides fragment during collision-induced tandem mass spectrometric (MS/MS) experiments in the positive ion mode. This aided in the structural characterization of potential organic hydroperoxides measured in the present study from SOA generated from α -pinene ozonolysis. Similarly, in the positive ion mode, a six-point calibration of the 1,2-ISPOOH was constructed in the range between 0.5 and 50 ppm. It was analysed along with the SOA samples produced from α -pinene ozonolysis.

2.2.1.4- Generation of Heterogeneously Oxidized 2-Methyltetrol Sulfates Aerosol

The experimental setup for generating and collecting aged particles from the heterogeneous \bullet OH oxidation of particulate 2-MTSs is illustrated in [Figure 2.3](#). Briefly, an aqueous solution of an authentic ammonium salt form of 2-MTSs was aerosolized into an oxidation flow reactor (OFR), conditioned at 91 ± 3 % RH and $21 \pm 1^\circ\text{C}$, by atomization. Varied \bullet OH concentrations in the OFR were generated through Uv irradiation ($\lambda = 254$ nm) of O_3 in the presence of water vapor. \bullet OH exposure levels ranged from 0 – 2.85×10^{12} molecules cm^{-3} s, and was achieved by varying the Uv lamp intensity, corresponding to an atmospheric age of 0 – 22 days (assuming an average atmospheric \bullet OH concentration of 1.5×10^6 molecules cm^{-3}).[219](#) Aged 2-MTS aerosol particles exiting the OFR were monitored in real-time by a SMPS, TSI Inc. to ensure the stability of aerosol concentrations. Aged particulate 2-MTSs were collected onto 47-mm Quartz filters (PALL Corp) at 4.0 L min^{-1} under each stabilized \bullet OH exposure conditions summarized in [Table 2.1](#).

Table 2.1. Summary of the experimental setup for the generation of heterogeneously $\cdot\text{OH}$ -mediated aged 2MTS aerosol used in the toxicological studies.

Sample/ Equivalent Aging Days	RH (%)	T (°C)	O ₃ (ppm)	UV photon flux (cm ⁻² .s ⁻¹)	$\cdot\text{OH}$ exposure (molecule. cm ⁻³)
0	92.6	20.3	2.7	0	0
5	93.4	20.8	2.7	2.54×10^{14}	6.43×10^{11}
12	87.0	21.2	2.8	7.40×10^{14}	1.51×10^{12}
22	90.0	22.3	2.7	1.49×10^{15}	2.85×10^{12}

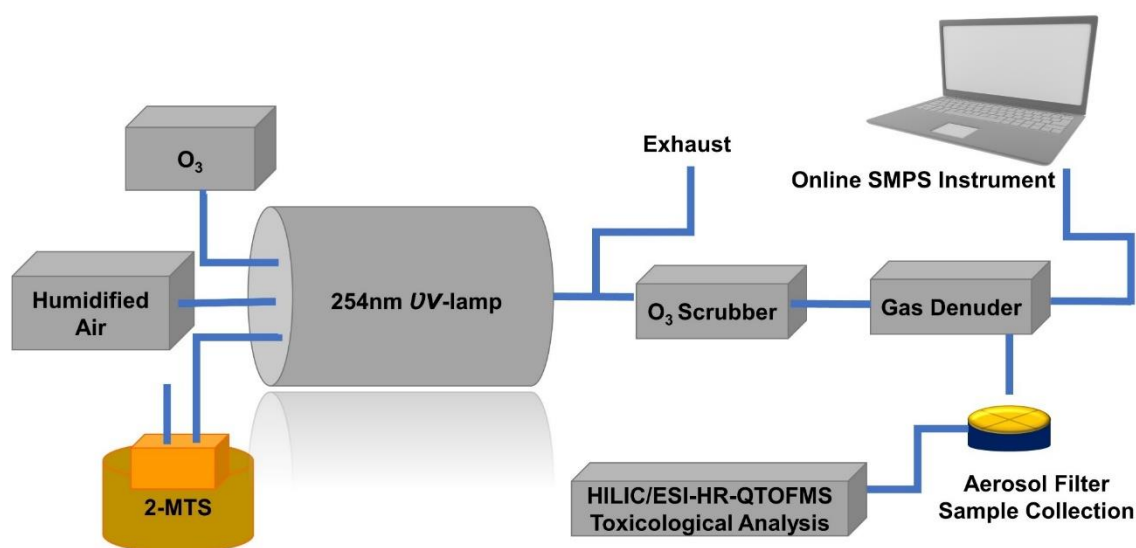


Figure 2.3. The experimental setup for heterogeneous $\cdot\text{OH}$ -mediated oxidation of particulate 2-MTSs with the PAM reactor.

Blank and sample quartz filters were stored in the dark at -20°C until extracted in methanol, blown dry, and reconstituted in Milli-Q water to achieve 50 mg mL^{-1} . A $10 \mu\text{L}$ aliquot of each reconstituted aqueous extract was preserved for analysis by ion chromatography (IC) to quantify $\text{Sulf}_{\text{inorg}}$, and for analysis by hydrophilic interaction liquid chromatography interfaced to electrospray ionization high-resolution quadrupole time-of-flight mass spec-

trometry (HILIC/ESI-HR-QTOFMS) to quantify OSs and other potential SOA constituents. Remaining aqueous extracts were used for biological assays. Detailed descriptions for the OFR, filter processing (or sample workup), and quantitative offline chemical analysis protocols have been described previously.[18](#), [124](#), [127](#)

2.2.1.5- Filter Extraction of 2MTS Originated Aged SOA Products

The blank and aerosol sample filters were extracted with 10 mL of high-purity LC/MS grade methanol by sonication for 45 min in pre-cleaned 22 mL scintillation vials. Prior to drying, extracts were filtered through 0.2- μm PTFE syringe filters to remove insoluble particles or quartz filter fibres. The methanol extracts were blown dry under a gentle N_2 (g) stream at ambient temperature. Dried extracts were then reconstituted with Milli-Q water to achieve an aqueous concentration of 50 mg mL^{-1} prior to the exposure studies with BEAS-2B cells. The total aerosol mass collected on quartz filters was determined based on SMPS- measured volume concentrations and total air volume collected through each filter. The density of aerosol for 0 day of aging was derived to match the chemical data with the standard purity. The density was calculated to be 1.27 g cm^{-3} . The total aerosol mass for the aged samples was then calculated using the new density and the fraction of each chemical component obtained in each sample.

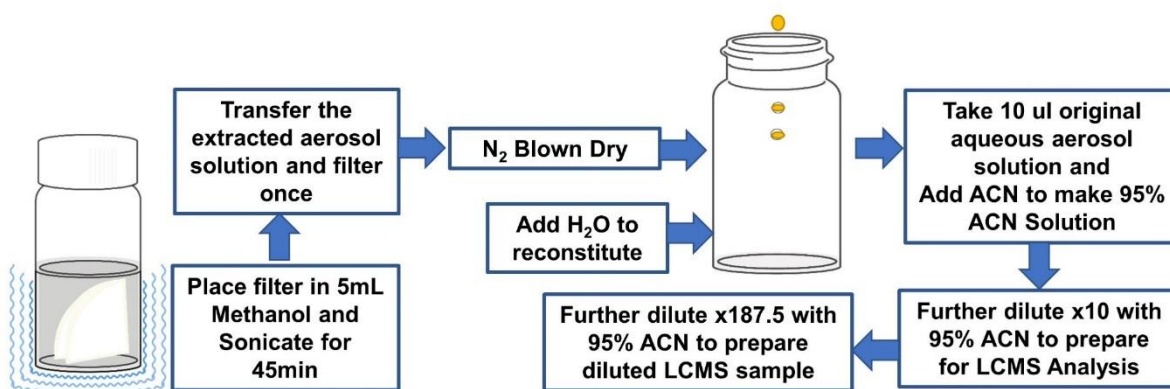


Figure 2.4. The filter extraction protocols were developed for the isolation of 2MTS-originated aged SOA products.

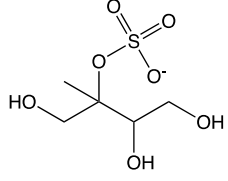
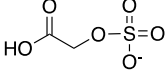
2.2.1.6- Chemical Analysis of Organosulfates

For HILIC/ESI-HR-QTOFMS analysis, a 10- μ L aliquot of each aqueous sample was withdrawn and diluted in 190 μ L acetonitrile to make a concentrated solution of the analytes, and further diluted by 187.5 times using 95:5 acetonitrile: Milli-Q water (ACN:H₂O) (v:v) to quantify deprotonated molecular ions associated with the particulate 2-MTSs and their corresponding heterogeneous *OH oxidation products. HILIC/ESI-HR-QTOFMS analysis was carried out on an Agilent 6500 Series UPLC system equipped with an ESI source interfaced to an Agilent 6250 Series Accurate Mass Q-TOFMS operated in negative ion mode. Detailed operating procedures (gradient elution program, mass calibration, tuning, and voltages) of the HILIC/ESI-HR-QTOFMS system have been previously described.[124](#), [127](#), [128](#), [220](#)

Two OS standards, which included 2-MTSs and glycolic acid sulfate (2MGS) (GAS, [M – H]⁻ ion at *m/z* 155), were analysed along with the samples to establish 6-point calibration curves for quantifications of other multifunctional OSs detected by HILIC/ESI-HR-QTOFMS. Similar to the approach adopted by Chen et al.,[220](#) the assignments of response factors of surrogate standards to detected OS products were based on retention time ([Table 2.2](#)). However, not all surrogate standards were analysed along with the samples in this work, so their response factors were derived from the absolute response factors of 2-MTSs determined here and the relative ionization efficiencies to 2-MTSs reported in our previous work.[220](#)

For ion chromatography (IC) analysis, an aliquot of each reconstituted aqueous sample was diluted by 400 times and 3600 times with Milli-Q water for SO₄²⁻ and NH₄⁺ quantifications, respectively. SO₄²⁻ was quantified by an anion-exchange IC system (ICS 3000, Thermo Scientific) equipped with an IonPac AS11-HC guard column (2×50 mm, Thermo Scientific) and anion-exchange column (2 × 250 mm, Thermo Scientific). The 35-min gradient program employed for the anion analysis has been described in our previous work.[18](#), [127](#) NH₄⁺ was quantified by a cation-exchange IC system (Aquion, Thermo Scientific) equipped with an IonPac CS16 guard column (5 × 50 mm, Thermo Scientific) and cation-exchange column (5×250 mm, Thermo Scientific). Methane sulfonic acid (MSA) was used as the eluent for the cation IC. NH₄⁺ elutes ~ 4.3 min using an 8-min isocratic eluting program with MSA concentration held constant at 20 mM. Ammonium sulfate (>99%, Sigma Aldrich) was used as the quantification standard for both the cation and anion exchange IC analyses.

Table 2.2. Quantification standards deployed for HILIC/ESI-HR-QTOFMS analyses.

Name	Structure	[M-H] ⁻	Purity	Retention Time (min)	Response Factor (ppm/Area)
2-methyltetrol sulfates (2-MTS)		C ₅ H ₁₁ O ₇ S ⁻	90.30%	5.5, 6.9	1.12×10 ⁻⁷
Glycolic acid sulfate (GAS)		C ₂ H ₃ O ₆ S ⁻	96.60%	23.96	1.29×10 ⁻⁶

2.2.1.7- Principal Component Analysis (PCA)

PCA was carried out on the 4 different heterogeneously aged particulate 2-MTS samples (Table 2.1) to reduce the dimension of the variables. 18 variables were introduced into the analysis (Sulf_{inorg} and OSs characterized by IC and HILIC/ESI-HR-QTOFMS, respectively), which generated 3 principal components (PCs). The PC that explained the total variance of 80% or above for all four aging points was selected for further analysis i.e., PC1.

2.2.1.8- Collection and analysis of mono-NPs in SOA and ambient PM_{2.5}

The aerosol part of the research was conducted in a close collaboration with the U.S. EPA. In brief, the SOA samples were obtained during the past 20 years in one of the U.S. EPA smog chambers [221](#), [222](#) by irradiating a series of individual aromatic hydrocarbons in the presence of NO_x. Subsequently, they were analyzed at the time of collection, and the resulting chromatograms were re-analyzed for the targeted NPs used in this study. The chambers were operated either in a static mode (as a conventional batch reactor) or, for experiments requiring large sampling volumes, in a dynamic mode (flow mode) to produce a steady-state concentrations of gas- and particle-phase reaction products.[223](#) Details on chamber operations, procedures, and instruments were reported in earlier studies.[221](#), [222](#)

Gas-phase species were collected with 60 cm, four-channel XAD4-coated annular denuders, and aerosol particles were collected onto 47-mm glass-fiber filters.²²³ The denuders were analyzed for organic compounds by extracting them in a 1:1 dichloromethane/methanol mixture, and then derivatized with a BSTFA/TMCS mixture.²²⁴ The aerosol samples were sonicated with methanol, and the dried extracts were derivatized with a BSTFA/TMCS mixture.²²³ The resulting derivatized extracts were analyzed by GC–MS on a ThermoQuest (Austin, TX) GC coupled with an ion-trap mass spectrometer. The temperature of the injector was held at 270 °C, and the GC was operated in splitless mode. A 60 m, 0.25 mm inner diameter, RTx-5MS column (Restek, Inc., Bellefonte, PA) with a 0.25- μm film thickness was used. The oven initial temperature was 84 °C for 1 min, which was increased by a temperature ramp of 8 °C min^{-1} to 200 °C, followed by a 2 min hold, and then the second ramp of 10 °C min^{-1} to 300 °C. The ion source, ion trap, and interface temperatures were 200, 200, and 300 °C, respectively. 2 μL of the extract was injected in methane chemical ionization (CI- CH_4) and/or electron impact (EI) modes.

Table 2.3. Initial reactants conditions of hydrocarbon (HC) and nitrogen oxides (NO_x) as well as the mass of SOA (mg) collected on the filters and analysed by GC-MS for selected representative smog chamber experiments.

Exp. ID	HC	Initial HC (ppmC)	Initial NO_x (ppb)	SOA mass (mg) / [SOA] ($\mu\text{g m}^{-3}$)	Phase analysed	Detected NPs
ER137 ^{S,*}	Toluene	5.44	293	8.85/54.95	GP; PP	2NP; 4NP
ER-343 ^D	Benzene	19.70	259	3.69/182.43	PP	4NP
MR092	Toluene	18.60	810	1.77/595.56	GP; PP	2NP; 4NP

* PP: particle-phase; GP: gas-phase; 2NP: 2-nitrophenol; 4NP: 4-nitrophenol; S: experiment conducted in static mode; D: experiment conducted in dynamic mode. Seed aerosol at 1 $\mu\text{g m}^{-3}$ was used. The initial NO_x during the irradiations was greater than 98% NO.

Additionally, ambient $\text{PM}_{2.5}$ samples were collected at several sites in the U.S. between 2003 and 2010. These were analyzed at the time of collection, and the resulting chromatograms were re-analyzed for the targeted NPs used in this study. Table 2.3 summarizes the field studies examined in this study for mono-NPs. Detailed descriptions of the field sites and sampling procedures are reported elsewhere.²²⁵⁻²²⁷ In brief, the $\text{PM}_{2.5}$ samples were collected onto pre-baked quartz-fiber filters for 24 h, whereupon the filters were

Soxhlet-extracted for 24-h in 50-mL dichloromethane/methanol mixture (1:1 v/v). Prior to extraction, known amounts of ketopinic acid (KPA) and D₅₀-tetracosane were spiked on each filter as internal and recovery standard, respectively. Each extract was evaporated to dryness under a gentle stream of N₂ (g) at room temperature, then derivatized for 1 h with 200 μL of *N, O*-bis- (trimethylsilyl)trifluoroacetamide: 1% trimethylchlorosilane (BSTFA) and 100 μL of pyridine at 70 °C. Chemical analyses of derivatized extracts were conducted using the same GC-MS used for chamber samples.

2.2.2- Model Eukaryotic Membranes

2.2.2.1- Preparation of Model Eukaryotic-Like Cell Membrane

For *in situ* analysis, two kinds of human lung cell-mimicking membranes were prepared, i.e., a membrane composed of DMPC(14:0-14:0) and the membrane comprised of an equimolar mixture of DMPC (14:0-14:0), DPPC (16:0-16:0), and POPC (16:0-18:1), named as the 3 × PC membrane. Phospholipids were dissolved separately in the chloroform: methanol (3:1 v/v) mixed solvent solution to form stock solutions. Sufficient volumes of stock solutions in a total amount of 1 mg phospholipids were combined in a vial. The solution was vortexed under the argon flow for 45 min until dry phospholipid film was formed on the walls of the vial. Dry phospholipid film was stored for 24 h in a desiccator before use. Then, 1 mL of MilliQ water was added to the dry phospholipid film, and the solution was sonicated at 45 °C for 30 min. As a result, hollow spheres of 25 nm to 100 nm in diameter, enveloped by a single lipid bilayer, were formed, named small uni-lamellar vesicles, SUVs. [228](#), [229](#) Such prepared SUVs solutions were used for the model biological cell membrane deposition. [230](#), [231](#)

2.2.2.2- Atomic Force Microscopy Imaging

The SUVs solution was drop-casted on a freshly cleaved mica surface. The deposition of the three × PC bilayer took 1 h. After that time, mica was gently washed by soaking a Kimwipe® with the excess solution and drop-casting fresh MilliQ water, repeatedly, for three times. Next, the sample was assembled in the AFM fluid cell, which was then filled with MilliQ water, and AFM measurements were performed immediately. Olympus BL-AC40TS probes (Oxford Instruments) of nominal resonant frequency $f = 110$ kHz, nominal

spring constant $k = 0.09 \text{ N m}^{-1}$, nominal tip end radius $R = 8 \text{ nm}$, were used after calibration. A calibration procedure was performed before each experiment and includes tip check scanning for tip end radius determination, deflection sensitivity measurement on freshly cleaved mica surface in MilliQ water, and thermal tune for the constant spring determination, performed in MilliQ water [232](#), [233](#). First, the bilayer was imaged in MilliQ water and then the NPs-mixture solution was injected to the AFM fluid cell and left for incubation. AFM imaging was performed for different incubation times. All AFM experiments were performed at $RT = 21 \text{ }^\circ\text{C}$.

2.2.3- *In vitro* Cell Cultures

2.2.3.1- A549 Cell

A549 cells were routinely cultured in the standard phenol red DMEM medium with, 10% FBS, 1%G/L and 1% P/S. Trypsin-EDTA (0.25% solution with phenol red was used to routinely detach the adherent cells for passaging and maintained at 37°C in a 5% CO_2 humidified incubator. Briefly, replenished medium was removed from ~80% confluent A549 cells in T75 flasks and cells were washed with 5mL of PBS. After removing the PBS, 5mL of Trypsin-EDTA was added for 5min to detach the cells. Trypsin was neutralized through 5mL of fresh medium. In around ~2mL of neutralized cells, 8mL of fresh DMEM medium was added to routinely culture the cells in T75 flask. A549 cells were maintained between 3-30 passages during the course of experiments. Cells were cryo-preserved in liquid nitrogen for long term storage in 10% DMSO in full DMEM medium.

2.2.3.2- BEAS-2B Cells

BEAS-2B cell were grown upto 80% confluency inside the T75 cell culture flasks in the BEGM medium. For passage, the depleted medium was discarded once or twice the week, cells washed with 5mL of pre-warmed (37°C) sterile PBS. 5mL of pre-warmed 0.05% trypsin-EDTA was added to the confluent cells and placed in the incubator for around 5-10 minutes and cells observed under the microscope for detachment. Trypsinized, detached cells were neutralized by adding 5mL of the BEGM medium, transferred to the falcon tubes and centrifuged at the 1000rpm (125 g^{-1}) between 5-10 min. The supernatant

was then discarded, and pelleted cells resuspended in 10mL of fresh BEGM medium and transferred to fresh T75 flask.

Prepare the storage stock as 20% DMSO in whole BEGM medium. To cryo-preserve the cells, medium was discarded, cells washed with PBS and trypsinized according to the protocol mentioned above. Pelleted cells were suspended in 1.5mL of medium and split into three vials containing a final concentration of cell suspension as: 0.5mL of medium + 0.5mL of storage stock. In this way, we had 10% DMSO as a final storage concentration. From one confluent T75 Flask, 3 cryopreservation vials of 1.5mL were prepared.

2.2.4- High Through-put Screening using Spectrophotometer

The end-point absorbance or fluorescence (depending upon the type of the analysis) was recorded using a spectrophotometer plate reader from BioTex Synergy HTX or Promega GloMax (Madison, WI). High-throughput analysis of the treated-cells was carried out inside the 96-well plates to observe for viability, proliferation and oxidative stress using fluorescence or absorbance mode as shown in Figure 2.6 below.

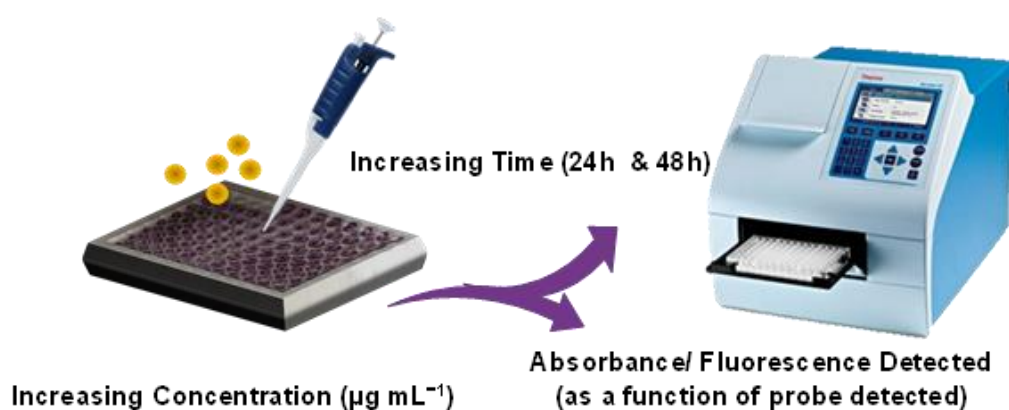


Figure 2.6. High-throughput spectrophotometer to detect the mean absorbance/fluorescence as a function of biological activity in the experimental and control lung cells.

2.2.4.1- Cell Count Optimization

For high-throughput assays, cells were plated in the 96 well plates and calibration curve with the MTT dye was drawn for further experiments. Briefly, cells were seeded in the 96 wells with increasing dilution and adhered to the bottom for 24 h. After 16 h, medium

was discarded and 100 μL of fresh medium and 10 μL of 5 mg mL^{-1} of MTT dye (dissolved in 1X PBS) was added. Cells were incubated at 37°C for 2-3 hours until they formed NAD(P)H-oxidoreductase reduced formazan insoluble crystals. The crystals were dissolved in 100 μL well⁻¹ of DMSO as a solubilizing agent and allowed to incubate for another 10min. The end-point absorbance was recorded using spectrophotometer (BioTex Synergy HTX) at 540 nm. Two non linear regression curves were then drawn (for A549 and BEAS-2B cells) as shown in **Figure 2.7** using Graphpad Prism version 9.2.0. The number of cells corresponding the specific optical density (OD) was used in the further experiments. For high-throughput screening assays, cells number corresponding to the absorbance of 0.5 was selected for further analysis.

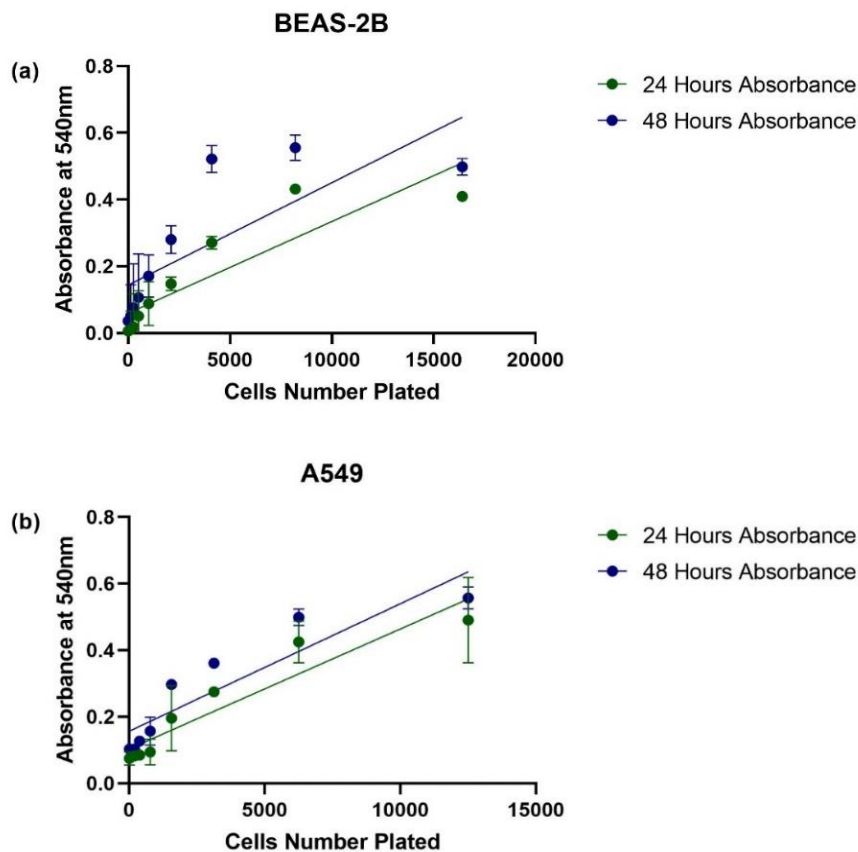


Figure 2.7. Cell count optimization for high-throughput analysis. (a) BEAS-2B and (b) A549 cells were seeded into 96-well plates in decreasing serial dilution, and corresponding OD was noted at 540nm after 24 h using an MTT dye.

2.2.4.2- Mitochondrial Toxicity Testing (MTT Assay)

Cells were seeded at 5000-8000 cells well⁻¹ for A549, and 10,000-12,000 cell well⁻¹ for BEAS-2B; these were allowed to adhere for at least 16 hours in 96-well plates. Cells were counted using trypan blue in automated Countess II Automated Cell Counter (Thermo Fisher Scientific). The cells were then replenished with 100 µL of fresh medium (complete BEGM for BEAS-2B cells, or DMEM (phenol-red free, reduced serum medium) supplemented with 5% FBS, 1% P/I, 1% L/G for A549 cells, and treated with various doses of 10 µL of individual α-pinene SOA molecular tracers (i.e., pinonic acid, pinic acid and MBTCA), a 3-component mixture of the same α-pinene SOA molecular tracers that had authentic standards (equal concentration/ volume ratio mixture), or the α-pinene SOA sample (all dissolved and prepared in double distilled and deionized water). Similarly, the cells were also treated with 2NP, 3NP, 4NP or their equimolar mixture, NS, NC, NG, or their equimolar mixture. Following 24 and 48 hours of exposure time, the medium was decanted from all the wells and fed with 100 µL of fresh medium, followed by the addition of 10 µL of 5 mg mL⁻¹ of MTT dye (dissolved in 1X PBS).

Cells were incubated at 37°C for 2-3 h until they formed NAD(P)H-oxido-reductase reduced formazan insoluble crystals. The crystals were dissolved in 100 µL well⁻¹ of DMSO as a solubilizing agent and allowed to incubate for another 10 minutes. The end-point absorbance was recorded using a spectrophotometer (BioTex Synergy HTX) at 540 nm with the background signal of DMSO subtracted from the recorded readings.

The final calculations for cellular proliferation rates were made as follows:

Cellular Proliferation rate (%)

$$= \frac{\text{Absorbance of Treated Cells at 540nm} - \text{Absorbance of the blank} \times 100}{\text{Absorbance of Untreated Cells at 540nm} - \text{Absorbance of the blank}}$$

where: *untreated cells* is the control without any aerosol treatment, while the *blank* is the medium without any cells.

2.2.4.3- Lactate Dehydrogenase Assay (LDH Assay)

The LDH enzyme is released by the dead cells and can be quantified to assess the percentage of cell death. The aerosol component treated A549, BEAS-2B were analysed for percentage cellular death following 24 and 48 hours of exposure to increasing concentration of the markers (i.e., NPs or BBA & their mixtures). The protocol recommended by the manufacturer was used to calculate LDH release. Briefly, after treatment time, the medium of the different treatment and control groups was transferred to black 96 well plates. To calculate the final release of LDH in the medium, 0.1% Triton-X 100 cells acted as a *Maximum* LDH control for the experiments. The cells without aerosol (10µL of DI water), acted as the *Spontaneous* LDH control. The final absorbance values were determined by calculating absorbance at 490 nm subtracted by absorbance at 680nm using Spectrophotometer Synergy HTX BioTex. The background absorbance of medium alone (blank) was subtracted from the absorbance of the treatment groups, maximum and spontaneous control groups. The final calculations were pursued in accordance with the formula:

$$\text{Percentage LDH Release Cytotoxicity} = \frac{\text{Compound treated LDH Activity} - \text{Spontaneous LDH Activity}}{\text{Maximum LDH Activity} - \text{Spontaneous LDH Activity}} \times 100$$

2.2.4.4- Resazurin Viability Assay

The Resazurin assay was performed to analyse the percentage of cellular proliferation following treatment with the increasing concentration of heterogeneously oxidized particulate 2-MTSs at four atmospherically relevant aging points, including 0, 5±3, 12 ±3 and 22 ±3 days. The exposure concentration was increased from 0.01 to 4000 µg mL⁻¹ to determine the IC₅₀ for the BEAS-2B cells following 24h and 48h exposures. For this assay, 10,000 cells well⁻¹ were seeded in black- walled 96-well plates and allowed to adhere overnight. Cells were then exposed to aqueous aerosol extracts and after desired treatment time, the conditioned medium was removed, 100- µL of fresh medium and 20-µL of 0.15 mg mL⁻¹ of resazurin were added to each well. Cells were incubated for 3 h, and fluorescence measured using a 560 nm excitation- 590 nm emission filter set in a microplate spectrophotometer Promega GloMax (Madison, WI).

Final calculations to determine cellular proliferation rate were made using the formula given below:

Cellular Proliferation rate (%)

$$= \frac{\text{Fluorescence of Treated Cells at 560 nm emission} - \text{Fluorescence of the blank}}{\text{Fluorescence of Positive Control Cells at 560nm} - \text{Fluorescence of the blank}} \times 100$$

where: the blank is the well with medium, and resazurin dye alone, and the positive control for viability is when cells were treated with blank filter extracts in DI water.

2.2.4.5- Carboxy-H₂DCF Assay

Carboxy-H₂DCFDA is a cell-permeant probe, which, upon deacetylation by cellular stresses and oxidation by ROS, is converted into green, fluorescent carboxy-DCF. To BEAS-2B and A549 control and nitrophenols treated cells in 96-well plates, resuspended in 100 μ L of cell culture medium, 100 μ L of PBS with 20 μ M of carboxy-H₂DCFDA were added and incubated for 15 min at 37°C in the dark. Working carboxy-H₂DCFDA concentration was 10 μ M. The exc.488 nm/em.525 nm filter was used to detect carboxy-DCF signal using fluorescent spectrophotometer at 4 h intervals up to 24 h of treatment.

2.2.4.6- Inhibitory Concentration-50 (IC₅₀) Calculations

The inhibitory concentration-50 (IC₅₀) is the concentration at which growth inhibition of half the cellular population occurs. The values for percentage cellular proliferation, as calculated through resazurin assay (2-MTS project) and MTT assay (α -pinene SOA project) was adjusted through fitting a non-linear dose response curve. The corresponding [aerosol concentration] v/s normalized response was plotted to estimate the IC₅₀ values following the aged particles at 24h or 48h of exposure. For the IC₅₀ values [Inhibitor] vs. normalized response, the following equation was used, with 95% confidence interval to obtain IC₅₀ and log-IC₅₀ values.

$$Y = \frac{100}{1 + X/IC_{50}}$$

The IC₅₀ was calculated using the SigmaPlot version 14.5 from the MTT data of three mono-nitrophenols and BBA components (LG, NS, NG, NC, and their equimolar mixture). The Hill's function was used to approximate the proliferation percentage vs. concentration and to estimate the IC₅₀ value equivalent to the *c* coefficient in the equation given below:

$$y = \frac{ax^b}{c^b + x^b} = \frac{a}{\left(\frac{c}{x}\right)^b + 1}$$

2.2.4.7- Statistical Analysis

The statistical analyses were performed using GraphPad Prism (Version 8.00 for Windows, GraphPad Software, La Jolla California USA, www.graphpad.com).

The data were analyzed for normality assumptions using one-way ANOVA and were presented as mean \pm standard deviation (SD) of at least three independent repetitions. For the concentration time-dependent MTT data, results were analyzed by using a one-way ANOVA followed by Tukey's post-hoc test. The results were considered statistically significant at p-value ≤ 0.05 for all exposure groups at two-time points.

In α -pinene SOA and its markers study, the Tukey's test allowed us to analyze the difference in the mean of treatment groups with the mean of untreated control cells. The significant difference at a particular concentration was reported as ⁺24 hour significant, ⁺⁺48 hour significant and ⁺⁺⁺significant difference amongst treatments at 24 and 48 hours. For image-J analyzed PI⁺ cells in α -pinene SOA treated SOA, the two way ANOVA with Šídák's multiple comparisons test was performed on the data set to determine the statistical significance between treated and untreated control cells, where $p \leq 0.05$ value was considered significant.

For MTT assay, resazurin assay and LDH assay, two way ANOVA followed by Tukey's post-hoc test was performed to analyze the difference in the mean of treatment groups with the mean of untreated control in the study with 2MTS, NPs and BBA.

2.2.5- Fluorescent Microscopy and Cellular Imaging

2.2.5.1- Phase Contrast Images

The fluorescence microscope (Nikon Eclipse T1-SAM, Japan) in phase contrast mode was used to acquire images of cells at 100 x lens magnification following treatment. Cells were incubated in the nitrophenol mixture for 24 and 48 h at various concentrations in 96 well plates. The nitrophenol mixture dosage was kept between 0.01 to 200 $\mu\text{g mL}^{-1}$

(0.01, 0.1, 1.0, 10, 100 and 200 $\mu\text{g mL}^{-1}$) and changes in cell morphology or cell count were observed under the microscope after 24 and 48 h of incubation. As a control experiment, the dose of 10 μL of double-distilled Milli-Q water in the absence of the nitrophenols was added to the BEAS-2B and A549 cells and imaged by fluorescence microscope.

2.2.5.2- Calcein-AM Propidium Iodide

The live-dead cell stain imaging was performed using Calcein-AM (1 mg mL^{-1} dissolved in DMSO for live cells) and propidium iodide (PI, 1 mg mL^{-1} in DI water for dead cells). The final Calcein AM:PI ratio of the fluorescent probe dissolved in PBS was 1:10 (100 $\mu\text{g mL}^{-1}$ for PI, and 1 $\mu\text{g mL}^{-1}$ for Calcein-AM). The fluorescent probe was added directly to 24 h and 48 h treated cells, respectively in 96-well plates without media removal. Calcein-AM is a cell-permeant non-fluorescent dye that converts into a fluorescent form through acetoxymethyl ester hydrolysis by cellular stresses. These stress activities are markers of the cell viability, rendering a green fluorescent and charged form of the probe that is well-retained in live cells. PI is a non-permeant DNA marker, unable to stain live cells, and only the cells with the damaged cell membrane (dead cells) appear as positive for PI. Images were acquired using fluorescence microscope (Nikon Eclipse T1-SAM, Japan) in TRITC and FITC filter range (Ti-FLC filters) at x100 magnification. High-resolution images were captured using Nikon DS-U2 digital sight (Japan). While capturing the image, cells were scanned at 6.8 gain settings, resolution of captured images was fixed at the fast-focus mode of 640 x 480 pixels. The scanning exposure in the Calcein-AM channel was kept fixed at 200 ms, while cells in the PI channel were scanned at the exposure of 400 ms. During an experiment, the plates were kept on the stage, maintained at 37°C using Linkam DC-60 thermo-controller. This approach was adopted for three projects included in this thesis: monoterpene SOA, NPs, and BBA.

2.2.5.3- Image-J Analysis

NIS-Elements imaging software was used for initial imaging, while final images were analyzed with NCBI's Image-J software, a freely available software at <https://imagej.net/Fiji>. All the images were captured at a fixed area of 600 x 800 μm using 10x objective lens in three modes: Calcein-AM + filter channel, PI+ filter channel and

phase-contrast brightfield mode. The PI+ BEAS-2B cells were calculated using particle size analysis function of image-J. The α -pinene ozonolysis SOA treated cells were normalized to untreated control cells population by capturing cellular density in the fixed area ($4.8 \times 10^4 \mu\text{m}^2$), as determined in three independent experiments.

2.2.6- Flow Cytometry Single Cell Analysis

Flow cytometry analysis was run to detect the changes in the cellular morphology, granularity, and biochemical signal at the single cell level. The analysis allows one for the quantification of cellular signal in a flow tube and allows the sorting based on:

1- Cells are sorted based on shape (morphology) and granularity/density (via the use of two type of detector, i.e., forward scatter detector FSD & side scatter detector SSD).

2- Functional assessment and sub-populations are sorted based on the cellular tagging with a fluorophore (Gating).

This approach allows for multiplexing and simultaneous detection of several signals in the treated and control cells. The principal of the flow cytometry measurement is summarized in [Figure 2.8](#).

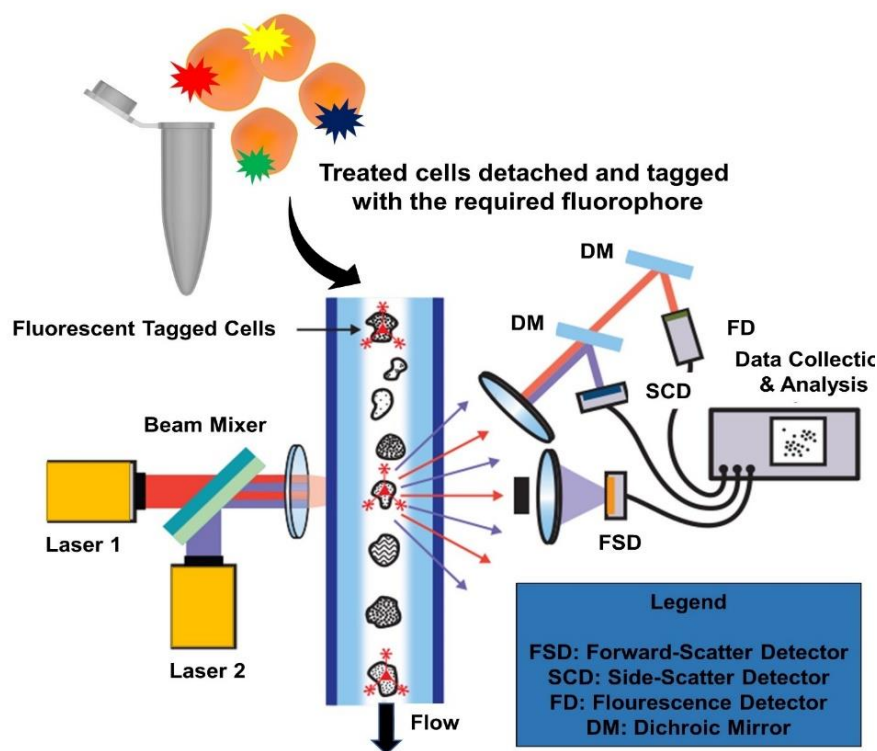


Figure 2.8. Simplified representation explaining the operation and working principle of a basic flow cytometer.

2.2.6.1- Sample Preparation for Flow Cytometric Analysis

For the flow cytometry analysis, BEAS-2B were seeded at $\sim 20,000$ cells well^{-1} for and A549 $\sim 10,000$ cell well^{-1} in 96 well plates and cells allowed to incubate with the compound for the course of the experiment: $100 \mu\text{g mL}^{-1}$ and $200 \mu\text{g mL}^{-1}$ of NPs or BBA components and their equimolar mixtures. For each of the experiments, cell medium was collected in pre-labelled centrifuge tubes. The wells were washed once with $50 \mu\text{L}$ of 1x PBS and collected again in the same centrifuge tubes. The cells were then trypsinized for 5-10 min using $50 \mu\text{L}$ of Trypsin-EDTA and collected in the centrifuge tubes as well. The cell suspension was then centrifuged at 300 g (gravity) for 5 min at 25°C . The supernatant was discarded, cells were re-suspended in $100 \mu\text{L}$ of fresh medium plus $100 \mu\text{L}$ of the fluorescent probe.

The CytoFLEX S Flow Cytometer (Beckman Coulter, USA) was used for sample acquisition, and data were recorded using CytExpert software. This instrument is a four-

laser flow cytometer equipped with forward scatter (FSC), side scatter (SSC), and 13 fluorescence detectors. During the data analysis, the aggregates were discarded using the forward scatter area (FSC-A) and height (FSC-H) signals, defining a "single cells" gate. Following this, the live cells were included in the final analysis. The double gate "live and single cells" was applied to all the measurements.

2.2.6.2- Annexin-V/Propidium Iodide Staining Assay

The Annexin-V/PI kit was prepared for analysis according to the instructions provided by the manufacturer. Briefly, 17.5 μL of annexin dye and 35 μL of PI were suspended in 3.5 mL of Annexin buffer, to prepare the stock solution. The Annexin buffer was supplied in the Annexin V kit in a 20X solution form. Daily, this was prepared at 1X in distilled water, discarding the unused solution. 10 μL of this stock was diluted in 100 μL of the Annexin buffer (Annexin V/PI solution). The trypsinized cells were centrifuged and resuspended in 100 μL of the Annexin V/PI solution and incubated at room temperature for 15 min in the dark. Treated (experimental) and untreated (control) cell groups (BEAS-2B and A549) were analysed for various parameters using CytoFLEX S Flow Cytometer (Beckman Coulter, USA) and data recorded using CytExpert software. Annexin V FITC was detected using the exc.488nm/em.525 nm filter, and PI with the exc.561 nm/em.610 nm filter.

The Annexin-V/ PI kit allows the fluorescent detection of apoptotic and necrotic cells through the specific binding of FITC labelled Annexin V to phosphatidylserine (PS), a negatively charged phospholipid located in the cytosolic side of plasma lipid bilayer. PS re-localization from the inner to the outer bilayer membrane is the early wide-spread event during the apoptosis. Hence Annexin V-FITC labelled cells were defined as early apoptotic cells, PI and Annexin V-FITC double-stained cells were late apoptosis/necrotic. In contrast, the single-cell PI-positive events were nude nuclei from the necrotic cells.

2.2.6.3- Tetramethyl rhodamine Methyl Ester Perchlorate (TMRM Assay)

TMRM is a cell-permeant, cationic dye actively sequestered by the living mitochondrial cells. Changes in TMRM signal indicate disruption of the mitochondrial function. The control and treated cells were incubated with 100 μL of 20 nM TMRM in PBS for 15 min

at 37 °C in the dark. The working TMRM concentration was 10 nM. Before the acquisition, DAPI was added to a final concentration of 1 $\mu\text{g mL}^{-1}$. The exc.561 nm/em.610 nm filter was used to detect TMRM, and exc.405/em.450 nm filter for DAPI detection. Only the DAPI -ve (live) cells were included in the analysis.

2.2.6.4- MitoSox Assay

MitoSox is a cell-permeant fluorogenic dye that produces red fluorescence in the presence of mitochondrial-specific superoxide. To BEAS-2B and A549 control and treated cells resuspended in 100 μL of cell culture medium, 100 μL of PBS 10 μM of MitoSox were added and incubated for 15 minutes at 37°C in the dark. Working MitoSox concentration was 5 μM . Before the acquisition, DAPI was added to a final concentration of 1 $\mu\text{g mL}^{-1}$. The exc.561 nm/em.610 nm filter was used to detect MitoSox, and exc.405/em.450 nm filter for DAPI detection.

2.2.6.5- Carboxy-H₂DCFH Analysis

Cells were analyzed 6 h post-aerosol exposure (α -pinene SOA) and 8 h post exposure to BBA components and their equimolar mixture. Conditioned cell medium was collected in pre-labeled centrifuge tubes, and the wells were washed once with 50 μL of 1x PBS and collected again in centrifuge tubes. The cells were then trypsinized for 5-10 min using 50 μL of Trypsin-EDTA and collected in centrifuge tubes. The cell suspension was then centrifuged at 300 g (gravity) for 5 min at 25°C. The supernatant was discarded, cells resuspended in 100 μL of fresh medium plus 100 μL of 10 μM of carboxy-H₂DCFDA, and 1 $\mu\text{g mL}^{-1}$ PI in 1x PBS. Treated (experimental) and untreated (control) cell groups (BEAS-2B and A549) were analyzed for increased oxidative stress signal using CytoFLEX S Flow Cytometer (Beckman Coulter, USA) and data recorded using CytExpert software.

Carboxy-H₂DCFDA is a non-fluorescent cell permeant probe. Upon deacetylation by cellular esterases and oxidation by ROS, the molecule is converted into carboxy-DCF, which has green fluorescence emission. The carboxy- H₂DCFDA signal was analysed in live and single cells using the exc.488 nm/ em.525 nm filter. First, the aggregates were discarded using the forward scatter area (FSA) and height (FSH) signals, defining a “single cells”

gate. PI signal was detected using the exc.561 nm/em.610 nm of the filter. PI+ cells were defined as dead cells and were discarded from the analysis, defining a “live cells” gate. The double gate “live and single cells” was applied to the carboxy-DCF measurement.

2.2.6.6- MitoPY1 Analysis

MitoPY1 is a fluorescent probe to detect mitochondrial hydrogen peroxide (H₂O₂). To BEAS-2B and A549 control and treated cells resuspended in 100 µL of cell culture medium, 100 µL of PBS 5 µM of MitoPY1 were added and incubated for 15 minutes at 37°C in the dark. Working MitoPY1 concentration was 2.5 µM. Before the acquisition, PI was added to a final concentration of 1 µg mL⁻¹. The exc.488 nm/em.525 nm filter was used to detect MitoPY1 and exc.561/em.610 nm filter for PI detection.

2.2.6.7- Statistical Analysis

The data were analyzed for normality assumptions using Graph-pad Prism version 9.1. One-way and two-way ANOVA are presented as mean ± standard deviation (SD) of at least three independent repetitions. The difference in the Annexin-V/PI treatment versus control was analyzed using the two-way ANOVA followed by Sidak’s multiple comparison tests. The fold changes relative to untreated control for TMRM analysis, MitoPY1, MitoSox, and carboxy-H₂DCFA were analyzed using one-way ANOVA followed by Dunnet’s multiple comparison tests. The values of $p \leq 0.05$ were considered significant in each of the tests, and values of up to **** $p \leq 0.0001$ significance were reported.

2.2.7- Confocal Microscopy Imaging

2.2.7.1- Oxidative Stress Studies

Aerosol exposed cells were qualitatively analysed for ROS using a Nikon A1 scanning laser confocal microscopy (Nikon, Olympus, Japan). Cells were seeded and incubated in µ-slide ibidi-polymer treated 8-well coverslip.

After the 8 h treatment with the aerosol markers, the conditioned medium was removed, and cells were washed with PBS; BEAS-2B cells were incubated in 290 µL well⁻¹ of fresh BEGM medium, while A549 cells were incubated in 290 µL well⁻¹ of live cell

imaging solution. The cells were loaded with 10 μL of the probe cocktail (diluted in PBS) for 15-30 min before performing the live-cell imaging. The final concentration of 10 μM of carboxy- H_2DCFDA , 5 μM of MitoSox, 5 μM of MitoPY1 and 10 μM of Hoechst 33342 were used for imaging the cells. Hoechst 33342 was used to stain the nucleus of the cells. **Figure 2.9** highlights the methodology adopted for the sample preparation for confocal imaging and the post-processing of acquired images.

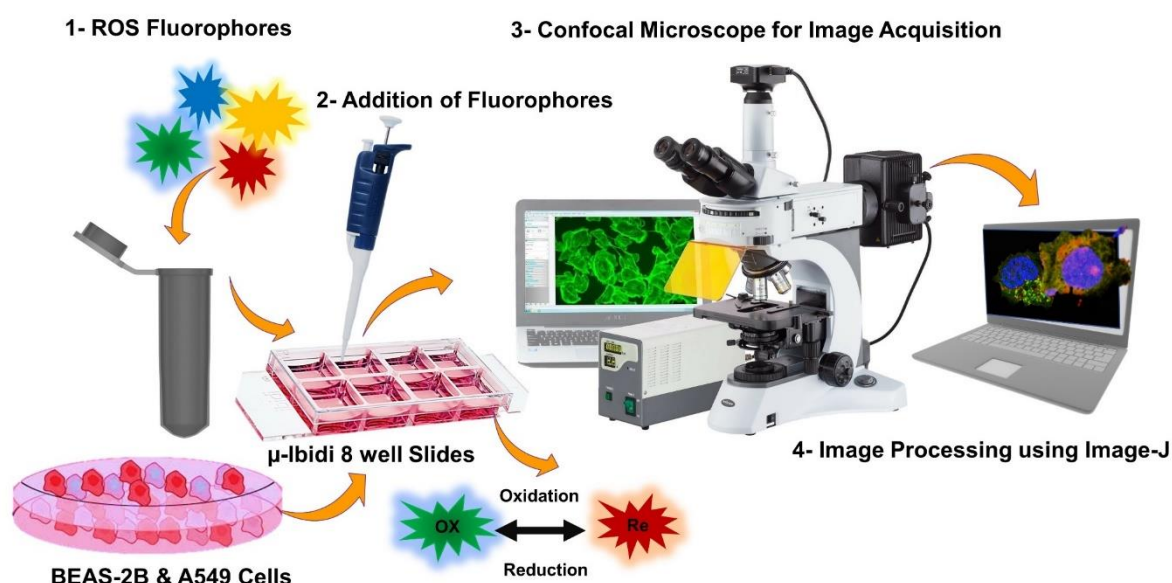


Figure 2.9. The summary of the method adopted for sample preparation, image analysis and processing in this part of the thesis. The aerosol markers treated cells were seeded in the μ -ibidi treated 8 well slides, fluorescent probes for ROS added and images for control and experimental groups analysed using confocal microscope. Finally, images were processed using Image J software.

For Hoechst-stained nucleus detection, 403.3 laser was used with exc.425nm/em475nm filter. Carboxy- H_2DCFDA and MitoPY1 signals were detected using 488 lasers with exc.500nm/em550nm filter. MitoSox signal was detected with 514.5 laser using filter of exc.570nm/em620nm. During the cellular imaging, the plates were kept on the stage, maintained at 37 $^{\circ}\text{C}$ using Linkam DC-60 thermo-controller, and images were captured with an oil immersion (x100 objective) lens. Images were captured in Galvano mode and analysed using NIS-Elements AR 4.13.04 software. Final images were merged and analysed using NIH Image-J software, freely available at <https://imagej.net/Fiji>.

2.2.8- Genomic Analysis

2.2.8.1- Cell Exposure

BEAS-2B cells were seeded at 200,000 cells well⁻¹ in tissue culture-coated 24-well plates. After allowing them to adhere overnight, cells were then exposed to 0.02, 0.2 and 2 mg mL⁻¹ of the four aerosol types (Table 2.1) as well as a positive control (blank filter extract in DI water). Four replicates from each treatment-type were tested for gene expression, pooled from two different experiments, to obtain both biological and technical replicates. The summary of steps carried out for genome analysis is summarized in Figure 2.10 below.

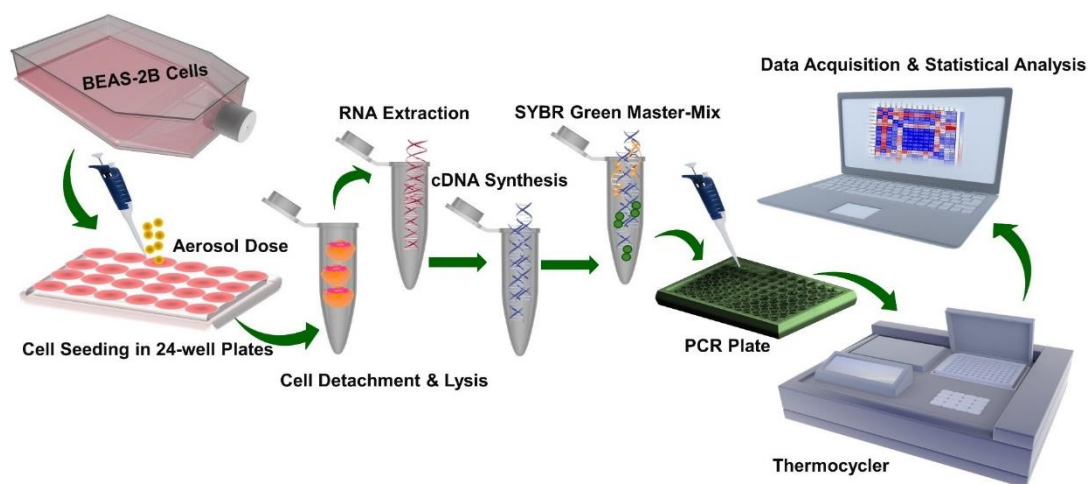


Figure 2.10. The summary of genome analysis following exposure to 2MTS and its aging products in the BEAS-2B cell lines. Briefly, cells were seeded in 24-well plates, aerosol dosed for 24 h. The cells were homogenized and lysed for RNA extraction. The cDNA was prepared, and RT-PCR analysis was carried out using SYBR-green. Finally, the data were acquired using thermocycler and analyzed using Graph-pad Prism.

2.2.8.1- RNA Extraction

Following 24 h of exposure, aerosol-treated and control cells using were harvested in 350 μ L of buffer RLT plus and placed in a QIAcube (Qiagen, Valencia CA). Total RNA extracted using Qiagen's All Prep DNA/RNA/miRNA Universal Kit following the manufacturer's protocol. Briefly, BME was added to RLT Plus (10 μ l BME per 1 ml Buffer RLT

Plus). All other buffers provided in the kit (FRN, RPE, AW1, and AW2) were also prepared.

To collect cells, we used 100 μL of 0.05% trypsin-EDTA to remove cells grown in a monolayer. Cells were then counted using a cell counter and transferred to an RNase-free centrifuge tube and centrifuge at 300 x g for min. We then utterly aspirated supernatant and added Buffer RLT Plus to each pellet (350 μL if $<5 \times 10^6$ cells; 600 μL if $5 \times 10^6 - 1 \times 10^7$ cells). The cell homogenate was vortexed to mix the cells and were homogenized by pipetting the lysate directly into a QIA-shredder spin column. They were then centrifuged for 2 min at top speed and lysate passed 5 times through a 20-gauge needle fitted to an RNase-free syringe. Nucleic acid extraction step followed. All-Prep DNA and All-Prep RNA mini spin column with collection tube and 1.5 mL collection tubes for RNA and DNA were pre-labelled. The homogenized lysate was transferred to All-Prep DNA mini spin column with collection tube and centrifuge for 30 sec at full speed. All-Prep DNA mini spin column were placed into a new collection tube and stored at 4°C. Flow-through was used for RNA extraction. For total RNA extraction, 80 μL Proteinase K was added to flow-through and pipetted up and down to mix. 350 μL 96-100% ethanol was added, and the sample was mixed well before incubating for 10 min at room temperature. Then we added 750 μL of 96-100% ethanol and mixed the sample well. Up to 700 μL of the sample was transferred to All-Prep RNA mini spin column with a collection tube. Centrifugation was carried out for 15 sec at full speed, and flow-through was discarded. This process was repeated until the entire sample had passed through the spin column. 500 μL of buffer RPE was added and centrifuge for 15 sec at full speed, and flow-through was again discarded. Following this, 80 μL of DNase mixture was directly added to the column and allowed to incubate at room temperature for 15 min. Next, 500 μL of buffer FRN was added to a column and centrifuged for 15 sec at full speed; at this step, flow-through was saved as it contained small RNAs.

For RNA extraction, the RNA spin column was placed into a new 2 mL collection tube. Flow-through from the previous step was added to a column and centrifuge for 15 sec at full speed. The flow-through was discarded, 500 μL of buffer RPE was added to the tube and centrifuged for 15 sec at full speed. Flow-through was discarded, and 500 μL of 96-100% ethanol was added and centrifuged for 2 min at full speed; again, the flow-through was discarded. RNA spin column was placed into new 2 mL collection tube and centrifuged for 2 min at full speed and flow-through discarded. RNA spin column was placed into new

1.5 mL collection tube and 50 μ L RNase-free water directly added onto the column. Centrifugation was carried out for 1 min at full speed to elute RNA.

The quality and quantity of total RNA were determined using NanoDrop-2000c spectrophotometer (ThermoScientific, Waltham, MA, USA) and samples stored at -80°C in nuclease-free water until further analysis.

2.2.8.2- Complementary DNA (cDNA) Preparation

The extracted RNA was used to synthesize 10 μ L of $20\text{ ng } \mu\text{L}^{-1}$ complementary DNA (cDNA) using Applied Biosystems' High-Capacity cDNA Reverse Transcription Kit, according to the manufacturer's protocol. Briefly, buffers were thawed at room temperature and enzymes (Reverse transcriptase, RNase inhibitor) placed on dry ice. The cDNA master mix was prepared in the Eppendorf tube as shown in Table 2.3 below and left on dry ice. 1X RT master mix was then combined with each sample. For this step, the PCR plate was placed on the cold block and 10 μ L of cDNA master mix to each well followed by 10 μ L of $200\text{ ng } \mu\text{L}^{-1}$ RNA to each well; PCR plate was sealed with the adhesive film and briefly centrifuge to eliminate air bubbles.

Table 2.3. Reaction master mix for cDNA preparation

	cDNA Reaction Master Mix	1X	26X
		1x (μ L)	26x (μ L)
1	10x RT Buffer	2	52
2	25x dNTP Mix	0.8	20.8
3	10x Random Primers	2	52
4	Reverse Transcriptase	1	26
5	RNase Inhibitor	1	26
6	Nuclease-free water	3.2	83.2
		10	260

The RT program was run as described in the following table 2.4. The final concentration of $2\text{ ng } \mu\text{L}^{-1}$ of cDNA was used for the RT-PCR analysis. The cDNA libraries created were stored at -20°C during the analysis.

Table 2.4. RT program to synthesize the cDNA from RNA.

Run RT Program				
	Step 1	Step 2	Step 3	Step 4
Temp	25	37	85	4
Time	10 min	120 min	5 min	hold

2.2.8.3- Real-Time PCR Gene Expression Analysis

This study included one house-keeping gene (ACTIN) and fourteen oxidative stress and inflammatory-associated genes. The reverse and forward primers for this current study were selected from the mRNA analysis-based studies on similar cell lines (BEAS-2B) using SYBR® Green RT-qPCR Kit. The forward and reverse primers were ordered from the Integrated DNA Technologies (USA) and reconstituted to a final working concentration of 3 μM before final dilution in the reaction mixture of RT-PCR 96-well plates.

Qiagen QuantiTect SYBR® Green RT-qPCR Kit was used to analyse the gene expression. Analysis and normalization of the NanoString raw data were conducted using nSolver Analysis Software v2.5 (NanoString Technologies). Briefly, 23 μl of RT-PCR master mix (table 6) and 2 μl of 2 $\text{ng } \mu\text{l}^{-1}$ (4 ng total) cDNA were pipetted into PCR Plate of master mix into corresponding wells within PCR plate.

Realtime RT-qPCR Ct values were then normalized against the geometric mean of housekeeping ACTIN, and fold changes in expression were calculated based on the $\Delta\Delta\text{CT}$ method.[234](#)

2.2.8.4- Statistical Analysis on Fold Change of Gene Expression

The statistical analyses were performed using GraphPad Prism (Version 9.2.0 for Windows, GraphPad Software, La Jolla California USA, www.graphpad.com). The difference in the fold change in the gene expression of treatment versus control cells was analysed for normality assumptions using ordinary two-way ANOVA, followed by Dunnett's multiple comparison test, and are presented as a Standard Error (SE) of four experimental repetitions and four technical replicates. The results were considered statistically significant at p -value ≤ 0.05 for all exposure groups against control cells where **** denotes $p < 0.0001$.

Table 2.5. The details of the forward and reverse primers for the reversed-transcriptase analysis included in the study.

Gene	Forward/ Reverse	Primer Sequence	Ref
NE2FL2	forward	GCTATGGAGACACACTACTTGG	235
	reverse	CCAGGACTTACAGGCAATTCT	
HMOX-1	forward	AGCTCTTTGAGGAGTTGCAGGA	236
	reverse	AGCTGAGTGTAAGGACCCATCG	
Catalase	forward	TCATGACATTTAATCAGGCA	237
	reverse	GTGTCAGGATAGGCAAAAAG	
GST	forward	CCATCTTTGAGAACACAGGT	237
	reverse	GAGAAGATTCGTGTGGACAT	
KEAP-2	forward	CGTCCTGCACAACACTGTATCT	235
	reverse	GTGTCTGTATCTGGGTCGTAAC	
SOD1	forward	TGTGGCCGATGTGTCTATTG	238
	reverse	GCGTTTCCTGTCTTTGTACTTTC	
SOD2	forward	CCTGGAACCTCACATCAACG	238
	reverse	GCTATCTGGGCTGTAACATCTC	
NQO-1	forward	GTGATATTCCAGTTCCCCCTGC	236
	reverse	AAGCACTGCCTTCTTACTCCGG	
GCLC	forward	GGAAGGAAGGTGTGTTTCCTGG	236
	reverse	ACTCCCTCATCCATCTGGCAA	
GCLM	forward	CCAGATGTCTTGAATGCACTG	236
	reverse	AGGACTGAACAGGCCATGTCA	
GSR	forward	TGGCACTTGCGTGAATGTTG	236
	reverse	CACATAGGCATCCCGCTTTTC	
IL-6	forward	CACAGACAGCCACTCACCTC	239
	reverse	AGCTCTGGCTTGTTCCCTCAC	
IL-8	forward	TCTGCAGCTCTGTGTGAAGGTG	239
	reverse	AATTTCTGTGTTGGCGCAGTG	
IL-10	forward	ATGCCCCAAGCTGAGAACCAAGACCCA	240
	reverse	TCTCAAGGGGCTGGGTCAGCTATCCCA	
Actin	forward	GGCGGACTATGACTTAGTTG	237
	reverse	AAACAACAATGTGCAATCAA	

Table 2.6. Final concentration of SYBR green and primers in the master mix.

Component	Starting Concentration	Final Concentration	Volume 1x (μL)	Volume 13x (μL)
Nuclease-free water	NA	NA	4	62
SYBR Green Master Mix	2x	1x	10	130
Forward Primer	3 μM	300 nM	2	36
Reverse Primer	3 μM	300 nM	2	36

2.2.8.5- Heat Map

Heat-maps were drawn to carry out the clustering of gene expression after exposure to the heterogeneously aged particulate 2MTS samples at 0.2, 0.2 and 2.0 mg mL⁻¹ concentration. These graphs show significantly fold increases or decreases in gene expression following the treatment where the range was between -20 to 60.

2.2.8.6- Multivariate Analysis and Pearson r Correlation Matrix

A multiple linear regression (MLR) model was used to predict the altered gene expression of BEAS-2B cells exposed to increasing concentrations of heterogeneously aged particulate 2-MTS samples by PC1. The gene expression was correlated by the following equation:

$$\text{Gene expression} \sim \text{Intercept } (\beta_0) + \beta_1 \times \text{PC1}$$

Where β_0 is the baseline gene expression, and β_1 is the change in gene expression following exposure to the increased heterogeneously aged particulate 2-MTS samples.

The IC₅₀ value and fold changes in gene expression were evaluated for the correlation with PC1 using Pearson R Correlation Matrix, where PC scores were either positively or negatively correlated with the IC₅₀ values at 24 and 48 h exposure. If r values were between 0.5 to 1, we assumed a positive strong correlation, while the values between -0.5 to -1 were assumed a negative strong correlation.

CHAPTER 3: Results and Discussion

The research undertaken during my Ph.D. studies resulted in four mutually inter-linked research projects. This chapter covers the essential results and findings of each project and the significant conclusions. The first section provides the toxicological profiling of three important atmospheric markers of α -pinene SOA. It compares it with the mixture of fresh α -pinene ozonolysis SOA in the BEAS-2B and A549 cells, respectively. The second section provides essential results obtained from the toxicological studies on heterogeneously OH radical-aged isoprene-derived 2MTS aerosol. The entire mixture of SOA-bound organo-sulfates (Oss) (aging time comparable to the atmospheric aging of 2MTS at 0 days, 5 days, 11 days, and 20 days) were exposed to the BEAS-2B cells at 24 hours. The corresponding dependence on gene expression with atmospheric aging was evaluated using the principal component and multivariate analysis. The third section assesses toxicological profiles of 2NP, 3NP, 4NP and their equimolar mixture in BEAS-2B and A549 cells, respectively. This includes the evaluation of the mono-nitrophenol in the ambient and smog chamber generated SOA samples followed by detailed cytotoxic evaluation in the lung cells. The fourth section is concerned with the toxicological profiling of four biomass burning aerosol (BBA) markers in the BEAS-2B and A549 cells, respectively. The markers were exposed to lung cells and a detailed toxicological assessment was carried out that included IC₅₀ calculations, mechanism of cell death elucidation, ROS, and mitochondrial dysfunction assessment.

3.1- Toxicological Profiling of α -Pinene Ozonolysis SOA and its Important Atmospheric Markers in the Lung Cells.

In recent years, changes in precursor molecule emissions from anthropogenic sources have increased PM_{2.5} emission and inadvertently contributed towards climatic change.²⁴¹ The global climatic change has also resulted in higher emission rates of biogenic VOCs due to increased temperatures and changes in plant metabolism.²¹⁷⁻²¹⁶ The resultant increase in atmospheric α -pinene SOA concentration requires the development of standards on minimal safe inhalation concentration (MSIC) from a public health perspective.⁹³ The objective of the present section was to determine the concentration and time-dependent responses of lung cells to known α -pinene SOA molecular tracers (i.e., pinic acid, pinonic acid, and MBTCA) and the full SOA mixture generated from α -pinene ozonolysis. To understand post-exposure responses, immortalized normal bronchial epithelial (BEAS-2B) cell line and cancer alveolar epithelial (A549) cell line were used as the lung cell models in the current study.²¹⁸ This comparison allowed us to investigate the potential toxicity of α -pinene-derived SOA compounds, including for multifunctional organic peroxides that could not be examined individually due to the lack of available authentic standards but could be examined as a mixture within the full SOA generated from α -pinene ozonolysis. The outline of the study is highlighted in **Figure 3.1** in next page.

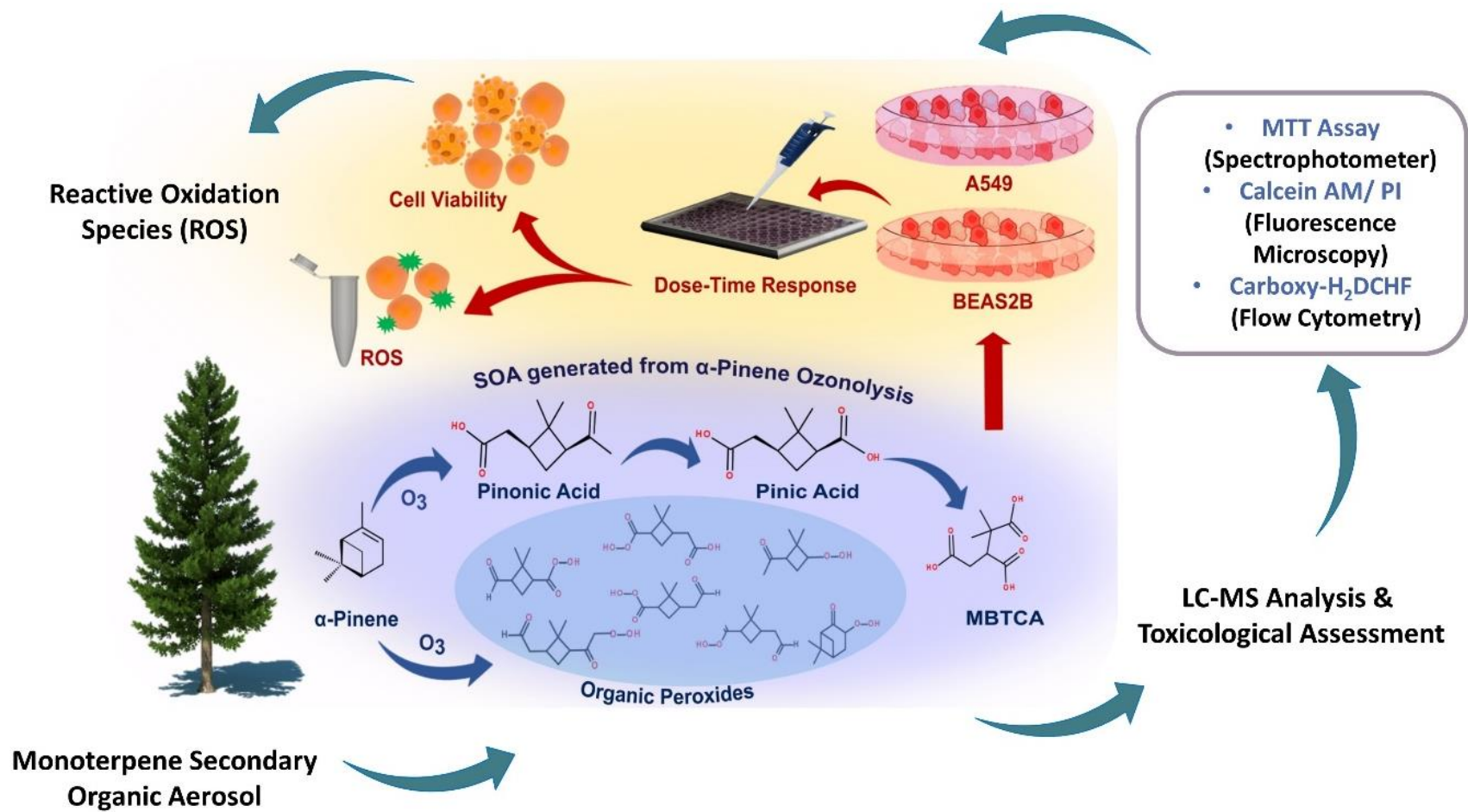


Figure 3.1.1. The key markers of α -pinene SOA and the mixture of α -pinene ozonolysis SOA were exposed to the lung cell lines. Changes in cellular proliferation rate and ROS buildup were two relevant endpoints studied.

3.1.1- Abstract α -pinene SOA Project

Secondary organic aerosol (SOA) is a major component of airborne fine particulate matter (PM_{2.5}) that contributes to adverse human health effects upon inhalation. Atmospheric ozonolysis of α -pinene, an abundantly emitted monoterpene from terrestrial vegetation, leads to significant global SOA formation; however, its impact on pulmonary pathophysiology remains uncertain. In this study, we quantified an increasing concentration-response of three well-established α -pinene SOA tracers (pinic, pinonic, and MBTCA) and a full mixture of α -pinene SOA in A549 (alveolar epithelial carcinoma) and BEAS-2B (bronchial epithelial normal) lung cell lines. The three aforementioned tracers contributed ~57% of the α -pinene SOA mass under our experimental conditions. Cellular proliferation, cell viability, and oxidative stress were assessed as toxicological endpoints. The three α -pinene SOA molecular tracers had insignificant responses in both cell types when compared with the α -pinene SOA (up to 200 $\mu\text{g mL}^{-1}$). BEAS-2B cells exposed to 200 $\mu\text{g mL}^{-1}$ of α -pinene SOA decreased cellular proliferation to ~ 70% and 44% at 24- and 48-hour post-exposure, respectively; no changes in A549 cells were observed. Inhibitory concentration-50 (IC₅₀) in BEAS-2B cells was found to be 912 and 230 $\mu\text{g mL}^{-1}$ at 24 and 48 hours, respectively. An approximate 4-fold increase in cellular oxidative stress was observed in BEAS-2B cells compared with untreated cells, suggesting that reactive oxygen species (ROS) buildup resulted in the downstream cytotoxicity following 24 hours of exposure to α -pinene SOA. Organic hydroperoxides that were identified in the α -pinene SOA samples likely contributed ROS and cytotoxicity. This study identifies the potential components of α -pinene SOA that likely modulate the oxidative stress response within lung cells.

3.1.2- Time-Dependent Increasing Concentration Response (ICR) using the MTT Assay

BEAS-2B and A549 cell lines were exposed to three α -pinene SOA molecular tracers (i.e., pinonic acid, pinic acid, and MBTCA), and α -pinene ozonolysis SOA. Exposure concentrations ranged from 0.01 to 200 $\mu\text{g mL}^{-1}$, with changes in cellular proliferation observed at 24- and 48-hour post-exposure time points (shown in blue and black bars, respectively, in Figures 3.1.2 and 3.1.4. Figure 3.1.2 shows the percent change in cellular proliferation normalized to the control in BEAS-2B cells following exposure to the α -pinene SOA molecular tracers, their equimolar mixture, and α -pinene ozonolysis SOA. Notably, the individual α -pinene SOA molecular tracers of pinonic acid (Figure 3.1.2a), pinic acid (Figure 3.1.2b), and MBTCA (Figure 3.1.2c), as well as their equimolar mixture (Figure 3.1.2d), did not induce any significantly quantifiable change in the cellular proliferation percentage up to the maximum exposure concentration of 200 $\mu\text{g mL}^{-1}$.

However, when BEAS-2B cells were exposed to 200 $\mu\text{g mL}^{-1}$ of the SOA mixture generated from α -pinene ozonolysis (as seen in Figure 3.1.2e), the proliferation decreased to 78% (compared to baseline control) after 24 hours of exposure and to 44% of untreated control cells after 48 hours of exposure. No significant difference was observed between the proliferation rates observed after 48 hours with 100 ($82\pm 12\%$) and 200 $\mu\text{g mL}^{-1}$ ($44\pm 12\%$) exposure concentrations. The calculated inhibitory concentration-50 (IC₅₀) values were 912 and 230 $\mu\text{g mL}^{-1}$ at 24 and 48 hours, respectively, in the BEAS-2B cells (Figure 3.1.3), suggesting the increased time of exposure decreased cellular viability.

The A549 cells responded differently than BEAS-2B cells when exposed to α -pinene SOA constituents under similar exposure concentration conditions. Unlike BEAS-2B cells, the A549 cells did not exhibit statistically significant differences in their proliferation relative to the untreated control following exposure to pinonic acid (Figure 3.1.4a), pinic acid (Figure 3.1.4b), their equimolar mixture (Figure 3.1.4d), and α -pinene ozonolysis SOA (Figure 3.1.4e). The only significant change in cellular proliferation percentage (relative to baseline control) was observed when MBTCA was exposed to A549 cells at 24 hours (Figure 3.1.4c).

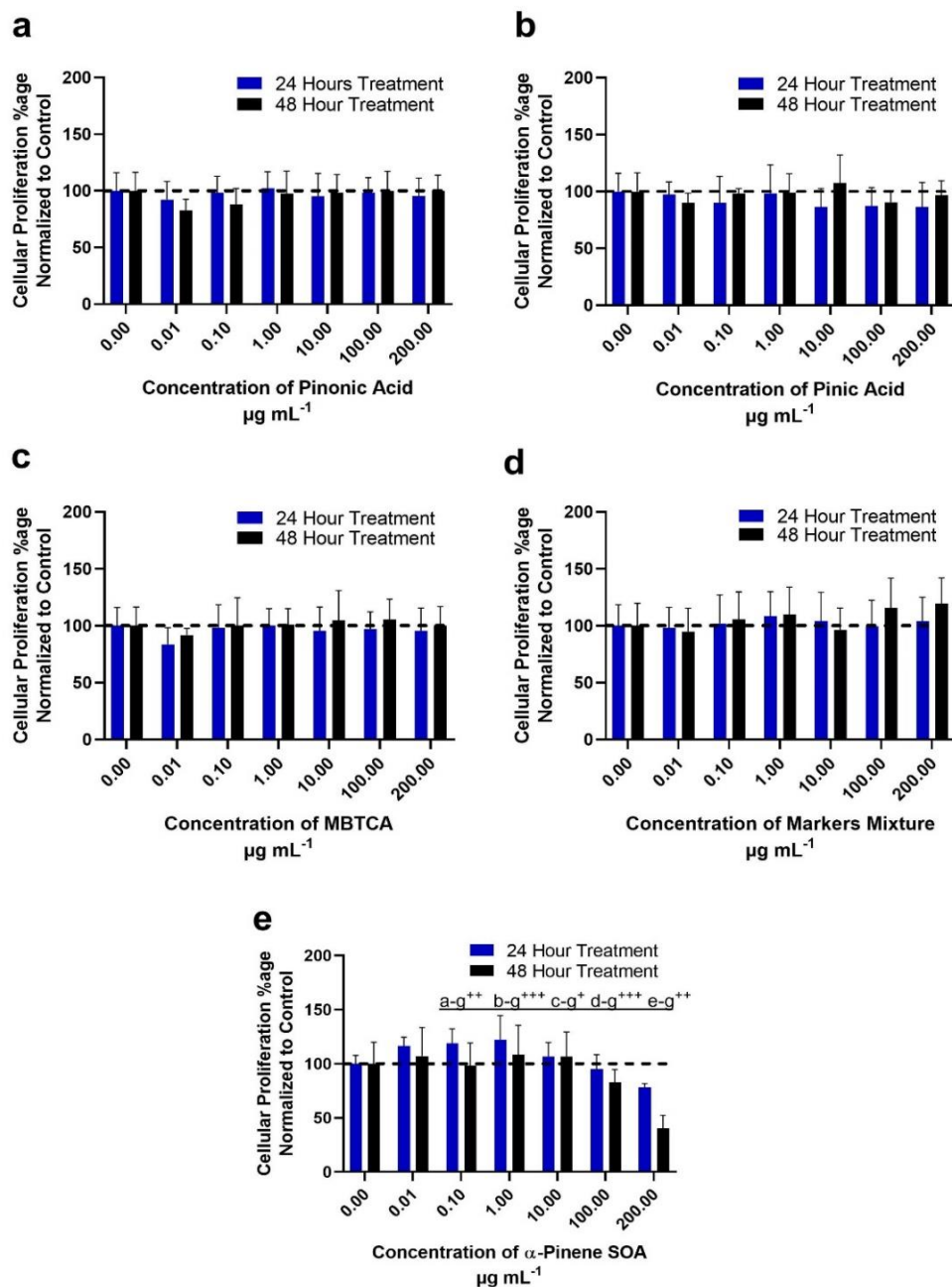


Figure 3.1.2. The percentage of cellular proliferation for BEAS-2B cells following treatment with pinonic acid/pinic acid/MBTCA and α -pinene SOA as determined through the MTT assay. The graphs show time-dependent concentration-response at 24 and 48 hours post-exposure, respectively of: (a) pinonic acid; (b) pinic acid; (c) MBTCA; (d) equimolar mixtures of pinonic and pinic acids with MBTCA; and (e) α -pinene ozonolysis SOA. The data is representative of three independent experiments normalized to untreated control cells for plotting these graphs. Figure 1e shows the effect of α -pinene ozonolysis SOA on cellular proliferation; a-g: 0-200 $\mu\text{g mL}^{-1}$, b-g: 0.01-200 $\mu\text{g mL}^{-1}$, c-g: 0.1-200 $\mu\text{g mL}^{-1}$, d-g: 1-200 $\mu\text{g mL}^{-1}$, e-g: 10-200 $\mu\text{g mL}^{-1}$ depicts significant difference in mean treatments. $P \leq 0.05$ where ⁺24 h significant, ⁺⁺ 48 h significant and ⁺⁺⁺ significant difference amongst treatments at 24 and 48 h.

	24 Hour Treatment	48 Hour Treatment
IC ₅₀	912.0	230.7
logIC ₅₀	2.960	2.363

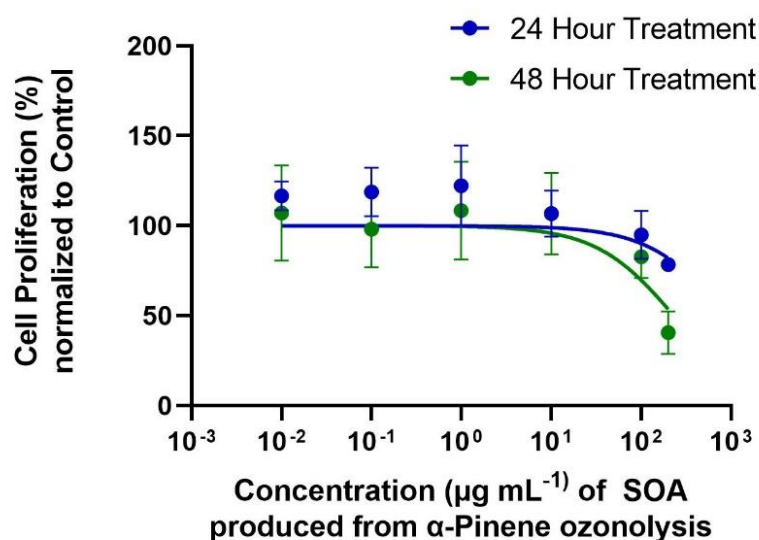


Figure 3.1.3. Inhibitory concentration-50 (IC₅₀) of SOA produced from a-pinene ozonolysis was found to be 912 and 230 µg mL⁻¹ for 48 and 24 h, respectively. logIC₅₀ was found to be 2.96 and 2.363 at the two different treatment time points in BEAS-2B cells.

The A549 cellular proliferation rate (metabolism) increased from 100% (untreated control) to 118% after exposure to 0.01 µg mL⁻¹ of MBTCA, then increased further to 124% after exposure to 0.1 µg mL⁻¹ and up to 140% after exposure to 1 µg mL⁻¹ of MBTCA; the proliferation decreased back to 103% at the 200 µg mL⁻¹ exposure concentration of MBTCA. Increased cellular proliferation at the 1 µg mL⁻¹ exposure concentration to 140% suggests that cells exhibited metabolic increase with MBTCA in a concentration-dependent manner. Following 48 hours of exposure to 0.01 µg mL⁻¹ of MBTCA, 139% cellular proliferation was observed, indicating a concentration-dependent exposure effect when compared with untreated control cells. **Figure 3.1.5.** shows the phase-contrast microscopy images of A549 cells treated with MBTCA, in increasing concentrations (0.01-200 µg mL⁻¹). The captured images at 24 and 48 hours did not exhibit much increase in cellular population compared with the untreated control cells. Hence, the rise in the MTT activity rate, which is a measure of mitochondrial activity, as depicted in **Figure 3.1.4c**, did not attribute to an increase in cell density following exposure to MBTCA, but rather indicates some mitochondrial metabolic changes within cells, following exposure at low concentrations only.

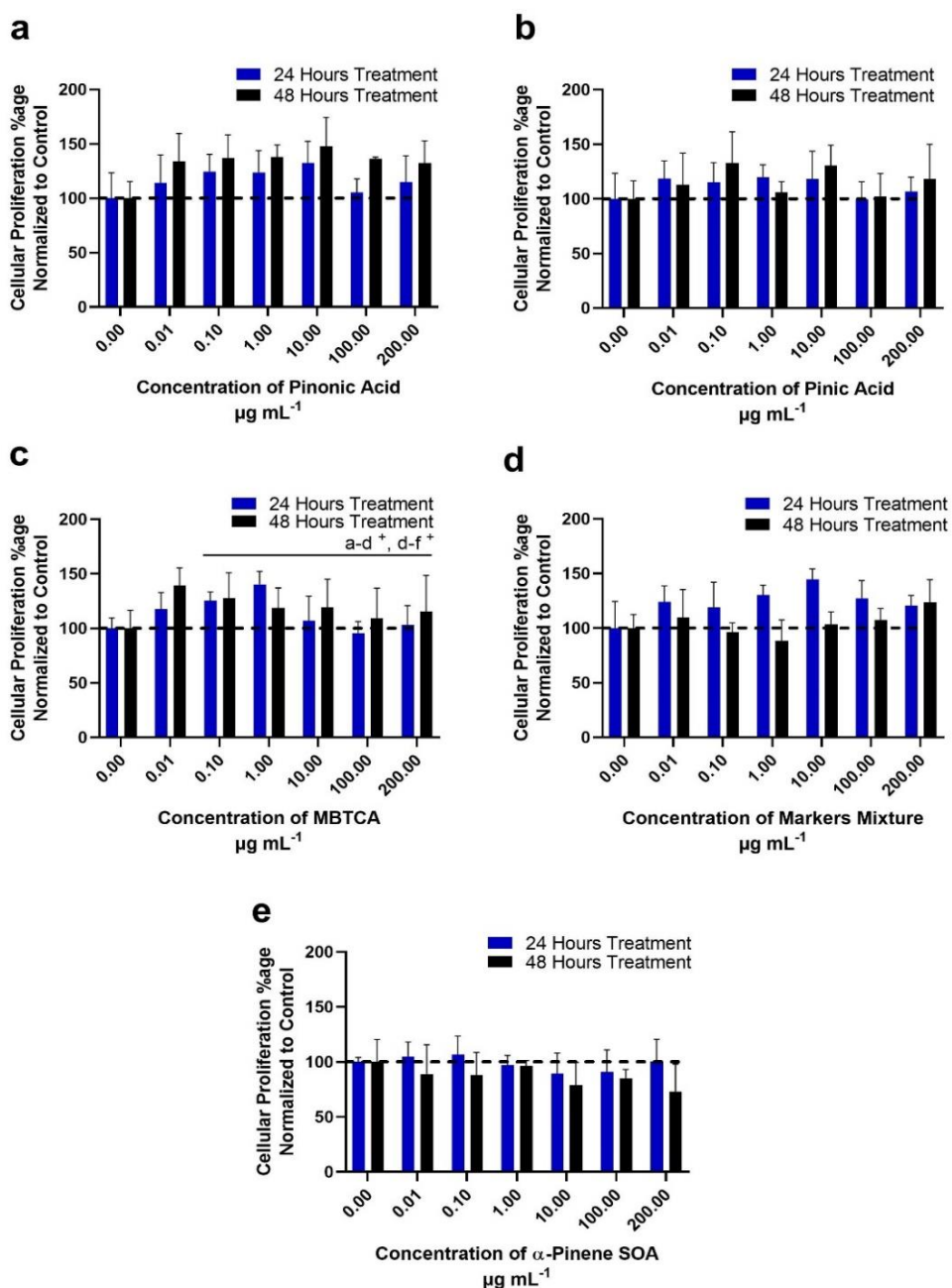


Figure 3.1.4. The percentage of cellular proliferation for A549 cells when treated with pinonic acid/pinic acid/MBTCA and α -pinene ozonolysis SOA as determined through the MTT assay. The graphs show time-dependent concentration responses at 24 and 48 hours post-exposure of: (a) pinonic acid; (b) pinic acid; (c) MBTCA; (d) equimolar mixtures of pinonic and pinic acids with MBTCA; and (e) α -pinene ozonolysis SOA. The data are representative of three independent experiments, which were normalized to untreated control cells for plotting these graphs. Note that A549 cell lines generally exhibited a higher cellular proliferation when compared to BEAS-2B cell lines for each molecular tracer, their mixture or its the SOA mixture from α -pinene ozonolysis. $P \leq 0.05$ where ⁺ 24 hour treatment significant, and a-d: 0-1 $\mu\text{g mL}^{-1}$ and d-f: 1-100 $\mu\text{g mL}^{-1}$ treatment group difference.

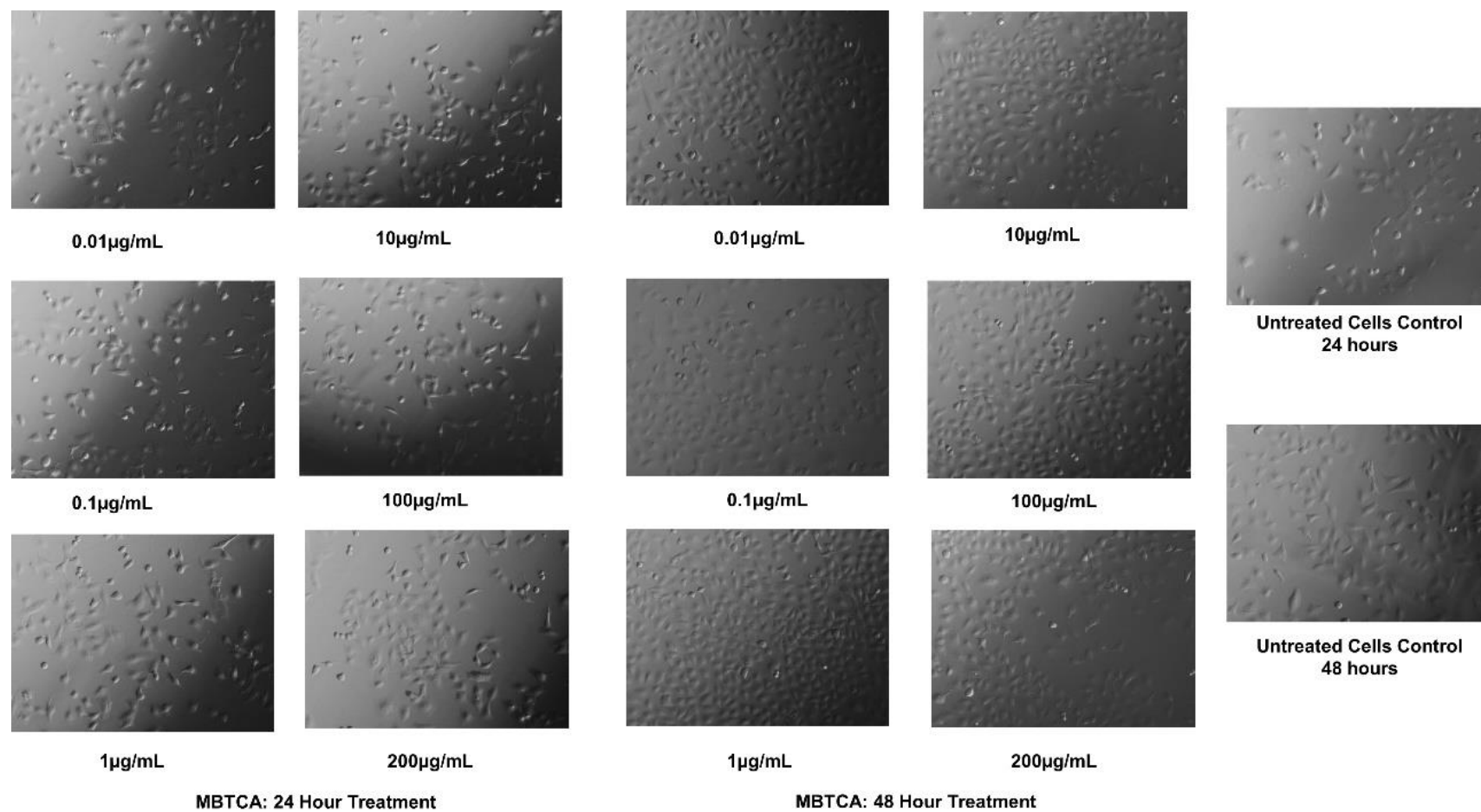


Figure 3.1.5. Inverted-phase microscopy (Nikon Eclipse T1-SAM, Japan) images of A549 cells treated with increasing concentrations of MBTCA at x100 magnification. The micrographs are scaled at 600 µm x 800 µm.

This study reports a time-dependent response of pinic acid/pinonic acid/MBTCA and their equimolar mixture and α -pinene ozonolysis SOA under increasing exposure concentrations. The MTT assay results revealed that pinic acid, pinonic acid, MBTCA, and their equimolar mixtures did not exhibit significant cellular toxicity and inhibition between the 0.01-200 $\mu\text{g mL}^{-1}$ dose range for up to 48 h of exposure in both A549 and BEAS-2B cells. A previous study by Gangwal et al.²⁴² used a multiple path particle dosimetry (MPPD) model to estimate the lung uptake of ultrafine particles (diameters $\leq 100\text{nm}$) ranges from 0.006 to 0.02 $\mu\text{g cm}^{-2}$ to a particle concentration of 100 mg m^{-3} at 24 hours exposure time.^{75, 242} To put these dose ranges in atmospheric context, we note that the lifetime uptake dosage of atmospheric ultrafine particles in the lungs is approximately 6.6 $\mu\text{g cm}^{-2}$.²⁴³ At an average daily inhaled volume of the air equal to *ca.* 25 cubic meters,²⁴⁴ the alveolar lung surface area of 100 m^2 , an aerosol particle deposition efficiency of 30% ($\sim 50\%$ for ultrafine particles),²⁴⁴ and an average mass concentration of ultrafine particles of 7.0 to 65.8 $\mu\text{g}\cdot\text{m}^{-3}$,²⁴⁵ the corresponding average daily lung exposure is approximately 7.5×10^{-4} $\mu\text{g cm}^{-2}$ in hot spot regions and 7.5×10^{-5} $\mu\text{g cm}^{-2}$ in ambient conditions as reported in Paur et al.²⁴³ The 24- and 72-hour clearance of inhaled ultrafine particles from the alveolar region is assumed to be negligible.^{244, 246}

The maximum exposure concentration used in the study is 200 $\mu\text{g mL}^{-1}$ which corresponds to 62.5 $\mu\text{g cm}^{-2}$ of total cell exposure. At 7.5×10^{-4} $\mu\text{g cm}^{-2} \text{ day}^{-1}$, this concentration is achieved in about 200 years of equivalent atmospheric exposure. The exposure dosage in the studied cell lines was higher than the environmentally relevant condition for acute exposure, helping us to assess the safety-index, i.e., the minimum concentration at which the α -pinene SOA and its markers can be exposed without significant contribution to ROS in human lung cells. Our results suggest that freshly aged α -pinene ozonolysis SOA might not induce considerable cytotoxicity upon acute exposure at environmentally relevant conditions; however, chronic exposure studies are essential to prelude long-term inhalation effects of the α -pinene ozonolysis SOA system. In addition to this, the α -pinene SOA constituents we report here can also contribute to the aged particles, which form as a result of chemical interaction between fresh α -pinene SOA and anthropogenic pollution. These may add to the increased ROS responses within lung cells during acute exposures. ^{94, 95}

3.1.3- Live/Dead Cell Staining Assay

To determine whether the changes in cellular proliferation are attributable to decreases in cell number (cell death) or conversely to proliferation inhibition (viability), the Calcein-AM/propidium iodide-based staining method was used, and cells were observed under the fluorescent microscope at x100 magnification. **Figure 3.1.6** shows the images of BEAS-2B cells treated with the well-established α -pinene SOA molecular tracers, their equimolar mixtures, and the α -pinene ozonolysis SOA.

Notably, the BEAS-2B cells did not undergo any morphological changes when treated with $200 \mu\text{g mL}^{-1}$ of pinonic acid, pinic acid, MBTCA, and their equimolar mixtures at the 24- and 48-h post-exposure conditions. This was confirmed through little, or no staining observed in the propidium iodide (PI) channel, which only stains the nucleus of cells with damaged cell membranes. However, there was increased PI staining when $200 \mu\text{g mL}^{-1}$ of the α -pinene ozonolysis SOA was added to the proliferating cells (**Figure 3.1.6b**). As exposure time increased from 24 to 48 h, more cells were stained with PI, and the BEAS-2B cells appeared more rounded and detached (as observed in the Calcein channel). The PI+ micro-graphs were analysed through image-J software to calculate that the PI+ cell population increased from 42 ± 10 cells at 24-h treatment to 151 ± 28 cells at 48-h treatment in the total captured area of $4.8 \times 10^4 \mu\text{m}^2$. The untreated control cells had 10 ± 2 and 12 ± 4 PI+ cells at 24 and 48 hours, respectively, within the same cellular density area (**Figure 3.1.6c**). This implies that the decrease in cellular proliferation observed in **Figure 3.1.2e** was due to increased cellular death. Hence, both the aerosol exposure concentration and time had a significant role in defining the cellular response in BEAS-2B cells.

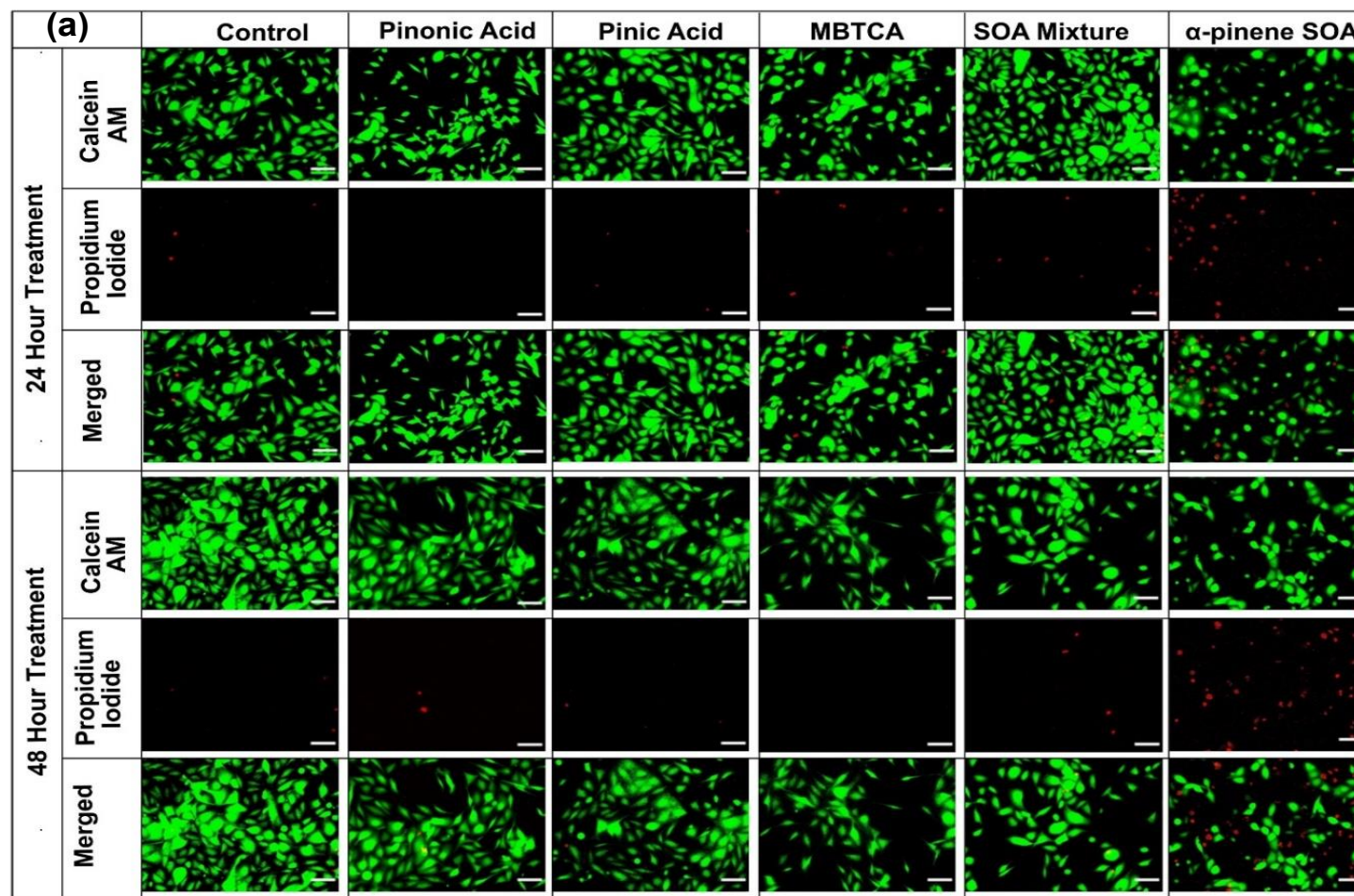


Figure 3.1.6. (a) Fluorescent microscopy images of BEAS-2B cells treated with well-established α -pinene SOA molecular tracers (i.e., pinonic acid, pinic acid, and MBTCA), their equimolar mixtures, and the α -pinene ozonolysis SOA at the $200 \mu\text{g mL}^{-1}$ exposure concentration at 24 h (upper panels) and 48 h (bottom panels). The cells were stained with Calcein AM (green) for live cells and propidium iodide (red) for dead cells. All the images were scaled to $50 \mu\text{m}$, and imaged at x100 magnification (to be continued..)

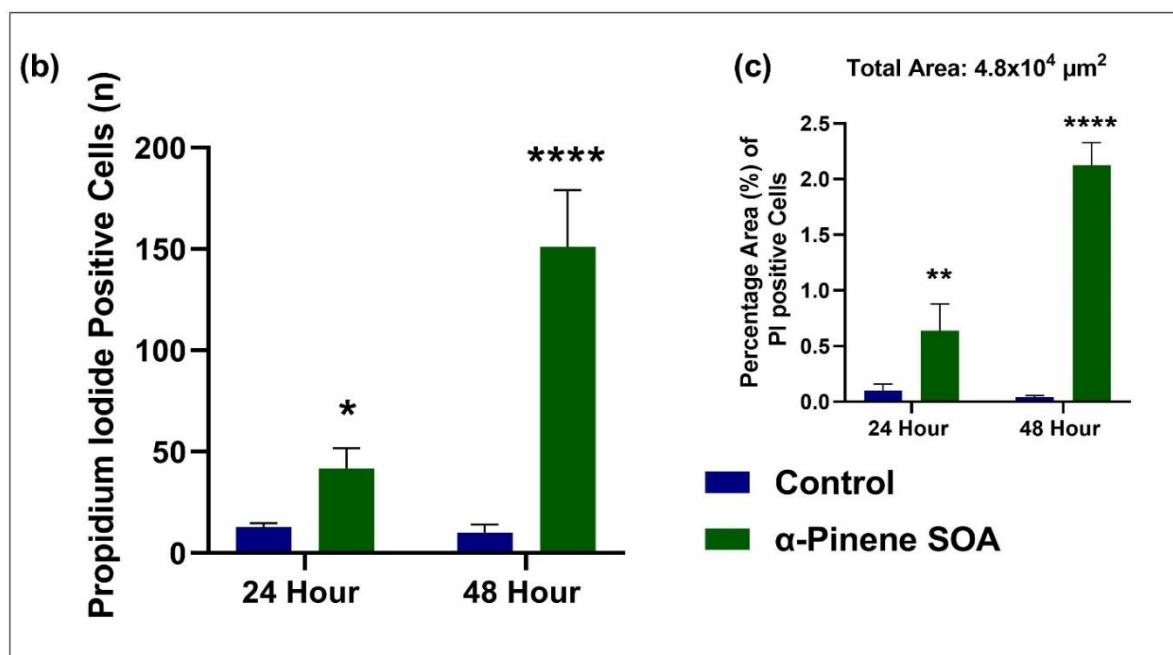


Figure 3.1.6. (continuation) (b) The graph shows an increase in the number of PI + cell population following treatment with α -pinene SOA when compared with untreated control at 24 and 48 h post exposure, as calculated through average of three micrographs, (c) The increase in the area percentage (%) of PI + cells in α -pinene SOA compared with untreated cell control. Note that for each experimental and control condition, a fixed area of $600 \times 800 \mu\text{m}^2$ was captured for each micrograph shown here. The average of PI+ cells was determined in $4.8 \times 10^4 \mu\text{m}^2$ area, normalized to the same area of the untreated control channel. Two way ANOVA with Šídák's multiple comparisons test was performed on the data set to determine the statistical significance of the change in signal when compared with untreated controls. The p -value < 0.05 was considered statistically significant for our analysis where **** indicates a p -value ≤ 0.0001

On the other hand, application of the Calcein-AM/PI staining method to A549 cells treated with the well-established α -pinene SOA tracers (i.e., pinonic acid, pinic acid, and MBTCA), their equimolar mixtures, and α -pinene ozonolysis SOA, had no significant changes observed in cellular viability. As shown in Figure 3.1.7, there was negligible PI staining at the 24 and 48 hours post-exposure times. The cells appeared confluent in the Calcein-AM channel, and the number of A549 cells in the treatment groups appeared the same as the untreated controls. This observation is consistent with our MTT assay data in Figure 3.1.4, suggesting no apparent change in A549 cell numbers after aerosol exposure. The phase-contrast microscopy images of α -pinene ozonolysis SOA treated A549 cells (Figure 3.1.8) confirmed the intact morphology, while cells treated with 0.1% Triton-X 100 had damaged cellular membrane.

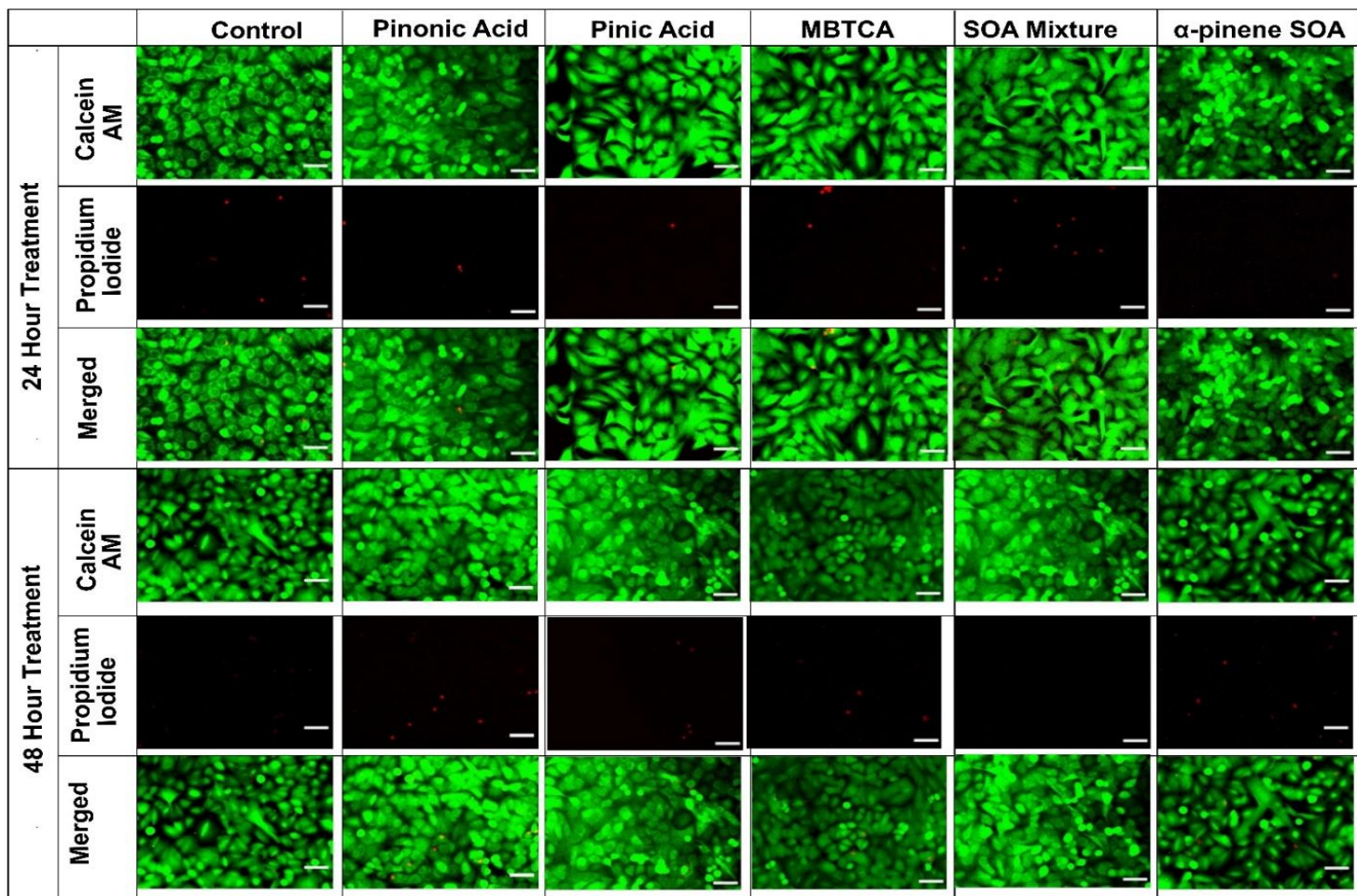


Figure 3.1.7. Fluorescent microscopy images of A549 cells treated with pinonic acid/pinic acid/MBTCA and α -pinene SOA at exposure to $200 \mu\text{g mL}^{-1}$ concentrations for 24 and 48 h. The cells were stained with Calcein-AM (green) for live cells and propidium iodide (red) for dead cells. Note that there is little to no cell death observed after treatment in A549 cells, and cellular density is not adversely affected even after 48 h of treatment. This implies in cancer lines, and the α -pinene SOA causes limited morphological changes. All the images are scaled to $50 \mu\text{m}$ size and imaged at x100 magnification

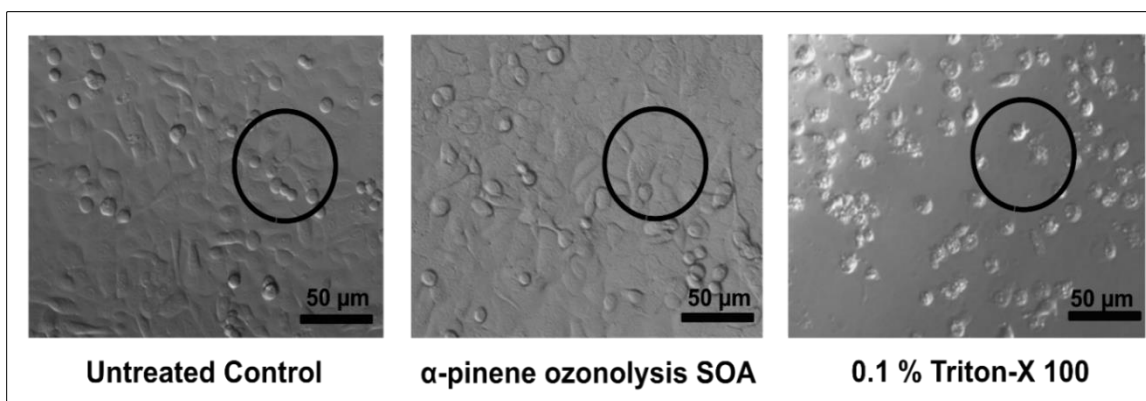


Figure 3.1.8. The phase-contrast microscopy micrograph of A549 cells at 24 h. The micrographs depict untreated control cells have similar morphology to α -pinene ozonolysis generated SOA treated A549. The positive control for cytotoxicity (Triton-X 100 treated cells) shows visible signs of cellular degradation.

Our study demonstrates that α -pinene ozonolysis SOA induced a clear cytotoxic response at the $200\text{-}\mu\text{g mL}^{-1}$ exposure concentration. Specifically, cellular viability in BEAS-2B cells decreased to 78% and 44% at 24 h and 48 h, respectively, of exposure time. A study by Moller et al.[13](#) reports that ultrafine particles of diameters ≤ 100 nm accumulate in the lung periphery, exhibiting 96% retention after 24 h of exposure and less clearance through the liver after 48 h of exposure. This suggests, even with lower exposure concentrations, lifetime exposures might lead to similar cellular fates as exhibited by the $200\text{-}\mu\text{g mL}^{-1}$ exposure concentration. The increased PI staining from α -pinene SOA shown in [Figure 3.1.6](#) demonstrated that the decrease in proliferation (%) was due to cellular death and not cellular growth/metabolic inhibition.

While BEAS-2B cells exhibited cellular toxicity following exposure to α -pinene ozonolysis SOA, A549 cells did not. These results are consistent with previous acellular (or chemical-based assay) oxidative stress studies, where low dithiothreitol (DTT) activity in α -pinene SOA was measured when compared with other biogenic and anthropogenic SOA systems.[113](#) No significant change in toxicity was observed with increasing mass of exposure of α -pinene ozonolysis SOA in A549 cells, implying *in vitro* cytotoxicity observed at higher concentration depends on the metabolic activity type of the cell lines.[247](#) Increasing the exposure time from 24 to 48 hours also did not induce significant changes in the toxicity profile in A549 cells. A notable part of this study was the MBTCA exposures in A549 cells. Cellular metabolic activity increased to 140% after exposure to $1\ \mu\text{g mL}^{-1}$ of MBTCA and

decreases with increasing exposure concentration and time. This suggests dosage-dependent metabolic stress induced by MBTCA in A549 cells,[247](#) as shown in [Figure 3.1.4c](#).

The differential response between cell lines could have been attributed to the inherent nature of A549 cancer cells that do not follow normal growth patterns of BEAS-2B (untreated) cells. Another reason could be that two cell types respond differently to pro-inflammatory tumor growth factor (TGF- β) stimuli.[248](#) MBTCA may also cause a slight increase in A549 cellular proliferation as the actively dividing cells to support energy-dependent respiration processes that use tricarboxylic acids (TCA) as intermediate substrates. The evidence suggests that MBTCA could act as a surrogate for TCA.[249](#) Furthermore, all cancer cells exhibit a hallmark of cancer known as the “Warburg effect” that is characteristically associated with higher glucose consumption and a higher rate of respiration.[250](#) Thus, MBTCA provided the intermediate reactants to support a higher rate of respiration and increasing cellular proliferation rate. Since MTT is a pH-sensitive compound, its darker color change is dependent on carbon dioxide production during the enhanced respiration rate of A549 cells.[251](#)

The alveolar and bronchial cells were insensitive to the molecular tracers of α -pinene SOA formation. Previous exposure studies with environmental pollutants (formaldehyde) in both BEAS-2B and A549 cells revealed that the acute exposure, without prior sensitization, did not induce significant changes.[252](#) But after sensitization with TNF- α , both cell lines responded differently to the environmental toxins (formaldehyde).[252](#) Another study revealed BEAS-2B cells tend to be more sensitive to PM₁₀ and PM_{2.5} exposure at the exact dosage than A549 cells.[253](#) The difference in cell cycle and metabolic response could be attributed to the over-expression of lung resistance-related protein (LRP) in A549 cells. At cytotoxic concentrations of drug/metabolite exposures, LRP levels remain unchanged.[254](#) However, increased LRP stimulation is observed at lower dosage concentrations and increasing exposure time.[254](#) A549 cells also have more antioxidant properties (Nrf2 expression), enhanced metabolic stress, and increased cellular proliferation following endogenous chemical exposure.[255](#)

The increase in cellular proliferation at lower concentrations could be attributed to A549 cells’ resistance to NRF-2 gene regulation. Homma et al.[255](#) reported that A549 cells are more resistant to drug exposure due to a mutation in the KEAP-1-NRF-2 (Antioxidant response gene) system. This mutation makes the A549 cells more resistant to external com-

pound exposure and NRF-2 activation increases the cellular proliferation rate. The dysregulation of the NRF-2 response system in A549 cell lines renders it more resistant to SOA exposure than BEAS-2B cell lines. As previous work by Lin et al.[70](#) suggests activation of NRF-2 related genes after exposure to isoprene-derived SOA in BEAS-2B cells, we speculated a similar antioxidant response in cells following α -pinene SOA exposure. The effect is not evident in A549 cells due to dysregulation of NRF-2 response in these cell types.

Furthermore, peroxiredoxin (Prx), an antioxidant protein that is known to over-express in A549 cells, is likely attributed to the differences in the cellular responses when compared to BEAS-2B cells.[256](#) All these factors could contribute to the differences in metabolic activity observed in A549 cells compared with BEAS-2B cells. LRP expression at the lower exposure concentration of MBTCA and increasing exposure time could be attributed towards higher metabolic activity at 1 and 0.01 $\mu\text{g mL}^{-1}$ exposure dosages at 24 and 48 hours, respectively. Another study revealed that the exposure to inhalable plasticizers led to the enlarged morphology of A549, increased proliferation, cell progression, and the loss of epithelial structure in a dosage-dependent manner.[257](#) This dosage-dependent exposure effect is lost with increased dosage, and cells regain their morphology and metabolic rate at the higher dosage. A549 cells become adaptive and refractory at higher concentrations used, hence limited changes in viability were observed at the 100-200 $\mu\text{g mL}^{-1}$ concentration range of MBTCA. This concentration-resistance of A549 cells is a characteristic behaviour, as shown in previous studies where cells become unresponsive to drugs after some time.[258](#) Our results suggest that MBTCA might induce metabolic changes in A549 cell lines at lower dosages, and time points shorter than 24 hours are worth investigating in future studies.

3.1.4- Oxidative Stress Measurements using Flow Cytometry

The cell lines were further assessed for changes in general oxidative stress using flow cytometric analysis and stained with carboxy- H_2DCFDA (i.e., ROS indicator) and propidium iodide (i.e., viability indicator). The percentage of live cell populations was observed to determine an overall change in oxidative stress within the cells that could be attributed to cell death. Since we observed cellular death in α -pinene ozonolysis SOA treated BEAS-2B cells after 24 h treatment ([Figure 3.1.6](#)), the 6 h time point was selected to determine whether the ROS build-up attributed to the cellular death, as previous studies demonstrated

the peak time ROS build-up to be around 4-8 h.²⁵⁹ The gating strategy, applied through the exclusion of cellular aggregates through FSA/FSH dot plot and further removal of PI+ cells from the final analysis, allowed us to include only single live cells in the analysis.

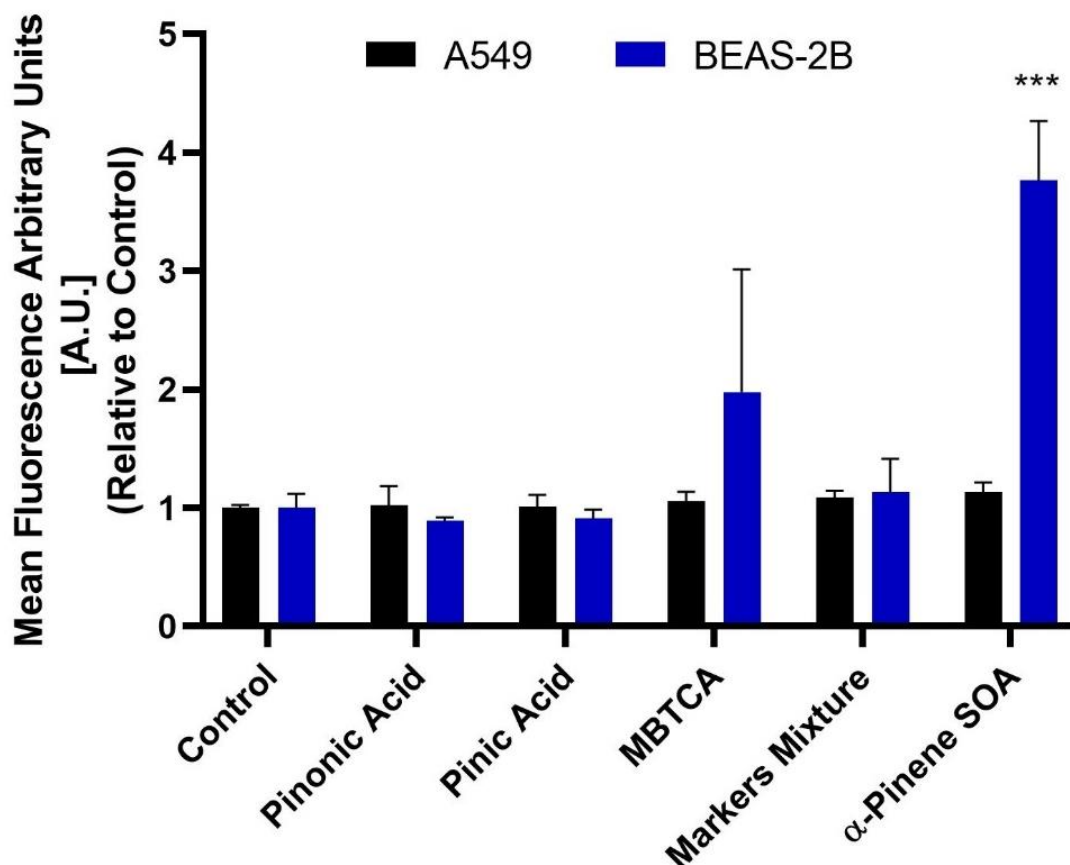


Figure 3.1.9. The fold change in general oxidative stress as a measure of carboxy- H_2DCFDA reduction signal relative to control. Measurements were made in A549 and BEAS-2B cell lines 6 hours post-exposure with α -pinene SOA molecular tracers, their equimolar mixture, and the α -pinene ozonolysis SOA through the flow cytometer. The change in signal, as determined through three independent experiments, were normalized to controls and a one-way ANOVA followed by Dunnett's post hoc test was performed on the data set to determine the statistical significance of the change in signal when compared with untreated controls. The p -value <0.05 was considered statistically significant for our analysis where *** indicates a p -value ≤ 0.001 .

As shown in **Figure 3.1.9**, A549 and BEAS-2B cells were treated with the highest aerosol exposure concentration of $200 \mu g mL^{-1}$, resulting in the graph shown as a change in the mean fluorescence signal relative to the untreated controls. The full SOA mixture

generated from α -pinene ozonolysis induced a 4-fold increase in the ROS-associated signal for the BEAS-2B cells exposed, suggesting an imbalance of oxidative stress response in cells within a few hours after exposure. The statistical analysis revealed MBTCA-treated cells were not significant when compared with untreated baseline controls. The remaining single-component exposures of the α -pinene SOA molecular tracers and their equimolar mixtures did not contribute towards any significant ROS changes in both the A549 and BEAS-2B cells. This indicates the presence of specific SOA components, found in the α -pinene ozonolysis SOA, might be an important contributor towards cellular death. As a result, we carefully examined the RPLC/ESI-HR-QTOFMS negative and positive ion mode mass spectrometric data acquired for the α -pinene ozonolysis SOA sample. An emphasis was given to SOA constituents other than pinic acid, pinonic acid, and MBTCA.

Additionally, we investigated the oxidative stress response of BEAS-2B and A549 cells following exposure to pinonic acid/pinic acid/MBTA, their equimolar mixtures, and α -pinene ozonolysis SOA. We did not observe any changes in ROS build-up within BEAS-2B or A549 cells when pinic acid, pinonic acid, and/or MBTCA were exposed to these cells. An 4-fold increase in carboxy-H₂DCFDA signal was observed in BEAS-2B cells treated with α -pinene ozonolysis SOA compared to the untreated control cells. This suggested that the cellular toxicity observed at 24 and 48 hours after the treatment was due to increased build-up of ROS in 6-hours -post-exposure. Other studies reveal that photochemical aging of SOA samples and loss of functionality of the SOA precursor might be attributed to ROS activity within the cells.[96-260](#) Previous studies reported increased pro-inflammatory gene expression i.e. interleukins 6 and 8 (IL-6, IL-8) and tumor necrosis factor- α (TNF α) when treated with α -pinene derived SOA.[96-98](#) Similarly, both heme oxygenase-1 (HMOX-1) and interleukin-8 (IL-8) genes involved in anti-oxidative stress and anti-inflammatory responses through NRF-2/KEAP-1 pathway, were slightly altered in the previous study by Ito et al.[69](#), when BEAS-2B and U937 macrophages were treated with freshly aged α -pinene ozonolysis SOA ([Table 3.1.1](#)).

Table 3.1.1. Comparison of previous toxicological studies associated with α -pinene SOA with the current study. Note that the fresh α -pinene SOA is generated through ozonolysis alone, while aged SOA is α -pinene SOA heterogeneously reacted with OH radicals

α -Pinene SOA system studied	Model used	Response Type Studied	Toxicological End Point	Conclusions	Consistent with current Study	Ref
Pinonic Acid Pinic Acid MBTCA Fresh α -pinene	A549 BEAS-2B	Cytotoxicity Oxidative Stress 24 & 48 hours 200 $\mu\text{g mL}^{-1}$	MTT Assay Calcein-AM/PI Staining H ₂ DCFDA	α -pinene SOA at $\mu\text{g mL}^{-1}$ induced high time-dependent cell death due to increased ROS	N/A	This Study
Fresh α -pinene	BEAS-2B	Lung Inflammatory response	IL-8 and Cytotoxicity	No significant change in IL-8 No toxicity	No	97
α -pinene+ NO _x + SO _x	Macrophages	Lung Macrophage response	Cytotoxicity IL-6, IL-8, and TNF- α Phagocytic Activity Wound Heal Assay	Decreased phagocytic activity	N/A	96
NO _x + NH ₃ α -pinene. SO _x + NO _x + NH ₃ α -pinene	Apo E ^{-/-} mice	Short term Cardiopulmonary response 7 days 250–300 mg m^{-3}	Gene expression of TBARS, HO-1, ET-1 & MMP-9	SO ₂ : Increased expression HO-1, MMP-9, and ET-1 No SO ₂ : Decreased expression	N/A	98
NO _x + α -pinene. SO _x + NO _x + α -pinene	Sprague-Dawley rats ApoE ^{-/-} mice	Short term Cardiopulmonary response 200 $\mu\text{g m}^{-3}$ 7 days	gene expression of TBARS, HO-1, ET-1 & MMP-9	Revealed limited biological response	N/A	76
NO _x + α -pinene Fresh and Aged α -pinene	DTT acellular	Oxidative potential response	Oxidative stress	Negligible or no response	Yes	113

NO _x + aged α -pinene Aged and Fresh α -pinene	Murine alveolar macrophages 0.1-10 μ g	Pro-inflammatory response and oxidative stress response	ROS/RNS production and levels of tumor necrosis factor- α (TNF- α) and interleukin-6 (IL-6)	Similar inflammatory response to all three conditions Negligible or no response	Yes	99
NO _x + α -pinene Fresh and Aged α -pinene	DTT acellular	Oxidative potential response	Oxidative stress	Negligible or no response	Yes	113
NO _x + aged α -pinene Aged and Fresh α -pinene	Murine alveolar macrophages 0.1-10 μ g	Pro-inflammatory response and oxidative stress response	ROS/RNS production and levels of tumor necrosis factor- α (TNF- α) and interleukin-6 (IL-6)	Similar inflammatory response to all three conditions Negligible or no response	Yes	99
Fresh & aged α -Pinene SOA	A549 cells ALI exposure system 0-14 μ g	Cellular Viability	LDH Assay	More decreased viability in aged than fresh sample	Yes	94

TBARS: thiobarbituric acid reactive substance, (HO)-1: heme-oxygenase, (ET)-1: endothelin, (MMP)-9: matrix metalloproteinase, (TNF- α): tumor necrosis factor- α , (I-6): interleukin-6, (IL-8): interleukin-8 and antioxidant response element (ARE)

On the other hand, an increase in ROS signals was not observed in A549 cells with similar treatments and concentrations, indicating that the oxidative stress response changes with cell lines. Our current study complements the data reported by Chowdhury et al.,⁹⁴ where increases in ROS were not observed in the A549 cells following exposure for both aged and fresh SOA generated from α -pinene ozonolysis. However, our study highlights the use of non-cancerous cell line models, such as normal BEAS-2B cells, to study the exposure effects, as A549 cells exhibited different cellular metabolism and dosage response than normal lung cells. Thus, careful selection of appropriate cell line models is important for toxicological assessments of SOA because the use of A549 cells by themselves may not provide sufficient information.⁹⁴⁻⁹⁵

3.1.5- RPLC/ESI-HR-QTOFMS Analysis of PAM-generated α -Pinene SOA

α -Pinene ozonolysis SOA showed increased ROS and cytotoxicity relative to pinic acid, pinonic acid, and MBTCA, respectively. As shown in **Figure 3.1.11**, these latter three α -pinene SOA molecular tracers account for $\sim 57\%$ by mass of the total SOA mass collected. Docherty et al.¹⁰⁵ and Surratt et al.¹²⁰ reported that organic peroxides of unknown molecular composition generated from α -pinene ozonolysis account for ~ 47 and 49% , respectively, of the total SOA mass. Here, we hypothesize that organic peroxides present in high yields²⁶¹⁻²⁶³ within α -pinene ozonolysis SOA are responsible for increased ROS and cytotoxicity content based on qualitatively similar trends observed for isoprene-derived hydroperoxides.¹³⁴ Organic peroxides (i.e., hydroxy hydroperoxides) present in our α -pinene ozonolysis SOA were identified using RPLC/ESI-HR-QTOFMS operated in the positive ion mode. As shown in **Table 3.1.2** and **Figure 3.1.12** seven multifunctional organic hydroperoxides are present in the SOA mass generated from α -pinene ozonolysis. These seven organic hydroperoxides potentially contributed towards increased cytotoxicity not observed with pinonic acid, pinic acid, and MBTCA.

To further support the chemical characterization of α -pinene-derived hydroperoxide structures shown in **Table 3.1.2** and **Figure 3.10**, we analysed a 1,2-ISOPROOH (2-hydroperoxy-2-methylbut-3-en-1-ol) authentic standard (which has a molecular weight of 118 g

mol⁻¹) by the RPLC/ESI-HR-QTOFMS method operated in the positive ion mode as a surrogate for the proposed α -pinene-derived organic hydroperoxides. By analyzing this model hydroperoxide standard with RPLC/ESI-HR-QTOFMS, we were able to determine how the hydroperoxides ionize and their typical neutral losses produced during MS/MS experiments. As shown in [Figure 3.1.10](#), we found that 1,2-ISOPPOOH was not only retained and detected as the $[M + \text{NH}_4^+]^+$ ion at a mass-to-charge ratio (m/z) 136 by the RPLC/ESI-HR-QTOFMS positive ion mode method, but it also produced neutral losses of 35 (i.e., loss of $\text{H}_2\text{O} + \text{NH}_3$) and 51 (i.e., loss of $\text{H}_2\text{O}_2 + \text{NH}_3$) during MS/MS experiments, which are consistent with neutral losses we observed for the proposed structures shown in [Table 3.1.2](#) and with a prior study by Zhou et al.[264](#) that applied atmospheric pressure chemical ionization-tandem mass spectrometry (APCI-MS/MS) operated in the positive mode.

All these observations bring to the conclusion that unknown compounds other than pinonic acid, pinic acid, and MBTCA that are present in α -pinene ozonolysis SOA induce cellular toxicity. Based on previous studies, including work from our group on complementary systems,[128](#) [262](#) the most likely candidate compounds are multifunctional organic peroxides that are generated from α -pinene ozonolysis. Several prior studies have revealed a significant organic peroxide contribution to SOA masses generated from α -pinene ozonolysis,[105](#) [120](#) including multifunctional organic peroxides.[92](#) As a result, we carefully examined our RPLC/ESI-HR-QTOF-MS data and found seven organic hydroperoxides (see [Table 3.1.2](#)) were detected at the molecular level in the full SOA mixture generated from α -pinene ozonolysis.

As shown in [Table 3.1.2](#), organic hydroperoxides were measured from this same SOA using RPLC/ESI-HR-QTOFMS operated in the positive ion mode ([Figure 3.1.12](#)), which explains some portion of the “other organics” not quantified at the molecular level by RPLC/ESI-HR-QTOFMS. Since we were lacking authentic standards for these organic hydroperoxides, currently we were not able to estimate their individual contributions to SOA loads.

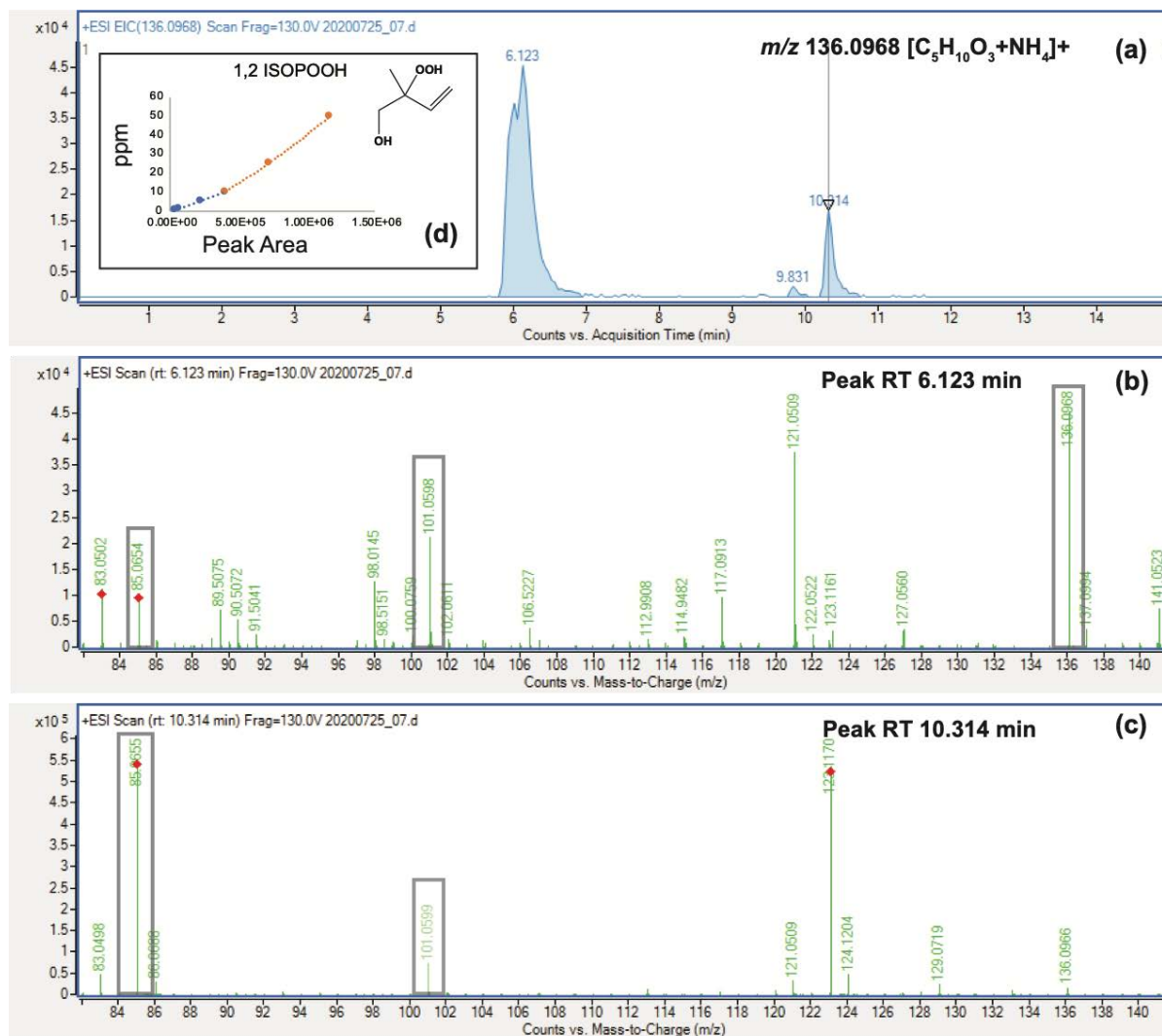
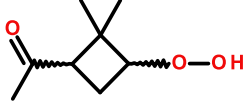
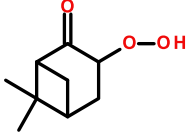
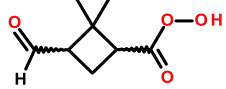
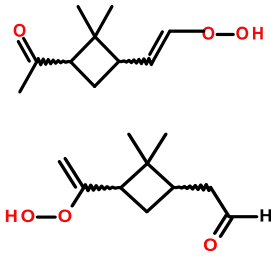
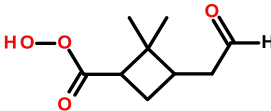
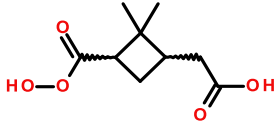
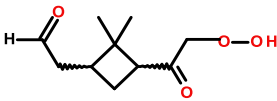


Figure 3.1.10. RPLC/ESI-HR-QTOFMS positive ion mode analysis of the 1,2-ISOPOOH standard demonstrates how organic hydroperoxides are detected and fragment during our ESI-HR-QTOFMS analyses: (a) the extracted ion chromatogram (EIC) of $[M+NH_4]^+$ ion at a mass-to-charge (m/z) 136 for 1,2-ISOPOOH; (b) the ESI mass spectrum taken for a chromatographic peak with the retention time (RT) of 6.123 min; (c) the electrospray (ESI) mass spectrum recorded for the chromatographic peak with the RT of 10.314 min; (d) the six-point calibration curve for 1,2-ISOPOOH in the concentration range between 0.5 and 50 ppm. Consistent with our previous study, the $[M+H]^+$ molecular ion was not seen in the full MS scan given the -OOH group being an unfavourable protonation site within ESI. Instead, the dehydrated molecular ion $[M + H - H_2O]^+$ (m/z 101) was observed. The presence of the $[M+NH_4]^+$ ion resulted from background NH_4^+ contamination in our system. Therefore, the neutral loss of 35 u (i.e., $NH_3 + H_2O$ loss from the $[M+NH_4]^+$ ion) may also contribute to the observed fragment ion at m/z 101. The fragment ion observed at m/z 85 can be explained by the neutral loss of 51 u (i.e., $NH_3 + H_2O_2$ loss of the $[M+NH_4]^+$ ion)

Table 3.1.2. Organic hydroperoxides identified in the SOA mass obtained from the ozonolysis of α -pinene in laboratory mimicking experiments using the PAM reactor.

[M + H] ⁺ ion		Retention Time (min)	Postulated structure(s)	Characteristic (+) ESI-MS/MS transitions	Ref
Formula	Theoretical/Acquired Mass				
C ₈ H ₁₅ O ₃	159.1021/159.1014	7.88		m/z 159 \rightarrow m/z 141 ($\Delta m = 28$: H ₂ O) m/z 159 \rightarrow m/z 125 ($\Delta m = 34$: H ₂ O ₂)	262
C ₉ H ₁₅ O ₃	171.1021/171.1011	8.90		m/z 171 \rightarrow m/z 153 ($\Delta m = 18$: H ₂ O) m/z 171 \rightarrow m/z 139 ($\Delta m = 32$: O ₂) m/z 171 \rightarrow m/z 111 ($\Delta m = 16$: O ₂ + CO)	105
C ₈ H ₁₃ O ₄	173.0814/173.0806	7.47		m/z 173 \rightarrow m/z 127 ($\Delta m = 46$: H ₂ O + CO) m/z 173 \rightarrow m/z 111 ($\Delta m = 62$: H ₂ O ₂ + CO) m/z 173 \rightarrow m/z 155 ($\Delta m = 28$: H ₂ O)	261 , 262
C ₁₀ H ₁₇ O ₃	185.1178/185.1170	9.53		m/z 185 \rightarrow m/z 139 ($\Delta m = 46$: H ₂ O + CO) m/z 185 \rightarrow m/z 151 ($\Delta m = 34$: H ₂ O ₂) m/z 185 \rightarrow m/z 167 ($\Delta m = 18$: H ₂ O)	262 , 263
C ₉ H ₁₅ O ₄	187.0970/187.0959	8.54		m/z 187 \rightarrow m/z 171 ($\Delta m = 16$: O) m/z 187 \rightarrow m/z 171 ($\Delta m = 18$: H ₂ O) m/z 187 \rightarrow m/z 153 ($\Delta m = 34$: H ₂ O ₂)	105

$C_8H_{13}O_5$	189.0763/189.0756	8.59		m/z 189 \rightarrow m/z 155 ($\Delta m = 34$: H_2O_2) m/z 189 \rightarrow m/z 127 ($\Delta m = 62$: $H_2O_2 + CO$) m/z 189 \rightarrow m/z 171 ($\Delta m = 18$: H_2O)	105 , 261
$C_{10}H_{17}O_4$	201.1127/201.1119	9.54		m/z 201 \rightarrow m/z 167 ($\Delta m = 34$: H_2O_2) m/z 201 \rightarrow m/z 139 ($\Delta m = 62$: $H_2O_2 + CO$) m/z 201 \rightarrow m/z 185 ($\Delta m = 16$: O)	261 , 262

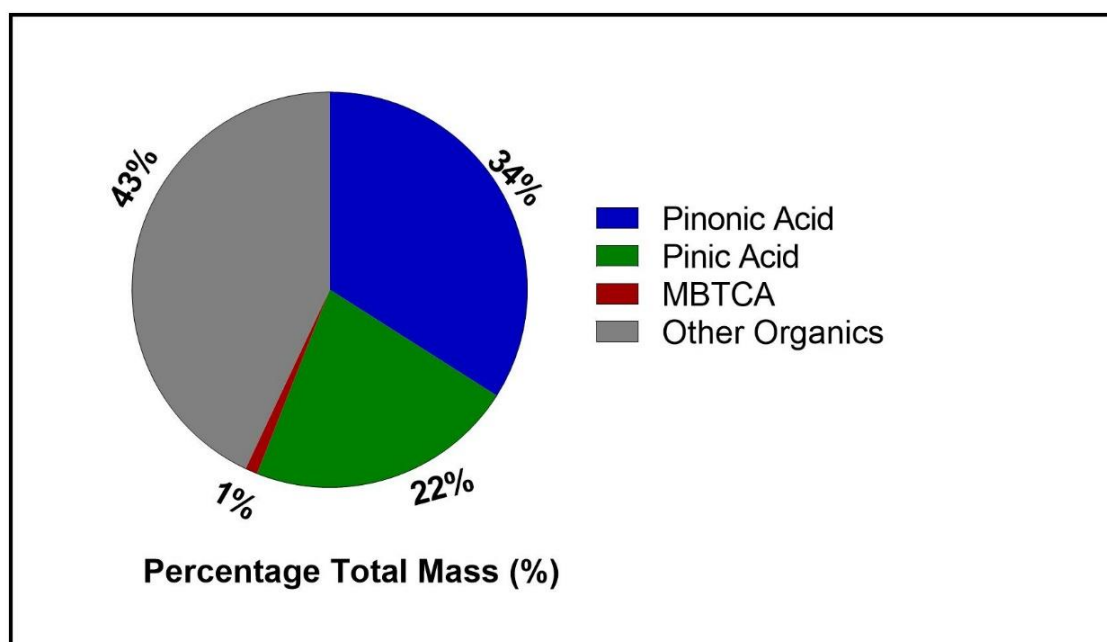
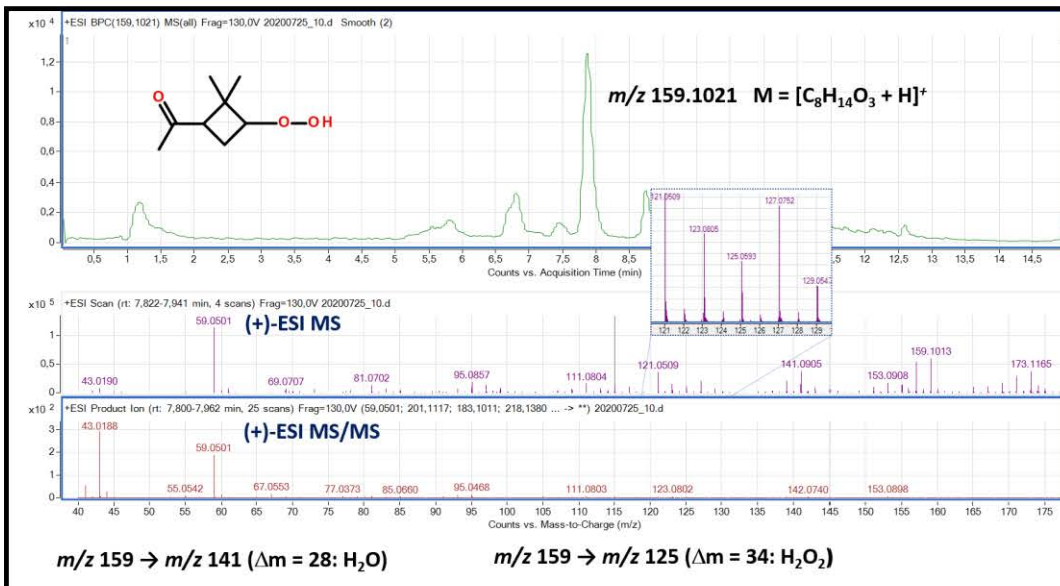


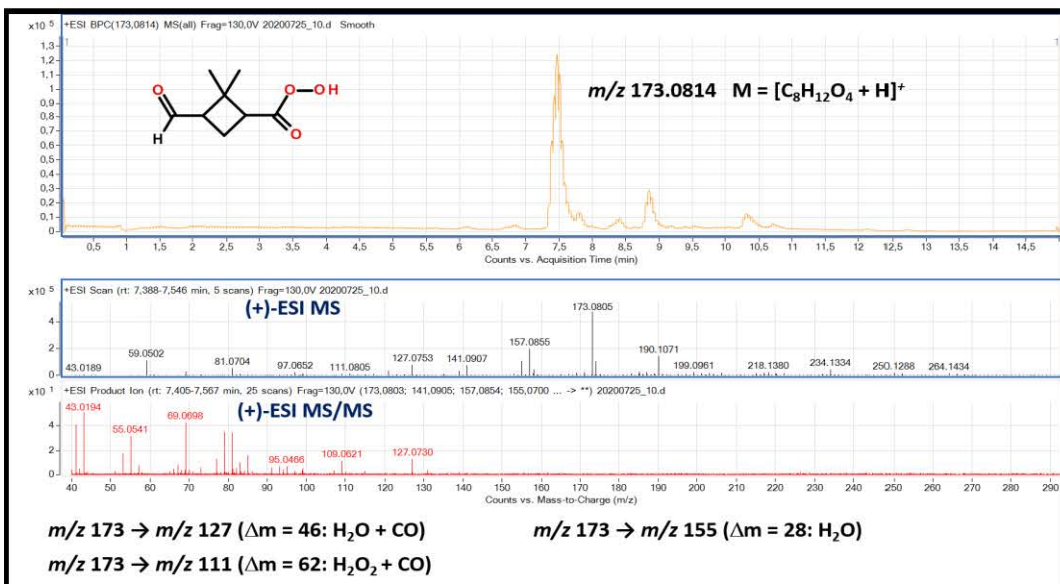
Figure 3.1.11. Pie chart showing the RPLC/ESI-HR-QTOFMS measurements of pinic, pinonic and MBTCA acids accounted for ~ 57 % of the total SOA mass produced from α -pinene ozonolysis. The SOA mass was determined by multiplying the total SOA volume measured in real-time with Scanning Mobility Particle Sizer by SOA density of 1.2 g cm^{-3} previously reported.[265](#)

Notably, pinic acid, pinonic acid, and MBTCA contributed to ~57% of the total SOA mass generated, and thus, the organic hydroperoxides measured here likely contribute to the mass closure, but this remains uncertain due to the lack of available authentic standards. Yet, there are other unidentified organics in the SOA sample that may also add to the ROS and cytotoxicity. Organic hydroperoxides generated from α -pinene ozonolysis are attributed to ROS removal by lung antioxidants, and hence, A549 cells with higher antioxidant proteins exhibited less toxic response at the exact dosage than the BEAS-2B cells. In another study, a positive correlation between the total organic peroxide concentration and ROS yield within surrogate lung fluid systems suggests that organic hydroperoxides may play an important role in ROS build up from biogenic SOA.[266](#)

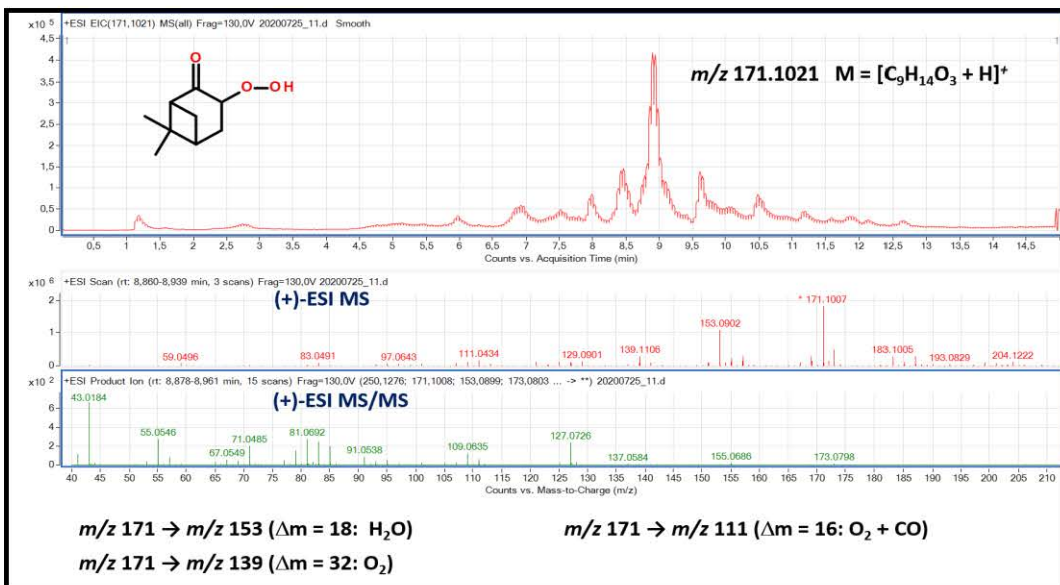
The prior work by Surratt et al. (2019) [134](#) examined the toxicity of varying chemical types of isoprene-derived SOA in BEAS-2B cells. Of various types of isoprene-derived SOA components, hydroxy-hydroperoxides, such as 1,2-ISOPOOH, was found to induce the strongest DTT and gene expression responses related to oxidative stress pathways. Overall, these studies suggested that multi-functional organic hydroperoxides are behind the strongest ROS responses within lung cells.



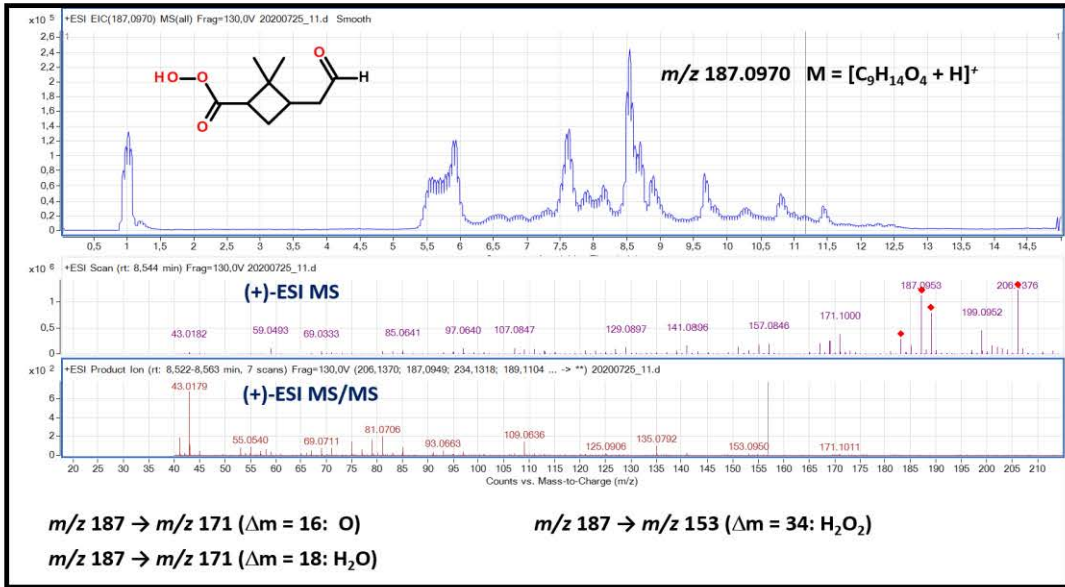
(b)



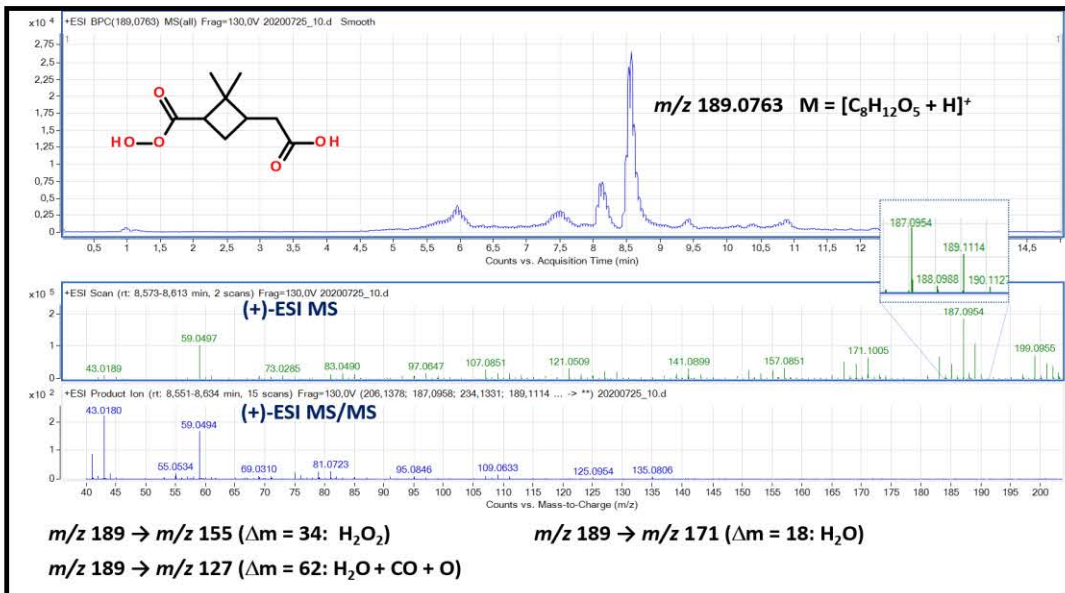
(c)



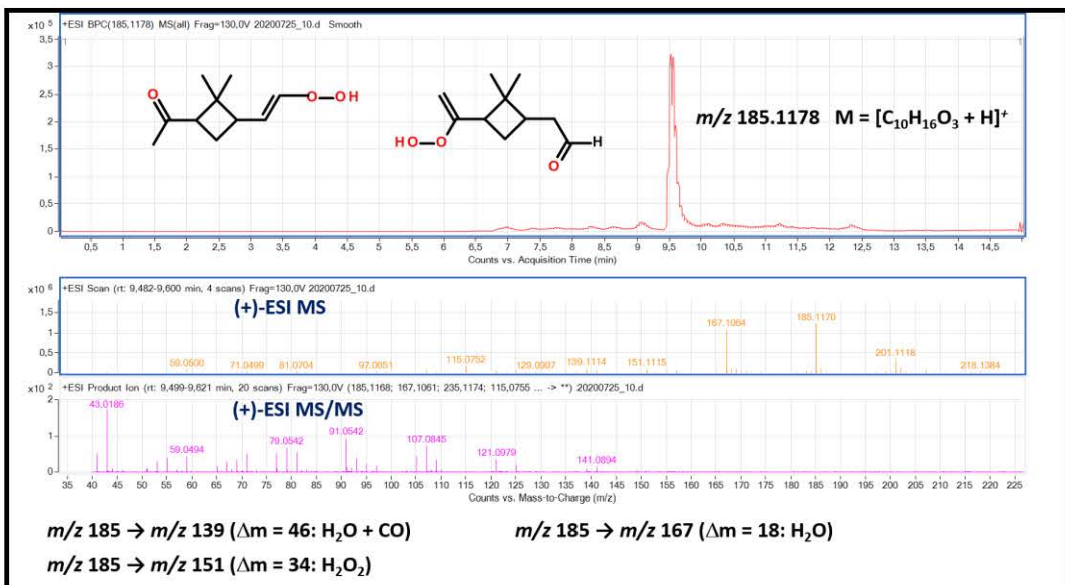
(d)



(e)



(f)



(g)

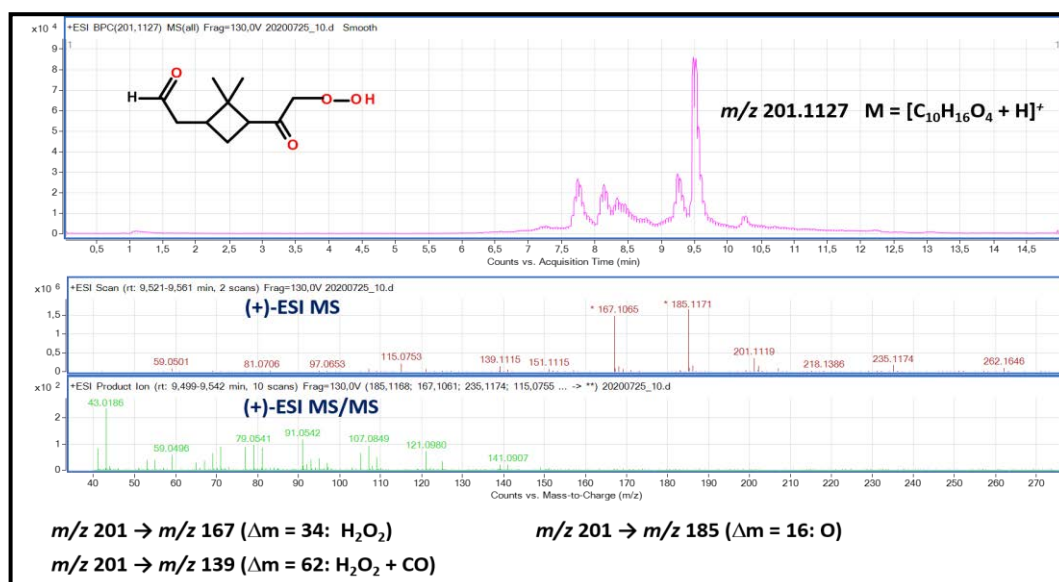


Figure 3.1.12. RPLC/ESI-HR-QTOFMS positive ion mode analysis data of the PAM-generated SOA from α -pinene ozonolysis revealed structures of organic hydroperoxides present during the exposures. Seven of these structures were tentatively identified through accurate mass measurements (HR) and tandem mass spectra (MS/MS). a-g.: the first panel of each figure shows the extracted ion chromatogram (EIC) for the $[M + H]^+$ ion associated with each organic hydroperoxide; the second panel is the positive electrospray full mass spectrum for the $[M + H]^+$ ion; the third panel is the product ion mass spectrum (MS/MS) for a given (diagnostic) $[M + H]^+$ ion.

3.1.6- Conclusion

Our results support the raised hypothesis and imply that identified particulate organic hydroperoxides from α -pinene ozonolysis may induce significant increases in ROS after exposure to the lung model systems. However, due to the lack of available authentic organic hydroperoxide standards from α -pinene ozonolysis, we cannot entirely rule out that other unidentified organics in the α -pinene ozonolysis SOA sample may also add to the ROS and cytotoxicity. For example, if the organic hydroperoxides identified in this study could be synthesized, then a toxicological assessment of these compounds could be conducted as well as the determinations of their mass contributions to the total SOA mixture generated from α -pinene ozonolysis.

3.2- Heterogeneous Oxidation Products of Particulate Isoprene Epoxydiol-Derived Methyltetrol Sulfates Increase the Oxidative Stress and Inflammatory Gene Responses in Human Lung Cells

In this section, we studied how the heterogeneous $\bullet\text{OH}$ -induced oxidation of isoprene-derived 2-MTS leads to the generation of multi-functional organosulfates that decreases the IC_{50} value with atmospheric aging in the BEAS-2B cells. The enhanced multi-functional organosulfates further alters the anti-inflammatory and anti-oxidative-stress gene responses in the cells as a function of composition/ structural dependence. Using the functional gene network of inflammation and oxidative stress-related genes from the previous studies with isoprene-derived SOA,[70](#) 14 genes were included in the current study. [Figure 3.2.1](#) summarizes the research outline of the project with corresponding techniques used in the current section.

Freshly-generated isoprene SOA derived from MAE, IEPOX and ISOPROOH, which are known isoprene SOA precursors, provided unique contributions to the induction of oxidative stress-related genes based on the chemical composition.[137](#) A recent study with viscous, photochemically-aged organic aerosol, anoxia was induced by the accumulation of O_2 within aerosol particles; ROS and carbon-centred radicals (CCR) accumulated within the interior of these viscous aerosol to overwhelm the O_2 .[267](#) Highly viscous 2-MTSs are surface active, and tend to be present at the aerosol particle surface in the presence of inorganic species.²⁵ As 2-MTSs typically mix with inorganic compounds in atmospheric $\text{PM}_{2.5}$, the accumulation of ROS and CCR may happen to 2-MTS-containing OA as it ages under certain atmospheric conditions. RH governs the viscosity of SOA and the potential accumulation of ROS,[127](#) [128](#) [267](#) and hence, under more humid conditions (such as inside lungs upon inhalation of $\text{PM}_{2.5}$), the ROS and organic shell of phase-separated aerosol particles collapse and may exacerbate negative health outcomes.[267](#) In current study, we hypothesize that the heterogeneous $\bullet\text{OH}$ oxidation of particulate 2-MTSs results in the formation of multifunctional OSs, which modifies the aerosol physiochemical properties.[127](#) As a result, these particulate multifunctional OSs, which are seen in $\text{PM}_{2.5}$ collected from urban areas affected by isoprene emissions, exhibit enhanced oxidative stress and inflammatory responses in human bronchial epithelial lung cell lines (BEAS-2B) when compared with its non-aged particulate 2-MTS precursor

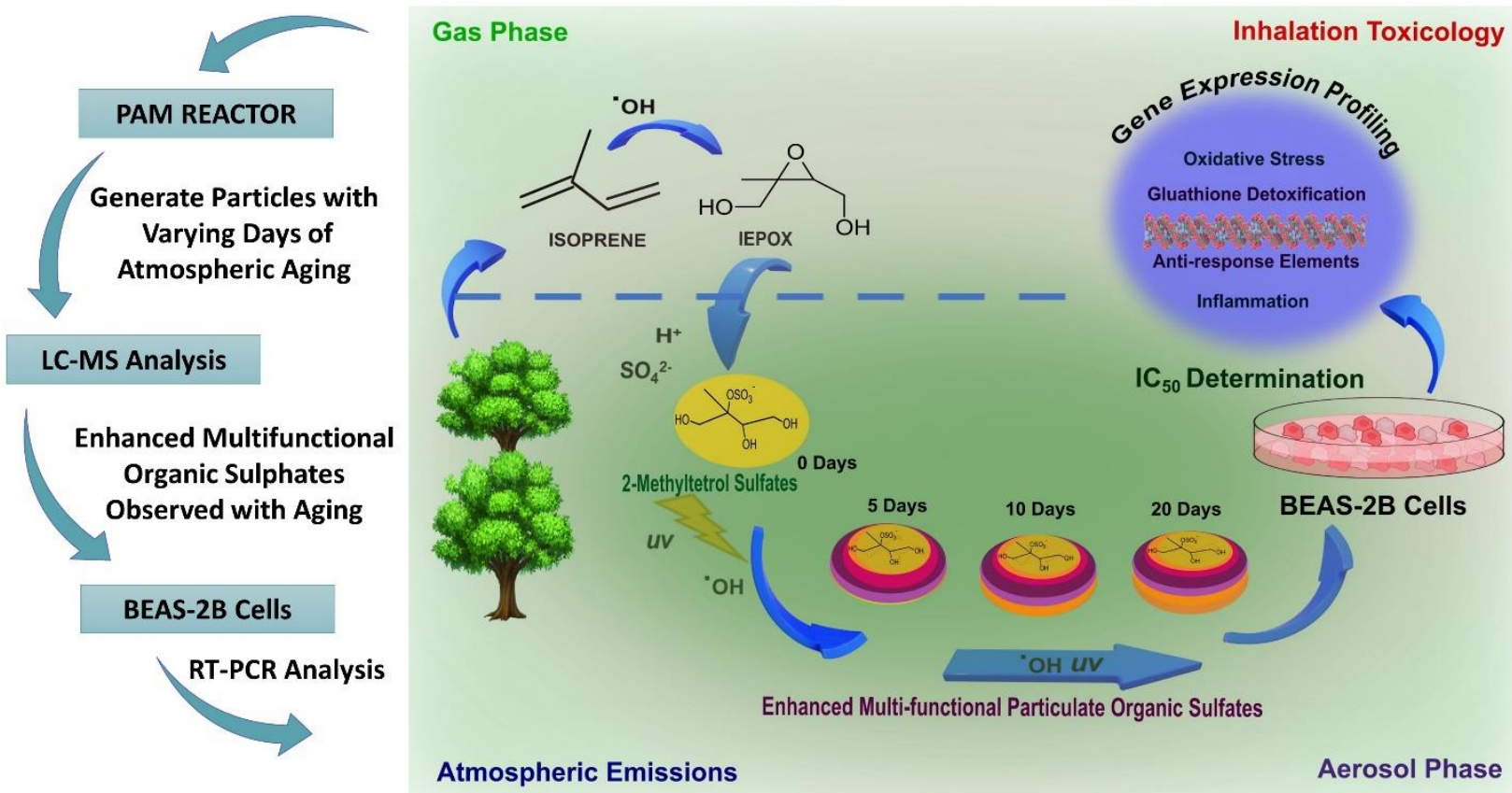


Figure 3.2.1. The BEAS-2B cell lines were exposed to the heterogeneously $\bullet\text{OH}$ radical-aged 2MTS particles, and the IC_{50} values and mRNA expression of inflammatory and oxidative stress-related genes were studied. The change in the biological end points was assessed as a function of increase in the atmospheric aging of the 2MTS.

3.2.1- Abstract 2MTS Project

Isoprene (C_5H_8) is the most abundant non-methane hydrocarbon emitted into Earth's atmosphere. Its further fate in the atmosphere, through $\bullet OH$ -mediated oxidation, is responsible for substantial contribution to fine secondary organic aerosol (SOA) masses. Specifically, particulate 2-methyltetrol sulfate diastereoisomers (MTSs) are the major SOA product formed via multiphase chemistry of isoprene-derived epoxy diols under low-nitrogen oxide conditions. We have recently demonstrated that their heterogeneous $\bullet OH$ oxidation leads to the formation of multifunctional particulate organosulfates (OSs), which are abundantly measured in atmospheric $PM_{2.5}$ samples. However, it remains unclear whether these processes (i.e., atmospheric chemical aging of $PM_{2.5}$) induce toxic effects within human lung cells. We demonstrate that inhibitory concentration-50 (IC_{50}) values decreased from the exposure to particulate 2-MTSs that were heterogeneously aged by $\bullet OH$ radicals from 0 to 22 days, indicating that the atmospheric chemical aging increased particulate toxicity in BEAS-2B lung cells. The lung cells exhibited concentration-dependent modulation of oxidative stress and inflammatory gene expression. The principal component analysis (PCA) revealed different patterns of correlation between gene expression and presence of OSs at various exposure concentrations. The basal expression of anti-ROS enzymes' genes (*NQO-1*, *SOD*, and *CAT*) signify that particulate 2-MTSs alone exhibited a strong ROS response within the treated cells. The exposure to heterogeneously-aged particulate 2-MTSs caused the upregulation of glutathione pathway genes (*GCLM* and *GCLC*) and anti-inflammatory *IL-10* gene.

3.2.2- Chemical Composition and PCA of Particulate 2-MTSs and its Aging Products

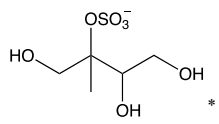
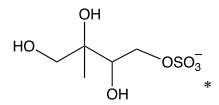
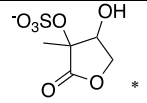
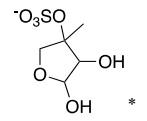
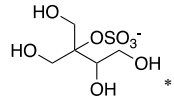
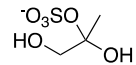
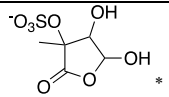
The relative abundances of specific constituents in the full aerosol mixture for 4 different heterogeneously-aged particulate 2-MTS samples (0, 5, 12 and 22 days of equivalent $\cdot\text{OH}$ exposures) are shown in [Figure 3.2.2. a](#). The proposed heterogeneous $\cdot\text{OH}$ oxidation mechanisms of particulate 2-MTSs were recently published,[127](#) and thus, will not be fully reiterated in this thesis. Briefly, heterogeneous $\cdot\text{OH}$ oxidation of particulate 2-MTSs initiates a cascade of organic peroxy radical ($\text{RO}_2\cdot$) reactions in the condensed phase through functionalization and fragmentation.[127](#) While fragmentation reactions result in the off-gassing of reaction products that are more volatile (e.g., acetic or formic acids) than the particulate 2-MTSs, which appears to recycle back particulate $\text{Sulf}_{\text{inorg}}$, functionalization reactions lead to the formation of low-volatility multifunctional OSs that remain in the particle phase. Substantial compositional changes were observed for the 2 predominant aerosol constituents, including 2-MTSs and $\text{Sulf}_{\text{inorg}}$, over the course of heterogeneous $\cdot\text{OH}$ -driven oxidation.

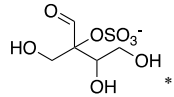
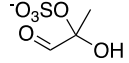
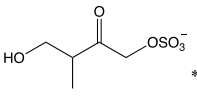
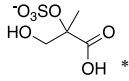
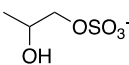
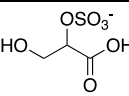
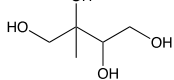
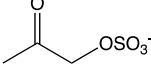
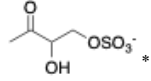
The total abundance of particulate OSs and $\text{Sulf}_{\text{inorg}}$ decreased from $\sim 80\%$ in non-aged 2MTS aerosol sample to 50% in 22 days aged aerosol sample. Previously reported particulate multifunctional OSs produced from the heterogeneous $\cdot\text{OH}$ oxidation of 2-MTSs, which included HILIC/ESI-HR-QTOFMS measured $[\text{M} - \text{H}]^-$ ions at m/z 213 ($\text{C}_5\text{H}_9\text{O}_7\text{S}^-$), 211 ($\text{C}_5\text{H}_7\text{O}_7\text{S}^-$), 171 ($\text{C}_3\text{H}_7\text{O}_6\text{S}^-$), 227 ($\text{C}_5\text{H}_7\text{O}_8\text{S}^-$), 229 ($\text{C}_5\text{H}_9\text{O}_8\text{S}^-$), 169 ($\text{C}_3\text{H}_5\text{O}_6\text{S}^-$), 199 ($\text{C}_4\text{H}_7\text{O}_7\text{S}^-$), 155 ($\text{C}_2\text{H}_3\text{O}_6\text{S}^-$), were observed to increase from 0 to 22 days.[127](#) Other HILIC/ESI-HR-QTOFMS observed $[\text{M} - \text{H}]^-$ ions at m/z 183 ($\text{C}_4\text{H}_7\text{O}_6\text{S}^-$), 153 ($\text{C}_3\text{H}_5\text{O}_5\text{S}^-$), 135 ($\text{C}_5\text{H}_{11}\text{O}_4^-$) 197 ($\text{C}_5\text{H}_9\text{O}_6\text{S}^-$) were impurities in the 2-MTSs standard, as they were present in the non-aged particulate 2-MTS sample (i.e., 0 days). The full list of observed compounds is summarized in [Table 3.2.1](#). Their identities were supported by elemental compositions determined from high-resolution mass fittings and extracted ion chromatograms (EICs) derived from the HILIC/ESI-HR-QTOFMS method; the identified compounds exhibited similar peak shapes and retention times to those previously reported for laboratory-generated and ambient IEPOX-SOA ([Figure 3.3.3](#)).[124](#), [127](#), [220](#) The fraction labelled “Unquantified” refers to the residual mass when comparing the HILIC-ESI-HR-QTOFMS or IC quantified tracers with the total mass calculated based on the SMPS data. The residual mass may result from insufficient recovery of certain semi-volatile organic compounds common to filter extraction/sample preparation steps, uncertainties in HILIC/ESI-HR-QTOFMS quantifications due to the lack of authentic standards for all

compounds, changes in aerosol densities that occurs for aged samples, or missing reaction products that are not well suited to HILIC/ESI-HR-QTOFMS detection.

The chemical composition characterized for the 4 different atmospherically aged aerosol samples were then input into principal component analysis (PCA) for two-dimensional (2-D) reduction of the data. The biplot of PCA in [Figure 3.2.2 b](#) explains the variance based on the atmospheric aging (along the x-axis, PC1) and the variance based on the chemical composition differences (along the y-axis, PC2). As shown in [Figure 3.2.2 c](#), three PC components explained the total variance of 82.37% for PC1, 12.72% for PC2 and 4.91% for PC3. For the multivariate linear regression model and Pearson r correlation studies, only PC1 was selected as it explained the total proportion of variance greater than 80%. As can be seen from the biplot in [Figure 3.2.2b](#), the PC1 showed a positive correlation value for 16 of the 18 variance values (i.e., $[M - H]^-$ ions at the m/z values) studied, while a negative correlation with 2 variance values (i.e., $[M - H]^-$ ions at 183 and associated with 2-MTSs). The exact variance with correlation of PC1 and PC2 values are summarized in [Table 3.2.2](#). When compared with the HILIC/ESI-HR-QTOFMS measured m/z values in [Figure 3.2.2a](#), it was noted that 2-MTSs and m/z 183 (main impurity, 10%) were predominant precursors in the non-aged (0 days aging of 2-MTSs) sample,¹²⁷ At the same time, the rest of the chemical components increased due to the heterogenous $\cdot\text{OH}$ oxidation of the non-aged samples. Hence, PC1 alone explained the variance resulting from the atmospheric chemical aging and reduced the components into aged and non-aged chemical products. [Table 3.3.3](#) summarizes the PC1 scores generated that were input into toxicological data (IC_{50} and gene expression).

Table 3.2.1. Organic compounds identified in heterogeneously •OH-mediated oxidized 2-MTS aerosol.

Name	Measured mass [M-H] ⁻	Formula [M-H] ⁻	Structure	O:C ratio	Retention Time (min)	Mass Error (ppm)	Changes to <u>OSC</u>
2-MTS	215.023	C ₅ H ₁₁ O ₇ S ⁻		1.4	2.6 3.2 5.5 6.9	3.72 2.79 5.11 7.42	0
215	215.0231	C ₅ H ₁₁ O ₇ S ⁻		1.4	9 10.4	6.73 12.85	0
211	210.991	C ₅ H ₇ O ₇ S ⁻		1.4	1.4 1.6	8.51 0.49	+0.80
213	213.007	C ₅ H ₉ O ₇ S ⁻		1.4	2.0 3.7 4.1	3.99 6.79 6.32	+0.40
231	231.018	C ₅ H ₁₁ O ₈ S ⁻		1.6	6.47	5.14	+0.40
171	170.997	C ₃ H ₇ O ₆ S ⁻		2	5.2 7.4	-3.39 9.41	+0.13
227	226.987	C ₅ H ₇ O ₈ S ⁻		1.6	1.9	-3.56	+1.2

229	229.002	C ₅ H ₉ O ₈ S ⁻		1.6	2.6 3.7 4.3	3.65 5.82 5.82	+0.80
169	168.981	C ₃ H ₅ O ₆ S ⁻		2	1.25 2.52	2.16 4.52	+0.80
197	197.013	C ₅ H ₉ O ₆ S ⁻		1.2	2.00, 2.63 3.42, 3.74 4.33	4.38, 3.37 -3.19, 5.9 5.39	0
199	198.992	C ₄ H ₇ O ₇ S ⁻		1.75	24.52	-6.52	+0.80
155	154.9695	C ₂ H ₃ O ₆ S ⁻		3	23.96	-22.76	+1.8
185	184.9745	C ₃ H ₅ O ₇ S ⁻		1.4	25.92	-8.6	+1.47
135	135.0663	C ₅ H ₁₁ O ₄ ⁻		0.8	4.45	4.53	0
153	152.9853	C ₃ H ₅ O ₅ S ⁻		1.67	1.33	1.85	+0.13
183	182.9969	C ₄ H ₇ O ₆ S ⁻		1.5	1.37	7.20	+0.3

* Additional isomeric structures are available.

\overline{OS}_C for the average oxidation state of an organic molecule and is calculated as $2O/C - H/C$.²⁶⁸ The original equation by Kroll et al. (2015) only considers organic molecules consisting of C, H, and O. In the calculation for OS, -OSO₃H was treated as -OH. The last column, “Changes to \overline{OS}_C ” is the difference between the \overline{OS}_C of the molecule and that of 2-MTSs

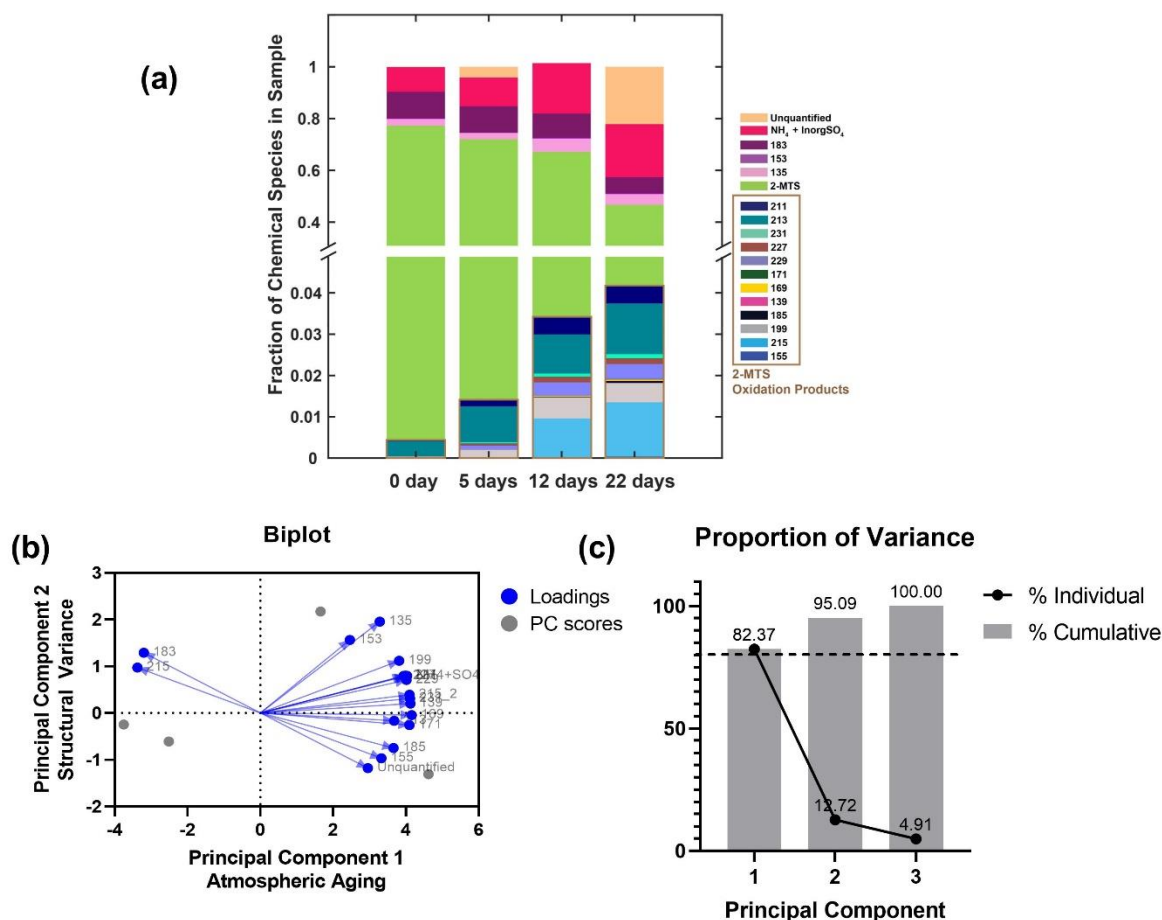


Figure 3.2.2. Chemical composition and principal component (PC) plots of particulate 2-MTSs under different OH exposure levels. (a) HILIC/ESI-HR-QTOFMS analysis to assess the changes to the chemical composition of particulate 2-MTSs with increased atmospheric chemical aging. The numbers in the legend are the nominal m/z values for monoisotopic deprotonated ions of the compounds characterized by HILIC/ESI-HR-QTOFMS. The fractional composition is calculated as the ratio of each identified species (organic and inorganic) to total particulate concentration. (b) 2-D reduction of the chemical composition (m/z values) using PC analysis so that the chemical structures present in the samples can be sorted based on the atmospheric chemical aging time. Note that the x-axis is positively correlated with the atmospheric aging. (c) Proportion of variance of the three PCs generated. PC scores were threshold at the point where percentage proportion of variance was $\sim 80\%$ or above, hence only PC1 was selected for further analysis.

Table 3.2.2. Variance v/s. PC correlation value, PC1 explains 82.37% of total variance for principal component analysis (PCA) and multiple linear regression.

Component Matrix		
	PC1	PC2
2-MTS	-0.95	0.30
211	0.96	0.25
213	0.88	-0.10
231	0.99	0.10
227	0.95	0.25
229	0.97	0.22
171	0.99	-0.16
169	0.10	-0.03
139	0.10	0.06
185	0.88	-0.45
199	0.92	0.35
183	-0.90	0.40
215	0.99	0.12
135	0.79	0.60
155	0.80	-0.58
153	0.60	0.48
NH ₄ ⁺ +SO ₄ ²⁻	0.97	0.25
Unquantified	0.71	-0.70

*Two components (PC1 & PC2) were extracted using PCA Method, while only PC1 was selected for further analysis in the study.

Table 3.2.3. PC 1 scores of the four different environmentally aged samples that were input into further analysis to generate a correlation between the chemical aging and toxicological data.

Corresponding Days of Atmospheric Aging in Days	0	5±3	10±3	20±3
PC1 scores	-3.75	-2.52	1.65	4.62

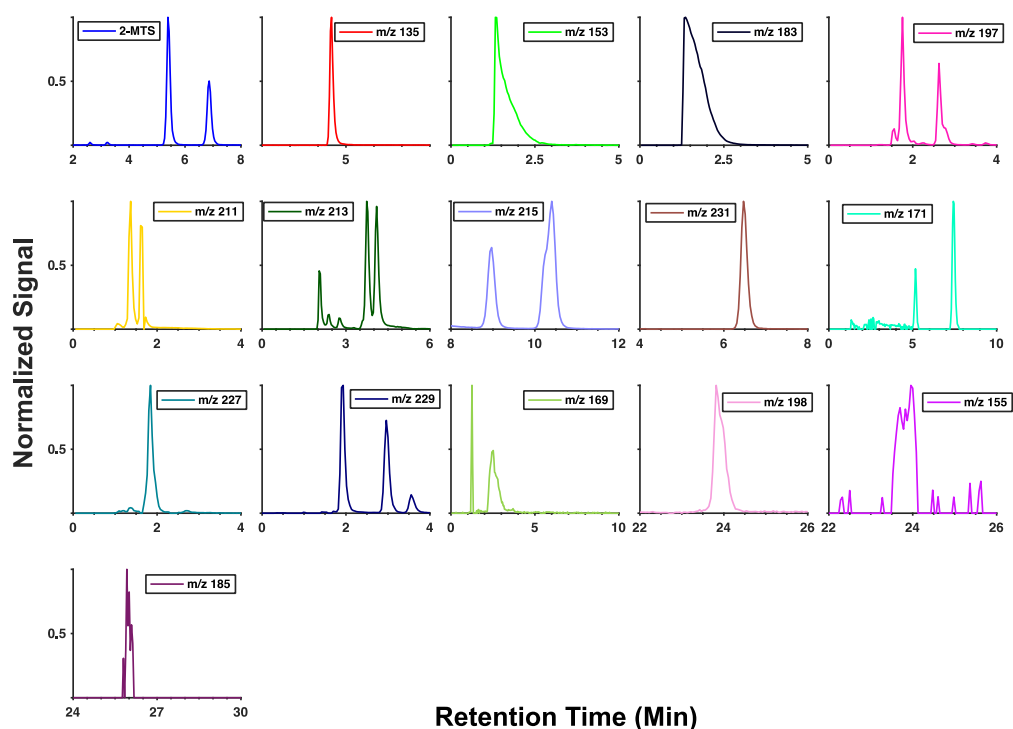


Figure 3.2.3. Extracted Ion Chromatograms (EICs) of organic components of aged 2-MTS aerosol acquired by HILIC/ESI-HR-QTOF mass spectrometry.

3.2.3- IC₅₀ Values of the 2-MTS and its Aging Products in BEAS-2B Cells

The BEAS-2B cells were treated with increased $\bullet\text{OH}$ -initiated heterogeneously aged 2-MTS aerosol in increasing concentrations of $0.01 \mu\text{g mL}^{-1}$ - $4000 \mu\text{g mL}^{-1}$. The cellular proliferation percentage (Figure 3.2.4) was then calculated as a function of blank filter-extract treated cells at 24 h and 48 h post exposure to the four different atmospherically aged aerosol (0, 5, 12 and 22 days).

As shown in Figure 3.2.5a, the IC₅₀ values estimated for 24 h exposures at 0, 5, 12, 22 days of heterogeneous $\bullet\text{OH}$ oxidation of particulate 2-MTSs was $\sim 230, 49, 25$ and 12 mg m L^{-1} , respectively. At 48 h exposures (Figure 3.2.5b) at 0, 5, 12, and 22 days of heterogeneous $\bullet\text{OH}$ oxidation of particulate 2-MTSs these IC₅₀ values mostly decreased to *ca.* $151, 44, 26$ and 5 mg m L^{-1} , respectively. At both exposure timepoints, IC₅₀ values decreased from exposure to particulate 2-MTSs, heterogeneously aged from 0 to 22 days, indicating that the atmospheric chemical age caused the particulate toxicity to increase. The cellular proliferation percentage graphs in Figures 3.2.4a and 3.2.4b show the two-way ANOVA, followed by Tukey's multiple comparison test, to determine the difference in the mean

effect of each exposure. The mean percentage proliferation following the exposure to different atmospherically aged 2-MTS particles was significant (p -value ≤ 0.001) between 0 days versus 5, 12, and 22 days at 24 h of exposure, while only significant (p -value ≤ 0.001) between 0 days and 22 days at 48 h of exposure.

The IC₅₀ values were then correlated with the PC1 values. The Pearson r correlation matrix in Figure 3.2.5c depicts the correlation between IC₅₀ values at 24 and 48 h of exposure with PC1. The matrix determined the IC₅₀ values at 24 h and 48 h exposure showed strong inverse correlation with PC1 (-0.76 and -0.81, respectively). This suggests that the IC₅₀ values decreased with increased heterogeneous $\cdot\text{OH}$ oxidation (or aging) of 2-MTS aerosols (i.e., IC₅₀ values at 0 days > 5 days > 12 days > 22 days). The correlations between IC₅₀ values with PC1 become more strongly inversed with increased exposure time.

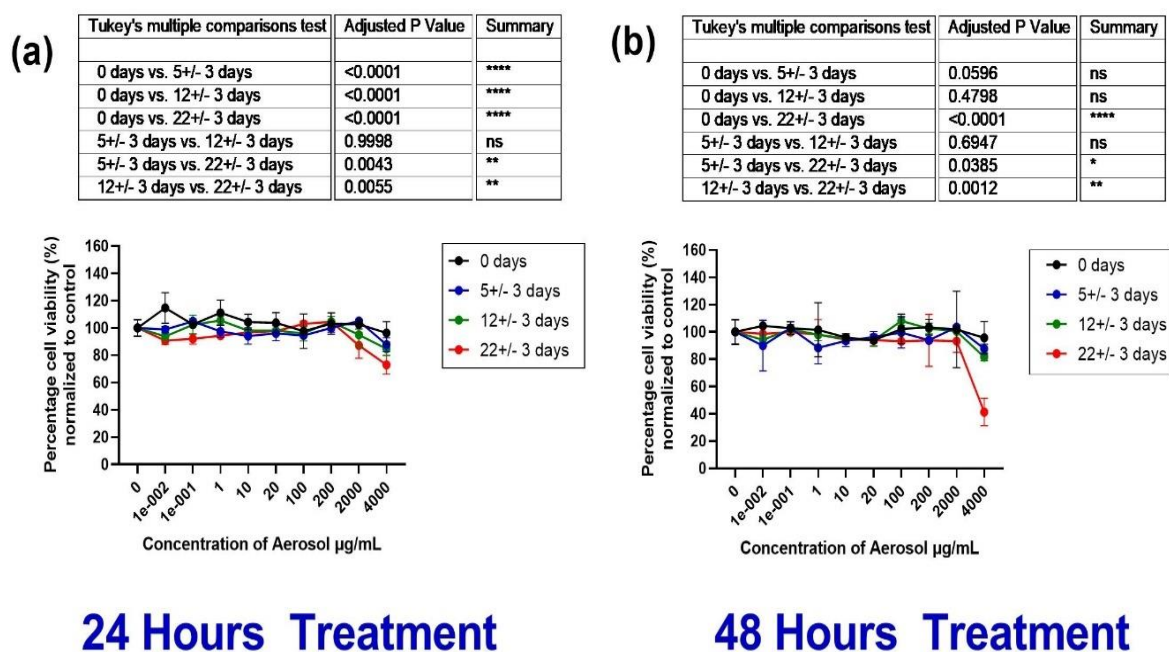


Figure 3.2.4. The percentage of proliferation for BEAS-2B cells when exposed to different atmospherically aged 2-MTS aerosols at 24 and 48 h of exposure. The difference in the mean proliferation values between different exposure types was analysed through 2-way ANOVA followed by Tukey's multiple comparison test. The value of **** denotes the p -value ≤ 0.0001 .

The IC₅₀ values of particulate 2-MTSs and its heterogeneously-aged •OH oxidation products are found to be in the mg mL⁻¹ concentration range in our current study; ambient MTS concentrations reported so far range ~ 69 – 2300 ng m⁻³ in known places that are heavily impacted by atmospheric oxidation chemistry of isoprene. [124](#), [128](#), [220](#), [269-271](#) This suggests that the exposure concentrations used in the lung cells are higher (~10²- 10³) than the environmentally relevant conditions. Furthermore, in previous section with the α-pinene SOA ozonolysis mixture exhibited IC₅₀ values of 912 and 230 μg mL⁻¹ in BEAS-2B cells at 24 and 48 h exposures, respectively.[73](#) Hence, particulate 2-MTSs and its heterogeneous •OH oxidation products appear less toxic in lung cells than α-pinene-derived SOA particles. However, the biological effects are seen even at lower exposure concentrations of 0.02 mg mL⁻¹, following 24 h of exposure. Hence, the chronic exposure to 2MTS and its heterogeneously •OH oxidation products may lead to underlying lung pathologies.

Another important aspect of our study is the inverse correlation between IC₅₀ and PC1, which implies that the formation of multi-functional OSs by atmospheric chemical aging mechanisms results in the formation of chemical structures that negatively affects lung cell growth. In our previous study with α-pinene SOA, ozonolysis of α-pinene created low-volatility particulate organic hydroperoxides that exhibited increased ROS and adversely affected cellular viability.[73](#) Chowdhury et al.[94](#), [95](#) also reported that higher ROS levels mediated cytotoxicity in aged-versus-fresh SOA samples. Similarly, in the study with naphthalene-derived secondary organic aerosol (NSOA),[272](#) altered toxicological profiles of NSOA were exhibited during atmospheric aging. Notably, we report a similar decrease in the cellular proliferation rate and IC₅₀ values with increased atmospheric aging of particulate 2-MTSs by heterogeneous •OH oxidation mechanisms, thereby highlighting the need to study the aerosol chemical aging processes in the atmosphere to predict the long-term exposure responses.

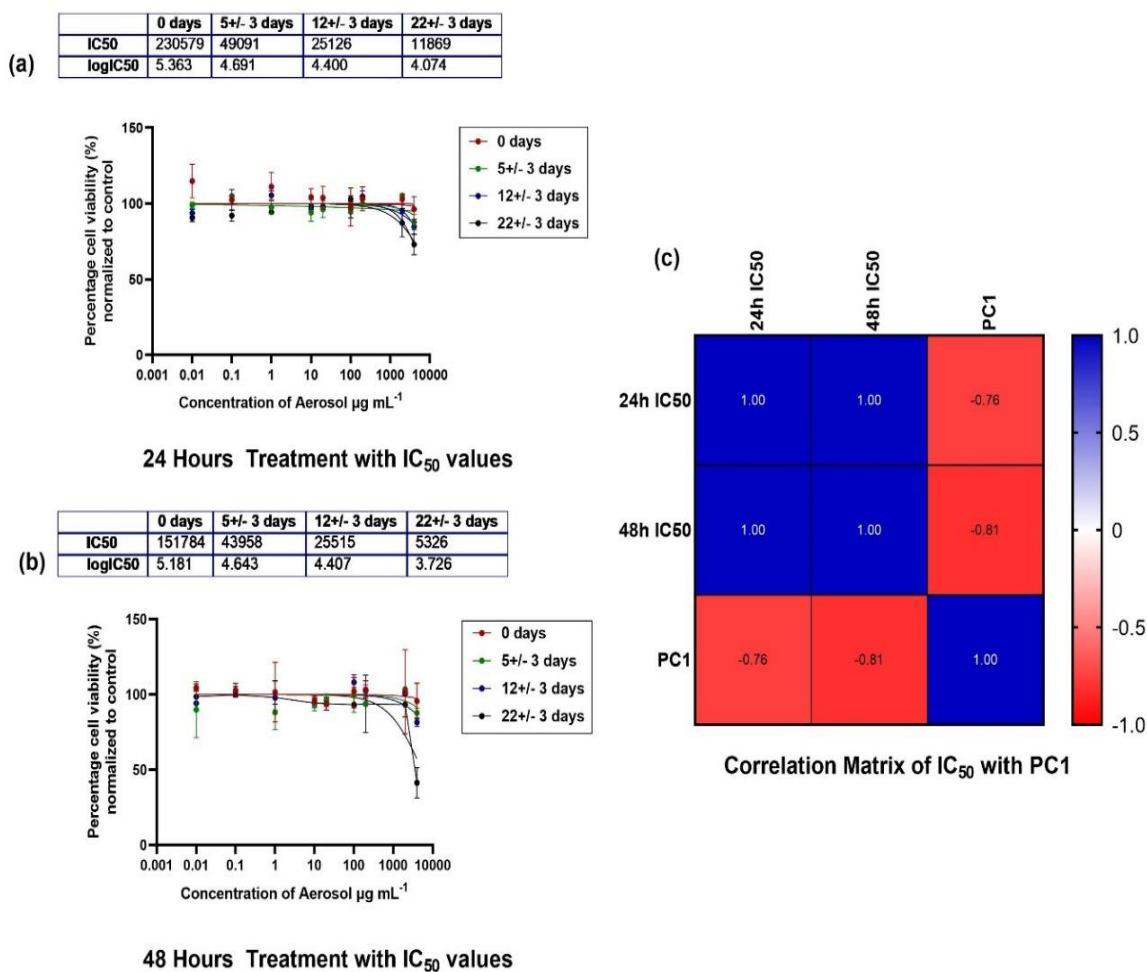


Figure 3.2.5. IC₅₀ values determined for particulate 2-MTSs heterogeneously oxidized by $\cdot\text{OH}$ at four atmospherically relevant aging time points (i.e., 0, 5 +/-3, 12 +/-3, and 22 +/-3 days) in the BEAS-2B cells. Cells were exposed to increasing concentrations of aerosol from 0.01- 4000 $\mu\text{g mL}^{-1}$ at 24 h and 48 h exposure to obtain the best-fit dose-inhibition curve. Cellular inhibition values were calculated using the resazurin assay and normalized to untreated-control BEAS-2B cells. Final IC₅₀ and log-IC₅₀ values were computed through the non-linear dose-response curve with 95% confidence interval (CI). (a) IC₅₀ and log-IC₅₀ values of BEAS-2B cells 24 h post-exposure, with corresponding best fit dose-inhibition curves. (b) IC₅₀ and log-IC₅₀ values at 48 h-post exposures in BEAS-2B cells with best-fit dose inhibition curve. (c) Pearson r correlation matrix of IC₅₀ values with PC1 shows the effect of atmospheric aging of particulate 2-MTSs on the IC₅₀ values at the 24 and 48 h exposure times.

3.2.4- Gene Expression Analysis after Exposure to 2MTS and its Heterogeneously Aged Oxidation Products in the BEAS-2B Cells

The BEAS-2B cells were exposed to the particulate 2-MTS and its heterogeneously aged aerosol components for 24 h, and gene expression (mRNA) analysis was conducted for 14 well-known genes from antioxidant, oxidative stress, glutathione, and inflammatory pathways as summarized [Figure 3.2.6](#). The genes included in the study were from anti-response elements (ARE) cluster, encoding for the NF-E2 p45-related factor 2 (Nrf2) and expressed by the *NFE2L2*; [273](#) this gene-expression is negatively regulated by Kelch-like ECH-associated protein 1 (*KEAP1*), a repressor protein that promotes Nrf-2 degradation. [274](#) Regulation of these genes is critical for the maintenance of oxidative stress, cellular redox, metabolic processes, protein homeostasis, and inflammation in the cells. [274](#) Nrf2 activation acts as a cytoprotectant against numerous chronic pathologies of the lung. [273](#) Glutathione (*GSH*) detoxification pathway is activated as a gene expression cascade response to ARE cluster; it encodes for the phase II detoxification enzymes inside the cells including glutathione (*GSH*), an important anti-oxidant factor, synthesized in the cells and involved in the removal of peroxides and xenobiotics. Three enzymes then catalyse the reduction of H_2O_2 by GSH into H_2O and GSSG. [275](#) Glutamate-cysteine ligase catalytic subunit (*GCLC*) and glutamate-cysteine ligase modifier subunit coding gene (*GCLM*) are important subunits for GSH synthesis in glutathione pathway; increased expression of *GCLC* elevate GSH in cells while increasing *GCLM/GCLC* ratio will further increase GSH. [276](#) Glutathione-S-transferases (*GST*) is an important enzyme in the same pathway that catalyses the conjugation of GSH with toxic oxidant compounds, and is associated with the regulation of chronic lung cell associated pathologies. [277](#) Glutathione reductase (*GSR*) regulates cellular GSH homeostasis by catalysing the reduction of GSSG to GSH. [278](#)

Other genes included in this study encode the superoxide dismutase enzymes, that efficiently metabolize the superoxide anions. Superoxide dismutase-1 (*SOD-1*) is found exclusively in the cytoplasm while superoxide dismutase-2 (*SOD-2*) is exclusive to mitochondrial spaces, and expressed in apoptosis and mitochondrial death pathways. [279](#) The phagocytosis of micro-organisms involves the production of ROS; one of the first enzymes involved in the ROS build up is nicotinamide adenine dinucleotide phosphate oxidase (NADPH) (*NOX*) that produces $^{\bullet}O_2^-$. [280](#) *IL-6* and *IL-8* are important pro-inflammatory chemokines and are the hallmark of atmospherically-induced airway inflammation. [281](#)

[282](#) Heme oxygenase (*HMOX-1*) is a protective factor with potent anti-inflammatory, anti-oxidant, and anti-proliferative effects.[283](#), [284](#) Interleukin-10 (*IL-10*) suppresses pro-inflammatory cytokines and induces anti-inflammatory effects.[285](#) The 14 genes included in the study are known to induce lung-associated pathologies in previous studies,[69](#), [70](#), [112](#), [134](#), [235](#), [282](#), [286](#), [287](#) and were used for initial toxicogenomic profiling following exposure to particulate 2-MTSs and its heterogeneously-aged particulate constituents produced by $\cdot\text{OH}$ at 24 h.

The fold change in mRNA expression was clustered in a heat map to observe the effect of atmospheric chemical aging of particulate 2-MTSs in the regulation of the genes. Our previous study identified significant expression of 29 oxidative stress- and inflammation-associated human genes, particularly from the Nrf-2 network when exposed to the full isoprene-derived SOA mixture.[70](#), [134](#) In current study, exposure to non-aged 2MTS particles (i.e., 0 days of heterogeneous $\cdot\text{OH}$ oxidation) resulted in the downregulation of *NFE2L2* mRNA expression, while significant upregulation was noted following the exposure to the 5, 12 and 22 days of heterogeneous $\cdot\text{OH}$ oxidation of particulate 2-MTSs at all three exposure concentrations ([Figure 3.2.7 a](#)). The *KEAP-1* expression was concentration-dependent, with the most significant fold-change decrease noted in the 0.02 mg mL^{-1} treated BEAS-2B cells ([Figure 3.2.7 b](#)). At the lowest exposure concentration, the *NFE2L2* was upregulated for 5, 12 and 22 days ([Figure 3.2.8](#)). The corresponding up-regulation of *KEAP-1* at a highest concentration (2.0 mg mL^{-1}) shows *NFE2L2* is negatively regulated by *KEAP-1* expression. This indicates at 24 h of exposure, the ARE gene cluster was activated for the *NFE2L2* expression at the lowest concentration, while *KEAP-1* expression at the highest concentration indicates the cells had basal expression of Nrf-2 before 24 h and cells are in phase II detoxification.[288](#) Nrf2 is a key factor in the regulation of the ARE-mediated activation of other defensive genes, including *NQO-1*, *GST*, and *HMOX-1*, antioxidant enzymes, cofactors, proteasomes, cytokines, chemokines, and drug transporters,[289](#) and its expression is negatively regulated (a delayed mechanism) by *KEAP-1* once associated secondary genes are switched on.[288](#)

Exposure to 2-Methyltetrol Sulfates and its Ageing Particles

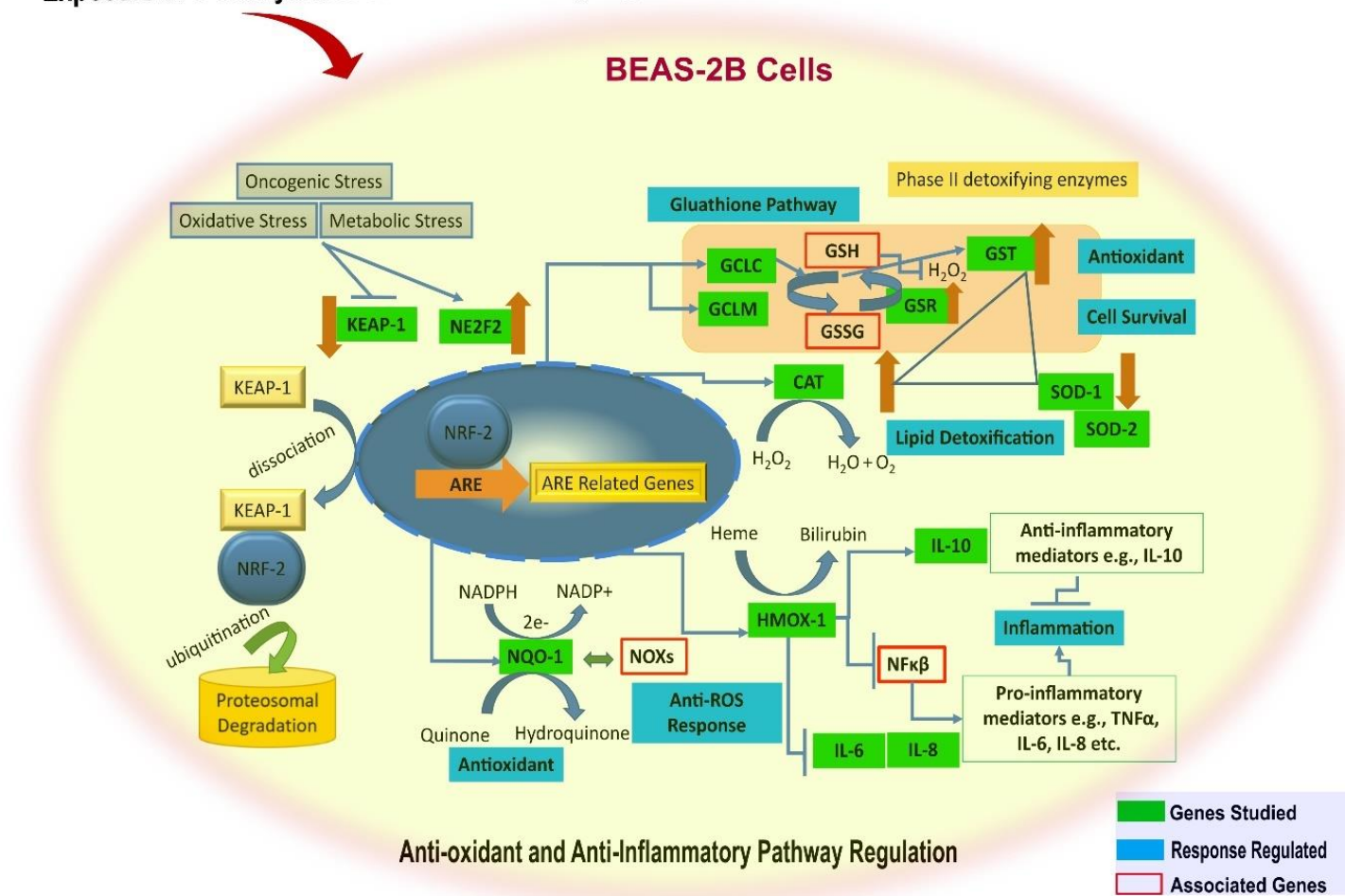


Figure 3.2.6. The gene map and signalling pathway of four antioxidant responses, oxidative stress response, glutathione detoxification responses, and inflammatory response included in the study. The cells were exposed to the enhanced multifunctional OS aerosol mixture at 0.02, 0.2 and 2 mg mL⁻¹ concentrations to determine the dosage effect on gene expression following exposure at 24 h. The genes are categorized into four clusters included in the study (a) The antioxidant response element (ARE) driven by two genes (i) *NFE2L2* (ii) *KEAP-1* (b) Inflammatory gene cluster including (i)

HMOX-1 (ii) *IL-6* (iii) *IL-8* and (iv) *IL-10* (c) Glutathione detoxification pathway including (i) *GST* (ii) *GSR* (iii) *GCLC* and (iv) *GCLM* and finally (d) Reactive oxygen species (ROS) mediated gene responses encoding for phase II detoxification enzymes were studied. These include (i) *NQO-1* (ii) *CAT* (iii) *SOD1* and (iv) *SOD*.

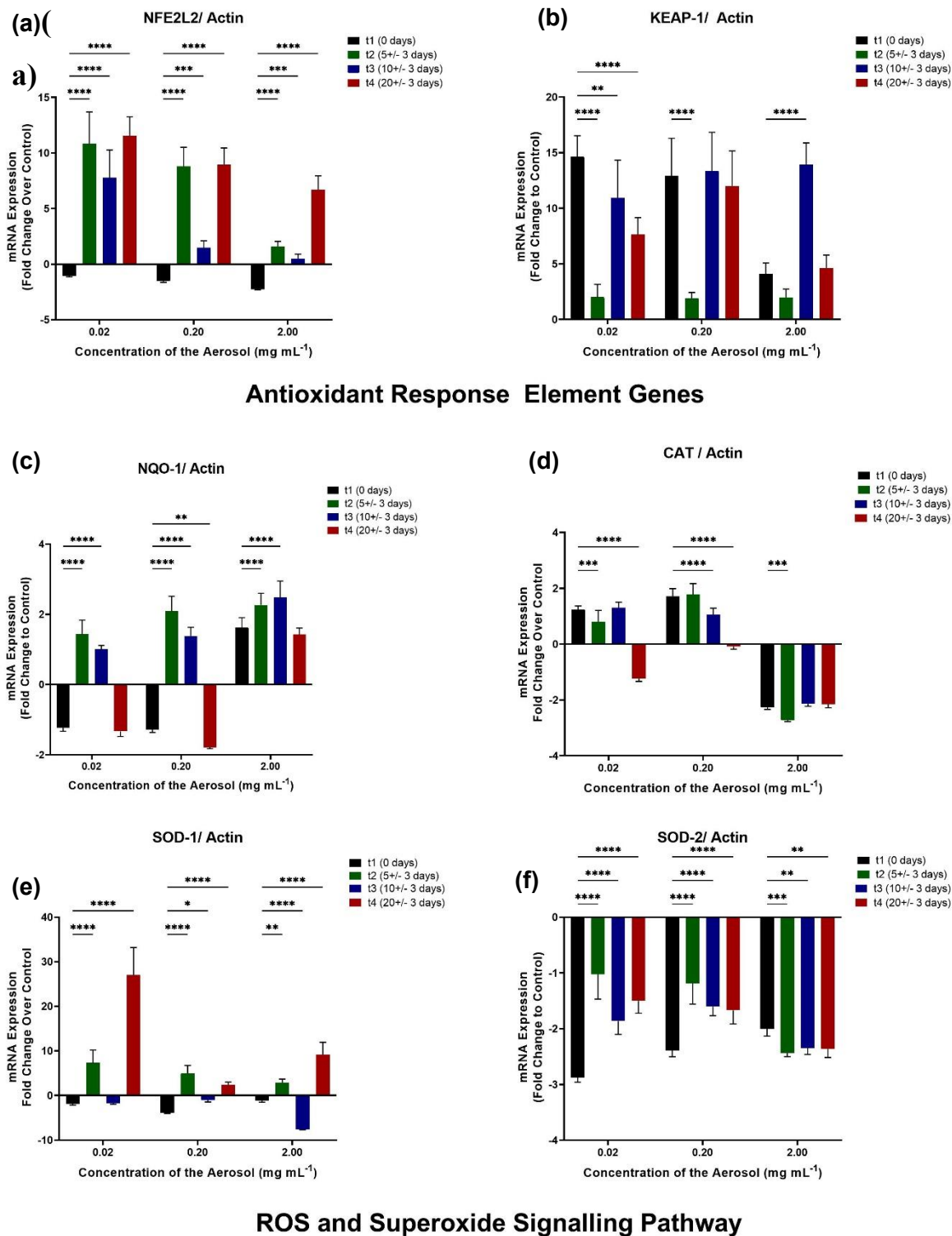
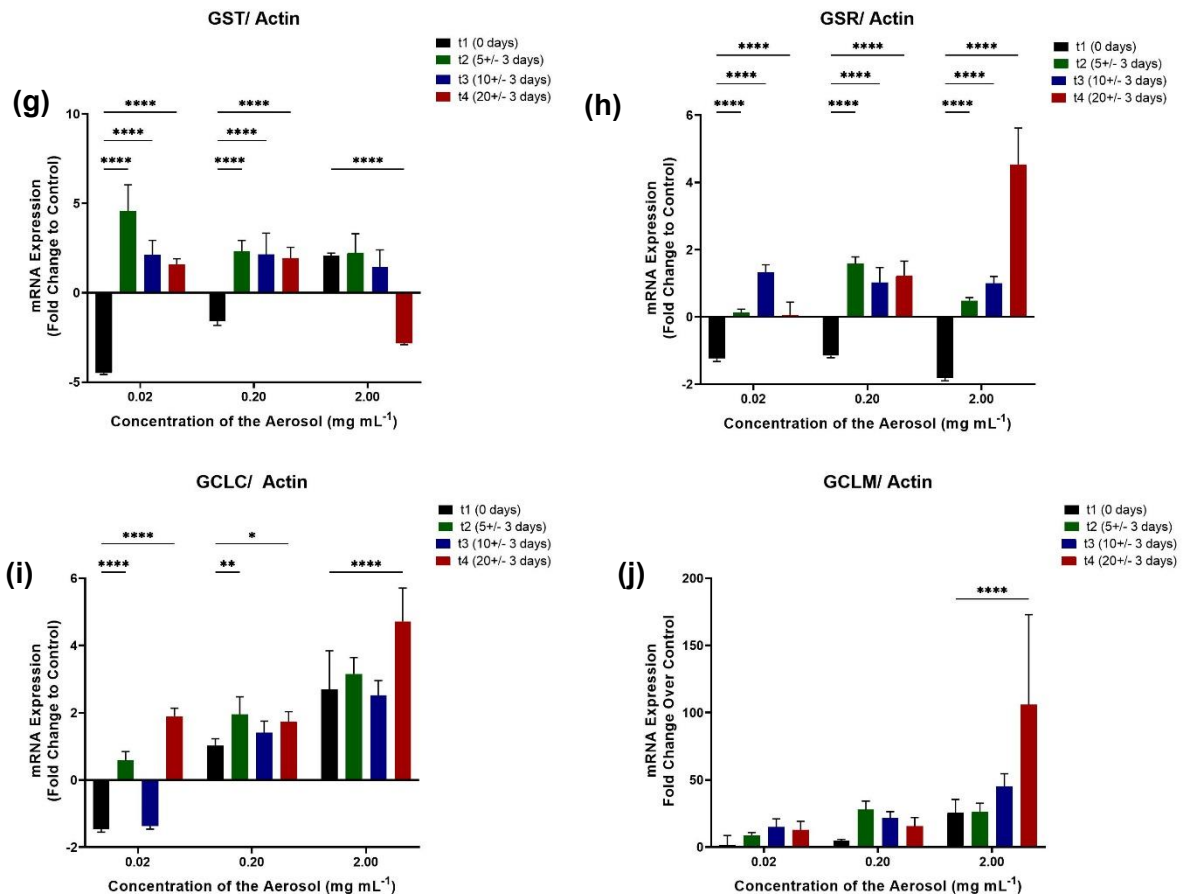


Figure 3.2.7. The fold change in the mRNA expression of the genes included in this study. Results were normalized to the aqueous extracts of blank filters (treated control) and the β -actin house-keeping gene. Increasing concentration (0.02, 0.20 and 2.00 mg mL⁻¹) of aerosol were exposed to BEAS-2B cells for 24 h, and fold changes in the mRNA expression were calculated for: (a) *NRF-2* (b) *KEAP-1* (c) *NQO-1* (d) *CAT* (e) *SOD-1* (f) *SOD-2* (to be continued).

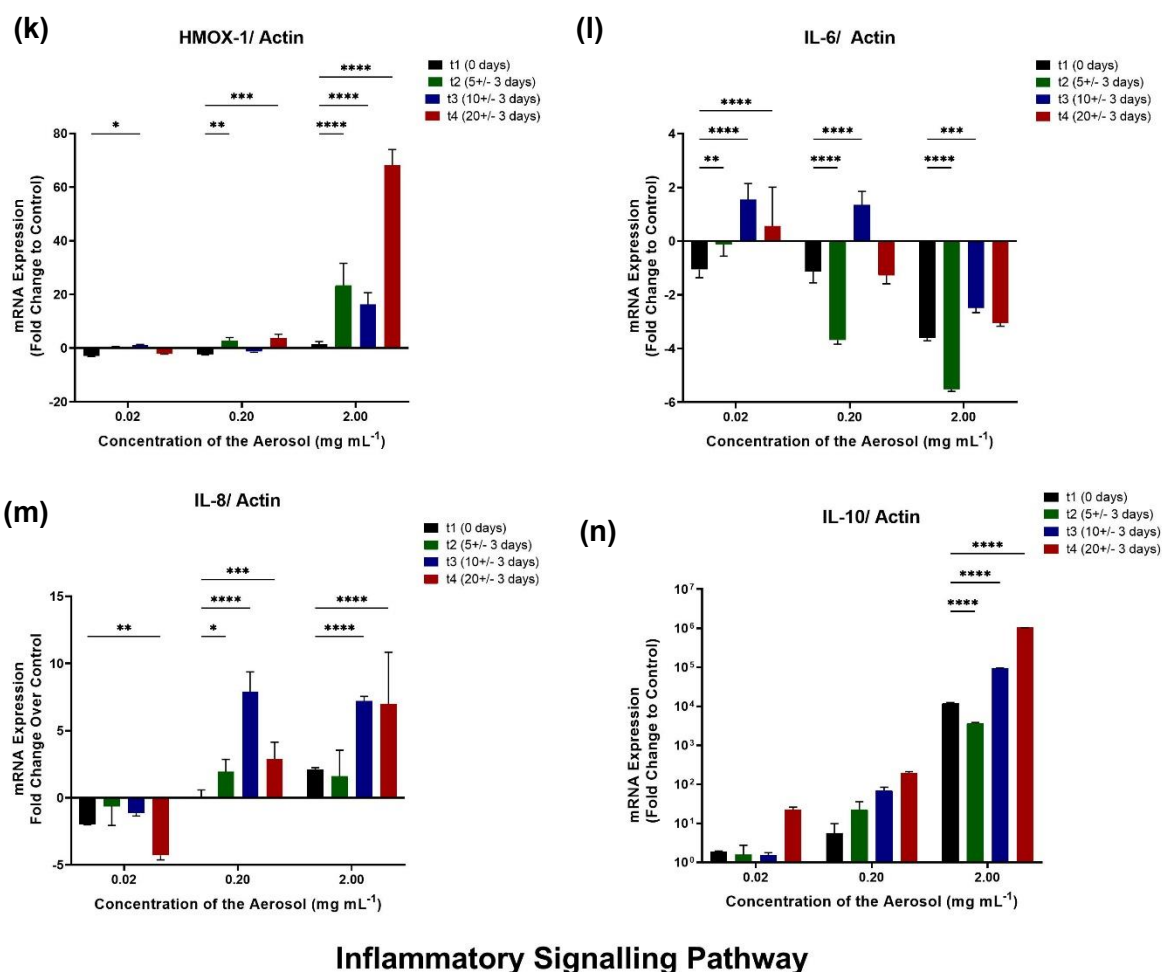


Glutathione Signalling Pathway

Figure 3.2.7 continuation. The fold change in the mRNA expression of the genes included in the study. (g) *GST* (h) *GSR* (i) *GCLC* (j) *GCLM*. The ordinary two-way ANOVA followed by Dunnett's multiple comparison test was run on the results to determine the statistical significance in the fold change of gene expression in the aged v/s non-aged 2MTS aerosol. The p -value ≤ 0.05 was considered statistically significant where p -value ≤ 0.0001 was denoted by ****

The increased atmospheric aging in a concentration-dependent manner noted a significant over-expression of IL-10 and HMOX-1 (Figure 3.2.7 k & n), while *IL-6* exhibited down-regulation (Figure 3.2.7 l). A concentration-dependent shift in the mRNA expression was noted from downregulation at the 0.02 mg mL⁻¹ dosage to upregulation at the 0.2 and 2.0 mg mL⁻¹ dosage (Figure 3.2.7 m) in *IL-8* expression. *HMOX-1* was upregulated in the 2.0 mg mL⁻¹ treatments for 5, 12 and 22 days, while 0 days did not exhibit an increase in expression (Figure 3.2.8). At lower concentrations, it was downregulated for all exposure types (i.e., 0-22 days). The downregulation of *IL-6* in the inflammatory response cluster for

all the exposure types and concentrations, and *IL-8* downregulation in lowest exposure concentrations (0.02 mg mL^{-1}) indicates that the pro-inflammatory cytokines are switched off.



Inflammatory Signalling Pathway

Figure 3.2.7 continuation: The fold change in the mRNA expression of the genes included in the study (k) HMOX-1 (l) IL-6 (m) IL-8 (n) IL-10. The ordinary two-way ANOVA followed by Dunnett's multiple comparison test was run on the results to determine the statistical significance in the fold change of gene expression in the aged v/s non-aged 2MTS aerosol. The p-value ≤ 0.05 was considered statistically significant where p-value ≤ 0.0001 was denoted by ****

Only 12- and 22-day exposure types at the higher concentrations (0.2 and 2.0 mg mL^{-1}) exhibited a fold increase in *IL-8* expression relative to control cells. There is a shift in *IL-10* expression from downregulation at the 0.02 mg mL^{-1} exposure concentration for 0 days, to upregulation at 12 and 22 days. The *IL-10* fold-change expression increases for all exposure types (0-22 days) for the 0.2 mg mL^{-1} and 2.0 mg mL^{-1} exposure concentra-

tions. This indicates the cells are shifting from pro-inflammatory to anti-inflammatory responses at higher concentrations of exposure and with increased days of heterogeneous $\cdot\text{OH}$ oxidation of particulate 2-MTSs. In previous studies, *HMOX-1* induction peaked at 6–8 h or 12 h, and returned to basal level at 24 h with cigarette smoke extracts.²⁹⁰ Downregulation of *HMOX-1* at lower exposure concentrations indicates that cells shifted from an anti-inflammatory and anti-apoptotic/anti-proliferative response to pro-inflammatory response.²⁹¹ *HO-1* gene expression is upregulated in several lung-associated pathologies, including IPF, ARDS, asthma²⁹² and COPD.²⁹³ At higher exposure concentrations with all exposure types (0–22 days of heterogeneous $\cdot\text{OH}$ oxidation), increased *HMOX-1* expression highlights the need for chronic exposure studies at atmospherically-relevant particulate concentrations of 2-MTSs and its associated multifunctional OSs products to preclude for the potential of long-term exposure effects associated with this gene in lung cells

The four genes involved in the glutathione pathway (Figure 3.2.7 g, h, i and j) exhibited increased mRNA fold-change expression relative to control with increased atmospheric aging of the 2MTS aerosol. The glutathione-detoxification pathway gene cluster in Figure 3.2.8 shows that the *GCLM* expression was upregulated at all three exposure concentrations and 4 exposure types (0–22 days of heterogeneous $\cdot\text{OH}$ oxidation of particulate 2-MTSs). The *GCLC* expression was also upregulated at 0.2 and 2.0 mg mL⁻¹. With increased heterogeneous $\cdot\text{OH}$ oxidation of particulate 2-MTSs, increased fold change in *GCLC* and *GCLM* expression was noted, implying that the heterogeneous $\cdot\text{OH}$ oxidation products enhanced gene expression compared with non-aged particulate 2-MTSs. *GSR* was downregulated with exposure to particulate 2-MTSs with 0 days of heterogeneous $\cdot\text{OH}$ oxidation at all concentrations. In contrast, at the highest concentration (2.0 mg mL⁻¹) a significant increase in *GSR* expression was noted at exposure to particulate 2-MTSs with 5, 12, and 22 days of heterogeneous $\cdot\text{OH}$ oxidation. The latter implies more conversion of *GSSG* into *GSH*. *GST* was only upregulated significantly with 0.02 and 0.2 mg mL⁻¹ exposure concentrations when 0 days of heterogeneous $\cdot\text{OH}$ oxidation was compared with 5, 12 and 22 days, possibly implying increased binding of certain aerosol chemical constituents with *GSH*.²⁷⁷ *GSH* induces response to oxidative stress and regulates pulmonary inflammation.²⁹⁴ There is evidence from previous studies that *GCLM* may influence diesel exhaust-particulate (DEP) or quantum-dot induced lung inflammation.²⁹⁵ ²⁹⁶ Another study shows cigarette smoke irreversibly modifies the *GSH* levels inside lung epithelial cell.²⁹⁷ *GCLM* and *GCLC* over-expression with increased heterogeneous $\cdot\text{OH}$ oxidation of particulate 2-MTSs indicates the

possibility of GSH accumulation in cells, which is crucial for lung homeostasis against environmental pollutants, and is associated with asthma, IPF, ARDS and inflammatory respiratory diseases in patients.[294](#)

As shown in [Figure 3.2.7 c & d](#) the *NQO-1* and *CAT* genes exhibited a concentration-dependent fold change in mRNA expression and differed between the different exposure types (0-22 days). *SOD-1* was upregulated at 5 and 22 days of heterogeneous $\cdot\text{OH}$ oxidation of particulate 2-MTSs, while it was downregulated with 0- and 12-day exposure types ([Figure 3.2.7 e](#)). *SOD-2* was significantly downregulated in all the exposure types ([Figure 3.2.7 f](#)). *NQO-1* expression increased with increasing heterogeneous $\cdot\text{OH}$ oxidation of particulate 2-MTSs at the 2.0 mg mL^{-1} exposure concentration ([Figure 3.2.8](#)). In lung cells, it contributes to ROS production, epithelial cell death, and disrupts alveolo-capillary barrier during hypoxia.[298](#) *CAT* expression was down-regulated after exposure to the most chemically aged particulate 2-MTSs (22 days) at all three exposure concentrations (0.02 , 0.2 and 2.0 mg mL^{-1}), while at the highest exposure concentration (2.0 mg mL^{-1}), all exposure types (0-22 days) resulted in the down-regulation. A previous COPD study on smokers revealed catalase was down-regulated in bronchiolar epithelium cells.[299](#) *SOD-1* was up-regulated when exposed to the 5 and 22 days of heterogeneous $\cdot\text{OH}$ oxidation of particulate 2-MTSs, while down-regulated with exposure to 0 and 12 days at all concentrations. The latter implies that exposure type (and thus, chemical composition) alters the regulation of the SOD enzymes in the cellular cytoplasm. *SOD-2* was down-regulated at all exposure types and concentrations. The down-regulation of *SOD* likely implies the dysregulation in superoxide regulation.[300](#) While *CAT*, *SOD-1* and *SOD-2* expression were downregulated in most of the exposure conditions, *NQO-1* was upregulated and ROS production/build-up occurred following 24 h of exposure.[298](#)

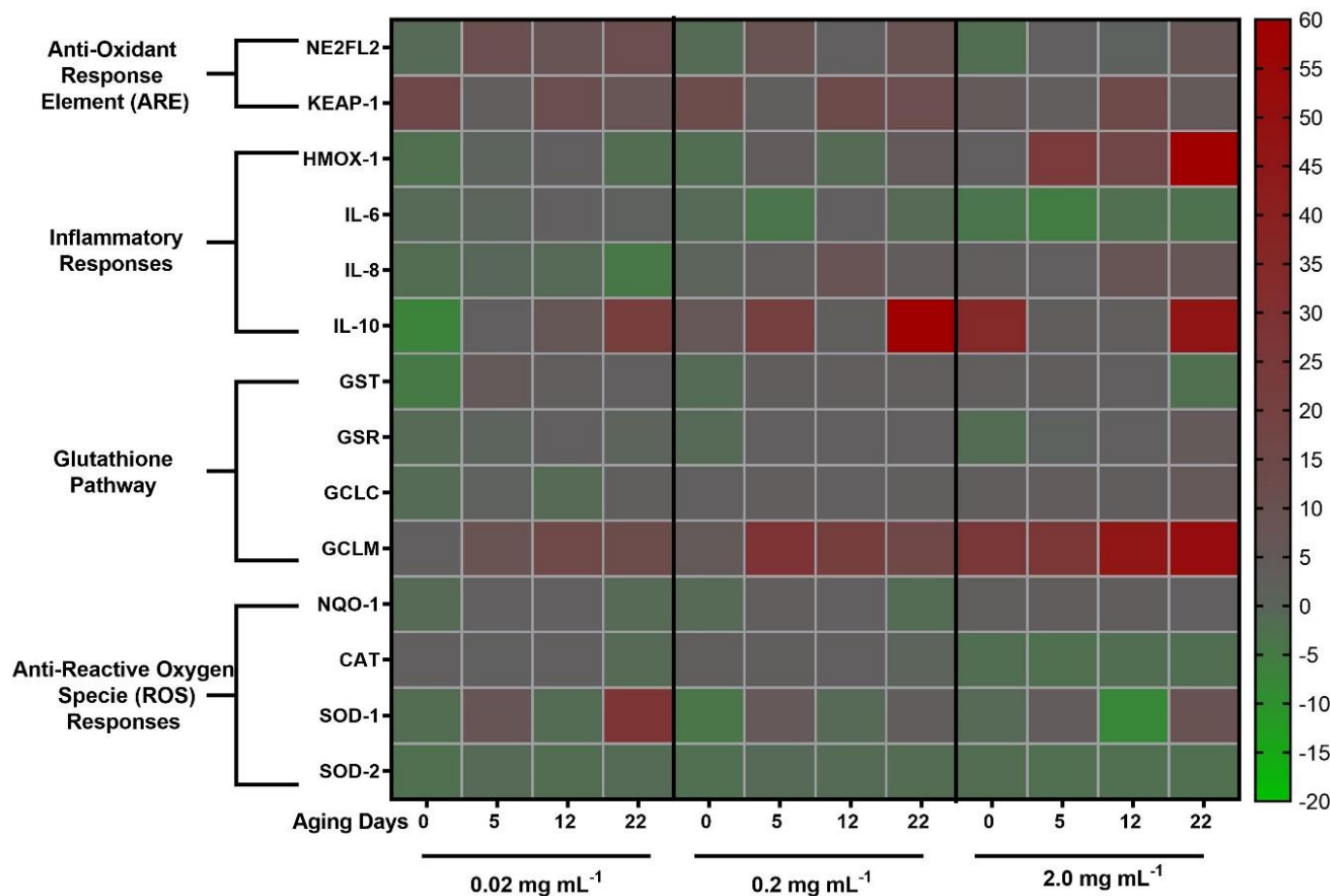


Figure 3.2.8. The heat map representing differential gene expression through clustering of samples by genes that were upregulated (red) or downregulated (green) following treatment with heterogeneously •OH-oxidized 2-MTS aerosol products at four atmospherically relevant aging points. The map summarizes the results of three exposure concentrations of 0.02, 0.2, and 2 mg mL⁻¹ in the BEAS-2B cells. Note that with exposure to increased atmospheric aging, the genes were significantly upregulated while 0 days aged particles exposure led to the downregulation of most gene clusters. The concentration-dependent response is also quite evident — the increased concentration of exposure caused the upregulation of most gene clusters. Finally, the different environmentally aged samples altered the gene expression differentially, implying the role of chemical composition as a driver of toxicogenomic profile in the study.

3.2.5- Multiple Linear Regression (MLR) Model and Altered Gene Expression

An MLR model was used to determine the significance of PC1 in driving changes in gene expression. Table 3.2.4 summarizes the results for this analysis, where β_0 (p -value ≤ 0.05) signified the basal gene expression dependence on exposure to non-aged components of particulate 2-MTSs (i.e., m/z 183 and 215), while β_1 (p -value ≤ 0.05) signified that PC1 dependence on exposure to HILIC/ESI-HR-QTOFMS measured m/z values corresponding to the heterogeneous $\cdot\text{OH}$ oxidation products of particulate 2-MTSs (as well as $\text{NH}_4^+ + \text{SO}_4^{2-}$) drove the differential gene expression in the exposed cells. As summarized in Table 3.2.2, exposure to different concentrations at four exposure types (i.e., 0-22 days of heterogeneous $\cdot\text{OH}$ oxidation of particulate 2-MTSs) changed the dependence of gene expression to PC1. At the 0.02 mg mL^{-1} exposure concentration, *GCLM* exhibited β_0 with p -value of 0.043, while *IL-10* exhibited β_1 with p -value of 0.045. At the 0.2 mg mL^{-1} exposure concentration, *CAT* (β_0 with p -value of 0.019 and β_1 with p -value of 0.044), *SOD-2* (β_0 with p -value of 0.028), *GCLC* (β_0 with p -value of 0.022), and *IL-10* (β_0 with p -value of 0.049 and β_1 with p -value of 0.052) altered genes showed a statistically-significant dependence on PC1. Similarly, at the 2.0 mg mL^{-1} exposure concentration, *NQO-1* (β_0 with p -value of 0.023), *CAT* (β_0 with p -value of 0.003), *SOD-2* (β_0 with p -value of 0.002), *GCLC* (β_0 with p -value of 0.0018), *GCLM* (β_0 with p -value of 0.001 and β_1 with p -value of 0.015) and *IL-6* (β_0 with p -value of 0.029) altered genes also showed a statistically-significant dependence on PC1.

The correlation matrix of gene expression with PC1 (summarized in Table 3.2.5 and Figure 3.2.9) further explains the effects of atmospheric chemical aging of particulate 2-MTSs on gene expression. *NFE2L2* was found to be directly and strongly correlated with PC1. *CAT* was inversely and strongly correlated with PC1 at 0.02 and 0.2 mg mL^{-1} exposure concentrations, while directly correlated at the 2.0 mg mL^{-1} exposure concentration. Genes involved in glutathione detoxification pathway (*GST*, *GSR*, *GCLC* and *GCLM*) were directly correlated with PC1. *IL-6*, *IL-8* and *IL-10* exhibited a concentration-dependent (and generally, strong) direct relation with PC1.

Our results show that particulate 2-MTSs and its heterogeneous $\cdot\text{OH}$ aging products generated a concentration-dependent effect on gene expression, and modulated the pathways activated. The 0.02 mg mL^{-1} exposure concentration affected the glutathione and anti-inflammatory response pathways with increased atmospheric chemical aging of particulate 2-MTSs, where the response at 22 days > 0 days. Similarly, *CAT* and *NQO-1*

were other pathways activated at higher exposure concentrations. In our previous studies,[70](#), [134](#), [136](#) we reported that the exposure to the full isoprene-derived SOA mixture caused genes from the NRF-2 and oxidative stress pathways to be differentially expressed ([Table 3.2.6](#)); however, none of the results showed the effect of atmospheric chemical aging on the gene expression or provide detailed gene pathway expression with corresponding chemical analysis.

In a study with gasoline derived PM_{2.5}, BEAS-2B cells, the effect of various components of gasoline on affecting gene expression was revealed through PC and multivariate analysis.[301](#) This prior study showed that the aromatic component in the fuel affected the gene expression, and hence, the toxicological responses were attributed to a specific chemical type of the exposed PM_{2.5} mixture. Similarly, in a study by Han et al.,[272](#) NSOA exposed in BEAS-2B cells revealed the effect of carbonyl components as a driver of post-translational toxicology following atmospheric chemical aging. Our current study demonstrates that the direct heterogeneous •OH oxidation of particulate 2-MTSs, which is a known and abundant SOA tracer in atmospheric PM_{2.5}, leads to dynamic genomic-level toxicity within BEAS-2B cells. The dependence of gene expression on PC1 varied with the exposure concentration, and thus, we determined how changing concentration altered the gene expression pathways in the BEAS-2B cells. Glutathione detoxification and *IL-10* expression (anti-inflammatory response)[285](#) pathways showed significant dependence on PC1. At higher concentrations, the pro-inflammatory response (*IL-6* expression)[286](#) pathway showed PC1 dependence, while basal expression of *NQO-1*, *SOD* and *CAT* signify that particulate 2-MTSs generally exhibited a strong ROS response within the treated cells. Our results confirm the up-regulation of second-phase detoxification enzyme genes following the exposure to particulate 2-MTSs.[298](#)

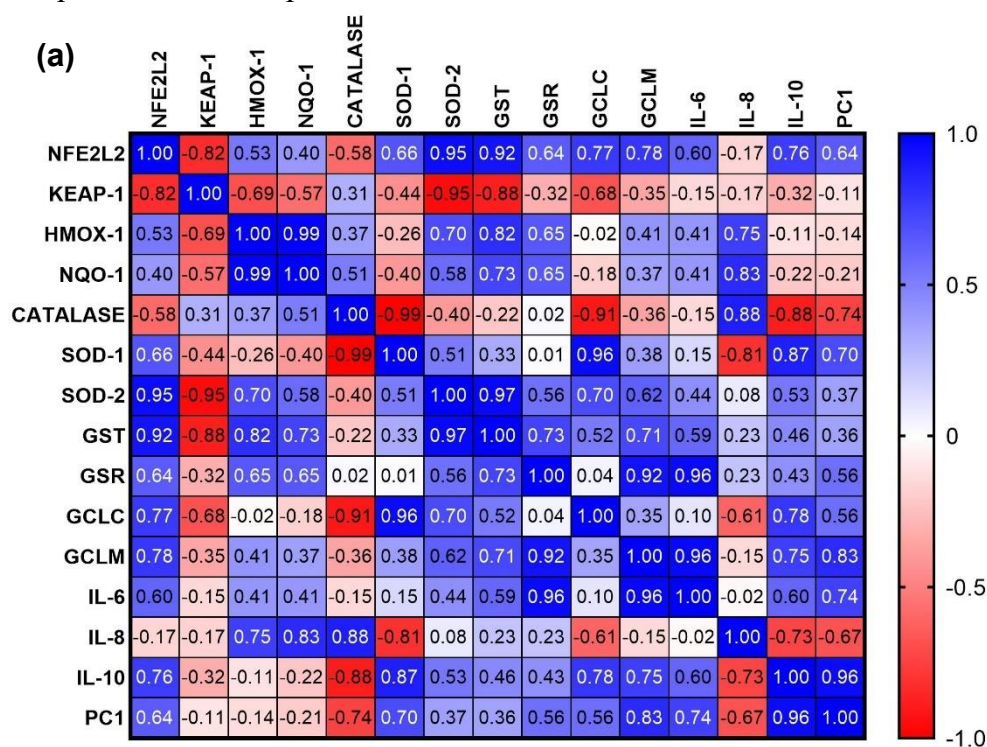
Table 3.2.4. A multiple linear regression model to predict the altered gene expression of BEAS2B cells exposed to increasing concentrations of atmospherically aged samples by Principal Component (PC) where **Gene expression** ~ **Intercept (β_0) + $\beta_1 \times P$.**

Gene ID	<i>NFE2L2</i>	<i>KEAP-1</i>	<i>HMOX-1</i>	<i>NQO-1</i>	<i>CAT</i>	<i>SOD-1</i>	<i>SOD-2</i>	<i>GST</i>	<i>GSR</i>	<i>GCLC</i>	<i>GCLM</i>	<i>IL-6</i>	<i>IL-8</i>	<i>IL-10</i>
0.02 mg mL⁻¹														
Intercept β_0 p-value	0.116	0.115	0.5350	0.975	0.394	0.322	0.0554	0.709	0.906	0.924	0.043 *	0.658	0.112	0.119
Standardized coefficient β_1 p-value	0.358	0.0892	0.8823	0.794	0.259	0.295	0.628	0.636	0.440	0.438	0.172	0.255	0.325	0.045 *
0.2 mg mL⁻¹														
Intercept β_0 p-value	0.2640	0.083	0.676	0.941	0.019 *	0.818	0.028*	0.324	0.403	0.022*	0.102	0.411	0.203	0.049 *
Standardized coefficient β_1 p-value	0.5520	0.618	0.520	0.711	0.044 *	0.744	0.7204	0.416	0.637	0.657	0.827	0.588	0.449	0.052 *
2.0 mg mL⁻¹														
Intercept β_0 p-value	0.324	0.175	0.535	0.023*	0.003 **	0.858	0.002**	0.417	0.217	0.018*	0.001**	0.029 *	0.150	0.242
Standardized coefficient β_1 p-value	0.162	0.609	0.882	0.806	0.411	0.673	0.484	0.131	0.070	0.314	0.015*	0.394	0.095	0.677

Table 3.2.5. Pearson R correlation values table explaining the relationship between the genes and PC1 following exposure to the concentration of 0.02 mg mL⁻¹, 0.2 mg mL⁻¹, and 2.0 mg mL⁻¹ of the aerosol in the BEAS-2B cells after 24h.

Pearson R Correlation value with PC1			
Gene ID	0.02 mg mL ⁻¹	0.2 mg mL ⁻¹	2.0 mg mL ⁻¹
<i>NFE2L2</i>	0.64*	0.45	0.84*
<i>KEAP-1</i>	-0.11	0.38	0.39
<i>HMOX-1</i>	-0.14	0.48	-0.09
<i>NQO-1</i>	-0.21	-0.29	-0.19
<i>CAT</i>	-0.74*	-0.96*	0.59*
<i>SOD-1</i>	0.70*	0.26	0.33
<i>SOD-2</i>	0.37	0.28	-0.52*
<i>GST</i>	0.36	0.58*	-0.87*
<i>GSR</i>	0.56*	0.54*	0.93*
<i>GCLC</i>	0.56*	0.34	0.69*
<i>GCLM</i>	0.83*	0.17	0.98*
<i>IL-6</i>	0.75*	0.41	0.60*
<i>IL-8</i>	-0.67*	0.55*	0.90*
<i>IL-10</i>	0.96*	0.95*	0.32

*The correlation values in bold fall between 0.5-1.0 and shows a strong correlation between the gene expression and PC1. The negative values show the inverse relation of genes with PC1, while positive values explain the direct link.



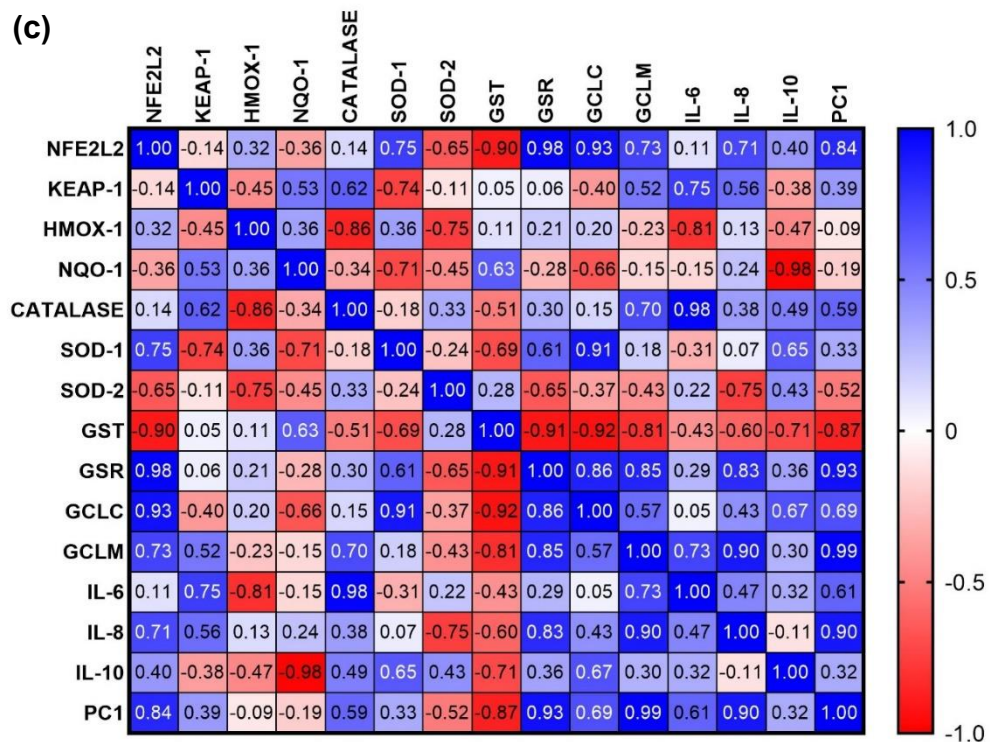
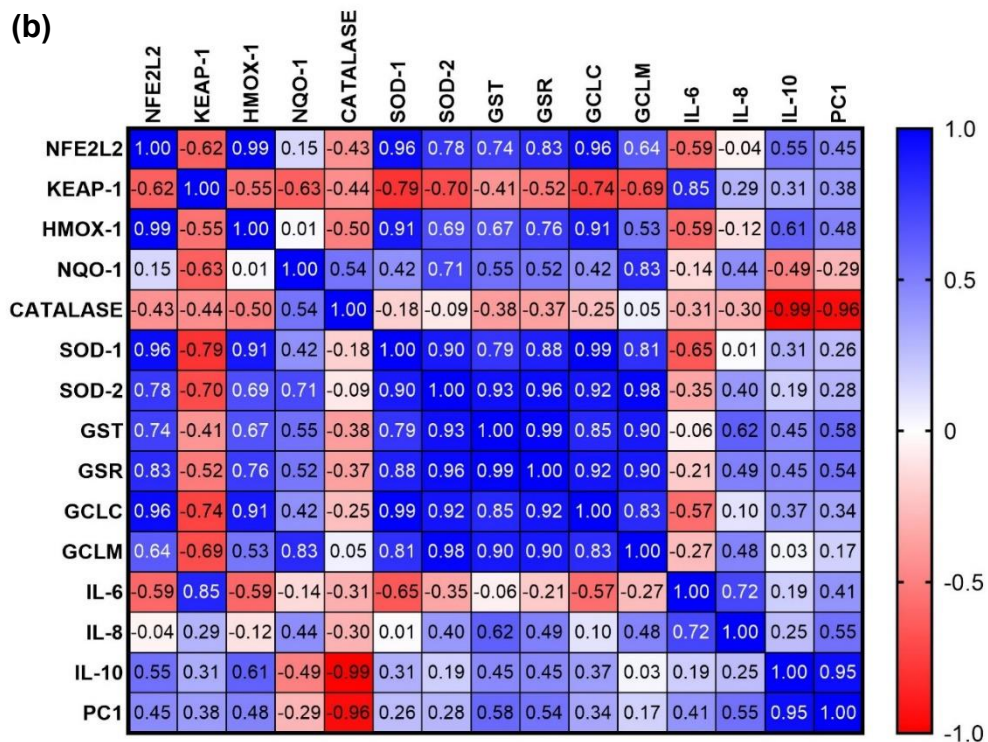


Figure 3.2.9. Pearson R correlation matrix explaining the relationship between the genes and PC1, and gene-gene expression following exposure to the concentration of (a) 0.02 mg mL⁻¹ (b) 0.2 mg mL⁻¹ and (c) 2.0 mg mL⁻¹ of the aerosol in the BEAS-2B cells after 24h.

Table 3.2.6. Previous toxicological studies on isoprene-derived SOA that correlates well with the findings obtained in the current study.

Isoprene SOA studied	Model Used	End Points Studied	Important Results	Ref
Isoprene NOx photochemical products	A549 cells	Cytotoxicity and IL-8 response	Increased LDH release and IL-8 expression	135
Ozonolysis products of isoprene	Mice Model	Airway Irritation	Maximum irritation in low-RH conditions, fresh mixtures	302
Oxidation products of isoprene	BALB/c mice	Upper Airway Irritation	Exposures to OPs did not cause enhanced upper airway irritation	303
Isoprene epoxy diols (IE-POX) and methacrylic acid epoxide (MAE) SOA	BEAS-2B	Cytotoxicity Oxidative Stress	MAE > toxicity than IE-POX 1 mg mL ⁻¹ for cytotoxicity NRF-2 pathway activated	136
High-NOx regime: 2-MG, MAE- and MACR Low-NOx regime, which yields 2-MT, IEPOX- and isoprene-derived SOA	DTT Chemical Assay	. DTT Chemical Assay	High-NOx conditions produce SOA that is more oxidizing compared low-NOx conditions	112
Isoprene epoxy diols (IE-POX) and methacrylic acid epoxide (MAE) SOA	BEAS-2B	Inflammatory/oxidative stress genes	29 miRNAs were identified as differentially expressed when exposed to IE-POX-derived SOA and 2 when exposed to MAE-derived SOA	138
Isoprene-derived photo-oxidation SOA in presence of acidified sulfate seed aerosols	BEAS-2B	Gene expression profiling of 84 oxidative stress and 249 inflammation-associated human genes	NRF-2 Activation at 0.1 mg mL ⁻¹	70
SOA derived from the various gaseous precursors (MAE, IEPOX, and ISO-POOH)	BEAS-2B	Changes in oxidative stress-related genes	MAE-derived SOA are the most potent inducer of oxidative stress-related gene	137
Isoprene-derived SOA	BEAS-2B	Interleukin 8 (IL-8) and cyclooxygenase 2 (COX-2)		75

3.2.6- Conclusion

The most significant change in the aerosol chemical composition resulting from the heterogeneous $\cdot\text{OH}$ oxidation of particulate 2-MTSs is the dramatic decrease in the 2-MTS aerosol mass fraction (90.5% to 60.5 % from 0 to 22 days, respectively). As a result, this likely explains why PC1 (containing the parent species) explained most of the variance. The yield of low-volatility multifunctional OSs from 2-MTSs was limited (i.e., up to 4% aerosol mass fraction in the most aged particulate 2-MTS samples at 22 days); however, the contribution of these species could be much higher owing to the fact that 25% of the aerosol mass remained unquantified and the low-volatility multifunctional OS products could have contributed much of this unassigned mass since we lacked authentic standards to quantify them by HILIC/ESI-HR-QTOFMS. Therefore, the toxicity of those multifunctional OSs is possibly overshadowed by the overwhelming decrease of 2-MTSs again. Previous atmospheric measurements have demonstrated that much higher particulate mass contributions from the multifunctional OS products identified during this study exist in $\text{PM}_{2.5}$, especially in urban areas that are also influenced by isoprene emissions. For example, OSs at m/z 211 ($\text{C}_5\text{H}_7\text{O}_7\text{S}^-$) and 213 ($\text{C}_5\text{H}_9\text{O}_7\text{S}^-$) are the second and third most abundant OSs following MTSs ($\sim 1/9$ by mass of the particulate MTSs, or their sum contributing $\sim 2\%$ of total particulate OC mass) in $\text{PM}_{2.5}$ samples collected from Atlanta, GA U.S. in summer.[269](#) This likely means particulate MTSs can become more aged or accumulate during atmospherically relevant lifetimes (from 2-3 weeks) of $\text{PM}_{2.5}$ in urban areas due to their low volatilities. The most aged sample that was attainable under our experimental setup (22 days of equivalent $\cdot\text{OH}$ exposure to particulate 2-MTSs) only corresponds to 3–8 equivalent aging days in an urban setting with a gas-phase $\cdot\text{OH}$ concentration of 4×10^6 — 1.1×10^7 molecules cm^{-3} . It is challenging to generate aged aerosol samples in our current experimental setup, hence, synthesizing the individual multifunctional low-volatility OS products will help to elucidate their toxicities. This may include studying combined toxicological effects in a mixture that is representative of their chemical composition in atmospheric $\text{PM}_{2.5}$. This study further showed the dependence of PC1 on gene expression. The direction for future studies includes the determination of exposure effects at a post-translational level as proteomic changes could be different from genomic-level changes.[272](#) Furthermore, toxicological studies using *in vivo* models can help better predict the systematic inflammation or irritation in the respiratory system. [302](#)
[303](#)

3.3- Mono-nitrophenols: Analysis for Atmospheric Prevalence and Toxicological Profiling in the Model Eukaryotic Membranes and Human Lung Cells

This thesis section is divided into two parts and covers the qualitative analysis on the source, emission, and prevalence of mono-NPs. It further provides toxicological assessment in the *in situ* eukaryotic cell membrane model following NP-mixture exposure and detailed comparative intra-cellular toxicity profiling in human lungs A549 and BEAS-2B cell lines. In the first part, we cover the exposure effects on the model eukaryotic lung cell membrane. In the second part, we provide details about the sources and *in vitro* toxicity mechanism of NPs exposure.

Biological cell membranes are overly complex systems; therefore, simplified models are necessary to facilitate the initial toxicological screening of potential membrane-disrupting compounds in the phospholipid-rich environment. In the first part of the study, done in collaboration with Marta Majewska at ICHF, PAS,[304](#) we presented electrochemical-based methodology (electrochemical impedance spectroscopy, EIS) combined with AFM, to screen the effects of a 2NP, 3NP and 4NP equimolar mixture on the model cell membrane supported on the atomically flat substrate, like mica and gold(111), which mimics the structure of eukaryotic membranes. The efficacy of these models was then supported by experiments performed on the BEAS-2B and A549 cell lines of lung origin. Our results showed that an equimolar mixture of 2NP, 3NP, and 4NP caused changes in the eukaryotic cell membrane potential at exposure concentrations above 100 $\mu\text{g ml}^{-1}$.[304](#) Our approach with EIS and AFM showed that exposure to NP mixtures leads to a profound rearrangement of model eukaryotic cell membrane structures, allowing for the internalization of NP and changes in cellular morphology. The cellular uptake of NPs provided evidence that an intrinsic cellular death mechanism is highly probable.[305](#)

In the second part of the study, a qualitative chemical analysis of selected NPs was conducted on ambient $\text{PM}_{2.5}$ collected from several ground sites around the U.S. as well as on SOA formed from the photooxidation of several aromatic hydrocarbons (i.e., benzene, toluene, *o*-xylene, *m*-xylene, 1,3,5-trimethylbenzene, 1,2,4-trimethylbenzene, ethylbenzene, naphthalene, 1-methylnaphthalene, 2-methylnaphthalene, and benzyl alcohol) conducted in the U.S. EPA smog chambers in the presence of NO_x . The detailed *in-vitro* toxicological assessment was then conducted to estimate the uptake of the identified NPs (i.e.,

2NP, 3NP, 4NP, and mixtures thereof) in the lung cell models and to understand the intracellular mechanisms following the initial exposure. The latter included the mechanism of cellular death and the underlying ROS build up, with a particular focus on mitochondrial dysfunction and mtROS. The study thoroughly compares the effects of cell exposure to mono-NPs and its equimolar mixture, highlighting the early biological changes in the lung cells. **Figure 3.3.1** summarizes the outline of the NP toxicology research in the current section of the thesis.

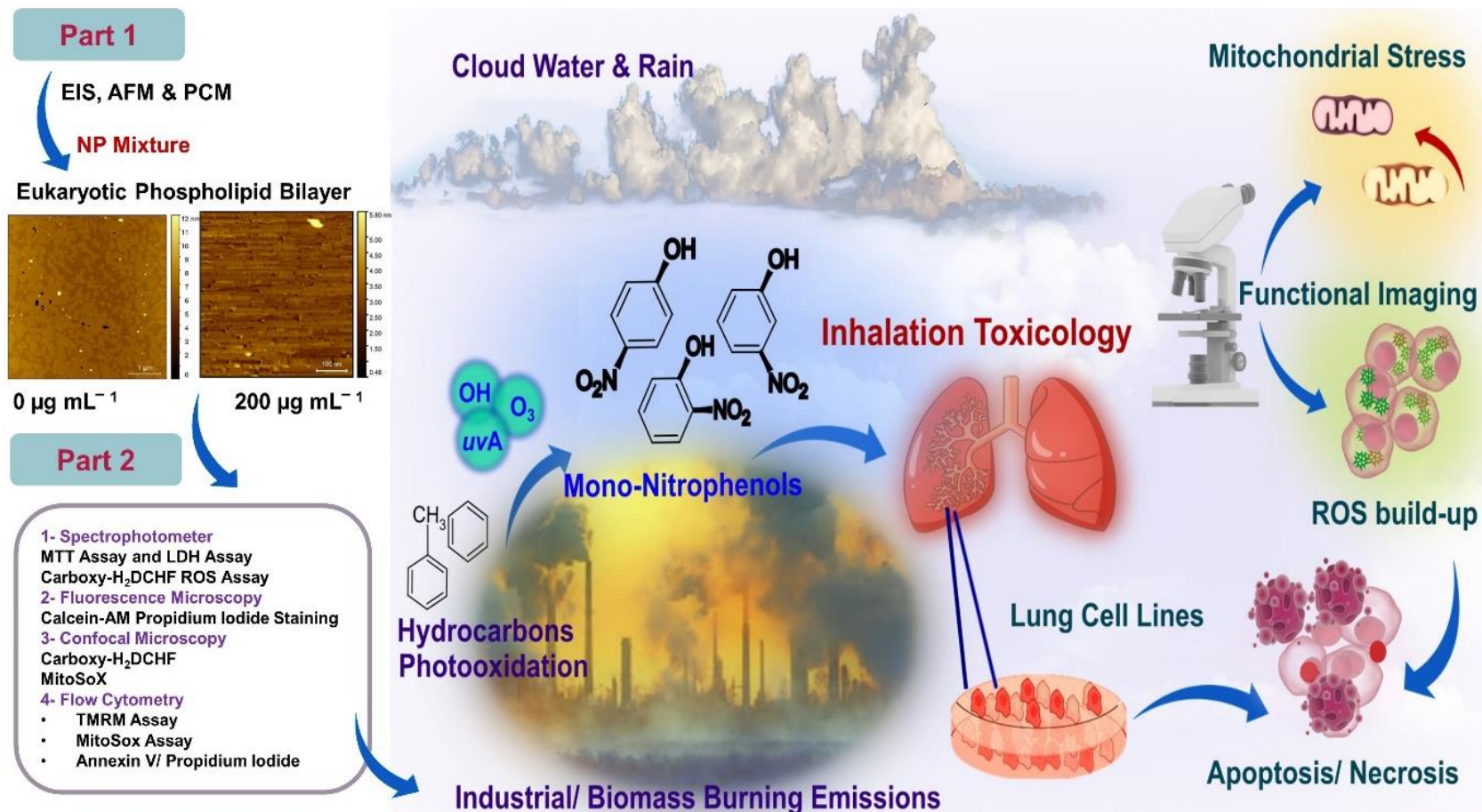


Figure 3.3.1. The mono-NPs were assessed for the toxicological responses in a two-part study. In part 1, we used the equimolar mixture of NP at 200 $\mu\text{g mL}^{-1}$ concentration in model eukaryotic phospholipid bilayer membrane and studied the corresponding changes through EIS and AFM. The NP were then exposed to A549 and BEAS-2B cells, and changes in cellular morphology were observed. In part 2, we used the functional toxicology approach to study intracellular changes in the BEAS-2B and A549 cells following exposure to 2NP, 3NP, 4NP, and equimolar NP mixture. We also qualitatively evaluated the mono-NP presence in the U.S. EPA field samples and smog chamber-generated aerosol from the photooxidation of aromatic hydrocarbons to understand their prevalence and emission source.

3.3.1- Abstract of NPs Project

Mono-nitrophenols (NPs) are a class of hazardous pollutants found in various environmental matrices, including ambient fine particulate matter (PM_{2.5}), agricultural residues, rainwater, wildfires, and industrial wastes. The first part of the study involves the use of model eukaryotic membranes to study the exposure effects of NP-mixture. After exposure to 200 µg mL⁻¹ concentration, the membrane developed pores to allow the internalization of the NPs, as determined through AFM. In the second part of the study, a qualitative chemical analysis of ambient PM_{2.5} and secondary organic aerosol (SOA) generated from the photooxidation of a series of monocyclic aromatic hydrocarbons in the U.S. EPA smog chamber was conducted. We then assessed the toxicity of these characterized fine particulate NPs and their equimolar mixture using normal bronchial epithelial (BEAS-2B) and alveolar epithelial cancer (A549) lung cell lines. The inhibitory concentration-50 (IC₅₀) was highest in the 2-nitrophenol (2NP) and lowest in 4NP-treated BEAS-2B cells at 24 and 48 h of exposure. 4NP, one of the most abundant observed in this study in ambient PM_{2.5} and SOA generated from the chamber studies, was found to be the most cytotoxic in both cell lines as determined through the lactate dehydrogenase (LDH) assay. The population of late apoptotic/necrotic BEAS-2B and A549 cells increased with the 3NP, 4NP and NP equimolar mixture treatments between 24-48 h, as determined through annexin-V/ fluorescein isothiocyanate (FITC) analysis. Cellular reactive oxygen species (ROS) regulation was altered, leading to cellular death post-exposure to 3NP, 4NP, and the NPs equimolar mixtures, while 2NP induced low ROS build up. An increased mitochondrial ROS signal following NPs exposure was only observed in BEAS-2B cells. Additionally, lung cells were analysed for the collapse of the mitochondrial membrane potential through the tetramethyl rhodamine methyl ester perchlorate (TMRM) assay. A decrease in TMRM signals was only significant in BEAS-2B cells with the highest decrease observed following 4NP exposure. Our results suggest that acute atmospheric exposures to NPs may not be toxic at ambient PM_{2.5} concentrations. However, future chronic studies with these NPs and their ambient PM_{2.5} mixtures are warranted to assess their contribution to lung-associated pathologies.

3.3.2- NPs Mixture and its effect on Eukaryotic Phospholipid Bilayer

The first part of the study involved the assessment of the exposure effects of equimolar NP-mixture on *in situ* model eukaryotic phospholipid bilayer. This study was carried out in collaboration with Dr Majewska at IPC PAS.[304](#) Details of the experimental procedure with electrochemical and atomic force microscopy (AFM) measurements have been published elsewhere.[304](#) A summary of the essential results is provided here.

- An equimolar mixture of 2NP, 3NP, and 4NP induced cytotoxicity in BEAS-2B and A549 cell lines at exposure concentrations around $100 \mu\text{g mL}^{-1}$.
- The cytotoxic effect of 2NP, 3NP, and 4NP mixture was confirmed through EIS, and AFM was performed on a model eukaryotic-like cell membrane.
- 2NP, 3NP, and 4NP equimolar mixture internalized through lung cell membrane disruption and may disintegrate by lipid extraction.

The model biological membrane mimics the structure of the eukaryotic membrane by optimization of cell surface phospholipids. The bronchial epithelial lung cells and adenocarcinoma human alveolar basal epithelium cells are known to be enriched in phosphatidylcholines (PC), which constitute ~60-80% of the lipids, followed by 7-15% phosphatidylglycerol (PG) (16:0-18:1) [306](#). Among PCs, 1,2-dimyristoyl-*sn*-glycero-3-phosphocholine, DMPC(14:0-14:0), 1-palmitoyl-2-oleoyl-*sn*-glycero-3-phosphocholine, POPC(16:0-18:1), and 1,2-dipalmitoyl-*sn*-glycero-3-phosphocholine, DPPC (16:0-16:0), are most abundant [307](#). Hence, for the *in-situ* studies, two kinds of model membranes were prepared, i.e., the membrane composed of DMPC (14:0-14:0) and the membrane comprised of an equimolar mixture of DMPC (14:0-14:0), DPPC (16:0-16:0), and POPC (16:0-18:1), named as the 3 × PC membrane as shown in [Figure 3.3.2](#)

The two types of membranes mimicked the lung cells we used for detailed *in vitro* studies, i.e., BEAS-2B and A549 cells. Electrochemical methods are widely applied to study well-known membrane-active compounds, e.g., antimicrobial peptides.[308-312](#) The exposed peptides usually exhibit defect-forming behaviour on model biological membranes, and this membrane-active effect was screened out with the cyclic voltammetry (CV) and electrochemical impedance spectroscopy (EIS) techniques.[313-315](#) The results from EIS and CV reported the 3 X PC layer (mimicking BEAS-2B cells) was more susceptible to degradation following NPs exposure when compared with the DMPC membrane alone.

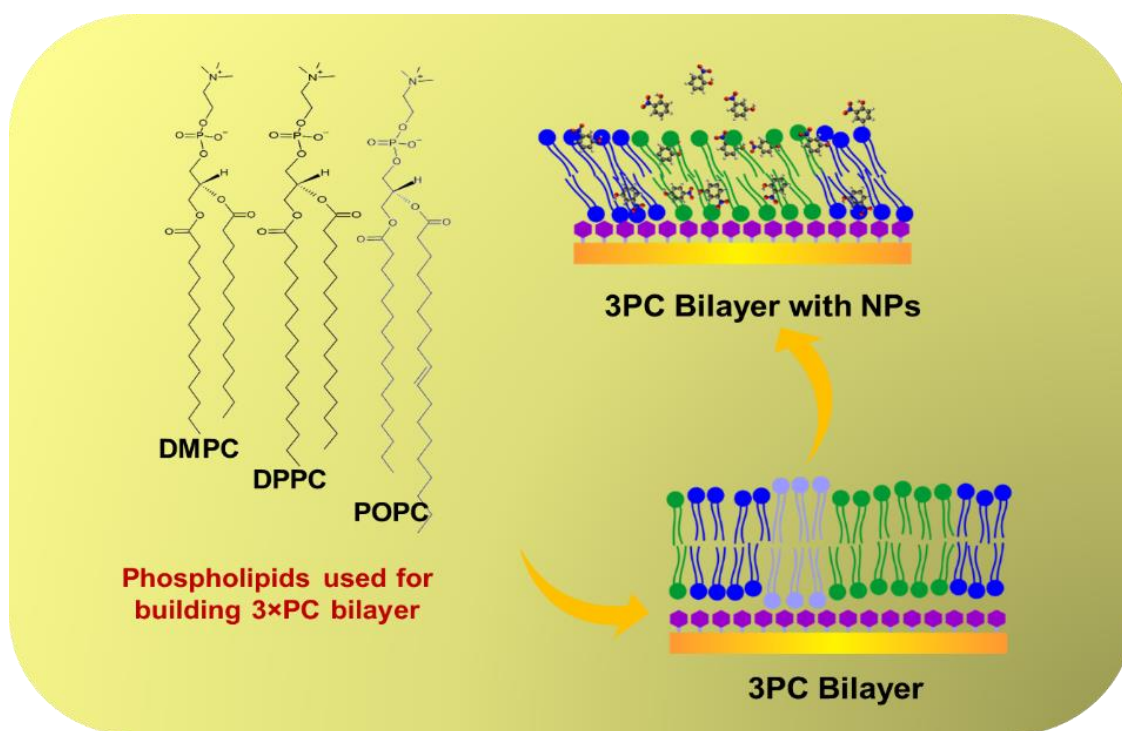


Figure 3.3.2. The composition of the 3 x PC (Phosphatidylcholines-based) model membrane used in the current study.

3.3.3- AFM Imaging of Model Eukaryotic Membrane Rearrangement following NP-Mixture Treatment

The AFM imaging revealed that the mixture of nitrophenols was active towards the 3 × PC membrane, thus confirming CV and EIS measurements in the study by Majewska et al.³⁰⁴ Figure 3.3.3 a and e shows the 3 × PC membrane before incubation in the equimolar NP-mixture solution. The image clearly indicates domains of different heights, indicating phase separation of phospholipids. The model membrane consisted of three kinds of phospholipids of different transition temperatures³¹⁶, i.e., 24°C, 41°C, and −2°C for DMPC, DPPC, and POPC, respectively. ³¹⁷ ³¹⁸ As a result, DMPC and DPPC phospholipids are in a gel phase, while POPC is in the liquid phase at room temperature (RT). The thickness of the 3 × PC bilayer was 6.0 ± 0.2 nm for the thicker domains, with 890 ± 110 pm average height differences between the thicker and thinner domains. This discrepancy in domain thickness is because of the different lengths of the acyl chains of the phospholipids used and the different phase states of the phospholipids at RT. DPPC was in

the fluid phase in which acyl chains are melted, thus forming the thinner domains. At the same time, DMPC and POPC were in the gel phase, where acyl chains are fully extended, thus forming thicker domains. The $3 \times$ PC bilayer became entirely disintegrated after 1-h incubation in a high concentration of the 2 mg mL^{-1} NP-mixture solution (Figure 3.3.3) which is tenfold more elevated than the concentration found in the atmosphere. [319-321](#)

To slow down the effectiveness of the NPs mixture interaction with the $3 \times$ PC membrane, the concentration of the NP-mixture was decreased. Figure 3.3.4 shows the AFM image of the $3 \times$ PC membrane before and after incubation in the $200\text{-}\mu\text{g mL}^{-1}$ NP-mixture solution at various times of exposure. The image is blurred because of rapid change in the liquidity of the membrane, but the individual pore-like structures in the bilayer are visible. It indicates that the NPs-mixture not only disrupted the bilayer but also made the bilayer less viscous during the initial activity.

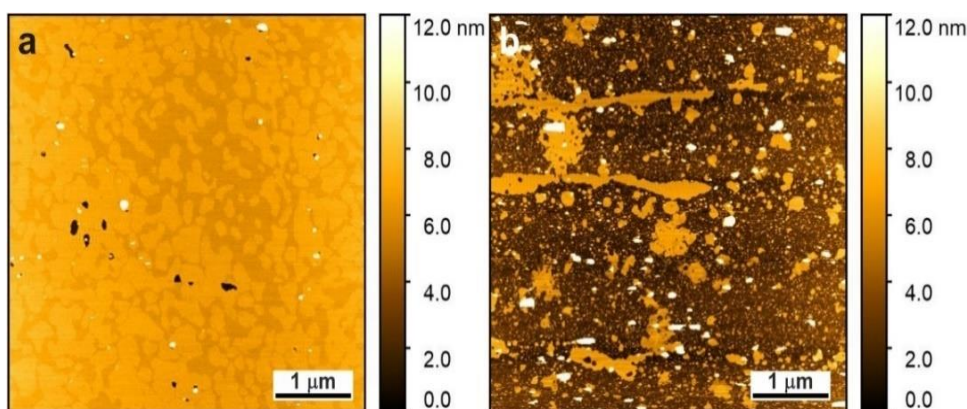


Figure 3.3.3. AFM images of the 3×PC bilayer deposited on mica, acquired in Milli-Q water (a) 0.01 M PBS (pH= 7.4) and (b) after 1 h incubation in the 2 mg mL⁻¹ NP-mixture.

Moreover, phospholipid domains, well visible for the 3 × PC membrane before incubation (**Figure 3.3.4 a & d**), disappeared after incubation in the NP-mixture solution (**Figure 3.3.4 b, c, e & f**), implying rapid reorganization or conformational changes of phospholipid molecules within the membrane. The similar behavior was observed for a variety of membrane-active peptides.[310](#)·[311](#)·[322](#)·[323](#) After 18 h (**Figure 3.3.4 e**) of incubation, phospholipid domains cover a smaller area. More uncovered areas of underlying mica are visible. After 24 h of incubation, more defects exposing mica are visible (**Figure 3.3.4 f**). It is difficult to find any phospholipid domains. The thickness of 3 × PC bilayer was initially determined to be 6.0 ± 0.2 nm, for the thicker domain, with 780 nm up to 1 nm height difference between the domains. After 24 h of incubation, the thickness of the bilayer was decreased to 3.5 ± 0.1 nm.

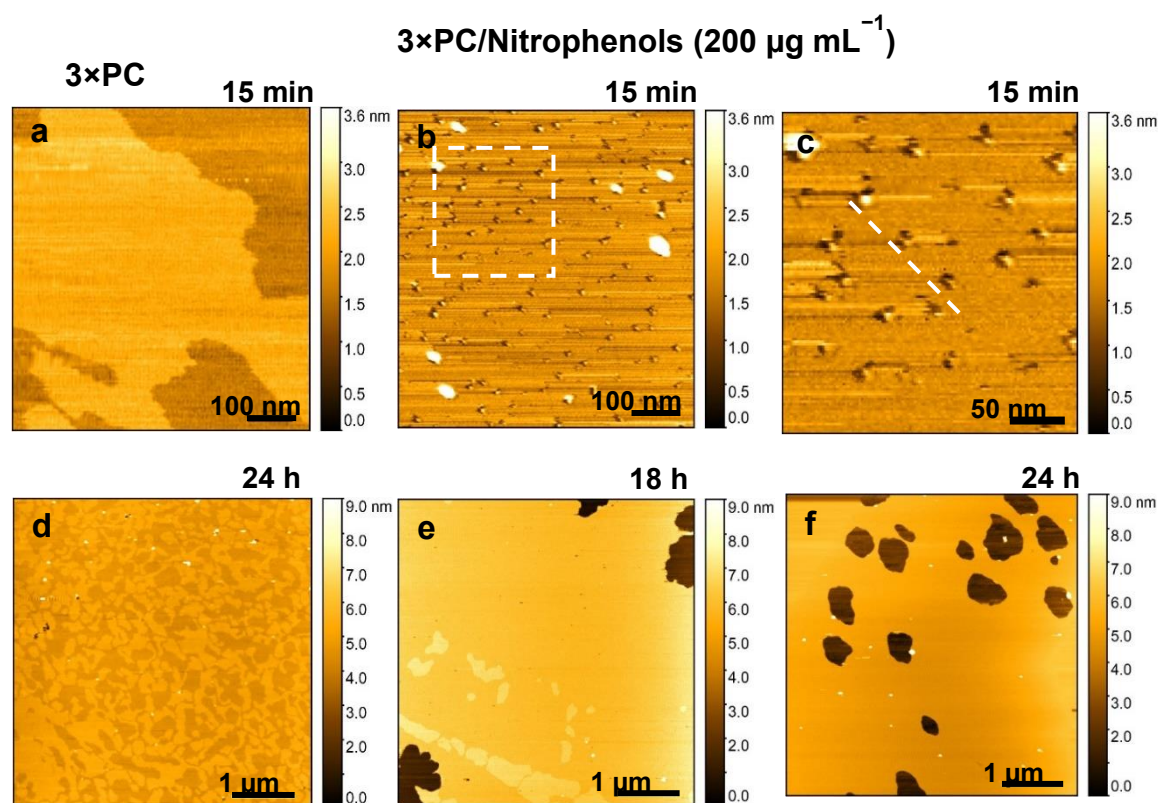


Figure 3.3.4. The AFM images of the $3 \times \text{PC}$ bilayer deposited on mica acquired in MilliQ water (a & d) in 0.01 M PBS (b & c) 15 min incubation in the 0.2 mg mL^{-1} NP-mixture (e) 18 h incubation in the 0.2 mg mL^{-1} NP-mixture and (f) 24 h incubation in the 0.2 mg mL^{-1} NP-mixture. The images in a, b & c were scanned at $1 \times 1 \mu\text{m}^2$ and the images in d, e & f were scanned at $5 \times 5 \mu\text{m}^2$ resolution.

Interestingly, the $3 \times \text{PC}$ bilayer was not disrupted immediately, but its thickness decreased to $3.5 \pm 0.1 \text{ nm}$ after 24 h of incubation in the $200\text{-}\mu\text{g mL}^{-1}$ NPs mixture solution (Figure 3.3.5). It may suggest that phospholipid acyl chains melt upon the interaction with the NPs, similar to the behaviour of the brain-like model membrane upon the interaction with amyloid beta.³¹³ Moreover, the NP-mixture activity is, most likely, concentration-dependent similarly to antimicrobial peptides.^{324, 325} Furthermore, this behaviour may suggest that NPs do not disintegrate the membrane at lower concentrations, but pass through it, changing its properties. This behavior would imply that nitrophenols can penetrate the biological cell and react with its interior.

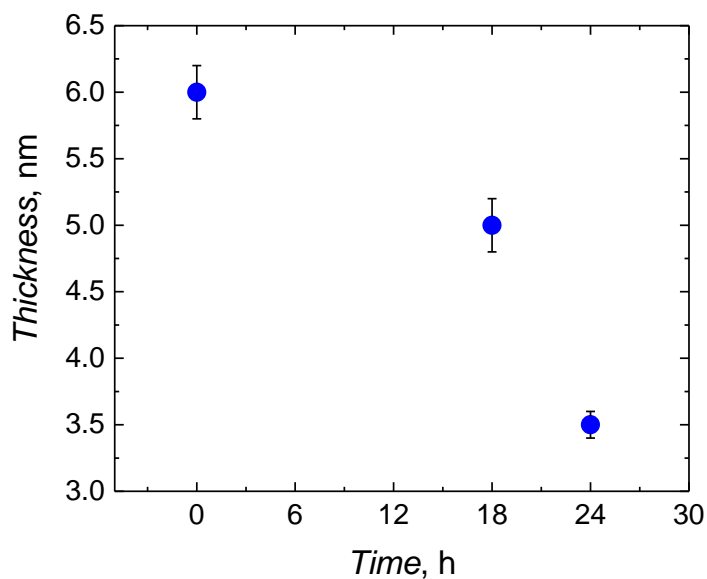


Figure 3.3.5. Change of the 3 × PC bilayer thickness after injection of 200 µg mL⁻¹ 3 × NP solution.

3.3.4- Phase-contrast Microscopy (PCM) Imaging of BEAS-2B and A549 cells Treated with NP-mixture

The cytotoxicity is observed as the change in a cellular shape from tapering elongated to round. These changes are because of the cellular cytoplasm disintegrates and the membrane collapse upon harmful activity. Moreover, 200 µg mL⁻¹ concentration exposure caused the treated cells to disintegrate completely, as observed in [Figure 3.3.6c and 3.3.6f](#). An increased number of disrupted cells with rounded morphology and disintegrated cell membranes was found after 48 h of exposure, as shown in [Figure 3.3.6f](#). These results suggest a time-dependent exposure effect on lung cells. They are in line with the previous study where the particulate matter (PM) of the wood smoke induces oxidative stress and cellular damage following exposure in A549 cells. [326](#)

[Figure 3.3.7](#) shows the BEAS-2B cell lines incubated in the 100 and 200 µg mL⁻¹ nitrophenols mixture solution for 24 h and 48 h. A significant decrease in the cell number is observed ([Figure 3.3.7 b, c, e, and f](#)), clearly indicating the cellular growth inhibition was induced following exposure to the nitrophenols mixture. The significant morphological changes were also visible, whereby cells appear more elongated in the control experiments ([Figure 3.3.7 a and d](#)) while rounder cells are observed in the treatment groups. The number of dead cells increases significantly after 48 h of incubation, as indicated by rounder morphology and cellular detachment in the treatment groups. Increased cell death and cell

membrane disruption were seen at $200 \mu\text{g mL}^{-1}$ when compared with $100 \mu\text{g mL}^{-1}$, indicating that increasing the concentration of aerosol induced increased cellular death. More round-shaped cells indicated the detachment of cells from the surface and the cellular death. Hence, there is an indication that the presence of the nitrophenols mixture induced cellular death through cell membrane damage in BEAS-2B and A549 cell models, which can be correlated with AFM and EIS data on the model eukaryotic-like cell membranes. The data correlates with air-pollutant $\text{PM}_{2.5}$ studies in BEAS-2B cells, whereby cellular stress and pro-inflammatory responses were observed following exposure. [327](#), [328](#)

The study revealed that increasing the concentration of NPs results in a substantial decrease in cellular viability and changes in cell morphology. At concentrations above $100 \mu\text{g mL}^{-1}$, both BEAS-2B and A549 cells undergo cellular death. The formation of membrane defects was observed for model eukaryotic-like cell membrane in the presence of NP-mixture, increasing permeation through the phospholipid bilayer composed of DMPC: DPPC: POPC (1:1:1 molar ratio). We observed rearrangement of phospholipid domains followed by the disappearance of some domains and the decrease of membrane area and thickness after 24 h exposure to $200 \mu\text{g mL}^{-1}$ NPs-mixture. In contrast, no such effects were observed for single DMPC phospholipid model membrane, suggesting that the nitrophenols mixture interacts preferentially with POPC and DPPC phospholipids, which are representative for human lung cells. Since no stable transmembrane channels were formed, only short-living pore-like structures, it implies that the interaction between nitrophenols and phospholipids occurs in the acyl chains region of the phospholipid bilayer and/or part of phospholipids are extracted from the phospholipid matrix. These results are supported by the selectivity of interacting nitrophenols with specific phospholipids, which differed only in the acyl chain lengths and saturation. At a high concentration of 2 mg mL^{-1} , exceeding tenfold levels found in the atmosphere, the model biological membrane is entirely disrupted by removing phospholipids from the substrate. The latter supports the mechanism of nitrophenols activity by disintegrating bilayer structure through phospholipids extraction. Thus, it implies their role in substantial cellular damage in the lungs when exposed to high concentrations of BBA.

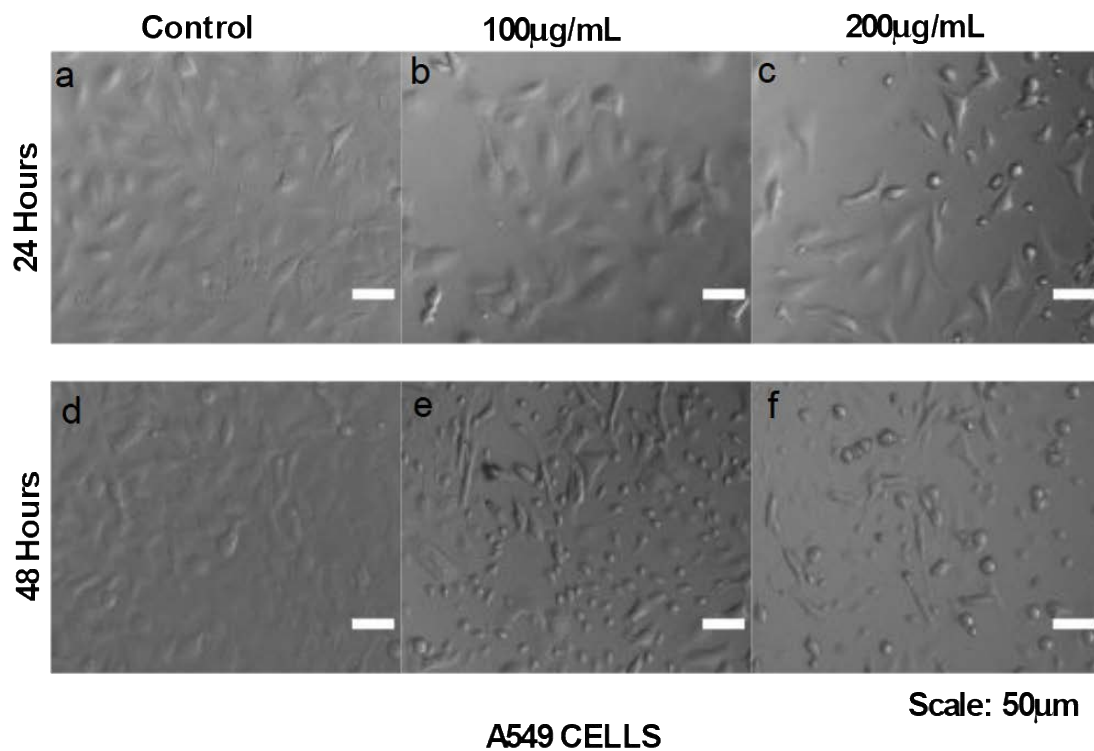


Figure 3.3.6. Phase-contrast microscopy images of A549 cell lines incubated for (a-c) 24 h and (d-f) 48 h in (a and d) the $0\text{-}\mu\text{g mL}^{-1}$ (control cells), (b and e) $100\ \mu\text{g mL}^{-1}$, (c and f) $200\ \mu\text{g mL}^{-1}$ NPs mixture solution. Images scale bars refer to $50\ \mu\text{m}$ distance.

These observations indicate that airborne NPs induce substantial changes in the cell membranes, which facilitate these pollutants to penetrate lung cells and develop lung-associated pathophysiology. A detailed mechanism of the intracellular changes following exposure is covered in further sections, together with the study of its environmental prevalence.

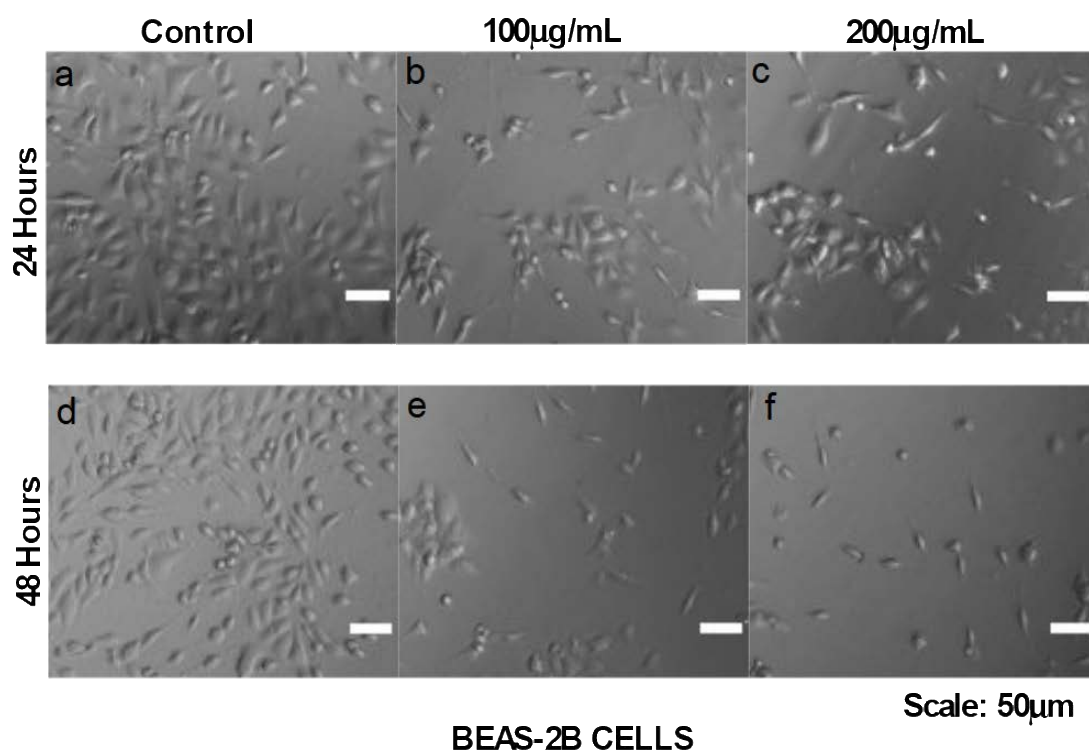


Figure 3.3.7. Phase-contrast microscopy images of BEAS-2B cell lines incubated for (a-c) 24 h and (d-f) 48 h in (a and d) the $0\text{-}\mu\text{g mL}^{-1}$ (control cells), (b and e) $100\ \mu\text{g mL}^{-1}$, (c and f) $200\ \mu\text{g mL}^{-1}$ NPs mixture solution. Images scale bars refer to $50\ \mu\text{m}$ distance.

3.3.5- Qualitative Analysis of Mono-NPs in Ambient PM_{2.5} and Smog Chamber-Generated SOA

The second part of the study provides evidence of mono-NPs in the field and lab-generated aerosol particle samples and their toxicological profiling in terms of cytotoxicity, OS, changes in the $\Delta\Psi_m$, and apoptosis. While the putative NPs can be found in field samples, they are most readily isolated and identified by laboratory experiments. In this part of the study, we report the detection of mono-NPs from the photooxidation of several aromatic hydrocarbons (i.e., toluene, benzene) in the EPA smog chamber under a wide range of conditions (relative humidity, acidic seed aerosol, and NO_x). We particularly emphasized the atmospheric relevance of NPs, especially 4NP, since it was readily detected in ambient PM_{2.5} samples and from our lab-generated SOA samples.

A subset of the experiments, representative of a large group conducted during the past 20 years at the US EPA, is summarized in [Table 2.3](#). It shows the initial reactant conditions (i.e., initial [hydrocarbon (aromatic)] and [NO_x]), SOA mass concentration (μg m⁻³) and SOA mass (mg) collected on filters) used for generating aromatic-derived SOA for GC-MS analysis of NPs. For selected experiments, the gas-phase chemical composition was also analysed. For completeness, additional experiments were analysed (i.e., *o*-xylene, *m*-xylene, 1,3,5-trimethylbenzene, 1,2,4-trimethylbenzene, ethylbenzene, naphthalene, 1-methylnaphthalene, 2-methylnaphthalene, and benzyl alcohol) in which NPs of interest in this study were not detected, although other NPs were detected. The initial reactant conditions and SOA collected in those experiments (not shown) are at the same order of magnitude as those reported in [Table 2.3](#).

NPs were analysed as silylated derivatives by a capillary GC-MS using the analytical technique previously reported [329](#), and their identities were confirmed using authentic standards. For example, [Figure 3.3.8](#) displays the total ion and extracted ion chromatograms (TICs and EICs, respectively) in the methane-chemical ionization mode (CI) associated with the gas phase and SOA particles generated from the oxidation of toluene in the presence of NO_x. [Figure 3.3.8](#) (middle and bottom panels) uses the selected ion (or EICs) at a mass-to-charge ratio (*m/z*) 212 to best illustrate the presence of mono-NPs. The mass spectra associated with 4NP are shown in [Figure 3.3.9](#) in EI mode (70 eV) (top), and CI mode (middle panel shows the authentic standard; and the bottom panel shows 4NP in toluene-derived SOA). 2NP, 3NP, and 4NP present similar mass spectra, but they elute at different GC-MS retention times. Note that the chromatographic peak associated with 4NP co-elutes with the internal standard peak of ketopinic acid (KPA); therefore, EICs at *m/z* 212, 196, and 182 ([Figure 3.3.9](#)) were used for positive identification of NPs in the chamber experiments, and particularly in the field studies. This is clearly illustrated in [Figure 3.3.8](#) (middle and bottom panels) for which KPA was not used. 4NP was observed in SOA generated from the laboratory oxidations of toluene, benzene, and *m*-cresol in the presence of NO_x, and in the gas-phase associated with toluene oxidation ([Table 2.3](#)). 2NP was only observed in toluene-derived SOA ([Figure 3.3.8](#)), and 3NP was not observed in any SOA system (including in the gas phase) re-examined here.

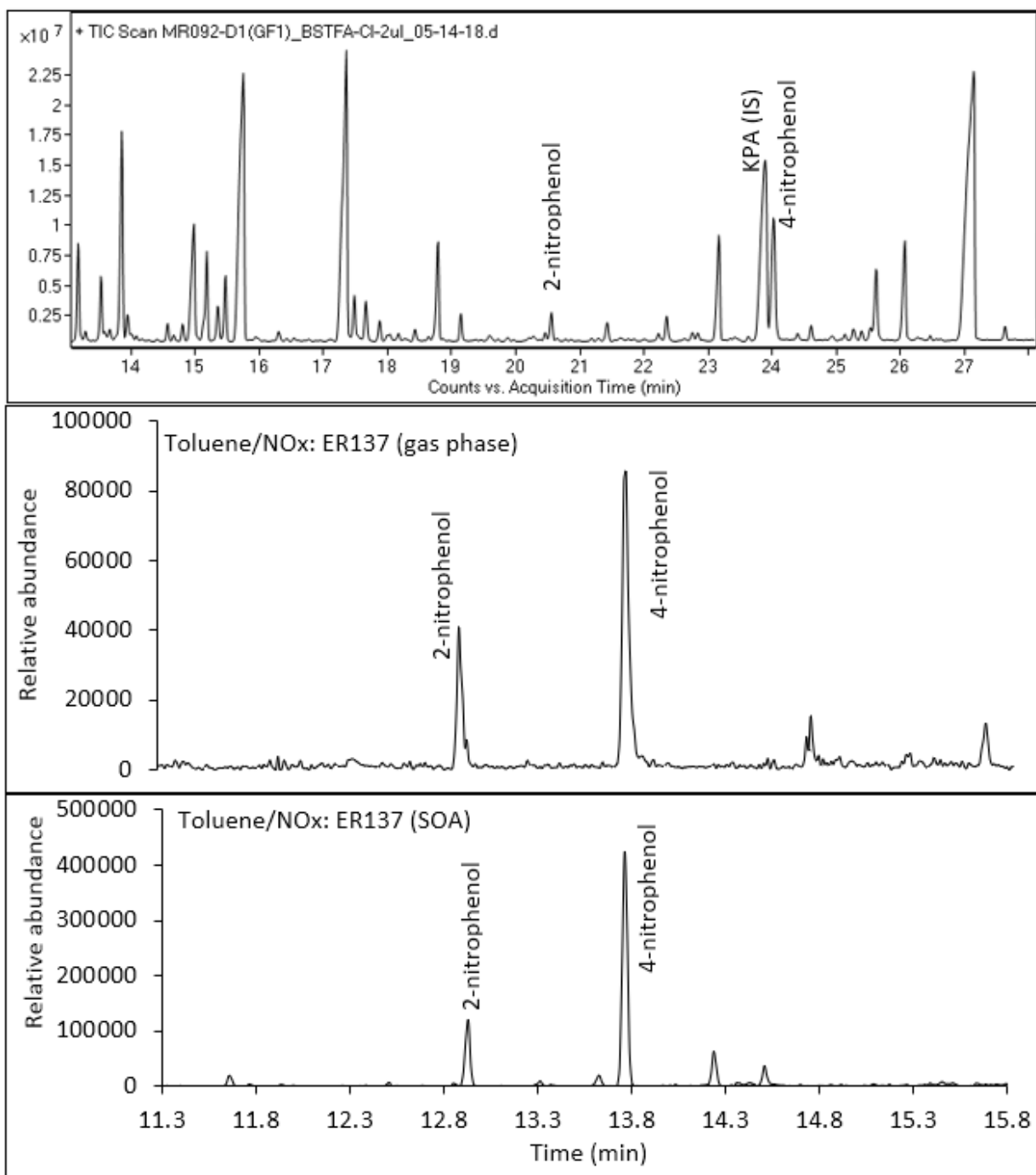


Figure 3.3.8. Total ion current TIC (top panel) and Extracted ion current EICs at m/z 212 (middle and bottom panels) GC-MS chromatograms were obtained for the silylated gas-phase products and SOA particles. The latter was generated from the photooxidation of toluene in the presence of NO_x . Top panel: TIC associated with gas-phase components from experiment MR092 showing co-elution of internal standard (IS) KPA and 4NP. EICs associated with ER137 (middle: gas-phase only; bottom: SOA), for which KPA was not used. These chamber samples were analysed at the time of collection, and the resulting chromatograms were re-analysed for the targeted NPs. Retention times may differ due to differing chromatographic conditions at the time of collection

Additionally, a similar qualitative analysis was conducted for ambient PM_{2.5} collected between 2003 and 2010 by our group at several sampling sites in the U.S. These previously collected field samples were analysed at the time of collection using the GC-MS method used for chamber samples discussed above, and the resulting chromatograms were re-analysed for the targeted NPs. **Table 3.3.1** summarizes results associated with these field studies. 4NP was the only mono-NP observed in these ambient PM_{2.5} samples, and only from the selected field sites outlined in **Table 3.3.1**. It was observed in the wintertime and in some urban areas in the summertime, consistent with its primary and/or secondary (or SOA) origin, as shown from the smog chamber experimental data.

Table 3.3.1. Ambient PM_{2.5} samples were analysed qualitatively in this study for mono-NPs. Only 4NP was detected, whereas 2NP and 3NP were not.

Date	Study Location	Site type/ landscape	4NP detected
Mar–Sep, 2003	Research Triangle Park, NC	Semi-rural	No
Mar–Sep, 2004	LADCO: Bondville, IL	Rural	Yes
Mar–Sep, 2004	LADCO: Cincinnati, OH	Urban	No
Mar–Sep, 2004	LADCO: Detroit, M	Urban	No
Mar–Sep, 2004	LADCO: E. St. Louis, IL	Industrial	No
Mar–Sep, 2004	LADCO: Northbrook, IL	Suburban	Yes
May–Aug, 2005	SEARCH: Atlanta, GA	Urban; residential	No
May–Aug, 2005	SEARCH: Birmingham, AL	Industrial; residential	No
May–Aug, 2005	SEARCH: Centreville, AL	Rural	No
May–Aug, 2005	SEARCH: Pensacola, FL	Suburban	No
Aug, 2005	SOAR: Riverside, CA	Urban	Yes
Mar–Sep, 2006	Research Triangle Park, NC	Semi-rural	No
Jul–Aug 2009 (summer)	CMAQS: Cleveland, OH	Industrial	No
Jul–Aug 2009 (summer)	CMAQS: Medina, OH	Rural	No
Feb 2010 (winter)	CMAQS: Cleveland, OH	Industrial	Yes
Feb 2010 (winter)	CMAQS: Medina, OH	Rural	Yes
May–Jun, 2010	CalNex: Bakersfield, CA	Urban; industrial	Yes
May–Jun, 2010	CalNex: Pasadena, CA	Urban; industrial	Yes

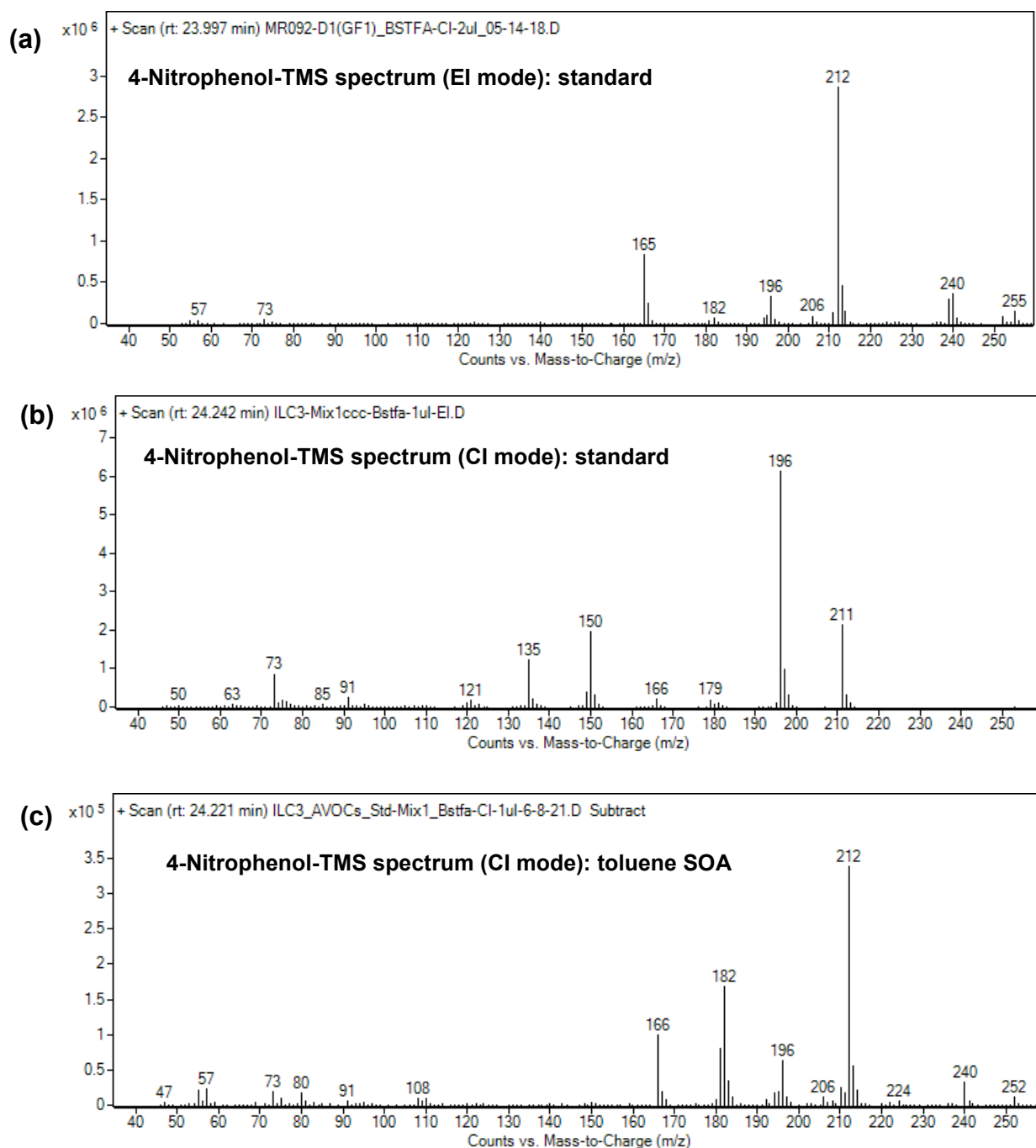


Figure 3.3.9: Mass spectra in (a) EI (70 EV, top panel) and (b) CI (middle panel) mode acquired for 4NP standard as trimethylsilyl (TMS) derivative. (c) MR092 smog chamber-generated SOA containing 4NP is shown in the bottom panel.

Table 3.3.2. Concentration of 2-nitrophenol (2NP) and 4-nitrophenol (4NP) in atmospheric compartments, including gas phase ($\mu\text{g m}^{-3}$) and aqueous phase ($\mu\text{g dm}^{-3}$).

Place	Phase	2NP			4NP			Year	Ref.
		Min	Max	Av.	Min	Max	Av.		
Air									
Milano	Gas						0.3		153 , 330
Milano, Center	Gas	0.130	0.177	0.139	0.042	0.163	0.085	Summer 1999	331
Milano, tunnel	Gas	0.232	1.139	0.641	0.387	0.993	0.642	Summer 1999	ibid
Lombardian, urban	Gas				0.094	0.163	0.118	Winter 1999	ibid
semi-rural	Gas						0.087		ibid
rural							0.042		ibid
Rome, city park	Gas			0.01			0.004	Spring 2003	160
Santiago, university	Gas	0.008	0.106	0.114	0.040	1.40	462	Sum 2010, 2011	332
Iowa city	Gas						0.001	2015	156
Clouds									
Great Dunn Fell	Gas	0.001	0.008		0.0001	0.02		May 1976	153 , 333
	Aqu	0.024	0.2		0.007	2.9			ibid
	Aqu			0.2			2.2	April 1993	ibid
Mount Brocken	Gas	0.01	0.50					1994	ibid
	Aqu			0.03			21		ibid
Vosges mountains	Aqu				1.66	16.27	5.46	1991	153 , 334
Rain									
Portland, OR	Gas	0.011	0.039	0.025					153 , 335
	Aqu	0.026	0.130	0.059					
Dübendorf, CH	Gas			0.35				1985	153 , 336
	Aqu			0.60					
Vosges mountains	Aqu				1.11	7.57	2.95	1991	153 , 334
Hannover	Aqu	0.03	0.68	0.18	1.2	19.5	5.7	1990	153 , 337
Western Germany	Aqu	0.1	1.4		2	16			153 , 338
Frankfurt	Aqu						24		ibid
Western Germany	Aqu				0.1	1.2			338
Lombardia	Aqu				12	29			331
Roskilde	Aqu				1	11.9	3.5		339
Oure	Aqu				0.1	5.4	1.2		ibid
Fog									
Ochswkopf Mt.	Aqu				0.0004	0.002	0.001	1988	153 , 340
Bayreuth Uni	Aqu				0.0007	0.0012	0.001	1988	ibid

Dew									
Santiago Uni	Aqu	Nd	237	25	Nd	629	71	Summer 2011	332
Snow									
Mount Melbourne (Antarctic)	Aqu			< LOD	< LOD	0.013	0.008		153 341

Table 3.3.3. Concentrations of 3-nitrophenol (3NP) in various environmental compartments, including the gas/particle phases ($\mu\text{g m}^{-3}$) and aqueous phase ($\mu\text{g dm}^{-3}$).

Place	Phase	3NP			Year	Ref.
		Min	Max	Av.		
Santiago Uni	Dew (aqu)	Nd	147	8	Summer 2011	332
Strasbourg, urban	Air + PM	Nd	0.003	0.0001		342
Schilt Heim, suburban	Air + PM	Nd	0.002	0.0002		
Erstein, rural	Air + PM	Nd	0.00005	0.000001		
Elsnig, ground water, lower level	Aqu			55		153 343

Table 3.3.4. Concentrations of 2NP and 4NP in ambient particulate matter ($\mu\text{g m}^{-3}$).

Place	Phase	2NP			4NP			Year	Ref.
		Min	Max	Av.	Min	Max	Av.		
NRI Kana-gawa		3.4 ^a	3.9 ^a		5.1 ^a	42 ^a	14.48 ^a		340 344
Hong Kong urban	PM _{2.5}				0	0.009	0.001		169
Detling, UK	PM _{0.13}						0.00002		169 345
Ljubljana, urban	PM ₁₀				0.0005	0.004	0.002	Winter 2010-2011	346
					0.0001	0.002	0.0002	Summer 2010-2011	ibid
Hamilton, Ontario	PM ₁				0.0002	0.002	0.0007	2000	347
Simcoe, Ontario	PM ₁				< LOD	0.002	0.0004	2000	ibid
Toronto, tunnel	PM ₁				0.003	0.025	0.009	2000	ibid
Iowa City	PM _{2.5}				0.0006	0.0005		2015	156

Mainz	PM ₁₀				0.0002	0.001	0.0008		348
Thessaloniki	PM ₁₀				0.0008	0.004	0.0026		ibid
Shanghai					0.151	0.768	0.304		349
Birmingham	PM _{2.5}	0.0001	0.0016		0.0001	0.0004		2007-2008	350
Melitz				< LOD	0.0008	0.0010		24 Jan 2012	351
					0.0001	0.0001		30 Aug 2012	ibid
					0.0005	0.0006		10 Oct 2012	ibid
Mainz	PM ₁₀	< LOD	0.009	0.002	< LOD	0.010	0.002	Summer 2007	352
	TSP	< LOD	0.009	0.002	< LOD	0.013	0.004	“	ibid
Rome, city park	PM ₅			0.0035			0.0178	Spring 2003	160
Paris		< 0.0001	10.863	0.0527	< 0.0001	0.0279	0.0069	2014-2015	353
Diesel	PM _{2.5}			Nd			0.004		354
Marine Diesel	PM _{2.5}			Nd			0.011		ibid
NIST 1649b urban	PM			< LOD			0.0024		ibid
NIST 1650b Diesel	PM			< LOD			0.072		ibid
Kladno, winter	PM ₁₀						0.00554		182
	PM _{2.5}						0.00301		ibid
Ostrava, winter	PM ₁₀						0.00906		ibid
	PM _{2.5}						0.00535		ibid
Ostrava, summer	PM ₁₀						0.00112		ibid
	PM _{2.5}						0.00085		ibid

^a mg g⁻¹

Table 3.3.5. Concentration of 2NP and 4NP in aquatic systems ($\mu\text{g dm}^{-3}$, aqueous phase).

Place	2NP			4NP			Ref.
	Min	Max	Av.	Min	Max	Av.	
Berlin	0.04	0.34		0.04	0.60		153 · 355
Antarctic lakes	< LOD	0.428	0.087	0.011	0.070	0.034	153 · 341
Elsnig, groundwater, upper level						15	153 · 343
Ibid, lower level						88	

The measured concentrations of these NPs in atmospheric samples varied significantly ([Tables 3.3.2- 3.3.5](#)), and our study provides evidence that 4NP is the most abundant form of mono-NPs. 4NP can form in $\text{PM}_{2.5}$ (or SOA, which is a major $\text{PM}_{2.5}$ component) either through the photochemical oxidations of toluene, benzene, and cresol emissions in the presence of NO_x . In ambient air, NP concentrations ranged between $0.008 - 1.139 \mu\text{g m}^{-3}$ for 2NP, and $0.040 - 1.400 \mu\text{g m}^{-3}$ for 4NP [331](#)·[332](#)·[356](#). Previously analysed ambient PM samples contained $0.0001 - 10.86 \mu\text{g m}^{-3}$ of 2NP [353](#), and $0.0002 - 0.768 \mu\text{g m}^{-3}$ of 4NP [348](#)·[349](#). Rainwater samples were measured to contain $0.026 - 1.4 \mu\text{g dm}^{-3}$ of 2NP [153](#)·[335](#)·[338](#), and $0.1 - 19.5 \mu\text{g dm}^{-3}$ of 4NP. [153](#)·[335](#)·[338](#) In cloud water, concentrations ranged between $0.024 - 0.200 \mu\text{g dm}^{-3}$ for 2NP [153](#)·[333](#), and $1.66 - 16.27 \mu\text{g dm}^{-3}$ for 4NP. [153](#)·[334](#) Exceptionally high concentrations of NPs were measured in the dew at the university campus in Santiago de Chile: up to $237 \mu\text{g dm}^{-3}$ of 2NP and $629 \mu\text{g dm}^{-3}$ of 4NP. [332](#) On the other hand, fog water contained only low amounts of 4NP: $0.0004 - 0.0012 \mu\text{g dm}^{-3}$.[153](#)·[340](#) 3NP was rarely detected: $0 - 147 \mu\text{g dm}^{-3}$ in dew in Santiago de Chile [332](#), and $0 - 0.003 \mu\text{g m}^{-3}$ total in air and PM at various European sites.[153](#)·[343](#) These data are consistent with our findings, where 4NP was the most atmospherically prevalent of the mono-NPs examined in this study.

3.3.6- Inhibitory Concentration-50 (IC₅₀) of NP

The BEAS-2B and A549 cells were treated with increasing concentrations (i.e., $0.01 - 200 \mu\text{g mL}^{-1}$) of 2NP, 3NP, and 4NP and their equimolar mixture. Changes in cellular proliferation percentage were calculated as a function of untreated control cells at 24 and 48 h exposure. As shown in [Figure 3.3.10](#), dose-response curves were generated to compute the IC₅₀ values for each of the treatment types in the two lung cell lines.

These data show that IC₅₀ values were lower in BEAS-2B cell lines (Figure 3.3.10 a, c, e, and g) when compared with A549 cell lines (Figure 3.3.10 b, d, f, and h). As shown in Figure 3.3.10 e, the lowest IC₅₀ value was found in 4NP-treated BEAS-2B cells (93 and 43 μg mL⁻¹ at 24 and 48 h exposure, respectively). This was followed by IC₅₀ values for 3NP (123 μg and 40 μg mL⁻¹ at 24 and 48 h exposure, respectively, Figure 3.3.10 c) and the NP mixtures (107 and 78 μg mL⁻¹ at 24 h and 48 h exposure, respectively, Figure 3.3.10 g). The highest IC₅₀ values were observed in the 2NP-treated BEAS-2B cells (397 and 31.93 mg mL⁻¹ at 24 h and 48 h exposure, respectively, Figure 3.3.10 a).

The IC₅₀ values in A549 cells were higher than BEAS-2B cells with the same treatment type. The inhibition curve was also different from that observed in BEAS-2B cells, and a significant decrease in proliferation rate was observed only after 48 h of treatment. The IC₅₀ value in 2NP-treated A549 cells was estimated to be $\sim 1.8 \times 10^8$ μg mL⁻¹ at 24 h and $\sim 6.3 \times 10^8$ μg mL⁻¹ at 48 h, as shown in Figure 3.3.10 b. 3NP-treated A549 cells exhibited an IC₅₀ value of 251 and 109 μg mL⁻¹ at 24 and 48 h exposure, respectively (Figure 3.3.10 d). The 4NP-treated A549 cells showed the IC₅₀ value of $\sim 3.5 \times 10^4$ μg mL⁻¹ at 24 h exposure and 552 μg mL⁻¹ after 48 h exposure (Figure 3.3.10 f). Finally, the NP mixture exhibited an IC₅₀ value of 223 and 122 μg mL⁻¹ at 24 and 48 h exposure, respectively (Figure 3.3.10 h).

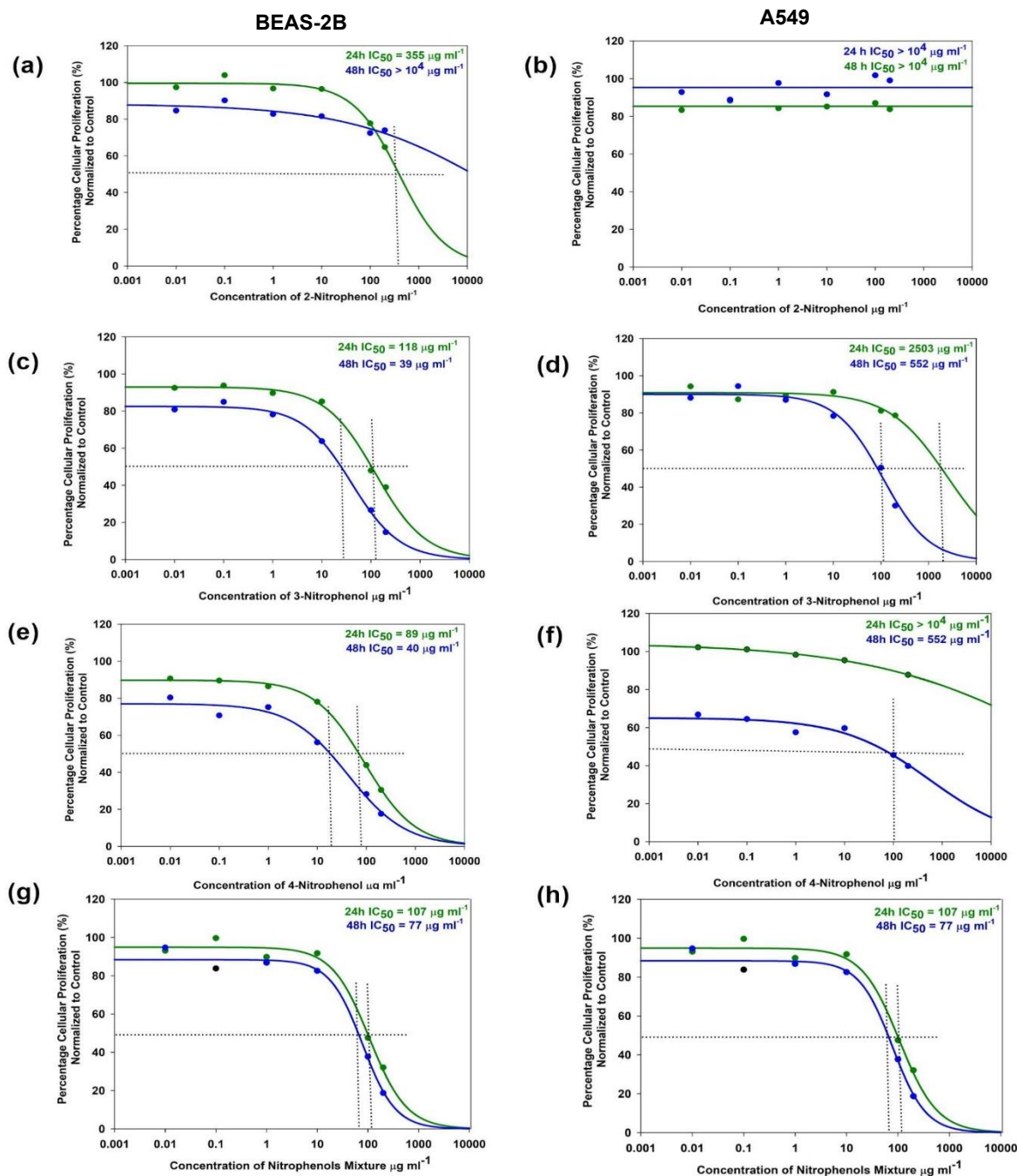


Figure 3.3.10. Percentage of cellular proliferation for the cells, as calculated through the MTT assay. The cells were treated with increasing concentrations of each of the NPs and their equimolar mixture (i.e., 0.01 - 200 $\mu\text{g mL}^{-1}$, and at 24 and 48 h exposures). The values were then fitted in the dose-response curve of the inhibitor versus normalized response to calculate the inhibitory concentration-50 (IC_{50}) values of various treatment types in the BEAS-2B and A549 cells. The graphs show normalized dose-response curves of the 2NP treatment in (a) BEAS-2B cells and (b) A549 cells; 3NP treatment in (c) BEAS-2B cells and (d) A549 cells; 4NP treatment in (e) BEAS-2B cells and (f) A549 cells; and NPs mixture treatment in (g) BEAS-2B cells and (h) A549 cells. Individual IC_{50} values of 2NP, 3NP, and 4NP, as well as their equimolar mixture, are shown for both A549 and BEAS-2B cell lines at 24 and 48 h exposures, calculated through the best-fit curve with 95% confidence interval. The dotted line represents the 50% inhibition point

The calculated IC₅₀ values of the NPs in two cell lines reported in the present study could be used to estimate the inhalation safety index. In section 3.1, we calculated the 200 µg mL⁻¹ concentration corresponds to 62.5 µg cm⁻² of cellular exposure, and thus, a similar approach was adopted herein to estimate NP exposures to cells (summarized in [Table 3.3.6](#)).⁷³ Furthermore, the MPPD model by Gangwal et al.²⁴² was used to estimate the lung uptake of ultrafine particles (≤ 100nm diameter). We predicted the uptake ranges from 0.006 to 0.02 µg cm⁻² to a particle concentration of 100 mg m⁻³ of these particle sizes at a 24 h exposure time. The estimated lung uptake was assumed to be 7.5 × 10⁻⁴ µg cm⁻² in the particles “hot spot” regions.⁷³ Using the same approach, we used the IC₅₀ values of each NP in BEAS-2B and A549 cell lines to estimate the inhibition response achieved in the number of years of continuous exposure, assuming negligible lung clearance rates ([Table 3.3.6](#)). IC₅₀ values were estimated to be lower in BEAS-2B cell lines when compared with A549 cells, implying BEAS-2B cells were more sensitive to NP exposures, a phenomenon found consistent with previous studies.^{73; 74} The continuous atmospheric exposure to the IC₅₀-equivalent concentration of 3NP and 4NP in BEAS-2B cells may result in similar lung inhibition effect in ~ 47 and 51 years, respectively.²⁴³ Exposure to other NPs required continuous exposure exceeding the lifetime; hence, we assume the atmospheric particulate concentrations of 2NP and the NPs mixture to be relatively safe. However, the NPs may exhibit different toxicological profiles following exposure to more chemically complex ambient PM_{2.5}, with varying atmospheric composition and concentration. In our study with individual chemical markers of α-pinene SOA and whole α-pinene ozonolysis SOA mixture,⁷³ we determined the SOA load was more toxic than its single components. Therefore, a further study on assessing the overall toxicity of real PM_{2.5} mixtures with NP tracers is called for.

Table 3.3.6. Exposure effects achieved in years in the two lung cell lines following 24 h and 48 h of exposure to the value corresponding to the IC₅₀ values of each nitrophenol and their equimolar mixture.

IC-50 Values Exposure Concentration		BEAS-2B		A549	
		24 Hours	48 Hours	24 Hours	48 Hours
2NP	Cell Exposure Concentration	397 µg mL ⁻¹ 124 µg cm ⁻²	31927 µg mL ⁻¹ 125 µg cm ⁻²	1.8 x 10 ⁸ µg mL ⁻¹ 5.6 x 10 ⁷ µg cm ⁻²	6.3 x 10 ⁸ µg mL ⁻¹ 2.0 x 10 ⁸ µg cm ⁻²
	Exposure effect Time	~ 452 years	~ 3600 years	~ 2.0 x 10 ⁸ years	~ 7.3 x 10 ⁸ years
3NP	Cell Exposure Concentration	123 µg mL ⁻¹ 40 µg cm ⁻²	40 µg mL ⁻¹ 13 µg cm ⁻²	2505 µg mL ⁻¹ 814 µg cm ⁻²	109 µg mL ⁻¹ 35 µg cm ⁻²
	Exposure effect Time	~ 146 years	~ 47 years	~ 2900 years	~ 128 years
4NP	Cell Exposure Concentration	93 µg mL ⁻¹ 30 µg cm ⁻²	43 µg mL ⁻¹ 13 µg cm ⁻²	3.5 x 10 ⁵ µg mL ⁻¹ ~1.1 x 10 ⁴ µg cm ⁻²	552 µg mL ⁻¹ 170 µg cm ⁻²
	Exposure effect Time	~ 110 years	~ 51 years	~ 41,000 years	~ 655 years
NP Mixtures	Cell Exposure Concentration	107 µg mL ⁻¹ 35 µg cm ⁻²	78 µg mL ⁻¹ 25 µg cm ⁻²	223 µg mL ⁻¹ 72 µg cm ⁻²	122 µg mL ⁻¹ 40 µg cm ⁻²
	Exposure effect Time	~ 127 years	~ 93 years	~ 265 years	~ 145 years

3.3.7- Analysis of Cytotoxicity in the Nitrophenols Treated Cells

The BEAS-2B and A549 cells were analyzed for cytotoxicity using the enzymatic marker of cellular death LDH, which is released by dead cells. [357](#) Figures 3.3.11 a, c, e, and g show the LDH release percentage bar-graph of the BEAS-2B cells treated with 0.1 - 200 µg mL⁻¹ of three individual NPs and their equimolar mixture, while Figures 3.3.11 b, d, f, and h show the LDH release percentage graphs in 0.1 - 200 µg mL⁻¹ of the NP-treated

A549 cells relative to the untreated control cells. The results depict how increasing exposure time enhances the percentage of cellular death in each of the treatment types. The 2NP, 3NP and 4NP treatments exhibited 10-30% increases in LDH release when compared with untreated controls using BEAS-2B cells. The NPs mixture treatment resulted in ~ 30-40% increase in LDH release in BEAS-2B cells, implying that the decrease in the percentage of cellular proliferation is attributed to cellular death and not inhibition.[358](#)

3NP-treated A549 cells resulted in a 30-40% increase in LDH release, as shown in [Figure 3.3.11 d](#). The treatment of these cells with 2NP resulted in an 18% increase in LDH release at 24 h exposure, while LDH release decreased to 10% at 48 h exposure ([Figure 3.3.11 b](#)). 4NP and the NPs mixture treatment at 200 $\mu\text{g mL}^{-1}$ resulted in a 10% increase in LDH release at 24 h, which increased to ~25% at 48 h exposure.

The increase in cellular death following exposure to the NPs was further confirmed through live/dead stain imaging using Calcein-AM (stains live cells only) and propidium iodide (PI, stains the nuclei of the dead cells) using 200 $\mu\text{g mL}^{-1}$ of exposure concentration. [Figure 3.3.12](#) shows the fluorescent microscopy micrographs of BEAS-2B cells treated with NPs, while [Figure 3.3.13](#) shows the micrographs of A549 treated cells. The BEAS-2B cells treated with 2NP exhibited only a slightly increased staining in the PI stain at 48 h exposure, compared with the untreated control, with few changes in Calcein-AM staining. As observed with the LDH assay, the number of dead cells increased at 48 h exposure of the BEAS-2B cells to 3NP. The cells treated with 4NP exhibited cellular growth inhibition followed by cellular death at 24 and 48 h of exposure, as can be seen by the lower number of cells found in the Calcein-AM channel compared with the untreated control at both exposure times. The slight increase in PI-stained cellular nuclei suggests cellular arrest, [359](#), followed by the cytotoxic response after the BEAS-2B cells with 4NP. The NPs mixture exhibited increased cellular death at 24 h exposure, as seen by the increased number of PI+ cells; the cellular inhibition followed, which allowed the smaller number of cells to be present with Calcein staining and the high number of cellular populations undergoing PI+ staining at 48 h exposure.

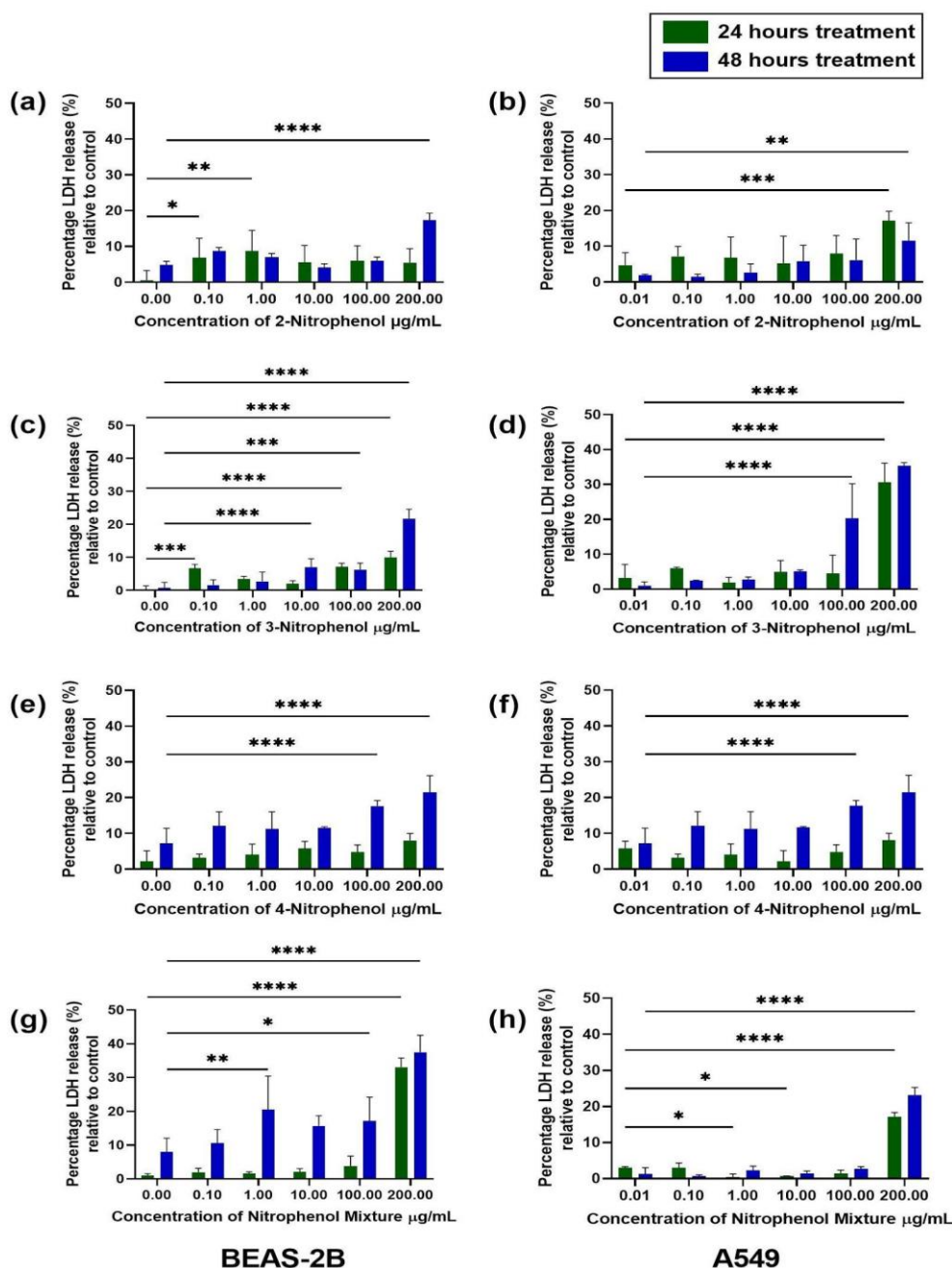


Figure 3.3.11. Percentage of cellular death as calculated through the LDH assay. LDH release was determined in both cell lines after exposure to increasing concentrations (0 – 200 $\mu\text{g mL}^{-1}$) of the three individual NPs and their equimolar mixture. (a) Percentage of BEAS-2B cell death in the four treatment types (normalized to untreated controls) at 24 and 48 h exposure, which shows increases in cellular death with longer exposure time. Note that the NPs mixture exhibited the highest percentage of cellular death (~30-40%) in all the treatment groups. (b) Percentage of A549 cell death determined by the LDH assay for the four treatment types after exposure to increasing concentration (0 – 200 $\mu\text{g mL}^{-1}$) to the NPs. The difference in the percentage of LDH release when compared with untreated (control) cells following 24 and 48 h exposure was statistically analysed through a two-way ANOVA, followed by Sidak's multiple comparison test. The p -value of <0.5 was considered statistically significant where **** corresponds to a p -value <0.0001 as depicted in graphs in (a-h).

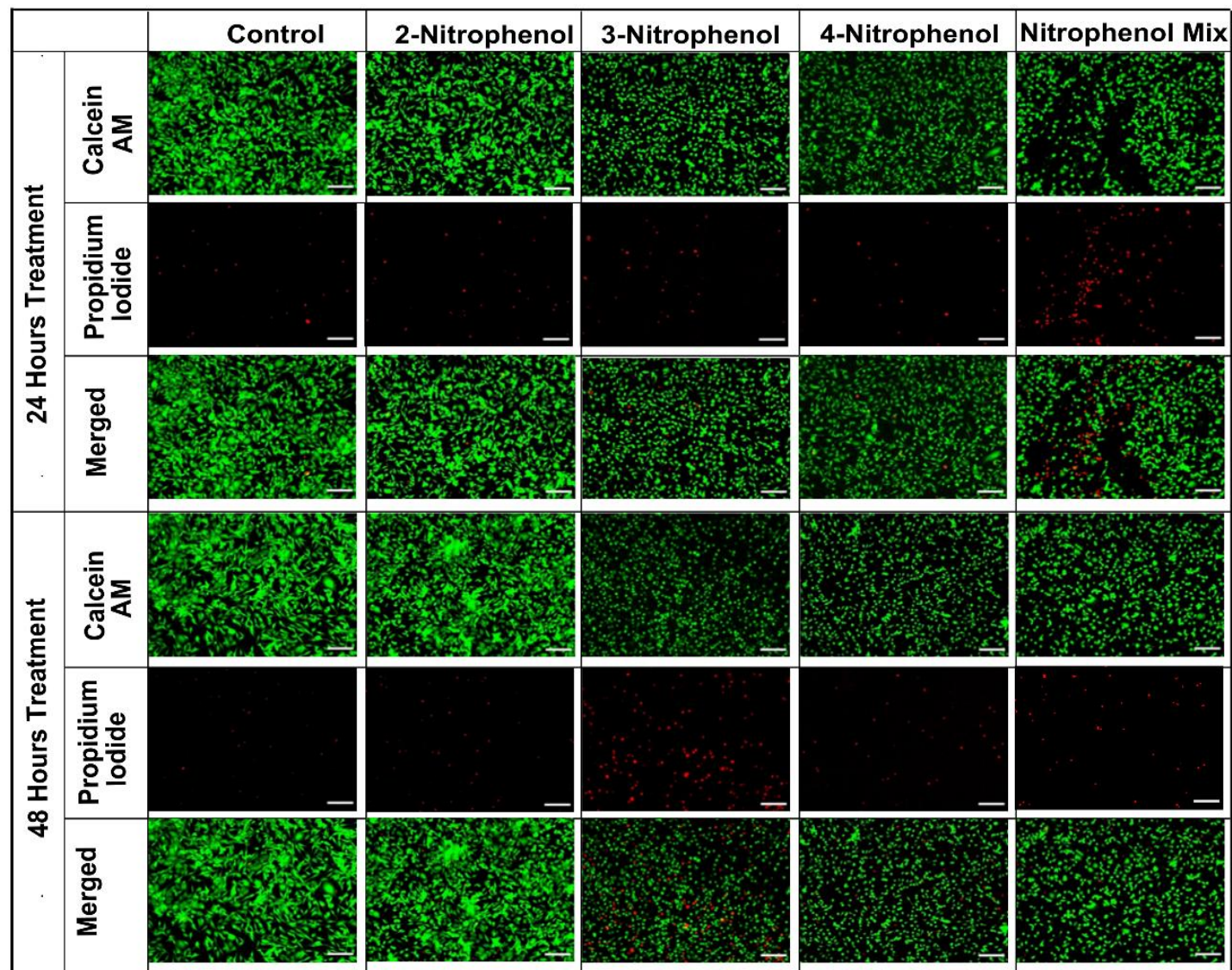


Figure 3.3.12. NP-treated BEAS-2B cells were visualized through Calcein-AM/ Propidium Iodide (live/dead) staining using fluorescence microscopy. The Calcein-AM (green) stained the live cells while propidium iodide (red) stained the dead cells and the merged channel shows the overlay of two images. The micrographs are scaled to a size of 50 μm . (a) The live/dead staining of BEAS-2B cells revealed the number of dead cells increased with increasing time of treatment; the highest number of cells were dead following exposure to the 4NP and the equimolar mixture of the NPs

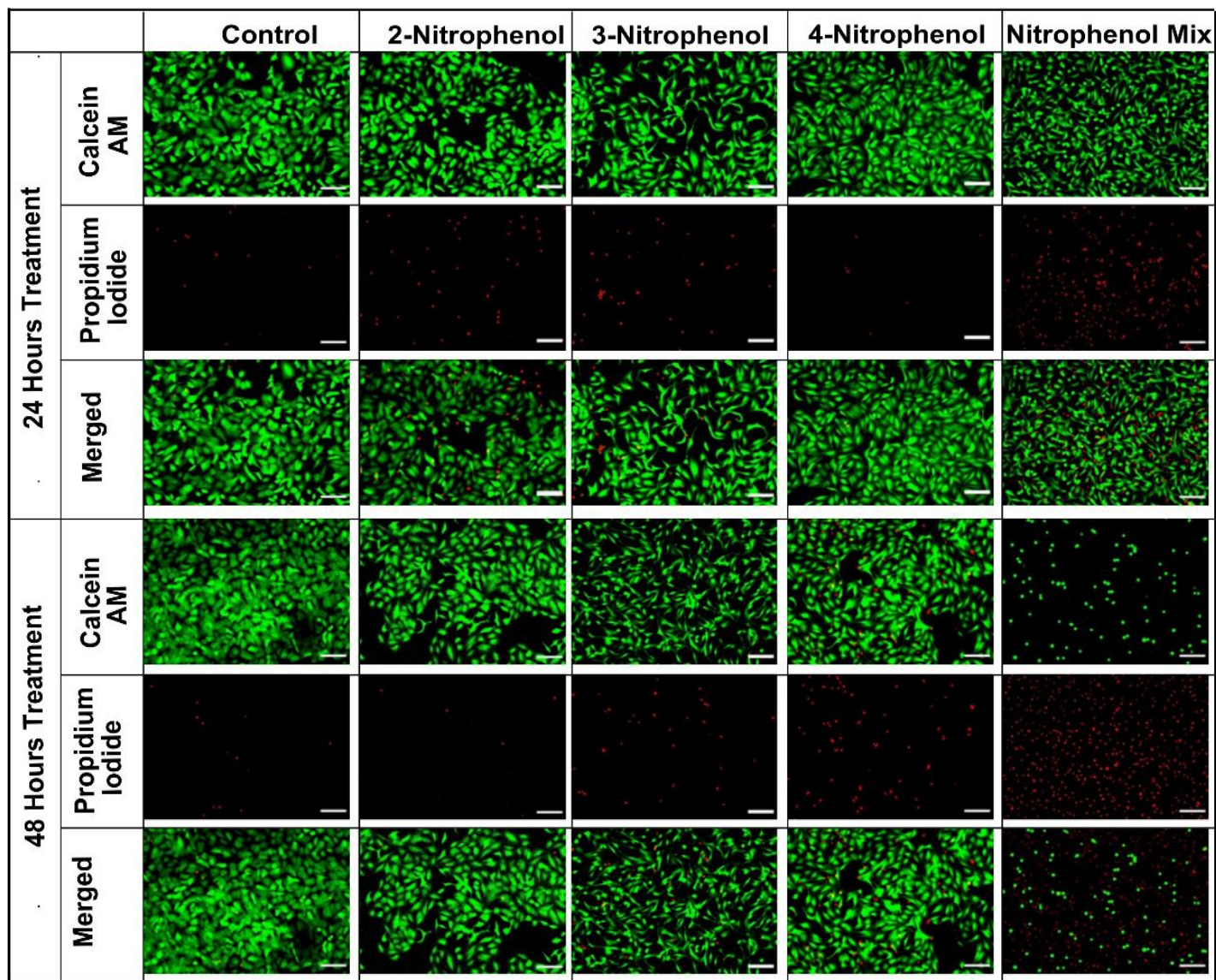


Figure 3.3.13. NP-treated A549 cells were visualized through Calcein-AM/ Propidium Iodide (live/dead) staining using fluorescence microscopy. The Calcein-AM (green) stained the live cells while propidium iodide (red) stained the dead cells and the merged channel shows the overlay of two images. The micrographs are scaled to a size of 50 μm . The live/dead staining of A549 cells revealed the number of dead cells increased with increasing time of treatment; the highest number of cells were dead following exposure to the 4NP and equimolar mixture of the NPs.

As shown in [Figure 3.3.13](#), the changes in A549 cellular morphology were less evident than in BEAS2B cells following treatments with various NPs and their equimolar mixture. 2NP-treated lung cells exhibited a slight increase in PI+ cells after 24 h exposure, while the cells recovered after 48 h exposure. The Calcein-AM stained cells in 48 h exposures were the same as in the untreated control. 3NP-treated A549 cells exhibited cellular growth inhibition and a slight increase in PI+ cells at 24 and 48 h exposure. The number of Calcein-AM + cells decreased compared with the untreated control at 48 h exposure; this could be attributed to cellular death and cellular growth inhibition.[358](#) A549 cells exposed to 4NP exhibited a high rate of cellular death at 48 h exposure, as can be seen through increased number PI+ cells in the PI channel. The NP mixture treated A549 cells exhibited increased PI+ cells following both 24 and 48 h exposure; the smaller number of cells in the merged channel depicts how the cells were undergoing cellular death even with 24 h exposure. The Calcein-AM + cells were almost negligible following 48 h exposure.

When studying the mechanisms of toxicity, the NPs exhibited a mix of inhibitory and cytotoxic effects in both cell lines, depending upon the treatment type. Each NP isomer exhibited different cytotoxic responses and intra-cellular OS mechanisms, where 4NP and 2NP was the most and least cytotoxic, respectively. A previous study on two isomers of nitro-polycyclic aromatic hydrocarbons (nitro-PAHs) revealed similar differential intra-cellular toxicological responses. [82](#) The NP mixture induced an additive effect of the three NP isomers, [360](#) as the IC₅₀ value was higher than the individual 3NP and 4NP values, but lower than the individual 2NP value in both BEAS-2B and A549 cells. The cytotoxic assessment revealed a mixture of inhibition and cytotoxic effects within the NP mixture-exposed lung cell. The cellular inhibition in the first 24 h exposure to 4NP followed an increased cellular death between 24-48 h, suggesting that high ROS and organelle dysfunction may have induced cellular death.

3.3.8- The Mechanism of Cellular Death: Apoptosis versus Necrosis

Flow cytometry analysis with Annexin-V/FITC- and PI-labelled cells were carried out at 24 and 48 h exposures to NPs treatments to elucidate the mechanism through which BEAS-2B and A549 cells undergo death following exposure to 200 µg mL⁻¹ of NPs. [Fig-](#)

ures 3.3.14 and 3.3.15 (*vide infra*) show dot plots of the BEAS-2B and A549 cellular populations, respectively, treated with: (i) deionized water as an untreated control; (ii) 2NP; (iii) 3NP; (iv) 4NP; and (v) equimolar mixtures of these NPs.

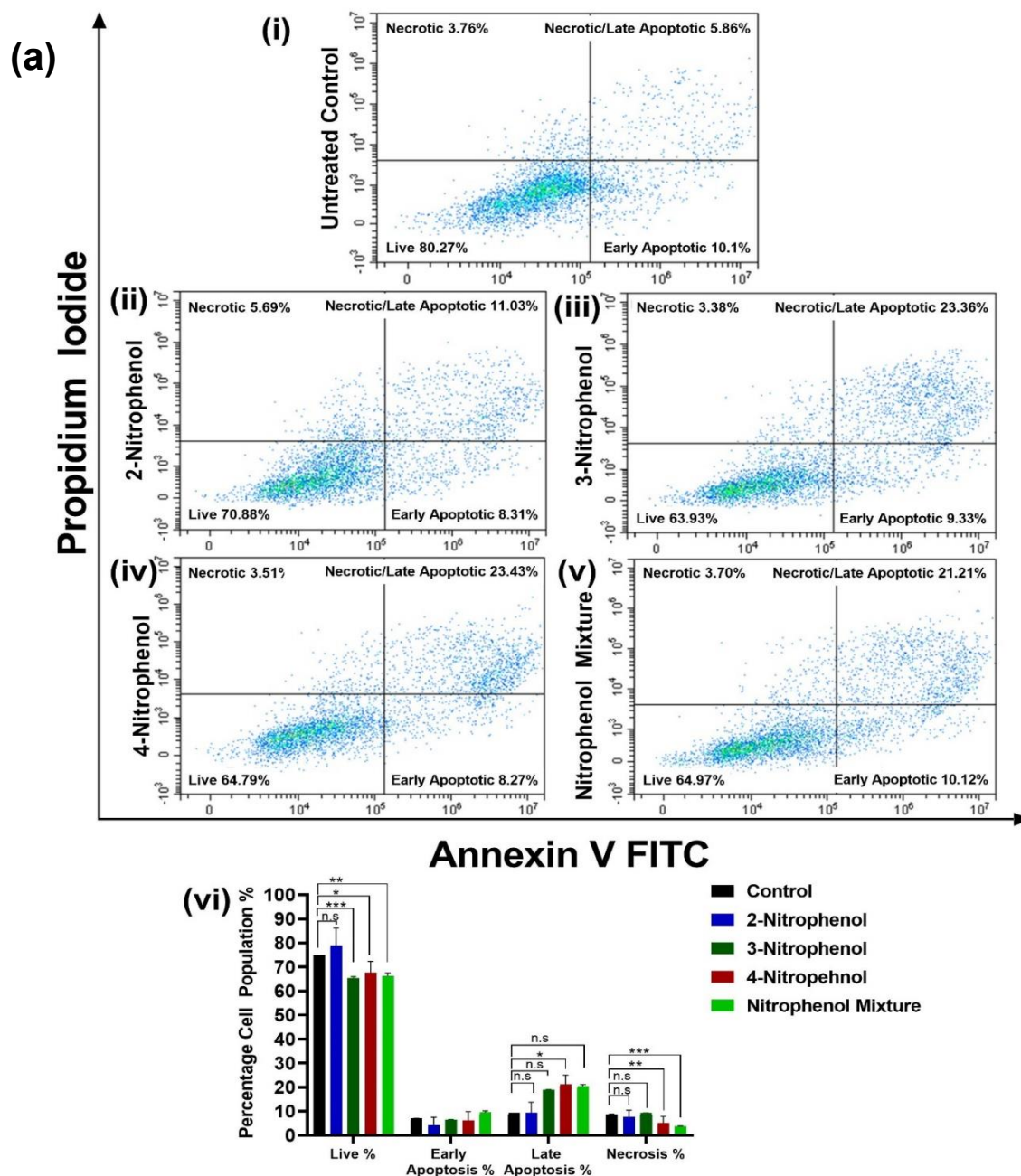


Figure 3.3.14. The Annexin-V/Propidium Iodide (PI) labelled cells reveal the percentage of live, apoptotic, or necrotic cellular populations of BEAS-2B cells at (a) 24 h exposure. These were analysed by flow cytometry, following treatment with: (i) untreated control (ii) 2NP (iii) 3NP (iv) 4NP and (v) the NP equimolar mixture. The dot-plots represent one treatment from each group, while the bar-graphs (vi) show the data from at least four-independent experiments and standard deviation plotted as error bars (to be continued)

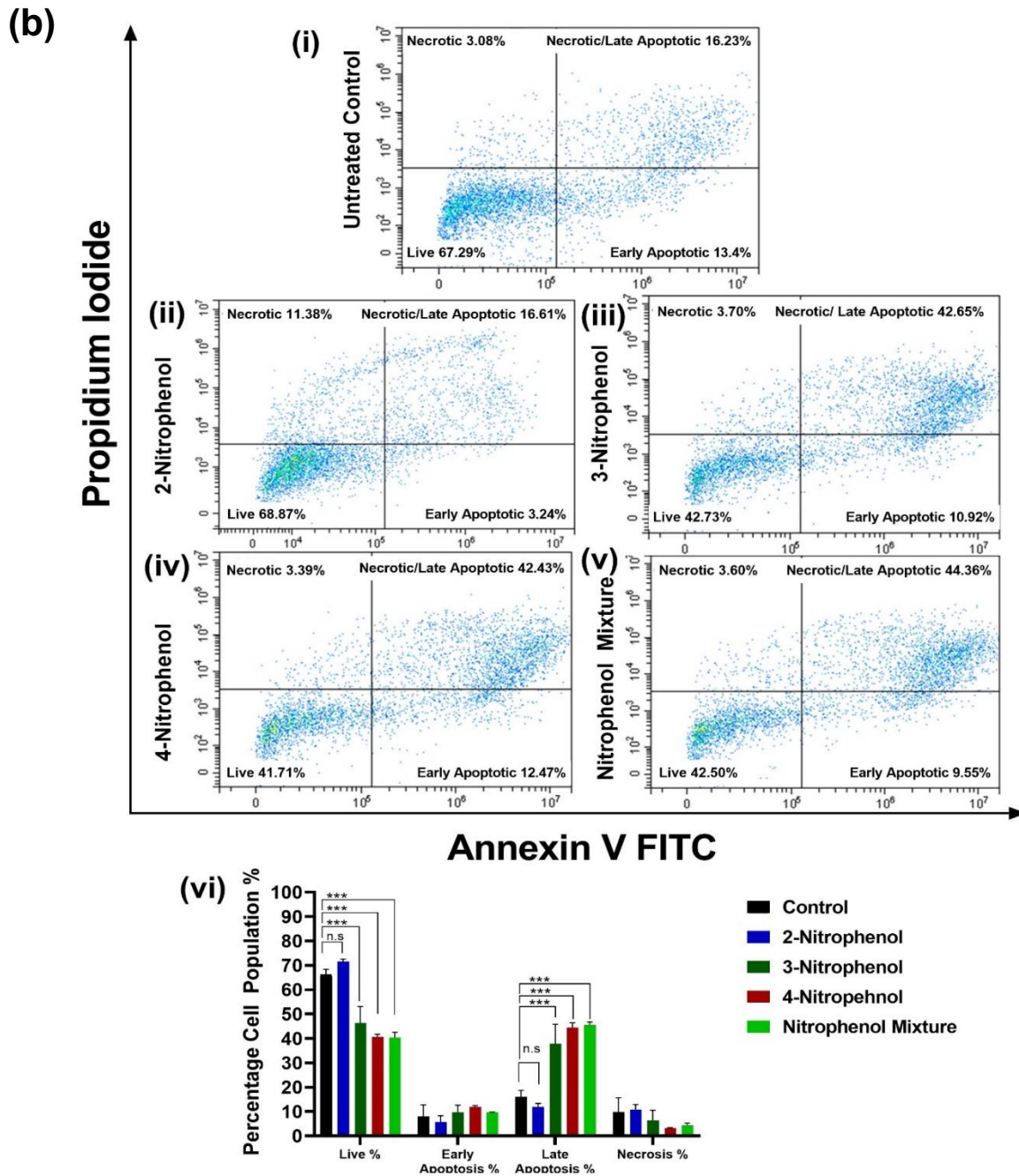


Figure 3.3.14 (continuation). (b) 48 h exposure. These were analysed by flow cytometry, following treatment with: (i) untreated control (ii) 2NP (iii) 3NP (iv) 4NP and (v) the NP equimolar mixture. Cells were treated with 200 $\mu\text{g mL}^{-1}$ of NPs, and the cellular populations were labelled with Annexin-V FITC and PI to determine the percentage of cells that are alive, in early apoptosis (Annexin-V FITC + cells), in late apoptosis and necrosis (Annexin-V FITC and PI + cells), and necrosis (PI + cells). The dot-plots represent one treatment from each group, while the bar-graphs (vi) show the data from at least four-independent experiments and standard deviation plotted as error bars. One-way ANOVA with Dunnett's multiple comparisons test was performed on the data set to determine the statistical significance of the change in signal when compared with untreated controls. A p -value <0.05 was considered statistically significant for our analysis, where *** indicates a p -value ≤ 0.001

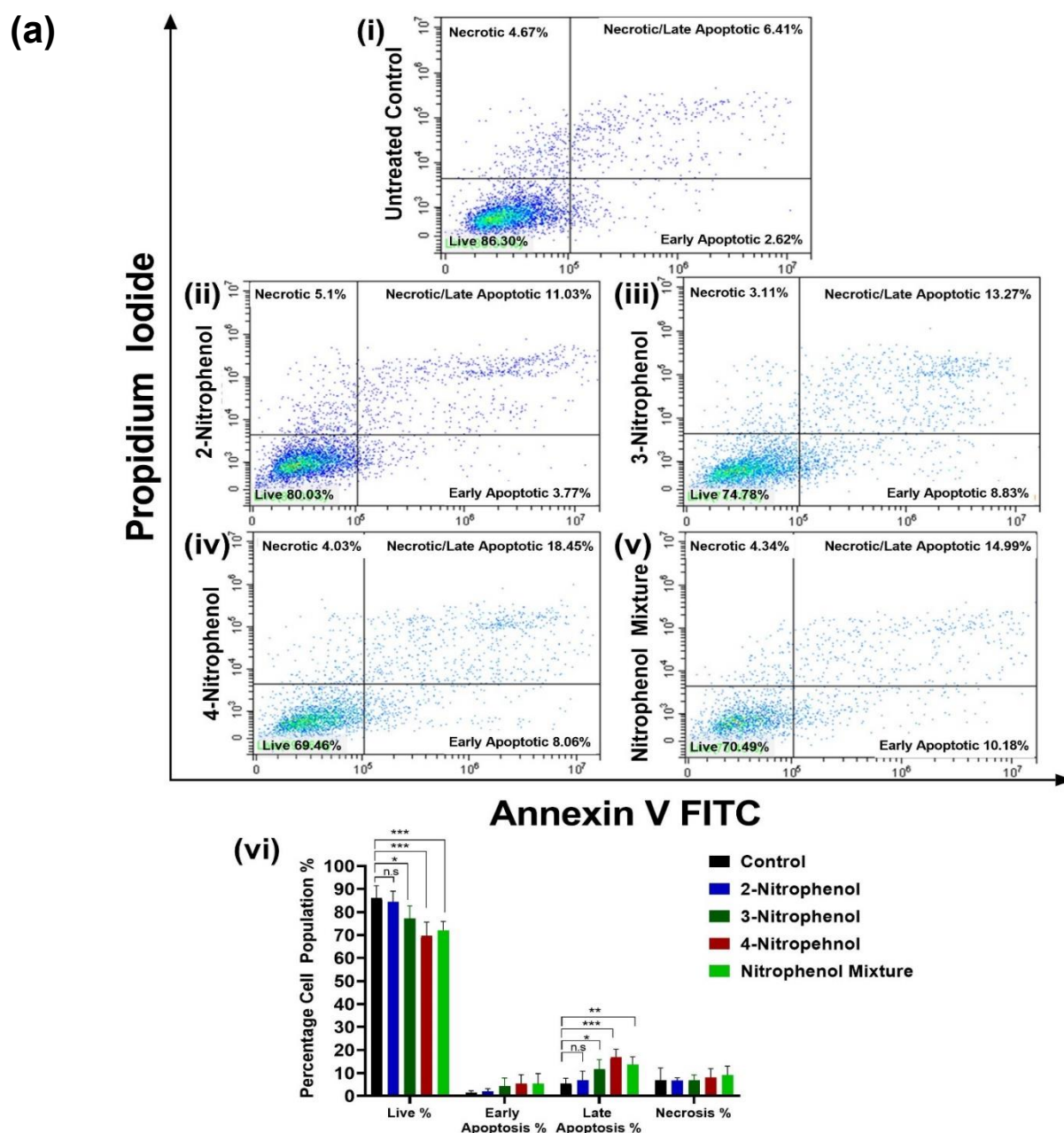


Figure 3.3.15. The Annexin-V/Propidium Iodide (PI) labelled cells to reveal the percentage of live, apoptotic, or necrotic cellular population of A549 cells at (a) 24 h of exposure was analysed through flow cytometry following treatment with the (i) untreated control (ii) 2NP (iii) 3NP (iv) 4NP and (v) the NP equimolar mixture. The dot-plots represent one treatment from each group, while the bar-graphs (vi) show the data from at least four independent experiments and standard deviation plotted as error bars. One-way ANOVA with Dunnett's multiple comparisons test was performed on the data set to determine the statistical significance of change in signal when compared with untreated controls. The p -value <0.05 was considered statistically significant for our analysis, where *** indicates a p -value ≤ 0.001 (to be continued)

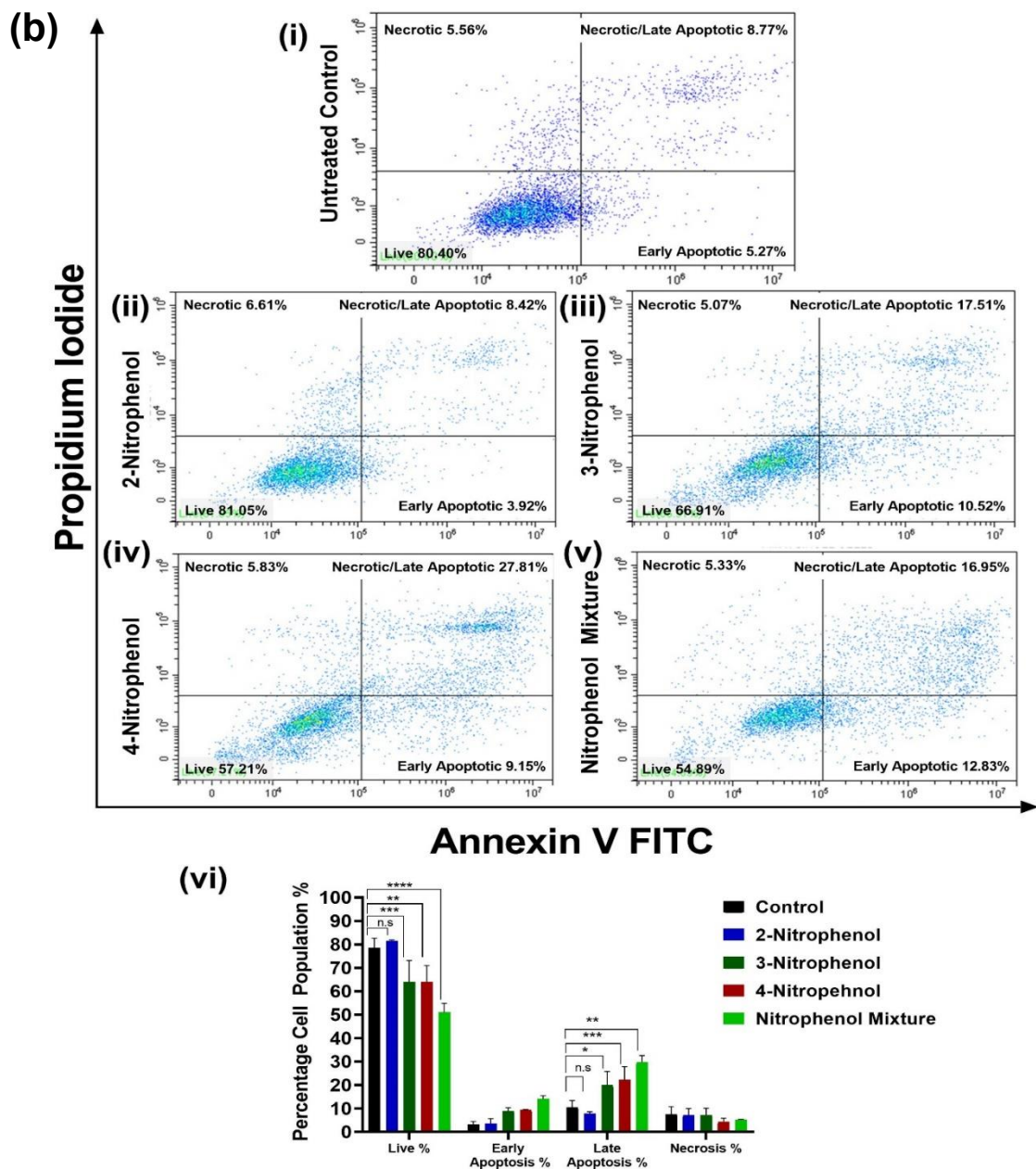


Figure 3.3.15 (continuation). The Annexin-V/Propidium Iodide (PI) labelled cells to reveal the percentage of live, apoptotic, or necrotic cellular population of A549 cells at (a) (b) 48 hours of exposure were analysed through flow cytometry following treatment with the (i) untreated control (ii) 2NP (iii) 3NP (iv) 4NP and (v) the NP equimolar mixture. The dot-plots represent one treatment from each group, while the bar-graphs (vi) show the data from at least four independent experiments and standard deviation plotted as error bars. One-way ANOVA with Dunnett's multiple comparisons test was performed on the data set to determine the statistical significance of change in signal when compared with untreated controls. The p -value <0.05 was considered statistically significant for our analysis, where *** indicates a p -value ≤ 0.001 .

Figure 3.3.14 a shows BEAS-2B cells at 24 h exposure; a significant increase in the percentage of the cellular population in late apoptosis/necrosis was only observed in the 3NP treatment (18.86 ± 0.2 % compared with 9.40 ± 0.024 % in the control cells). A significant decrease in the percentage of the live population was observed for 3NP, 4NP, and the NPs mixture treatment (65.34 ± 0.6 , 67.6 ± 4.8 and 66.25 ± 1.3 %, respectively) compared with untreated controls (74.87 ± 0.03 %). However, the percentage of live cells in 2NP-treated cells did not decrease significantly (78.8 ± 7.4 %).

When the exposure times were increased to 48 h, the percentage of the cellular population of BEAS-2B cells in the late apoptosis/necrosis phase increased significantly for 3NP, 4NP, and NP mixture (as shown in Figure 3.3.14 b). 37.8 ± 8.0 and 44.4 ± 2.0 % of the cellular population was found in the late apoptosis/necrosis region for the 3NP and 4NP treatments, respectively, and 45.54 ± 1.18 % of cells in the NP mixture treatment. The percentage of live cell populations decreased significantly to 46.23 ± 6.8 , 40.59 ± 1.1 , and 40.35 ± 2.2 % in the 3NP, 4NP, and NP mixture-treated groups, respectively. The 2NP treatment did not exhibit statistically significant changes in the cellular population (71.6 ± 0.98 %) compared with the untreated controls (66.39 ± 2 %). The A549 cells treated with NPs exhibited a similar increase in late apoptotic/necrotic cellular population as observed in BEAS-2B cells (Figure 3.3.15 a). The 24 h exposures to $200 \mu\text{g mL}^{-1}$ of NPs resulted in a statistically significant decrease in live-cell population percentages: specifically, 77.19 ± 5.5 , 69.61 ± 6.0 and 71.96 ± 4.0 % in the 3NP-, 4NP- and NP equimolar mixture-treated cells, respectively (as shown in Figure 3.3.15). Notably, the 2NP treatment did not exhibit statistically significant changes in the live cellular population (84.48 ± 4.5 %), compared with the untreated control (86.19 ± 5.2 %). The percentage of mixed late apoptotic/necrotic populations increased to 11.71 ± 4.2 , 16.88 ± 3.5 , and 13.64 ± 3.4 % for the 3NP, 4NP and NP equimolar mixture treatments, respectively.

Finally, the A549 cells treated with NPs for 48 h exhibited a statistically significant decrease in the live cell population percentage for 3NP, 4NP and the equimolar NP mixture; specifically, they decreased to 64 ± 9.2 , 64.09 ± 6.9 and 51 ± 3.9 %, respectively (Figure 3.3.15 b). Subsequently, the percentage of mixed late apoptotic/necrotic cellular populations increased statistically significantly from 10.48 ± 3.0 % for untreated control cells to 19.93 ± 5.8 , 22.23 ± 5.6 , and 29.76 ± 2.8 % for the 3NP-, 4NP- and NP mixture-treated cells, respectively. 2NP-treated lung cells did not exhibit a statistically significant changes

in the percentage of the cellular populations (7.8 ± 0.72 %) as of late apoptotic/necrotic cells.

Apoptosis, also known as “programmed cell death,” is one of the most studied cellular death mechanisms,[361](#), and morphologically different from necrotic cellular death. The mechanism of cellular death (apoptosis) was the same in the 3NP-, 4NP- and NP mixture-treated cells; however, BEAS-2B cells treated with 3NP underwent apoptosis within 24 h of exposure, while 4NP-treated BEAS-2B and A549 cells increased in necrosis/late apoptosis colonies between 24-48 h of treatment. This suggests that cell growth inhibition in the 4NP-treated lung cells for the first 24 h led to apoptosis, and then after 48 h a mixture of apoptotic and necrotic cells emerged. This is because in cell cultured *in vitro*, the necrosis is a state following late apoptosis,[362](#) hence the intensity of the effect noted in 4NP is strongest when compared with other NPs. The time- and dose-dependent apoptotic and intracellular ROS build-up effects are seen with previous ambient PM, PM_{2.5} and PM_{0.3} and black carbon (BC) emission studies,[286](#) [363](#) implying disruption in the intracellular ROS and mtROS system to induce apoptosis through “intrinsic pathway”.[361](#) As our previous work reported the changes in cellular membranes after exposures to equimolar mixtures of NPs;[304](#) specifically, the internalization of NPs took place to exhibit molecular-level cellular changes. Hence, the induction of apoptosis via activation of internal apoptotic pathway [361](#) is suggested in our study following exposure to 3NP, 4NP, and an equimolar mixture of NPs. Biochemically, the cellular membrane has a similar structure to the mitochondrial membrane, [364](#) hence, the observed effects on membrane models can be valid for mitochondrial membrane as well. Thereby, we observe changes in $\Delta\Psi_m$.

3.3.9- The Build-up of Oxidative Stress following Nitrophenol Exposure

Oxidative stress (OS) results from the imbalance between pro-oxidant and antioxidant systems in the cell, ultimately pushing the cell towards pro-oxidation mechanisms.[365](#) The changes in the cellular OS and the build-up of ROS before the cellular death event were determined using ROS-specific dyes. The quantitative analysis for general ROS build-up was performed with the carboxy-H₂DCHF dye. Changes in general ROS were monitored every 4 h (up to 24 h) with the various NP exposure groups (as shown in [Figure 3.3.16](#)). [Figures 3.3.16 a & b](#) show the BEAS-2B cells treated with 100 and 200 $\mu\text{g mL}^{-1}$, respectively, and [Figure S5b](#) of 2NP, 3NP, 4NP and the NP mixture. [Figures 3.3.16 c & d](#) show

the A549 cells treated with 100 and 200 $\mu\text{g mL}^{-1}$, respectively, of 2NP, 3NP, 4NP, and the NP mixture.

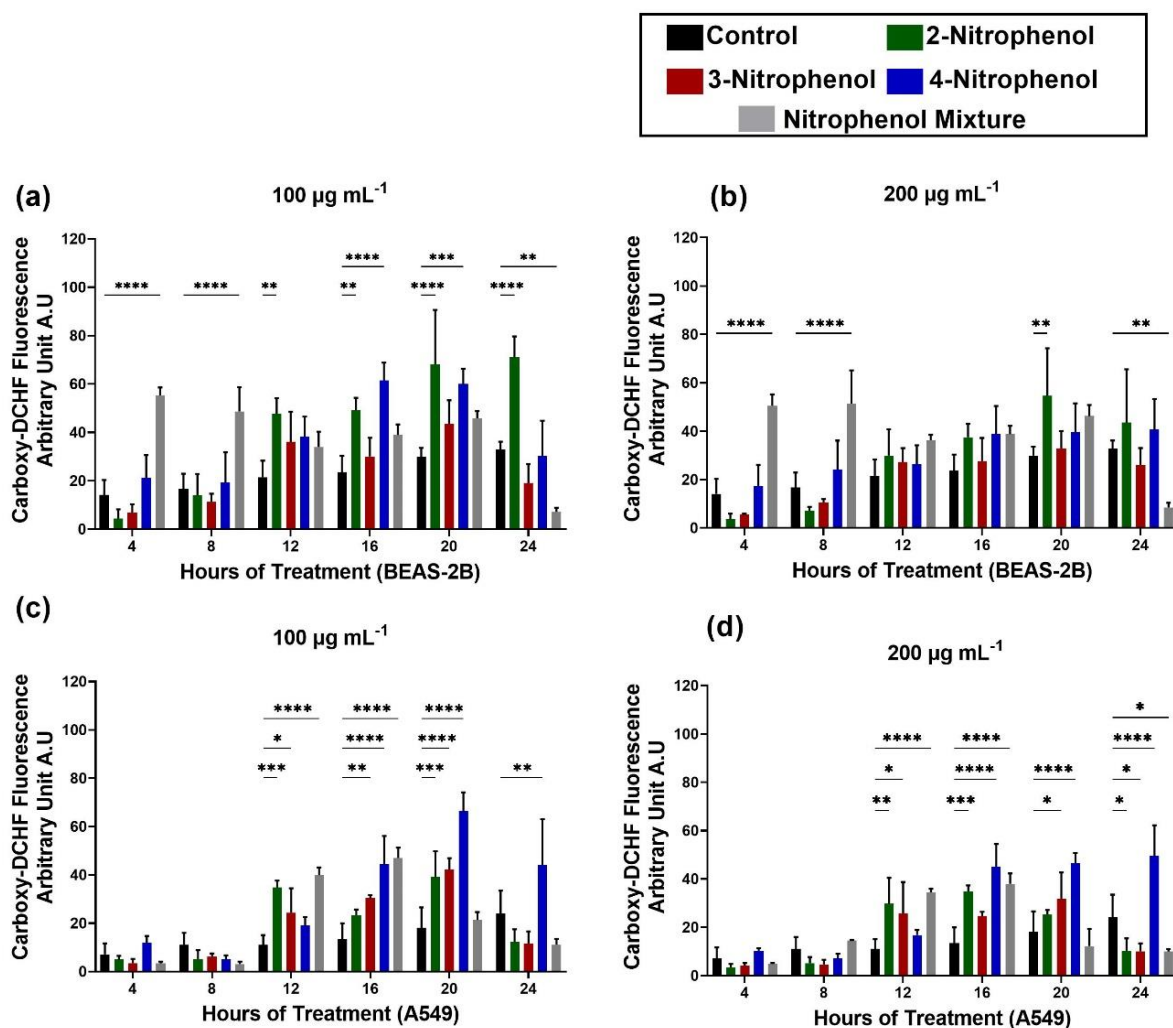


Figure 3.3.16. (a) The change in carboxy- H_2DCHF signal was determined using spectrophotometer plate-reader after every four hours up to 24 hours post exposure using the concentration of NPs as (a) 100 $\mu\text{g mL}^{-1}$ in BEAS-2B; (b) 200 $\mu\text{g mL}^{-1}$ in BEAS-2B; (c) 100 $\mu\text{g mL}^{-1}$ in A549; and (d) 200 $\mu\text{g mL}^{-1}$ in A549 of the 2NP, 3NP, and 4NP as well as their equimolar mixture. The increase in the carboxy- H_2DCHF signal relative to the untreated control was analysed statistically through two-way ANOVA followed by Dunnett's multiple comparison test. The p -value < 0.05 was considered statistically significant for our analysis where **** indicates a p -value ≤ 0.0001 .

After exposure to 100 and 200 $\mu\text{g mL}^{-1}$ of 2NP, a significant increase in general ROS signal was observed only between 12-20 h of treatment in the BEAS-2B and A549 cell lines. The ROS signals decreased after 20 h, implying that the cells were able to resolve the exposure effects, and hence, cellular death was not observed in the 2NP-treated cells.

The carboxy-DCF signal peaked for 3NP-treated A549 cells around 12-16 h post-exposure, whereas the signals peaked for 3NP-treated BEAS-2B cells around 12-20 h post-exposure. In 4NP-exposed lung cells, ROS signals peaked around 16-20 h and 12-24 h in BEA-2B and A549 cells, respectively. The NP equimolar mixture exposure induced the highest increase in general ROS signals; ROS signals peaked between 4-8 h post exposure, while decreasing significantly after 12 h post exposure in BEAS-2B treated cells. In A549 cells treated with the NP equimolar mixture, the ROS signals peaked around 12-16 h and decreased significantly between 20-24 h post exposure. The peak fluorescent intensity was higher in A549 cells when compared with BEAS-2B cells.

The graphs shown in [Figure 3.3.17](#) suggest an increase in MitoSox (mitochondrial superoxide) signal when treated with $200 \mu\text{g mL}^{-1}$ of NPs in (a) BEAS-2B and (b) A549 cells at 8 h post-exposure. The 3NP-, 4NP- and the equimolar NP mixture-treated BEAS-2B cells exhibited an increase in signal around 6-8 arbitrary unit (A.U). In contrast, only a significant increase in signal (2 A.U) was observed in the equimolar NP mixture treated A549 cells.

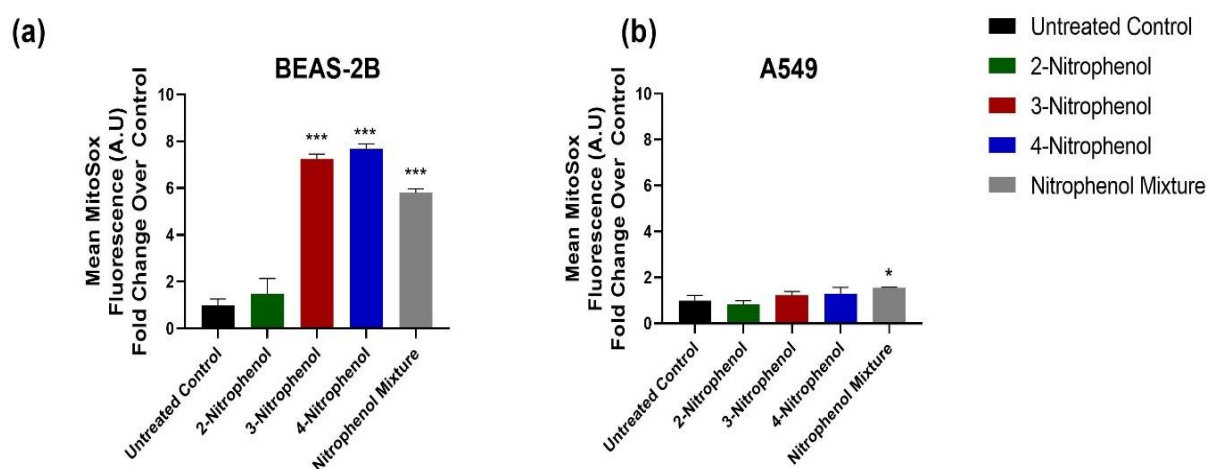


Figure 3.3.17. The change in MitoSox signal was further analyzed through flow cytometry. MitoSox fluorescence was observed as a function of change in mitochondrial superoxide production following treatment with $200 \mu\text{g mL}^{-1}$ of the 2NP, 3NP, and 4NP as well as their equimolar mixture after 8 hours of exposure in (a) BEAS-2B cell lines; and (b) A549 cell lines. One-way ANOVA, followed by Dunnett's multiple comparison test, was run on the untreated control versus treatment group to analyze the significant difference in the fold change of fluorescence signal, where the p -value <0.05 was considered statistically significant for our analysis, and *** indicates a p -value ≤ 0.001 .

Figures 3.3.18 a & b show the confocal microscopy micrographs of BEAS-2B- and A549-treated cells, respectively. The cells were imaged following 8h exposure to the NPs and were stained with the ROS-related dyes to visualize the localization and build-up of ROS-associated signals. The Hoechst dye was used to stain the nucleus of the cells (blue colored) so that ROS signals generated from the live cells (co-observed in the brightfield micrographs) were only captured. The carboxy-DCF signals (stained green in the micrographs) highlights the regions with general ROS build-up. Finally, cells were stained with the MitoSox dye (red-colored) to qualitatively observe the build-up of mitochondrial-associated super-oxide signals. The merged micrographs show the overlay of general ROS signals with the mitochondrial superoxide signals to determine if the mitochondrial superoxide signals or other ROS signals contributed to the cellular death observed at 24 or 48 h exposure. In case of increased MitoSox signals followed by the apoptotic signals generated (as shown in Figure 3.3.14 & 3.3.15), the possibility of the intrinsic apoptotic pathway being switched-on following the exposure can be precluded as of the cellular toxicology mechanism.[361](#)

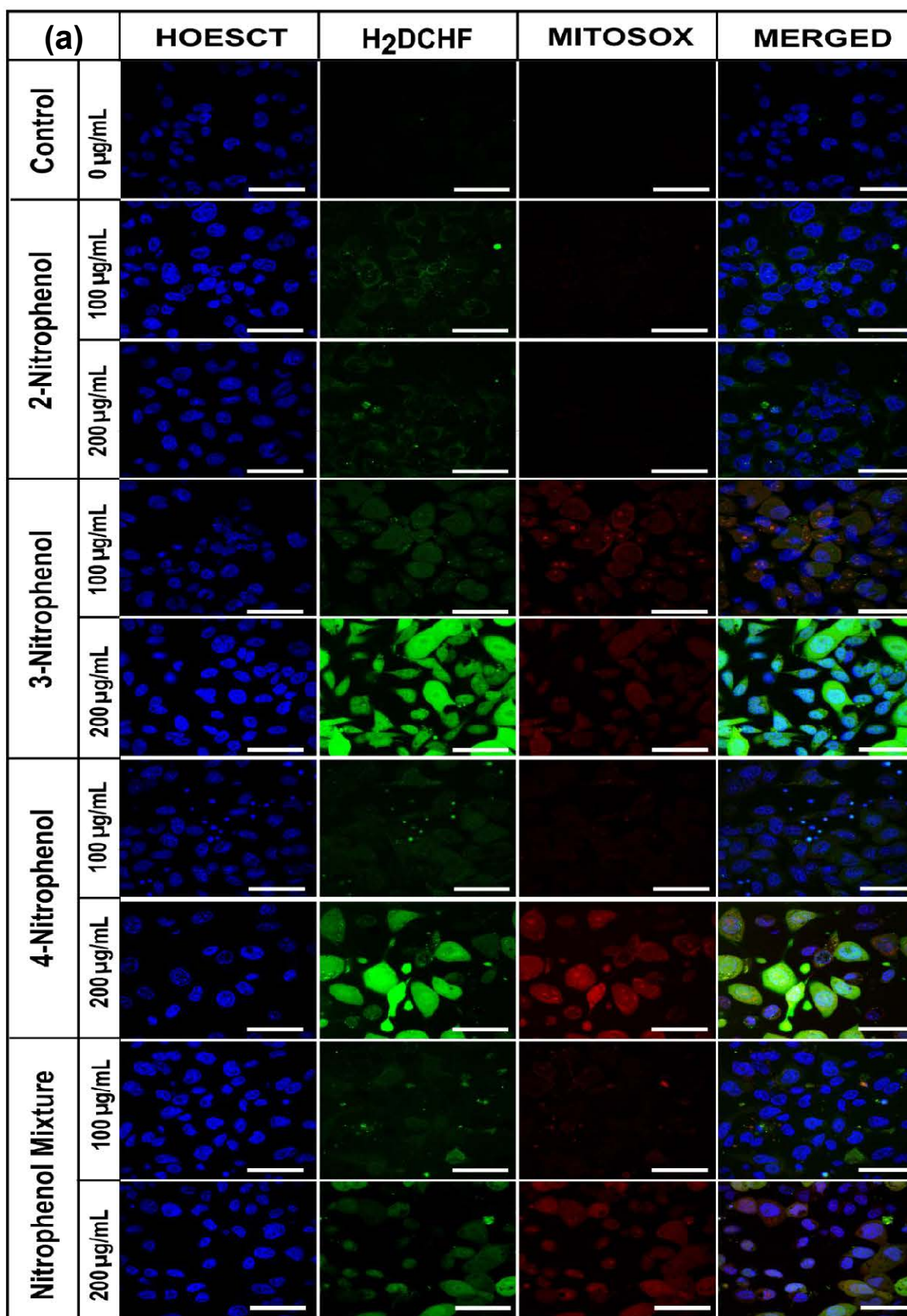
In the BEAS-2B cells (Figure 3.3.18 a) treated with 2NP, the micrographs revealed a slight build-up of general ROS signals (green dots) after 8 h of treatment in 100 and 200 $\mu\text{g mL}^{-1}$ NP exposures. In contrast, no MitoSox-associated signals were observed in the treated cells. Similarly, in A549 cells (Figure 3.3.18 a), a slight increase in ROS build-up was only observed in the 200- $\mu\text{g mL}^{-1}$ NP treatments after 8 h exposure.

3NP-treated BEAS-2B cells (Figure 3.3.18 a) had increased general ROS signals (green region) and mitochondrial superoxide-associated signals (red region); signal strengths increased when exposure concentration was increased from 100 to 200 $\mu\text{g mL}^{-1}$. In 3NP-treated A549 cells (Figure 3.3.18 b), although the general ROS signals were observed to increase with enhanced exposure concentration, the MitoSox signals were not observed. This implied that the mitochondrial superoxide was not increased in the A549 cells after 8 h exposure.

In 4NP-treated BEAS-2B cells (Figure 3.3.18 a), general ROS signals (green) increased with increasing exposure concentrations, while mitochondrial superoxide-associated signals (red) were only observed in the 200- $\mu\text{g mL}^{-1}$ NP exposures. In A549 cells (Figure 3.3.18 b), general and ROS signals only increased in the 200- $\mu\text{g mL}^{-1}$ NP exposures.

Finally, the exposures to the equimolar NPs mixture in BEAS-2B cells ([Figure 3.3.18 a](#)) resulted in increased general- and mitochondrial-specific ROS signals, and signal strengths increased when the NP mixture concentration increased from 100 to 200 $\mu\text{g mL}^{-1}$. In A549 cells ([Figure 3.3.18 b](#)), the cells exhibited a similar increase in general- and mitochondrial-specific ROS signals, increasing NP exposure concentrations.

Lung epithelial cells lining the respiratory pathways are uniquely vulnerable to endogenous (cellular oxidases, mitochondrial and phagocytic bursts, etc.) and exogenous oxidants (xenobiotics, pathogens, and air pollutants).³⁶⁶ Therefore, ROS induced by the imbalance in anti-oxidant and oxidant response regulations may be the underlying factor for adverse lung effects following exposure to urban pollutants.³⁶⁷ The persistent induction of ROS and pro-survival responses may contribute to the progression of diseases following exposure to atmospheric $\text{PM}_{2.5}$.²⁸⁷ The individual exposure to each of the three NP isomers (2NP, 3NP, and 4NP) as well as their equimolar mixture resulted in increased signals of general ROS; however, 2NP-treated lung cells recovered within 24 h exposure, and hence, cellular death was not observed following exposure to 200 $\mu\text{g mL}^{-1}$ concentration of 2NP. ROS includes free radicals, e.g., hydroxyl ($\cdot\text{OH}$), superoxide ($\text{O}_2^{\cdot-}$) and nonradicals (e.g., hydrogen peroxide (H_2O_2)) that can increase OS within cells, and can cause mitochondria to promote cellular apoptosis.²⁸⁶ The 3NP-, 4NP- and the NPs equimolar mixture-treated cells peaked with ROS in 12-20 h of exposure, implying down-signalling increases ROS that contributed towards cellular apoptosis at 24 h exposure to both 100 and 200 $\mu\text{g mL}^{-1}$ concentrations.



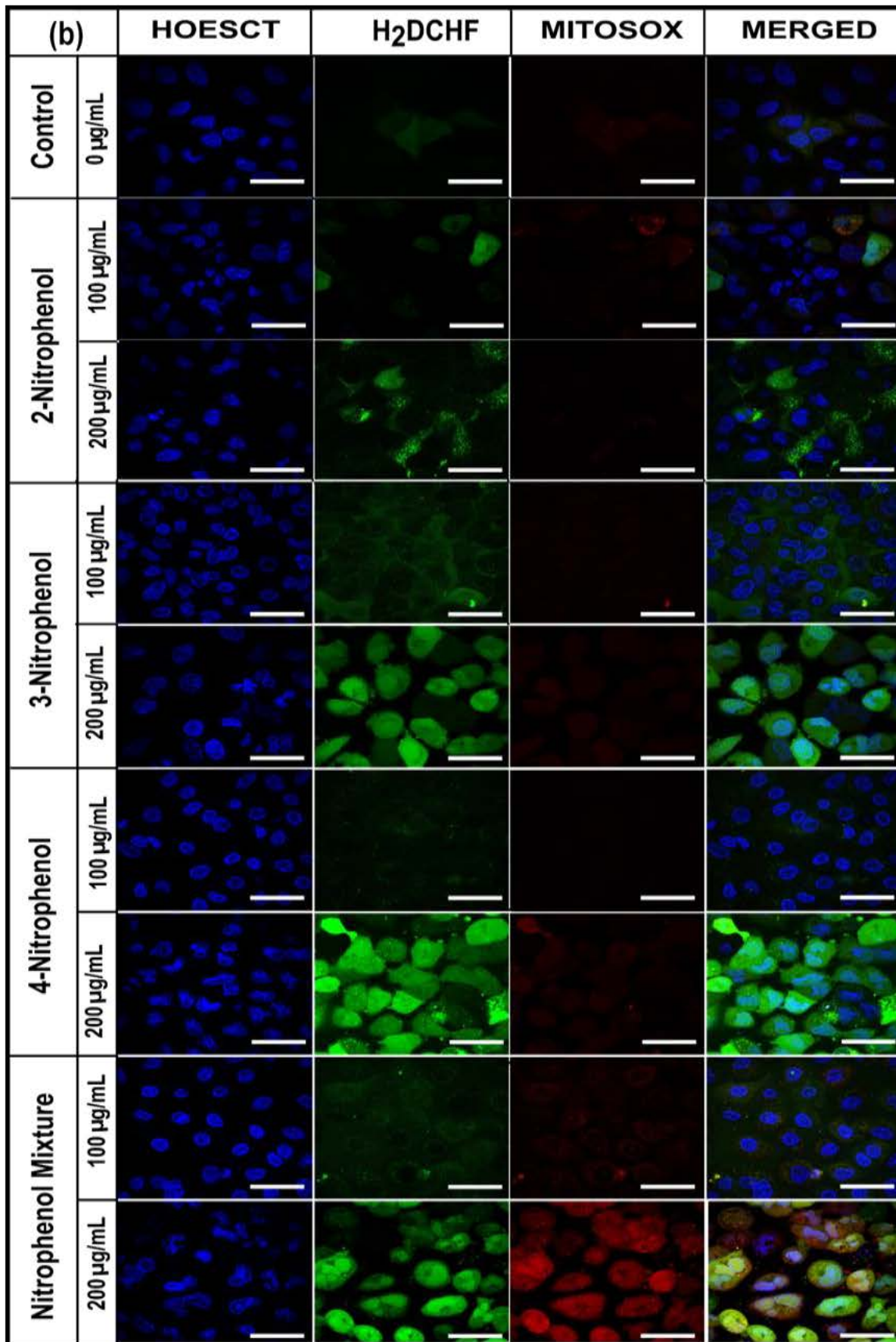


Figure 3.3.18. OS signals were detected following the NP treatments to determine the intracellular changes. The confocal microscopy micrographs were obtained to qualitatively

observe the changes in OS-related signals following exposure to both 100 and 200 $\mu\text{g mL}^{-1}$ of the NPs in (a) BEAS-2B cell lines; and (b) A549 cell lines after 8 h exposure. The Hoechst dye was used to stain the nucleus of the live cells, which were then analysed for general ROS build-up (carboxy- H_2DCHF) and mitochondrial superoxide (MitoSox) signals. The merged channel allowed for visual analysis of the signals generated from general ROS build-up in the cells and those specific to mitochondria through an overlay of the three micrograph channels. The micrographs in the figure are scaled to a size of 25 μm .

3.3.10- Changes in Mitochondrial Membrane Potential ($\Delta\Psi\text{m}$)

TMRM is a cell-permeant dye that is sequestered by the active mitochondria ($\Delta\Psi\text{m}$) [368](#). The decrease in $\Delta\Psi\text{m}$ is indicative of a collapse of the proton gradient in mitochondrial membrane [369](#). Changes in $\Delta\Psi\text{m}$ provide critical information on mitochondrial health. An increase in mitochondrial-specific superoxide and a decrease in $\Delta\Psi\text{m}$ may indicate mitochondrial dysfunction that arises after NP exposures; the exposure inadvertently leads to the “switching-on” of the intrinsic apoptotic pathway [361](#). As shown in [Figure 3.3.19 \(iii, iv and v\)](#), 24 h exposures to 3NP, 4NP, and the equimolar NPs mixture in BEAS-2B cells resulted in decreased TMRM signals when compared with the untreated (basal) controls [Figure 3.3.19 \(i\)](#).

There was no change in the $\Delta\Psi\text{m}$ signal following exposure to 2NP (as shown in [Figure 3.3.19 \(ii\)](#)). The A549 cells treated with the NPs showed no change in the $\Delta\Psi\text{m}$ signals ([Figure 3.3.20](#)). The treatment with the positive control (FCCP) resulted in the decreased $\Delta\Psi\text{m}$ signals when compared with the basal cells (as shown in [Figures 3.3.19 \(vi\) and 3.3.20 \(vi\)](#)).

The build-up of mitochondrial $\text{O}_2^{\cdot-}$ is a further indication of ROS imbalance, as mitochondria are important modulators and regulators of oxidation-reduction processes.[87](#) In addition, moderately reactive $\text{O}_2^{\cdot-}$ is detoxified by mitochondrial superoxide dismutase (SOD) to less toxic H_2O_2 .[367](#) Hence, mtROS build-up indicates the cells are undergoing mitochondrial dysfunction that may ultimately lead to the build-up of general ROS signals within cells, impaired electron transport function, followed by the collapse in the mitochondrial membrane potential.[88](#) Significant mtROS was observed in the 3NP-, 4NP- and the NP equimolar mixture-treated BEAS-2B cells, implying collapse of mitochondrial membrane potential that ultimately led to the intrinsic apoptosis induction within the treated cells.

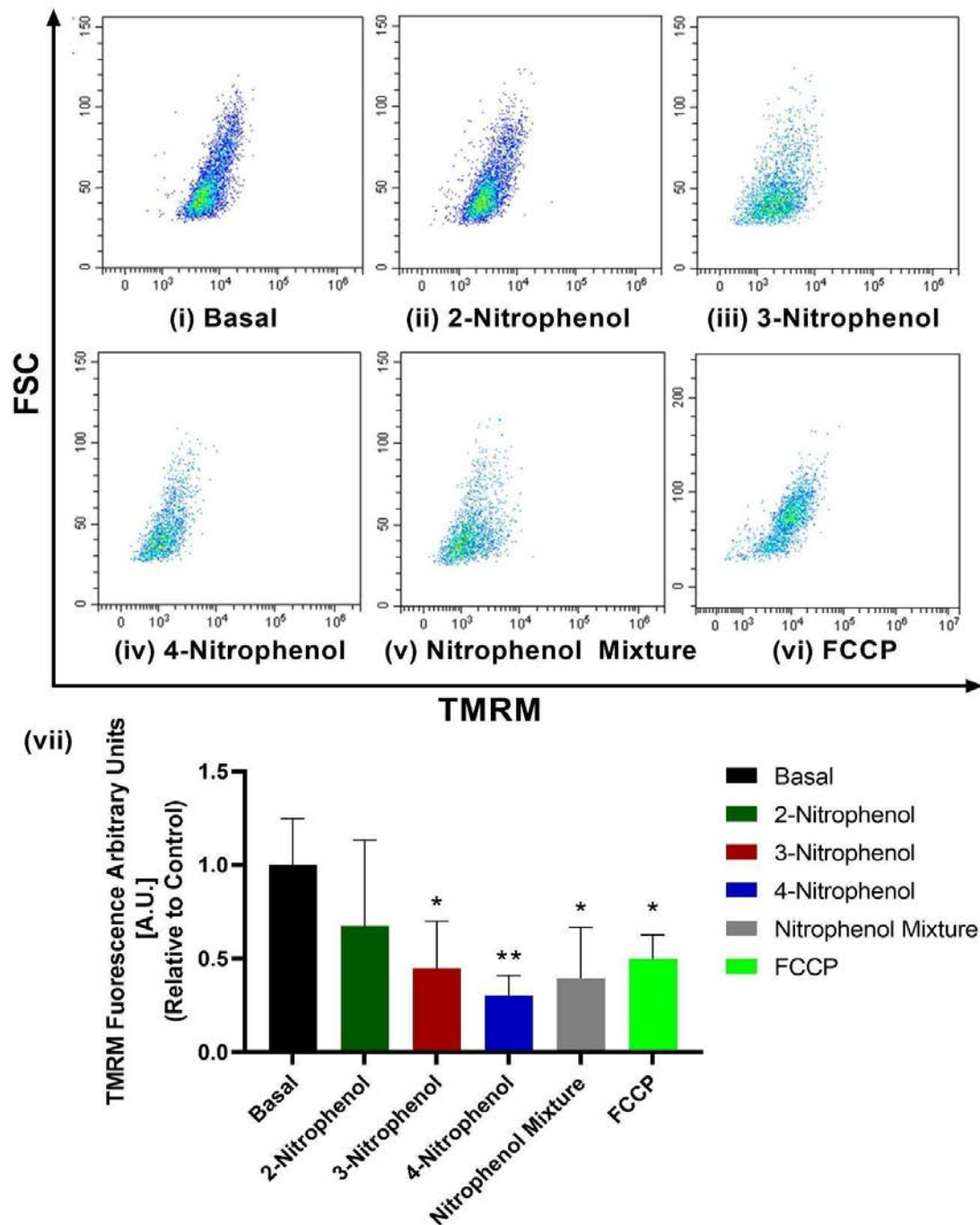


Figure 3.3.19. The cells were treated with the 200- $\mu\text{g mL}^{-1}$ of 2NP, 3NP, 4NP and their equimolar mixture at 24 h exposure, where decreases in $\Delta\Psi_m$ were detected as a function of decreases in TMRM through flow cytometry in BEAS-2B cells; Ordinary one-way ANOVA followed by Dunnett's multiple comparison test was performed to analyse the significant difference between the untreated controls and treatment groups. A p -value < 0.05 was considered statistically significant for our analysis, where ** indicates a p -value ≤ 0.01 . Carbonyl cyanide 4-(trifluoromethoxy) phenylhydrazone (FCCP) is a positive control to detect decreases in the $\Delta\Psi_m$.

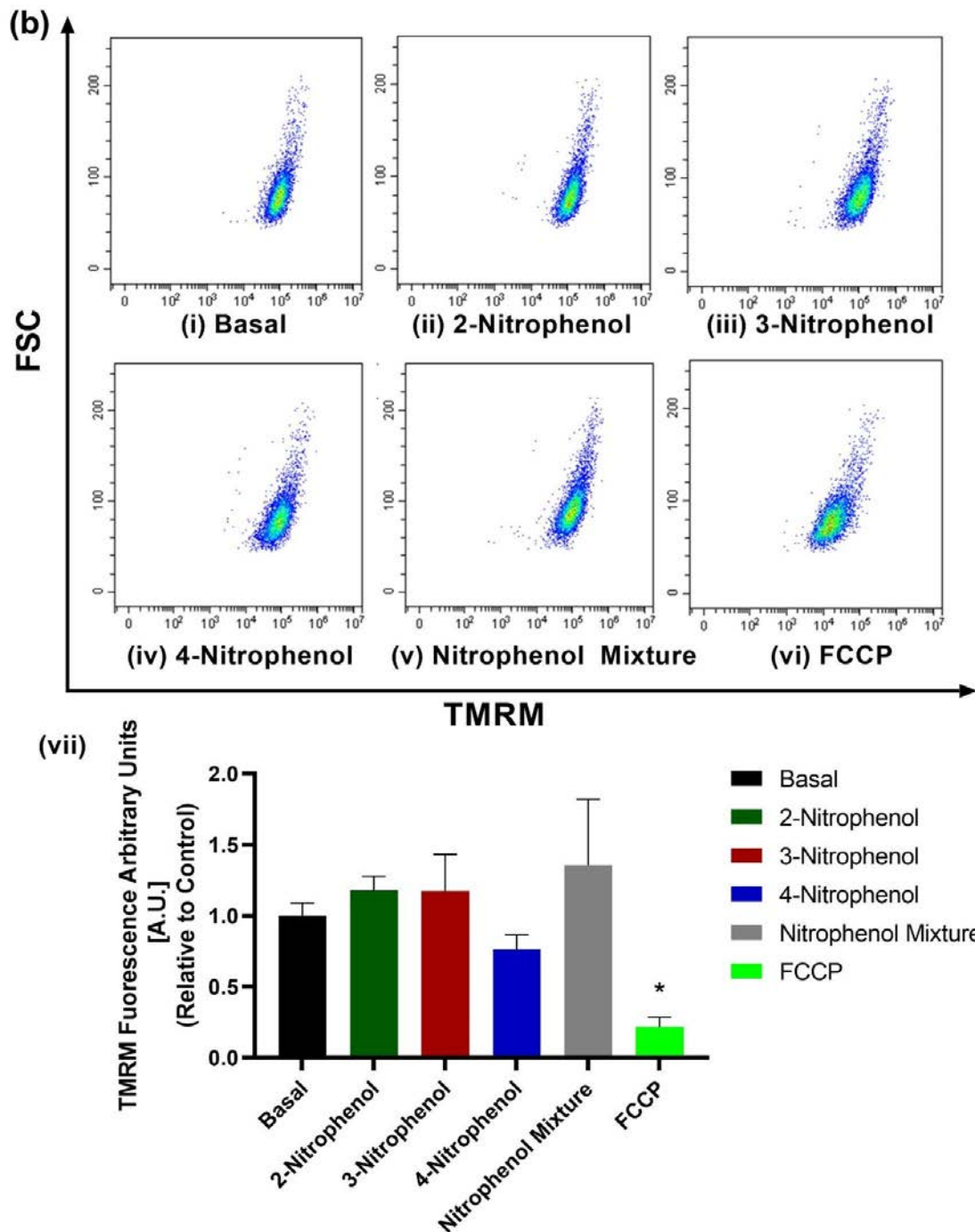


Figure 3.3.20. The cells were treated with the $200\text{-}\mu\text{g mL}^{-1}$ of 2NP, 3NP, 4NP and their equimolar mixture at 24 h exposure, where decreases in $\Delta\Psi_m$ were detected as a function of decreases in TMRM through flow cytometry in A549 cells; Ordinary one-way ANOVA followed by Dunnett's multiple comparison test was performed to analyse the significant difference between the untreated controls and treatment groups. A p -value <0.05 was considered statistically significant for our analysis, where ** indicates a p -value ≤ 0.01 . FCCP is a positive control to detect decreases in the $\Delta\Psi_m$.

The ROS build-up in A549 cells was lower than in BEAS-2B cells, and can be attributed to different metabolic, proliferative, and higher “respiratory” effects in the cancer cell lines.²⁵⁰⁻³⁷⁰ Since dysmorphic mitochondria are also associated with chronic respiratory diseases including asthma, allergy, bronchitis and pulmonary hypertension,³⁷¹ the NP exposure effects at sub-organelle levels may indicate that disruptions in mitochondrial membrane functioning, warranting future chronic exposure studies using IC₅₀ concentrations to resolve underlying lung pathophysiology.

3.3.11- Conclusion

Mono-NPs are pollutant tracers in ambient PM_{2.5} and smog chamber-generated SOA. The cellular growth inhibition effect following exposures to NPs can be correlated with the intracellular ROS and mtROS build-up. Significantly, the 3NP- and 4NP-treated BEAS-2B cells induced the highest growth inhibition and mtROS build-up, followed by apoptosis between 24-48 h of exposure. The 4NP exposure was the most abundant for most environmental and smog-chamber-generated samples and exhibited the highest toxicological response. These findings are important from an atmospheric perspective as acute exposure to the NPs in case of accidental emissions, such as wildfires, industrial settings, smog-generated SOA particles, and water spillages, may expose human populations to higher-than-normal NPs concentrations. There is a need to monitor the NP concentrations in primary and secondary source regions so that acute exposure effects within lungs could be estimated. As our calculations estimate years of exposure to generate inhibitory effects on cell lines, chronic exposure studies are warranted as human lungs are more complex than the *in vitro* systems.

3.4- Primary versus Secondary Organic Emissions of Biomass Burning Aerosol: Nitrated Aromatic Components induce Mitochondrial Stress and Apoptosis in Human Lung Cells

This section of the thesis covers the toxicological assessment of four biomass burning aerosol (BBA) markers, which include levoglucosan (LG), 3-nitrosalicylic acid (3NS), 4-nitroguaiacol (4NG) and 4-nitrocatechol (4NC), and their equimolar mixtures. In a previous study by Tuet et al.,[208](#) it was reported that the oxidative potential (OP), deduced from a chemical based assay, of BBA emissions induced higher reactive oxygen species (ROS)/reactive nitrogen species (RNS) than any other organic aerosol (OA) type collected from ambient and/or lab-generated aerosol samples with LG concentration as a predictor of OP. Herein, we report the toxicological profiling of LG versus nitroaromatic compounds (NACs) in BEAS-2B and A549 cells as a predictor of changes in cellular stress, proliferation rate and ROS following exposure. We also conducted both time- and dose-dependent response studies to elucidate the mechanism through which lung cells undergo cell death and molecular changes behind it. Finally, by using the 4 BBA tracers in an equimolar mixture as a model for BB emissions, we predict how NACs govern a vital role in driving the toxicology within the lung cells.

The IC₅₀ values for each BBA component are provided in both BEAS-2B and A549 cells, emphasizing the percentage of cell proliferation rate, the release of lactate dehydrogenase (LDH) as a percentage of untreated control, and morphological changes in cells through Calcein-AM/PI (live/dead) staining (as observed under a microscope). In the next step, changes in the mitochondrial and general ROS balance at a single cell level were determined using flow cytometry and confocal microscopy. Finally, we propose the mechanism of cellular death, because of the change in ROS balance and mitochondrial membrane potential ($\Delta\Psi_m$).

Figure 3.4.1 summarizes the paradigm of the presented research. The chapter is divided into five sub-sections to provide a detailed toxicological profile of each of the BBA markers in the lung cells. It concludes with comparing their toxicology responses following exposure to 100 $\mu\text{g mL}^{-1}$ and 200 $\mu\text{g mL}^{-1}$ concentration, respectively.

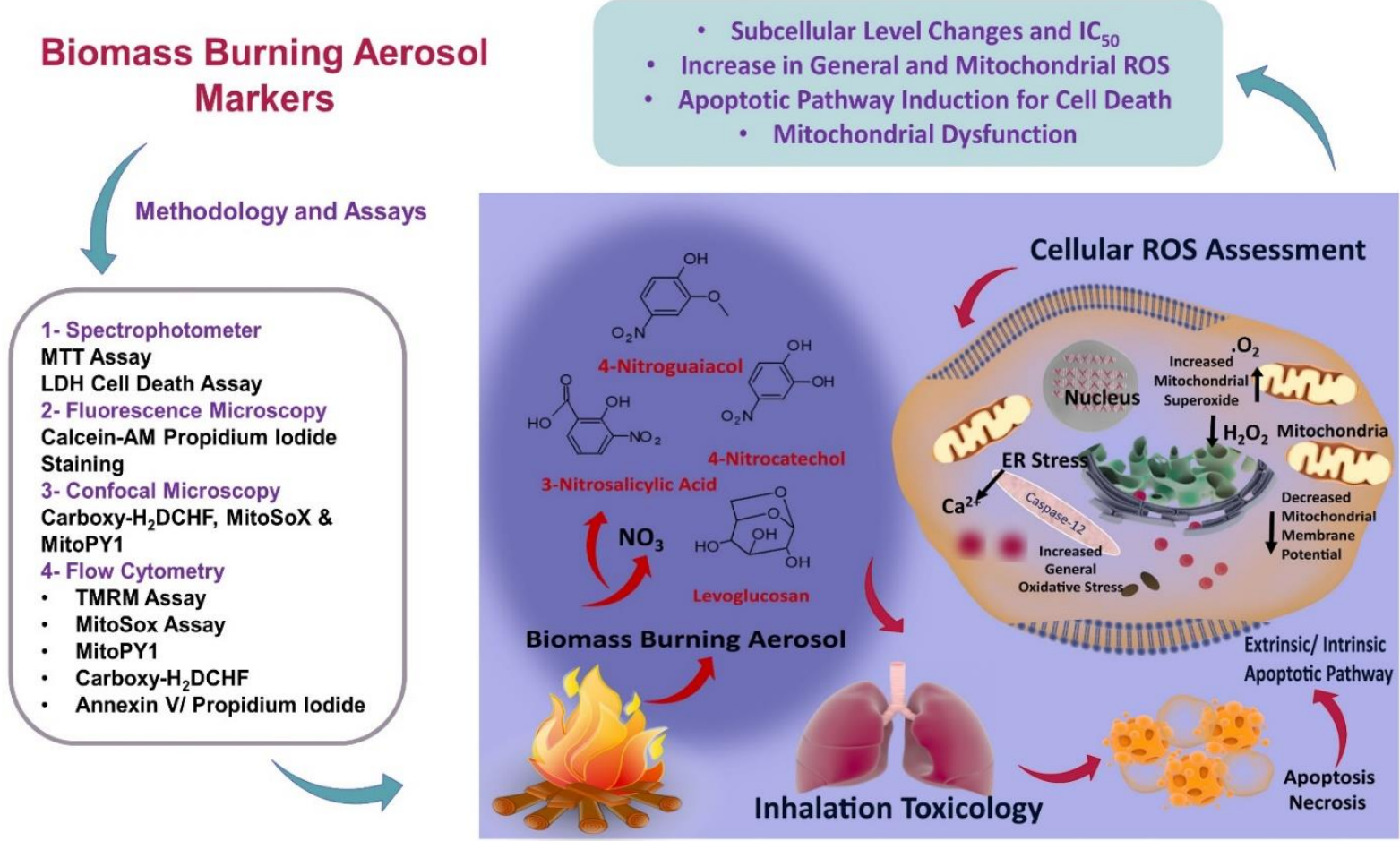


Figure 3.4.1. The study design for the current section of the thesis. We provided detailed toxicological profiling of four BBA components i.e., LG, NS, NC and NG and their equimolar mixture (4BBA) in the BEAS-2B and A549 cells, with special focus on the mitochondrial dysfunction as a driver of cellular ROS.

3.4.1- Abstract of BBA Project

Globally, biomass burning (BB) processes result in 10-15 Tg yr⁻¹ of organic carbon (OC) emissions into the atmosphere. The UV-light absorbing OC component contains a group of poorly characterized nitrated aromatic compounds (NACs). The latter are relevant secondary organic aerosol (SOA) components of urban biomass burning aerosol (BBA), which involve nitrogen oxides (NO_x) – as key reactants. The present work determines the inhalation toxicity profile of the primary BBA emission marker, levoglucosan (LG), in the A549 and BEAS-2B lung cells and compares it with the toxicology of three important NACs, which includes NS, NC, NG and 4BBA. Inhibitory concentration-50 (IC₅₀) in the cells was determined for NC and showed the lowest 24 h IC₅₀, whereas NS revealed the lowest 48 h IC₅₀ in BEAS-2B cells. LG had the highest IC₅₀ value in both cell lines. Lactate dehydrogenase (LDH) release assay revealed ~ 80% of cellular death after exposure to 100-200 µg mL⁻¹ of NC, implying it to be the most toxic to cells at 24 h and 48 h of exposure. An increase in general reactive oxygen species (ROS) inside the treated cells was observed with LG, NG, and NC, and their equimolar mixture treatment, while NS-treated cells showed ROS efflux in the cellular vicinity. A change in TMRM signal was observed with increasing time for NC, NG, LG, and 4BBA exposure, indicating the collapse of mitochondrial membrane potential in the lung cells. Increased TMRM signals for NS-treated cells were only observed around 48 h. This observation was well correlated with the increased mitochondrial ROS signals, including superoxide and hydrogen-peroxide in most treatment types, implying mitochondrial dysfunction as a predominant factor inducing cellular death in the BBA-treated cells. Annexin-V/ Propidium Iodide (PI) staining of the BBA-treated cell population revealed cells entering apoptosis at varying times following exposure to each of the markers. In contrast, NC-treated cells entered apoptosis at a short duration of 6 h, when 200 µg mL⁻¹ exposure concentration was used. This study provides strong evidence that OA-bound components, such as LG from BB emissions, exhibit ROS originating from mitochondria. In contrast, NC is the most toxic of all NACs studied. We recommend using NC concentration from ambient BBA emissions as a predictor of adverse effects following inhalation. Furthermore, we emphasize the need to control the emission rates of NACs into the atmosphere due to their potential inhalation toxicity. Their atmospheric release can be controlled by regulating NO_x levels and decreasing instances of BB.

3.4.2- Toxicological Profile of LG

3.4.2.1- IC₅₀ and Cellular Death Analysis in LG-Treated Lung Cells

The LG-treated BEAS-2B (Figure 3.4.2) and A549 (Figure 3.4.3) cells were analyzed for percentage of cellular viability using the MTT assay, and the corresponding IC₅₀ values were calculated using an increasing concentration of LG (0.01 – 200 µg mL⁻¹). This was followed by the determination of the percentage of cellular death following exposure to 0.01 – 200 µg mL⁻¹ of LG using the LDH assay, and morphological changes were assessed by using the Calcein-AM/ PI staining under the fluorescence microscope. The IC₅₀ values for LG-treated BEAS-2B cells were calculated using the proliferation rate percentage from the MTT assay, and was found to be ~ 2546 and ~ 3 x 10⁷ µg mL⁻¹ at 24 h and 48 h, of exposure respectively (Figure 3.4.2a).

The IC₅₀ values for LG-treated A549 cells were calculated to be ~ 4.4 x 10⁸ and ~ 1.6 x 10⁸ µg mL⁻¹ at 24 h and 48 h, respectively, of exposure (Figure 3.4.3a). As shown in Figures 3.4.2b and 3.4.3b, exposure to the 1.0 and 10 µg mL⁻¹ of LG in the BEAS-2B and A549 cells, respectively, resulted in a slight increases (around 5-10%) in the LDH release percentage. This effect was only observed at 24 h of exposure. No such increase was observed at higher concentrations as confirmed by the Calcein-AM/PI-stained cellular micrographs in Figures 3.4.2c and 3.4.3c.

The BEAS-2B cellular morphology remained intact as the untreated control when exposed to the 100 and 200 µg mL⁻¹ of LG at 24 and 48 h exposures, as seen through the Calcein-AM-stained cells channel. No significant increase in PI-stained cells were observed at both 24 and 48 h of treatment. However, for the A549 cells, a slight increase in the PI channel staining was observed at 24 h exposure with the 100 µg mL⁻¹ treatment, and the cellular morphology (as observed in the bright-field channel) was distorted. The combined LDH, cellular imaging and IC₅₀ data shows that LG-treated BEAS-2B and A549 cells exhibited a concentration-dependent effect on cellular viability, and the inhibitory effect was more evident in BEAS-2B cells. In contrast, the concentration-dependent cellular death was observed in A549 cell lines. The decrease in the LG-treated BEAS-2B cells proliferation rate percentage suggests the possibility of metabolic stress inside the cells that causes inhibition in the growth rate relative to control, as the cytotoxic effect is negligible at the studied concentrations.³⁷² Likewise, the percentage proliferation rate in the A549

cells is not affected significantly relative to control even with a slight increase in the cytotoxicity- this suggests a high metabolic rate coupled with cellular death in the cancer cells.[373](#)

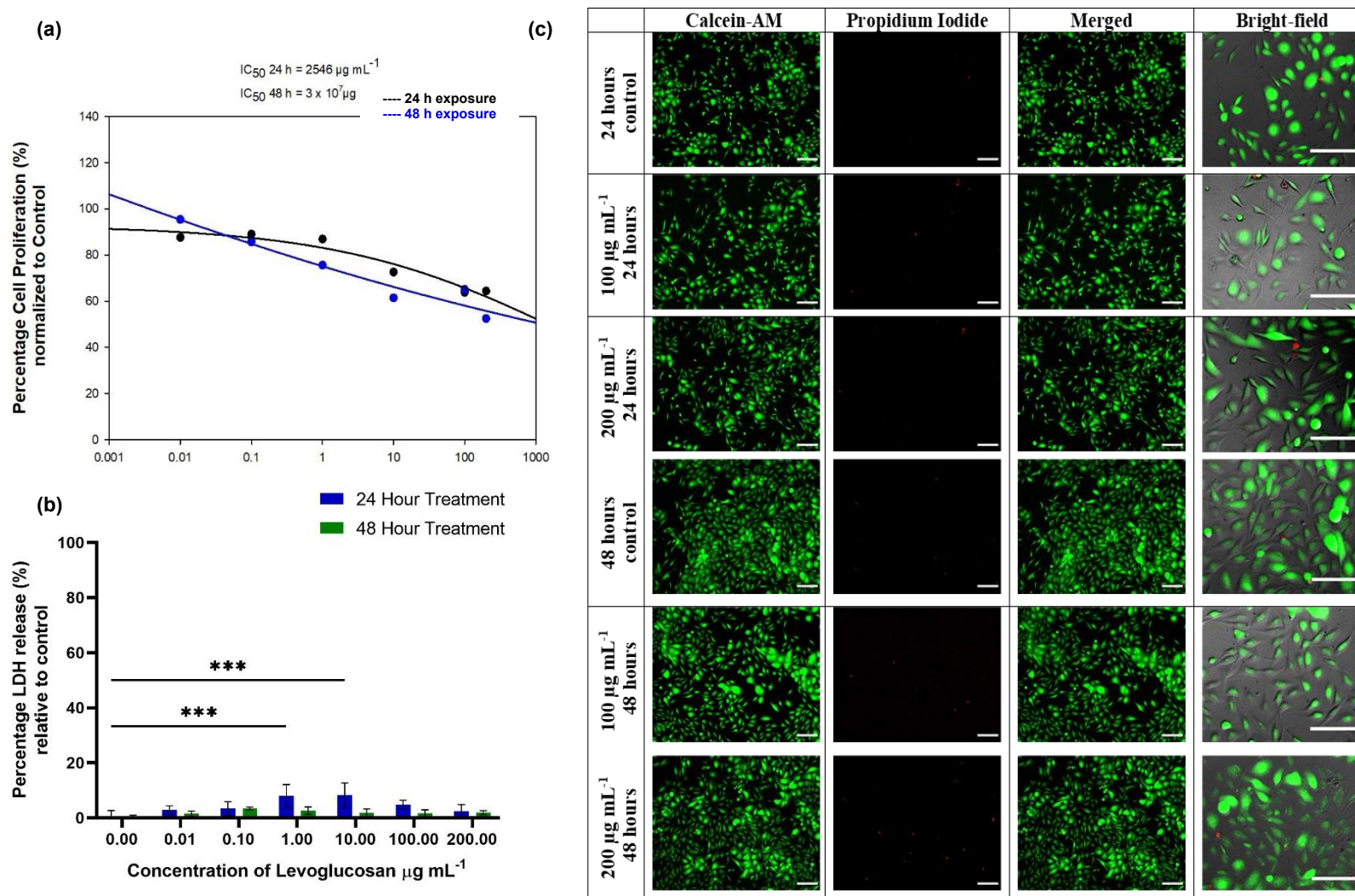


Figure 3.4.2. Cellular viability and death analyses in the BEAS-2B cell lines following exposure to LG: (a) IC₅₀ values of LG at 24 and 48 h exposure; (b) LDH analysis at 24 and 48 h exposure; and (c) The Calcein-AM/PI staining of cells treated with 100 and 200 µg mL⁻¹ of LG at 24 h and 48 h exposure. Micrographs are scaled to 50-µm in size.

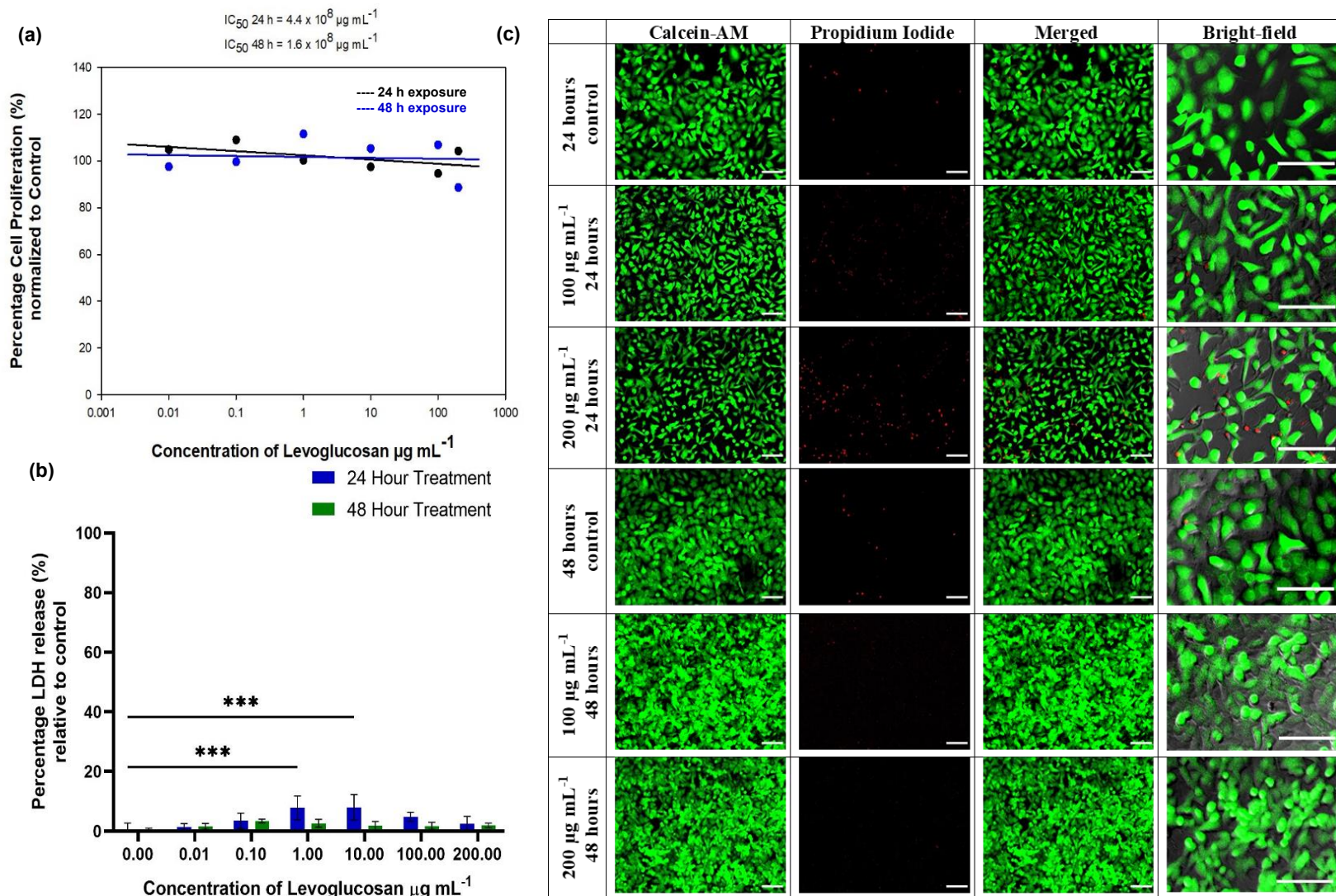
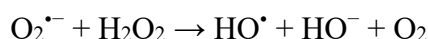


Figure 3.4.3. Cellular viability and death analysis in the A549 cell lines following exposure to LG: (a) IC_{50} values of LG-treated cells at 24 and 48 h exposure (b) LDH analysis at 24 and 48 h exposure; and (c) The Calcein-AM/PI staining of cells treated with 100 and 200 $\mu\text{g mL}^{-1}$ of LG at 24 and 48 h exposure. Micrographs are scaled to 50- μm in size.

3.4.2.2- General and Mitochondrial ROS buildup in LG-Treated Lung Cells

The mitochondrial membrane potential ($\Delta\Psi_m$) is essential for the functionality of many cellular organelles.³⁷⁴ The prime role of $\Delta\Psi_m$ is to drive ATP synthesis by oxidative phosphorylation, and its magnitude (basal level ~ 120 – 180 mV, negative inside of the membrane) is determined by the balance between its generation (as an electrons passing through the respiratory chain as oxygen) and its consumption by ATP synthesis and other potential dissipative processes.³⁷⁵ Hence, $\Delta\Psi_m$ is an important indicator of mtROS and cellular energetics.³⁷⁵ $\Delta\Psi_m$ is decreased in case of enhanced ATP production, thermogenesis (or energy dissipating) process and as a result of mitochondrial dysfunction.^{375; 376} An increase in $\Delta\Psi_m$ may be attributed to low ATP production and upregulation of proton pumps in the inner mitochondrial membrane.³⁷⁵⁻³⁷⁷ Such an increase can also be attributed to the intrinsic pathway of cellular apoptosis (through the release of cytochrome c),³⁷⁶ cancer progression, aging and mtROS redox.^{377; 378} The mild depolarization of $\Delta\Psi_m$ is associated with decreased mtROS production as ROS homeostasis process inside the cells.³⁷⁹ The mtROS controls homeostasis of the whole cell, and the rate of mitochondrial $O_2^{\cdot-}$ and H_2O_2 is determined by mtSOD (enzyme scavenging $O_2^{\cdot-}$ from mitochondria);³⁷⁸ the overall reaction is summarized in the equation below:



The redox-optimized ROS balance hypothesis³⁸⁰ states that physiological mtROS (and subsequent cellular ROS) signalling occurs within an optimized cellular condition, and mtROS increase at either the extreme of high $\Delta\Psi_m$ or low $\Delta\Psi_m$, thereby indicating that anti-ROS system of the cell is compromised following exposure to endogenous compounds (in the case of this thesis, the BBA markers).³⁸¹

The LG-treated BEAS-2B and A549 cells were analysed for ROS changes. The change in general cellular ROS was determined through carboxy- H_2DCHF dye, while changes in the mitochondrial ROS determined through MitoSox assay and MitoPY1 dye. Furthermore, alterations in mitochondrial membrane potential ($\Delta\Psi_m$) were determined through the TMRM assay. **Figure 3.4.4** shows the changes in the cellular ROS and mtROS of the BEAS-2B cells treated with LG following 8 h the exposure. **Figure 3.4.4a** shows the flow cytometric TMRM analysis of the BEAS-2B cells treated with LG at 12, 24 and 48 h of exposure at the $200\text{-}\mu\text{g mL}^{-1}$ treatment concentration. At 12 h, the TMRM fluorescence signal ($\Delta\Psi_m$) increased to ~ 1.25 over the control, while no significant change was observed at 24 h. The $\Delta\Psi_m$ decreased to ~ 0.8 over the controls at 48 h exposure. As shown in **Figure**

3.4.4b, the MitoSox signal increased to ~1.6 over the controls following exposure to the LG concentration of 100 and 200 $\mu\text{g mL}^{-1}$ at 8 h exposure. As shown in Figure 3.4.4c, no significant increase in carboxy- H_2DCHF signal was observed following exposure to 100 $\mu\text{g mL}^{-1}$ of LG at 8 h, while ~1.4-fold increase in the signal was observed when compared to controls when the exposure concentration of LG was increased to 200 $\mu\text{g mL}^{-1}$.

The images of ROS-fluorophores tagged in BEAS-2B cells, treated with LG, were acquired through confocal microscopy as shown in Figure 3.4.4d. The upper channels show the changes in general ROS and mtROS in BEAS-2B cells treated with 200 $\mu\text{g mL}^{-1}$ of LG at 8 h of the exposure. An increased carboxy- H_2DCHF signal was observed, which closely overlays with the MitoSox signal. In the lower channel, which uses the MitoPY1 stain, no change in the signal was observed in the LG-treated lung cells, while increased MitoSox signal was observed.

The increase in the $\Delta\Psi\text{m}$ during the first 12 h of exposure was associated with a subsequent increase in MitoSox signal. The latter indicates that low ATP production³⁷⁵ was likely, and hence, consistent with the decrease in the cellular proliferation rate (as determined through MTT assay) shown in Figure 3.4.2. This could be attributed towards low mitochondrial functionality, as negligible cellular death was observed at higher exposure concentration.³⁸² Mild depolarization of $\Delta\Psi\text{m}$ at 48 h of the exposure indicates the decrease in the mtROS production,³⁷⁹ especially since no cellular death was observed at 48 h of exposure. Hence, the decreased $\Delta\Psi\text{m}$ suggests that the cells are trying to recover from increased cellular ROS and mtROS production during the first 24 h of LG exposure.

In the A549 cells treated with 200 $\mu\text{g mL}^{-1}$ of LG, there was no significant change observed in the TMRM signal at 12, 24 and 48 h of exposure (as shown in Figure 3.4.5a). However, as shown in Figure 3.4.5b, a ~1.5-fold increase in MitoSox signal was observed following treatment with 200 $\mu\text{g mL}^{-1}$ of LG at 8 h of exposure. The change in the carboxy- H_2DCHF signal was non-significant in the 200- $\mu\text{g mL}^{-1}$ exposure to LG after 8 h, while a slight decrease of ~0.8-fold change compared with controls was observed following exposure to 100 $\mu\text{g mL}^{-1}$ of LG (as shown in Figure 3.4.5c). The confocal microscopy images of the LG-treated A549 cells at 8 h of the exposure reveals increased carboxy- H_2DCHF and MitoSox signals in panel 1 when compared with untreated controls. As shown in Figure 3.4.5d, the signal observed in carboxy- H_2DCHF channel was due to the mtROS since both the MitoSox and MitoPY1 signals were observed in panel 2, and the merged images of MitoSox with carboxy- H_2DCHF depict similar signals overlaying each other.

The A549 cells were more resistant than BEAS2B to the changes in ROS, as reported in previous sections of the thesis.⁷³ Slight increases in mtROS (as a function of MitoSox signal at 8 h) indicates the slight mitochondrial membrane leakage of $O_2^{\cdot-}$, and likely explains the increased PI staining at 24 h of exposure in **Figure 3.4.3c**. However, this effect was not strong enough to cause a change in $\Delta\Psi_m$, and cells appear to recover at 48 h of the exposure.

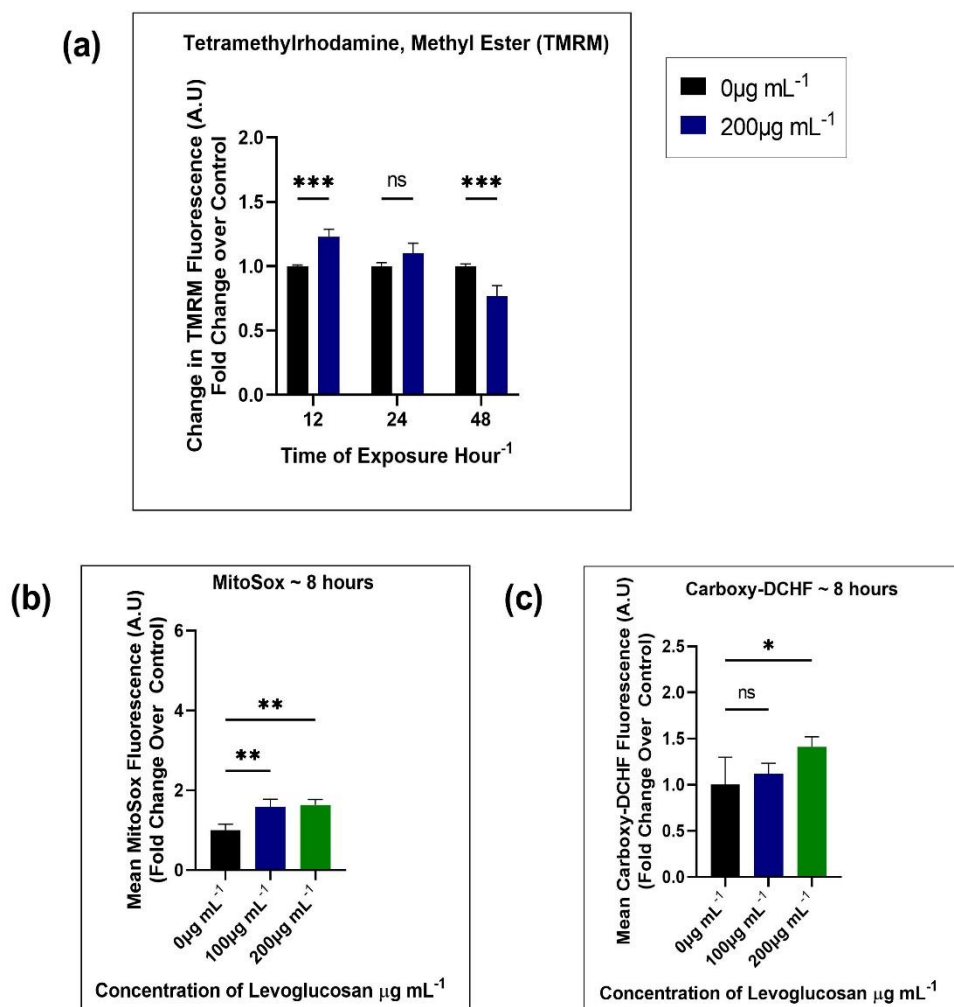


Figure 3.4.4. The general ROS and mtROS analysis in the BEAS-2B cell lines after exposure to LG using flow cytometry and confocal microscopy: (a) Changes in TMRM fluorescence compared to controls following treatment with 200 µg mL⁻¹ LG at 12, 24 and 48 h of exposure; (b) Fold change in MitoSox signal with 100 and 200 µg mL⁻¹ of LG exposure at 8 h of exposure; and (c) Fold change in carboxy H₂DCHF signal with 100 and 200 µg mL⁻¹ of LG exposure at 8 h (to be continued on the next page).

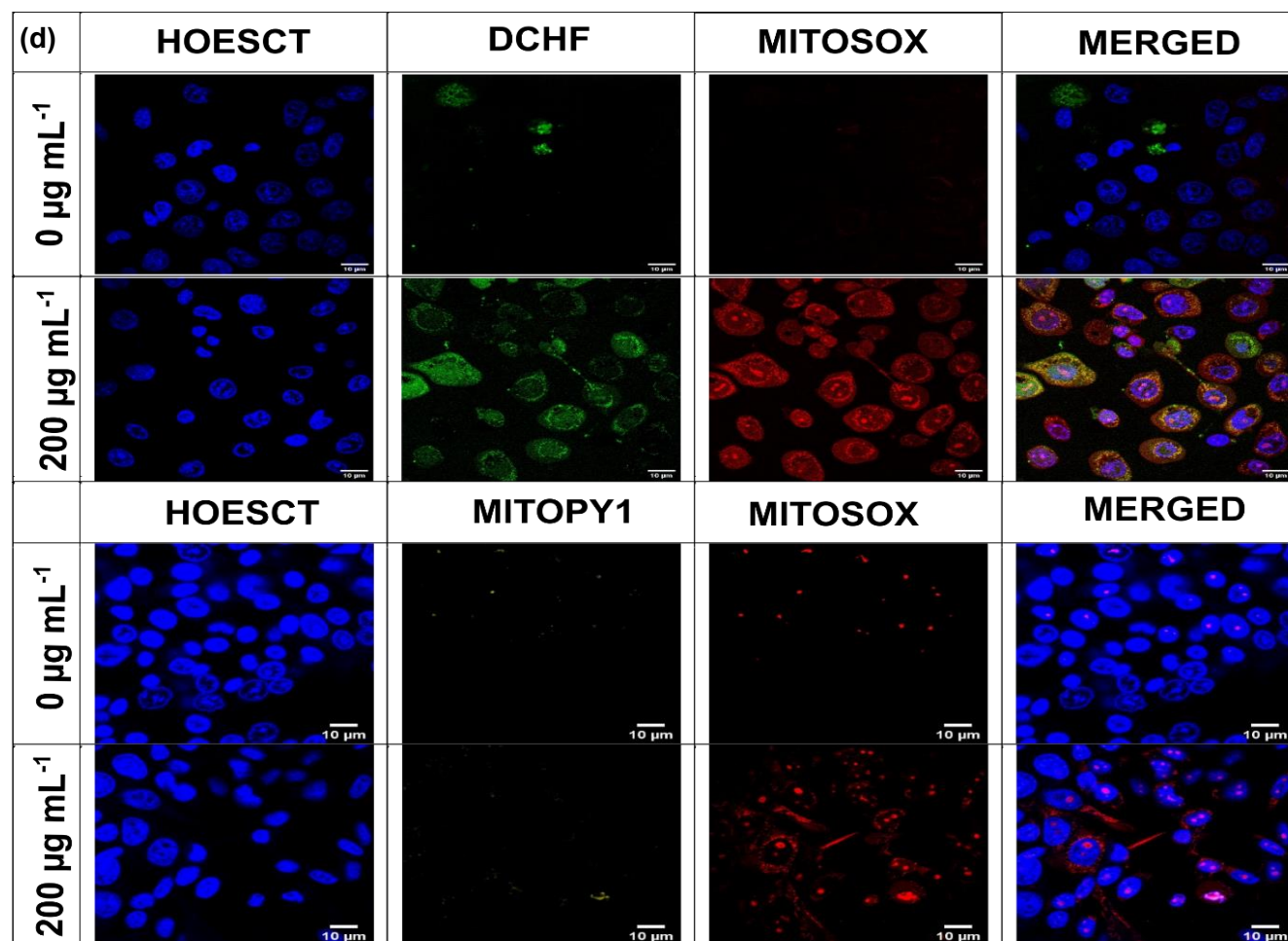


Figure 3.4.4 continuation. (d) Confocal imaging of cells treated with 200 $\mu\text{g mL}^{-1}$ of LG at 8 h of the exposure stained with the carboxy H₂DCHF and MitoSox dye in panel 1 and MitoPY1 and MitoSox in panel 2. The cellular nucleus was stained with Hoechst. Micrographs are scaled to 10- μm sizes.

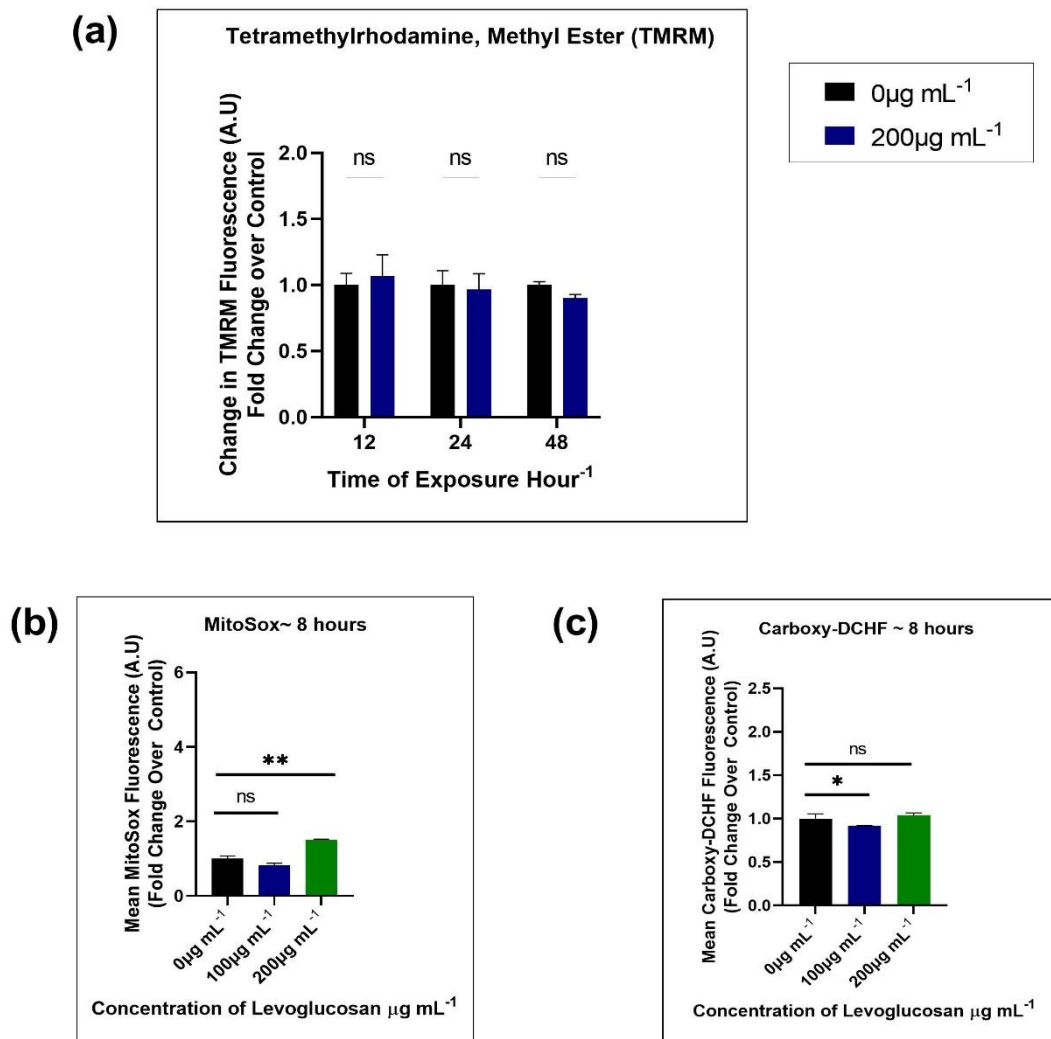


Figure 3.4.5. The general ROS and mtROS analysis in the A549 cell lines after exposure to LG using flow cytometry and confocal microscopy: (a) Changes in TMRM fluorescence compared to controls following treatment with 200 µg mL⁻¹ LG at 12, 24 and 48 h of exposure; (b) Fold changes in the MitoSox signals with 100 and 200 µg mL⁻¹ of LG exposure at 8 h; and (c) Fold changes in the carboxy H₂DCHF signals with 100 µg mL⁻¹ and 200 µg mL⁻¹ of LG exposure at 8 h (to be continued on the next page).

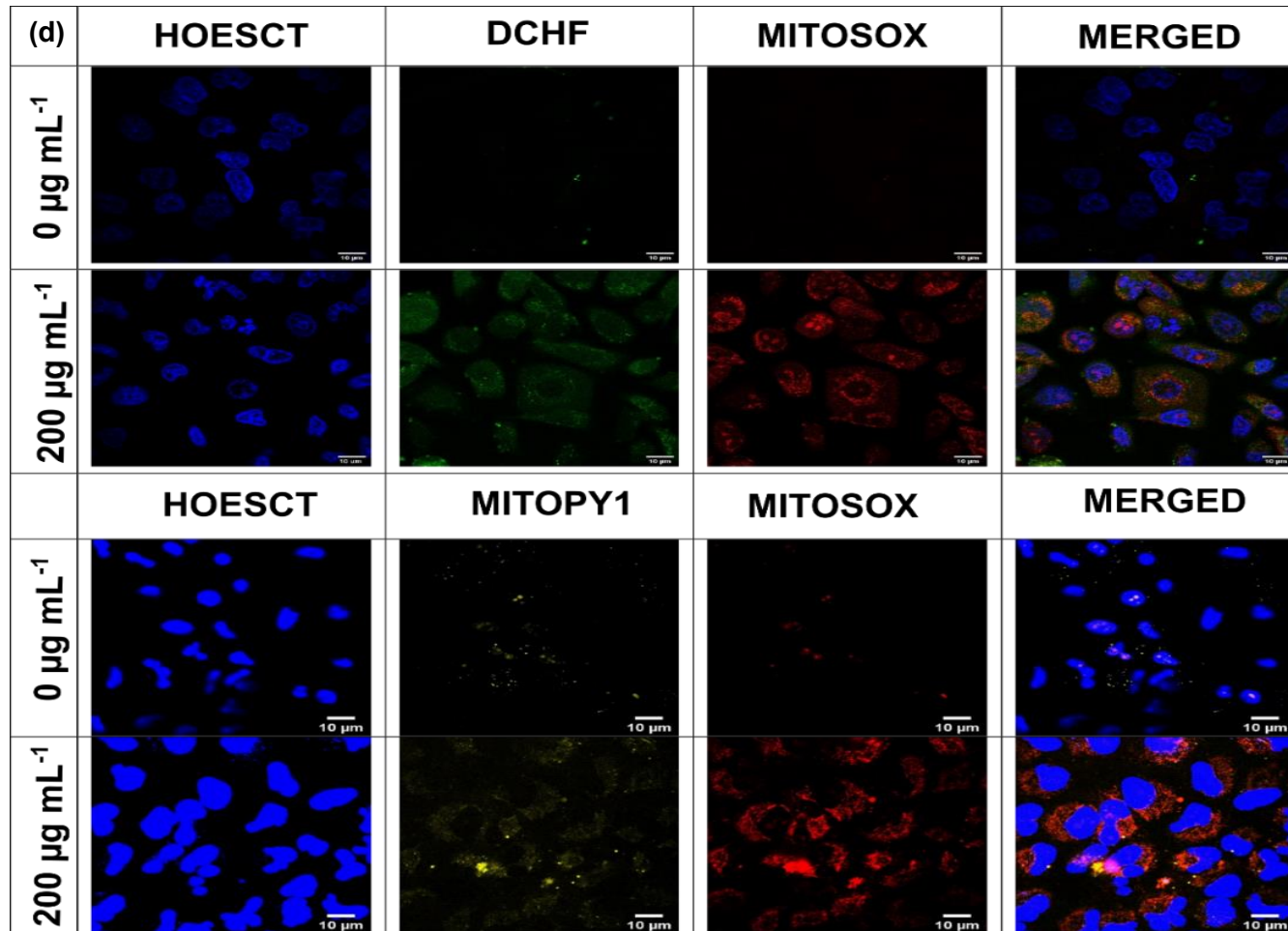


Figure 3.4.5 continuation (d) Confocal imaging of cells treated with 200 $\mu\text{g mL}^{-1}$ of LG at 8 h of exposure stained with the carboxy H₂DCHF and MitoSox dye in panel one and MitoPY1 and MitoSox in panel 2. The cellular nucleus was stained with Hoechst stain. Micrographs are scaled to 10 μm

3.4.2.3- Mechanism of Cell Death in LG-Treated Lung Cells

The cells undergoing cellular death through apoptosis have distinct attributes that include chromatin (or DNA) condensation, blebbing of the cell plasma membrane (apoptotic bodies), nuclear fragmentation, and phosphatidylserine (PS) exposure on the outside of the cell membrane.³⁸³ This intrinsic apoptotic pathway (triggered by intracellular signaling and factors) is further regulated by changes in the $\Delta\Psi_m$, DNA damage, caspase induction and ROS increase.³⁸³⁻³⁸⁵ On the contrary, necrosis is characterized by cytoplasmic swelling and is a consequence of extreme physiochemical stress. It is associated with unwanted loss of cells from organs, inflammation, and rupture of the plasma membrane followed by organelle matrix in the extra-cellular vicinity.³⁸³

The BEAS-2B cells treated with $200\ \mu\text{g mL}^{-1}$ of LG were analyzed for the mechanism of cellular death using the Annexin-V/PI staining. At 12 h of the exposure, a slight increase in the late apoptotic/necrotic cellular population was observed (15%) when compared with untreated controls (10%). At the same time, the percentage of live cells decreased from 75% in the untreated controls to ~71% in the treated cells. However, at 24 h of exposure, the percentage of live cells increased and no significant change in the percentage of other populations was observed. As shown in [Figure 3.4.6.](#), the 48 h of the exposure to LG also did not exhibit much difference in the percentage population compared with the untreated controls. The increase in the MitoSox signal in the BEAS-2B cells at ~8 h of the exposure and increased $\Delta\Psi_m$ at 12 h of the exposure (as exhibited in [Figure 3.4.4](#)) may help to explain the evidence of the apoptotic/necrotic cell population³⁸² in the early stages of exposure. Still, only 5% increase in the population was observed which is restored to normal in the later stages of LG exposures. These data further confirms that the decrease in cellular proliferation rate at 24 h and 48 h of exposure observed in [Figure 3.4.2](#) is due to mitochondrial stress.

As shown in [Figure 3.4.7.](#), in A549 cells treated with the $200\text{-}\mu\text{g mL}^{-1}$ of LG, there was no significant changes observed in the cellular population compared with the untreated controls at 12, 24 or 48 h of the exposure.

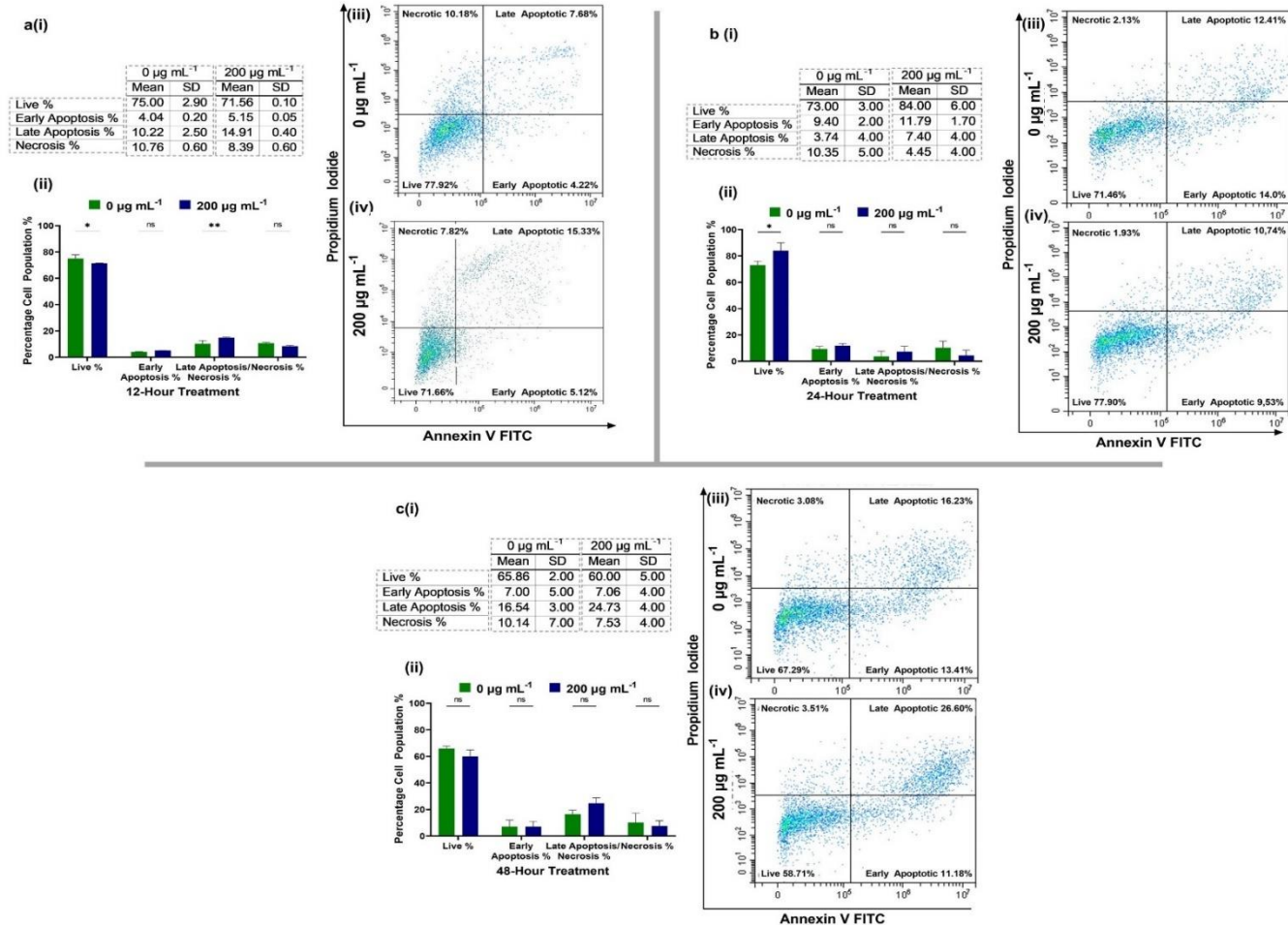


Figure 3.4.6. Annexin-V/PI staining of LG-treated BEAS-2B cells was conducted to evaluate the mechanism of cellular death following exposure to 200 $\mu\text{g mL}^{-1}$ of LG at: (a) 12 h; (b) 24 h; and (c) 48 h exposure. The table in (i) represents the average of experiments performed; (ii) the bar-graph represents the percentage cellular population in either live, early apoptotic, late apoptotic/necrotic, and necrotic phases; and the dot plot represents the sample of one experiment for (iii) the control group and (iv) the treatment group.

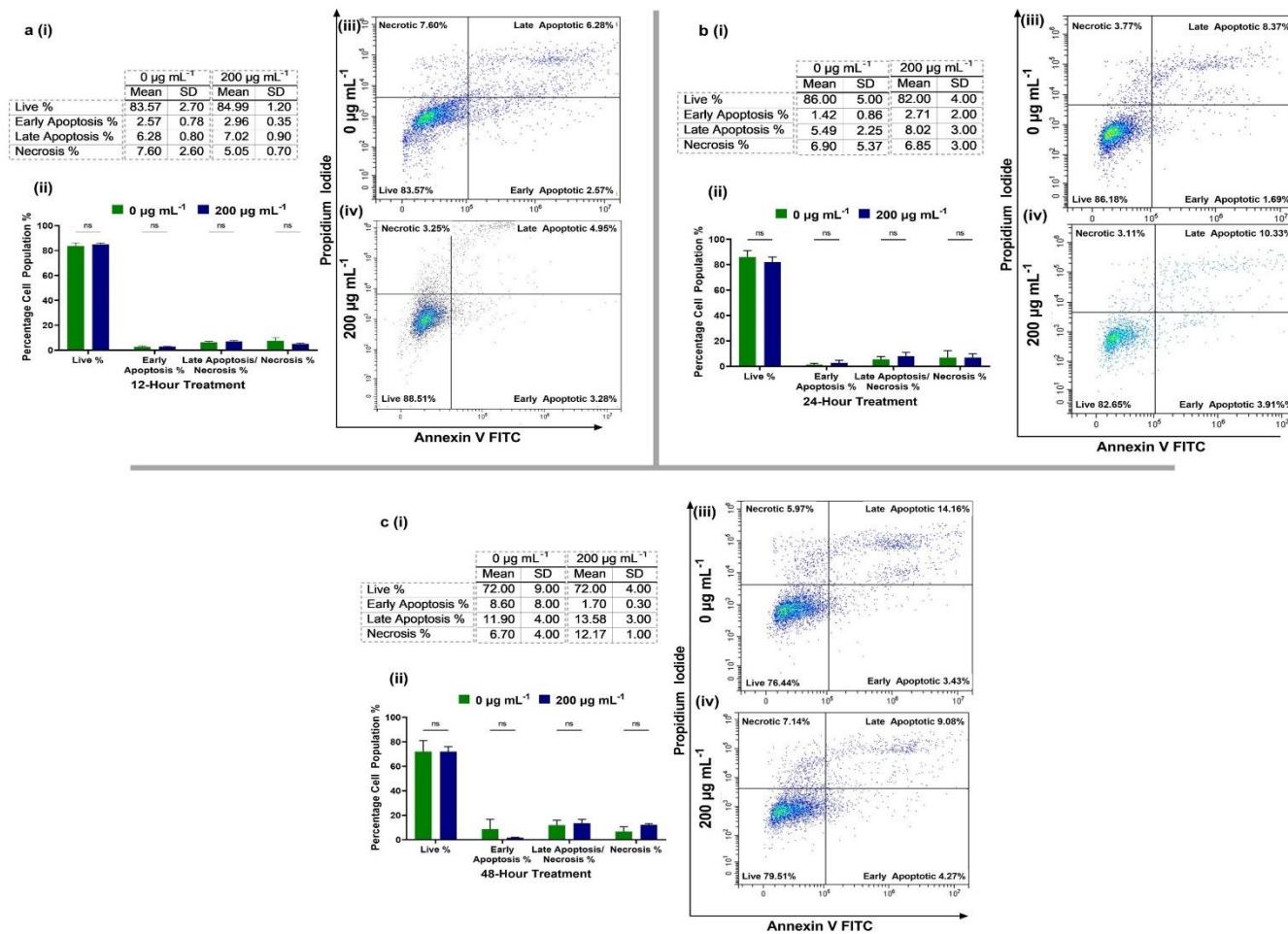


Figure 3.4.7. Annexin-V/PI staining of LG-treated A549 cells to evaluate the mechanism of cellular death following exposure to the 200- $\mu\text{g mL}^{-1}$ concentration of LG at: (a) 12 h; (b) 24 h; and (c) 48 h exposure. The table in (i) represents the average of experiments performed; (ii) the bar-graph represents the percentage cellular population in either live, early apoptotic, late apoptotic/necrotic, and necrotic phases; and the dot plot represents the sample of one experiment for (iii) the control group and (iv) the treatment group.

3.4.3- Toxicological Profile of NS

3.4.3.1- IC₅₀ and Cellular Death Analysis in NS-Treated Lung Cells

The NS-treated BEAS-2B (Figure 3.4.8) and A549 cells (Figure 3.4.9) were analyzed for cellular viability percentage using an increasing concentration of NS (0.01 – 200 $\mu\text{g mL}^{-1}$). The IC₅₀ values for NS-treated BEAS-2B cells were found to be $\sim 695 \mu\text{g mL}^{-1}$ and $\sim 0.16 \mu\text{g mL}^{-1}$ at 24 and 48 h, respectively, of the exposure (Figure 3.4.8a). The IC₅₀ values for NS-treated A549 cells were calculated to be ~ 279 and $\sim 2.02 \times 10^8 \mu\text{g mL}^{-1}$ at 24 and 48 h, respectively, of exposure (Figure 3.4.9a). The inhibitory effect evident in the first 24 h of exposure in A549 cells recovered at 48 h, and thus, a higher IC₅₀ value was noted.

Exposure to the 100 and 200 $\mu\text{g mL}^{-1}$ of NS in the BEAS-2B and A549 cells resulted in a slight increases (around 10-15%) in the LDH release percentage as shown in Figures 3.4.8b and 3.4.9b, respectively. This effect was observed at both 24 h and 48 h of exposure. The increase in cellular death were observed at higher concentrations as confirmed by the Calcein-AM/ PI stained cellular micrographs shown in Figures 3.4.8c and 3.4.9c respectively.

The BEAS-2B cellular morphology remained intact as the untreated controls when exposed to the 100 and 200 $\mu\text{g mL}^{-1}$ of NS at 24 h and 48 h (as seen through the Calcein-AM stained cells channel in Figure 3.4.8c. No significant increases in the PI-stained cells were observed at both 24 and 48 h of exposure. However, for the A549 cells, a slight increase in the PI channel staining was observed at 24 h exposure with 100 and 200 $\mu\text{g mL}^{-1}$ of NS, and the cellular morphology (as observed in the bright-field channel) was distorted. At 48 h of treatment, A549 cells exhibited only a slight increase in the PI channel staining, thereby depicting the cytotoxic effect shown by NS exposure was recovered at 48 h.

The small increase in the LDH release percentage in BEAS-2B cells was attributed to cell death following immediate exposure at a time of the exposure less than 24 h. The cells underwent a decreased proliferation rate after 48 h of exposure (Figure 3.4.8a), but significant cell death was not observed in the BEAS-2B cells. This is confirmed by the bright-field images in Figure 3.4.8b, as slightly less numbers of cells were found for 100 $\mu\text{g mL}^{-1}$ of NS exposure. The cell numbers recovered at higher concentrations of exposure

200 $\mu\text{g mL}^{-1}$, thereby indicating that mitochondrial stress and proliferation inhibition had occurred.³⁷⁸ ³⁸² A higher number of cellular death was observed in A549 cell lines (Figure 3.4.9c), as evident from increased PI staining and at 48 h of exposure. At the same time, we noticed a continuous inhibitory effect of ~80% proliferation rate with 0.01-200 $\mu\text{g mL}^{-1}$ of NS exposure.

The combined LDH, cellular imaging and IC_{50} data show that NS-treated BEAS-2B and A549 cells exhibited a concentration-dependent effect on cellular viability, and the inhibitory effect was more evident in BEAS-2B cells. Concentration-dependent cellular death was only observed in A549 cell lines.

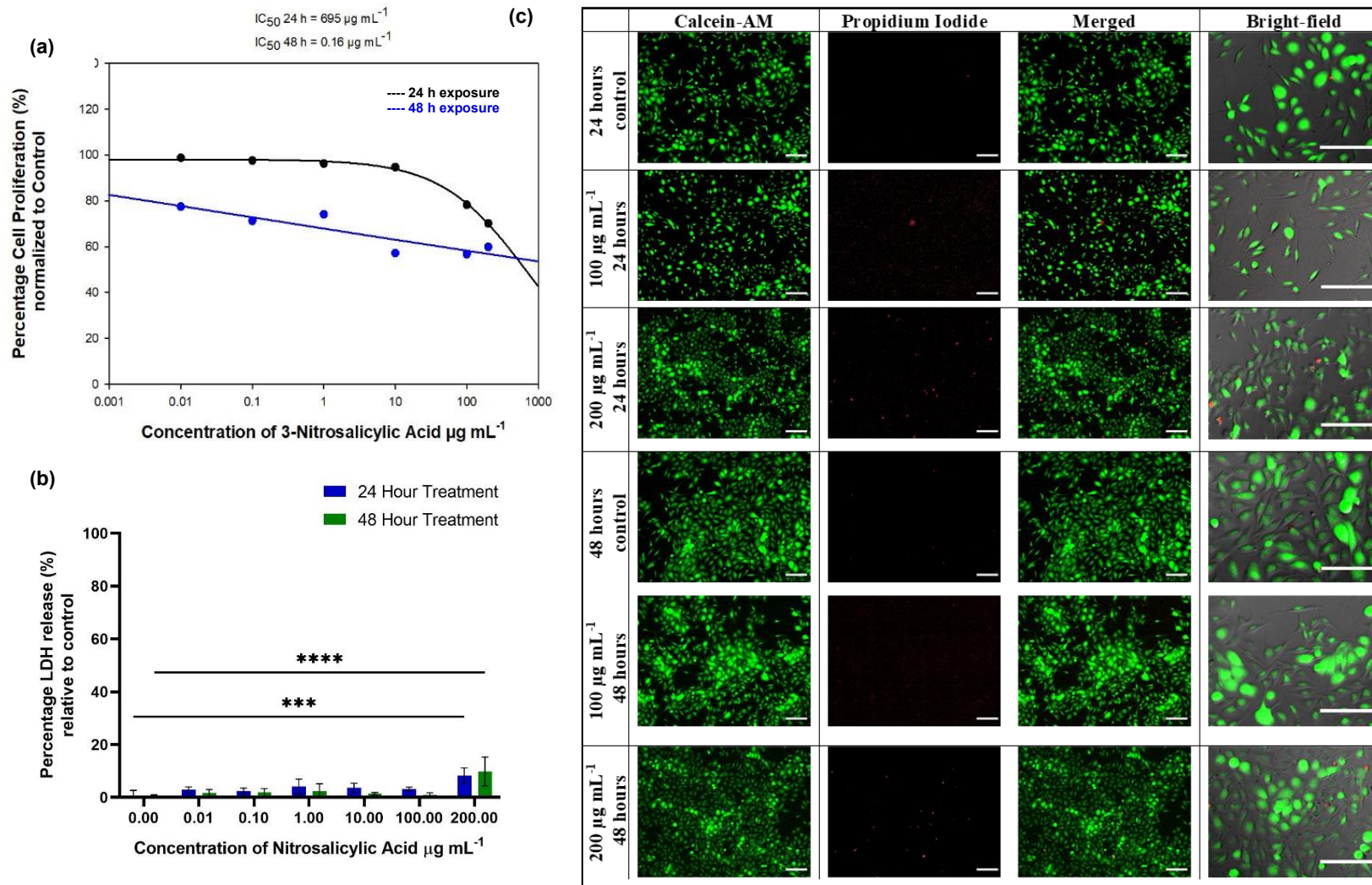


Figure 3.4.8. The cellular viability and death analysis in the BEAS-2B cell lines following exposure to NS: (a) IC_{50} values of at 24 and 48 h of exposure; (b) LDH analysis at 24 and 48 h of exposure; (c) The Calcein-AM/PI staining of cells treated with 100 and 200 $\mu\text{g mL}^{-1}$ of 3NS at 24 and 48 h of exposure. The micrographs are scaled to 50- μm in size.

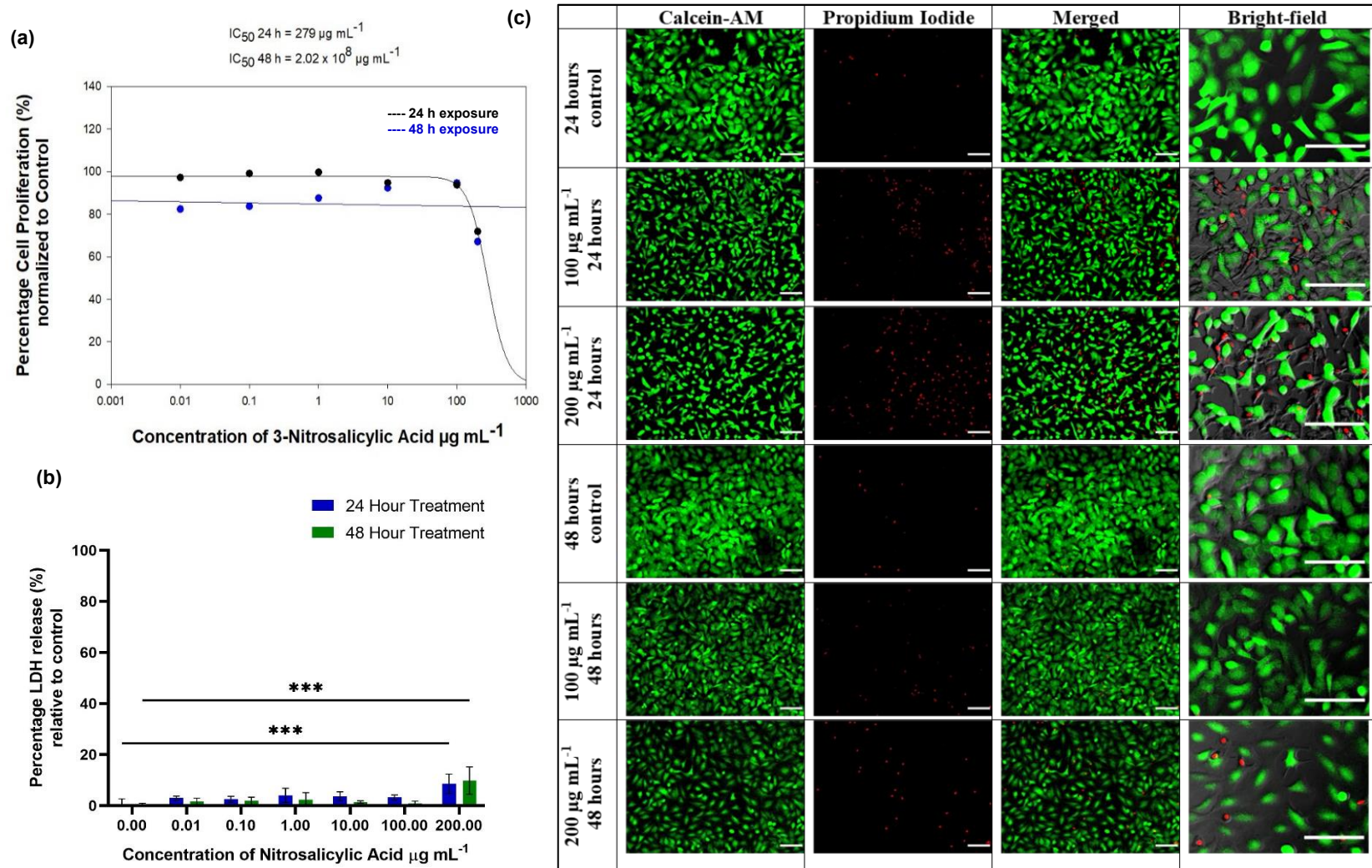


Figure 3.4.9. The cellular viability and death analysis in the A549 cell lines following exposure to NS: (a) IC_{50} values of NS at 24 and 48 h of exposure (b) LDH analysis at 24 and 48 h of exposure; and (c) The Calcein-AM/PI staining of cells treated with 100 and 200 $\mu\text{g mL}^{-1}$ of NS at 24 and 48 h of exposure. The micrographs are scaled to 50- μm in size.

3.4.3.2- General and Mitochondrial ROS buildup in NS-Treated Lung Cells

The NS-treated BEAS-2B and A549 cells were analysed for changes in the cellular ROS and mtROS. **Figure 3.4.10** shows the changes in the cellular ROS and mtROS observed for the BEAS-2B cells treated with NS following the 8 h of exposure. **Figure 3.4.10a** shows the $\Delta\Psi_m$ analyses of the BEAS-2B cells treated with $200\ \mu\text{g mL}^{-1}$ of 3NS at 12, 24 and 48 h of exposure. The only significant increase in $\Delta\Psi_m$ was observed at 48 h of exposure, where ~ 1.6 -fold increase in the signal was observed when compared with untreated controls. The MitoSox signal increased to ~ 2.4 over controls following exposure to $200\ \mu\text{g mL}^{-1}$ of NS (as shown in **Figure 3.4.10b** at 8 h of exposure). An ~ 1.4 -fold increase in the carboxy- H_2DCHF signal was observed following exposure to $200\ \mu\text{g mL}^{-1}$ of 3NS at 8 h, while no change in the ROS signal was observed after exposure to $100\ \mu\text{g mL}^{-1}$ of 3NS (as shown in **Figures 3.4.10b & c**).

The confocal images of the BEAS-2B cells treated with NS are shown in **Figure 3.4.10d**. The upper channels show the general ROS and mitochondrial $\text{O}_2^{\cdot-}$ production in BEAS-2B cells treated with $200\ \mu\text{g mL}^{-1}$ of NS at the 8 h of exposure, while lower panel shows the NS-treated lung cells at the 8 h of exposure that shows changes in the mitochondrial H_2O_2 and $\text{O}_2^{\cdot-}$. The increased carboxy- H_2DCHF signals were observed in the NS-treated lung cells. However, there is a high ROS signal outside the cells. The MitoSox signals were confined to the inside of cells, implying that in the merged upper channel of **Figure 3.4.10d** that cellular inhibition (as seen in **Figure 3.4.8a**) could be attributed to a high ROS activity. The latter results in the expulsion of ROS from inside the cells and they develop a resistance to the NS exposures.[88](#); [259](#) It also explains the low cellular death at 24 and 48 h of the exposure to NS in **Figures 3.4.8b & c**. In the lower channel of **Figure 3.4.10d**, increased MitoPY1 signals were observed in the NS-treated lung cells, which is correlated with increased MitoSox signals. Together with the increased $\Delta\Psi_m$ observed in **Figure 3.4.10a** at 48 h and high mtROS associated signal, the inhibition effect of the MTT assay could be explained.[371](#); [382](#) The overall mitochondrial activity was impaired following the NS treatments without causing significant alterations in the BEAS-2B cellular viability.

As shown in **Figure 3.4.11a**, for the A549 cells treated with $200\ \mu\text{g mL}^{-1}$ of NS there was no significant change observed in the TMRM signals at 12, 24 and 48 h of exposure. However, as shown in **Figure 3.4.11b**, ~ 1.2 and ~ 1.6 -fold increases in MitoSox signals were observed following treatments with 100 and $200\ \mu\text{g mL}^{-1}$ of NS, respectively, at the

8 h of exposure. As shown in **Figure 3.4.11c**, changes in the carboxy-H₂DCHF signals were insignificant after exposure to 100 and 200 $\mu\text{g mL}^{-1}$ of NS at the 8 h exposure.

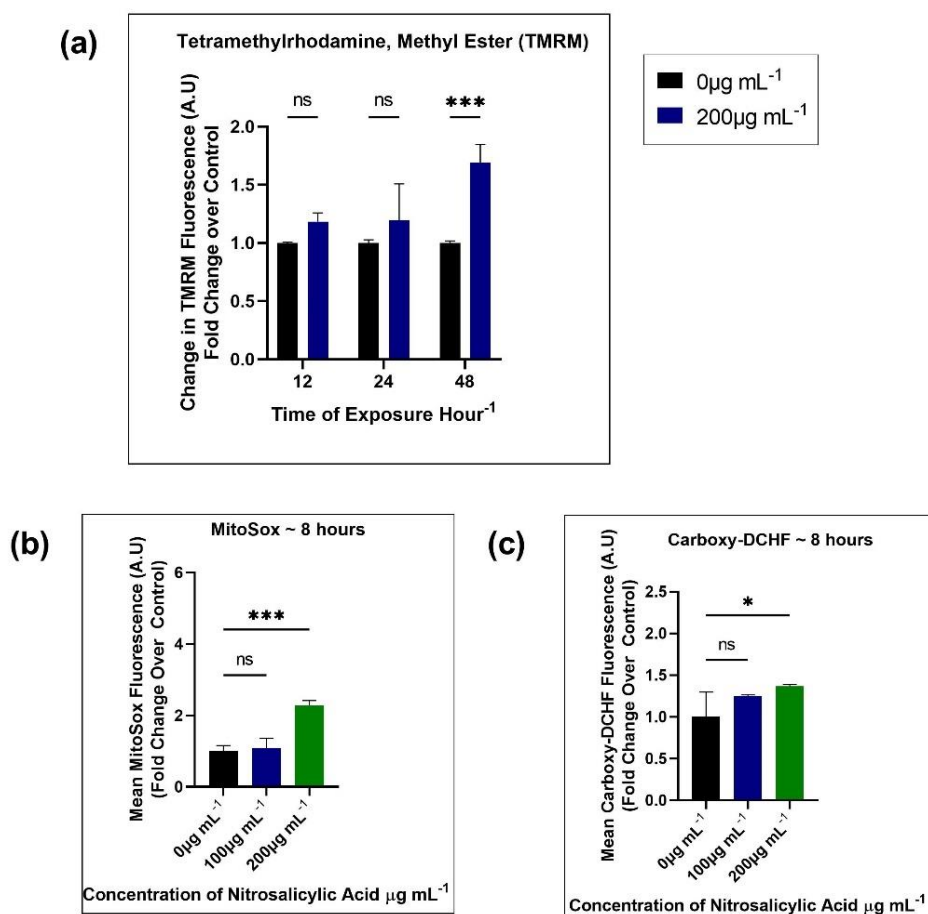


Figure 3.4.10. The general ROS and mtROS analysis in the BEAS-2B cell lines after exposure to NS using flow cytometry and confocal microscopy: (a) Changes in the TMRM fluorescence compared to controls following treatment with 200 $\mu\text{g mL}^{-1}$ of NS at 12, 24 and 48 h of exposure; (b) Fold changes in the MitoSox signals with 100 and 200 $\mu\text{g mL}^{-1}$ of NS exposure at 8 h; (c) Fold changes in carboxy-H₂DCHF signals with 100 and 200 $\mu\text{g mL}^{-1}$ of NS exposure at 8 h (to be continued on next page).

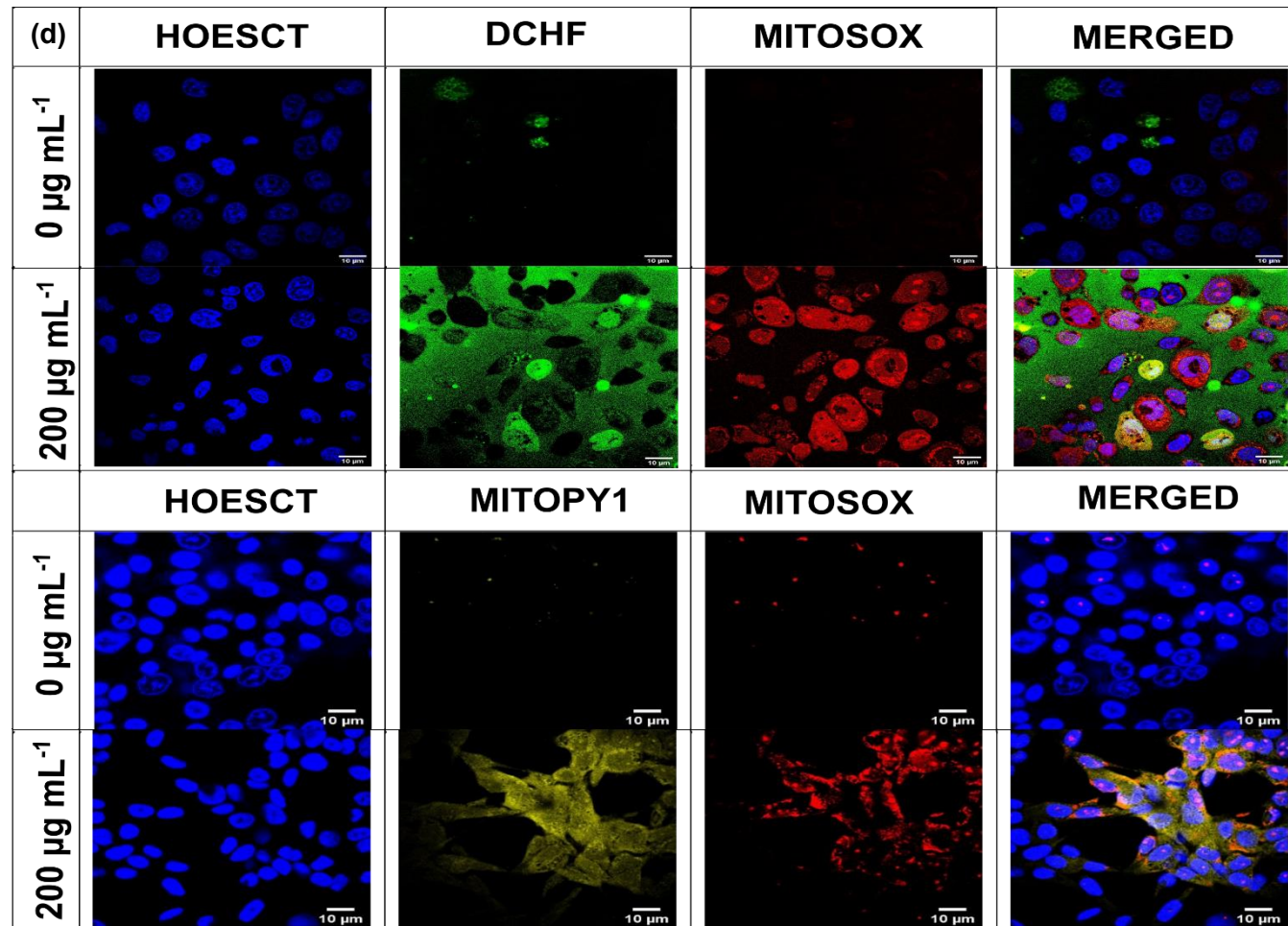


Figure 3.4.10 (continuation). (d) Confocal imaging of BEAS-2B cells treated with 200 $\mu\text{g mL}^{-1}$ of NS at the 8 h of exposure stained with the carboxy H₂DCHF and MitoSox dye in panel 1, and MitoPY1 and MitoSox in panel 2. The cellular nucleus was stained with Hoechst. Micrographs are scaled to 10- μm in size.

As shown in **Figure 3.4.11d**, the confocal microscopy images of the NS-treated A549 cells at 8 h of the exposure shows slightly increased carboxy-H₂DCHF and MitoSox signals in panel 1 when compared with the untreated controls. The signals observed in the carboxy-H₂DCHF channel were outside of the A549 cells, implying a similar mechanism of ROS expulsion of cells,³⁶⁶⁻³⁷⁸ which was also shown above for the BEAS-2B cells. In the lower panel of **Figure 3.4.11d**, increased mtROS signals were associated to increased MitoSox signals. Slightly increased MitoPY1 signals were also observed. The merged images of MitoSox with MitoPY1 depict similar signals overlaying each another (as shown in **Figure 3.4.11d**).

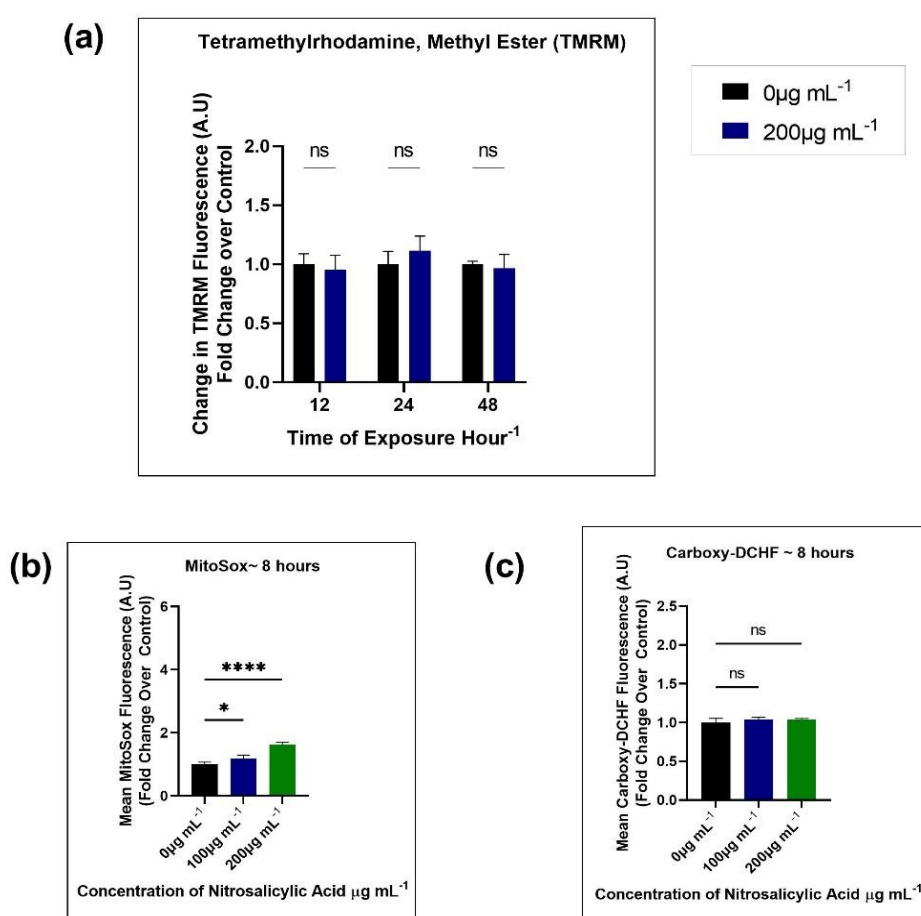


Figure 3.4.11. The general ROS and mtROS analysis in the A549 cell lines after exposure to NS using flow cytometry and confocal microscopy: (a) Changes in TMRM fluorescence compared to controls following treatment with 200 µg mL⁻¹ NS at 12, 24 and 48 h of exposure; (b) Fold changes in MitoSox signals with 100 and 200 µg mL⁻¹ of NS exposures at 8 h; (c) Fold changes in carboxy-H₂DCHF signals with 100 and 200 µg mL⁻¹ of NS exposures at 8 h (to be continued on next page).

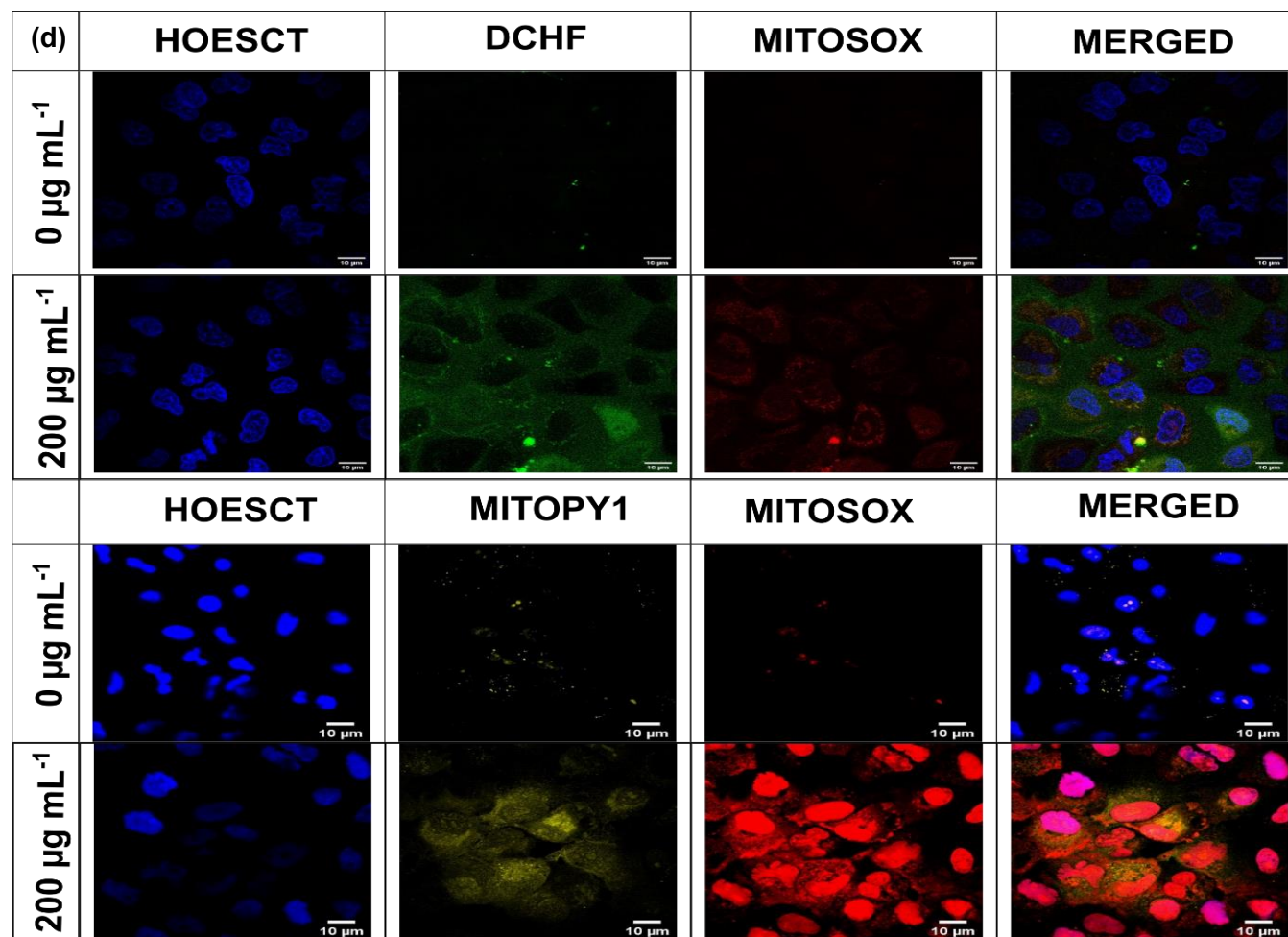


Figure 3.4.11 (continuation). (d) Confocal imaging of A549 cells treated with 200 $\mu\text{g mL}^{-1}$ of NS at the 8 h of exposure stained with the carboxy H₂DCHF and MitoSox dyes in panel 1, and MitoPY1 and MitoSox dyes in panel 2. The cellular nucleus was stained with Hoechst. Micrographs are scaled to 10 μm -sizes.

3.4.3.3- Mechanism of Cell Death in the NS-Treated Lung Cells

The BEAS-2B cells treated with $200 \mu\text{g mL}^{-1}$ of NS were analysed for the mechanism of cellular death using the Annexin-V/PI staining. At 12 h of exposure, slight increases in the late apoptotic/necrotic cellular populations were observed (16%) when compared with untreated controls (10%), while the percentage of the live cells decreased from 75% in the untreated controls to $\sim 70\%$ in the treated cells. The percentage of the necrotic cell populations in the NS-treated cells decreased to $\sim 6\%$ from $\sim 11\%$ in the control cells. The low necrotic cell populations in the first 12 h of exposure indicated a high anti-ROS activity, as confirmed by the high ROS expulsion from the BEAS-2B cells observed in panel 1 of [Figure 3.4.11d](#). This finding indicates that cells were shifting the cellular metabolism signal towards survival from cellular growth following exposure to NS.[365](#)

However, at 24 h of NS exposure, the percentage of late apoptotic/necrotic cells increased to $\sim 13.5\%$ from $\sim 3.8\%$ in the control cells. No substantial changes in the percentage of other populations were observed. This shows that the dysfunctional cells with impaired ROS machinery were dying, as cells try to undergo cell survival and through anti-oxidative stress mechanisms, expelled the ROS from inside the cells.[365](#) [381](#) The 48 h exposure to NS also did not exhibit much change in the percentages of cellular population when compared with untreated controls (as shown in [Figure 3.4.12](#)). This implies that the cells are in late apoptotic/necrotic phases between 0-12 h of exposure to NS, and recover from the initial exposure between 24 - 48 h post exposure.[365](#)

In the A549 cells treated with the $200\text{-}\mu\text{g mL}^{-1}$ of NS there were no significant changes in the cellular populations when compared with the untreated controls at 12, 24 or 48 h of exposure (as shown in [Figures 3.4.13 a and c](#)). The high cell survival rates could be attributed to the high anti-ROS activities observed in the exposed cells (see [Figure 3.4.11d](#)) through the accumulation of ROS outside of the cells as a result of anti-ROS response mechanisms.[288](#)

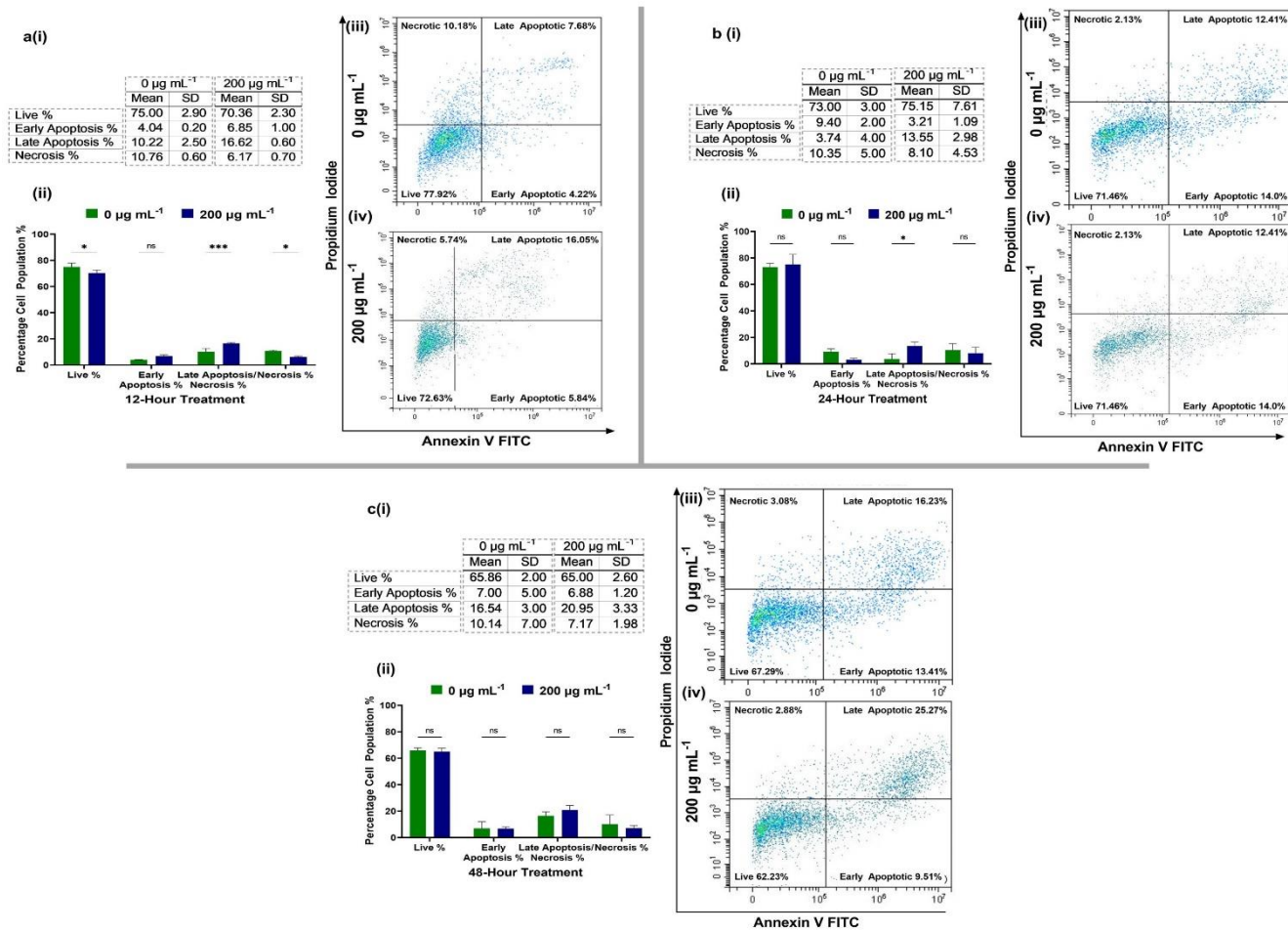


Figure 3.4.12. Annexin-V/PI staining of NS-treated BEAS-2B cells to evaluate the mechanism of cellular death following exposure to the 200- $\mu\text{g mL}^{-1}$ of NS at: (a) 12 h; (b) 24 h; and (c) 48 h of exposure. The table in (i) represents the average of experiments performed; (ii) the bar-graph represents the cellular population percentages in either live, early apoptotic, late apoptotic necrotic and necrotic phases; and the dot-plot represents the sample of one experiment for (iii) the control group and (iv) the treatment group.

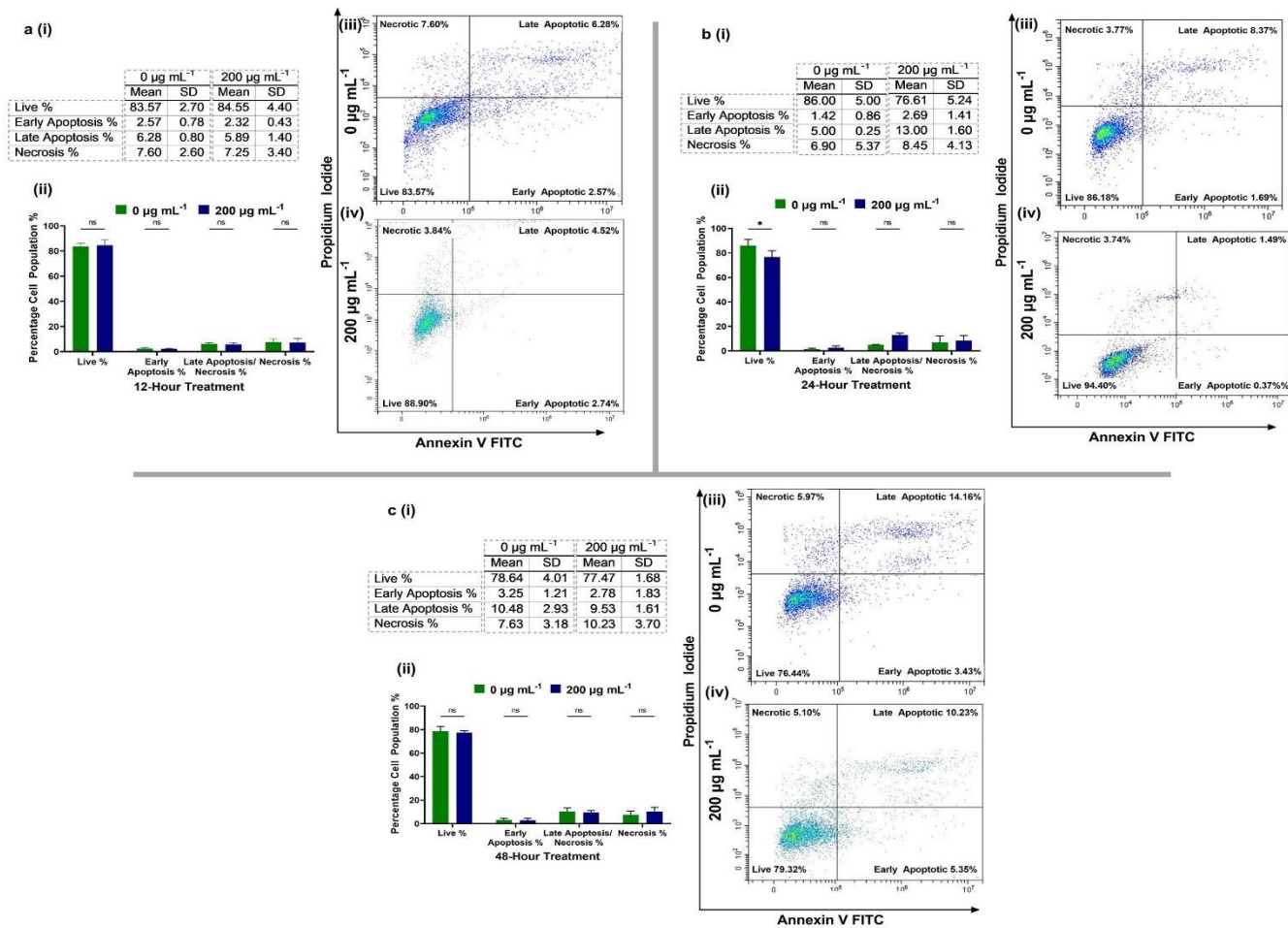


Figure 3.4.13. Annexin-V/PI staining of NS-treated A549 cells to evaluate the mechanism of cellular death following exposure to the 200- $\mu\text{g mL}^{-1}$ of NS at: (a) 12 h; (b) 24 h; and (c) 48 h of exposure. The table in (i) represents the average of experiments performed; (ii) the bar-graph represents the cellular population percentages in either live, early apoptotic, late apoptotic/necrotic, and necrotic phases; and the dot-plots represent the sample of one experiment for (iii) the control group and (iv) the treatment group.

3.4.4- Toxicological Profile of NG

3.4.4.1- IC₅₀ and Cellular Death Analysis in NG-Treated Lung Cells

The NG-treated BEAS-2B (Figure 3.4.14) and A549 cells (Figure 3.4.15) were analyzed for cellular viability percentages using an increasing concentration of NG (0.01 – 200 $\mu\text{g mL}^{-1}$). The IC₅₀ values for NG-treated BEAS-2B cells were determined to be ~ 159 and ~ 154 $\mu\text{g mL}^{-1}$ at 24 and 48 h, respectively, of exposure (Figure 3.4.14a). The IC₅₀ values for NG-treated A549 cells were determined to be ~ 320 and ~ 2.8 x 10⁸ $\mu\text{g mL}^{-1}$ at 24 and 48 h, respectively, of exposure (Figure 3.4.15a). The inhibitory effect was evident in the first 24 h of exposure in A549 cells, and recovered at 48 h. The latter is consistent with a higher IC₅₀ value calculated at 48 h.

Exposure to 100 and 200 $\mu\text{g mL}^{-1}$ of NG in the BEAS-2B and A549 cells resulted in an increased percentages of LDH release of ~20-40% (as shown in Figure 3.4.14b and Figure 3.4.15b, respectively). Increases in cellular death were observed at both concentrations, as confirmed by the Calcein-AM/PI stained cellular micrographs shown in Figure 3.4.14c and Figure 3.4.15c.

The BEAS-2B cells undergo cellular death after exposure to 200 $\mu\text{g mL}^{-1}$ concentration of NG at 24 and 48 h of exposure, as observed by the Calcein-AM stained cells. A significant increase in the PI-stained cells were observed at both 24 and 48 h of the exposure. At 48 h of exposure, increased cellular inhibition and death were evident, as lower numbers of cells were present than untreated controls in the Calcein-AM and bright-field merged channels.³⁸⁶ However, for A549 cells, an increase in the PI-staining channel were observed at 24 and 48 h of exposure with 100 and 200 $\mu\text{g mL}^{-1}$ of NG, and the cellular morphology (as observed in the bright-field channel) was distorted. At 48 h of exposure, A549 cells exhibited increases in the PI-staining channel, with corresponding increases in the Calcein-AM staining, thereby depicting that cells were trying to recover from the cytotoxic effect exhibited by NG exposures at 24 and 48 h.²⁸⁸ The combined LDH, cellular imaging and IC₅₀ data show that NG-treated BEAS-2B and A549 cells exhibited a concentration-dependent effect on cellular viability and cytotoxicity.

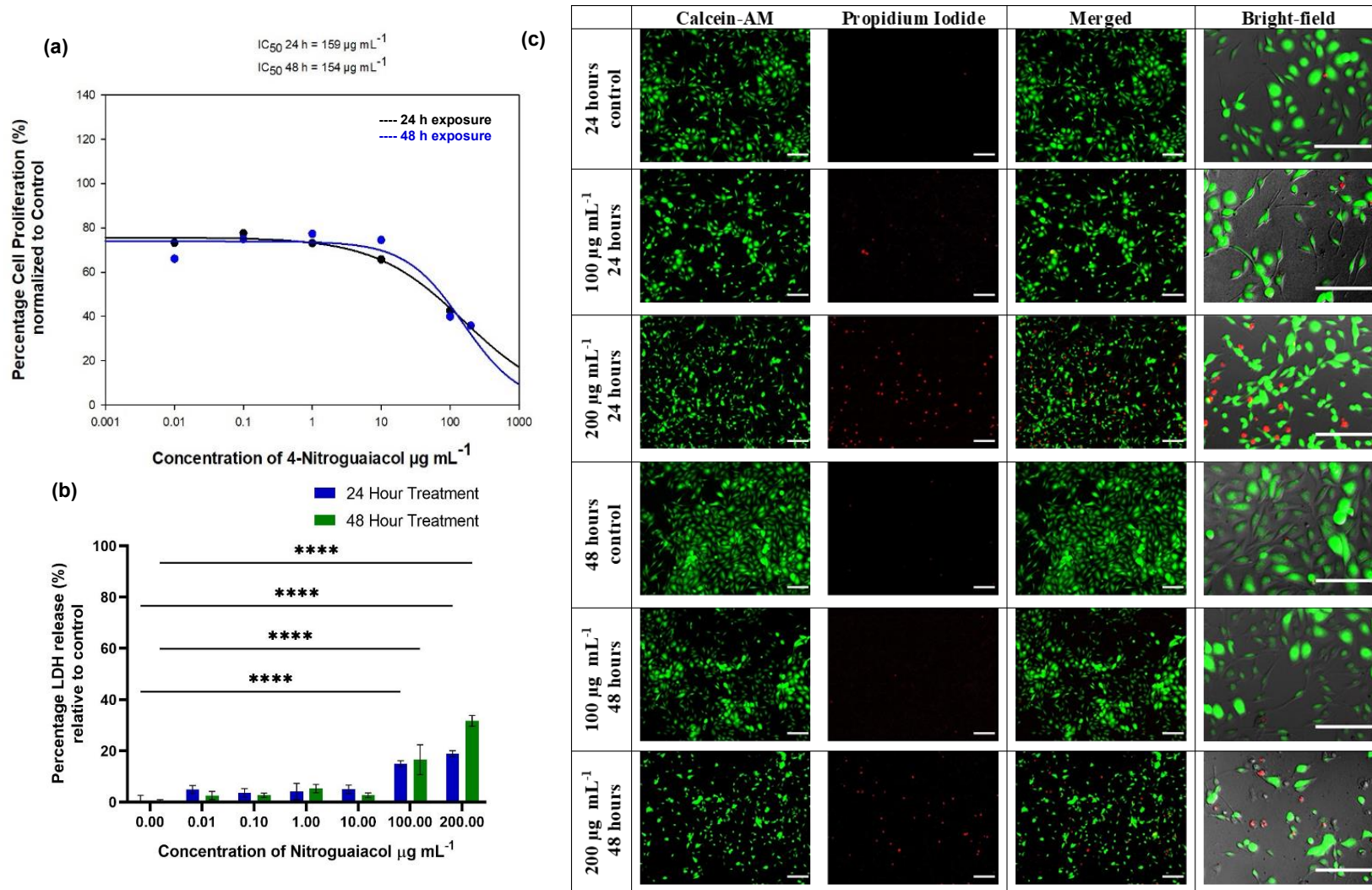


Figure 3.4.14. The cellular viability and death analysis in the BEAS-2B cell lines following exposure to NG: (a) IC_{50} values at 24 and 48 h the exposure; (b) LDH analysis at 24 and 48 h of the exposure (c) The Calcein-AM/PI staining of cells treated with 100 and 200 $\mu\text{g mL}^{-1}$ of NG at 24 and 48 h of the exposure. The micrographs are scaled to 50- μm in size.

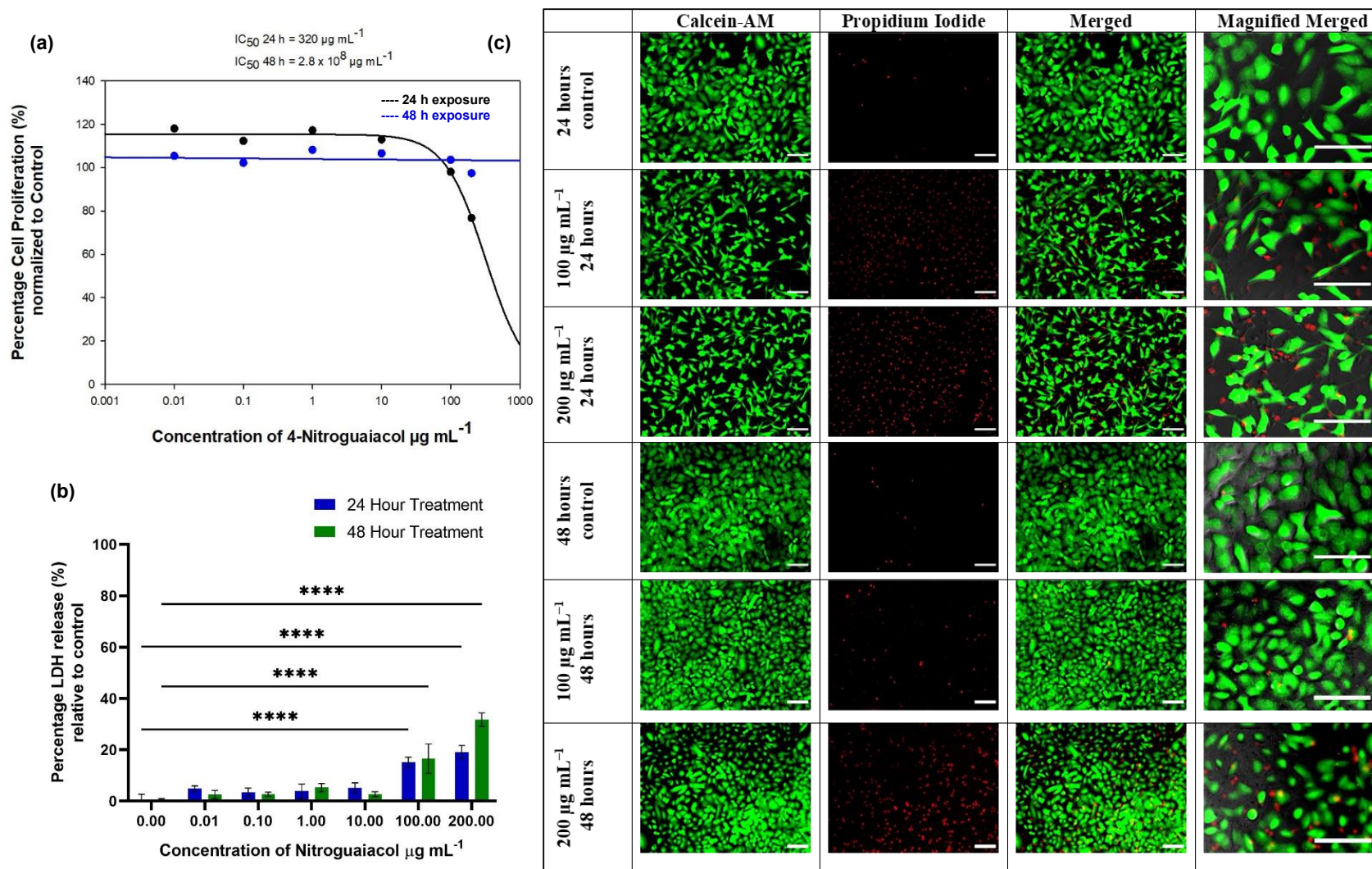


Figure 3.4.15. The cellular viability and death analysis in the A549 cell lines following exposure to NG: (a) IC_{50} values at 24 and 48 h of the exposure; (b) LDH analysis at 24 and 48 h of the exposure; and (c) The Calcein-AM/PI staining of cells treated with 100 and 200 $\mu\text{g mL}^{-1}$ of NG at 24 and 48 h of the exposure. The micrographs are scaled to 50- μm in size.

3.4.4.2- General and Mitochondrial ROS buildup in NG-Treated Lung Cells

The NG-treated BEAS-2B and A549 cells were analysed for the changes in the cellular ROS and mtROS. **Figure 3.4.16** shows the changes in the cellular ROS and mtROS of the BEAS-2B cells treated with NG following 8 h of exposure. The $\Delta\Psi_m$ analysis is shown in **Figure 3.4.16a** for BEAS-2B cells treated with $200 \mu\text{g mL}^{-1}$ of NG at 12, 24 and 48 h of exposure. A significant increase in $\Delta\Psi_m$ were observed at 12, 24 and 48 h of the exposure, where ~ 1.25 to ~ 1.35 -fold increase in the signals were observed compared to the untreated controls. The MitoSox signals increased from ~ 1.8 to ~ 2 -fold over the control (as shown in **Figure 3.4.16b**), especially following the 8 h of exposure to 100 and $200 \mu\text{g mL}^{-1}$ of 4NG, respectively. An estimated ~ 1.6 -fold increase in the carboxy- H_2DCHF signal was observed following exposure to $200 \mu\text{g mL}^{-1}$ of NG at the 8 h of exposure, while no changes in the ROS signal were observed after exposure to $100 \mu\text{g mL}^{-1}$ of NG (as shown in **Figure 3.4.16c**).

The confocal images of the BEAS-2B cells treated with NG are shown in **Figure 3.4.16d**. The upper channels show the general ROS and mitochondrial $\text{O}_2^{\cdot-}$ production in BEAS-2B cells treated with $200 \mu\text{g mL}^{-1}$ of NG at the 8 h of exposure, while lower panels showed the 4NG- treated cells at 8 h, implying changes in the mitochondrial H_2O_2 and $\text{O}_2^{\cdot-}$. Increased carboxy- H_2DCHF signals were observed in the NG-treated cells. The MitoSox signals also increased, implying in the merged upper channel in **Figure 3.4.16d**, that cellular inhibition and death as seen in **Figure 3.4.14a** could be attributed to high ROS activity.³⁸² In the lower channel of **Figure 3.4.16d**, increased MitoPY1 and MitoSox signals were observed in the 4NG-treated cells. Considering, the increased $\Delta\Psi_m$ signals observed in **Figure 3.4.16a** and the high mtROS-associated signals, the inhibition and cytotoxic effect could be explained. The overall mitochondrial activity was impaired following NG treatments, with significant changes in the cellular viability of BEAS-2B cells (through apoptosis).³⁶¹

In the A549 cells treated with $200 \mu\text{g mL}^{-1}$ of NG, there was no significant changes observed in the TMRM signals at 12 and 24 h of exposure, while at 48 h of exposure ~ 0.8 -fold decreases in the $\Delta\Psi_m$ signals were observed (**Figure 3.4.17a**). No change in MitoSox signals were observed with $100 \mu\text{g mL}^{-1}$ of NG, while ~ 1.3 -fold increases in the MitoSox signals were observed following exposure to $200 \mu\text{g mL}^{-1}$ of NG at 8 h of the exposure as shown in **Figure 3.4.17b**. The change in the carboxy- H_2DCHF signal was insignificant after exposure to $100 \mu\text{g mL}^{-1}$ of NG, while slight but significant increases of ~ 1.1 -fold were

observed with $200 \mu\text{g mL}^{-1}$ of NG (as shown in [Figure 3.4.17c](#)). The confocal microscopy images of the NG-treated A549 cells at the 8 h of exposure shows slightly increased carboxy- H_2DCHF and MitoSox signals in panel 1 when compared with the untreated controls (as shown in [Figure 3.4.17d](#)). In the lower panel, increased MitoPY1 and MitoSox signals indicate that there is mtROS imbalance in NG-treated cells. The decrease in $\Delta\Psi\text{m}$ signals at 48 h confirms the slight mitochondrial membrane depolarization, as well as likely leakage of H_2O_2 and $\text{O}_2^{\cdot-}$ to the cellular matrix, and hence, resultant cellular death.[365](#), [377](#)

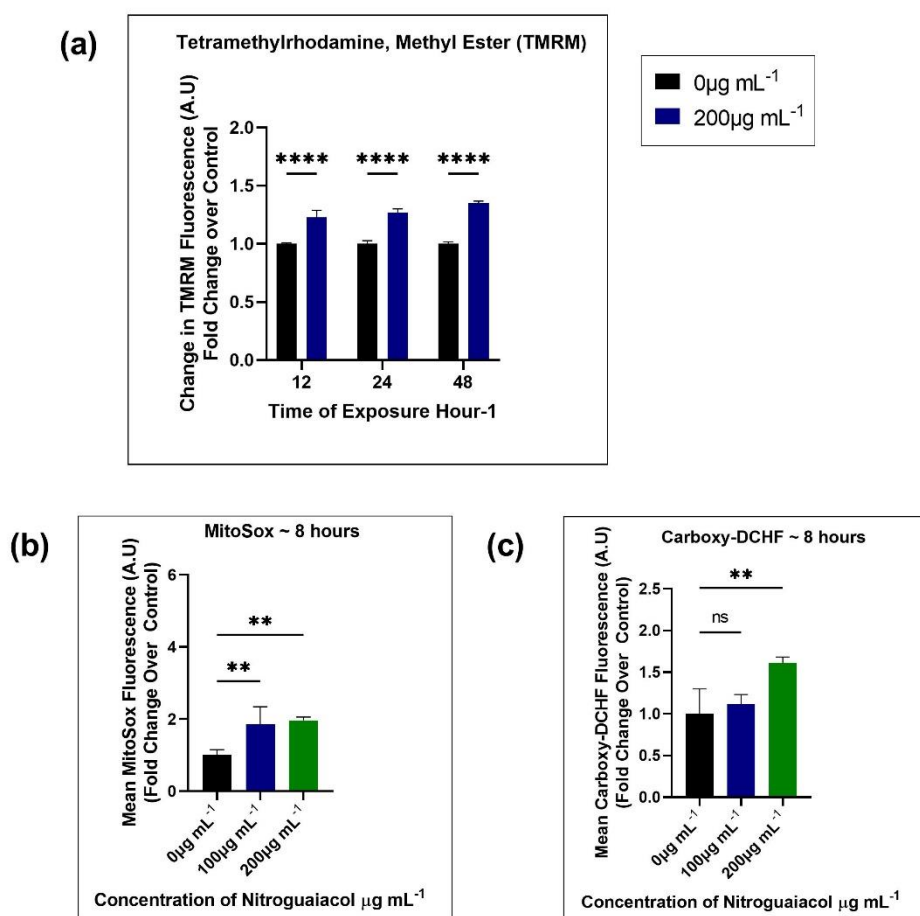


Figure 3.4.16. The general ROS and mtROS analysis in the BEAS-2B cell lines after exposure to NG using flow cytometry and confocal microscopy: (a) Changes in TMRM fluorescence signals compared to controls following treatment with $200 \mu\text{g mL}^{-1}$ of NG at 12, 24 and 48 h of the exposures; (b) Fold changes in MitoSox signals with 100 and $200 \mu\text{g mL}^{-1}$ of NG at 8 h of the exposure; (c) Fold changes in the carboxy H_2DCHF signals with 100 and $200 \mu\text{g mL}^{-1}$ of NG at 8 h of the exposure (to be continued on next page).

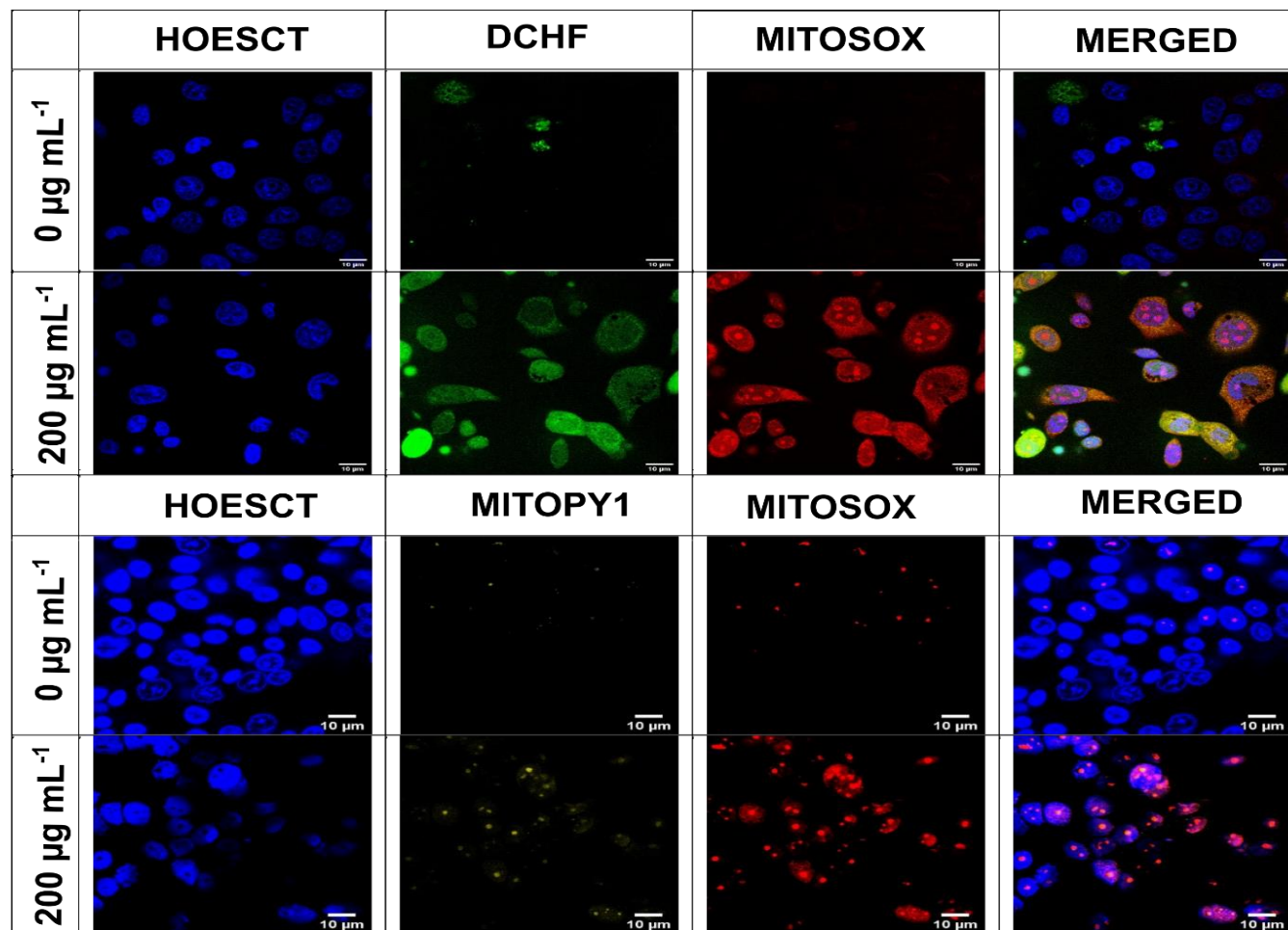


Figure 3.4.16 (continuation). (d) Confocal imaging of BEAS-2B cells treated with 200 $\mu\text{g mL}^{-1}$ of NG at the 8 h of exposure stained with the carboxy- H_2DCHF and MitoSox dyes in panel 1, and MitoPY1 and MitoSox dyes in panel 2. The cellular nucleus was stained with Hoechst. Micrographs are scaled to 10- μm in size.

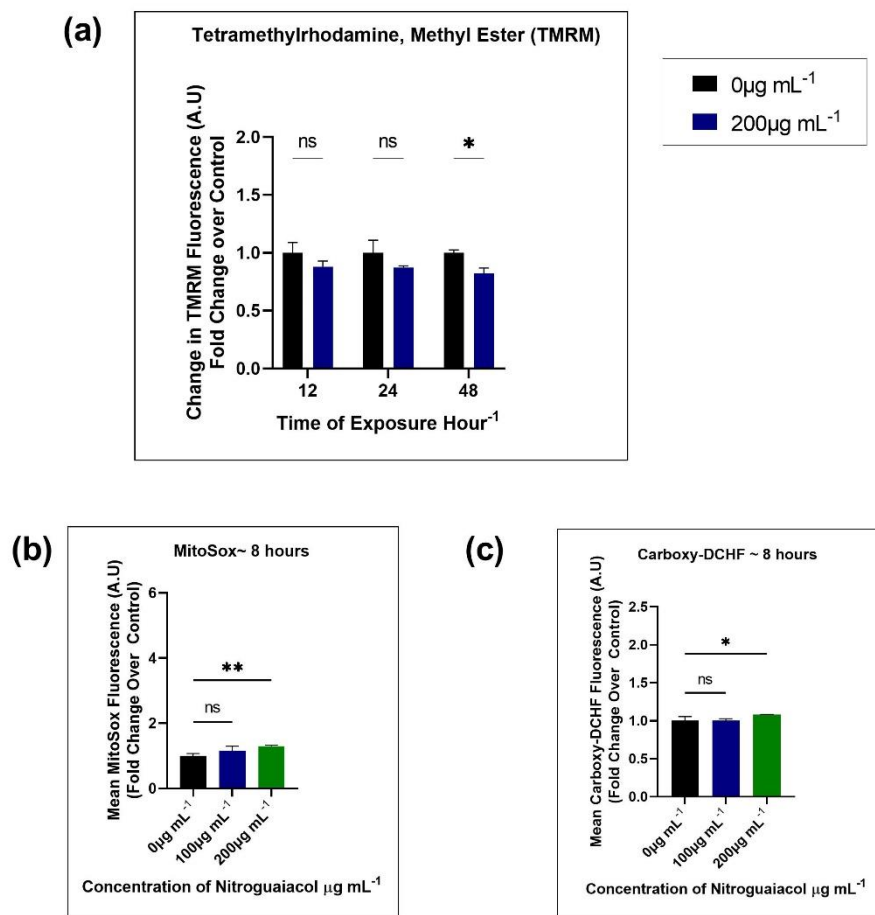


Figure 3.4.17. The general ROS and mtROS analysis in the A549 cell lines after exposure to NG using flow cytometry and confocal microscopy: (a) Changes in TMRM fluorescence signals compared to controls following treatment with 200 µg mL⁻¹ of NG at 12, 24 and 48 h of exposure; (b) Fold changes in the MitoSox signals with 100 and 200 µg mL⁻¹ of NG exposure at 8 h (c) Fold changes in the carboxy H₂DCHF signals with 100 µg mL⁻¹ and 200 µg mL⁻¹ of NG exposure at 8 h (to be continued on next page).

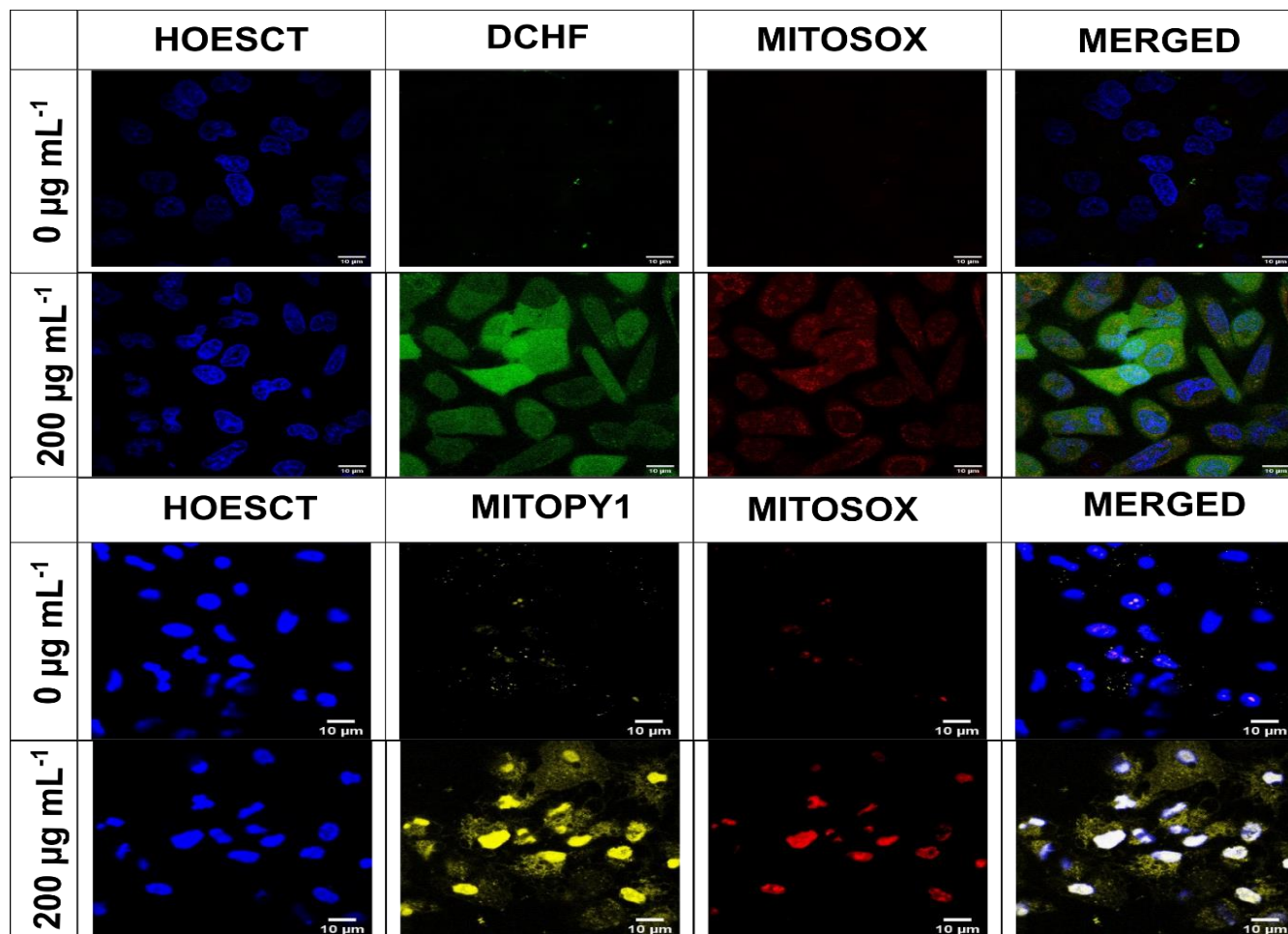


Figure 3.4.17 (continued). (d) Confocal imaging of A549 cells treated with 200 $\mu\text{g mL}^{-1}$ of NG at 8 h of exposure stained with the carboxy H_2DCHF and MitoSox dyes in panel 1, and MitoPY1 and MitoSox dyes in panel 2. The cellular nucleus was stained with Hoechst. Micrographs are scaled to 10- μm sizes.

3.4.4.3- Mechanism of Cellular Death Following NG Treatments

The BEAS-2B cells treated with $200 \mu\text{g mL}^{-1}$ of NG were analyzed for the mechanism of cellular death by using Annexin-V/PI staining. At 12 h of the exposure, there was no significant change in the cellular populations compared with the untreated control cells (Figure 3.4.18a). However, at 24 h of NG exposure, the percentage of late apoptotic/necrotic cells increased to ~12.9% from ~3.8% in the control cells. No significant change in the percentages of other cellular populations were observed (as shown in Figure 3.4.18b). After the 48 h of NG exposure, the percentage of late apoptotic/necrotic cells increased to ~23.6% from ~16.5% in the control cells, and live cell populations decreased from 68% in control cells to 60% in NG-exposed cells (as shown in Figure 3.4.18c). Overall, this implies that the cells are in the late apoptotic/necrotic phase between 24-48 h of exposure to 4NG.

In the A549 cells treated with the $200\text{-}\mu\text{g mL}^{-1}$ of NG there was a slight increase in the live cell populations (88%) compared to the untreated controls at 12 h (83%). A decrease in the necrotic cell populations from 7.6% in control cells to 3.12% in NG-exposed cells was also observed (Figure 3.4.19a). However, at 24 h of exposure, the percentage of live cells decreased from 86% in control cells compared to 72% of NG-exposed cells. The late apoptotic/necrotic cell populations increased from 16.5% in NG-exposed cells from 5.5% in control cells (Figure 3.4.19b). No significant changes in the cell populations were observed in the NG-exposed cells at 48 h as shown in Figure 3.4.19c.

The increase in $\Delta\Psi\text{m}$ signals between 12 - 48 h with subsequent increases in mtROS signals at 8 h of exposure indicates that the mitochondrial dysfunction contributed towards induction of apoptosis³⁶⁵ in the NG-treated BEAS-2B cells between 24-48 h of exposure. The latter was confirmed by high PI staining shown in Figure 3.4.14. This apoptosis response is delayed in the A549 cells since they undergo growth inhibition in the 24 h exposure (as shown in Figure 3.4.15), and subsequently exhibit the $\Delta\Psi\text{m}$ depolarization at 48 h exposure with a corresponding increase in PI staining. Increase in apoptosis/necrosis cell populations were also observed at 48 h of the exposure.³⁸³

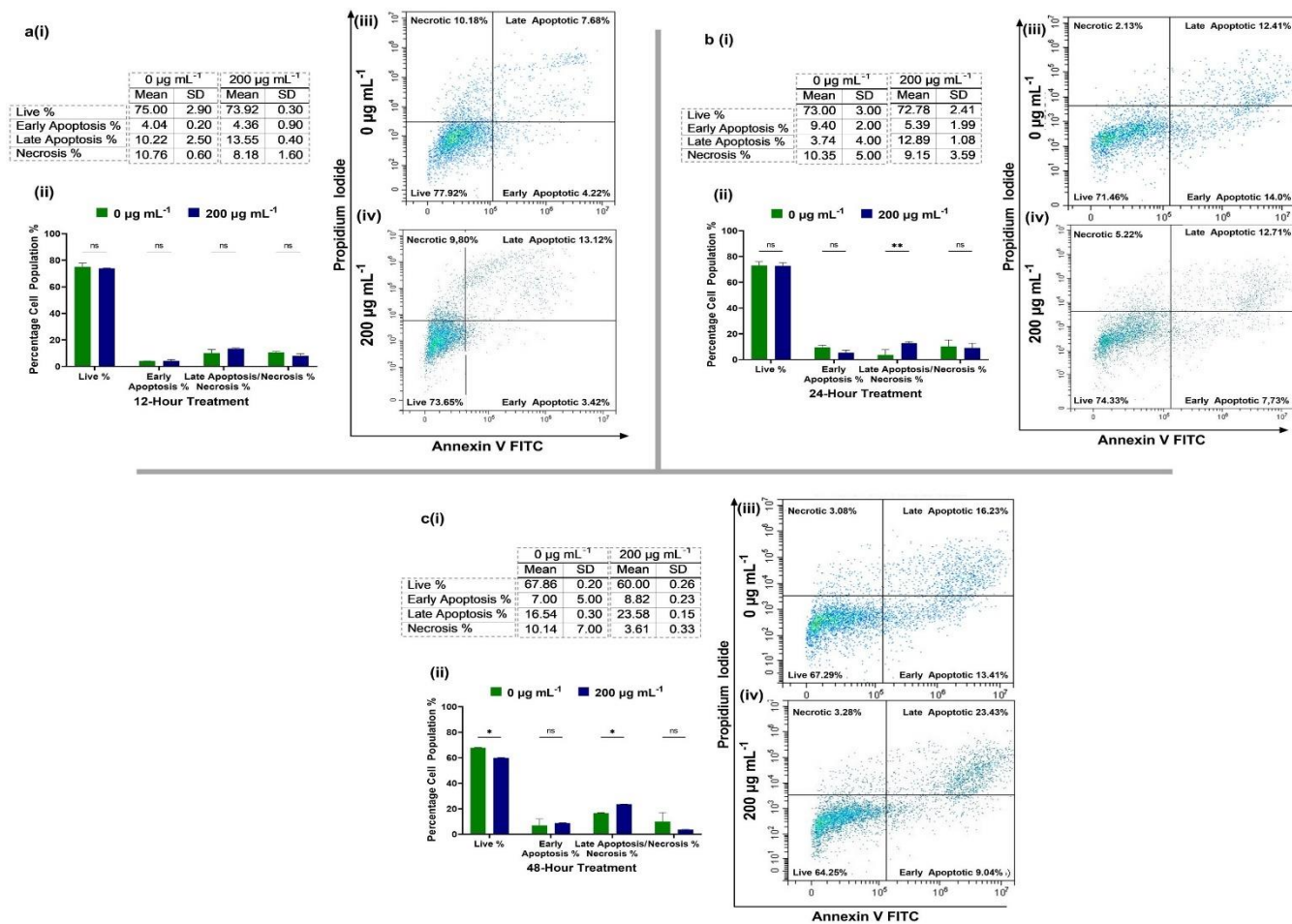


Figure 3.4.18. Annexin-V/PI staining of NG-treated BEAS-2B cells to evaluate the mechanism of cellular death following exposure to the 200- $\mu\text{g mL}^{-1}$ of NG at: (a) 12 h; (b) 24 h; and (c) 48 h of the exposure. The table in (i) represents the average of experiments performed; (ii) the bar-graph represents the cellular population percentages in either live, early apoptotic, late apoptotic/necrotic, and necrotic phases; and the dot-plots represent the sample of one experiment for (iii) the control group and (iv) the treatment group.

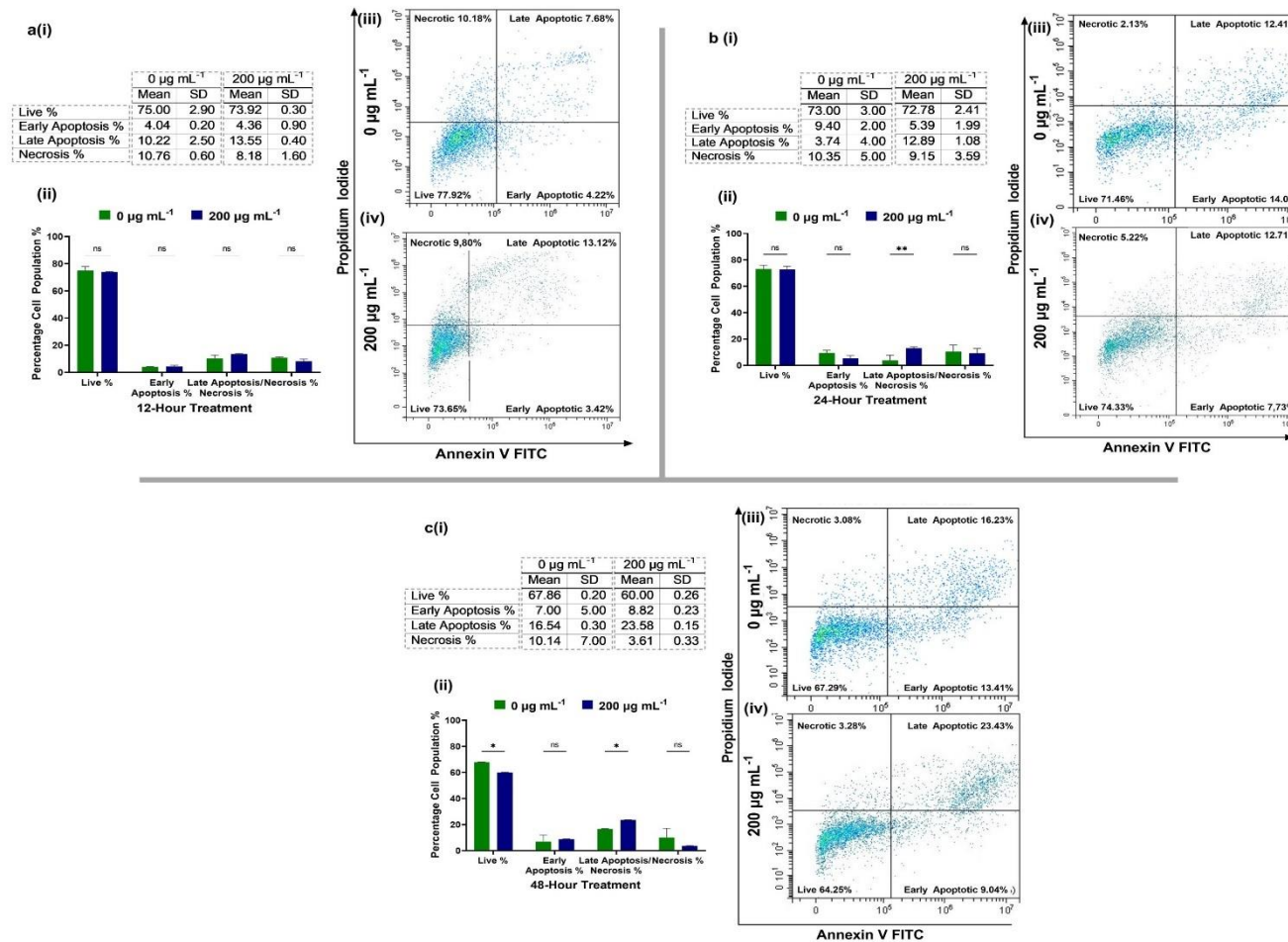


Figure 3.4.19. Annexin-V/PI staining of NG-treated A549 cells to evaluate the mechanism of cellular death following exposure to the 200- $\mu\text{g mL}^{-1}$ of NG at: (a) 12 h; (b) 24 h; and (c) 48 h of the exposure. The table in (i) represents the average of experiments performed; (ii) the bar-graph represents the cellular population percentages in either live, early apoptotic, late apoptotic/necrotic, and necrotic phases; and the dot-plots represent the sample of one experiment for (iii) the control group and (iv) the treatment group.

3.4.5- Toxicological Profiling of NC

3.4.5.1- IC₅₀ Profiles and Cellular Death Analyses of NC-Treated Lung Cells

The NC-treated BEAS-2B (Figure 3.4.20) and A549 cells (Figure 3.4.21) were analyzed for cellular viability percentages using an increasing concentration of NC (0.01 – 200 $\mu\text{g mL}^{-1}$). The IC₅₀ values for NC-treated BEAS-2B cells were found to be ~ 30 and ~ 8.8 $\mu\text{g mL}^{-1}$ at 24 and 48 h of the exposure, respectively (Figure 3.4.20a). The percentage proliferation rate of the BEAS-2B cells at the 0.1-200 $\mu\text{g mL}^{-1}$ of NC remained $\leq 80\%$ following exposure, implying the cellular inhibitory effect was posed by NC even at the lowest concentration of exposure (0.01 $\mu\text{g mL}^{-1}$). The IC₅₀ values determined for NC-treated A549 cells were ~ 335 and ~ 79 $\mu\text{g mL}^{-1}$ at 24 and 48 h, respectively, of exposure (Figure 3.4.21a).

The rate of the cellular death analysis followed IC₅₀ calculations upon the exposure to 0.01 – 200 $\mu\text{g mL}^{-1}$ of NC using LDH assay. The exposure to the 100 and 200 $\mu\text{g mL}^{-1}$ of NC in the BEAS-2B and A549 cells resulted in 20-80% of LDH release percentages at 24 and 48 h of exposure (as shown in Figures 3.4.20b and 3.4.21b, respectively).

Morphological changes were determined by using Calcein-AM/PI staining under the fluorescence microscope (as shown in Figures 3.4.20c and 3.4.21c). The BEAS-2B cells became rounder and detached when exposed to the 100 and 200 $\mu\text{g mL}^{-1}$ of NC at 24 and 48 h of exposure, as observed in the Calcein-AM stained channel. Increases in the PI-stained lung cells were observed at both 24 and 48 h of treatment (Figure 3.4.20c). In the A549 cells, an increase in the PI channel staining was observed at 24 h, and 48 h of exposure with 100 $\mu\text{g mL}^{-1}$ and 200 $\mu\text{g mL}^{-1}$ exposure, and the cellular morphology (as observed in the bright-field channel) was distorted. The combined LDH, cellular imaging and IC₅₀ data showed that NC-treated BEAS-2B and A549 cells exhibited a concentration-dependent effect on cellular viability and death.

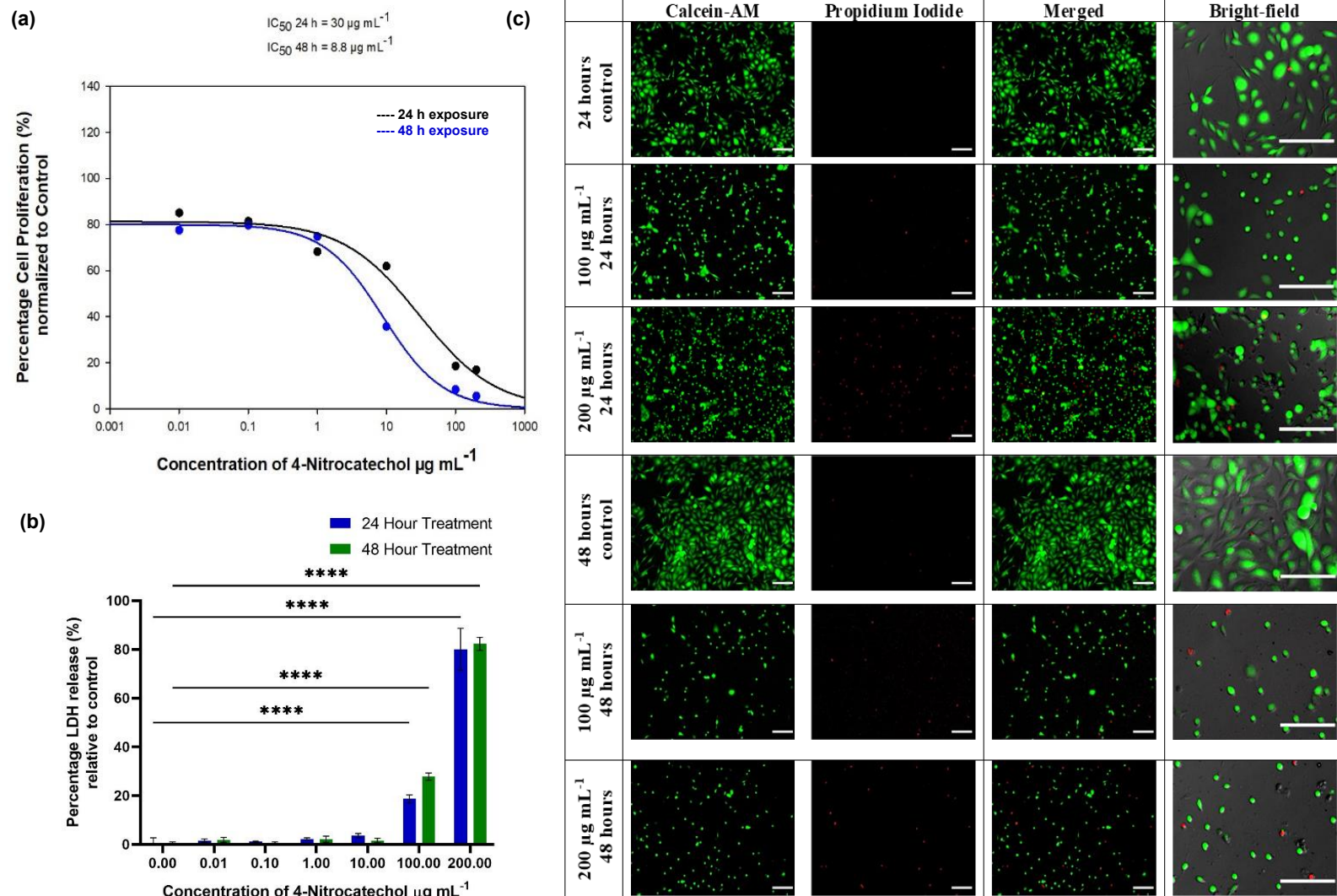


Figure 3.4.20. The cellular viability and death analysis in the BEAS-2B cell lines following exposure to NC: (a) IC_{50} values at 24 and 48 h of the exposure; (b) LDH analysis at 24 and 48 h of the exposure (c) The Calcein-AM/PI staining of cells treated with $100 \mu\text{g mL}^{-1}$ and $200 \mu\text{g mL}^{-1}$ of NC at 24 and 48 h of the exposure. The micrographs are scaled to $50\text{-}\mu\text{m}$ in size

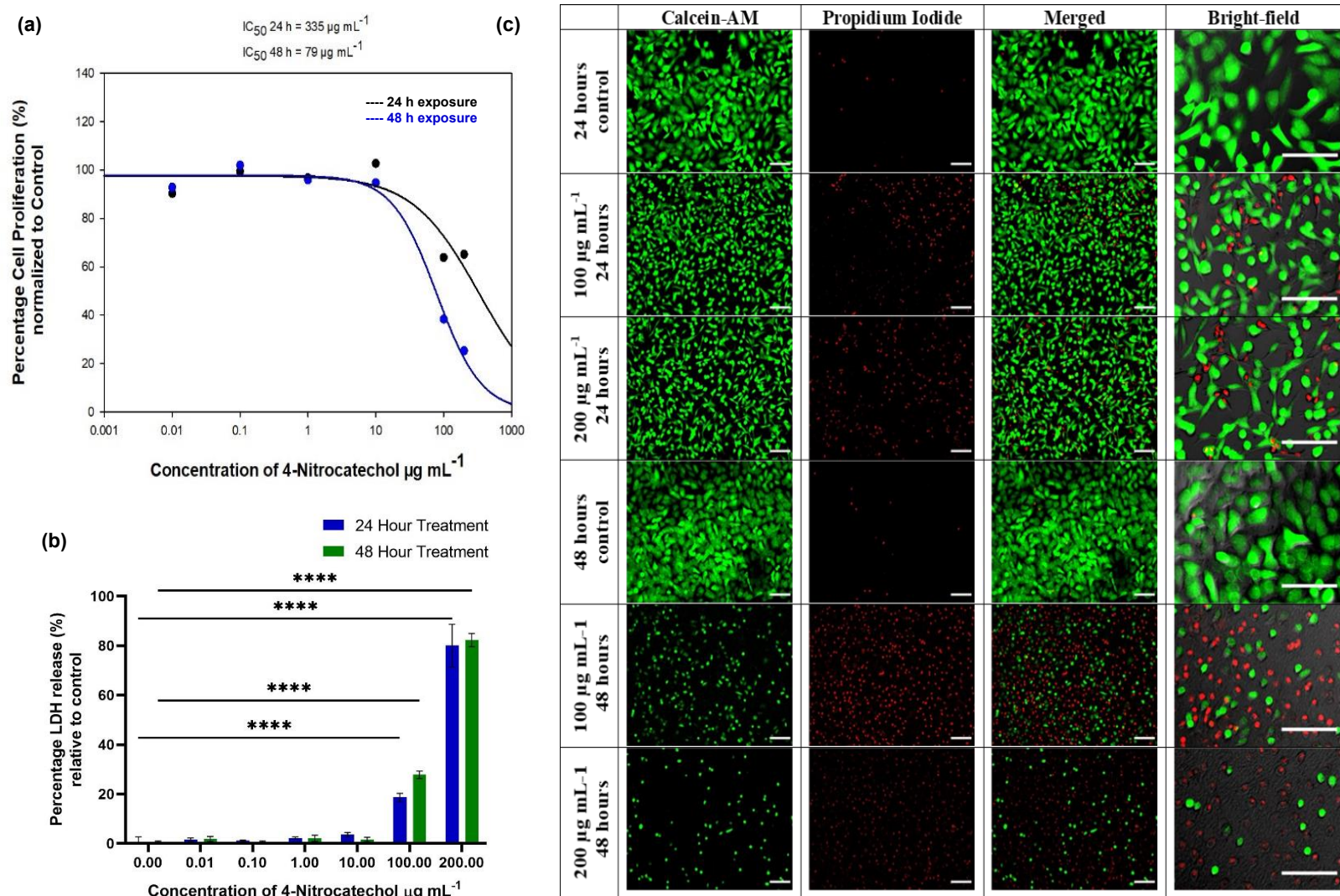


Figure 3.4.21. The cellular viability and death analysis in the A549 cell lines following exposure to NC: (a) IC_{50} values at 24 and 48 h of the exposure; (b) LDH analysis at 24 and 48 h of the exposure (c) The Calcein-AM/PI staining of cells treated with 100 and 200 $\mu\text{g mL}^{-1}$ of NC at 24 and 48 h of the exposure. The micrographs are scaled to 50- μm in size.

3.4.5.2- General and Mitochondrial ROS build-up in NC-Treated Lung Cells

The NC-treated BEAS-2B and A549 cells were analysed for the changes in the cellular ROS and mtROS. [Figure 3.4.22](#) shows the changes in the cellular ROS and mtROS of the BEAS-2B cells treated with NC and [Figure 3.4.23](#) shows the ROS changes in the A549 cells. The flow cytometric TMRM analysis in [Figure 3.4.22a](#) showed the BEAS-2B cells treated with NC at 6 h, 12 h, 24 h and 48 h of exposure to 100 $\mu\text{g mL}^{-1}$ and 200 $\mu\text{g mL}^{-1}$ concentration. A significant decrease in $\Delta\Psi\text{m}$ was observed in 200 $\mu\text{g mL}^{-1}$ exposed cells, starting at 6 h of exposure where the signal decreased to 0.5 when compared to the untreated control. It further decreased to 0.1 from 12 h to 48 h of exposure. The $\Delta\Psi\text{m}$ decreased to 0.7 relative to untreated control between 6 h to 24 h and decreased further to 0.2 at 48 h when NC of concentration 100 $\mu\text{g mL}^{-1}$ was exposed to the cells. The MitoPY1 signal in the BEAS-2B cells increased to ~ 1.3 when exposed to both 100 $\mu\text{g mL}^{-1}$ and 200 $\mu\text{g mL}^{-1}$ concentrations of NC after 8 h as shown in [Figure 3.4.22b](#). The MitoSox signal increased to ~ 2.2 over control following exposure to the NC concentration of 100 $\mu\text{g mL}^{-1}$ and further increased ~ 4.8 fold after exposure to 200 $\mu\text{g mL}^{-1}$ at 8 h of exposure as shown in [Figure 3.4.22c](#). An almost ~ 1.6 fold increase in carboxy- H_2DCHF signal was observed following exposure to 200 $\mu\text{g mL}^{-1}$ of NC while no significant change in the ROS signal was observed after exposure to 100 $\mu\text{g mL}^{-1}$ of NC at 8 h as shown in [Figure 3.4.22d](#).

The confocal microscopy images of BEAS-2B cells, treated with NC are shown in [Figure 3.4.22d](#). The upper channels show the general ROS and mitochondrial $\text{O}_2^{\cdot-}$ production in BEAS-2B cells treated with 200 $\mu\text{g mL}^{-1}$ of NC at 8 h while lower panel shows the NC treated cells at 8 h showing changes in the mitochondrial H_2O_2 and $\text{O}_2^{\cdot-}$. The increased carboxy H_2DCHF signal was observed in the NC-exposed cells. The MitoSox signal also increased, implying in the merged upper channel in [Figure 3.4.22d](#), that cellular inhibition and death as seen in [Figure 3.4.21a](#) could be attributed to high mtROS activity. In the lower channel of [Figure 3.4.22d](#), an increased MitoPY1 and MitoSox signals were observed in the NC exposed cells. Together with the decrease of $\Delta\Psi\text{m}$ observed in [Figure 3.4.22a](#) and the high mtROS associated signal, the cytotoxic effect of NC could be explained. The overall mitochondrial activity was impaired following NC exposure, which contributed to the BEAS-2B cells viability.[377](#)

The flow cytometric TMRM analysis in [Figure 3.4.23a](#) showed the A549 cells treated with NC at 6 h, 12 h, 24 h and 48 h when exposed to 100 $\mu\text{g mL}^{-1}$ and 200 $\mu\text{g mL}^{-1}$

concentrations, respectively. A decrease in $\Delta\Psi_m$ signal was observed in $100\ \mu\text{g mL}^{-1}$ and $200\ \mu\text{g mL}^{-1}$ exposed cells, between 6 h -24 h of exposure where signal decreased to 0.7 compared to the untreated control. This further decreased significantly to $\Delta\Psi_m$ of 0.3 of the control cells at the 48 h of exposure. The MitoPY1 signal in the A549 cells increased significantly to ~ 1.2 when exposed to $200\ \mu\text{g mL}^{-1}$ concentrations of NC after 8 h as shown in [Figure 3.4.23b](#). The MitoSox signal increased to ~ 1.3 over control following exposure to the NC concentration of $100\ \mu\text{g mL}^{-1}$ and further increased ~ 2.1 fold after the exposure to $200\ \mu\text{g mL}^{-1}$ at 8 h of the exposure as shown in [Figure 3.4.23c](#). An ~ 0.9 - and 0.75 -fold decrease in carboxy- H_2DCHF signals were observed following exposure to $100\ \mu\text{g mL}^{-1}$ and $200\ \mu\text{g mL}^{-1}$ of NC at 8 h as shown in [Figure 3.4.23d](#).

The confocal microscopy images of A549 cells, treated with NC are shown in [Figure 3.4.23e](#). A slightly increased carboxy H_2DCHF signal was observed in the NC-treated cells. The MitoSox signal also increased, implying in the merged upper channel that mitochondrial ROS also contributed to the general cellular ROS signal of carboxy H_2DCHF . In the lower channel of [Figure 3.4.23e](#), an increased MitoPY1 and MitoSox signal was observed in the NC treated cells. Along with the decreased $\Delta\Psi_m$ observed in [Figure 3.4.22a](#) and high mtROS associated signal, the cytotoxic effect of NC exposure in A549 cells could be explained.

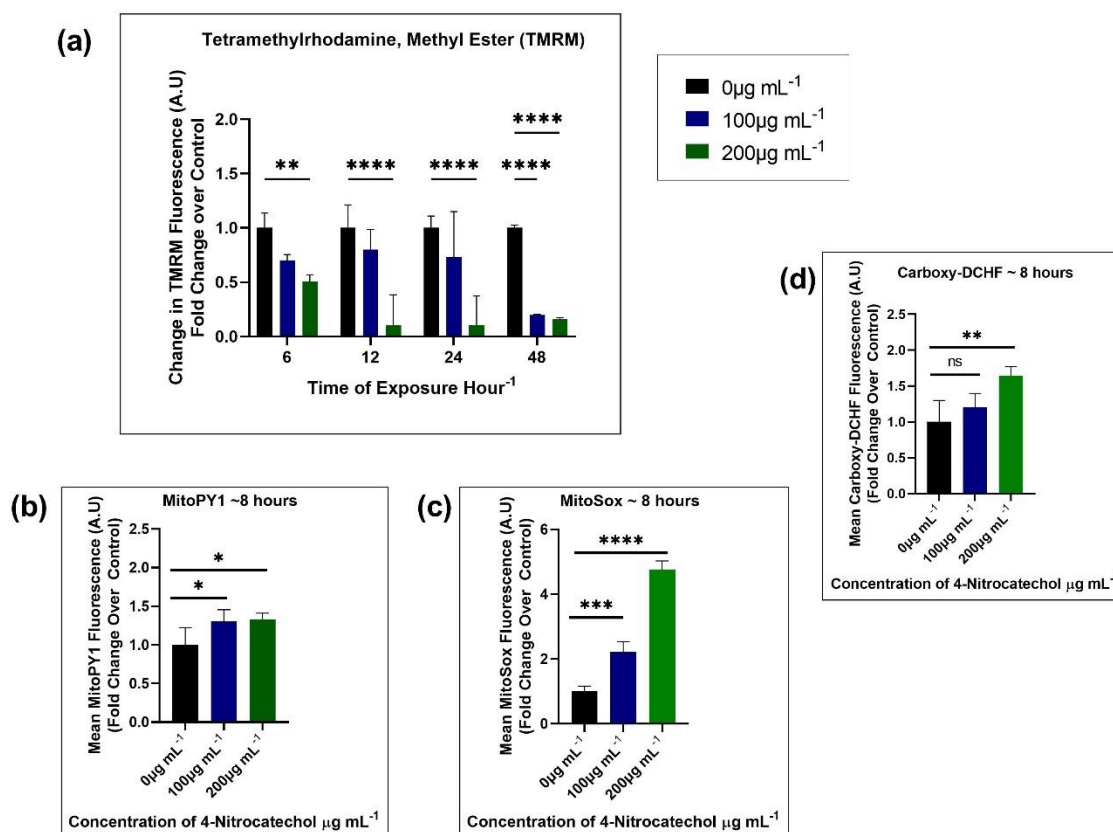


Figure 3.4.22: The general and mtROS analysis in the BEAS-2B cell lines after exposure to NC (a) Changes in TMRM fluorescence compared to control following treatment with 200 µg mL⁻¹ NC at 6 h, 12 h, 24 h and 48 h of the exposure (b) Fold change in MitoPY1 signal with 100 µg mL⁻¹ and 200 µg mL⁻¹ of NC exposure at 8 h (c) Fold change in MitoSox signal with 100 µg mL⁻¹ and 200 µg mL⁻¹ of NC exposure at 8 h (d) Fold change in carboxy H₂DCHF signal with 100 µg mL⁻¹ and 200 µg mL⁻¹ of NC exposure at 8 h (to be continued on next page).

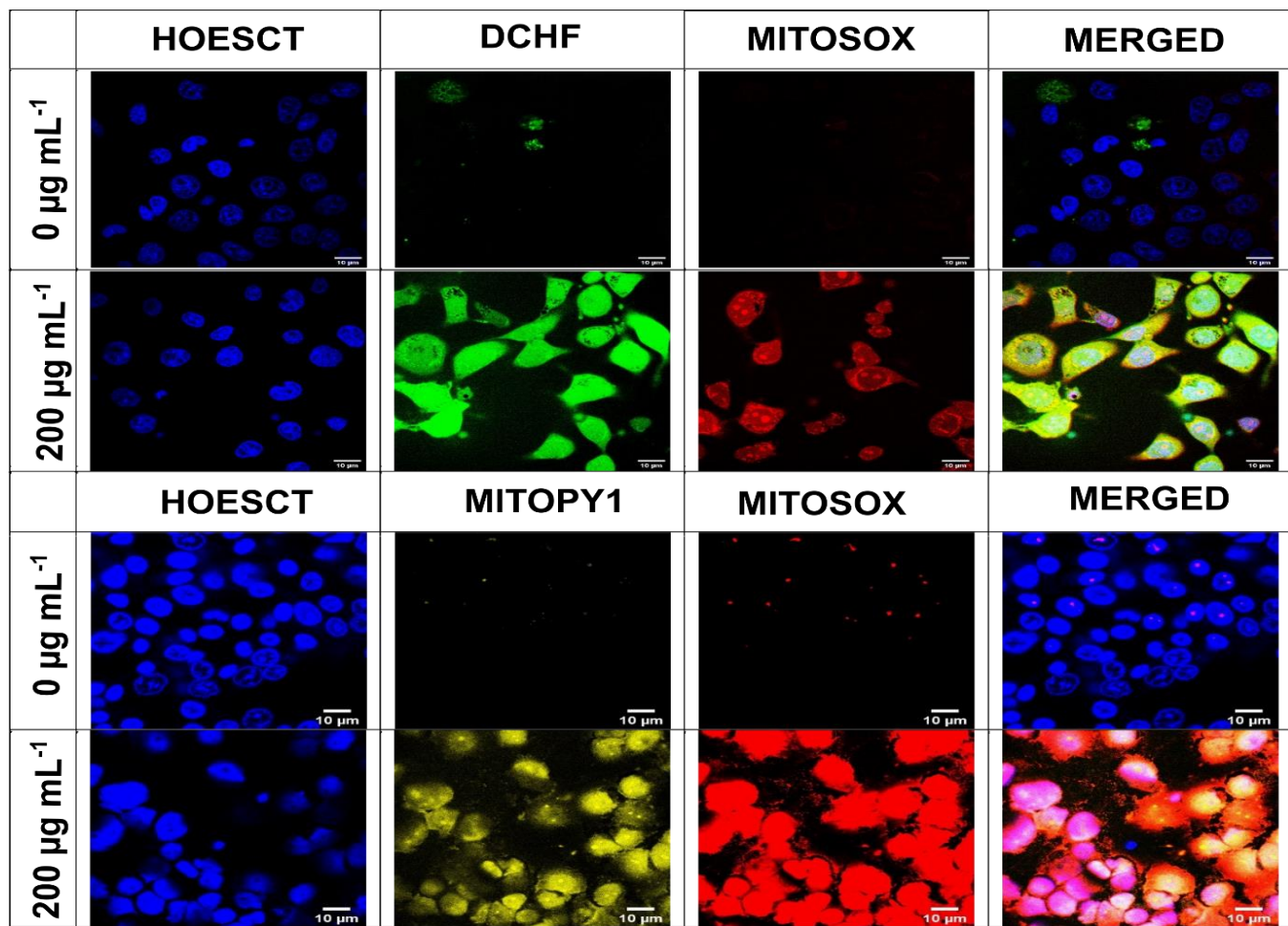


Figure 3.4.22 (continuation): (d) Confocal imaging of cells treated with 200 $\mu\text{g mL}^{-1}$ of NC at the 8 h of exposure stained with the carboxy H_2DCHF and MitoSox dye in panel one and MitoPY1 and MitoSox in panel 2. The cellular nucleus was stained with Hoechst. Micrographs are scaled to 10 μm in size.

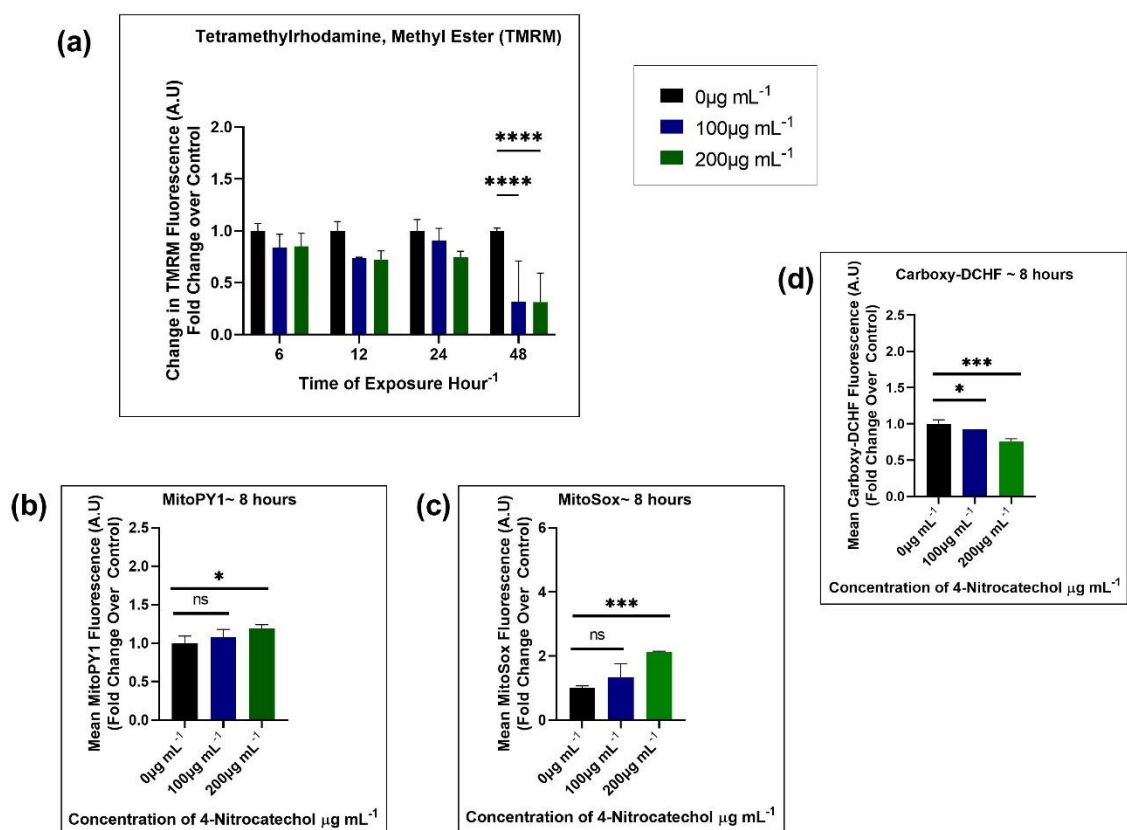


Figure 3.4.23: The general and mtROS analysis in the A549 cell lines after exposure to NC (a) Changes in TMRM fluorescence compared to control following treatment with 200 µg mL⁻¹ NC at 6 h, 12 h, 24 h and 48 h of the exposure (b) Fold change in MitoPY1 signal with 100 µg mL⁻¹ and 200 µg mL⁻¹ of the NC exposure at 8 h (c) Fold change in MitoSox signal with 100 µg mL⁻¹ and 200 µg mL⁻¹ of the NC exposure at 8 h (d) Fold change in carboxy H₂DCHF signal with 100 µg mL⁻¹ and 200 µg mL⁻¹ of the NC exposure at 8 h (to be continued on next page).

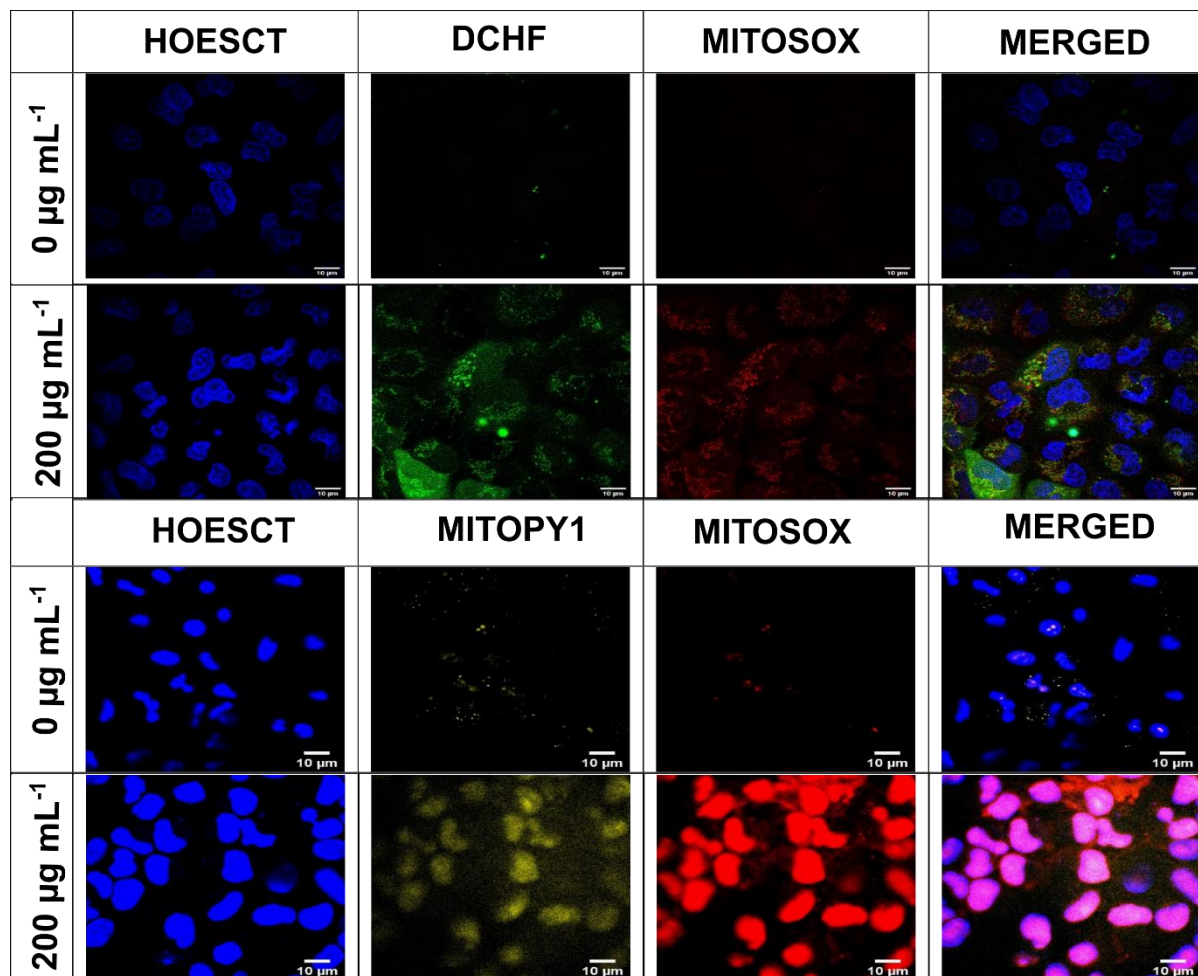


Figure 3.4.23 (continuation): (d) Confocal imaging of cells treated with 200 $\mu\text{g mL}^{-1}$ of the NC at 8 h of the exposure stained with the carboxy H_2DCHF and MitoSox dye in panel one and MitoPY1 and MitoSox in panel 2. The cellular nucleus was stained with Hoechst. Micrographs are scaled to 10 μm in size.

3.4.4.1- Mechanism of Cellular Death following NC Treatments

The BEAS-2B cells treated with $200 \mu\text{g mL}^{-1}$ of NC were analysed for the mechanism of cellular death using the Annexin-V/ PI staining. At 6 h of the exposure, there was no significant change in the cellular population compared with the control BEAS-2B cells (Figure 3.4.24a). This was further confirmed by the Calcein-AM/PI staining (using fluorescence microscopy) in Figure 3.4.25. The Figure 3.4.25a shows the control BEAS-2B cells where no sign of apoptosis/ necrosis is observed. However, the Figure 3.4.25b showed the NC-exposed cells at 6 h and early apoptotic cells appeared but the general cell population remained viable. At the 12 h of exposure, the percentage of live cells decreased from ~75% in the control cells to the ~62.5% in the NC-exposed cells. The early apoptotic cell population increased from ~4% in the control cells to ~10% in the NC-exposed cells while late apoptotic/necrotic cells increased from ~10% in the control cells to ~17% in the NC-treated cells (Figure 3.4.24b). The micrographs of NC-exposed BEAS-2B cells in Figure 3.4.25c confirmed the apoptotic cell population and the emergence of small apoptotic bodies (or round vesicles) at 12 h of treatment. There is also the presence of PI-stained cells, strong evidence of the naked-nuclei following cellular death. At 24 h of exposure, the percentage of live cells decreased from ~75% in the control cells to ~63% in NC-exposed cells. The early apoptotic cell population increased from ~4% in the control cells to ~12% in the NC-exposed cells while late apoptotic/necrotic cells increased from ~8% in the control cells to ~22% in the NC-treated cells (Figure 3.4.24c). The cells were entering from the early to the late apoptotic stage as confirmed by the images in Figure 3.4.25d. A smaller number of live cells were present in the 24 h treated NC samples as there were more rounder cells present (detached from the bottom) and apoptotic bodies were evident in the micrograph. At 48 h of exposure, the percentage of live cells decreased from ~67% in the control cells to ~49% in NC-exposed cells. The early apoptotic cell population remained same as control as in NC-exposed cells (8%). In comparison, the late apoptotic/necrotic cells increased significantly from ~15% in the control cells to ~34% in the NC-treated cells (Figure 3.4.24d). The cells entered the late-apoptotic phase from early apoptosis as confirmed by the images in Figure 3.4.25e & f. The NC-treated cells micrograph at 48 h (Figure 3.4.25e), exhibited a high number of round cells with the PI-stained naked cellular nuclei. The apoptotic bodies were not present as most of the cells had already entered the late stage of apoptosis while the Figure 3.4.25f of 48 h control cells showed intact BEAS-2B cells.

The A549 cells treated with $200 \mu\text{g mL}^{-1}$ of NC were also analysed for the mechanism of cellular death using the Annexin-V/ PI staining and fluorescence microscopy (Figure 3.4.26 & Figure 3.4.27). At 6 h of the exposure, the percentage of live cells decreased from ~83% in the control cells to the ~77% in NC-exposed cells. The early apoptotic cell population increased from ~5.8% in the control cells to ~10% in the NC-exposed cells while late apoptotic/necrotic cells increased from ~10% in the control cells to ~17% in the NC-treated cells (Figure 3.4.26a). The Figure 3.4.27a shows the control A549 cells at 6 h where no sign of apoptosis/ necrosis is observed. However, the Figure 3.4.27b shows the NC-exposed cells at 6 h and early apoptotic cells appeared. At 12 h of exposure, the percentage of live cells decreased from ~72% in the control cells to ~59% in NC-exposed cells. The early apoptotic cell population increased from ~4% in the control cells to ~7% in the NC-exposed cells while late apoptotic/necrotic cells increased from ~10% in the control cells to ~24% in the NC-exposed cells (Figure 3.4.26b). The micrographs of NC-exposed A549 cells in Figure 3.4.27c confirmed the presence of apoptotic cells and emergence of small apoptotic bodies (or round vesicles)³⁸³ at 12 h of treatment. At 24 h of exposure, the percentage of live cells decreased from ~89% in the control cells to the ~59% in NC-exposed cells. The early apoptotic cells increased from ~1% in the control cells to ~12% in the NC-exposed cells while late apoptotic/necrotic cells increased from ~5.6% in the control cells to ~26% in the NC-exposed cells (Figure 3.4.26c). The cells were present in the early and late apoptotic stage as confirmed by the images in Figure 3.4.27d. A smaller number of live cells were present in the 24 h exposed NC samples as there are more rounder cells and most of them had apoptotic bodies as evident in the micrograph. At 48 h of exposure, the percentage of live cells decreased from ~80% in the control cells to the ~25% in NC-exposed cells. The early apoptotic cell population increased from 4% in control to 13% NC-exposed cells. In comparison, late apoptotic/necrotic cells increased significantly from ~10% in the control cells to ~60% in the NC-exposed cells (Figure 3.4.24d). This suggested that most NC-exposed A549 entered the late-apoptotic phase from early apoptosis at 48 h of the exposure as confirmed by the images in Figure 3.4.25e & f. The micrograph recorded for NC-exposed cells at 48 h (Figure 3.4.25e), exhibits rounder cells and the PI-stained naked cellular nuclei. A small number of cells with apoptotic bodies were also present while the Figure 3.4.25f of 48 h control cells showed the intact A549 cells.

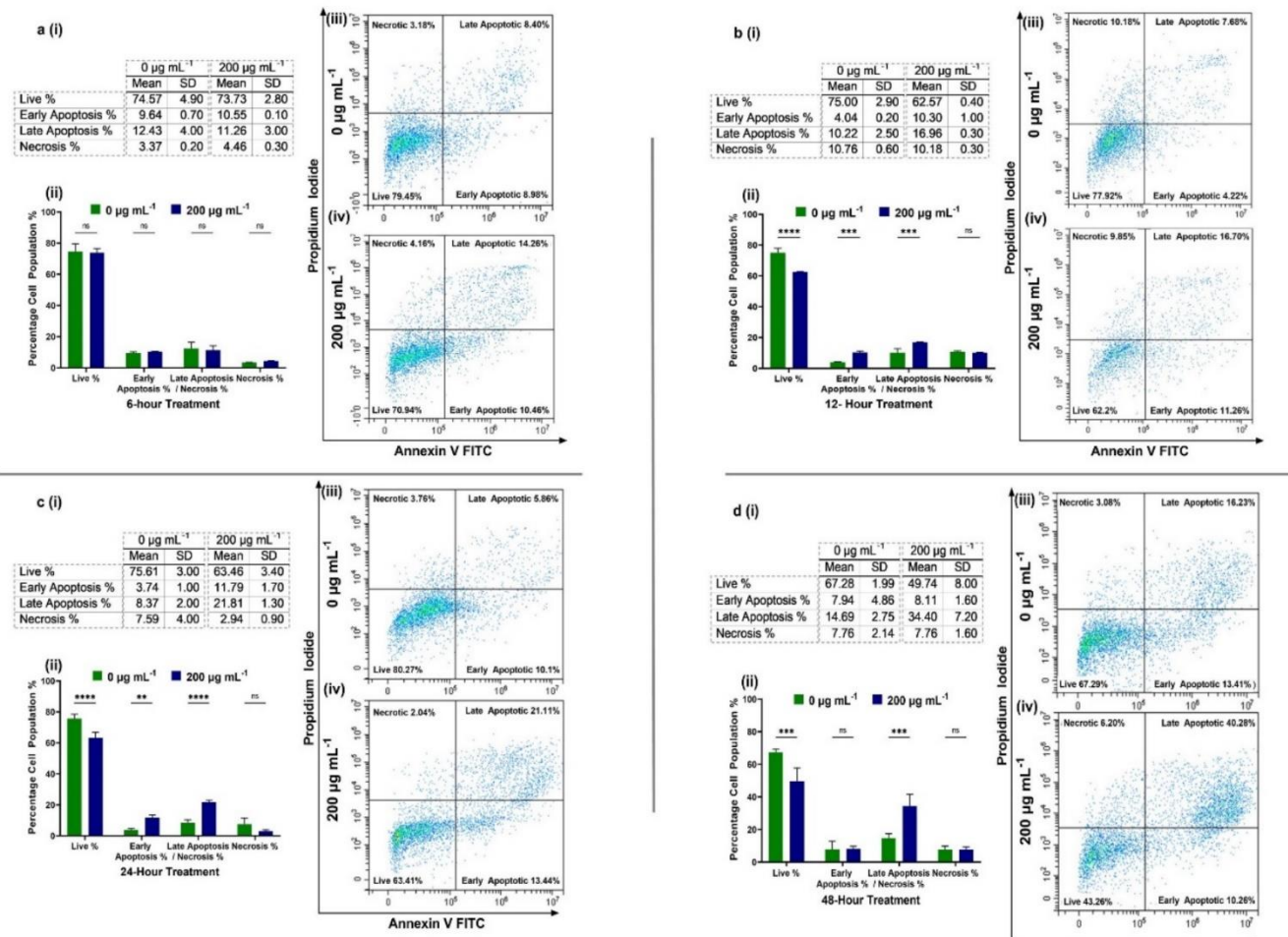


Figure 3.4.24. Annexin-V/ PI staining of NC treated BEAS-2B cells to see the mechanism of cellular death following exposure to the 200 $\mu\text{g mL}^{-1}$ concentration at (a) 6 h (b) 12 h (c) 24 h and (d) 48 h of the treatment. The table in (i) represents the average of experiments performed (ii) the bar-graph represents the percentage cellular population in either live, early apoptotic, late apoptotic/ necrotic, and necrotic phase and the dot plot represents the sample of one experiment for (iii) control group (iv) the treatment group.

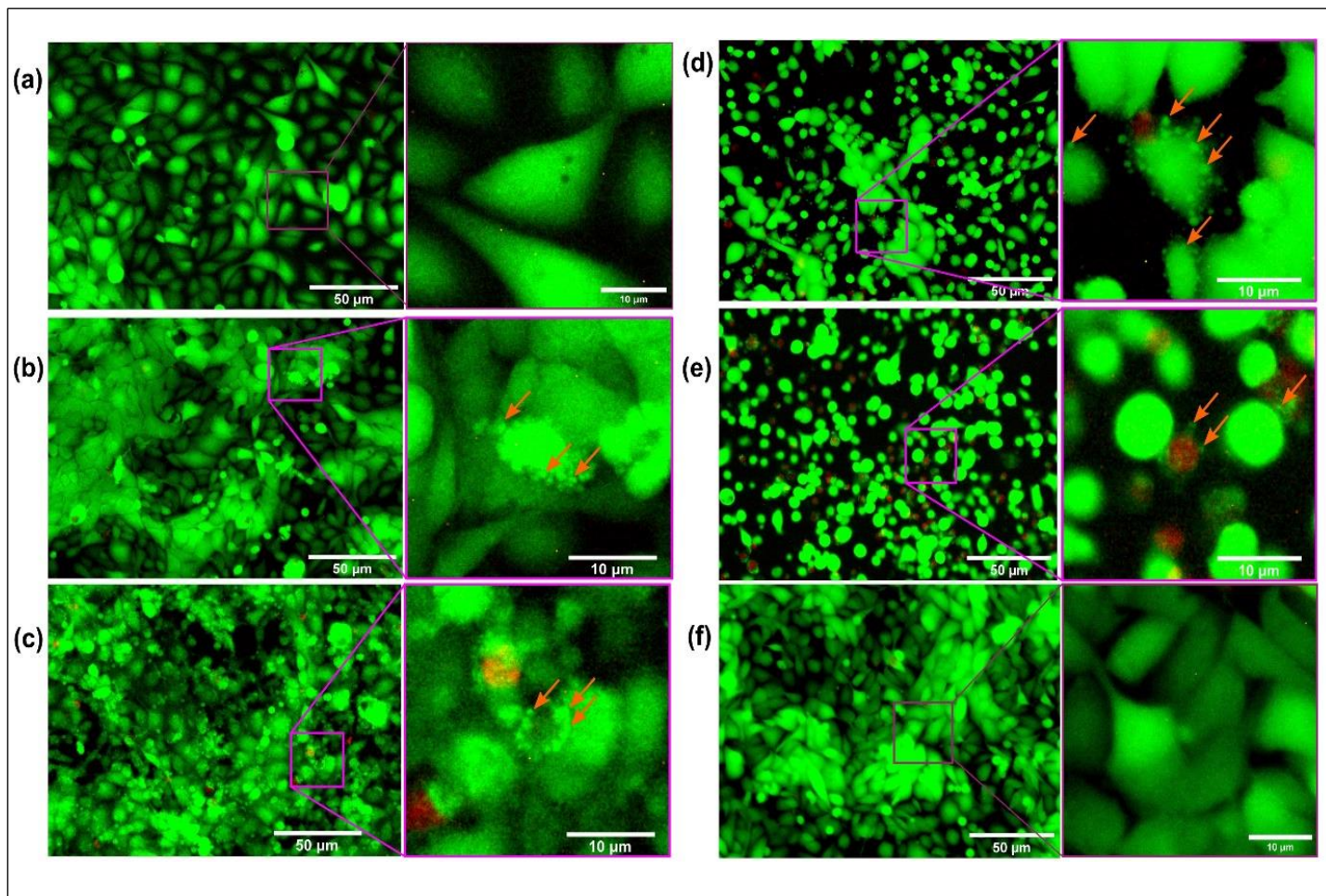


Figure 3.4.25. The BEAS-2B stained with Calcein-AM/PI were observed under the fluorescent microscope to see the formation of apoptotic bodies after exposure to $200 \mu\text{g mL}^{-1}$ (a) untreated control of cells at 6 h (b) the NC exposed cells at 6 h (c) the NC-exposed cells at 12 h (d) the NC-exposed cells at 24 h (e) the NC-exposed cells at 48 h and (f) the untreated control cells at 48 h. The images in left are scaled to $50 \mu\text{m}$ and zoomed images scaled to $10 \mu\text{m}$ in size.

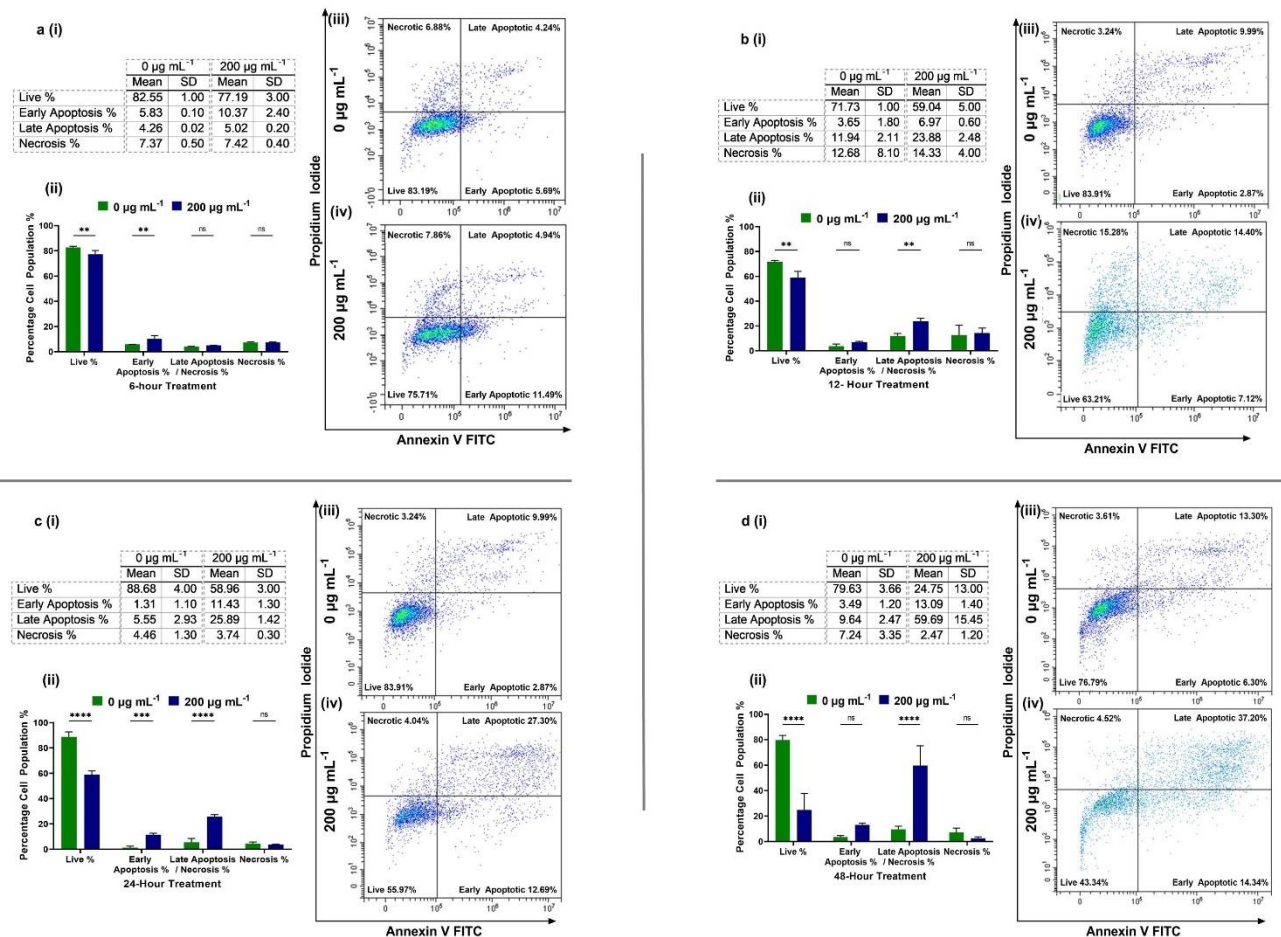


Figure 3.4.26. Annexin-V/ PI staining of NC treated A549 cells to see the mechanism of cellular death following exposure to the 200 $\mu\text{g mL}^{-1}$ concentration at (a) 6 h (b) 12 h (c) 24 hand (d) 48 h of the treatment. The table in (i) represents the average of experiments performed (ii) the bar-graph represents the percentage cellular population in either live, early apoptotic, late apoptotic/ necrotic, and necrotic phase and the dot plot represents the sample of one experiment for (iii) control group (iv) the treatment group.

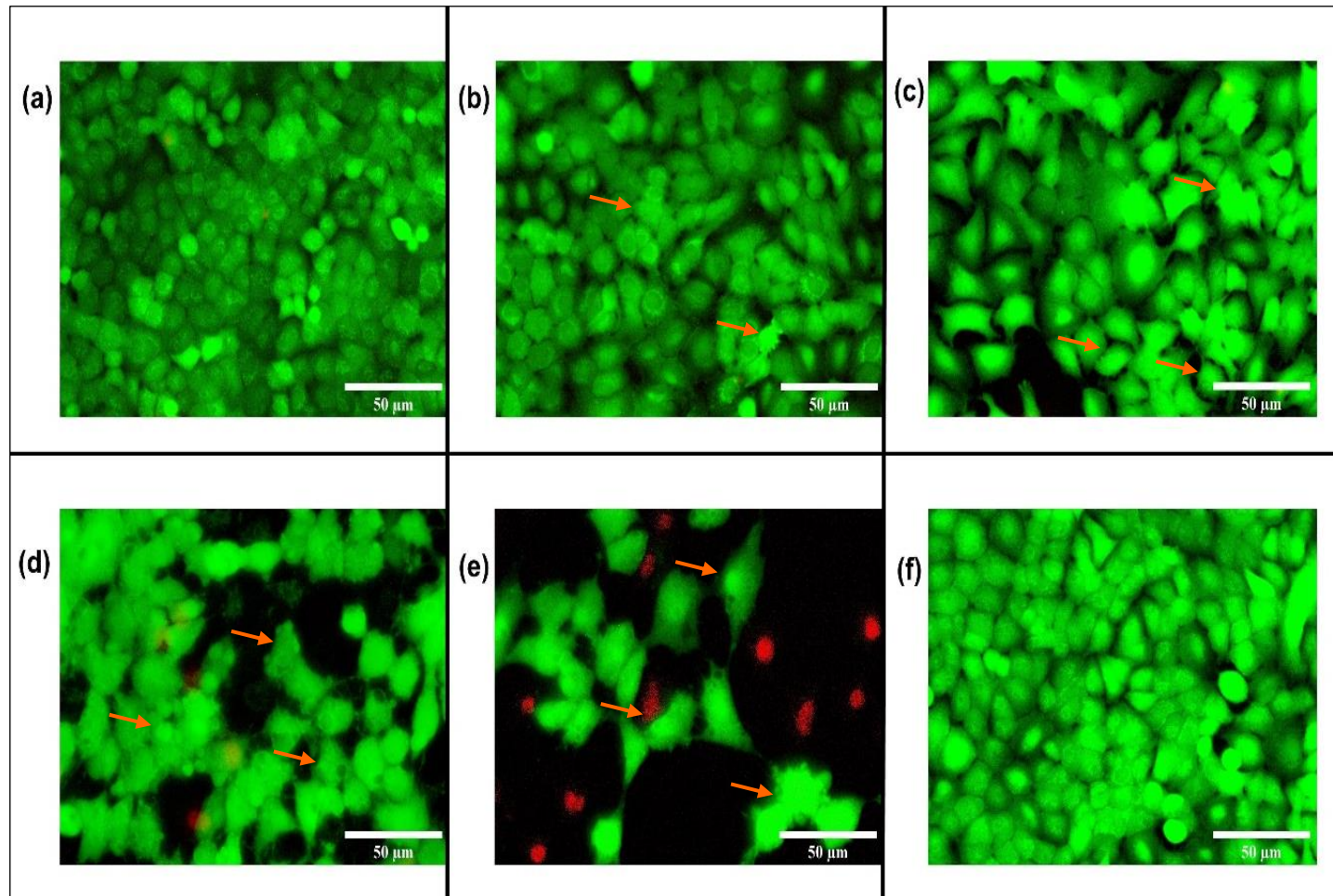


Figure 3.4.27. The A549 stained with the Calcein-AM, PI were observed under the fluorescent microscope to see the formation of apoptotic bodies after exposure to $200 \mu\text{g mL}^{-1}$ (a) untreated control of cells at 6 h (b) the NC exposed cells at 6 h (c) the NC-exposed cells at 12 h (d) the NC-exposed cells at 24 h (e) the NC-exposed cells at 48 h and (f) the untreated control cells at 48 h. The images are scaled to $50 \mu\text{m}$ in size.

3.4.6- Toxicological Profiling of the 4BBA Mixtures

3.4.6.1- IC₅₀ Profiles and Cellular Death Analyses of the 4BBA-Treated Lung Cells

Next, we decided to research the lung cell toxicity induced by the equimolar mixture of the four biomass burning aerosol components (4BBA), which were discussed in previous chapters. The 4BBA treated BEAS-2B cells (Figure 3.4.28) and A549 cells (Figure 3.4.29) were analyzed for percentage cellular viability using an increasing concentration of 4BBA (0.01 – 200 $\mu\text{g mL}^{-1}$). The IC₅₀ values for 4BBA treated BEAS-2B cells were $\sim 63 \mu\text{g mL}^{-1}$ at 24 h and $\sim 34 \mu\text{g mL}^{-1}$ at 48 h of exposure (Figure 3.4.28a). The percentage proliferation rate of the BEAS-2B at the 0.1-200 $\mu\text{g mL}^{-1}$ remained $\leq 74\%$ following exposure to 4BBA at 48 h, implying the inhibitory effect posed by 4BBA even at the lowest concentration of exposure. The IC₅₀ values for 4BBA treated A549 cells were calculated to be $\sim 208 \mu\text{g mL}^{-1}$ at 24 h and $\sim 120 \mu\text{g mL}^{-1}$ at 48 h of exposure respectively (Figure 3.4.29a). The percentage proliferation rate of the cells at the 0.1-200 $\mu\text{g mL}^{-1}$ exposure concentration remained $\leq 80\%$ following exposure to 4BBA at 48 h.

The percentage of cellular death analysis followed IC₅₀ calculations upon exposure to the 0.01 – 200 $\mu\text{g mL}^{-1}$ of 4BBA using LDH assay. The exposure to the 100 $\mu\text{g mL}^{-1}$ and 200 $\mu\text{g mL}^{-1}$ of 4BBA in the BEAS-2B and A549 resulted in 20-40% of LDH release percentage at 24 h and 48 h of exposure as shown in Figure 3.4.27b and Figure 3.4.28b respectively.

Morphological changes following the exposure were noted using Calcein-AM/ PI staining under the fluorescence microscope as shown in Figure 3.4.27c and Figure 3.4.28c. The BEAS-2B cells turned rounder and detached when exposed to the 100 $\mu\text{g mL}^{-1}$ and 200 $\mu\text{g mL}^{-1}$ of 4BBA at 24 h and 48 h, as observed in the Calcein-AM stained channel. An increase in the PI-stained cells was observed at both 24 h and 48 h of exposure (Figure 3.4.27c). In 4BBA exposed A549 cells, an increase in the PI-stained channel was observed at 24 h and 48 h of exposure and the cellular morphology (as observed in the bright-field channel) was distorted. The combined LDH, cellular imaging and IC₅₀ data show that 4BBA-treated BEAS-2B and A549 cells exhibited a concentration-dependent effect on cellular viability and cellular death.

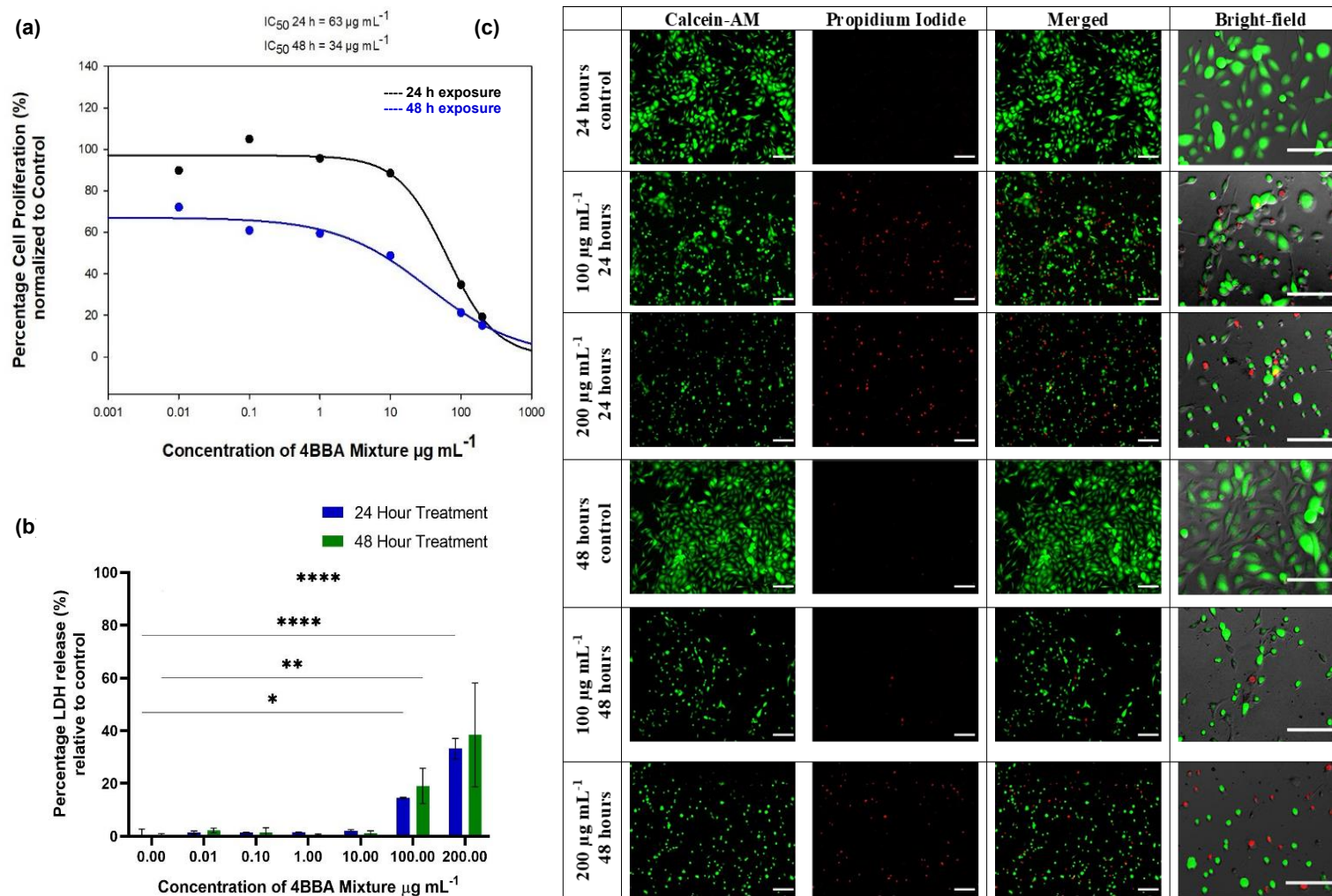


Figure 3.4.28: The cellular viability and death analysis in the BEAS-2B cell lines following exposure to the 4BBA(a) IC_{50} values of 4BBA at 24 h and 48 h of the exposure (b) LDH analysis at 24 h and 48 h of the exposure (c) The Calcein-AM/PI staining of cells treated with $100 \mu\text{g mL}^{-1}$ and $200 \mu\text{g mL}^{-1}$ of 4BBA at 24 h and 48 h of the exposure. The micrographs are scaled to $50 \mu\text{m}$ in size.

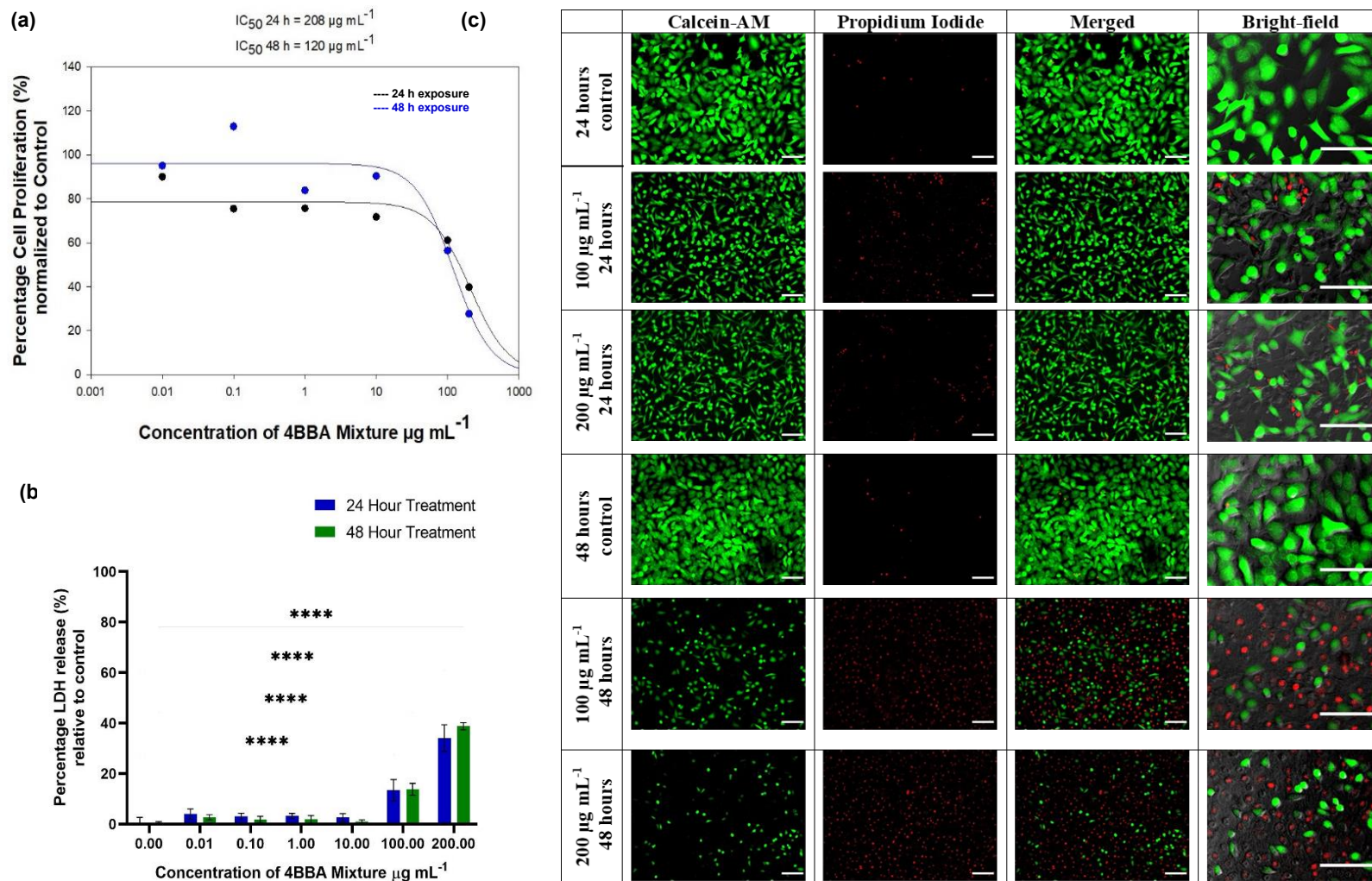


Figure 3.4.29: The cellular viability and death analysis in the A549 cell lines following exposure to the 4BBA (a) IC_{50} values of 4BBA at 24 h and 48 h of the exposure (b) LDH analysis at 24 h and 48 h of the exposure (c) The Calcein-AM/PI staining of cells treated with 100 $\mu\text{g mL}^{-1}$ and 200 $\mu\text{g mL}^{-1}$ of 4BBA at 24 h and 48 h of the exposure. The micrographs are scaled to 50 μm in size.

3.4.6.2- General and Mitochondrial ROS build-up in the 4BBA Mixture-Treated Lung Cells

The 4BBA-treated BEAS-2B and A549 cells were analysed for the changes in the cellular ROS and mtROS. **Figure 3.4.30** shows the changes in the cellular ROS and mtROS of the BEAS-2B cells exposed to 4BBA and **Figure 3.4.31** shows the ROS changes in the A549 cells. The flow cytometric TMRM analysis in **Figure 3.4.30a** showed the BEAS-2B cells treated with 4BBA at 12 h, 24 h and 48 h of exposure to 200 $\mu\text{g mL}^{-1}$ concentration. A significant decrease in $\Delta\Psi\text{m}$ was observed in 200 $\mu\text{g mL}^{-1}$ exposed cells, starting 24 h of exposure where signal decreased to 0.87 of the untreated control. The $\Delta\Psi\text{m}$ decreased to 0.7 of the control at 48 h of the exposure. The MitoSox signal increased to ~ 2.0 over the control following exposure to the 4BBA concentration of 100 $\mu\text{g mL}^{-1}$ and further increased to ~ 2.2 fold after exposure to 200 $\mu\text{g mL}^{-1}$ at 8 h of the exposure as shown in **Figure 3.4.30b**. An almost 1.5-fold increase in carboxy- H_2DCHF signal was observed following the exposure to 200 $\mu\text{g mL}^{-1}$ of 4BBA while no significant changes in the ROS signals were observed after the exposure to 100 $\mu\text{g mL}^{-1}$ of 4BBA at 8 h as shown in **Figure 3.4.30c**.

The confocal microscopy images of BEAS-2B cells, treated with the 4BBA are shown in **Figure 3.4.30d**. The upper channels show the general ROS and mitochondrial $\text{O}_2^{\cdot-}$ production in the BEAS-2B cells exposed with 200 $\mu\text{g mL}^{-1}$ of 4BBA at 8 h while lower panel shows the 4BBA exposed cells at 8 h showing changes in the mitochondrial H_2O_2 and $\text{O}_2^{\cdot-}$. The increased carboxy H_2DCHF signal was observed in the 4BBA treated cells. The MitoSox signal also increased, implying in the merged upper channel in **Figure 3.4.30d**, cellular inhibition and death could be attributed to high ROS activity. In the lower channel of **Figure 3.4.30d**, an increased MitoPY1 and MitoSox signals were observed in the 4BBA exposed cells. Together with the decreased $\Delta\Psi\text{m}$ observed in **Figure 3.4.30a** and high mtROS associated signal, the cytotoxicity could be explained. The overall mitochondrial activity was impaired following 4BBA treatment, contributing to the BEAS-2B cells decreased viability.

The flow cytometric TMRM analysis in **Figure 3.4.31a** showed the A549 cells treated with 4BBA at 12 h, 24 h and 48 h when exposed to 200 $\mu\text{g mL}^{-1}$ concentration. A decrease of $\Delta\Psi\text{m}$ was observed between 24 h -48 h of the exposure where signal decreased to ~ 1.4 and ~ 2.1 respectively when compared with the untreated control. The MitoSox signal increased to ~ 1.2 over control following exposure to the 4BBA concentration of 200

$\mu\text{g mL}^{-1}$ at the 8 h of exposure as shown in Figure 3.4.31b. An ~ 0.9 decrease in carboxy- H_2DCHF signal was observed following exposure to $100 \mu\text{g mL}^{-1}$ and fold change increased to ~ 1.2 following exposure to $200 \mu\text{g mL}^{-1}$ of 4BBA at 8 h as shown in Figure 3.4.31d.

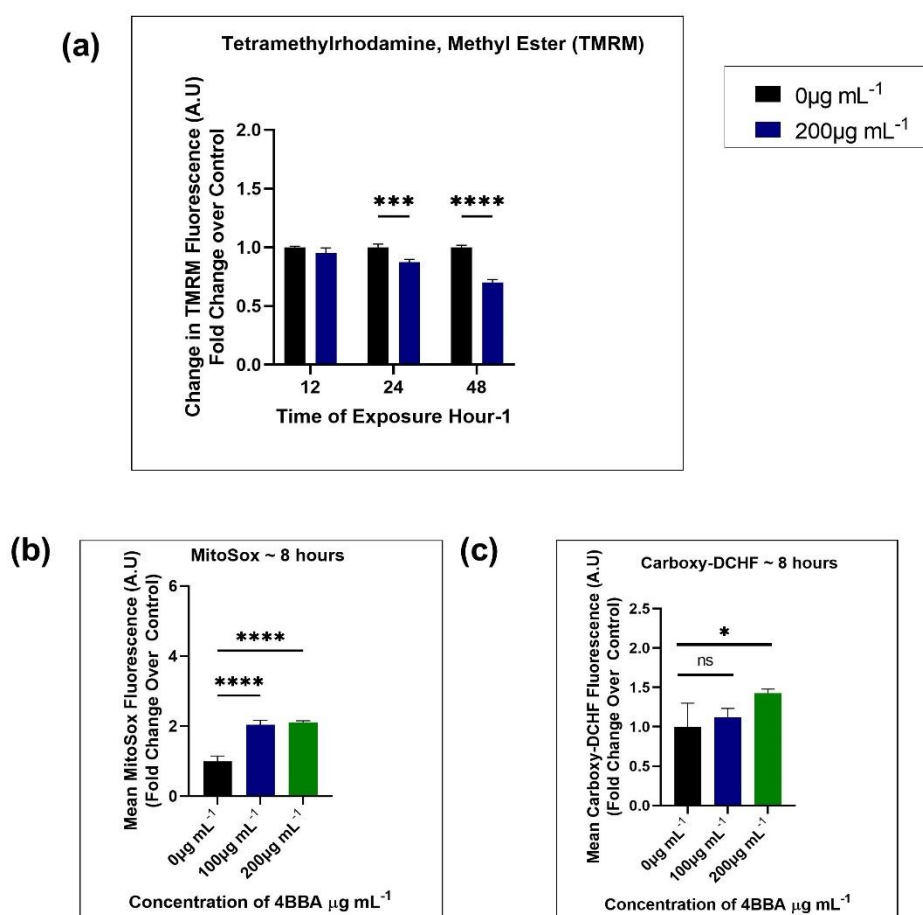


Figure 3.4.30: The general and mtROS analysis in the BEAS-2B cell lines after exposure to 4BBA using flow cytometer and confocal microscopy (a) Changes in TMRM fluorescence compared to control following treatment with $200 \mu\text{g mL}^{-1}$ 4BBA at 12 h, 24 h and 48 h of the exposure (b) Fold change in MitoSox signal with 100 and $200 \mu\text{g mL}^{-1}$ of the 4BBA exposure at 8 h (c) Fold change in the carboxy H_2DCHF signal with $100 \mu\text{g mL}^{-1}$ and $200 \mu\text{g mL}^{-1}$ of 4BBA exposure at 8 h (to be continued on next page)

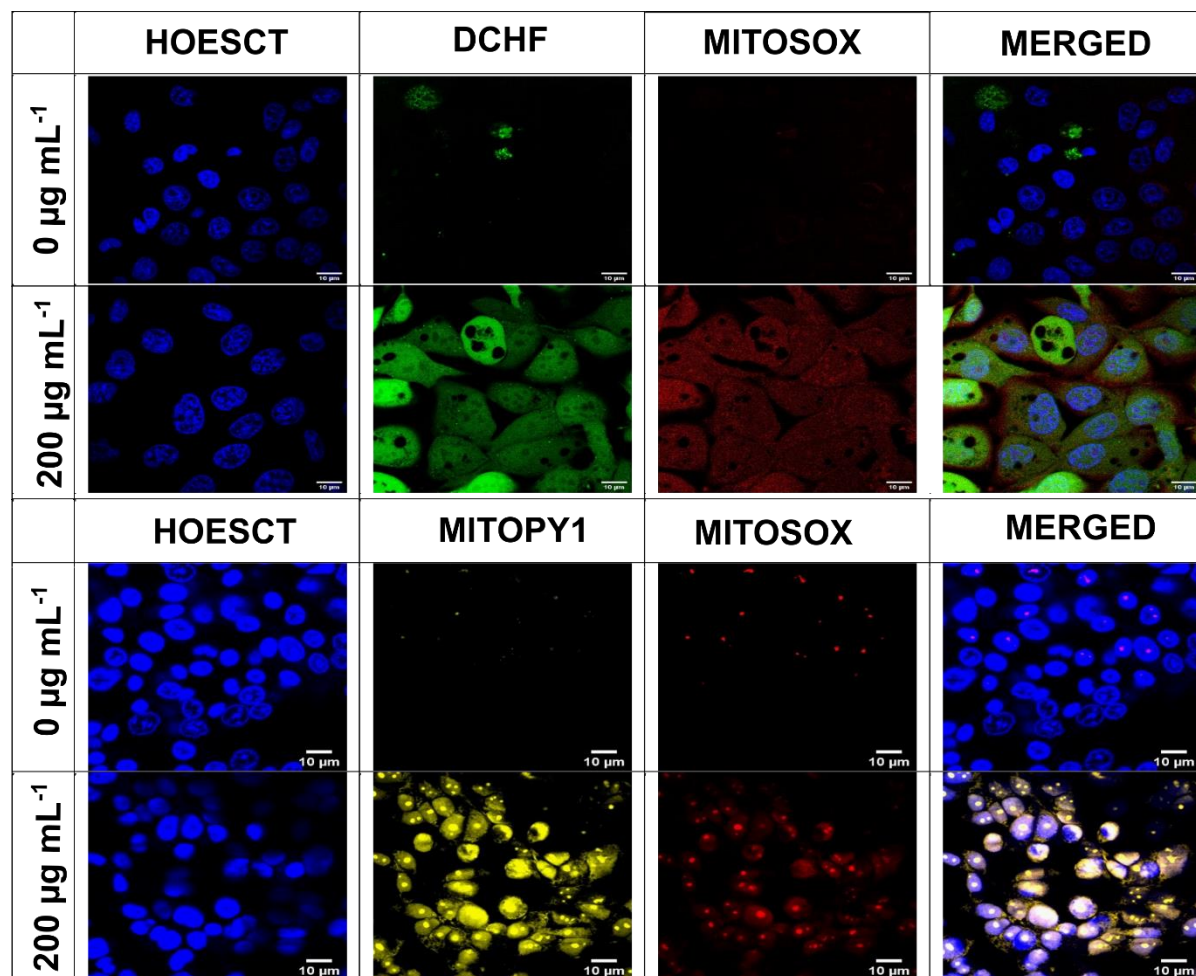


Figure 3.4.30 (continuation): (d) Confocal imaging of BEAS-2B cells treated with 200 $\mu\text{g mL}^{-1}$ of 4BBA at 8 h of the exposure stained with the carboxy H₂DCHF and MitoSox dye in panel one and MitoPY1 and MitoSox in panel 2. The cellular nucleus was stained with Hoechst. Micrographs are scaled to 10 μm in size.

The confocal microscopy images of A549 cells, exposed to 4BBA are shown in **Figure 3.4.31d**. The increase in carboxy H₂DCHF signal was observed in the 4BBA exposed cells. The MitoSox signal also increased, implying in the merged upper channel that mitochondrial ROS also contributed to the general cellular ROS signal of carboxy H₂DCHF but there was also evidence of the general ROS signal in the cells where MitoSox signal was not observed. In the lower channel of **Figure 3.4.31d**, an increased MitoPY1 and MitoSox signals were observed in the 4BBA treated cells. Together with the decreased $\Delta\Psi_m$ observed in **Figure 3.4.31a** and high mtROS associated signal, the cytotoxic effect of 4BBA exposure in A549 cells could be explained and resulted in the apoptosis of the cells, covered in the previous section of the thesis.

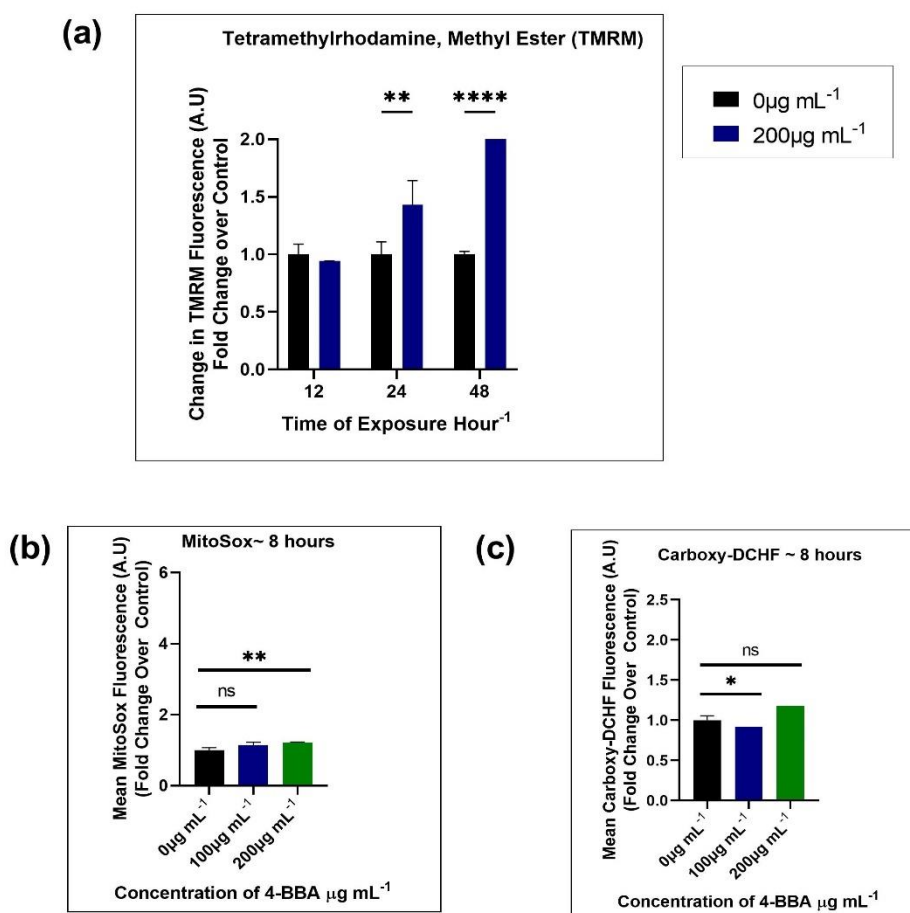


Figure 3.4.31: The general and mtROS analysis in the A549 cell lines after exposure to the 4BBA using flow cytometer and confocal microscopy (a) Changes in TMRM fluorescence compared to the control following treatment with 200 µg mL⁻¹ 4BBA at 12 h, 24 h and 48 h of the exposure (b) Fold change in MitoSox signal with 100 µg mL⁻¹ and 200 µg mL⁻¹ of 4BBA exposure at 8 h (c) Fold change in carboxy H₂DCHF signal with 100 µg mL⁻¹ and 200 µg mL⁻¹ of 4BBA exposure at 8 h (to be continued on next page)

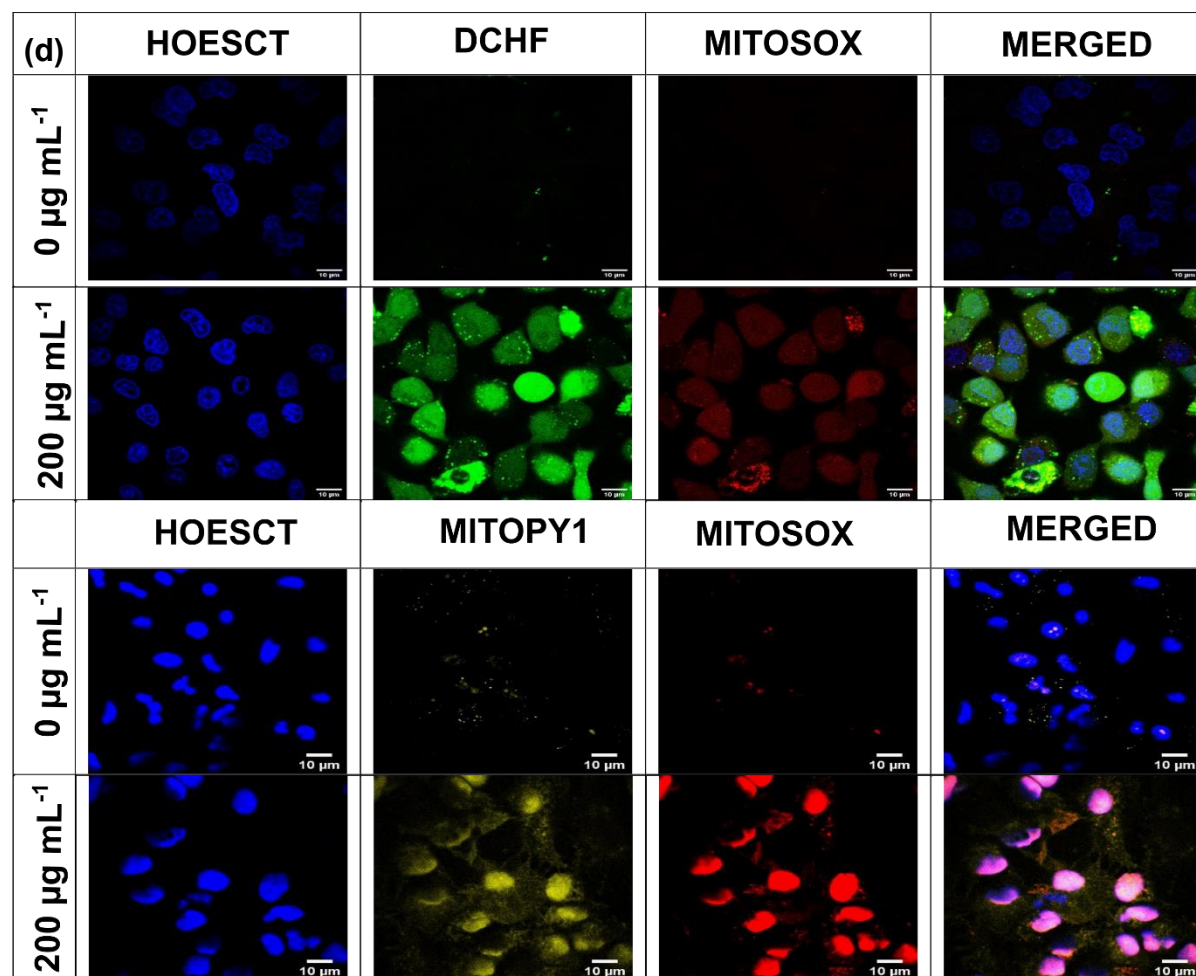


Figure 3.4.31 (continuation): (d) Confocal imaging of A549 cells treated with 200 $\mu\text{g mL}^{-1}$ of 4BBA at 8 h of the exposure stained with the carboxy H_2DCHF and MitoSox dye in panel one and MitoPY1 and MitoSox in panel 2. The cellular nucleus was stained with Hoechst. Micrographs are scaled to 10 μm in size.

3.4.6.3- Mechanism of Cellular Death Following the 4BBA Mixture Treatments

The BEAS-2B cells treated with $200 \mu\text{g mL}^{-1}$ of 4BBA were analysed for the mechanism of cellular death using the Annexin-V/ PI staining. At 12 h of exposure, the live cell population decreased from 75% in control cells to 70% of the 4BBA exposed cells. The late apoptotic/ necrotic cells population increased from $\sim 10\%$ of control to $\sim 18\%$ in the 4BBA exposed cells (Figure 3.4.32a). At 24 h of 4BBA exposure, the live cell population decreased from 73% of control cells to 64.5% of the 4BBA treated cells and the percentage of late apoptotic/necrotic cells increased to $\sim 24\%$ from $\sim 3.8\%$ in the control cells as seen in Figure 3.4.32b. At the 48-h exposure to 4BBA, the percentage of late apoptotic/necrotic cells increased to $\sim 38.5\%$ from $\sim 16.5\%$ in the control cells and live cell population decreased from 68% of control cells to $\sim 49\%$ of 4BBA-exposed cells as seen in Figure 3.4.32c. This implies that the cells are in late apoptotic/ necrotic phase between 12-48 h of exposure and early apoptosis event took place in the first 12 h of the exposure.

In the A549 cells treated with the $200\text{-}\mu\text{g mL}^{-1}$ of 4BBA there was a slight decrease in the necrotic cell population from 7.6% of control cells to the 2.4% of 4BBA exposed cells (Figure 3.4.33a). However, at 24 h of exposure, the percentage of live cells decreased from 86% of control cells to 73.5% of 4BBA-exposed cells and late apoptotic/ necrotic cell population increased to 13.73% in 4BBA-exposed cells from 5.5% of the control cells (Figure 3.4.33b). At 48 h of exposure, the percentage of live cells decreased from 79% of control cells to 62.67% of 4BBA-exposed cells; early apoptotic cells increased from 3.25% in the control cells to 14.5% in the 4BBA-exposed cells and late apoptotic/ necrotic cell population increased from 10.5% of the control cells to 19% of 4BBA treated cells (Figure 3.4.33c). As explained in previous chapters, the mtROS and cellular energetics changes contributed to the apoptosis induction in the 4BBA exposed BEAS-2B and A549 cells.

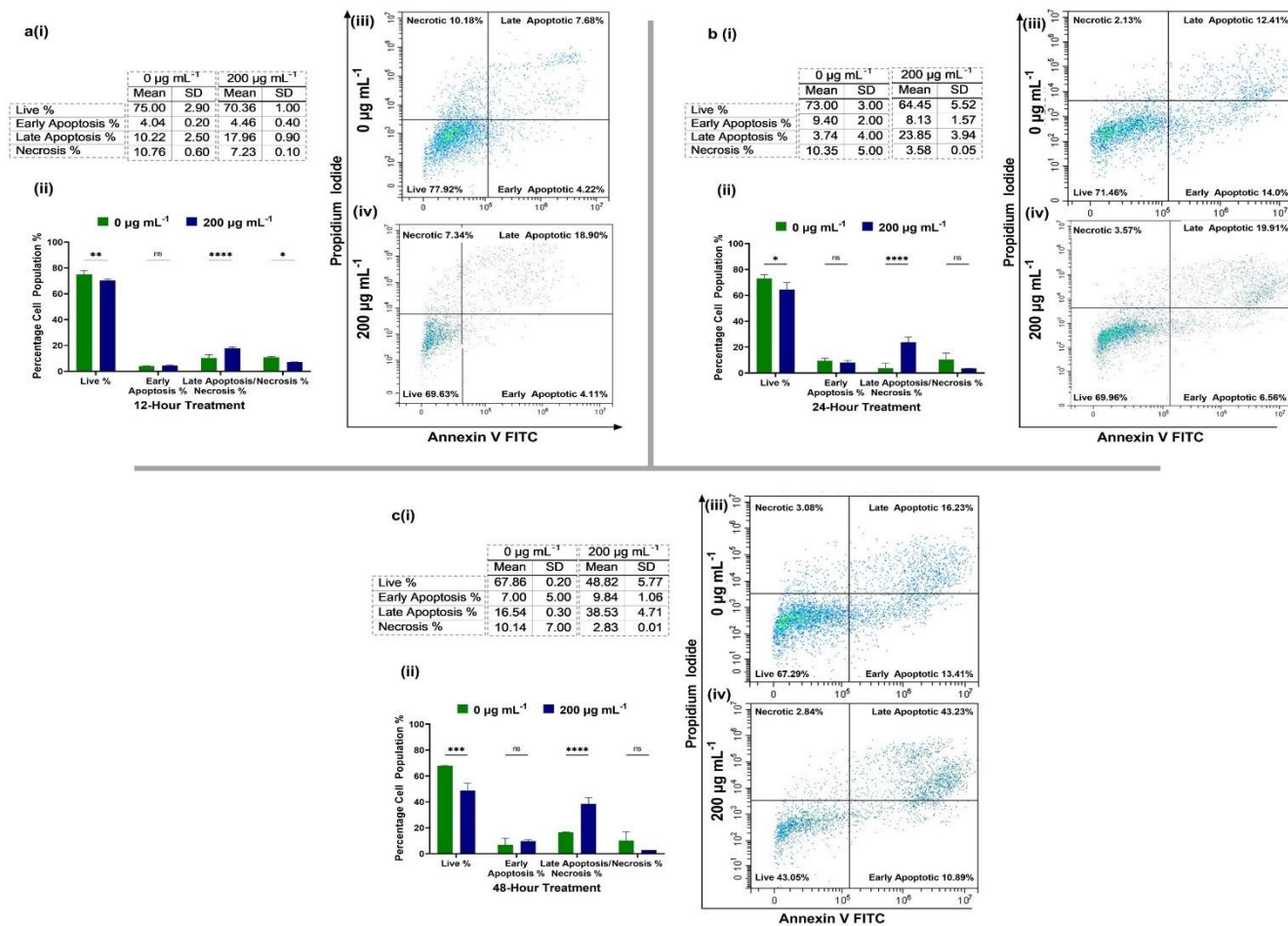


Figure 3.4.32: Annexin-V/ PI staining of 4BBA treated BEAS-2B cells to see the mechanism of cellular death following exposure to the 200 $\mu\text{g mL}^{-1}$ concentration at (a) 12 h (b) 24 h and (c) 48 h of the exposure. The table in (i) represents the average of experiments performed (ii) the bar-graph represents the percentage cellular population in either live, early apoptotic, late apoptotic/ necrotic, and necrotic phase and the dot plot represents the sample of one experiment for (iii) control group (iv) the treatment group

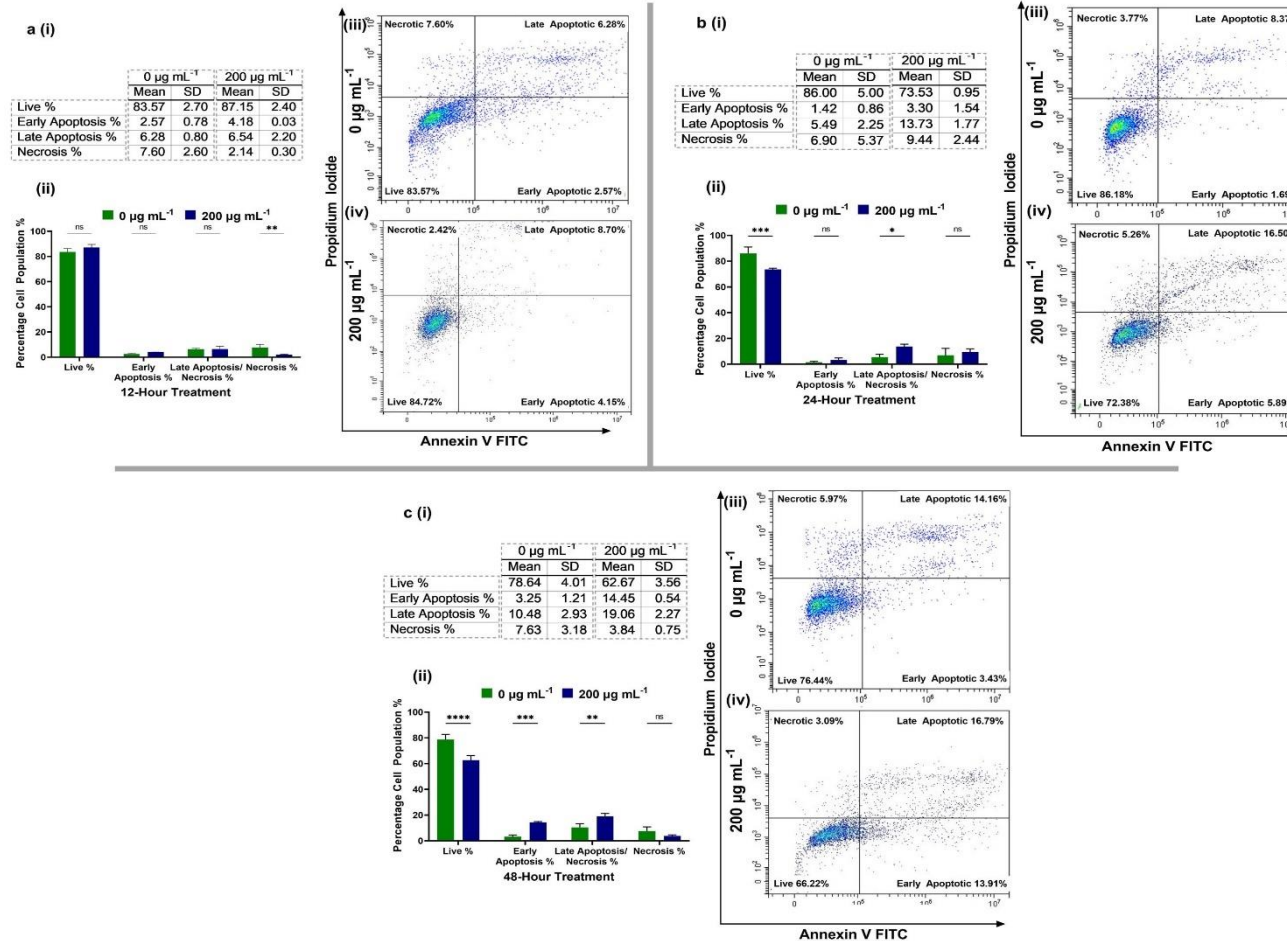


Figure 3.4.33: Annexin-V/ PI staining of 4BBA treated A549 cells to see the mechanism of cellular death following exposure to the 200 $\mu\text{g mL}^{-1}$ concentration at (a) 12 h (b) 24 h and (c) 48 h of the exposure. The table in (i) represents the average of experiments performed (ii) the bar-graph represents the percentage cellular population in either live, early apoptotic, late apoptotic/ necrotic, and necrotic phase and the dot plot represents the sample of one experiment for (iii) control group (iv) the treatment group.

3.4.1- Comparative Toxicology of the BBA markers and Conclusions

The majority of particulate matter-bound compounds in the ambient air have unknown health effects.³⁸⁷ The BBA emissions from wildfire and smoke that inflict adverse effects upon inhalation are NACs.³⁸⁸ As the most essential components of the light-absorbing compounds of the BB emission in one study were found to be nitrophenols and NACs, ³⁸⁹ the current project provides a detailed toxicological profile of the four important BB emissions markers and their equimolar mixture. As discussed in the previous **section (3.1 and 3.3)**, the inhalation safety index of the SOA and NPs was provided through lung uptake of ultrafine particles using the multiple path particle dosimetry (MPPD) model by Gangwal et al.²⁴² Using a similar approach, we calculated the toxicological response achieved in the number of years following exposure to the dose equivalent to the IC₅₀ of each of the studied marker, as summarized in **Table 3.4.1**.

LG did not provide a high cellular inhibition response (for both cell lines) as the number of years to exhibit the response similar to the treated cells corresponds to thousands of years. NS, however, provided an increased inhibition response in BEAS-2B cell lines as the inhibitory response equivalent to IC₅₀ of 48 h (exposure concentration 0.05 $\mu\text{g cm}^{-2}$) could be achieved in ~ 0.2 years of exposure. Similarly, NG exhibited a similar response in hundreds of years in both BEAS-2B and A549 cells as the IC₅₀ value for NG was higher when compared with NS but lower than LG. NC was most cytotoxic in both A549 and BEAS-2B cell lines as 48 h IC₅₀ value for BEAS-2B was found to be around 2.8 $\mu\text{g cm}^{-2}$ exposure concentration and continuous exposure of 10 years can exhibit a similar response as that observed in the BEAS-2B. The 4BBA revealed 11 $\mu\text{g cm}^{-2}$ 48 h IC₅₀ in the BEAS-2B with ~ 40 years required to achieve the similar effect. In the ambient samples collected from fires over central and eastern US, the total simulated BBA concentrations ranged from 1 $\mu\text{g}\cdot\text{m}^{-3}$ to 5 $\mu\text{g}\cdot\text{m}^{-3}$.³⁹⁰ This indicates at higher instances of emissions (such as wildfire and smoke), the emissions of the NACs, including NC, NS and NG included in the study could exceed the threshold and may induce the effect at lower time than the one estimated in our study.

In the study on the exposure effects of the human lung cells on the PM₁₀ from Amazonian Forest fires, oxidative stress, autophagy, DNA damage, cell cycle arrest, increased necrosis/apoptosis, and increased pro-inflammatory response was noted.³⁹¹ In our study, we were able to determine which of OA-bound components exhibited a change in ROS,

mitochondrial dysfunction, and also the induction of apoptosis/ necrosis at exact concentration and exposure times (which varied with the type of NACs marker included in the study). The summary of prior studies on BBA emission can be found in [Table 3.4.2](#).

LG did not exhibit significant changes in the cellular viability at 48 h. However, when studied at 12 h, it induced apoptosis in the BEAS-2B cells, which recovered in the long-term exposure. However, we report increased mtROS and changes in $\Delta\Psi_m$ throughout the exposure (12 h- 48 h); hence underlying mitochondrial dysfunction and subsequent underlying lung pathophysiologies could be attributed to the continuous exposure to LG.[85](#) Having known the exact exposure effects of LG is important as new BB emissions (including the cellulose combustion) contain an abundant amount of LG and is frequently used as the reference point for BB.[389](#) [392](#) LG increase the ROS and alter the cellular metabolism following the inhalation.[208](#) [393](#) It is not as toxic as NACs. Still, our study provided an important insight into the altered ROS mechanism following LG exposure, and we were able to correlate the exposure responses in the two lung cells.¹ LG is the "fingerprint" marker in the BB primary emissions[393](#). Its overall contribution in the exposed mass of biomass burning emissions are essential for comparing other NACs toxicological responses.[392](#) LG percentage is higher in the wildfire smoldering events.[388](#)

The NO_x concentration is almost 30-70% higher in flaming combustion when compared with smoldering combustion, and NACs are known to be predominant in the flaming events.[147](#) [388](#) In the wildfire plumes from Northern California, sugar-like components were most abundant, followed by mono-carboxylic acids and aromatic components.[394](#) The wood combustion product exhibited a decreased proliferation in A549 in one study at 125 $\mu\text{g mL}^{-1}$ exposure concentration.[77](#) In another study, it was revealed that PM from different fuels and combustion phases have appreciable differences in lung toxic and mutagenic potency. On a mass basis, flaming samples were more active.[202](#) The NS induced a cellular inhibitory effect at a concentration between 100-200 $\mu\text{g mL}^{-1}$ due to an imbalance between anti-ROS and ROS response, as clear from our results in BEAS-2B and A549 cell lines. The continuous exposure results in increased $\Delta\Psi_m$ between 12h to 48 h, which subsequently results in the increased BEAS-2B apoptosis and necrosis population. NS also exhibited the temporal emission, where day-time emissions from BB were higher than at night and summer concentrations were higher than at winters; NS are emitted from anthropogenic VOCs oxidation.[395](#) Hence, understanding the emission effects of NS can give us an estimate of its long term exposure effects in regions of high emission rates.

Similarly, the NG was observed to be a slow-acting toxicant (EC_{50} after 30 min incubation with *Vibrio Fischer* are in the range from 16.7 mg L^{-1} to 102 mg L^{-1}), with relatively high estimated hazardous concentrations ($10\text{--}15 \text{ mg L}^{-1}$) in one study.[209](#) We report the high mtROS and cellular ROS at much lower exposure concentrations ($\mu\text{g mg L}^{-1}$) following exposure to NG. Increased apoptosis was observed at the exposure time of 24 h -48 h, which is a consequence of increased $\Delta\Psi_m$ throughout the exposure in the BEAS-2B cells.

Based on the results obtained, we hypothesize that NC is the most critical SAO component that drives the toxicity in the 4BBA mixture. The catechol is emitted from wildfires due to lignin pyrolysis, and gas-phase reaction products show that under moderate NO_x conditions, NC is formed in the presence of OH radicals, and one study show NC to be the sole reaction product.[388](#) NC was found to be abundant in aged plumes, with the temporal variation in its formation similar to primary BBA tracers.[387](#) In another study, NC was formed as primary emissions from BB during fall (correlations between NC and LG were found) and as SOA during winter/ fall.[395](#) In our study, we found increased apoptosis even after the 6 h exposure. The depolarization of $\Delta\Psi_m$ at increasing exposure time ($100\text{--}200 \mu\text{g mg L}^{-1}$ concentration) in the BEAS-2B cells shows that acute exposure effect with NC induces mitochondrial dysfunction, which subsequently results in the apoptosis induction in the treated cells.

The NACs from winter and summer aerosol samples from an urban location in Ljubljana, Slovenia, identified 12 NACs, 4 of which were included in the study. NC and methyl-NC were the most abundant components.[195](#) The concentration in the winter samples was ~310 times higher than summer samples and were attributed to BB activity, as confirmed by the fingerprint of BB (LG) presence in the samples.[195](#) NC was also present in abundance in the PM_{2.5} samples from Budapest and K-puszta, Hungary, and Rondônia, Brazil, with the highest concentration present in the BB samples from Brazil.[145](#) A study cohort reports that PM_{2.5} from wildfire emission is more toxic to human lungs than any other SOA system, and we report similar results.[200](#)

While previous studies highlighted that the adverse effects for both primary and aged BB particles and seemed to result from a combined effect of several chemical particle constituents,[206](#) we were able to demonstrate that individual NACs exhibited different toxicological response at different dosages and time of exposure, the 4BBA mixture exhibited a profile more closer to the most cytotoxic component (NC). In our study we highlighted the use

of NC as an important marker that drives the cellular toxicology following exposure to BB emissions.

Table 3.4.1. The exposure effects achieved in years in the two lung cell lines following 24 h and 48 h of exposure to the IC₅₀ values of each BBA marker and its equimolar mixture studied in the current project.

IC ₅₀ Values		BEAS-2B Cells		A549 Cells	
		24 Hours	48 Hours	24 Hours	48 Hours
LG	Cell Exposure Concentration	2546 µg mL ⁻¹ 796 µg cm ⁻²	3 x 10 ⁷ µg mL ⁻¹ 9.4 x 10 ⁶ µg cm ⁻²	4.4 x 10 ⁸ µg mL ⁻¹ 1.4 x 10 ⁸ µg cm ⁻²	1.6 x 10 ⁸ µg mL ⁻¹ 5.0 x 10 ⁷ µg cm ⁻²
	Exposure effect Time	~ 2900 years	~ 3.4 x 10 ⁷ years	~ 5.1 x 10 ⁸ years	~ 1.8x 10 ⁸ years
NS	Cell Exposure Concentration	695 µg mL ⁻¹ 217 µg cm ⁻²	0.16 µg mL ⁻¹ 0.05 µg cm ⁻²	279 µg mL ⁻¹ 87 µg cm ⁻²	2.02 x 10 ⁸ µg mL ⁻¹ 6.3 x 10 ⁷ µg cm ⁻²
	Exposure effect Time	~ 792 years	~ 0.2 years	~ 318 years	2.3 x 10 ⁸ ~ years
NG	Cell Exposure Concentration	159 µg mL ⁻¹ 50 µg cm ⁻²	154 µg mL ⁻¹ 48 µg cm ⁻²	320 µg mL ⁻¹ 100 µg cm ⁻²	2.8 x 10 ⁸ µg mL ⁻¹ 8.8 x 10 ⁷ µg cm ⁻²
	Exposure effect Time	~ 183 years	~ 175 years	~ 365 years	~ 3.2 x 10 ⁸ years
NC	Cell Exposure Concentration	30 µg mL ⁻¹ 9 µg cm ⁻²	8.8 µg mL ⁻¹ 2.8 µg cm ⁻²	335 µg mL ⁻¹ 104 µg cm ⁻²	79 µg mL ⁻¹ 25 µg cm ⁻²
	Exposure effect Time	~ 33 years	~ 10 years	~ 380 years	~ 91 years
4BBA	Cell Exposure Concentration	63 µg mL ⁻¹ 20 µg cm ⁻²	34 µg mL ⁻¹ 11 µg cm ⁻²	208 µg mL ⁻¹ 65 µg cm ⁻²	120 µg mL ⁻¹ 37.5 µg cm ⁻²
	Exposure effect Time	~73 years	~40 years	~237 years	~137 years

Table 3.4.2. The literature on BBA samples from different sources and their subsequent toxicological effects in various models.

Type of Emission Source	Model Type	Response Studied	Important Conclusion	Ref
Fir and beech pellets burnt in domestic appliances	A549 cells THP-1 cells	LDH CXCL8 (IL-8) Oxidative stress DNA damage	IL-8 release: more effect with late combustion, Actin polymerization in particles uptake, Modest dose-dependent DNA lesions observed, Combustion conditions modulate toxicity	17
Wildfire-specific PM _{2.5}	Study Cohort	Respiratory hospital admissions.	Wildfire-specific PM _{2.5} can cause a more significant impact on respiratory health than PM _{2.5} from other sources	200
Nitrated-polycyclic aromatic hydrocarbons (nitro-PAHs) and diesel exhaust particle extracts (DEPE)	Hepa1c1c7 cells	Lipid peroxidation DNA adduct formation Apoptosis	P53 accumulation, Apoptosis induction, Potential carcinogenicity, and mutagenicity	201
Flaming vs. smoldering phases of five biomass fuels (red oak, peat, pine needles, pine, and eucalyptus)	Acute lung toxicity in mice and mutagenicity in Salmonella	Lung toxicity EF (neutrophil/mass of fuel burned)	PM from different fuels and combustion phases have appreciable differences in lung toxic and mutagenic potency, and on a mass basis, flaming samples are more active, whereas smoldering samples had a greater effect when EFs were considered	202
PM samples from a countryside city, Limeira, Brazil, influenced by heavy traffic and sugar cane biomass burning.	Salmonella/microsome micro-suspension mutagenicity assay using TA98, YG1041, and TA1538, with and without metabolic activation	Mutagenicity testing	High mutagenicity rates are speculated when the PM from sugarcane production is mixed with PM from traffic.	203
Wood smoke PM from operating wood stoves in the rural area.	A549 and THP-1 cell lines	ROS/ RNS Pro-inflammatory response DNA, lipid, protein damage Self-defense signal	Dose-dependent formation of ROS DNA damage in terms of strand breaks. Chemoattractant protein-1, Interleukin-8, and tumor necrosis factor- α , as well as the oxidative stress gene heme oxygenase-1, was upregulated	204
Primary and atmospherically aged wood combustion particles	Human bronchial epithelial (HBE) and BEAS-2B cell lines	LDH, IL-6, IL-8, HMOX-1, COX-2	Adverse effects were observed for both primary and aged particles and seemed to result from a combined effect of several chemical particle constituents.	206

Water-soluble fraction of pyrolyzed wood tar aerosols	Mice model and BEAS-2B	Cell Death Lipid peroxidation ROS Mitochondrial damage	ROS build-up and Nrf2 mediated antioxidant response noted, MDA was increased, apoptotic bodies observed with mitochondrial degradation	207
Guaiacol, 4-nitroguaiacol, 6-nitroguaiacol, and dinitroguaiacol.	V. Fischer bioluminescence acute toxicity test	Effective concentrations EC50	4NG was observed to be a slow-acting toxicant (EC50 after 30 min incubation with <i>V. Fischer</i> are in the range from 16.7 to 102 mg L ⁻¹ , the toxicity is increasing in the order GUA < 6NG < 4NG < DNG), with high estimated hazardous concentrations HC5 (10–15 mg L ⁻¹)	209
Biomass burning aerosol from the Brazilian Amazon.	Murine alveolar macrophages (MH-S) Chemical Assay	ROS/ RNS DTT Assay	Compared to ambient samples and laboratory-generated SOA, BBA induced higher levels of ROS/RNS. The correlation was observed between ROS/RNS and levoglucosan.	208
Wood-combustion-related biomass burning nanoparticles	A549 lung cells	Cytotoxicity Behavioural parameters Physical Parameters	At 125 µg/mL, decreased cell proliferation compared to the control was noted. Exposure to higher concentrations (250 and 500 µg/mL) changed cell perimeter, optical thickness for smoldering and flaming particles, and led to decreased migration, motility, and motility speed of cells	77
Particulate Matter (PM2.5) from Biomass Combustion	BEAS-2B cells	Proliferation ROS/ RNS Cancer drug resistance	no impact on cellular viability and proliferation, increased intracellular reactive oxygen species (ROS) level, increased nrf-2 expression, molecular defense mechanisms, which prevent cellular damage	287
PM ₁₀ from Amazon region	A549 cell line	Cell viability ROS generation Inflammation Autophagy Cell cycle arrest DNA damage Apoptosis/ necrosis induction	200 and 400 µg mL ⁻¹ induced increased ROS, cell cycle inhibition and mitochondrial ROS Exposure effect achieved in dose and time-dependent manner, induction of pro-inflammatory response, apoptosis and necrosis were both induced, DNA damage and cell cycle arrest was noted	391

CHAPTER 4: Research Summary and Future Prospective

The Ph.D. thesis research conducted in four inter-linked and multidisciplinary projects was designed to determine the potential inhalation exposure effects of ambient SOA components on human lung cells. Several studies in the past provided evidence of the adverse exposure effects of the systems included in this research through various *in vitro* and *in vivo* models. However, there have been limited studies that provide detailed toxicological profiles of individual markers and their mixtures in the same cellular model. Our results help to fill this gap.

The results obtained from the monoterpene-derived SOA study revealed that organic peroxides from α -pinene ozonolysis SOA likely induced ROS in the lung cells. At the same time, the individual SOA organic acid markers, including MBTCA, did not exhibit any changes in the cellular viability or ROS. The exposure of BEAS-2B cell lines to α -pinene ozonolysis SOA showed changes in cellular viability and ROS. In contrast, exposure to A549 cells at the same concentration and exposure time did not exhibit any change. This data suggests that A549 cells responded differently to the exposure compared to the BEAS-2B cell lines, thereby emphasizing the need for careful selection of cellular models for *in vitro* studies.

The atmospheric aging of particulate 2-MTS modulates the gene expression pathways from the KEAP-1/ NRF-2 cluster. The basal-level gene expression (with 2MTS expression alone) includes ROS enzymes and inflammatory gene cascades. The downregulation of mitochondrial superoxide enzymes in the treated cells indicates the antioxidant activity and cell survival response. Furthermore, the glutathione detoxification pathway exhibits higher gene upregulation than the untreated control with increased heterogeneous $\cdot\text{OH}$ -mediated oxidation (or atmospheric chemical aging) of particulate 2-MTSs. The exposure of fine particulate 2-MTSs with enhanced multifunctional OSs also change the gene expression from pro-inflammatory to anti-inflammatory pathways; this observation suggests that changes in the chemical composition of the aerosol particles due to atmospheric chemical aging through heterogeneous $\cdot\text{OH}$ oxidation drive the IC_{50} and gene expression in the exposed BEAS-2B cells.

Of all mono-NPs in the atmosphere, 4NP is the most abundant of monocyclic SOA-bound species and smog chamber-generated aerosol. It also exhibited the lowest IC_{50} value and highest cellular death in both the BEAS-2B and A549 cells. The NP mixture induced

apparent changes in the model eukaryotic membrane by forming “hole-like” structures, as verified by electrochemical and microscopic techniques, thereby causing the internalization of these pollutants. The mono-NPs exhibited different toxicological profiles in the two cell lines. Increased cellular ROS and mtROS were evident in the BEAS-2B cells exposed to the mono-NPs and their equimolar mixture. At the same time, the 2NP-treated A549 cells did not exhibit much changes, thereby emphasizing exposure of OA and their markers result in the different cellular/ biochemical behaviour in different cell types. The apoptotic/necrotic population of cells increased significantly between 24 h to 48 h for most exposure types with 200 $\mu\text{g mL}^{-1}$ concentration.

The BBA markers exhibited a time- and concentration-dependent toxicological response in both the BEAS-2B and A549 cells. While the three NACs markers studied (NS, NG, NC) revealed different fold changes in TMRM, general ROS, and mtROS expression, the overall change was higher when compared with LG, a POA marker for BB emissions. The NC was most toxic as it exhibited apoptosis induction even after 6 h of exposure to 200 $\mu\text{g mL}^{-1}$ of the pollutant. A significant increase in mtROS with all four BBA markers and their mixture was reported in both A549 and BEAS-2B cells. Monitoring the environmental concentrations of LG and NC in wildfire- or BBA-impacted regions may help predict the adverse effects of exposure in the lungs. The NACs from BBA emissions were most toxic to the BEAS-2B cells when compared to all other aerosol systems studied in this thesis, as determined through IC_{50} values (summarized in [Table 5.1](#)).

As summarized in Table 5.1, the lowest IC_{50} value was exhibited by the NACs in the BEAS-2B cells, including NC, NS, NG, 4NP, 3NP, and 4BBA. This was followed by the IC_{50} of α -pinene ozonolysis SOA (attributed to the organic peroxides in this aerosol mixture), and the particulate 2-MTSs were found to be safer at the atmospherically-relevant exposure concentrations as their IC_{50} values were found to be in mg mL^{-1} . Although this value gives us an estimate of the relative toxicity of the components/markers and mixtures of OA in different systems at acute exposure of 24 h and 48 h only, there is a need to develop mechanisms for the chronic studies. The exposure to the OA from different systems induced ROS at the concentration much lower than the IC_{50} values, thereby emphasizing the need to study other cellular responses at different hours of exposure to exactly determine the inhalation effects. This may include addition of different *in vitro* models such as primary lung cell lines from healthy individuals or cells from the patients including cystic fibrosis, lung cancer or even smoker’s lungs. It will allow us to address questions

related to environmental health susceptibility in general and immuno-compromised population. The current work focused on the early biological changes following exposure to lung cells, but detailed mechanistic insight can be provided by looking at proteome level or metabolite level expression.

Thereby, future directions of the study include:

- 1- Chronic exposure studies using *in vivo* models to determine the life-time inhalation effects of the examined aerosol systems.
- 2- An alternate study approach could be the inclusion of 3-D organoids, which mimic the organ behaviour more closely than the 2-D cell culture systems included in this study.
- 3- The focus of the current study was on toxicological screening of individual markers or laboratory-generated SOA mixtures; future research directions may include toxicological profiling with ambient aerosol samples from the regions heavily impacted by these aerosol systems.
- 4- The Earth's atmosphere combines the origin of PM_{2.5}-bound pollutants from different sources; thus, studying individual SOA components and their mixtures may build up the strategy for predicting the toxicological profiles relevant for atmospheric conditions.
- 5- Inclusion of other endpoints such as metabolic or proteome-wide changes following SOA exposure can help us determine functional or proteome level changes inside the cells.
- 6- Finally, the future perspective may include the exposure impact of the aerosol in different organ systems- this includes cardiovascular and neuronal systems to predict the acute and chronic effect on cardiological and vascular functioning and the brain and its functionalities.

Table 5.1. Summary of IC₅₀ values in the BEAS-2B cells from four studied systems.

The Aerosol Type Studied	IC ₅₀ at 24 h	IC ₅₀ at 48 h
α-pinene SOA		
α -pinene ozonolysis SOA	912 $\mu\text{g mL}^{-1}$	230 $\mu\text{g mL}^{-1}$
Heterogeneously $\cdot\text{OH}$ oxidized 2MTSs		
0 days	230 mg mL^{-1}	151 mg mL^{-1}
5 days	49 mg mL^{-1}	44 mg mL^{-1}
12 days	25 mg mL^{-1}	26 mg mL^{-1}
22 days	12 mg mL^{-1}	5 mg mL^{-1}
Mono-NPs		
2NP	397 mg mL^{-1}	31.93 mg mL^{-1}
3NP	123 $\mu\text{g mL}^{-1}$	40 $\mu\text{g mL}^{-1}$
4NP	93 $\mu\text{g mL}^{-1}$	43 $\mu\text{g mL}^{-1}$
NP-mixture	107 $\mu\text{g mL}^{-1}$	78 $\mu\text{g mL}^{-1}$
BBA		
LG	2.6 mg mL^{-1}	3 x 10 ⁴ mg mL^{-1}
NS	695 $\mu\text{g mL}^{-1}$	0.16 $\mu\text{g mL}^{-1}$
NG	159 $\mu\text{g mL}^{-1}$	154 $\mu\text{g mL}^{-1}$
NC	30 $\mu\text{g mL}^{-1}$	8.8 $\mu\text{g mL}^{-1}$
4BBA	63 $\mu\text{g mL}^{-1}$	34 $\mu\text{g mL}^{-1}$

CHAPTER 5: References

1. Manahan, S., *Environmental chemistry*. CRC Press: 2017.
2. Heal, M. R.; Kumar, P.; Harrison, R. M., Particles, air quality, policy and health. *Chem Soc Rev* **2012**, *41* (19), 6606-30.
3. Morakinyo, O. M.; Mokgobu, M. I.; Mukhola, M. S.; Hunter, R. P., Health Outcomes of Exposure to Biological and Chemical Components of Inhalable and Respirable Particulate Matter. *International journal of environmental research and public health* **2016**, *13* (6), 592.
4. EPA, Health and Environmental Effects of Particulate Matter (PM). Agency, U. S. E. P., Ed. EPA: US, 2018.
5. Jacobson, M. C.; Hansson, H. C.; Noone, K. J.; Charlson, R. J., Organic atmospheric aerosols: Review and state of the science. *Reviews of Geophysics* **2000**, *38* (2), 267-294.
6. Hallquist, M.; Wenger, J. C.; Baltensperger, U.; Rudich, Y.; Simpson, D.; Claeys, M.; Dommen, J.; Donahue, N.; George, C.; Goldstein, A., The formation, properties and impact of secondary organic aerosol: current and emerging issues. *Atmospheric chemistry and physics* **2009**, *9* (14), 5155-5236.
7. Brunekreef, B.; Holgate, S. T., Air pollution and health. *The lancet* **2002**, *360* (9341), 1233-1242.
8. Burnett, R.; Chen, H.; Szyszkowicz, M.; Fann, N.; Hubbell, B.; Pope, C. A.; Apte, J. S.; Brauer, M.; Cohen, A.; Weichenthal, S.; Coggins, J.; Di, Q.; Brunekreef, B.; Frostad, J.; Lim, S. S.; Kan, H.; Walker, K. D.; Thurston, G. D.; Hayes, R. B.; Lim, C. C.; Turner, M. C.; Jerrett, M.; Krewski, D.; Gapstur, S. M.; Diver, W. R.; Ostro, B.; Goldberg, D.; Crouse, D. L.; Martin, R. V.; Peters, P.; Pinault, L.; Tjepkema, M.; van Donkelaar, A.; Villeneuve, P. J.; Miller, A. B.; Yin, P.; Zhou, M.; Wang, L.; Janssen, N. A. H.; Marra, M.; Atkinson, R. W.; Tsang, H.; Quoc Thach, T.; Cannon, J. B.; Allen, R. T.; Hart, J. E.; Laden, F.; Cesaroni, G.; Forastiere, F.; Weinmayr, G.; Jaensch, A.; Nagel, G.; Concin, H.; Spadaro, J. V., Global estimates of mortality associated with long-term exposure to outdoor fine particulate matter. *Proceedings of the National Academy of Sciences* **2018**, *115* (38), 9592-9597.
9. EEA, Air quality in Europe — 2020 report. Agency, E. E., Ed. 2020.
10. WHO, E. F., Ambient (outdoor) air pollution. 2nd May 2018 ed.; 2018.
11. Xing, Y.-F.; Xu, Y.-H.; Shi, M.-H.; Lian, Y.-X., The impact of PM_{2.5} on the human respiratory system. *J Thorac Dis* **2016**, *8* (1), E69-E74.
12. Landrigan, P. J.; Fuller, R.; Acosta, N. J. R.; Adeyi, O.; Arnold, R.; Basu, N.; Baldé, A. B.; Bertollini, R.; Bose-O'Reilly, S.; Boufford, J. I.; Breysse, P. N.; Chiles, T.; Mahidol, C.; Coll-Seck, A. M.; Cropper, M. L.; Fobil, J.; Fuster, V.; Greenstone, M.; Haines, A.; Hanrahan, D.; Hunter, D.; Khare, M.; Krupnick, A.; Lanphear, B.; Lohani,

B.; Martin, K.; Mathiasen, K. V.; McTeer, M. A.; Murray, C. J. L.; Ndahimananjara, J. D.; Perera, F.; Potočnik, J.; Preker, A. S.; Ramesh, J.; Rockström, J.; Salinas, C.; Samson, L. D.; Sandilya, K.; Sly, P. D.; Smith, K. R.; Steiner, A.; Stewart, R. B.; Suk, W. A.; van Schayck, O. C. P.; Yadama, G. N.; Yumkella, K.; Zhong, M., The Lancet Commission on pollution and health. *The Lancet* **2018**, *391* (10119), 462-512.

13. Möller, W.; Felten, K.; Sommerer, K.; Scheuch, G.; Meyer, G.; Meyer, P.; Häussinger, K.; Kreyling, W. G., Deposition, Retention, and Translocation of Ultrafine Particles from the Central Airways and Lung Periphery. *American Journal of Respiratory and Critical Care Medicine* **2008**, *177* (4), 426-432.

14. Wang, J. L.; Zhang, Y. H.; Shao, M.; Liu, X. L.; Zeng, L. M.; Cheng, C. L.; Xu, X. F., Quantitative relationship between visibility and mass concentration of PM_{2.5} in Beijing. *J Environ Sci (China)* **2006**, *18* (3), 475-81.

15. Requia, W. J.; Jhun, I.; Coull, B. A.; Koutrakis, P., Climate impact on ambient PM_{2.5} elemental concentration in the United States: A trend analysis over the last 30 years. *Environment International* **2019**, *131*, 104888.

16. Council., P. M. N. R., Global Sources of Local Pollution: An Assessment of Long-Range Transport of Key Air Pollutants to and from the United States. The National Academies Press: Washington, DC, 2010. .

17. Corsini, E.; Budello, S.; Marabini, L.; Galbiati, V.; Piazzalunga, A.; Barbieri, P.; Cozzutto, S.; Marinovich, M.; Pitea, D.; Galli, C. L., Comparison of wood smoke PM_{2.5} obtained from the combustion of FIR and beech pellets on inflammation and DNA damage in A549 and THP-1 human cell lines. *Archives of Toxicology* **2013**, *87* (12), 2187-2199.

18. Tomaz, S.; Cui, T.; Chen, Y.; Sexton, K. G.; Roberts, J. M.; Warneke, C.; Yokelson, R. J.; Surratt, J. D.; Turpin, B. J., Photochemical cloud processing of primary wildfire emissions as a potential source of secondary organic aerosol. *Environmental science & technology* **2018**, *52* (19), 11027-11037.

19. Jathar, S. H.; Sharma, N.; Bilzback, K. R.; Pierce, J. R.; Vanhanen, J.; Gordon, T. D.; Volckens, J., Emissions and radiative impacts of sub-10 nm particles from biofuel and fossil fuel cookstoves. *Aerosol Science and Technology* **2020**, *54* (10), 1231-1243.

20. Known and Unexplored Organic Constituents in the Earth's Atmosphere. *Environmental Science & Technology* **2007**, *41* (5), 1514-1521.

21. Turpin, B. J.; Huntzicker, J. J., Identification of secondary organic aerosol episodes and quantitation of primary and secondary organic aerosol concentrations during SCAQS. *Atmospheric Environment* **1995**, *29* (23), 3527-3544.

22. Kroll, J. H.; Seinfeld, J. H., Chemistry of secondary organic aerosol: Formation and evolution of low-volatility organics in the atmosphere. *Atmospheric Environment* **2008**, *42* (16), 3593-3624.

23. Nozière, B.; Kalberer, M.; Claeys, M.; Allan, J.; D'Anna, B.; Decesari, S.; Finessi, E.; Glasius, M.; Grgić, I.; Hamilton, J. F.; Hoffmann, T.; Iinuma, Y.; Jaoui, M.; Kahnt, A.; Kampf, C. J.; Kourchev, I.; Maenhaut, W.; Marsden, N.; Saarikoski, S.; Schnelle-

Kreis, J.; Surratt, J. D.; Szidat, S.; Szmigielski, R.; Wisthaler, A., The Molecular Identification of Organic Compounds in the Atmosphere: State of the Art and Challenges. *Chemical Reviews* **2015**, *115* (10), 3919-3983.

24. Adams, P. J.; Seinfeld, J. H., Predicting global aerosol size distributions in general circulation models. *Journal of Geophysical Research: Atmospheres* **2002**, *107* (D19), AAC 4-1-AAC 4-23.

25. Kanakidou, M.; Seinfeld, J. H.; Pandis, S. N.; Barnes, I.; Dentener, F. J.; Facchini, M. C.; Van Dingenen, R.; Ervens, B.; Nenes, A.; Nielsen, C. J.; Swietlicki, E.; Putaud, J. P.; Balkanski, Y.; Fuzzi, S.; Horth, J.; Moortgat, G. K.; Winterhalter, R.; Myhre, C. E. L.; Tsigaridis, K.; Vignati, E.; Stephanou, E. G.; Wilson, J., Organic aerosol and global climate modelling: a review. *Atmos. Chem. Phys.* **2005**, *5* (4), 1053-1123.

26. Gantt, B.; Meskhidze, N., The physical and chemical characteristics of marine primary organic aerosol: a review. *Atmospheric Chemistry and Physics* **2013**, *13* (8), 3979-3996.

27. Sindelarova, K.; Granier, C.; Bouarar, I.; Guenther, A.; Tilmes, S.; Stavrou, T.; Muller, J. F.; Kuhn, U.; Stefani, P.; Knorr, W., Global data set of biogenic VOC emissions calculated by the MEGAN model over the last 30 years. *Atmos. Chem. Phys.* **2014**, *14* (17), 9317-9341.

28. Heald, C. L.; Henze, D. K.; Horowitz, L. W.; Feddema, J.; Lamarque, J. F.; Guenther, A.; Hess, P. G.; Vitt, F.; Seinfeld, J. H.; Goldstein, A. H.; Fung, I., Predicted change in global secondary organic aerosol concentrations in response to future climate, emissions, and land use change. *Journal of Geophysical Research: Atmospheres* **2008**, *113* (D5).

29. Guenther, A. B.; Jiang, X.; Heald, C. L.; Sakulyanontvittaya, T.; Duhl, T.; Emmons, L. K.; Wang, X., The Model of Emissions of Gases and Aerosols from Nature version 2.1 (MEGAN2.1): an extended and updated framework for modeling biogenic emissions. *Geosci. Model Dev.* **2012**, *5* (6), 1471-1492.

30. Griffin, R. J.; Cocker III, D. R.; Seinfeld, J. H.; Dabdub, D., Estimate of global atmospheric organic aerosol from oxidation of biogenic hydrocarbons. *Geophysical Research Letters* **1999**, *26* (17), 2721-2724.

31. Hunter, J. F.; Day, D. A.; Palm, B. B.; Yatavelli, R. L. N.; Chan, A. W. H.; Kaser, L.; Cappellin, L.; Hayes, P. L.; Cross, E. S.; Carrasquillo, A. J., Comprehensive characterization of atmospheric organic carbon at a forested site. *Nature Geoscience* **2017**, *10* (10), 748-753.

32. Weber, R. J.; Sullivan, A. P.; Peltier, R. E.; Russell, A.; Yan, B.; Zheng, M.; De Gouw, J.; Warneke, C.; Brock, C.; Holloway, J. S., A study of secondary organic aerosol formation in the anthropogenic influenced southeastern United States. *Journal of Geophysical Research: Atmospheres* **2007**, *112* (D13).

33. Anderson, H. R., Air pollution and mortality: A history. *Atmospheric Environment* **2009**, *43* (1), 142-152.

34. Wilkins, E. T., Air pollution and the London fog of December, 1952. *Journal of the Royal Sanitary Institute* **1954**, 74 (1), 1-21.
35. Bell, M. L.; Davis, D. L., Reassessment of the lethal London fog of 1952: novel indicators of acute and chronic consequences of acute exposure to air pollution. *Environmental health perspectives* **2001**, 109 (suppl 3), 389-394.
36. Jacobs, E. T.; Burgess, J. L.; Abbott, M. B., The Donora smog revisited: 70 years after the event that inspired the clean air act. *American journal of public health* **2018**, 108 (S2), S85-S88.
37. Dockery, D. W.; Pope, C. A.; Xu, X.; Spengler, J. D.; Ware, J. H.; Fay, M. E.; Ferris Jr, B. G.; Speizer, F. E., An association between air pollution and mortality in six US cities. *New England journal of medicine* **1993**, 329 (24), 1753-1759.
38. Samet, J. M.; Dominici, F.; Curriero, F. C.; Coursac, I.; Zeger, S. L., Fine particulate air pollution and mortality in 20 US cities, 1987–1994. *New England journal of medicine* **2000**, 343 (24), 1742-1749.
39. Schraufnagel, D. E.; Balmes, J. R.; Cowl, C. T.; De Matteis, S.; Jung, S.-H.; Mortimer, K.; Perez-Padilla, R.; Rice, M. B.; Riojas-Rodriguez, H.; Sood, A.; Thurston, G. D.; To, T.; Vanker, A.; Wuebbles, D. J., Air Pollution and Noncommunicable Diseases: A Review by the Forum of International Respiratory Societies 2019; Environmental Committee, Part 1: The Damaging Effects of Air Pollution. *CHEST* **2019**, 155 (2), 409-416.
40. Lim, S. S.; Vos, T.; Flaxman, A. D.; Danaei, G.; Shibuya, K.; Adair-Rohani, H.; AlMazroa, M. A.; Amann, M.; Anderson, H. R.; Andrews, K. G., A comparative risk assessment of burden of disease and injury attributable to 67 risk factors and risk factor clusters in 21 regions, 1990–2010: a systematic analysis for the Global Burden of Disease Study 2010. *The lancet* **2012**, 380 (9859), 2224-2260.
41. Makri, A.; Stilianakis, N. I., Vulnerability to air pollution health effects. *International journal of hygiene and environmental health* **2008**, 211 (3-4), 326-336.
42. Katsouyanni, K.; Touloumi, G.; Samoli, E.; Gryparis, A.; Le Tertre, A.; Monopoli, Y.; Rossi, G.; Zmirou, D.; Ballester, F.; Boumghar, A.; Anderson, H. R.; Wojtyniak, B.; Paldy, A.; Braunstein, R.; Pekkanen, J.; Schindler, C.; Schwartz, J., Confounding and effect modification in the short-term effects of ambient particles on total mortality: results from 29 European cities within the APHEA2 project. *Epidemiology* **2001**, 12 (5), 521-31.
43. Katsouyanni, K.; Schwartz, J.; Spix, C.; Touloumi, G.; Zmirou, D.; Zanobetti, A.; Wojtyniak, B.; Vonk, J. M.; Tobias, A.; Ponka, A.; Medina, S.; Bacharova, L.; Anderson, H. R., Short term effects of air pollution on health: a European approach using epidemiologic time series data: the APHEA protocol. *J Epidemiol Community Health* **1996**, 50 Suppl 1 (Suppl 1), S12-S18.
44. Samet, J. M.; Zeger, S. L.; Dominici, F.; Curriero, F.; Coursac, I.; Dockery, D. W.; Schwartz, J.; Zanobetti, A., The national morbidity, mortality, and air pollution study. *Part II: morbidity and mortality from air pollution in the United States Res Rep Health Eff Inst* **2000**, 94 (pt 2), 5-79.

45. Samet, J. M.; Dominici, F.; Zeger, S. L.; Schwartz, J.; Dockery, D. W., The National Morbidity, Mortality, and Air Pollution Study. Part I: Methods and methodologic issues. *Research report (Health Effects Institute)* **2000**, (94 Pt 1), 5-14.
46. Pinkerton, K. E.; Green, F. H.; Saiki, C.; Vallyathan, V.; Plopper, C. G.; Gopal, V.; Hung, D.; Bahne, E. B.; Lin, S. S.; Menache, M. G., Distribution of particulate matter and tissue remodeling in the human lung. *Environmental Health Perspectives* **2000**, *108* (11), 1063-1069.
47. Yang, L.; Li, C.; Tang, X., The Impact of PM_{2.5} on the Host Defense of Respiratory System. *Frontiers in Cell and Developmental Biology* **2020**, *8*, 91.
48. Xu, D.; Chen, Y.; Wu, L.; He, S.; Xu, P.; Zhang, Y.; Luo, J.; Ye, X.; Chen, Z.; Wang, X.; Lou, X., Acute effects of ambient PM_{2.5} on lung function among schoolchildren. *Scientific Reports* **2020**, *10* (1), 4061.
49. Li, R.; Zhou, R.; Zhang, J., Function of PM_{2.5} in the pathogenesis of lung cancer and chronic airway inflammatory diseases. *Oncol Lett* **2018**, *15* (5), 7506-7514.
50. Meier, R.; Cascio, W. E.; Ghio, A. J.; Wild, P.; Danuser, B.; Riediker, M., Associations of short-term particle and noise exposures with markers of cardiovascular and respiratory health among highway maintenance workers. *Environ Health Perspect* **2014**, *122* (7), 726-32.
51. Huang, W.; Wang, G.; Lu, S. E.; Kipen, H.; Wang, Y.; Hu, M.; Lin, W.; Rich, D.; Ohman-Strickland, P.; Diehl, S. R.; Zhu, P.; Tong, J.; Gong, J.; Zhu, T.; Zhang, J., Inflammatory and oxidative stress responses of healthy young adults to changes in air quality during the Beijing Olympics. *Am J Respir Crit Care Med* **2012**, *186* (11), 1150-9.
52. van EEDEN, S. F.; Tan, W. C.; Suwa, T.; Mukae, H.; Terashima, T.; Fujii, T.; Qui, D.; Vincent, R.; Hogg, J. C., Cytokines involved in the systemic inflammatory response induced by exposure to particulate matter air pollutants (PM₁₀). *American journal of respiratory and critical care medicine* **2001**, *164* (5), 826-830.
53. Wang, J.; Tang, B.; Liu, X.; Wu, X.; Wang, H.; Xu, D.; Guo, Y., Increased monomeric CRP levels in acute myocardial infarction: a possible new and specific biomarker for diagnosis and severity assessment of disease. *Atherosclerosis* **2015**, *239* (2), 343-9.
54. Du, Y.; Xu, X.; Chu, M.; Guo, Y.; Wang, J., Air particulate matter and cardiovascular disease: the epidemiological, biomedical and clinical evidence. *J Thorac Dis* **2016**, *8* (1), E8-E19.
55. Martinelli, N.; Olivieri, O.; Girelli, D., Air particulate matter and cardiovascular disease: a narrative review. *Eur J Intern Med* **2013**, *24* (4), 295-302.
56. Chan, S. H.; Van Hee, V. C.; Bergen, S.; Szpiro, A. A.; DeRoo, L. A.; London, S. J.; Marshall, J. D.; Kaufman, J. D.; Sandler, D. P., Long-Term Air Pollution Exposure and Blood Pressure in the Sister Study. *Environ Health Perspect* **2015**, *123* (10), 951-8.

57. Strosnider, H. M.; Chang, H. H.; Darrow, L. A.; Liu, Y.; Vaidyanathan, A.; Strickland, M. J., Age-specific associations of ozone and fine particulate matter with respiratory emergency department visits in the United States. *American journal of respiratory and critical care medicine* **2019**, *199* (7), 882-890.
58. Yadav, A. K.; Kumar, K.; Kasim, M. H. A.; Singh, M. P.; Parida, S. K.; Sharan, M., Visibility and incidence of respiratory diseases during the 1998 haze episode in Brunei Darussalam. In *Air Quality*, Springer: 2003; pp 265-277.
59. Donaldson, K.; Beswick, P. H.; Gilmour, P. S., Free radical activity associated with the surface of particles: a unifying factor in determining biological activity? *Toxicology letters* **1996**, *88* (1-3), 293-298.
60. Mehta, M.; Chen, L.-C.; Gordon, T.; Rom, W.; Tang, M.-s., Particulate matter inhibits DNA repair and enhances mutagenesis. *Mutation Research/Genetic Toxicology and Environmental Mutagenesis* **2008**, *657* (2), 116-121.
61. Brown, D. M.; Donaldson, K.; Borm, P. J.; Schins, R. P.; Dehnhardt, M.; Gilmour, P.; Jimenez, L. A.; Stone, V., Calcium and ROS-mediated activation of transcription factors and TNF- α cytokine gene expression in macrophages exposed to ultrafine particles. *American Journal of Physiology-Lung Cellular and Molecular Physiology* **2004**, *286* (2), L344-L353.
62. Sigaud, S.; Goldsmith, C.-A. W.; Zhou, H.; Yang, Z.; Fedulov, A.; Imrich, A.; Kobzik, L., Air pollution particles diminish bacterial clearance in the primed lungs of mice. *Toxicology and applied pharmacology* **2007**, *223* (1), 1-9.
63. Kelly, F. J.; Fussell, J. C., Size, source and chemical composition as determinants of toxicity attributable to ambient particulate matter. *Atmospheric environment* **2012**, *60*, 504-526.
64. Dix, D. J.; Houck, K. A.; Martin, M. T.; Richard, A. M.; Setzer, R. W.; Kavlock, R. J., The ToxCast program for prioritizing toxicity testing of environmental chemicals. *Toxicol. Sci.* **2006**, *95* (1), 5-12.
65. Connors, K. A.; Beasley, A.; Barron, M. G.; Belanger, S. E.; Bonnell, M.; Brill, J. L.; de Zwart, D.; Kienzler, A.; Krailler, J.; Otter, R.; Phillips, J. L.; Embry, M. R., Creation of a curated aquatic toxicology database: EnviroTox. *Environ. Toxicol. Chem.* **2019**, *38* (5), 1062-1073.
66. Cihák, R., REACH - an overview. *Interdiscip. Toxicol.* **2009**, *2* (2), 42-44.
67. Doke, S. K.; Dhawale, S. C., Alternatives to animal testing: A review. *Saudi Pharm J* **2015**, *23* (3), 223-229.
68. Zavala, J.; Freedman, A. N.; Szilagyi, J. T.; Jaspers, I.; Wambaugh, J. F.; Higuchi, M.; Rager, J. E., New Approach Methods to Evaluate Health Risks of Air Pollutants: Critical Design Considerations for In Vitro Exposure Testing. *International journal of environmental research and public health* **2020**, *17* (6), 2124.

69. Ito, T.; Bekki, K.; Fujitani, Y.; Hirano, S., The toxicological analysis of secondary organic aerosol in human lung epithelial cells and macrophages. *Environmental Science and Pollution Research* **2019**, *26* (22), 22747-22755.
70. Lin, Y. H.; Arashiro, M.; Clapp, P. W.; Cui, T.; Sexton, K. G.; Vizuete, W.; Gold, A.; Jaspers, I.; Fry, R. C.; Surratt, J. D., Gene Expression Profiling in Human Lung Cells Exposed to Isoprene-Derived Secondary Organic Aerosol. *Environ Sci Technol* **2017**, *51* (14), 8166-8175.
71. Raudoniute, J.; Stasiulaitiene, I.; Kulvinskiene, I.; Bagdonas, E.; Garbaras, A.; Krugly, E.; Martuzevicius, D.; Bironaite, D.; Aldonyte, R., Pro-inflammatory effects of extracted urban fine particulate matter on human bronchial epithelial cells BEAS-2B. *Environmental Science and Pollution Research* **2018**, *25* (32), 32277-32291.
72. Raudoniute, J.; Stasiulaitiene, I.; Kulvinskiene, I.; Bagdonas, E.; Garbaras, A.; Krugly, E.; Martuzevicius, D.; Bironaite, D.; Aldonyte, R., Pro-inflammatory effects of extracted urban fine particulate matter on human bronchial epithelial cells BEAS-2B. *Environ. Sci. Pollut. Res.* **2018**, *25* (32), 32277-32291.
73. Khan, F.; Kwapiszewska, K.; Zhang, Y.; Chen, Y.; Lambe, A. T.; Kołodziejczyk, A.; Jalal, N.; Rudzinski, K.; Martínez-Romero, A.; Fry, R. C.; Surratt, J. D.; Szmigielski, R., Toxicological Responses of α -Pinene-Derived Secondary Organic Aerosol and Its Molecular Tracers in Human Lung Cell Lines. *Chemical Research in Toxicology* **2021**, *34* (3), 817-832.
74. Zhang, S.; Li, X.; Xie, F.; Liu, K.; Liu, H.; Xie, J., Evaluation of whole cigarette smoke induced oxidative stress in A549 and BEAS-2B cells. *Environmental Toxicology and Pharmacology* **2017**, *54*, 40-47.
75. Arashiro, M.; Lin, Y. H.; Sexton, K. G.; Zhang, Z.; Jaspers, I.; Fry, R. C.; Vizuete, W. G.; Gold, A.; Surratt, J. D., In vitro exposure to isoprene-derived secondary organic aerosol by direct deposition and its effects on COX-2 and IL-8 gene expression. *Atmos. Chem. Phys.* **2016**, *16* (22), 14079-14090.
76. McDonald, J. D.; Doyle-Eisele, M.; Campen, M. J.; Seagrave, J.; Holmes, T.; Lund, A.; Surratt, J. D.; Seinfeld, J. H.; Rohr, A. C.; Knipping, E. M., Cardiopulmonary response to inhalation of biogenic secondary organic aerosol. *Inhalation toxicology* **2010**, *22* (3), 253-265.
77. Lima de Albuquerque, Y.; Berger, E.; Li, C.; Pardo, M.; George, C.; Rudich, Y.; Głogowski, A., The Toxic Effect of Water-Soluble Particulate Pollutants from Biomass Burning on Alveolar Lung Cells. *Atmosphere* **2021**, *12* (8), 1023.
78. Mazuryk, O.; Stochel, G.; Brindell, M., Variations in Reactive Oxygen Species Generation by Urban Airborne Particulate Matter in Lung Epithelial Cells | Impact of Inorganic Fraction. *Frontiers in Chemistry* **2020**, *8*, 1132.
79. Judson, R.; Houck, K.; Martin, M.; Richard, A. M.; Knudsen, T. B.; Shah, I.; Little, S.; Wambaugh, J.; Woodrow Setzer, R.; Kothiyia, P.; Phuong, J.; Filer, D.; Smith, D.; Reif, D.; Rotroff, D.; Kleinstreuer, N.; Sipes, N.; Xia, M.; Huang, R.; Crofton, K.; Thomas, R. S., Editor's Highlight: Analysis of the Effects of Cell Stress and Cytotoxicity

on In Vitro Assay Activity Across a Diverse Chemical and Assay Space. *Toxicological sciences : an official journal of the Society of Toxicology* **2016**, *152* (2), 323-339.

80. Qu, J.; Li, Y.; Zhong, W.; Gao, P.; Hu, C., Recent developments in the role of reactive oxygen species in allergic asthma. *J Thorac Dis* **2017**, *9* (1), E32-E43.

81. Jiang, N.; Wen, H.; Zhou, M.; Lei, T.; Shen, J.; Zhang, D.; Wang, R.; Wu, H.; Jiang, S.; Li, W., Low-dose combined exposure of carboxylated black carbon and heavy metal lead induced potentiation of oxidative stress, DNA damage, inflammation, and apoptosis in BEAS-2B cells. *Ecotoxicology and Environmental Safety* **2020**, *206*, 111388.

82. Øya, E.; Øvrevik, J.; Arlt, V. M.; Nagy, E.; Phillips, D. H.; Holme, J. A., DNA damage and DNA damage response in human bronchial epithelial BEAS-2B cells following exposure to 2-nitrobenzanthrone and 3-nitrobenzanthrone: role in apoptosis. *Mutagenesis* **2011**, *26* (6), 697-708.

83. Janssen Nicole, A. H.; Hoek, G.; Simic-Lawson, M.; Fischer, P.; van Bree, L.; ten Brink, H.; Keuken, M.; Atkinson Richard, W.; Anderson, H. R.; Brunekreef, B.; Cassee Flemming, R., Black Carbon as an Additional Indicator of the Adverse Health Effects of Airborne Particles Compared with PM10 and PM2.5. *Environmental Health Perspectives* **2011**, *119* (12), 1691-1699.

84. Pan, L.; Wu, S.; Li, H.; Xu, J.; Dong, W.; Shan, J.; Yang, X.; Chen, Y.; Shima, M.; Deng, F.; Guo, X., The short-term effects of indoor size-fractioned particulate matter and black carbon on cardiac autonomic function in COPD patients. *Environment International* **2018**, *112*, 261-268.

85. Cloonan, S. M.; Choi, A. M., Mitochondria in lung disease. *J Clin Invest* **2016**, *126* (3), 809-20.

86. Liu, X.; Zhao, X.; Li, X.; Lv, S.; Ma, R.; Qi, Y.; Abulikemu, A.; Duan, H.; Guo, C.; Li, Y.; Sun, Z., PM2.5 triggered apoptosis in lung epithelial cells through the mitochondrial apoptotic way mediated by a ROS-DRP1-mitochondrial fission axis. *Journal of Hazardous Materials* **2020**, *397*, 122608.

87. Piantadosi, C. A.; Suliman, H. B., Mitochondrial Dysfunction in Lung Pathogenesis. *Annu Rev Physiol* **2017**, *79*, 495-515.

88. Liu, X.; Chen, Z., The pathophysiological role of mitochondrial oxidative stress in lung diseases. *J Transl Med* **2017**, *15* (1), 207.

89. Glasius, M.; Goldstein, A. H., Recent discoveries and future challenges in atmospheric organic chemistry. ACS Publications: 2016.

90. Guenther, A.; Karl, T.; Harley, P.; Wiedinmyer, C.; Palmer, P.; Geron, C., Estimates of global terrestrial isoprene emissions using MEGAN (Model of Emissions of Gases and Aerosols from Nature). **2006**.

91. Geron, C.; Rasmussen, R.; R. Arnts, R.; Guenther, A., A review and synthesis of monoterpene speciation from forests in the United States. *Atmospheric Environment* **2000**, *34* (11), 1761-1781.

92. Ehn, M.; Thornton, J. A.; Kleist, E.; Sipilä, M.; Junninen, H.; Pullinen, I.; Springer, M.; Rubach, F.; Tillmann, R.; Lee, B.; Lopez-Hilfiker, F.; Andres, S.; Acir, I.-H.; Rissanen, M.; Jokinen, T.; Schobesberger, S.; Kangasluoma, J.; Kontkanen, J.; Nieminen, T.; Kurtén, T.; Nielsen, L. B.; Jørgensen, S.; Kjaergaard, H. G.; Canagaratna, M.; Maso, M. D.; Berndt, T.; Petäjä, T.; Wahner, A.; Kerminen, V.-M.; Kulmala, M.; Worsnop, D. R.; Wildt, J.; Mentel, T. F., A large source of low-volatility secondary organic aerosol. *Nature* **2014**, *506* (7489), 476-479.
93. Rohr, A. C., The health significance of gas- and particle-phase terpene oxidation products: A review. *Environment International* **2013**, *60*, 145-162.
94. Chowdhury, P. H.; He, Q.; Carmieli, R.; Li, C.; Rudich, Y.; Pardo, M., Connecting the Oxidative Potential of Secondary Organic Aerosols with Reactive Oxygen Species in Exposed Lung Cells. *Environmental Science & Technology* **2019**, *53* (23), 13949-13958.
95. Chowdhury, P. H.; He, Q.; Lasitza Male, T.; Brune, W. H.; Rudich, Y.; Pardo, M., Exposure of Lung Epithelial Cells to Photochemically Aged Secondary Organic Aerosol Shows Increased Toxic Effects. *Environmental Science & Technology Letters* **2018**, *5* (7), 424-430.
96. Gaschen, A.; Lang, D.; Kalberer, M.; Savi, M.; Geiser, T.; Gazdhar, A.; Lehr, C.-M.; Bur, M.; Dommen, J.; Baltensperger, U.; Geiser, M., Cellular Responses after Exposure of Lung Cell Cultures to Secondary Organic Aerosol Particles. *Environmental Science & Technology* **2010**, *44* (4), 1424-1430.
97. Jang, M.; Ghio, A. J.; Cao, G., Exposure of BEAS-2B Cells to Secondary Organic Aerosol Coated on Magnetic Nanoparticles. *Chemical Research in Toxicology* **2006**, *19* (8), 1044-1050.
98. Lund, A. K.; Doyle-Eisele, M.; Lin, Y.-H.; Arashiro, M.; Surratt, J. D.; Holmes, T.; Schilling, K. A.; Seinfeld, J. H.; Rohr, A. C.; Knipping, E. M., The effects of α -pinene versus toluene-derived secondary organic aerosol exposure on the expression of markers associated with vascular disease. *Inhalation toxicology* **2013**, *25* (6), 309-324.
99. Tuet, W. Y.; Chen, Y.; Fok, S.; Champion, J. A.; Ng, N. L., Inflammatory responses to secondary organic aerosols (SOA) generated from biogenic and anthropogenic precursors. *Atmospheric Chemistry and Physics* **2017**, *17* (18), 11423.
100. Hoffmann, T.; Bandur, R.; Marggraf, U.; Linscheid, M., Molecular composition of organic aerosols formed in the α -pinene/O₃ reaction: Implications for new particle formation processes. *Journal of Geophysical Research: Atmospheres* **1998**, *103* (D19), 25569-25578.
101. Glasius, M.; Lahaniati, M.; Calogirou, A.; Di Bella, D.; Jensen, N. R.; Hjorth, J.; Kotzias, D.; Larsen, B. R., Carboxylic Acids in Secondary Aerosols from Oxidation of Cyclic Monoterpenes by Ozone. *Environmental Science & Technology* **2000**, *34* (6), 1001-1010.
102. Rodigast, M.; Mutzel, A.; Schindelka, J.; Herrmann, H., A new source of methylglyoxal in the aqueous phase. *Atmos. Chem. Phys.* **2016**, *16* (4), 2689-2702.

- 103.Szmigielski, R.; Surratt, J. D.; Gómez-González, Y.; Van der Veken, P.; Kourtshev, I.; Vermeulen, R.; Blockhuys, F.; Jaoui, M.; Kleindienst, T. E.; Lewandowski, M.; Offenberg, J. H.; Edney, E. O.; Seinfeld, J. H.; Maenhaut, W.; Claeys, M., 3-methyl-1,2,3-butanetricarboxylic acid: An atmospheric tracer for terpene secondary organic aerosol. *Geophysical Research Letters* **2007**, *34* (24).
- 104.Müller, L.; Reinnig, M.-C.; Naumann, K.; Saathoff, H.; Mentel, T.; Donahue, N.; Hoffmann, T.; Keutsch, F., Formation of 3-methyl-1, 2, 3-butanetricarboxylic acid via gas phase oxidation of pinonic acid--a mass spectrometric study of SOA aging. *Atmospheric Chemistry & Physics* **2012**, *12* (3).
- 105.Docherty, K. S.; Wu, W.; Lim, Y. B.; Ziemann, P. J., Contributions of organic peroxides to secondary aerosol formed from reactions of monoterpenes with O₃. *Environmental science & technology* **2005**, *39* (11), 4049-4059.
- 106.Kristensen, K.; Enggrob, K. L.; King, S. M.; Worton, D.; Platt, S.; Mortensen, R.; Rosenoern, T.; Surratt, J.; Bilde, M.; Goldstein, A., Formation and occurrence of dimer esters of pinene oxidation products in atmospheric aerosols. *Atmos. Chem. Phys* **2013**, *13* (7), 3763-3776.
- 107.Kristensen, K.; Cui, T.; Zhang, H.; Gold, A.; Glasius, M.; Surratt, J., Dimers in α -pinene secondary organic aerosol: effect of hydroxyl radical, ozone, relative humidity and aerosol acidity. *Atmos. Chem. Phys* **2014**, *14* (8), 4201-4218.
- 108.Surratt, J. D.; Kroll, J. H.; Kleindienst, T. E.; Edney, E. O.; Claeys, M.; Sorooshian, A.; Ng, N. L.; Offenberg, J. H.; Lewandowski, M.; Jaoui, M.; Flagan, R. C.; Seinfeld, J. H., Evidence for Organosulfates in Secondary Organic Aerosol. *Environmental Science & Technology* **2007**, *41* (2), 517-527.
- 109.Lopez-Hilfiker, F.; Mohr, C.; D'Ambro, E. L.; Lutz, A.; Riedel, T. P.; Gaston, C. J.; Iyer, S.; Zhang, Z.; Gold, A.; Surratt, J., Molecular composition and volatility of organic aerosol in the Southeastern US: implications for IEPOX derived SOA. *Environmental science & technology* **2016**, *50* (5), 2200-2209.
- 110.Lopez-Hilfiker, F.; Mohr, C.; Ehn, M.; Rubach, F.; Kleist, E.; Wildt, J.; Mentel, T. F.; Carrasquillo, A.; Daumit, K.; Hunter, J., Phase partitioning and volatility of secondary organic aerosol components formed from α -pinene ozonolysis and OH oxidation: the importance of accretion products and other low volatility compounds. **2015**.
- 111.Jeong, S.-C.; Cho, Y.; Song, M.-K.; Lee, E.; Ryu, J.-C., Epidermal growth factor receptor (EGFR)—MAPK—nuclear factor(NF)- κ B—IL8: A possible mechanism of particulate matter(PM) 2.5-induced lung toxicity. *Environmental Toxicology* **2017**, *32* (5), 1628-1636.
- 112.Kramer, A. J.; Rattanavaraha, W.; Zhang, Z.; Gold, A.; Surratt, J. D.; Lin, Y.-H., Assessing the oxidative potential of isoprene-derived epoxides and secondary organic aerosol. *Atmospheric Environment* **2016**, *130*, 211-218.
- 113.Tuet, W. Y.; Chen, Y.; Xu, L.; Fok, S.; Gao, D.; Weber, R. J.; Ng, N. L., Chemical oxidative potential of secondary organic aerosol (SOA) generated from the photooxidation

of biogenic and anthropogenic volatile organic compounds. *Atmospheric Chemistry & Physics* **2017**, *17*, 839.

114. Kim, V.; Oros, M.; Durra, H.; Kelsen, S.; Aksoy, M.; Cornwell, W. D.; Rogers, T. J.; Criner, G. J., Chronic Bronchitis and Current Smoking Are Associated with More Goblet Cells in Moderate to Severe COPD and Smokers without Airflow Obstruction. *PloS one* **2015**, *10* (2), e0116108.

115. Santus, P.; Corsico, A.; Solidoro, P.; Braido, F.; Di Marco, F.; Scichilone, N., Oxidative stress and respiratory system: pharmacological and clinical reappraisal of N-acetylcysteine. *COPD* **2014**, *11* (6), 705-717.

116. St. Clair, J. M.; Rivera-Rios, J. C.; Crouse, J. D.; Knap, H. C.; Bates, K. H.; Teng, A. P.; Jørgensen, S.; Kjaergaard, H. G.; Keutsch, F. N.; Wennberg, P. O., Kinetics and Products of the Reaction of the First-Generation Isoprene Hydroxy Hydroperoxide (ISOPOOH) with OH. *The Journal of Physical Chemistry A* **2016**, *120* (9), 1441-1451.

117. Riva, M.; Budisulistiorini, S. H.; Chen, Y.; Zhang, Z.; D'Ambro, E. L.; Zhang, X.; Gold, A.; Turpin, B. J.; Thornton, J. A.; Canagaratna, M. R.; Surratt, J. D., Chemical Characterization of Secondary Organic Aerosol from Oxidation of Isoprene Hydroxyhydroperoxides. *Environmental Science & Technology* **2016**, *50* (18), 9889-9899.

118. Claeys, M.; Graham, B.; Vas, G.; Wang, W.; Vermeylen, R.; Pashynska, V.; Cafmeyer, J.; Guyon, P.; Andreae, M. O.; Artaxo, P., Formation of secondary organic aerosols through photooxidation of isoprene. *Science* **2004**, *303* (5661), 1173-1176.

119. Surratt, J. D.; Chan, A. W. H.; Eddingsaas, N. C.; Chan, M.; Loza, C. L.; Kwan, A. J.; Hersey, S. P.; Flagan, R. C.; Wennberg, P. O.; Seinfeld, J. H., Reactive intermediates revealed in secondary organic aerosol formation from isoprene. *Proceedings of the National Academy of Sciences* **2010**, *107* (15), 6640-6645.

120. Surratt, J. D.; Murphy, S. M.; Kroll, J. H.; Ng, N. L.; Hildebrandt, L.; Sorooshian, A.; Szmigielski, R.; Vermeylen, R.; Maenhaut, W.; Claeys, M., Chemical composition of secondary organic aerosol formed from the photooxidation of isoprene. *The Journal of physical chemistry A* **2006**, *110* (31), 9665-9690.

121. Budisulistiorini, S. H.; Baumann, K.; Edgerton, E. S.; Bairai, S. T.; Mueller, S.; Shaw, S. L.; Knipping, E. M.; Gold, A.; Surratt, J. D., Seasonal characterization of submicron aerosol chemical composition and organic aerosol sources in the southeastern United States: Atlanta, Georgia, and Look Rock, Tennessee. *Atmospheric Chemistry and Physics* **2016**, *16* (8), 5171-5189.

122. Xu, L.; Guo, H.; Boyd, C. M.; Klein, M.; Bougiatioti, A.; Cerully, K. M.; Hite, J. R.; Isaacman-VanWertz, G.; Kreisberg, N. M.; Knute, C., Effects of anthropogenic emissions on aerosol formation from isoprene and monoterpenes in the southeastern United States. *Proceedings of the National Academy of Sciences* **2015**, *112* (1), 37-42.

123. Glasius, M.; Bering, M. S.; Yee, L. D.; de Sá, S. S.; Isaacman-VanWertz, G.; Wernis, R. A.; Barbosa, H. M. J.; Alexander, M. L.; Palm, B. B.; Hu, W.; Campuzano-Jost, P.; Day, D. A.; Jimenez, J. L.; Shrivastava, M.; Martin, S. T.; Goldstein, A. H.,

Organosulfates in aerosols downwind of an urban region in central Amazon. *Environmental Science: Processes & Impacts* **2018**, 20 (11), 1546-1558.

124. Cui, T.; Zeng, Z.; dos Santos, E. O.; Zhang, Z.; Chen, Y.; Zhang, Y.; Rose, C. A.; Budisulistiorini, S. H.; Collins, L. B.; Bodnar, W. M.; de Souza, R. A. F.; Martin, S. T.; Machado, C. M. D.; Turpin, B. J.; Gold, A.; Ault, A. P.; Surratt, J. D., Development of a hydrophilic interaction liquid chromatography (HILIC) method for the chemical characterization of water-soluble isoprene epoxydiol (IEPOX)-derived secondary organic aerosol. *Environmental Science: Processes & Impacts* **2018**, 20 (11), 1524-1536.

125. Hettiyadura, A. P. S.; Stone, E. A.; Kundu, S.; Baker, Z.; Geddes, E.; Richards, K.; Humphry, T., Determination of atmospheric organosulfates using HILIC chromatography with MS detection. *Atmospheric Measurement Techniques* **2015**, 8 (6), 2347-2358.

126. Hughes, D. D.; Christiansen, M. B.; Milani, A.; Vermeuel, M. P.; Novak, G. A.; Alwe, H. D.; Dickens, A. F.; Pierce, R. B.; Millet, D. B.; Bertram, T. H.; Stanier, C. O.; Stone, E. A., PM_{2.5} chemistry, organosulfates, and secondary organic aerosol during the 2017 Lake Michigan Ozone Study. *Atmospheric Environment* **2021**, 244, 117939.

127. Chen, Y.; Zhang, Y.; Lambe, A. T.; Xu, R.; Lei, Z.; Olson, N. E.; Zhang, Z.; Szalkowski, T.; Cui, T.; Vizuete, W., Heterogeneous hydroxyl radical oxidation of isoprene-epoxydiol-derived methyltetrol sulfates: plausible formation mechanisms of previously unexplained organosulfates in ambient fine aerosols. *Environmental Science & Technology Letters* **2020**, 7 (7), 460-468.

128. Riva, M.; Chen, Y.; Zhang, Y.; Lei, Z.; Olson, N. E.; Boyer, H. C.; Narayan, S.; Yee, L. D.; Green, H. S.; Cui, T.; Zhang, Z.; Baumann, K.; Fort, M.; Edgerton, E.; Budisulistiorini, S. H.; Rose, C. A.; Ribeiro, I. O.; e Oliveira, R. L.; dos Santos, E. O.; Machado, C. M. D.; Szopa, S.; Zhao, Y.; Alves, E. G.; de Sá, S. S.; Hu, W.; Knipping, E. M.; Shaw, S. L.; Duvoisin Junior, S.; de Souza, R. A. F.; Palm, B. B.; Jimenez, J.-L.; Glasius, M.; Goldstein, A. H.; Pye, H. O. T.; Gold, A.; Turpin, B. J.; Vizuete, W.; Martin, S. T.; Thornton, J. A.; Dutcher, C. S.; Ault, A. P.; Surratt, J. D., Increasing Isoprene Epoxydiol-to-Inorganic Sulfate Aerosol Ratio Results in Extensive Conversion of Inorganic Sulfate to Organosulfur Forms: Implications for Aerosol Physicochemical Properties. *Environmental Science & Technology* **2019**, 53 (15), 8682-8694.

129. Tiiva, P.; Faubert, P.; Michelsen, A.; Holopainen, T.; Holopainen, J. K.; Rinnan, R., Climatic warming increases isoprene emission from a subarctic heath. *New Phytol* **2008**, 180 (4), 853-63.

130. Turner, D. P.; Baglio, J. V.; Wones, A. G.; Pross, D.; Vong, R.; McVeety, B. D.; Phillips, D. L., Climate change and isoprene emissions from vegetation. *Chemosphere* **1991**, 23 (1), 37-56.

131. Rohr, A. C.; Shore, S. A.; Spengler, J. D., Repeated exposure to isoprene oxidation products causes enhanced respiratory tract effects in multiple murine strains. *Inhalation toxicology* **2003**, 15 (12), 1191-1207.

132. Wilkins, C. K.; Clausen, P. A.; Wolkoff, P.; Larsen, S. T.; Hammer, M.; Larsen, K.; Hansen, V.; Nielsen, G. D., Formation of strong airway irritants in mixtures of

isoprene/ozone and isoprene/ozone/nitrogen dioxide. *Environmental health perspectives* **2001**, *109* (9), 937-941.

133. Wilkins, C. K.; Wolkoff, P.; Clausen, P. A.; Hammer, M.; Nielsen, G. D., Upper airway irritation of terpene/ozone oxidation products (TOPS). Dependence on reaction time, relative humidity and initial ozone concentration. *Toxicology letters* **2003**, *143* (2), 109-114.

134. Jason D Surratt, Y.-H.-L., Maiko Arashiro, William G Vizuete, Zhenfa Zhang, Avram Gold, Ilona Jaspers, Rebecca C Fry *Understanding the Early Biological Effects of Isoprene-Derived Particulate Matter Enhanced by Anthropogenic Pollutants*; March 2019, 2019.

135. Doyle, M.; Sexton Kenneth, G.; Jeffries, H.; Bridge, K.; Jaspers, I., Effects of 1,3-Butadiene, Isoprene, and Their Photochemical Degradation Products on Human Lung Cells. *Environmental Health Perspectives* **2004**, *112* (15), 1488-1495.

136. Lin, Y.-H.; Arashiro, M.; Martin, E.; Chen, Y.; Zhang, Z.; Sexton, K. G.; Gold, A.; Jaspers, I.; Fry, R. C.; Surratt, J. D., Isoprene-derived secondary organic aerosol induces the expression of oxidative stress response genes in human lung cells. *Environmental Science & Technology Letters* **2016**, *3* (6), 250-254.

137. Arashiro, M.; Lin, Y.-H.; Zhang, Z.; Sexton, K. G.; Gold, A.; Jaspers, I.; Fry, R. C.; Surratt, J. D., Effect of secondary organic aerosol from isoprene-derived hydroxyhydroperoxides on the expression of oxidative stress response genes in human bronchial epithelial cells. *Environmental Science: Processes & Impacts* **2018**, *20* (2), 332-339.

138. Eaves, L. A.; Smeester, L.; Hartwell, H. J.; Lin, Y.-H.; Arashiro, M.; Zhang, Z.; Gold, A.; Surratt, J. D.; Fry, R. C., Isoprene-Derived Secondary Organic Aerosol Induces the Expression of MicroRNAs Associated with Inflammatory/Oxidative Stress Response in Lung Cells. *Chemical research in toxicology* **2019**, *33* (2), 381-387.

139. Inomata, S.; Fushimi, A.; Sato, K.; Fujitani, Y.; Yamada, H., 4-Nitrophenol, 1-nitropyrene, and 9-nitroanthracene emissions in exhaust particles from diesel vehicles with different exhaust gas treatments. *Atmospheric Environment* **2015**, *110*, 93-102.

140. Lu, C.; Wang, X.; Dong, S.; Zhang, J.; Li, J.; Zhao, Y.; Liang, Y.; Xue, L.; Xie, H.; Zhang, Q.; Wang, W., Emissions of fine particulate nitrated phenols from various on-road vehicles in China. *Environmental Research* **2019**, *179*, 108709.

141. Rubio, M. A.; Bustamante, P.; Vásquez P., Y., Atmospheric phenolic derivatives as tracers in an urban area. *Journal of the Chilean Chemical Society* **2019**, *64* (2), 4407-4411.

142. Lin, P.; Bluvshstein, N.; Rudich, Y.; Nizkorodov, S. A.; Laskin, J.; Laskin, A., Molecular Chemistry of Atmospheric Brown Carbon Inferred from a Nationwide Biomass Burning Event. *Environmental Science & Technology* **2017**, *51* (20), 11561-11570.

143. Lin, P.; Aiona, P. K.; Li, Y.; Shiraiwa, M.; Laskin, J.; Nizkorodov, S. A.; Laskin, A., Molecular Characterization of Brown Carbon in Biomass Burning Aerosol Particles. *Environmental Science & Technology* **2016**, *50* (21), 11815-11824.

144. Iinuma, Y.; Böge, O.; Gräfe, R.; Herrmann, H., Methyl-Nitrocatechols: Atmospheric Tracer Compounds for Biomass Burning Secondary Organic Aerosols. *Environmental Science & Technology* **2010**, *44* (22), 8453-8459.
145. Claeys, M.; Vermeylen, R.; Yasmeeen, F.; Gomez-Gonzalez, Y.; Chi, X.; Maenhaut, W.; Meszaros, T.; Salma, I., Chemical characterisation of humic-like substances from urban, rural and tropical biomass burning environments using liquid chromatography with UV/vis photodiode array detection and electrospray ionisation mass spectrometry. *Environmental Chemistry* **2012**, *9* (3), 273-284.
146. Bluvshstein, N.; Lin, P.; Flores, J. M.; Segev, L.; Mazar, Y.; Tas, E.; Snider, G.; Weagle, C.; Brown, S. S.; Laskin, A.; Rudich, Y., Broadband optical properties of biomass-burning aerosol and identification of brown carbon chromophores. *Journal of Geophysical Research: Atmospheres* **2017**, *122* (10), 5441-5456.
147. Xie, M.; Chen, X.; Hays, M. D.; Holder, A. L., Composition and light absorption of N-containing aromatic compounds in organic aerosols from laboratory biomass burning. *Atmos. Chem. Phys.* **2019**, *19* (5), 2899-2915.
148. Laskin, A.; Laskin, J.; Nizkorodov, S. A., Chemistry of Atmospheric Brown Carbon. *Chemical Reviews* **2015**, *115* (10), 4335-4382.
149. Jay, K.; Stieglitz, L., Identification and quantification of volatile organic components in emissions of waste incineration plants. *Chemosphere* **1995**, *30* (7), 1249-1260.
150. EPA, Interim Reregistration Eligibility Decision for Methyl Parathion, Case No. 0153. Office of Prevention, P. a. T. S., Ed. United States Environmental Protection Agency: Washington D.C., 20460, 2006.
151. WHO *Parathion in drinking-water. Background document for development of WHO guidelines for drinking-water quality.*; World Health Organization: Geneva, 2004.
152. Boehncke, A.; Koennecker, G.; Mangelsdorf, I.; Wibbertmann, A. *Mononitrophenols*; World Health Organization: Geneva, 2000; pp 1-43.
153. Harrison, M. A. J.; Barra, S.; Borghesi, D.; Vione, D.; Arsene, C.; Iulian Olariu, R., Nitrated phenols in the atmosphere: a review. *Atmospheric Environment* **2005**, *39* (2), 231-248.
154. Lin, P.; Laskin, J.; Nizkorodov, S. A.; Laskin, A., Revealing Brown Carbon Chromophores Produced in Reactions of Methylglyoxal with Ammonium Sulfate. *Environmental Science & Technology* **2015**, *49* (24), 14257-14266.
155. Xie, M.; Hays, M. D.; Holder, A. L., Light-absorbing organic carbon from prescribed and laboratory biomass burning and gasoline vehicle emissions. *Scientific Reports* **2017**, *7* (1), 7318.
156. Al-Naiema, I. M.; Stone, E. A., Evaluation of anthropogenic secondary organic aerosol tracers from aromatic hydrocarbons. *Atmos. Chem. Phys.* **2017**, *17* (3), 2053-2065.

157. Vione, D.; Maurino, V.; Minero, C.; Pelizzetti, E., Aqueous atmospheric chemistry: Formation of 2,4-dinitrophenol upon nitration of 2-nitrophenol and 4-nitrophenol in solution. *Environ. Sci. Technol.* **2005**, *39* (20), 7921-7931.
158. Vione, D.; Maurino, V.; Minero, C.; Pelizzetti, E.; Harrison, M. A. J.; Olariu, R.; Arsene, C., Photochemical reactions in the tropospheric aqueous phase and on particulate matter. *Chem Soc Rev* **2006**, *35* (5), 441-53.
159. Xie, M.; Chen, X.; Holder, A. L.; Hays, M. D.; Lewandowski, M.; Offenberg, J. H.; Kleindienst, T. E.; Jaoui, M.; Hannigan, M. P., Light absorption of organic carbon and its sources at a southeastern U.S. location in summer. *Environmental Pollution* **2019**, *244*, 38-46.
160. Cecinato, A.; Di Palo, V.; Pomata, D.; Tomasi Scianò, M. C.; Possanzini, M., Measurement of phase-distributed nitrophenols in Rome ambient air. *Chemosphere* **2005**, *59* (5), 679-683.
161. Li, M.; Wang, X.; Lu, C.; Li, R.; Zhang, J.; Dong, S.; Yang, L.; Xue, L.; Chen, J.; Wang, W., Nitrated phenols and the phenolic precursors in the atmosphere in urban Jinan, China. *Science of The Total Environment* **2020**, *714*, 136760.
162. Hartter, D. R., The use and importance of nitroaromatic chemicals in the chemical industry. In *Toxicity of Nitroaromatic Compounds*, Chemical Industry, Institute of Toxicology, Washington DC, 1985; pp 1-14.
163. Goi, A.; Trapido, M., Comparison of advanced oxidation processes for the destruction of 2, 4-dinitrophenol. In *Proc. Estonian Acad. Sci. Chem.*, Estonia, 2001; Vol. 50, pp 5-17.
164. Rippen, G.; Zietz, E.; Frank, R.; Knacker, T.; Klöpffer, W., Do airborne nitrophenols contribute to forest decline? *Environ. Technol. Let.* **1987**, *8* (1-12), 475-482.
165. An, Y. F.; Geng, X. R.; Mo, L. H.; Liu, J. Q.; Yang, L. T.; Zhang, X. W.; Liu, Z. G.; Zhao, C. Q.; Yang, P. C., The 3-methyl-4-nitrophenol (PNMC) compromises airway epithelial barrier function. *Toxicology* **2018**, *395*, 9-14.
166. EPA Priority Pollutants. <http://water.epa.gov/scitech/methods/cwa/pollutants.cfm> (accessed 27-10-2014).
167. EPA The original list of hazardous air pollutants. <http://www.epa.gov/ttn/atw/188polls.html> (accessed 29-10-2014).
168. Keith, L.; Telliard, W., ES&T Special Report: Priority pollutants: I-a perspective view. *Environmental Science & Technology* **1979**, *13* (4), 416-423.
169. Chow, K. S.; Huang, X. H. H.; Yu, J. Z., Quantification of nitroaromatic compounds in atmospheric fine particulate matter in Hong Kong over 3 years: field measurement evidence for secondary formation derived from biomass burning emissions. *Environmental Chemistry* **2016**, *13* (4), 665-673.

170. Lu, C.; Wang, X.; Li, R.; Gu, R.; Zhang, Y.; Li, W.; Gao, R.; Chen, B.; Xue, L.; Wang, W., Emissions of fine particulate nitrated phenols from residential coal combustion in China. *Atmospheric Environment* **2019**, *203*, 10-17.
171. Gramatica, P.; Santagostino, A.; Bolzacchini, E.; Rindone, B., Atmospheric monitoring, toxicology and QSAR modelling of nitrophenols. *Fresenius Environ. Bull.* **2002**, *11* (10a), 757-762.
172. Purohit, V.; Basu, A. K., Mutagenicity of nitroaromatic compounds. *Chem. Res. Toxicol.* **2000**, *13* (8), 673-92.
173. Schafer, K. S.; Reeves, M.; Spitzer, S.; Kegley, S. E. *Chemical trespass pesticides in our bodies and corporate accountability*; Pesticide Action Network North America: San Francisco, 2004.
174. Vernot, E. H.; MacEwen, J. D.; Haun, C. C.; Kinkead, E. R., Acute toxicity and skin corrosion data for some organic and inorganic compounds and aqueous solutions. *Toxicology and Applied Pharmacology* **1977**, *42* (2), 417-423.
175. Zhang, D.-P.; Wu, W.-L.; Long, H.-Y.; Liu, Y.-C.; Yang, Z.-S., Voltammetric behavior of o-nitrophenol and damage to DNA. *International Journal of Molecular Sciences* **2008**, *9* (3), 316-326.
176. Eichenbaum, G.; Johnson, M.; Kirkland, D.; O'Neill, P.; Stellar, S.; Bielawne, J.; DeWire, R.; Areia, D.; Bryant, S.; Weiner, S.; Desai-Krieger, D.; Guzzie-Peck, P.; Evans, D. C.; Tonelli, A., Assessment of the genotoxic and carcinogenic risks of p-nitrophenol when it is present as an impurity in a drug product. *Regulatory Toxicology and Pharmacology* **2009**, *55* (1), 33-42.
177. Yalkowsky, S. H.; He, Y.; Jain, P., *Handbook of Aqueous Solubility Data*. J. Wiley & Sons: New York, 2001; Vol. 1-2.
178. Information, N. C. f. B. PubChem Compound Summary for CID 980, 4-Nitrophenol. <https://pubchem.ncbi.nlm.nih.gov/compound/4-Nitrophenol> (accessed 21-06-2021).
179. Information, N. C. f. B. PubChem Compound Summary for CID 11137, 3-Nitrophenol. <https://pubchem.ncbi.nlm.nih.gov/compound/3-Nitrophenol> (accessed 21-06-2021).
180. Information, N. C. f. B. PubChem Compound Summary for CID 6947, 2-Nitrophenol. <https://pubchem.ncbi.nlm.nih.gov/compound/2-Nitrophenol> (accessed 21-06-2021).
181. Calas, A.; Uzu, G.; Martins, J. M. F.; Voisin, D.; Spadini, L.; Lacroix, T.; Jaffrezo, J.-L., The importance of simulated lung fluid (SLF) extractions for a more relevant evaluation of the oxidative potential of particulate matter. *Scientific Reports* **2017**, *7* (1), 11617.
182. Kitanovski, Z.; Hovorka, J.; Kuta, J.; Leoni, C.; Prokeš, R.; Sáňka, O.; Shahpoury, P.; Lammel, G., Nitrated monoaromatic hydrocarbons (nitrophenols, nitrocatechols, nitrosalicylic acids) in ambient air: levels, mass size distributions and inhalation bioaccessibility. *Environmental Science and Pollution Research* **2020**.

183. Akagi, S. K.; Yokelson, R. J.; Wiedinmyer, C.; Alvarado, M. J.; Reid, J. S.; Karl, T.; Crouse, J. D.; Wennberg, P. O., Emission factors for open and domestic biomass burning for use in atmospheric models. *Atmos. Chem. Phys.* **2011**, *11* (9), 4039-4072.
184. Bond, T. C.; Streets, D. G.; Yarber, K. F.; Nelson, S. M.; Woo, J. H.; Klimont, Z., A technology-based global inventory of black and organic carbon emissions from combustion. *Journal of Geophysical Research: Atmospheres* **2004**, *109* (D14).
185. Ramanathan, V.; Crutzen, P. J.; Kiehl, J. T.; Rosenfeld, D., Aerosols, climate, and the hydrological cycle. *science* **2001**, *294* (5549), 2119-2124.
186. Bond, T. C.; Bergstrom, R. W., Light absorption by carbonaceous particles: An investigative review. *Aerosol science and technology* **2006**, *40* (1), 27-67.
187. Bond, T.; Venkataraman, C.; Masera, O., Global atmospheric impacts of residential fuels. *Energy for Sustainable Development* **2004**, *8* (3), 20-32.
188. Ito, A.; Sudo, K.; Akimoto, H.; Sillman, S.; Penner, J. E., Global modeling analysis of tropospheric ozone and its radiative forcing from biomass burning emissions in the twentieth century. *Journal of Geophysical Research: Atmospheres* **2007**, *112* (D24).
189. Pfister, G. G.; Wiedinmyer, C.; Emmons, L. K., Impacts of the fall 2007 California wildfires on surface ozone: Integrating local observations with global model simulations. *Geophysical Research Letters* **2008**, *35* (19).
190. Alvarado, M. J.; Prinn, R. G., Formation of ozone and growth of aerosols in young smoke plumes from biomass burning: 1. Lagrangian parcel studies. *Journal of Geophysical Research: Atmospheres* **2009**, *114* (D9).
191. Yokelson, R. J.; Crouse, J. D.; DeCarlo, P. F.; Karl, T.; Urbanski, S.; Atlas, E.; Campos, T.; Shinozuka, Y.; Kapustin, V.; Clarke, A. D., Emissions from biomass burning in the Yucatan. *Atmospheric Chemistry and Physics* **2009**, *9* (15), 5785-5812.
192. Xie, M.; Chen, X.; Hays, M. D.; Holder, A. L., Composition and light absorption of nitroaromatic compounds in organic aerosols from laboratory biomass burning 2.
193. Bertrand, A.; Stefenelli, G.; Jen, C. N.; Pieber, S. M.; Bruns, E. A.; Ni, H.; Temime-Roussel, B.; Slowik, J. G.; Goldstein, A. H.; El Haddad, I.; Baltensperger, U.; Prévôt, A. S. H.; Wortham, H.; Marchand, N., Evolution of the chemical fingerprint of biomass burning organic aerosol during aging. *Atmos. Chem. Phys.* **2018**, *18* (10), 7607-7624.
194. Wang, Y.; Hu, M.; Wang, Y.; Zheng, J.; Shang, D.; Yang, Y.; Liu, Y.; Li, X.; Tang, R.; Zhu, W., The formation of nitro-aromatic compounds under high NO_x and anthropogenic VOC conditions in urban Beijing, China. *Atmospheric Chemistry and Physics* **2019**, *19* (11), 7649-7665.
195. Kitanovski, Z.; Grgić, I.; Vermeulen, R.; Claeys, M.; Maenhaut, W., Liquid chromatography tandem mass spectrometry method for characterization of monoaromatic nitro-compounds in atmospheric particulate matter. *Journal of Chromatography A* **2012**, *1268*, 35-43.

196. Tiwari, J.; Tarale, P.; Sivanesan, S.; Bafana, A., Environmental persistence, hazard, and mitigation challenges of nitroaromatic compounds. *Environmental Science and Pollution Research* **2019**, 1-18.
197. Lauraguais, A.; Coeur-Tourneur, C.; Cassez, A.; Deboudt, K.; Fourmentin, M.; Choël, M., Atmospheric reactivity of hydroxyl radicals with guaiacol (2-methoxyphenol), a biomass burning emitted compound: Secondary organic aerosol formation and gas-phase oxidation products. *Atmospheric environment* **2014**, *86*, 155-163.
198. Iinuma, Y.; Keywood, M.; Herrmann, H., Characterization of primary and secondary organic aerosols in Melbourne airshed: The influence of biogenic emissions, wood smoke and bushfires. *Atmospheric Environment* **2016**, *130*, 54-63.
199. Ford, B.; Val Martin, M.; Zelasky, S. E.; Fischer, E. V.; Anenberg, S. C.; Heald, C. L.; Pierce, J. R., Future Fire Impacts on Smoke Concentrations, Visibility, and Health in the Contiguous United States. *Geohealth* **2018**, *2* (8), 229-247.
200. Aguilera, R.; Corringham, T.; Gershunov, A.; Benmarhnia, T., Wildfire smoke impacts respiratory health more than fine particles from other sources: observational evidence from Southern California. *Nature communications* **2021**, *12* (1), 1-8.
201. Landvik, N. E.; Gorria, M.; Arlt, V. M.; Asare, N.; Solhaug, A.; Lagadic-Gossmann, D.; Holme, J. r. A., Effects of nitrated-polycyclic aromatic hydrocarbons and diesel exhaust particle extracts on cell signalling related to apoptosis: Possible implications for their mutagenic and carcinogenic effects. *Toxicology* **2007**, *231* (2), 159-174.
202. Kim, Y. H.; Warren, S. H.; Krantz, Q. T.; King, C.; Jaskot, R.; Preston, W. T.; George, B. J.; Hays, M. D.; Landis, M. S.; Higuchi, M., Mutagenicity and lung toxicity of smoldering vs. flaming emissions from various biomass fuels: implications for health effects from wildland fires. *Environmental health perspectives* **2018**, *126* (1), 017011.
203. Alves, D. K. M.; Kummrow, F. b.; Cardoso, A. A.; Morales, D. A.; Umbuzeiro, G. A., Mutagenicity profile of atmospheric particulate matter in a small urban center subjected to airborne emission from vehicle traffic and sugar cane burning. *Environmental and molecular mutagenesis* **2016**, *57* (1), 41-50.
204. Danielsen, P. H. g.; Muller, P.; Jensen, K. A.; Sharma, A. K.; Wallin, H. k.; Bossi, R.; Autrup, H.; Muhave, L.; Ravanat, J.-L.; Briedl, J. J., Oxidative stress, DNA damage, and inflammation induced by ambient air and wood smoke particulate matter in human A549 and THP-1 cell lines. *Chemical research in toxicology* **2011**, *24* (2), 168-184.
205. Kim, Y. H.; King, C.; Krantz, T.; Hargrove, M. M.; George, I. J.; McGee, J.; Copeland, L.; Hays, M. D.; Landis, M. S.; Higuchi, M., The role of fuel type and combustion phase on the toxicity of biomass smoke following inhalation exposure in mice. *Archives of toxicology* **2019**, *93* (6), 1501-1513.
206. Krapf, M.; KČnzi, L.; Allenbach, S.; Bruns, E. A.; Gavarini, I.; El-Haddad, I.; Slowik, J. G.; PrĆvĆt, A. S. H.; Drinovec, L.; MoÄnik, G. a., Wood combustion particles induce adverse effects to normal and diseased airway epithelia. *Environmental science: processes & impacts* **2017**, *19* (4), 538-548.

207. Pardo, M.; Li, C.; He, Q.; Levin-Zaidman, S.; Tsoory, M.; Yu, Q.; Wang, X.; Rudich, Y., Mechanisms of lung toxicity induced by biomass burning aerosols. *Particle and fibre toxicology* **2020**, *17* (1), 1-15.
208. Tuet, W. Y.; Liu, F.; de Oliveira Alves, N.; Fok, S.; Artaxo, P.; Vasconcellos, P.; Champion, J. A.; Ng, N. L., Chemical Oxidative Potential and Cellular Oxidative Stress from Open Biomass Burning Aerosol. *Environmental Science & Technology Letters* **2019**.
209. Pflieger, M.; Krofli, A., Acute toxicity of emerging atmospheric pollutants from wood lignin due to biomass burning. *Journal of hazardous materials* **2017**, *338*, 132-139.
210. Kołodziejczyk, A.; Pyrcz, P.; Pobudkowska, A.; Błaziak, K.; Szmigielski, R., Physicochemical Properties of Pinic, Pinonic, Norpinic, and Norpinonic Acids as Relevant α -Pinene Oxidation Products. *J. Phys. Chem. B* **2019**, *123* (39), 8261-8267.
211. Kołodziejczyk, A.; Pyrcz, P.; Błaziak, K.; Pobudkowska, A.; Sarang, K.; Szmigielski, R., Physicochemical Properties of Terebic Acid, MBTCA, Diaterpenylic Acid Acetate, and Pinanediol as Relevant α -Pinene Oxidation Products. *ACS Omega* **2020**, *5* (14), 7919-7927.
212. Zhang, Y.; Sanchez, M. S.; Douet, C.; Wang, Y.; Bateman, A. P.; Gong, Z.; Kuwata, M.; Renbaum-Wolff, L.; Sato, B. B.; Liu, P. F.; Bertram, A. K.; Geiger, F. M.; Martin, S. T., Changing shapes and implied viscosities of suspended submicron particles. *Atmos. Chem. Phys.* **2015**, *15* (14), 7819-7829.
213. Zhang, Y.; Chen, Y.; Lambe, A. T.; Olson, N. E.; Lei, Z.; Craig, R. L.; Zhang, Z.; Gold, A.; Onasch, T. B.; Jayne, J. T.; Worsnop, D. R.; Gaston, C. J.; Thornton, J. A.; Vizuete, W.; Ault, A. P.; Surratt, J. D., Effect of Aerosol-Phase State on Secondary Organic Aerosol Formation from the Reactive Uptake of Isoprene-Derived Epoxydiols (IEPOX). *Environ. Sci. Technol. Lett.* **2018**, *5* (3), 167-174.
214. Lambe, A. T.; Ahern, A. T.; Williams, L. R.; Slowik, J. G.; Wong, J. P. S.; Abbatt, J. P. D.; Brune, W. H.; Ng, N. L.; Wright, J. P.; Croasdale, D. R.; Worsnop, D. R.; Davidovits, P.; Onasch, T. B., Characterization of aerosol photooxidation flow reactors: heterogeneous oxidation, secondary organic aerosol formation and cloud condensation nuclei activity measurements. *Atmos. Meas. Tech.* **2011**, *4* (3), 445-461.
215. Zhang, Y.; Chen, Y.; Lambe, A. T.; Olson, N. E.; Lei, Z.; Craig, R. L.; Zhang, Z.; Gold, A.; Onasch, T. B.; Jayne, J. T.; Worsnop, D. R.; Gaston, C. J.; Thornton, J. A.; Vizuete, W.; Ault, A. P.; Surratt, J. D., Effect of the Aerosol-Phase State on Secondary Organic Aerosol Formation from the Reactive Uptake of Isoprene-Derived Epoxydiols (IEPOX). *Environmental Science & Technology Letters* **2018**, *5* (3), 167-174.
216. Zhang, H.; Yee, L. D.; Lee, B. H.; Curtis, M. P.; Worton, D. R.; Isaacman-VanWertz, G.; Offenberg, J. H.; Lewandowski, M.; Kleindienst, T. E.; Beaver, M. R.; Holder, A. L.; Lonneman, W. A.; Docherty, K. S.; Jaoui, M.; Pye, H. O. T.; Hu, W.; Day, D. A.; Campuzano-Jost, P.; Jimenez, J. L.; Guo, H.; Weber, R. J.; de Gouw, J.; Koss, A. R.; Edgerton, E. S.; Brune, W.; Mohr, C.; Lopez-Hilfiker, F. D.; Lutz, A.; Kreisberg, N. M.; Spielman, S. R.; Hering, S. V.; Wilson, K. R.; Thornton, J. A.; Goldstein, A. H., Monoterpenes are the largest source of summertime organic aerosol in

the southeastern United States. *Proceedings of the National Academy of Sciences* **2018**, *115* (9), 2038.

217. Carslaw, K.; Boucher, O.; Spracklen, D.; Mann, G.; Rae, J.; Woodward, S.; Kulmala, M., A review of natural aerosol interactions and feedbacks within the Earth system. *Atmospheric Chemistry & Physics* **2010**, *10* (4).

218. Upadhyay, S.; Palmberg, L., Air-Liquid Interface: Relevant In Vitro Models for Investigating Air Pollutant-Induced Pulmonary Toxicity. *Toxicological Sciences* **2018**, *164* (1), 21-30.

219. Mao, J.; Ren, X.; Brune, W. H.; Olson, J. R.; Crawford, J. H.; Fried, A.; Huey, L. G.; Cohen, R. C.; Heikes, B.; Singh, H. B.; Blake, D. R.; Sachse, G. W.; Diskin, G. S.; Hall, S. R.; Shetter, R. E., Airborne measurement of OH reactivity during INTEX-B. *Atmos. Chem. Phys.* **2009**, *9* (1), 163-173.

220. Chen, Y.; Dombek, T.; Hand, J.; Zhang, Z.; Gold, A.; Ault, A. P.; Levine, K. E.; Surratt, J. D., Seasonal Contribution of Isoprene-Derived Organosulfates to Total Water-Soluble Fine Particulate Organic Sulfur in the United States. *ACS Earth and Space Chemistry* **2021**.

221. Offenberg, J. H.; Kleindienst, T. E.; Jaoui, M.; Lewandowski, M.; Edney, E. O., Thermal properties of secondary organic aerosols. *Geophysical research letters* **2006**, *33* (3).

222. Docherty, K. S.; Corse, E. W.; Jaoui, M.; Offenberg, J. H.; Kleindienst, T. E.; Krug, J. D.; Riedel, T. P.; Lewandowski, M., Trends in the oxidation and relative volatility of chamber-generated secondary organic aerosol. *Aerosol Science and Technology* **2018**, *52* (9), 992-1004.

223. Jaoui, M.; Lewandowski, M.; Docherty, K.; Offenberg, J.; Kleindienst, T., Atmospheric oxidation of 1, 3-butadiene: characterization of gas and aerosol reaction products and implications for PM 2.5. *Atmospheric Chemistry and Physics* **2014**, *14* (24), 13681-13704.

224. Jaoui, M.; Kleindienst, T. E.; Lewandowski, M.; Edney, E. O., Identification and quantification of aerosol polar oxygenated compounds bearing carboxylic or hydroxyl groups. 1. Method development. *Analytical Chemistry* **2004**, *76* (16), 4765-4778.

225. Kleindienst, T. E.; Jaoui, M.; Lewandowski, M.; Offenberg, J. H.; Lewis, C. W.; Bhave, P. V.; Edney, E. O., Estimates of the contributions of biogenic and anthropogenic hydrocarbons to secondary organic aerosol at a southeastern US location. *Atmospheric Environment* **2007**, *41* (37), 8288-8300.

226. Lewandowski, M.; Piletic, I. R.; Kleindienst, T. E.; Offenberg, J. H.; Beaver, M. R.; Jaoui, M.; Docherty, K. S.; Edney, E. O., Secondary organic aerosol characterisation at field sites across the United States during the spring–summer period. *International Journal of Environmental Analytical Chemistry* **2013**, *93* (10), 1084-1103.

227. Jaoui, M.; Szmigielski, R.; Nestorowicz, K.; Kolodziejczyk, A.; Sarang, K.; Rudzinski, K. J.; Konopka, A.; Bulska, E.; Lewandowski, M.; Kleindienst, T. E., Organic

hydroxy acids as highly oxygenated molecular (HOM) tracers for aged isoprene aerosol. *Environmental science & technology* **2019**, *53* (24), 14516-14527.

228.Rideau, E.; Dimova, R.; Schwille, P.; Wurm, F. R.; Landfester, K., Liposomes and polymersomes: a comparative review towards cell mimicking. *Chem. Soc. Rev.* **2018**, *47* (23), 8572-8610.

229.Barenholz, Y.; Gibbes, D.; Litman, B. J.; Goll, J.; Thompson, T. E.; Carlson, F. D., A simple method for the preparation of homogeneous phospholipid vesicles. *Biochemistry* **1977**, *16* (12), 2806-2810.

230.Reviakine, I.; Brisson, A., Formation of supported phospholipid bilayers from unilamellar vesicles investigated by atomic force microscopy. *Langmuir* **2000**, *16* (4), 1806-1815.

231.Pawłowski, J.; Juhaniwicz, J.; Güzeloğlu, A.; Søk, S., Mechanism of lipid vesicles spreading and bilayer formation on a Au(111) surface. *Langmuir* **2015**, *31* (40), 11012-11019.

232.Lévy, R.; Maaloum, M., Measuring the spring constant of atomic force microscope cantilevers: thermal fluctuations and other methods. *Nanotechnology* **2002**, *13*, 33-37.

233.Hutter, J. L.; Bechhoefer, J., Calibration of atomic-force microscope tips. *Review of Scientific Instruments* **1993**, *64* (7), 1868-1873.

234.Livak, K. J.; Schmittgen, T. D., Analysis of relative gene expression data using real-time quantitative PCR and the 2(-Delta Delta C(T)) Method. *Methods* **2001**, *25* (4), 402-8.

235.Frias, D. P.; Gomes, R. L. N.; Yoshizaki, K.; Carvalho-Oliveira, R.; Matsuda, M.; Junqueira, M. S.; Teodoro, W. R.; Vasconcellos, P. C.; Pereira, D. C. A.; Conceição, P. R. D.; Saldiva, P. H. N.; Mauad, T.; Macchione, M., Nrf2 positively regulates autophagy antioxidant response in human bronchial epithelial cells exposed to diesel exhaust particles. *Sci Rep* **2020**, *10* (1), 3704.

236.Lian, F.; Wang, X. D., Enzymatic metabolites of lycopene induce Nrf2-mediated expression of phase II detoxifying/antioxidant enzymes in human bronchial epithelial cells. *International journal of cancer* **2008**, *123* (6), 1262-1268.

237.Park, E.-J.; Choi, J.; Park, Y.-K.; Park, K., Oxidative stress induced by cerium oxide nanoparticles in cultured BEAS-2B cells. *Toxicology* **2008**, *245* (1-2), 90-100.

238.Seriani, R.; de Souza, C. E. C.; Krempel, P. G.; Frias, D. P.; Matsuda, M.; Correia, A. T.; Ferreira, M. Z. J.; Alencar, A. M.; Negri, E. M.; Saldiva, P. H. N., Human bronchial epithelial cells exposed in vitro to diesel exhaust particles exhibit alterations in cell rheology and cytotoxicity associated with decrease in antioxidant defenses and imbalance in pro-and anti-apoptotic gene expression. *Environmental Science and Pollution Research* **2016**, *23* (10), 9862-9870.

239.Homma, T.; Kato, A.; Hashimoto, N.; Batchelor, J.; Yoshikawa, M.; Imai, S.; Wakiguchi, H.; Saito, H.; Matsumoto, K., Corticosteroid and cytokines synergistically

enhance toll-like receptor 2 expression in respiratory epithelial cells. *American journal of respiratory cell and molecular biology* **2004**, *31* (4), 463-469.

240.Lim, S.; Caramori, G.; Tomita, K.; Jazrawi, E.; Oates, T.; Chung, K.; Barnes, P.; Adcock, I., Differential expression of IL-10 receptor by epithelial cells and alveolar macrophages. *Allergy* **2004**, *59* (5), 505-514.

241.Fuzzi, S.; Baltensperger, U.; Carslaw, K.; Decesari, S.; Denier van der Gon, H.; Facchini, M. C.; Fowler, D.; Koren, I.; Langford, B.; Lohmann, U., Particulate matter, air quality and climate: lessons learned and future needs. *Atmospheric chemistry and physics* **2015**, *15* (14), 8217-8299.

242.Gangwal, S.; Brown, J. S.; Wang, A.; Houck, K. A.; Dix, D. J.; Kavlock, R. J.; Hubal, E. A. C., Informing selection of nanomaterial concentrations for ToxCast in vitro testing based on occupational exposure potential. *Environmental health perspectives* **2011**, *119* (11), 1539-1546.

243.Paur, H.-R.; Cassee, F. R.; Teeguarden, J.; Fissan, H.; Diabate, S.; Aufderheide, M.; Kreyling, W. G.; Hänninen, O.; Kasper, G.; Riediker, M.; Rothen-Rutishauser, B.; Schmid, O., In-vitro cell exposure studies for the assessment of nanoparticle toxicity in the lung—A dialog between aerosol science and biology. *Journal of Aerosol Science* **2011**, *42* (10), 668-692.

244.ICRP, Human respiratory tract model for radiological protection. A report of a Task Group of the International Commission on Radiological Protection. **1994**, *1995;25(3-4):iii*] (0146-6453 (Print)).

245.de Jesus, A. L.; Rahman, M. M.; Mazaheri, M.; Thompson, H.; Knibbs, L. D.; Jeong, C.; Evans, G.; Nei, W.; Ding, A.; Qiao, L.; Li, L.; Portin, H.; Niemi, J. V.; Timonen, H.; Luoma, K.; Petäjä, T.; Kulmala, M.; Kowalski, M.; Peters, A.; Cyrus, J.; Ferrero, L.; Manigrasso, M.; Avino, P.; Buonano, G.; Reche, C.; Querol, X.; Beddows, D.; Harrison, R. M.; Sowlat, M. H.; Sioutas, C.; Morawska, L., Ultrafine particles and PM_{2.5} in the air of cities around the world: Are they representative of each other? *Environment International* **2019**, *129*, 118-135.

246.Kreyling, W. G.; Semmler-Behnke, M.; Möller, W., Ultrafine Particle–Lung Interactions: Does Size Matter? *Journal of Aerosol Medicine* **2006**, *19* (1), 74-83.

247.Chang, J.-S.; Chang, K. L. B.; Hwang, D.-F.; Kong, Z.-L., In vitro cytotoxicity of silica nanoparticles at high concentrations strongly depends on the metabolic activity type of the cell line. *Environmental science & technology* **2007**, *41* (6), 2064-2068.

248.Haghi, M.; Hittinger, M.; Zeng, Q.; Oliver, B.; Traini, D.; Young, P. M.; Huwer, H.; Schneider-Daum, N.; Lehr, C. M., Mono- and Cocultures of Bronchial and Alveolar Epithelial Cells Respond Differently to Proinflammatory Stimuli and Their Modulation by Salbutamol and Budesonide. *Mol Pharm* **2015**, *12* (8), 2625-32.

249.Aljawhary, D.; Zhao, R.; Lee, A. K. Y.; Wang, C.; Abbatt, J. P. D., Kinetics, Mechanism, and Secondary Organic Aerosol Yield of Aqueous Phase Photo-oxidation of α -Pinene Oxidation Products. *The Journal of Physical Chemistry A* **2016**, *120* (9), 1395-1407.

250. Wang, S. J.; Zhao, J. K.; Ren, S.; Sun, W. W.; Zhang, W. J.; Zhang, J. N., Wogonin affects proliferation and the energy metabolism of SGC-7901 and A549 cells. *Exp Ther Med* **2019**, *17* (1), 911-918.
251. Vistica, D. T.; Skehan, P.; Scudiero, D.; Monks, A.; Pittman, A.; Boyd, M. R., Tetrazolium-based assays for cellular viability: a critical examination of selected parameters affecting formazan production. *Cancer Res* **1991**, *51* (10), 2515-20.
252. Persoz, C.; Achard, S.; Momas, I.; Seta, N., Inflammatory response modulation of airway epithelial cells exposed to formaldehyde. *Toxicology letters* **2012**, *211* (2), 159-163.
253. Gualtieri, M.; Øvrevik, J.; Holme, J. A.; Perrone, M. G.; Bolzacchini, E.; Schwarze, P. E.; Camatini, M., Differences in cytotoxicity versus pro-inflammatory potency of different PM fractions in human epithelial lung cells. *Toxicology in Vitro* **2010**, *24* (1), 29-39.
254. Berger, W.; Elbling, L.; Micksche, M., Expression of the major vault protein LRP in human non-small-cell lung cancer cells: Activation by short-term exposure to antineoplastic drugs. *International Journal of Cancer* **2000**, *88* (2), 293-300.
255. Homma, S.; Ishii, Y.; Morishima, Y.; Yamadori, T.; Matsuno, Y.; Haraguchi, N.; Kikuchi, N.; Satoh, H.; Sakamoto, T.; Hizawa, N., Nrf2 enhances cell proliferation and resistance to anticancer drugs in human lung cancer. *Clinical Cancer Research* **2009**, *15* (10), 3423-3432.
256. Chang, J. W.; Lee, S. H.; Lu, Y.; Yoo, Y. J., Transforming growth factor- β 1 induces the non-classical secretion of peroxiredoxin-I in A549 cells. *Biochemical and Biophysical Research Communications* **2006**, *345* (1), 118-123.
257. Rafael-Vázquez, L.; García-Trejo, S.; Aztatzi-Aguilar, O. G.; Bazán-Perkins, B.; Quintanilla-Vega, B., Exposure to diethylhexyl phthalate (DEHP) and monoethylhexyl phthalate (MEHP) promotes the loss of alveolar epithelial phenotype of A549 cells. *Toxicology letters* **2018**, *294*, 135-144.
258. Barr, M. P.; Gray, S. G.; Hoffmann, A. C.; Hilger, R. A.; Thomale, J.; O'Flaherty, J. D.; Fennell, D. A.; Richard, D.; O'Leary, J. J.; O'Byrne, K. J., Generation and Characterisation of Cisplatin-Resistant Non-Small Cell Lung Cancer Cell Lines Displaying a Stem-Like Signature. *PloS one* **2013**, *8* (1), e54193.
259. Tan, S.; Sagara, Y.; Liu, Y.; Maher, P.; Schubert, D., The regulation of reactive oxygen species production during programmed cell death. *J Cell Biol* **1998**, *141* (6), 1423-1432.
260. Saffari, A.; Daher, N.; Shafer, M. M.; Schauer, J. J.; Sioutas, C., Global Perspective on the Oxidative Potential of Airborne Particulate Matter: A Synthesis of Research Findings. *Environmental Science & Technology* **2014**, *48* (13), 7576-7583.
261. Reinnig, M. C.; Warnke, J.; Hoffmann, T., Identification of organic hydroperoxides and hydroperoxy acids in secondary organic aerosol formed during the ozonolysis of different monoterpenes and sesquiterpenes by on-line analysis using atmospheric pressure chemical ionization ion trap mass spectrometry. *Rapid Communications in Mass Spectrometry* **2014**, *28* (12), 1423-1432.

Spectrometry: An International Journal Devoted to the Rapid Dissemination of Up-to-the-Minute Research in Mass Spectrometry **2009**, 23 (11), 1735-1741.

262. Zhou, S.; Rivera-Rios, J. C.; Keutsch, F. N.; Abbatt, J. P., Identification of organic hydroperoxides and peroxy acids using atmospheric pressure chemical ionization–tandem mass spectrometry (APCI-MS/MS): application to secondary organic aerosol. *Atmospheric Measurement Techniques* **2018**, 11 (5), 3081.

263. Zhang, D.; Zhang, R., Ozonolysis of α -pinene and β -pinene: kinetics and mechanism. *The Journal of chemical physics* **2005**, 122 (11), 114308.

264. Zhou, S.; Rivera-Rios, J. C.; Keutsch, F. N.; Abbatt, J. P. D., Identification of organic hydroperoxides and peroxy acids using atmospheric pressure chemical ionization–tandem mass spectrometry (APCI-MS/MS): application to secondary organic aerosol. *Atmos. Meas. Tech.* **2018**, 11 (5), 3081-3089.

265. Faiola, C. L.; Buchholz, A.; Kari, E.; Yli-Pirilä, P.; Holopainen, J. K.; Kivimäenpää, M.; Miettinen, P.; Worsnop, D. R.; Lehtinen, K. E. J.; Guenther, A. B.; Virtanen, A., Terpene Composition Complexity Controls Secondary Organic Aerosol Yields from Scots Pine Volatile Emissions. *Scientific reports* **2018**, 8 (1), 3053-3053.

266. Tong, H.; Lakey, P. S. J.; Arangio, A. M.; Socorro, J.; Shen, F.; Lucas, K.; Brune, W. H.; Pöschl, U.; Shiraiwa, M., Reactive Oxygen Species Formed by Secondary Organic Aerosols in Water and Surrogate Lung Fluid. *Environmental Science & Technology* **2018**, 52 (20), 11642-11651.

267. Alpert, P. A.; Dou, J.; Corral Arroyo, P.; Schneider, F.; Xto, J.; Luo, B.; Peter, T.; Huthwelker, T.; Borca, C. N.; Henzler, K. D.; Schaefer, T.; Herrmann, H.; Raabe, J. r.; Watts, B.; Krieger, U. K.; Ammann, M., Photolytic radical persistence due to anoxia in viscous aerosol particles. *Nature Communications* **2021**, 12 (1), 1769.

268. Kroll, J. H.; Lim, C. Y.; Kessler, S. H.; Wilson, K. R., Heterogeneous oxidation of atmospheric organic aerosol: kinetics of changes to the amount and oxidation state of particle-phase organic carbon. *The Journal of Physical Chemistry A* **2015**, 119 (44), 10767-10783.

269. Hettiyadura, A. P. S.; Al-Naiema, I. M.; Hughes, D. D.; Fang, T.; Stone, E. A., Organosulfates in Atlanta, Georgia: anthropogenic influences on biogenic secondary organic aerosol formation. *Atmospheric Chemistry and Physics* **2019**, 19 (5), 3191-3206.

270. Budisulistiorini, S.; Li, X.; Bairai, S. T.; Renfro, J.; Liu, Y.; Liu, Y. J.; McKinney, K. A.; Martin, S. T.; McNeill, V. F.; Pye, H. O. T., Examining the effects of anthropogenic emissions on isoprene-derived secondary organic aerosol formation during the 2013 Southern Oxidant and Aerosol Study (SOAS) at the Look Rock, Tennessee ground site. *Atmospheric Chemistry and Physics* **2015**, 15 (15), 8871-8888.

271. Rattanavaraha, W.; Chu, K.; Budisulistiorini, S. H.; Riva, M.; Lin, Y.-H.; Edgerton, E. S.; Baumann, K.; Shaw, S. L.; Guo, H.; King, L., Assessing the impact of anthropogenic pollution on isoprene-derived secondary organic aerosol formation in PM 2.5 collected from the Birmingham, Alabama, ground site during the 2013 Southern Oxidant and Aerosol Study. *Atmospheric chemistry and physics* **2016**, 16 (8), 4897-4914.

- 272.Han, J.; Wang, S.; Yeung, K.; Yang, D.; Gu, W.; Ma, Z.; Sun, J.; Wang, X.; Chow, C.-W.; Chan, A. W. H.; Peng, H., Proteome-wide effects of naphthalene-derived secondary organic aerosol in BEAS-2B cells are caused by short-lived unsaturated carbonyls. *Proceedings of the National Academy of Sciences* **2020**, *117* (41), 25386.
- 273.Cuadrado, A.; Manda, G.; Hassan, A.; Alcaraz, M. J.; Barbas, C.; Daiber, A.; Ghezzi, P.; León, R.; López, M. G.; Oliva, B., Transcription factor NRF2 as a therapeutic target for chronic diseases: a systems medicine approach. *Pharmacological reviews* **2018**, *70* (2), 348-383.
- 274.Cuadrado, A.; Rojo, A. I.; Wells, G.; Hayes, J. D.; Cousin, S. P.; Rumsey, W. L.; Attucks, O. C.; Franklin, S.; Levonen, A.-L.; Kensler, T. W.; Dinkova-Kostova, A. T., Therapeutic targeting of the NRF2 and KEAP1 partnership in chronic diseases. *Nature Reviews Drug Discovery* **2019**, *18* (4), 295-317.
- 275.Ralat, L. A.; Manevich, Y.; Fisher, A. B.; Colman, R. F., Direct evidence for the formation of a complex between 1-cysteine peroxiredoxin and glutathione S-transferase π with activity changes in both enzymes. *Biochemistry* **2006**, *45* (2), 360-372.
- 276.Choi, J.; Liu, R.-M.; Kundu, R. K.; Sangiorgi, F.; Wu, W.; Maxson, R.; Forman, H. J., Molecular mechanism of decreased glutathione content in human immunodeficiency virus type 1 Tat-transgenic mice. *Journal of Biological Chemistry* **2000**, *275* (5), 3693-3698.
- 277.Fletcher, M. E.; Boshier, P. R.; Wakabayashi, K.; Keun, H. C.; Smolenski, R. T.; Kirkham, P. A.; Adcock, I. M.; Barton, P. J.; Takata, M.; Marczin, N., Influence of glutathione-S-transferase (GST) inhibition on lung epithelial cell injury: role of oxidative stress and metabolism. *American Journal of Physiology-Lung Cellular and Molecular Physiology* **2015**, *308* (12), L1274-L1285.
- 278.Carlberg, I.; Mannervik, B., [59] Glutathione reductase. *Methods in enzymology* **1985**, *113*, 484-490.
- 279.Zelko, I. N.; Mariani, T. J.; Folz, R. J., Superoxide dismutase multigene family: a comparison of the CuZn-SOD (SOD1), Mn-SOD (SOD2), and EC-SOD (SOD3) gene structures, evolution, and expression. *Free Radical Biology and Medicine* **2002**, *33* (3), 337-349.
- 280.Vignais, P. V., The superoxide-generating NADPH oxidase: structural aspects and activation mechanism. *Cellular and Molecular Life Sciences CMLS* **2002**, *59* (9), 1428-1459.
- 281.Aris, R. M.; Christian, D.; Hearne, P. Q.; Kerr, K.; Finkbeiner, W. E.; Balmes, J. R., Ozone-induced airway inflammation in human subjects as determined by airway lavage and biopsy. *Am Rev Respir Dis* **1993**, *148* (5), 1363-72.
- 282.Bromberg, P. A., Mechanisms of the acute effects of inhaled ozone in humans. *Biochimica et Biophysica Acta (BBA) - General Subjects* **2016**, *1860* (12), 2771-2781.

283. Islam, T.; McConnell, R.; Gauderman, W. J.; Avol, E.; Peters, J. M.; Gilliland, F. D., Ozone, Oxidant Defense Genes, and Risk of Asthma during Adolescence. *American Journal of Respiratory and Critical Care Medicine* **2008**, *177* (4), 388-395.
284. Exner, M.; Minar, E.; Wagner, O.; Schillinger, M., The role of heme oxygenase-1 promoter polymorphisms in human disease. *Free Radic Biol Med* **2004**, *37* (8), 1097-104.
285. Borish, L., IL-10: Evolving concepts. *Journal of Allergy and Clinical Immunology* **1998**, *101* (3), 293-297.
286. Badran, G.; Verdin, A.; Grare, C.; Abbas, I.; Achour, D.; Ledoux, F.; Roumie, M.; Cazier, F.; Courcot, D.; Lo Guidice, J.-M.; Garçon, G., Toxicological appraisal of the chemical fractions of ambient fine (PM_{2.5-0.3}) and quasi-ultrafine (PM_{0.3}) particles in human bronchial epithelial BEAS-2B cells. *Environmental Pollution* **2020**, *263*, 114620.
287. Merk, R.; Heßelbach, K.; Osipova, A.; Popadić, D.; Schmidt-Heck, W.; Kim, G.-J.; Günther, S.; Piñeres, A. G.; Merfort, I.; Humar, M., Particulate Matter (PM_{2.5}) from Biomass Combustion Induces an Anti-Oxidative Response and Cancer Drug Resistance in Human Bronchial Epithelial BEAS-2B Cells. *International Journal of Environmental Research and Public Health* **2020**, *17* (21), 8193.
288. Niture, S. K.; Kaspar, J. W.; Shen, J.; Jaiswal, A. K., Nrf2 signaling and cell survival. *Toxicology and applied pharmacology* **2010**, *244* (1), 37-42.
289. Dhakshinamoorthy, S.; Long, D. J., 2nd; Jaiswal, A. K., Antioxidant regulation of genes encoding enzymes that detoxify xenobiotics and carcinogens. *Curr Top Cell Regul* **2000**, *36*, 201-16.
290. Guan, S. P.; Tee, W.; Ng, D. S. W.; Chan, T. K.; Peh, H. Y.; Ho, W. E.; Cheng, C.; Mak, J. C.; Wong, W. S. F., Andrographolide protects against cigarette smoke-induced oxidative lung injury via augmentation of Nrf2 activity. *British Journal of Pharmacology* **2013**, *168* (7), 1707-1718.
291. Otterbein, L. E.; Soares, M. P.; Yamashita, K.; Bach, F. H., Heme oxygenase-1: unleashing the protective properties of heme. *Trends Immunol* **2003**, *24* (8), 449-55.
292. Harju, T.; Soini, Y.; Paakko, R.; Kinnula, V. L., Up-regulation of heme oxygenase-I in alveolar macrophages of newly diagnosed asthmatics. *Respir Med* **2002**, *96* (6), 418-23.
293. Fredenburgh, L. E.; Perrella, M. A.; Mitsialis, S. A., The role of heme oxygenase-1 in pulmonary disease. *American journal of respiratory cell and molecular biology* **2007**, *36* (2), 158-165.
294. Biswas, S. K.; Rahman, I., Environmental toxicity, redox signaling and lung inflammation: The role of glutathione. *Molecular Aspects of Medicine* **2009**, *30* (1), 60-76.
295. Weldy, C. S.; White, C. C.; Wilkerson, H.-W.; Larson, T. V.; Stewart, J. A.; Gill, S. E.; Parks, W. C.; Kavanagh, T. J., Heterozygosity in the glutathione synthesis gene Gclm increases sensitivity to diesel exhaust particulate induced lung inflammation in mice. *Inhalation toxicology* **2011**, *23* (12), 724-735.

296. McConnachie, L. A.; Botta, D.; White, C. C.; Weldy, C. S.; Wilkerson, H.-W.; Yu, J.; Dills, R.; Yu, X.; Griffith, W. C.; Faustman, E. M.; Farin, F. M.; Gill, S. E.; Parks, W. C.; Hu, X.; Gao, X.; Eaton, D. L.; Kavanagh, T. J., The Glutathione Synthesis Gene *Gclm* Modulates Amphiphilic Polymer-Coated CdSe/ZnS Quantum Dot Induced Lung Inflammation in Mice. *PloS one* **2013**, *8* (5), e64165.
297. van der Toorn, M.; Smit-de Vries, M. P.; Slebos, D. J.; de Bruin, H. G.; Abello, N.; van Oosterhout, A. J.; Bischoff, R.; Kauffman, H. F., Cigarette smoke irreversibly modifies glutathione in airway epithelial cells. *Am J Physiol Lung Cell Mol Physiol* **2007**, *293* (5), L1156-62.
298. Bernard, K.; Hecker, L.; Luckhardt, T. R.; Cheng, G.; Thannickal, V. J., NADPH Oxidases in Lung Health and Disease. *Antioxidants & Redox Signaling* **2013**, *20* (17), 2838-2853.
299. Betsuyaku, T.; Fuke, S.; Inomata, T.; Kaga, K.; Morikawa, T.; Odajima, N.; Adair-Kirk, T.; Nishimura, M., Bronchiolar epithelial catalase is diminished in smokers with mild COPD. *European Respiratory Journal* **2013**, *42* (1), 42.
300. Kinnula, V. L.; Crapo, J. D., Superoxide dismutases in the lung and human lung diseases. *Am J Respir Crit Care Med* **2003**, *167* (12), 1600-19.
301. Ahmed, C. M. S.; Yang, J.; Chen, J. Y.; Jiang, H.; Cullen, C.; Karavalakis, G.; Lin, Y.-H., Toxicological responses in human airway epithelial cells (BEAS-2B) exposed to particulate matter emissions from gasoline fuels with varying aromatic and ethanol levels. *Science of The Total Environment* **2020**, *706*, 135732.
302. Wilkins, C. K.; Wolkoff, P.; Clausen, P. A.; Hammer, M.; Nielsen, G. D., Upper airway irritation of terpene/ozone oxidation products (TOPS). Dependence on reaction time, relative humidity and initial ozone concentration. *Toxicology letters* **2003**, *143* (2), 109-14.
303. Rohr, A. C.; Wilkins, C. K.; Clausen, P. A.; Hammer, M.; Nielsen, G. D.; Wolkoff, P.; Spengler, J. D., Upper airway and pulmonary effects of oxidation products of (+)-alpha-pinene, d-limonene, and isoprene in BALB/c mice. *Inhalation toxicology* **2002**, *14* (7), 663-84.
304. Majewska, M.; Khan, F.; Pieta, I. S.; Wróblewska, A.; Szmigielski, R.; Pieta, P., Toxicity of selected airborne nitrophenols on eukaryotic cell membrane models. *Chemosphere* **2021**, *266*, 128996.
305. Cao, X.; Fu, M.; Bi, R.; Zheng, X.; Fu, B.; Tian, S.; Liu, C.; Li, Q.; Liu, J., Cadmium induced BEAS-2B cells apoptosis and mitochondria damage via MAPK signaling pathway. *Chemosphere* **2021**, *263*, 128346.
306. Zemski Berry, K. A.; Murphy, R. C.; Kosmider, B.; Mason, R. J., Lipidomic characterization and localization of phospholipids in the human lung. *J. Lipid Res.* **2017**, *58* (5), 926-933.
307. Kyle, J. E.; Clair, G.; Bandyopadhyay, G.; Misra, R. S.; Zink, E. M.; Bloodsworth, K. J.; Shukla, A. K.; Du, Y.; Lillis, J.; Myers, J. R.; Ashton, J.; Bushnell, T.; Cochran,

M.; Deutsch, G.; Baker, E. S.; Carson, J. P.; Mariani, T. J.; Xu, Y.; Whitsett, J. A.; Pryhuber, G.; Ansong, C., Cell type-resolved human lung lipidome reveals cellular cooperation in lung function. *Sci. Rep.* **2018**, *8* (1), 13455.

308.Su, Z.; Leitch, J. J.; Lipkowski, J., Electrode-supported biomimetic membranes: An electrochemical and surface science approach for characterizing biological cell membranes. *Curr. Opin. Electrochem.* **2018**, *12*, 60-72.

309.Lipkowski, J., Biomimetics: a new research opportunity for surface electrochemistry. *J. Solid State Electr.* **2020**.

310.Juhaniewicz, J.; Sek, S., Atomic force microscopy and electrochemical studies of melittin action on lipid bilayers supported on gold electrodes. *Electrochim. Acta* **2015**, *162* (0), 53-61.

311.Juhaniewicz-Dębińska, J.; Tymecka, D.; Sęk, S., Lipopeptide-induced changes in permeability of solid supported bilayers composed of bacterial membrane lipids. *J. Electroanal. Chem.* **2018**, *812*, 227-234.

312.Su, Z.; Shodiev, M.; Jay Leitch, J.; Abbasi, F.; Lipkowski, J., In situ electrochemical and PM-IRRAS studies of alamethicin ion channel formation in model phospholipid bilayers. *J. Electroanal. Chem.* **2018**, *819*, 251-259.

313.Mrdenovic, D.; Su, Z.; Kutner, W.; Lipkowski, J.; Pieta, P., Alzheimer's disease-related amyloid β peptide causes structural disordering of lipids and changes the electric properties of a floating bilayer lipid membrane. *Nanoscale Advances* **2020**.

314.Raila, T.; Penkauskas, T.; Jankunec, M.; Dreizas, G.; Meškauskas, T.; Valincius, G., Electrochemical impedance of randomly distributed defects in tethered phospholipid bilayers: Finite element analysis. *Electrochim. Acta* **2019**, *299*, 863-874.

315.Valincius, G.; Mickevicius, M., Chapter two - tethered phospholipid bilayer membranes: an interpretation of the electrochemical impedance response. In *Advances in Planar Lipid Bilayers and Liposomes*, Iglič, A.; Kulkarni, C. V.; Rappolt, M., Eds. Academic Press: 2015; Vol. 21, pp 27-61.

316.Feigenson, G. W., Phase diagrams and lipid domains in multicomponent lipid bilayer mixtures. *Biochim. Biophys. Acta* **2009**, *1788* (1), 47-52.

317.Silvius, J. R., Thermotropic phase transitions of pure lipids in model membranes and their modifications by membrane proteins. In *Lipid-protein interactions*, John Wiley & Sons, Inc.: New York, 1982.

318.Avanti Polar Lipids, I. Phase transition temperatures for glycerophospholipids. <https://avantilipids.com/tech-support/physical-properties/phase-transition-temps> (accessed 23 Jul).

319.Kahnt, A.; Behrouzi, S.; Vermeylen, R.; Safi Shalamzari, M.; Vercauteren, J.; Roekens, E.; Claeys, M.; Maenhaut, W., One-year study of nitro-organic compounds and their relation to wood burning in PM10 aerosol from a rural site in Belgium. *Atmos. Environ.* **2013**, *81*, 561-568.

320. Wang, Y.; Hu, M.; Wang, Y.; Zheng, J.; Shang, D.; Yang, Y.; Liu, Y.; Li, X.; Tang, R.; Zhu, W.; Du, Z.; Wu, Y.; Guo, S.; Wu, Z.; Lou, S.; Hallquist, M.; Yu, J. Z., The formation of nitro-aromatic compounds under high NO_x and anthropogenic VOC conditions in urban Beijing, China. *Atmos. Chem. Phys.* **2019**, *19* (11), 7649-7665.
321. Wang, X.; Gu, R.; Wang, L.; Xu, W.; Zhang, Y.; Chen, B.; Li, W.; Xue, L.; Chen, J.; Wang, W., Emissions of fine particulate nitrated phenols from the burning of five common types of biomass. *Environ. Pollut.* **2017**, *230*, 405-412.
322. Juhaniwicz-Dębińska, J.; Tymecka, D.; Sęk, S., Diverse effect of cationic lipopeptide on negatively charged and neutral lipid bilayers supported on gold electrodes. *Electrochim. Acta* **2019**, *298*, 735-744.
323. Kycia, A. H.; Wang, J.; Merrill, A. R.; Lipkowski, J., Atomic force microscopy studies of a floating-bilayer lipid membrane on a Au(111) surface modified with a hydrophilic monolayer. *Langmuir* **2011**, *27* (17), 10867-10877.
324. Johansson, J.; Gudmundsson, G. H.; Rottenberg, M. E.; Berndt, K. D.; Agerberth, B., Conformation-dependent antibacterial activity of the naturally occurring human peptide LL-37. *J. Biol. Chem.* **1998**, *273* (6), 3718-3724.
325. Last, N. B.; Schlamadinger, D. E.; Miranker, A. D., A common landscape for membrane-active peptides. *Protein Sci.* **2013**, *22* (7), 870-882.
326. Danielsen, P. H.; Møller, P.; Jensen, K. A.; Sharma, A. K.; Wallin, H.; Bossi, R.; Autrup, H.; Mølhav, L.; Ravanat, J. L.; Briedé, J. J.; de Kok, T. M.; Loft, S., Oxidative stress, DNA damage, and inflammation induced by ambient air and wood smoke particulate matter in human A549 and THP-1 cell lines. *Chem. Res. Toxicol.* **2011**, *24* (2), 168-84.
327. Dergham, M.; Lepers, C.; Verdin, A.; Billet, S.; Cazier, F.; Courcot, D.; Shirali, P.; Garçon, G., Prooxidant and proinflammatory potency of air pollution particulate matter (PM_{2.5-0.3}) produced in rural, urban, or industrial surroundings in human bronchial epithelial cells (BEAS-2B). *Chem. Res. Toxicol.* **2012**, *25* (4), 904-919.
328. Abbas, I.; Badran, G.; Verdin, A.; Ledoux, F.; Roumie, M.; Lo Guidice, J. M.; Courcot, D.; Garçon, G., In vitro evaluation of organic extractable matter from ambient PM_{2.5} using human bronchial epithelial BEAS-2B cells: Cytotoxicity, oxidative stress, pro-inflammatory response, genotoxicity, and cell cycle deregulation. *Environ. Res.* **2019**, *171*, 510-522.
329. Jaoui, M.; Lewandowski, M.; Offenbergh, J. H.; Colon, M.; Docherty, K. S.; Kleindienst, T. E., Characterization of aerosol nitroaromatic compounds: Validation of an experimental method. *Journal of Mass Spectrometry* **2018**, *53* (8), 680-692.
330. Belloli, R.; Barletta, B.; Bolzacchini, E.; Meinardi, S.; Orlandi, M.; Rindone, B., Determination of toxic nitrophenols in the atmosphere by high-performance liquid chromatography. *Journal of Chromatography A* **1999**, *846* (1), 277-281.
331. Belloli, R.; Bolzacchini, E.; Clerici, L.; Rindone, B.; Sesana, G.; Librando, V., Nitrophenols in air and rainwater. *Environ. Eng. Sci.* **2006**, *23* (2), 405-415.

332. Rubio, M. A.; Lissi, E.; Herrera, N.; Pérez, V.; Fuentes, N., Phenol and nitrophenols in the air and dew waters of Santiago de Chile. *Chemosphere* **2012**, *86* (10), 1035-1039.
333. Lüttke, J.; Levsen, K.; Acker, K.; Wieprecht, W.; Möller, D., Phenols and Nitrated Phenols in Clouds at Mount Brocken. *International Journal of Environmental Analytical Chemistry* **1999**, *74* (1-4), 69-89.
334. Levsen, K.; Behnert, S.; Mußmann, P.; Raabe, M.; Prieß, B., Organic Compounds In Cloud And Rain Water. *International Journal of Environmental Analytical Chemistry* **1993**, *52* (1-4), 87-97.
335. Leuenberger, C.; Ligocki, M. P.; Pankow, J. F., Trace organic compounds in rain. 4. Identities, concentrations, and scavenging mechanisms for phenols in urban air and rain. *Environmental Science & Technology* **1985**, *19* (11), 1053-1058.
336. Leuenberger, C.; Czuczwa, J.; Tremp, J.; Giger, W., Nitrated phenols in rain: Atmospheric occurrence of phytotoxic pollutants. *Chemosphere* **1988**, *17* (3), 511-515.
337. Levsen, K.; Behnert, S.; Prieß, B.; Svoboda, M.; Winkeler, H.-D.; Zietlow, J., Organic compounds in precipitation. *Chemosphere* **1990**, *21* (9), 1037-1061.
338. Rippen, G.; Zietz, E.; Frank, R.; Knacker, T.; Klöpffer, W., Do airborne nitrophenols contribute to forest decline? *Environmental Technology Letters* **1987**, *8* (1-12), 475-482.
339. Asman, W. A. H.; Jørgensen, A.; Bossi, R.; Vejrup, K. V.; Bügel Mogensen, B.; Glasius, M., Wet deposition of pesticides and nitrophenols at two sites in Denmark: measurements and contributions from regional sources. *Chemosphere* **2005**, *59* (7), 1023-1031.
340. Richartz, H.; Reischl, A.; Trautner, F.; Hutzinger, O., Nitrated phenols in fog. *Atmospheric Environment. Part A. General Topics* **1990**, *24* (12), 3067-3071.
341. Vanni, A.; Pellegrino, V.; Gamberini, R.; Calabria, A., An Evidence for Nitrophenols Contamination in Antarctic Fresh-Water and Snow. Simultaneous Determination of Nitrophenols and Nitroarenes at ng/L Levels. *International Journal of Environmental Analytical Chemistry* **2001**, *79* (4), 349-365.
342. Delhomme, O.; Morville, S.; Millet, M., Seasonal and diurnal variations of atmospheric concentrations of phenols and nitrophenols measured in the Strasbourg area, France. *Atmos. Pollut. Res.* **2010**, *1*, 16-22.
343. Wennrich, L.; Efer, J.; Engewald, W., Gas chromatographic trace analysis of underivatized nitrophenols. *Chromatographia* **1995**, *41* (5), 361-366.
344. Nojima, K.; Kawaguchi, A.; Ohya, T.; Kanno, S.; Hirobe, M., Studies on Photochemical Reaction of Air Pollutants. X. Identification of Nitrophenols in Suspended Particulates. *Chemical & Pharmaceutical Bulletin* **1983**, *31* (3), 1047-1051.
345. Mohr, C.; Lopez-Hilfiker, F. D.; Zotter, P.; Prévôt, A. S. H.; Xu, L.; Ng, N. L.; Herndon, S. C.; Williams, L. R.; Franklin, J. P.; Zahniser, M. S.; Worsnop, D. R.; Knighton, W. B.; Aiken, A. C.; Gorkowski, K. J.; Dubey, M. K.; Allan, J. D.; Thornton,

J. A., Contribution of Nitrated Phenols to Wood Burning Brown Carbon Light Absorption in Detling, United Kingdom during Winter Time. *Environmental Science & Technology* **2013**, *47* (12), 6316-6324.

346. Kitanovski, Z.; Grgic, I.; Vermeylen, R.; Claeys, M.; Maenhaut, W., Liquid chromatography tandem mass spectrometry method for characterization of monoaromatic nitro-compounds in atmospheric particulate matter. *J. Chromatogr. A* **2012**, *1268*, 35-43.

347. Irei, S.; Stupak, J.; Gong, X.; Chan, T.-W.; Cox, M.; McLaren, R.; Rudolph, J., Molecular marker study of particulate organic matter in Southern Ontario air. *Journal of Analytical Methods in Chemistry* **2017**, *2017*, 19.

348. Kitanovski, Z.; Shahpoury, P.; Samara, C.; Voliotis, A.; Lammel, G., Composition and mass size distribution of nitrated and oxygenated aromatic compounds in ambient particulate matter from southern and central Europe – implications for the origin. *Atmos. Chem. Phys.* **2020**, *20* (4), 2471-2487.

349. Li, X.; Jiang, L.; Hoa, L. P.; Lyu, Y.; Xu, T.; Yang, X.; Iinuma, Y.; Chen, J.; Herrmann, H., Size distribution of particle-phase sugar and nitrophenol tracers during severe urban haze episodes in Shanghai. *Atmospheric Environment* **2016**, *145*, 115-127.

350. Özel, M. Z.; Hamilton, J. F.; Lewis, A. C., New sensitive and quantitative analysis method for organic nitrogen compounds in urban aerosol samples. *Environmental Science & Technology* **2011**, *45* (4), 1497-1505.

351. Teich, M.; Pinxteren, D.; Herrmann, H., Determination of nitrophenolic compounds from atmospheric particles using hollow-fiber liquid-phase microextraction and capillary electrophoresis/mass spectrometry analysis. *Electrophoresis* **2014**, *35* (9), 1353-1361.

352. Zhang, Y. Y.; Müller, L.; Winterhalter, R.; Moortgat, G. K.; Hoffmann, T.; Pöschl, U., Seasonal cycle and temperature dependence of pinene oxidation products, dicarboxylic acids and nitrophenols in fine and coarse air particulate matter. *Atmos. Chem. Phys.* **2010**, *10* (16), 7859-7873.

353. Lanzafame, G. M.; Srivastava, D.; Favez, O.; Bandowe, B. A. M.; Shahpoury, P.; Lammel, G.; Bonnaire, N.; Alleman, L. Y.; Couvidat, F.; Bessagnet, B.; Albinet, A., One-year measurements of secondary organic aerosol (SOA) markers in the Paris region (France): Concentrations, gas/particle partitioning and SOA source apportionment. *Science of The Total Environment* **2021**, *757*, 143921.

354. Yassine, M. M.; Suski, M.; Dabek-Zlotorzynska, E., Characterization of benzene polycarboxylic acids and polar nitroaromatic compounds in atmospheric aerosols using UPLC-MS/MS. *Journal of Chromatography A* **2020**, *1630*, 461507.

355. Schmidt-Bäumler, K.; Heberer, T.; Stan, H.-J., Occurrence and distribution of organic contaminants in the aquatic system in Berlin. Part II: Substituted phenols in Berlin surface water. *Acta hydrochimica et hydrobiologica* **1999**, *27* (3), 143-149.

356. Belloli, R.; Barletta, B.; Bolzacchini, E.; Meinardi, S.; Orlandi, M.; Rindone, B., Determination of toxic nitrophenols in the atmosphere by high-performance liquid chromatography. *Journal of Chromatography A* **1999**, *846* (1-2), 277-281.

357. Legrand, C.; Bour, J. M.; Jacob, C.; Capiamont, J.; Martial, A.; Marc, A.; Wudtke, M.; Kretzmer, G.; Demangel, C.; Duval, D., Lactate dehydrogenase (LDH) activity of the number of dead cells in the medium of cultured eukaryotic cells as marker. *Journal of biotechnology* **1992**, *25* (3), 231-243.
358. Pucci, B.; Kasten, M.; Giordano, A., Cell cycle and apoptosis. *Neoplasia* **2000**, *2* (4), 291-299.
359. Wu, J.; Shi, Y.; Asweto, C. O.; Feng, L.; Yang, X.; Zhang, Y.; Hu, H.; Duan, J.; Sun, Z., Fine particle matters induce DNA damage and G2/M cell cycle arrest in human bronchial epithelial BEAS-2B cells. *Environmental Science and Pollution Research* **2017**, *24* (32), 25071-25081.
360. Lin, Z.; Zhong, P.; Yin, K.; Zhao, D.; Wang, L.; Yu, H., Use of the IC50 for predicting joint toxic effects of mixtures. *Bull Environ Contam Toxicol* **2004**, *72* (3), 571-8.
361. Elmore, S., Apoptosis: a review of programmed cell death. *Toxicol Pathol* **2007**, *35* (4), 495-516.
362. Fink, S. L.; Cookson, B. T., Apoptosis, pyroptosis, and necrosis: mechanistic description of dead and dying eukaryotic cells. *Infection and immunity* **2005**, *73* (4), 1907-1916.
363. An, J.; Zhou, Q.; Wu, M.; Wang, L.; Zhong, Y.; Feng, J.; Shang, Y.; Chen, Y., Interactions between oxidative stress, autophagy and apoptosis in A549 cells treated with aged black carbon. *Toxicology in Vitro* **2019**, *54*, 67-74.
364. Klhlbrandt, W., Structure and function of mitochondrial membrane protein complexes. *BMC Biology* **2015**, *13* (1), 89.
365. Martindale, J. L.; Holbrook, N. J., Cellular response to oxidative stress: signaling for suicide and survival. *Journal of cellular physiology* **2002**, *192* (1), 1-15.
366. Wright, D. T.; Cohn, L. A.; Li, H.; Fischer, B.; Li, C. M.; Adler, K. B., Interactions of oxygen radicals with airway epithelium. *Environmental health perspectives* **1994**, *102 Suppl 10* (Suppl 10), 85-90.
367. Oh, S. M.; Kim, H. R.; Park, Y. J.; Lee, S. Y.; Chung, K. H., Organic extracts of urban air pollution particulate matter (PM2.5)-induced genotoxicity and oxidative stress in human lung bronchial epithelial cells (BEAS-2B cells). *Mutation Research/Genetic Toxicology and Environmental Mutagenesis* **2011**, *723* (2), 142-151.
368. Chazotte, B., Labeling mitochondria with TMRM or TMRE. *Cold Spring Harbor Protocols* **2011**, *2011* (7), pdb-prot5641.
369. Zorova, L. D.; Popkov, V. A.; Plotnikov, E. Y.; Silachev, D. N.; Pevzner, I. B.; Jankauskas, S. S.; Babenko, V. A.; Zorov, S. D.; Balakireva, A. V.; Juhaszova, M., Mitochondrial membrane potential. *Analytical biochemistry* **2018**, *552*, 50-59.

- 370.Homma, S.; Ishii, Y.; Morishima, Y.; Yamadori, T.; Matsuno, Y.; Haraguchi, N.; Kikuchi, N.; Satoh, H.; Sakamoto, T.; Hizawa, N.; Itoh, K.; Yamamoto, M., Nrf2 Enhances Cell Proliferation and Resistance to Anticancer Drugs in Human Lung Cancer. *Clinical Cancer Research* **2009**, *15* (10), 3423-3432.
- 371.Rowlands, D. J., Mitochondria dysfunction: A novel therapeutic target in pathological lung remodeling or bystander? *Pharmacol Ther* **2016**, *166*, 96-105.
- 372.Costa, A. N.; Moreno, V.; Prieto, M. J.; Urbano, A. M.; Alpoim, M. C., Induction of morphological changes in BEAS-2B human bronchial epithelial cells following chronic sub-cytotoxic and mildly cytotoxic hexavalent chromium exposures. *Mol Carcinog* **2010**, *49* (6), 582-91.
- 373.Zhang, Y.; Darland, D.; He, Y.; Yang, L.; Dong, X.; Chang, Y., Reduction Of Pm2.5 Toxicity On Human Alveolar Epithelial Cells A549 By Tea Polyphenols. *J Food Biochem* **2018**, *42* (3).
- 374.Polster, B. M.; Nicholls, D. G.; Shealinna, X. G.; Roelofs, B. A., Use of potentiometric fluorophores in the measurement of mitochondrial reactive oxygen species. *Methods in enzymology* **2014**, *547*, 225-250.
- 375.Logan, A.; Pell, V. R.; Shaffer, K. J.; Evans, C.; Stanley, N. J.; Robb, E. L.; Prime, T. A.; Chouchani, E. T.; CochemĆ, H. M.; Fearnley, I. M.; Vidoni, S.; James, A. M.; Porteous, C. M.; Partridge, L.; Krieg, T.; Smith, R. A. J.; Murphy, M. P., Assessing the Mitochondrial Membrane Potential in Cells and InĀ Vivo using Targeted Click Chemistry and Mass Spectrometry. *Cell Metab* **2016**, *23* (2), 379-385.
- 376.Murphy, M. P., How mitochondria produce reactive oxygen species. *Biochemical journal* **2009**, *417* (1), 1-13.
- 377.Smith, R. A. J.; Hartley, R. C.; CochemĆ, H. M.; Murphy, M. P., Mitochondrial pharmacology. *Trends in Pharmacological Sciences* **2012**, *33* (6), 341-352.
- 378.Indo, H. P.; Yen, H.-C.; Nakanishi, I.; Matsumoto, K.-I.; Tamura, M.; Nagano, Y.; Matsui, H.; Gusev, O.; Cornette, R.; Okuda, T.; Minamiyama, Y.; Ichikawa, H.; Suenaga, S.; Oki, M.; Sato, T.; Ozawa, T.; Clair, D. K. S.; Majima, H. J., A mitochondrial superoxide theory for oxidative stress diseases and aging. *J Clin Biochem Nutr* **2015**, *56* (1), 1-7.
- 379.Vyssokikh, M. Y.; Holtze, S.; Averina, O. A.; Lyamzaev, K. G.; Panteleeva, A. A.; Marey, M. V.; Zinovkin, R. A.; Severin, F. F.; Skulachev, M. V.; Fasel, N.; Hildebrandt, T. B.; Skulachev, V. P., Mild depolarization of the inner mitochondrial membrane is a crucial component of an anti-aging program. *Proceedings of the National Academy of Sciences* **2020**, *117* (12), 6491.
- 380.Aon, M. A.; Cortassa, S.; O'Rourke, B., Redox-optimized ROS balance: a unifying hypothesis. *Biochimica et Biophysica Acta (BBA)-Bioenergetics* **2010**, *1797* (6-7), 865-877.

381. Li, X.; Fang, P.; Mai, J.; Choi, E. T.; Wang, H.; Yang, X.-f., Targeting mitochondrial reactive oxygen species as novel therapy for inflammatory diseases and cancers. *Journal of Hematology & Oncology* **2013**, *6* (1), 19.
382. Antico Arciuch, V. G.; Elguero, M. a. E.; Poderoso, J. J.; Carreras, M. a. C., Mitochondrial regulation of cell cycle and proliferation. *Antioxidants & redox signaling* **2012**, *16* (10), 1150-1180.
383. Krysko, D. V.; Vanden Berghe, T.; Dä€™Herde, K.; Vandenabeele, P., Apoptosis and necrosis: Detection, discrimination and phagocytosis. *Methods* **2008**, *44* (3), 205-221.
384. Hongmei, Z., *Extrinsic and intrinsic apoptosis signal pathway review*. InTechOpen: 2012.
385. Wu, C.-C.; Bratton, S. B., Regulation of the Intrinsic Apoptosis Pathway by Reactive Oxygen Species. *Antioxidants & Redox Signaling* **2012**, *19* (6), 546-558.
386. Künzi, L.; Krapf, M.; Daher, N.; Dommen, J.; Jeannet, N.; Schneider, S.; Platt, S.; Slowik, J. G.; Baumlin, N.; Salathe, M.; Prévôt, A. S. H.; Kalberer, M.; Strähl, C.; Dübng, L.; Sioutas, C.; Baltensperger, U.; Geiser, M., Toxicity of aged gasoline exhaust particles to normal and diseased airway epithelia. *Scientific Reports* **2015**, *5* (1), 11801.
387. Liang, Y.; Jen, C. N.; Weber, R. J.; Misztal, P. K.; Goldstein, A. H., Chemical composition of PM_{2.5} in October 2017 Northern California wildfire plumes. *Atmos. Chem. Phys.* **2021**, *21* (7), 5719-5737.
388. Finewax, Z.; de Gouw, J. A.; Ziemann, P. J., Identification and Quantification of 4-Nitrocatechol Formed from OH and NO₃ Radical-Initiated Reactions of Catechol in Air in the Presence of NO_x: Implications for Secondary Organic Aerosol Formation from Biomass Burning. *Environmental Science & Technology* **2018**, *52* (4), 1981-1989.
389. Desyaterik, Y.; Sun, Y.; Shen, X.; Lee, T.; Wang, X.; Wang, T.; Collett Jr, J. L., Speciation of "brown" carbon in cloud water impacted by agricultural biomass burning in eastern China. *Journal of Geophysical Research: Atmospheres* **2013**, *118* (13), 7389-7399.
390. Kodros, J. K.; Papanastasiou, D. K.; Paglione, M.; Masiol, M.; Squizzato, S.; Florou, K.; Skyllakou, K.; Kaltsonoudis, C.; Nenes, A.; Pandis, S. N., Rapid dark aging of biomass burning as an overlooked source of oxidized organic aerosol. *Proceedings of the National Academy of Sciences* **2020**, *117* (52), 33028.
391. de Oliveira Alves, N.; Vessoni, A. T.; Quinet, A.; Fortunato, R. S.; Kajitani, G. S.; Peixoto, M. S. e.; de Souza Hacon, S.; Artaxo, P.; Saldiva, P.; Menck, C. F. M., Biomass burning in the Amazon region causes DNA damage and cell death in human lung cells. *Scientific reports* **2017**, *7* (1), 1-13.
392. Bertrand, A.; Stefenelli, G.; Jen, C. N.; Pieber, S. M.; Bruns, E. A.; Ni, H.; Temime-Roussel, B.; Slowik, J. G.; Goldstein, A. H.; Haddad, I. E., Evolution of the chemical fingerprint of biomass burning organic aerosol during aging. *Atmospheric Chemistry and Physics* **2018**, *18* (10), 7607-7624.

393. Simoneit, B. R. T.; Schauer, J. J.; Nolte, C. G.; Oros, D. R.; Elias, V. O.; Fraser, M. P.; Rogge, W. F.; Cass, G. R., Levoglucosan, a tracer for cellulose in biomass burning and atmospheric particles. *Atmospheric Environment* **1999**, *33* (2), 173-182.

394. Liang, Y.; Sengupta, D.; Campmier, M. J.; Lunderberg, D. M.; Apte, J. S.; Goldstein, A. H., Wildfire smoke impacts on indoor air quality assessed using crowdsourced data in California. *Proceedings of the National Academy of Sciences* **2021**, *118* (36), e2106478118.

395. Ikemori, F.; Nakayama, T.; Hasegawa, H., Characterization and possible sources of nitrated mono- and di-aromatic hydrocarbons containing hydroxyl and/or carboxyl functional groups in ambient particles in Nagoya, Japan. *Atmospheric Environment* **2019**, *211*, 91-102.



B.546/22



ICChF

Institute of Physical Chemistry PAS

Biblioteka Instytutu Chemii Fizycznej PAN

F-B-546/22



80000000343608